

DTIC FILE COPY

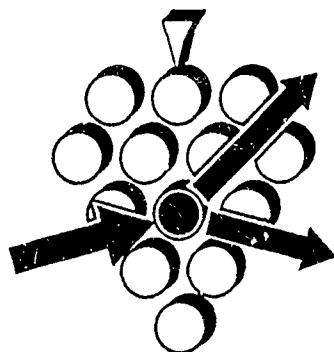
UNIVERSITY OF BORDEAUX

~~UNIVERSITY OF BORDEAUX~~  
EDISON HOUSE

Unlimited

1

AD-A218 399



BORDEAUX  
20 - 25 JULY 1986

DTIC  
ELECTE  
FEB 20 1990  
S D & D

ABSTRACTS

90 02 16 023

# 9TH. INTERNATIONAL SYMPOSIUM ON GAS KINETICS

DISTRIBUTION STATEMENT A

Approved for public release  
Distribution Unlimited

Under the auspices of the Gas Kinetics Group  
of the Royal Society of Chemistry of Great Britain  
and the Division de Chimie-Physique de la Société Française de Chimie.

---

### INTERNATIONAL ORGANISING COMMITTEE

F. BARONNET (Nancy)	R. MARX (Orsay)
G. LE BRAS (Orléans)	M.J. PILLING (Oxford)
R. LESCLAUX (Bordeaux)	I.W.M. SMITH (Birmingham)

### LOCAL ORGANISING COMMITTEE

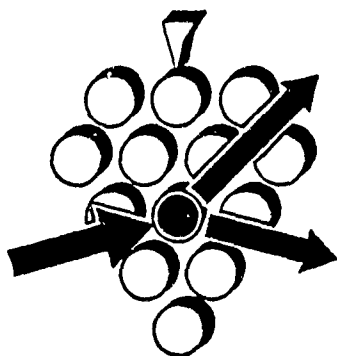
F. CARALP	G. DORTHE	J.C. RAYEZ
P. CAUBET	P. HALVICK	M.T. RAYEZ
M. COSTES	R. LESCLAUX	B. VEYRET
M. DESTRIAU	C. NAULIN	

Chas. T. H.

Approved for public release;  
distribution unlimited.

9 0 01 18 0 27

UNIVERSITY OF BORDEAUX



**BORDEAUX**  
**20 - 25 JULY 1986**

## **ABSTRACTS**

# **9TH. INTERNATIONAL SYMPOSIUM ON GAS KINETICS**

*Under the auspices of the Gas Kinetics Group  
of the Royal Society of Chemistry of Great Britain  
and the Division de Chimie-Physique de la Société Française de Chimie.*



## CONFERENCE PROGRAMME

Registration and scientific sessions will take place in the grounds of the law school of the University, avenue Léon Duguit.

### SUNDAY 20 JULY

16.00 - 21.00

19.00 - 21.00

Registration

Get-together and buffet in the Conference Hall

STATEMENT "A" per D. Tyrell

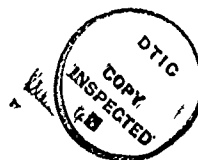
AFOSR/XCTD (~~136~~)

TELECON

2/16/90

CG

Accession For	
NTIS CRA&I	<input checked="" type="checkbox"/>
DTIC TAB	<input type="checkbox"/>
Unannounced	<input type="checkbox"/>
Justification	
By <i>per call</i>	
Distribution /	
Availability Codes	
Dist	Avail and/or Special
<i>A-1</i>	



MONDAY 21 JULY

09.00 - 09.20 Official Welcome

→ Partial continuity

SESSION A - THEORY AND DYNAMICS

09.20 - 10.00 A1 Dynamical bottlenecks and tunneling path for chemical reactions;  
D.G. Truhlar

10.00 - 10.20 A2 Study of the  $H + H_2$  ( $V = 1$ ) reaction and its isotopic analogs.  
V.B. Rozenshtein, Y.M. Gershenzon,  
A.V. Ivanov, S.D. Ilin, S.I. Kucheryavii and  
S.Y. Umanskii

10.20 - 10.40 A3 Reduced dimensionality rate constant calculations for  $O(^3P) + H_2$  ( $D_2$ , HD)  $\rightarrow$  OH (OD) + H(D) : comparison between theory and experiment.  
A.F. Wagner, T.H. Dunning, Jr. and  
J.M. Bowman

10.40 - 11.20 Coffee

11.20 - 11.40 A4 Reactions on attractive potential energy surfaces : connections between rate and potential parameters.  
J. Troe

11.40 - 12.00 A5 A theoretical prediction of rate coefficients for reactions involving intermediate complex formation.  
J.A. Miller, C.F. Melius and N.J. Brown

12.00 - 12.20 A6 The dynamics of the reactions of  $O(^1D_2)$  with hydrogen-containing halocarbons.  
P.M. Aker, B. Niefer, J.J. Sloan and  
H. Heydtmann.

MONDAY 21 JULY

12.20 - 12.40 A7 LIF measurements on product state distributions in radical-radical reactions.  
B.J. Orr, I.W.M. Smith and R.P. Tuckett

13.00 Lunch

SESSION B - MOLECULAR BEAMS

14.30 - 15.10 B1 Reactivity of Van der Waals complexes;  
C. Jouvet, M.C. Duval, W.H. Breckenridge,  
B. Soep

15.10 - 15.30 B2 The dynamics of reactive collisions of atomic carbon.  
G. Dorthé, M. Costes, C. Naulin, Ph. Caubet,  
C. Vaucamps and G. Nouchi

15.30 - 15.50 B3 Molecular beam study of the radical group effect in the  $K + RI \rightarrow KI + R$  ( $R = CH_3, C_2H_5, nC_3H_7$ ) reactive collisions.  
V. Saez Rabanos, F.J. Aoiz, V.J. Herrero,  
E. Verdasco and A. González Urena

15.50 - 16.10 B4 Laser induced fluorescence study of reactions of Ca with  $CH_3I$  and  $CF_3I$  in the molecular beam-gas apparatus.  
Guo-zhong He, Jue Wang, R.S. Tse and Nan-quan Lou

16.10 - 16.40 Coffee

16.40 - 17.00 B5 Energy and angular momentum disposal in chemiluminescent electronically excited atomic reactions;  
K. Johnson, A. Kvaran, J.P. Simons and P.A. Smith

MONDAY 21 JULY

- 17.00 - 17.40 B6 Topological study on three and four atom indirect exchange reactions. Application to the processes  $C(^3P) + NO(X^2\Pi)$  and  $C(^3P) + N_2O(X^1\Sigma^+)$ .  
M.T. Rayez, P. Halvick, B. Duguay and J.C. Rayez
- 17.40 - 18.00 B7 Dynamical processes of detachment in  $Cl^-/H_2$ .  
M. Barat, J.C. Brenot, M. Durup-Ferguson, J. Fayeton, J.C. Houver and J.B. Ozenne
- 19.00 Reception at City Hall.

TUESDAY 22 JULY

SESSION C - ATMOSPHERIC REACTIONS -

09.00 - 09.40 C1 Some current problems in atmospheric trace gas chemistry, the role of chemical kinetics;  
R.A. Cox

09.40 - 10.00 C2 Absolute rate constants for the gas-phase reaction of  $\text{NO}_3$  radicals with reduced sulfur compounds.  
T.J. Wallington, R. Atkinson, A.M. Winer and J.N. Pitts

10.00 - 10.20 C3 Thermal stability of peroxy nitrates.  
A. Reimer and F. Zabel

10.20 - 10.40 C4 The sticking of gas molecules to water surfaces.  
J. Gardner, L. Sharfman, Y.G. Adewuyi  
P. Davidovits, M.S. Zahniser, D.R. Worsnop and C.E. Kolb

10.40 - 11.20 Coffee

11.20 - 11.40 C5 Discharge flow determination of the rate constants for the reactions  $\text{OH} + \text{SO}_2 + \text{He}$  and  $\text{HOSO}_2 + \text{O}_2$ .  
D. Martin, J.L. Jourdain and G. Le Bras

11.40 - 12.00 C6 High resolution Fourier transform spectroscopy of gas phase radicals and reaction products.  
J.B. Burkholder, P.D. Hammer and C.J. Howard

12.00 - 12.20 C7 Kinetics and mechanism of atmospheric  $\text{CS}_2$  oxidation.  
A.R. Ravishankara, E.R. Lovejoy, N.S. Wang, C.J. Howard, P.H. Whine, J.M. Nicovich and A.J. Hynes

11

TUESDAY 22 JULY

12.20 - 12.40 C8 Examination of the temperature dependence for the reaction of OH radicals with heterocyclic aromatics (imidazole, furan, pyrrole and thiophene) and the unimolecular decay of the adducts imidazole-OH and thiophene-OH.

F. Witte and C. Zetzsch

13.00 Lunch

SESSION D - UNIMOLECULAR REACTIONS -

14.30 - 15.10 D1 The chemical dynamics of highly vibrationally excited molecules;  
F.F. Crim

15.10 - 15.30 D2 Mode selectivity in reactions induced by vibrational overtone excitation.  
J.E. Baggott, D.W. Law, P.D. Lightfoot and I.M. Mills

15.30 - 15.50 D3 Analytic solution of relaxation in a system with exponential transition probabilities.  
W. Forst and Guo-Ying Xu

15.50 - 16.10 D4 Mode specificity in intramolecular vibrational relaxation and unimolecular reactions: a semi-classical analysis.  
V. Aquilanti, S. Cavalli and G. Grossi

16.10 - 16.50 Coffee

16.50 - 17.10 D5 The "a priori" calculation of collisional energy transfer in highly vibrationally excited molecules.  
K.F. Lim and R.G. Gilbert

✓

## TUESDAY 22 JULY

- 17.10 - 17.30 D6 Multiphoton ionization studies on collisional energy transfer and unimolecular reactions of excited benzene derivatives.  
H.G. Löhmannsröben, K. Luther and K. Reihs
- 17.30 - 17.50 D7 Is propylene oxide cation radical behaving non-ergodically in its dissociation reactions ?  
C. Lifshitz, T. Peres, N. Ohmichi, I. Pri-Bar and L. Radom
- 17.50 - 18.10 D8 Energy selected ion chemistry by photoelectron photoion coincidence and laser induced dissociation.  
T. Baer, L. Bunn, S. Olesik and J.C. Morrow
- 18.30 Dinner
- 19.20 - 20.10 F. KAUFMAN Memorial Conference by D.M. Golden.

## SESSION E -- POSTER SESSIONS

- 20.10 - 21.00 Odd numbers.
- 21.00 - 21.50 Even numbers.
- E1 Direct versus indirect microscopic mechanisms in the Li + HF reaction : an isotopic and orientational study.  
J.M. Alvarino, F.J. Basterrechea and A. Lagana
- E2 A trajectory surface-hopping study of  $\text{Cl}^- + \text{H}_2$  reactive collisions.  
M. Sizun, E.A. Gislason and G. Parlant
- E3 Quasiclassical trajectory study of  $\text{X} + \text{H}_2$  type reactions on realistic potential energy surfaces.  
B. Laszlo, G. Lendvay and T. Bérces
- E4 Dynamics of Collision-Induced Dissociation.  
J.E. Dove, M.E. Mandy, N. Sathyamurthy and T. Joseph

Vi

## TUESDAY 22 JULY

- E5 A dynamical investigation of the Li + HCl reaction.  
A. Lagana, E. Garcia, J.M. Alvarino and P. Palmieri
- E6 Theoretical study of the  $O(^3P) + CS_2$  gas phase reaction. Potential energy hypersurface.  
R. Sayos, M. Gonzalez, J. Bofill and A. Aguilar
- E7 Molecular beams studies of atom-molecule interactions : the adiabatic route from scattering information to anisotropic potentials.  
V. Aquilanti, L. Beneventi, G. Grossi and F. Vecchiocattivi
- E8 Reactive collision of  $O + H_2$  produced with excited states in a crossed beam experiment.  
A. Lebéhot, J. Marx, F. Aguillon and R. Campargue
- E9 Rotational excitation of the MgCl reaction product in the harpooning  $Mg(^1S) + Cl_2$  reaction.  
B. Bourguignon, M.A. Gargoura, J. McCombie, J. Rostas and G. Taieb.
- E10  $A(^2\Sigma^+)$  production by 193 nm photolysis of nitrous acid.  
D. Solgadi, F. Lahmani, E. Hontzopoulos and C. Fotakis
- E11 U.V. photoexcitation of rovibrationally excited NO.  
J. Deson, C. Lalo, F. Lempereur, J. Masanet and J. Tardieu de Maleissye
- E12 193 nm photolysis of ammonia : The intermediate in the 2-photon formation of  $NH(A^3\Pi)$ .  
R.D. Kenner, F. Rohrer, R. Browarzik, A. Kaes and F. Stuhl
- E13 Photodissociation of molecular beams of chlorinated benzene derivatives.  
T. Ichimura, Y. Mori, H. Shinohara and N. Nishi
- E14 Single- and two-photon dissociation of  $CClF_2NO$  in the visible.  
J.A. Dyet, M.R.S. McCoustra and J. Pfab
- E15  $HgBr(B \rightarrow X)$  fluorescence emission induced by KrF laser multiphoton dissociation of  $HgBr_2$ .  
P. Papagiannakopoulos and D. Zevgolís
- E16 Picosecond laser fluorescence study of the collisionless photodissociation of nitrocompounds at 266 nm.  
J.C. Mialocq and J.C. Stephenson
- E17 Product Vibrational State Distributions in the Photodissociation of Iodine - Rare Gas Clusters.  
J.M. Philippoz, H. Van den Bergh and R. Monot
- E18 Vibrational and electronic collisional relaxation of  $C_2(d^3\Pi_g, v')$  and  $(C^1\Pi_g, v')$  states.  
P. Bartolomé, M. Castillejo, J.M. Figuera and M. Martin

U71



## TUESDAY 22 JULY

- E19 The collisional quenching of  $\text{Ca}(4s3d(^1D_2))$  by  $\text{H}_2$  and  $\text{D}_2$ .  
D. Husain and G. Roberts
- E20 Collisional Electronic Quenching of  $\text{OH}(A^2\Sigma^+)$  radical.  
A. Vegiri, S.C. Farantos, P. Papagiannakopoulos and C. Fotakis
- E21 Collisional quenching of  $\text{OH}(A^2\Sigma^+, v' = 0)$  by  $\text{NH}_3$  from 250-1400K.  
J.B. Jeffries, R.A. Copeland and D.R. Crosley
- E22 Formation of  $\text{XeCl}(B^2\Sigma_{1/2})$  and  $\text{XeI}(B^2\Sigma_{1/2})$  by reaction of electronically excited  $\text{ICl}$  with  $\text{Xe}$ .  
J.P.T. Wilkinson, E.A. Kerr, R.J. Donovan, D. Shaw and I. Munro
- E23 Quenching of  $\text{NO}_3(^2E')$  by  $\text{N}_2$ : a potential photochemical source of  $\text{N}_2\text{O}$ .  
K.G. Pettrich, F. Ewig and R. Zellner
- E24 The electron swarm method as a tool to investigate the three-body electron attachment processes.  
I. Szamrej, I. Chrzascik and M. Forys
- E25 The role of Van der Waals dimers in the electron capture processes.  
I. Szamrej, I. Chrzascik and M. Forys
- E26 Reactions of ion-pair states of  $\text{Cl}_2$ .  
E. Hontzopoulos and C. Fotakis
- E27 The association reactions of  $\text{NO}^+$  with  $\text{NO}$  and  $\text{N}_2$  in  $\text{N}_2$  carrier gas.  
R.R. Burke and I. McLaren
- E28 Hot atoms in ionosphere.  
I.K. Larin and V.L. Talrose
- E29 The Chemistry of Sodium in the Mesosphere: Absolute Rates of the Reactions  $\text{Na} + \text{O}_3 \rightarrow \text{NaO} + \text{O}_2$  and  $\text{NaO} + \text{O} \rightarrow \text{Na}(^2P_J, ^2S_{1/2}) + \text{O}_2$ .  
J.M.C. Plane, D. Husain and P. Marshall.
- E30 Parameters of Activation Barriers for Hydrogen Atom Transfer Reactions from Curved Arrhenius Plots.  
H. Furue and P.D. Pacey
- E31 Mass spectrometric determination of rate constants and mechanism of atomic fluorine reactions in gas phase.  
N.I. Butkovskaya, E.S. Vasiliyev, I.I. Morozov and V.L. Talrose
- E32 Kinetic study by mass spectrometry of the reaction of hydrogen atoms with isobutane in the range 295-407 K.  
J.P. Sawerysyn, C. Lafage, B. Meriaux and A. Tighezza
- E33 Kinetics of some gas phase muonium addition reactions between 155 and 500 K.  
D.M. Garner, M. Senba, I.D. Reid, D.G. Fleming, D.J. Arseneau, R.J. Mikula and L. Lee

Viii

## TUESDAY 22 JULY

- E34 Rate constant measurements for the reactions of ground state atomic oxygen with tetramethylethylene,  $299\text{ K} \leq T \leq 1005\text{ K}$ , and isobutene,  $296\text{ K} \leq T \leq 1019\text{ K}$ .  
J.F. Smalley, R.B. Klemm and F.L. Nesbitt
- E35 A discharge flow-mass spectrometry study of the rates of the reactions of diacetylene with atomic oxygen and atomic chlorine.  
M. Mitchell, J. Brunning, W. Payne and L. Stief
- E36 Reaction of  $\text{O}(^3\text{P}) + \text{SiH}_4$  in the gas phase.  
O. Horie, P. Potzinger and B. Reimann
- E37 Rate constant for the reaction of  $\text{O}(^3\text{P})$  with 1-butene ;  $300 < T < 900\text{ K}$ .  
R.B. Klemm, F.L. Nesbitt and J.F. Smalley
- E38 Direct measurements of the reactions  $\text{NH}_2 + \text{H}_2 \rightleftharpoons \text{NH}_3 + \text{H}$  at temperatures from 670 to 1000 K.  
W. Hack and P. Rouveirolles
- E39 Laser studies of gallium atom reaction kinetics.  
S.A. Mitchell, P.A. Hackett, D.M. Rayner and M. Cantin
- E40 Reaction kinetics of gas-phase boron atoms and boron monoxide with oxygen.  
R.C. Oldenborg and L. Baughcum
- E41 Pulsed laser photolysis study of the  $\text{O} + \text{ClO}$  reaction.  
J.M. Nicovich, P.H. Wine and A.R. Ravishankara
- E42 The kinetics of  $\text{ClO}$  decay and spectroscopy of species formed.  
R.A. Cox, J.M. Davies and G.D. Hayman
- E43 Kinetic study of the reactions of  $\text{N}_2\text{O}_5$  with  $\text{OH}$ ,  $\text{HO}_2$ ,  $\text{Cl}$  and  $\text{ClO}$ .  
A. Mellouki, G. Poulet and G. Le Bras
- E44 The reactivity of the nitrate radical with alkynes and some other molecules.  
C. Canosa-Mas, S.J. Smith, S. Toby and R.P. Wayne
- E45 The gas phase reaction of ethyl radicals with  $\text{NO}_2$ .  
I. Shanahan
- E46 Kinetic measurements on the  $\text{NO} + \text{NO}_2 = \text{N}_2\text{O}_3$  reaction using a pulsed photolysis - IR laser absorption technique.  
I.W.M. Smith and G. Yarwood
- E47 Temperature and pressure dependence of the rate constant for the association reaction  $\text{CF}_3 + \text{O}_2 + \text{M} \rightarrow \text{CF}_3\text{O}_2 + \text{M}$ .  
F. Caralp, A.M. Dognon and R. Lesclaux
- E48  $\text{CX}_3 - \text{O}_2$  Bond Dissociation Energies  
L. Batt and P. Stewart,

ix

## TUESDAY 22 JULY

- E49 Dissociation energy of C-O bond in the  $\text{CF}_3\text{O}_2$  radical.  
V.I. Vedenev, M.Y. Goldenberg and M.A. Teitelboim
- E50 Relative rate studies for reactions of silylene.  
C.D. Eley, H.M. Frey, M.C.A. Rowe, R. Walsh and I.M. Watts
- E51 Detection of radicals in the photo-oxidation of aldehydes.  
G.K. Moortgat, J.P. Burrows, G.S. Tyndall, W. Schneider, R.A. Cox, B. Veyret and K. McAdam
- E52 Optical detection of  $\text{OH}(\Sigma^+)$  radicals during oxidation of ethylene in a jet-stirred reactor.  
A. Chakir, F. Gaillard, P. Dagaut, M. Cathonnet, J.C. Boettner and H. James
- E53 Probe sampling and ESR detection of labile species for kinetics studies in flames.  
J.F. Pauwels, M. Carlier and L.R. Sochet
- E54 Two-photon laser-excited fluorescence study of H and O atoms : temperature-dependent quenching and laser photolysis for combustion applications.  
U. Meier, K. Kohse-Höinghaus and Th. Just
- E55 An expert system for gas phase reaction mechanisms.  
P.B. Ayscough, D.L. Baulch and S.J. Chinnick
- E56 Simulation of the three P-T explosion limits in the  $\text{H}_2 - \text{O}_2$  system including detailed chemistry and multi-species transport.  
U. Maas and J. Warnatz
- E57 Study of reaction mechanisms by sensitivity analysis.  
T. Turanyi, T. Bérces and S. Vajda
- E58 Implementation of the rapid equilibrium approximation on a computer for kinetics in complex systems.  
R.A. Alberty
- E59 The selfreaction of  $\text{CH}_2\text{OH}$  — radicals and the  $\text{CH}_3\text{OH} - \text{Cl} - \text{Cl}_2$  system.  
H.H. Grotheer, G. Riekert and Th. Just
- E60 The role of decomposition reactions in flames.  
J. Vandooren, B. Walravens and P.J. Van Tiggelen
- E61 Pyrolysis of cyclohexane/n-decane/steam mixtures at ca.  $810^\circ\text{C}$ .  
F. Billaud and E. Freund
- E62 High temperature pyrolysis of toluene at very low initial concentrations.  
M. Braun-Unkhoff and P. Frank

X

TUESDAY 22 JULY

- E63 Kinetic study and modelling of propene hydrogenation-hydrogenolysis  
in pyrex vessels at about 500°C.  
J.M. Beral, C. Richard and R. Martin
- E64 Kinetics of the hydrogenation of propylene at 950 K.  
D. Perrin and M.H. Back
- E65 The chain  $\text{NF}_2$  reactions.  
Y.R. Bedjanian, Y.M. Gershenzon, O.P. Kishkovitch and V.B. Rozenshtein

WEDNESDAY 23 JULY

SESSION F - EXCITED STATES

- 09.00 - 09.40 F1 Transient gain-versus-absorption laser probing of spin-orbit states, kinetics and dynamics;  
S.R. Leone
- 09.40 - 10.00 F2 Energy partitioning in the electronically excited NO formed by the photolysis of the NO dimer.  
O. Kajimoto, K. Honma, Y. Achiba, K. Shobatake and K. Kimura
- 10.00 - 10.20 F3 The Raman spectrum of predissociating H<sub>2</sub>S.  
K. Kleinermanns and R. Suntz
- 10.20 - 11.00 Coffee
- 11.00 - 11.20 F4 Vibrational and rotational distributions of the CO product of H + CO(v = 0, J ≈ 0) with hot hydrogen atoms.  
P.L. Houston
- 11.20 - 11.40 F5 Energy disposal in O(<sup>1</sup>D) + NH<sub>3</sub> → NH<sub>2</sub> + OH reaction.  
S.G. Cheskis, A.A. Iogansen, P.V. Kulakov A.A. Titov and O.M. Sarkisov
- 11.40 - 12.00 F6 Formation and reactions of electronically excited HCl.  
M.A. Brown, P.C. Cartwright, R.J. Donovan, P.R.R. Langridge-Smith, K.P. Lawley
- 12.00 - 12.20 F7 ArF-laser photolysis of hydrazoic acid : formation and kinetics of NH(C<sup>1</sup>II).  
F. Rohrer and F. Stuhl
- 12.30 Lunch

WEDNESDAY 23 JULY

13.45	Excursions (departure from university).
20.00	Banquet

THURSDAY 24 JULY

Session G  
**SESSION G : BIMOLECULAR REACTIONS**

- 09.00 - 09.40 G1 Recent advances in free radical kinetics of oxygenated hydrocarbon species;  
R. Zellner
- 09.40 - 10.00 G2 Structure-reactivity relationships in the reaction series  $\text{OH} + \text{RCHO}$ .  
S. Dobé, T. Bérces and F. Marta
- 10.00 - 10.20 G3 On gas phase kinetics probed by a diode laser.  
R.J. Balla and L. Pasternack
- 10.20 - 10.40 G4 Kinetic microwave spectroscopy of reaction intermediates : atomic oxygen reactions with olefins.  
S. Koda, S. Tsuchiya, Y. Endo, C. Yamada and E. Hirota
- 10.40 - 11.20 Coffee
- 11.20 - 11.40 G5 Kinetics of the  $\text{CH}_3 + \text{D}$  reaction : an anomalous isotope effect.  
M. Brouard and M.J. Pilling
- 11.40 - 12.00 G6 The reaction  $\text{O}_2^+ + \text{CH}_4 \rightarrow \text{H}_2\text{COOH}^+ + \text{H}$ .  
E.E. Ferguson
- 12.00 - 12.20 G7 Kinetics of ion molecule reactions at very low temperature : the cresu technique.  
C. Rebrion, J.B Marquette, B.R. Rowe and G. Dupeyrat
- 12.20 - 12.40 G8 Neutral reactions on ions.  
A.A. Viggiano, C.A. Deakyne and J.F. Paulson
- 13.00 Lunch

XIV

THURSDAY 24 JULY

SESSION H — HIGH TEMPERATURE REACTIONS —

- 14.30 - 15.10 H1 Integration of theory and experiment in high-temperature chemical kinetics;  
D. Gutman
- 15.10 - 15.30 H2 The mechanism of the reaction  $C_2H_5 + O_2 \rightarrow C_2H_4 + HO_2$ .  
R.R. Baldwin, K. McAdam and R.W. Walker
- 15.30 - 15.50 H3 Hydroxyl-radical reactions with unsaturated hydrocarbons : effects of deuterium substitution.  
F.P. Tully, A.T. Droege and J.E.M. Goldsmith
- 15.50 - 16.10 H4 OH + olefin reaction rates at high temperatures.  
G.P. Smith
- 16.10 - 16.50 Coffee
- 16.50 - 17.10 H5 The ketenyl yield of the elementary reaction of ethyne with atomic hydrogen at  $T = 280 - 550$  K.  
J. Peeters, M. Schaekers and C. Vinckier
- 17.10 - 17.30 H6 The reaction of CH radicals with  $H_2$  from 372 to 675 K.  
S. Zabarnick, J.W. Fleming and M.C. Lin
- 17.30 - 17.50 H7 A direct study of the reaction  $CH_2(X^3B_1) + C_2H_4$  in the temperature range  $296\text{ K} < T < 728\text{ K}$ .  
T. Böhland and F. Temps



## THURSDAY 24 JULY

17.50 - 18.10 H8 Kinetics and thermodynamics of the reaction  
 $\text{H} + \text{NH}_3 \rightleftharpoons \text{NH}_2 + \text{H}_2$  by the flash photolysis-shock tube technique.  
J.W. Sutherland and J.V. Michael

18.30 Dinner

## SESSION I – POSTER SESSIONS

20.00 - 20.50 Odd numbers.

20.50 - 21.40 Even numbers.

- 11 Reaction of atomic hydrogen with monosubstituted halomethanes. A MNDO analysis of the importance of the different channels.  
M. Gonzalez, R. Sayos, J. Bofill and M. Alberti
- 12 Experimental determination of the energy distribution in photodecomposition. Diazirines and diazocompounds.  
M.J. Avila, J.M. Figuera, J. Medina and J.C. Rodriguez
- 13 A study of energy transfer processes at the collision of a polyatomic molecule with an inert gas atom by the method of classical trajectories.  
V.I. Vedenev, M.Y. Goldenberg, A.A. Levitsky, L.S. Polak and S.Y. Umansky
- 14 Transition-state theory calculations for reactions of OH with haloalkanes. II. Haloethanes.  
N. Cohen
- 15 Theoretical studies of hydrogen atom addition to carbon monoxide and the thermal dissociation of the formyl radical.  
A.F. Wagner and L.B. Harding
- 16 Resonant electronic excitation in electron- $\text{O}_2$  collision.  
D. Teillet-Billy, L. Malegat and J.P. Gauyacq
- 17 Van der Waals, charge transfer and "mixed" states of molecular complexes formed in supersonic jets.  
M. Castella, A. Tramer and F. Piuze

## THURSDAY 24 JULY

- 18 Electronic structure of mercury-argon complexes.  
O. Benoist d'Azy, W.H. Breckenridge, M.C. Duval, C. Jouvét and B. Soep
- 19 Reactions of metastable rare gas atoms with  $N_2O$  ; chemiluminescence of  $RgO^*$  ;  $Rg = Xe, Kr, Ar$ .  
A. Kvaran, A. Luoviksson, W.S. Hartree and J.P. Simons
- 110 A lifetime study on the second maximum of predissociation of the iodine  $B^3 \Pi(O_u^+)$  state.  
F. Castano, E. Martinez and M.T. Martinez
- 111 Measurement of rotational energy transfer rates for  $HD(v = 1)$  in collisions with thermal  $HD$ .  
D.W. Chandler and R.L. Farrow
- 112 Laser induced fluorescence of  $SiH_2 A^1 B_1 - X^1 A_1$  in the supersonic free jet.  
K. Obi and S. Mayama
- 113 High temperature collisional energy transfer in highly vibrationally excited molecules. II. Isotope effects in iso-propyl bromide systems.  
T.C. Brown, K.D. King and R.G. Gilbert
- 114 Unimolecular reactions following single uv-photon and multi ir-photon excitation.  
B. Abel, B. Herzog, H. Hippler and J. Troe
- 115 Laser pyrolysis of dimethylnitramine and dimethylnitrosamine.  
S.E. Nigenda, A.C. Gonzalez, D.F. McMillen and D.M. Golden
- 116 IR laser-induced decomposition of oxetanes and alkanols.  
K.A. Holbrook, G.A. Oldershaw, C.J. Shaw and P.E. Dyer
- 117 Use of Doppler broadening by the 254 nm Hg absorption line to monitor  $v \rightarrow r, t$  energy transfer in vibrationally excited gases.  
W. Braun, M.D. Scheer, R.J. Cvetanovic and V. Kaufman
- 118 Analysis of multiple decompositions in chemically activated reactions.  
P.R. Westmoreland, J.B. Howard and J.P. Longwell
- 119 Wavelength dependent isomerization of allyl isocyanide.  
J. Segall and R.N. Zare
- 120 A study of the effect of excess energy on the collisional deactivation of highly vibrationally excited 7-ethylcycloheptatriene.  
Gui-Yung Chung and R.W. Carr, Jr

XVII

## THURSDAY 24 JULY

- I21 A simple FTIR instrument for emission studies.  
P. Biggs, F.J. Holdsworth, G. Marston and R.P. Wayne
- I22 Multiphoton ionization as a kinetic probe.  
H.H. Nelson and B.R. Weiner
- I23 Intracavity detection applied to reaction rate measurements.  
J.E. Allen, Jr. and W.D. Brobst
- I24 On the errors of arrhenius parameters and estimated rate constant values.  
K. Héberger, S. Kemény and T. Vidoczy
- I25 The National Bureau of Standards chemical kinetics data base.  
J.T. Herron and R.J. Cvetanovic
- I26 Spectroscopy of  $\text{HO}_2$  and  $\text{CH}_3\text{O}_2$  radicals and kinetics of their mutual reaction.  
K. McAdam, H. Forges and B. Veyret
- I27 The kinetics of hydroxyl radical reactions with alkanes studied under atmospheric conditions.  
S.J. Harris and J.A. Kerr
- I28 Rate constant and mechanism of the reaction  $\text{OH} + \text{HCOOH}$ .  
G.S. Jolly, D.J. McKenney, D.L. Singleton, G. Paraskevopoulos and A.R. Bossard
- I29 The reactions of hydroxyl radicals with aromatic compounds.  
D.L. Baulch, I.M. Campbell and S.M. Saunders
- I30 Measurement of the rate constant of the reaction  $\text{OH} + \text{H}_2\text{S} \rightarrow \text{products}$  in the range 243 - 473 K by discharge flow laser induced fluorescence.  
P. Devolder, C. Lafage and L.R. Sochet
- I31 Reactions of OH radicals with reduced sulphur compounds.  
I. Barnes, V. Bastian and K.H. Becker
- I32 Reactions of hydroxyl radicals with sulphur containing compounds.  
P. Pagsberg, O.J. Nielsen, J. Treacy, L. Nelson and H. Sidebottom
- I33 Rate constants for the reactions of OD with  $\text{DNO}_3$  and  $\text{NO}_2$ .  
A.R. Bossard, D.L. Singleton and G. Paraskevopoulos
- I34 The kinetics of the reactions of the hydroxyl radical with molecular chlorine and bromine.  
R.B. Boodaghians, I.W. Hall and R.P. Wayne

YVIII

## THURSDAY 24 JULY

- I35 Reactions of OH radicals with acetates and glycols.  
D. Hartmann, D. Rhäsa, A. Gédra and R. Zellner
- I36 Kinetics of the reactions of SH with NO<sub>2</sub> and O<sub>2</sub>.  
R.A. Stachnik and M.J. Molina
- I37 Laser-induced fluorescence studies of the CH<sub>3</sub>S radical.  
G. Black and L.E. Jusinski
- I38 Oxidation of the H<sub>2</sub>S by the atmosphere components.  
V.P. Bulatov, M.Z. Kozliner and O.M. Sarkisov
- I39 Relaxation and reactions of NCO (X<sup>2</sup> II).  
C.J. Astbury, G. Hancock and K.G. McKendrick
- I40 Kinetic measurements of the NCO radical reaction with ethene over an extended temperature range.  
R.A. Perry
- I41 Direct rate studies of HCO radical reactions.  
J.E. Baggott, H.M. Frey, P.D. Lighfoot and R. Walsh
- I42 Reactions of CH(X<sup>2</sup> II) radicals with selected species at low pressure.  
K.H. Becker, P. Wiesen and K.D. Bayes
- I43 The temperature and pressure dependence of the reaction : CH<sub>3</sub> + O<sub>2</sub> + M → CH<sub>3</sub>O<sub>2</sub> + M.  
M. Keiffer, M.J. Pilling and M.J.C. Smith
- I44 Kinetics of the reactions of polyatomic free radicals with molecular chlorine.  
R.S. Timonen, J.J. Russell and D. Gutman
- I45 On the methyl radical-initiated thermal reaction of 2,3-dimethyl-butene-2.  
T. Körtvélyesi and L. Seres
- I46 Rate constants for some hydrocarbon radical combinations.  
L. Seres and A. Nacsá
- I47 Kinetics of the chlorination of C<sub>2</sub>H<sub>5</sub>Br and the competitive bromination of C<sub>2</sub>H<sub>5</sub>Cl, CH<sub>3</sub>CHCl<sub>2</sub>, C<sub>2</sub>H<sub>5</sub>Br, and CH<sub>3</sub>CHBr<sub>2</sub>.  
E. Tschuikow-Roux, D.R. Salomon, F. Faraji and K. Miyokawa
- I48 The chemistry of triplet vinylidene radicals : reaction with molecular oxygen.  
A. Fahr and A.H. Laufer

XIX

## THURSDAY 24 JULY

- 149 On the kinetics and thermochemistry of cyanoacetylene and the ethynyl radical.  
J.B. Halpern and G.E. Miller
- 150 The radical-radical  $\text{NF}_2$  reactions.  
Y.R. Bedjanian, Y.M. Gershenzon, O.P. Kishkovitch and V.B. Rozenshtein
- 151 Formation of molecular hydrogen by the thermal decomposition of n-dialkylperoxides in oxygen.  
K.A. Sahetchian, A. Heiss, R. Rigny and J. Tardieu de Maleissye
- 152 Reaction mechanisms for decomposition of energetic materials.  
C.F. Melius and J.S. Binkley
- 153 The pressure dependent decomposition of the trifluoromethoxy radical.  
L. Batt, M. MacKay, I.A.B. Reid and P. Stewart
- 154 Synthesis and Pyrolysis of Perfluoroazo -2- propane.  
K.V. Scherer Jr., L. Batt and P. Stewart
- 155 Experimental and theoretical study of the ethyl radical unimolecular dissociation.  
Y. Simon, J.F. Foucaut and G. Scacchi
- 156 The photochemical and thermal decomposition of some simple  $\alpha$  - dicarbonyl compounds in the gas phase.  
R.A. Back
- 157 UV-laser induced decomposition of 1,2-dichloropropane.  
M. Schneider, R. Weller and J. Wolfrum
- 158 The thermal decomposition of unsymmetrical dimethylhydrazine.  
K. Brezinsky, F.L. Dryer, D. Schmitt and D. Lourme
- 159 Oxidation of formaldehyde at low oxygen concentration.  
M. Vanpee, K. Sahetchian, V. Viossat and J. Chamboux
- 160 Pseudoflame front for methane in a lean methane air mixture.  
M. Vanpee
- 161 Dilute hydrocarbon oxidation in the presence of the  $\text{CO}/\text{H}_2\text{O}/\text{O}_2$  reaction between 960 - 1250 K at 1 atm.  
R.A. Yetter and F.L. Dryer
- 162 Kinetic and chemical study of the gas-phase oxidation of isobutane and propane.  
B. Vogin, G. Scacchi and F. Baronnet

X X

THURSDAY 24 JULY

- 163 A simplified chemical kinetic reaction mechanism for propane oxidation.  
A.Y. Abdalla, J.C. Boettner, M. Cathonnet, P. Dagaut and F. Gaillard
- 164 Gas-phase oxidation of benzene and derivatives ; formation and further  
conversion of phenols.  
R. Louw and P. Mulder
- 165 High-temperature propane oxidation.  
R.I. Moshkina, S.S. Polyak and L.B. Romanovich
- 166 The initial stage of methane oxidation at high pressures.  
V.I. Vedenev, M.Y. Goldenberg, N.I. Gorban', M.A. Teitelboim

XXI

FRIDAY 25 JULY

09.00 - 09.40 POLANYI Memorial Conference : Bond dissociation energies : a continuing story.  
S.W. Benson

*cont'd*  
SESSION J - COMPLEX REACTIONS. (AW)

09.40 - 10.00 J1 Kinetics of the halogen catalysed elimination of HCl from 1, 1, 1-trichloroethane.  
A.S. Rodgers and J. Perus

10.00 - 10.20 J2 Computer programs and data bases for the kinetics of gas phase reactions.  
G.M. Côme, G. Scacchi, Ch. Muller,  
P.M. Marquaire and P. Azay

10.20 - 10.40 J3 The thermal decomposition of n-hexane.  
F.E. Imbert and R.M. Marshall

10.40 - 11.20 Coffee

11.20 - 11.40 J4 Chain kinetics in igniting hydrocarbon-air mixtures studied by transient OH fluorescence following photolytic perturbation.  
C. Morley and L.J. Kirsh

11.40 - 12.00 J5 Modeling nitric oxide formation in combustion.  
A. Miller

12.00 - 12.20 J6 Modelling of the gas phase free radical chemistry of the plasma etching process :  
CF<sub>4</sub> and CF<sub>3</sub>/O<sub>2</sub> mixtures.  
I.C. Plumb and K.R. Ryan

12.20 - 12.40 J7 Reaction of CF<sub>3</sub> radicals on SiO<sub>2</sub> and Si surfaces between 300 - 600 K.  
R. Robertson, M.J. Rossi and D.M. Golden

XX ii

**FRIDAY 25 JULY**

12.40 Concluding remarks.

13.00 Lunch

End of conference.



DYNAMICAL BOTTLENECKS AND TUNNELING  
PATHS FOR CHEMICAL REACTIONS

Donald G. Truhlar  
Department of Chemistry, University of Minnesota,  
Minneapolis, Minnesota 55455 U.S.A.

I will present the concepts involved in variational transition state theory and multidimensional semiclassical tunneling calculations. Emphasis will be placed on vibrationally adiabatic potential curves, free energy of activation profiles, and a least-action variational principle for the analytic continuation of classical mechanics to tunneling regimes. The concepts will be illustrated by applications to determine dynamical bottlenecks and tunneling probabilities for microcanonical, thermal, and state-selected reaction rates.

This work is supported in part by the United States Department of Energy, Office of Basic Energy Sciences.

Study of the  $H + H_2(v=1)$  reaction and its isotopic analogs.

Rozenshtein V.B., Gershenzon Yu.M., Ivanov A.V., Il'in S.D.,

Kucheryavii S.I., Umanskii S.Ya

Institute of Chemical Physics, Moscow 117977, USSR

The goal of the present study is to determine the rate constants of different channels of the reactions of vibrationally excited hydrogen molecules with hydrogen atoms and its isotopic analogs. The rate constants of following processes have been measured ( $k_i$  in  $\text{cm}^3/\text{molecule s}$ ):

1.  $H + H_2(v=1) \begin{cases} \rightarrow H_2(v=0) + H \\ \rightarrow H + H_2(v=0) \end{cases}$ ,  $k_1 = 5 \cdot 10^{-11} \exp(-1450/T)$ ,  
255-300 K
2.  $D + H_2(v=1) \rightarrow DH(v=1) + H$ ,  $k_2 = 2.1 \cdot 10^{-10} \exp(-1600/T)$ ,  
254-367 K
3.  $D + H_2(v=1) \rightarrow DH(v=0) + H$ ,  $k_3 = 1.0 \cdot 10^{-10} \exp(-1550/T)$ ,  
254-367 K
4.  $D + H_2(v=1) \rightarrow D + H_2(v=0)$ ,  $k_4 \leq 2.7 \cdot 10^{-13}$ , 254 - 300 K
5.  $H + D_2(v=1) \rightarrow HD(v=1) + D$ ,  $k_5 = 4.8 \cdot 10^{-10} \exp(-3325/T)$ ,  
298-367 K
6.  $H + D_2(v=1) \rightarrow HD(v=0) + D$ ,  $k_6 = 1.3 \cdot 10^{-10} \exp(-2125/T)$ ,  
298-367 K
7.  $H + D_2(v=1) \rightarrow H + D_2(v=0)$ ,  $k_7 = 3 \cdot 10^{-11} \exp(-2125/T)$ ,  
298-367 K
8.  $D + D_2(v=1) \begin{cases} \rightarrow D_2(v=0) + D \\ \rightarrow D + D_2(v=0) \end{cases}$ ,  $k_8 \leq 1.0 \cdot 10^{-13}$ , 300 K

The experiments were carried out in a flow-tube apparatus. Atoms were produced in microwave discharge. Vibrationally excited  $H_2$  and  $D_2$  molecules were generated in quartz furnace or in microwave discharge. The H- and D- concentrations were measured by EPR method. The thermometric method was used to measure the concentrations of  $H_2(v=1)$  and  $D_2(v=1)$  molecules.

There were the experimental conditions the V-V exchange between HD( $v=1$ ) molecules and H<sub>2</sub>( $v=0$ ) or D<sub>2</sub>( $v=0$ ) molecules proceeded or was absent. This gave us an opportunity to find the rates of different channels of the reactions studied.

The results obtained are in a good agreement with the results of the recent theoretical studies.

**Reduced Dimensionality Rate Constant Calculations for  
 $\text{O}(^3\text{P}) + \text{H}_2(\text{D}_2, \text{HD}) \rightarrow \text{OH}(\text{OD}) + \text{H}(\text{D})$ :  
Comparison between Theory and Experiment**

A. F. Wagner, T. H. Dunning, Jr. and J. M. Bowman\*  
Argonne National Laboratory  
Argonne, IL 60439  
USA

Exact quantum dynamics and quasiclassical trajectory dynamics calculations on an *ab initio* and a semiempirical LEPS collinear effective potential energy surface are presented. The surfaces adiabatically incorporate the bending degree of freedom. All hydrogenic isotopic combinations of the  $\text{O}(^3\text{P}) + \text{H}_2$  reaction are examined. The results display the effects of skew angle and adiabatic barriers. The collinear dynamics studies are incorporated with reduced dimensionality techniques into transition state theory to produce fully dimensional rate constants for comparison to experiment. The results for the *ab initio* surface are in near quantitative agreement with available experimental results. The results for the semiempirical surface are less satisfactory. In particular, even though the two potential energy surfaces have almost exactly the same barrier to reaction, the experimental isotope effects alone (ie., ratios of rate constants) clearly distinguish between these two surfaces. These calculations can also be compared favorably with variational transition state theory rate constant calculations by Truhlar and Garrett.

\*Consultant. Permanent address: Emory University, Atlanta, GA., 30322, USA

Reactions on Attractive Potential Energy Surfaces:  
Connections between Rate and Potential Parameters.

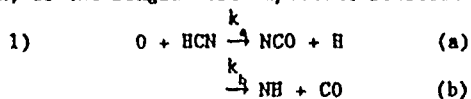
J. Troe

Institut für Physikalische Chemie der Universität Göttingen,  
Tammannstraße 6, D-3400 Göttingen, Germany

Simple short-range/long-range switching models of attractive potential energy surfaces are implemented in the statistical adiabatic channel model. By explicit determination of channel eigenvalues, state-resolved channel threshold energies are determined and investigated with respect to their dependence on the potential parameters. The treatment is applied to thermal ion-molecule capture processes over very wide temperature ranges (1 - 1000 K), to elementary thermal bimolecular reactions with redissociation of the collision complex ( $O + OH \rightleftharpoons O_2 + H$  and other examples), to thermal radical and ion recombination processes at high pressures, and to state-resolved simple bond fission reactions of excited neutral and ionic molecules. With known short-range and long-range potential data, the model becomes free from further adjustable parameters. In a series of thermal reactions, the comparison with experimental results indicates excellent agreement over very wide temperature ranges.

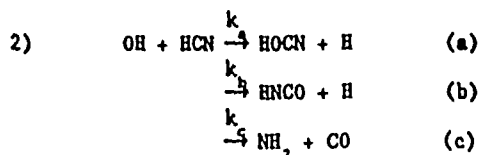
and

The emphasis in this work is on the prediction of rate coefficients and branching ratios for chemical reactions that occur over one or more potential wells. Such reactions are complicated by a number of factors. One factor is that the complex formed initially from the reactants may isomerize any number of times and each isomer may dissociate into several different product channels. In the first two projects discussed here, we use the strong-coupling (or RRKM) approximation to treat two such reactions important in the nitrogen chemistry of flames. In the third project, we use quasi-classical trajectory methods to elucidate the apparent violation of the strong-coupling approximation in the reaction  $O + OH \rightarrow O + H$ . This latter reaction, viewed from the reverse direction, is the single most important reaction in combustion

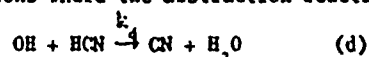


- (a) Canonical theory, CT
- (b) Canonical theory with Wigner tunneling correction, CT-W
- (c) Microcanonical theory,  $\mu$ CT (conserves energy)
- (d) Microcanonical/J - conservative theory,  $\mu$ JT (conserves energy and angular momentum)
- (e) Microcanonical/J - conservative theory with one-dimensional tunneling,  $\mu$ JT-T.

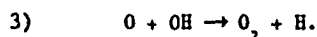
At the high end of the temperature range investigated (500 K to 2500 K), the experimental results available are predicted accurately by even the crudest theoretical treatment (canonical theory). At lower temperatures, the theoretical predictions, at all levels of approximation, using the basic BAC-HP4 parameters are too low. However, adjustments to the BAC-HP4 energy barriers within their anticipated error limits lead to satisfactory agreement with experiment over the entire temperature range. At high temperature, both  $k$  and  $k_b$  are independent of the level of approximation of the statistical theory. At low temperature, the total rate coefficient,  $k_t = k + k_b$ , is also relatively independent of the level of approximation. However, at low  $T$  the branching ratio  $k/(k + k_b)$  strongly depends on energy and angular momentum conservation and on tunneling. Each successive refinement in the theory produces larger values of  $k_t$ .



We have treated these reactions using CT,  $\mu\text{JT}$ , and  $\mu\text{JT-T}$  with BAC-MP4 potential parameters. As shown in Fig. 1, our prediction for  $k = k_a + k_b + k_c$  is in excellent agreement with the high-temperature flame results. We find that  $k_a$  is the dominant part of  $k$  at high temperature, whereas  $k_b$  is dominant at low temperature;  $k_c$  is never more than 10 percent of the total. Energy and angular momentum conservation have no effect on either  $k_a$  or  $k_b$ ; however, tunneling has a very large effect on  $k_b$  at the low end of the temperature range investigated (500 K to 250 K). As indicated by Fig. 1, the importance of this reaction in flame chemistry is limited to conditions where the abstraction reaction



is nearly equilibrated.



We have compared quasi-classical trajectory calculations of this rate coefficient (Meliuss-Blint potential) with experiment and with the variational transition-state theory calculations of Rai and Truhlar using the same potential. The most important result of this study is that all the discrepancy with experiment of the VTST predictions is made up by the trajectories. Most of the difference is due to recrossing effects, apparently violating the strong-coupling (RRKM) assumption. Figure 2 shows the comparisons.

<sup>†</sup> Author to whom correspondence should be addressed.

\* Work supported by the U.S. Department of Energy, Office of Basic Energy Sciences, Division of Chemical Sciences.

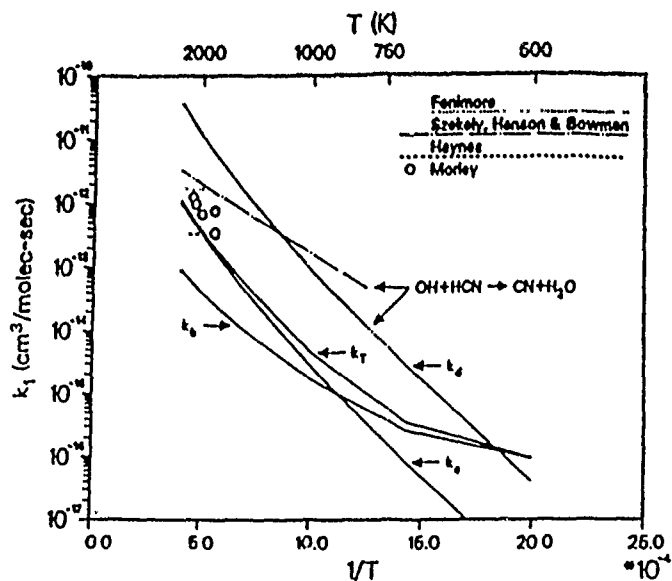


Figure 1. Comparison of experimental and theoretical results. The experimental results are from Fenimore, Haynes, Morley and Szekely, Hanson and Bowman.

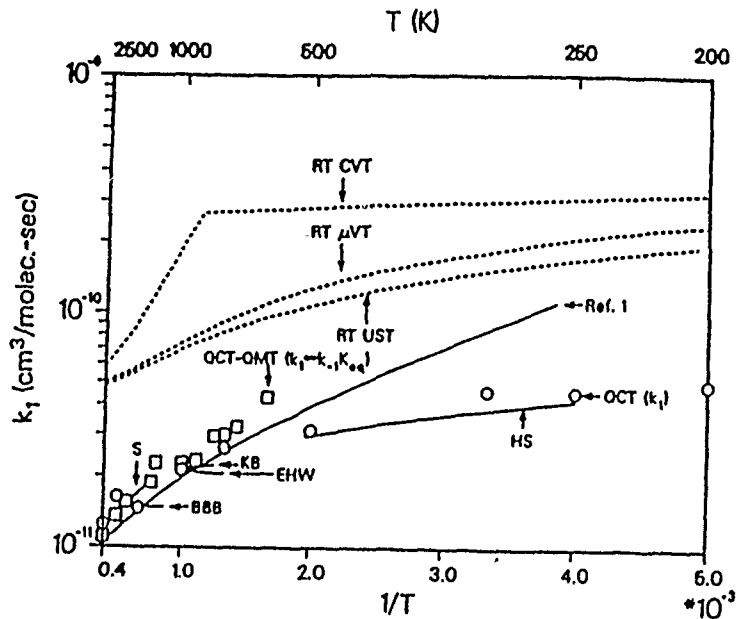


Figure 2. Arrhenius plot of  $k_{1,0} + OH \xrightarrow{k_{1,1}} O_2 + H$ . Variational transition state theory results are from Raj and Truhlar (RT). Trajectory results are from J. A. Miller, *J. Chem. Phys.* 74, 5120 (1981), (marked Ref. 1 on the figure) and from this work. Experimental results are from Smith and Howard (HS), Schott (S), Grabbs, Belles and Brokaw (BBB), Eberius, Hoyermann and Wagner (EHW), and Kurzius and Boudart (KB).



The Dynamics of the Reactions of  $O(^1D_2)$  with  
Hydrogen-Containing Halocarbons

P.H. Aker, B. Niefer and J.J. Sloan  
National Research Council of Canada  
100 Sussex Drive, Ottawa, Ontario, Canada K1A 0R6

and

H. Heydtmann  
Institut f. Physikalische Chemie  
J.W. Goethe-Universitat  
D-6000 Frankfurt/Main, West Germany

We have used an implementation of time-resolved Fourier transform spectroscopy, recently developed in this laboratory, to study the dynamics of U.V. laser-initiated reactions of  $O(^1D_2)$  with several small hydrogen-containing freons. The reagent atoms are prepared in the  $^1D_2$  electronic state with a narrow translational energy distribution by the 248 nm laser photofragmentation of ozone. State- and time-resolved observations of the products are made via low-pressure Fourier transform infrared emission spectroscopy. The instrument used for this is a slightly-modified commercial Fourier transform spectrometer to which a timing computer has been added. This timing computer monitors the operation of the computer in the commercial instrument and synchronizes the initiation of the reaction with the operation of the interferometer. As a result, the high-resolution infrared spectra of the reaction products are measured at a known time after the creation of the  $O(^1D_2)$  reagent. The time-dependences of the energy distributions give both the initial product energy distributions and the way these change due to gas phase energy transfer processes. This permits the considerable (throughput and multiplex) advantages of the Fourier transform technique to be used in kinetics and dynamics measurements.

Presently, the accuracy of the time-resolved measurement is limited to about  $\pm 5$  microseconds. The spectral resolution is limited to about  $0.02 \text{ cm}^{-1}$ . The experiments are carried out in the millitorr pressure range so that the collision time approximately matches the minimum time-resolution. In most experiments, the products can be observed before vibrational deactivation occurs and in selected cases, before rotational deactivation as well. Energy transfer information can also be obtained using this technique. By increasing the pressure in the reaction chamber and by delaying the observation time, the number of gas phase collisions involving the products can be increased in a known, controllable way. Thus observations of the distributions can be made at known times during their deactivation and the way in which their shapes change during deactivation can be observed directly. Using a master equation or other suitable procedure, this information can be used to obtain detailed energy transfer rate constants.

This technique has previously been applied to the measurement of energy partitioning in the reactions of  $O(^1D_2)$  with several small molecules. The first study was the reaction with  $H_2$ . Here, the product  $OH(^2\Pi, v', J')$  was

observed at a minimum time corresponding to about 10 gas kinetic collisions after its formation. Although the OH deactivation probability in collisions with ozone is very high, this measurement provided the initial vibrational distribution for the reaction. The rotational distribution had been thermalized before observation, however. The observed vibrational distribution,  $P(v'=1:2:3:4) = 0.29:0.32:0.25:0.13$ , is slightly inverted, suggesting specific, rather than statistical energy partitioning. These results, combined with dynamical calculations and laser-induced fluorescence measurements of the rotational distributions made in other laboratories, provide a complete picture of the reaction dynamics. The very high rotational excitation observed in the laser induced fluorescence experiments suggests an insertion mechanism which forms highly-excited HOH. The inverted vibrational distribution dictates that this intermediate exists for only one or two vibrational periods before decomposing into OH and H. Thus, although this reaction is an insertion, it has the same time scale as a direct abstraction in which products are formed in a single OHH collision without the formation of the HOH intermediate.

The work to be discussed in this Symposium involves reactions of  $O(^1D_2)$  with small hydrogen-containing halocarbons. These are all very fast and are typical of many similar reactions which make a substantial contribution to the chemistry of the ozone layer through the  $HO_x$  and  $ClO_x$  cycles. The initial measurements include the reactions with  $CHCl_3$ ,  $CHF_3$  and  $CHF_2Cl$ . These systems are more complicated than the triatomic case as they have the possibility for multiple reaction channels forming chemically different products. In addition, the vibrational deactivation rates in collisions with the unused halocarbon reagents are high and there is the possibility for fast secondary reactions among the radical products of the primary reaction. All of these factors complicate the interpretation of the long-time behaviour observed in these systems. In the work to be discussed, we have observed two primary reaction branches - one a direct abstraction forming OH and one an addition-elimination in which the primary product is a hydrogen halide. Work in other laboratories has suggested that there is also a channel in which the halogen oxide is formed directly, but this process would not be observable in our experiment.

In the  $CHCl_3$  reaction, the branching ratios indicate that the direct hydrogen abstraction channel and the addition-elimination (forming HCl) have comparable importance. The dynamics of the two channels, however, are not the same. The initial distribution of the HCl is very "cold" - the vibrational populations decrease rapidly with increasing vibrational level. This indicates that the interaction time for this process is long and a statistical amount of the large reaction exoergicity (650 kJ/mole) is retained by the  $COCl_2$  fragment. CO is also observed as an initial product of this reaction, suggesting that the energized  $COCl_2$  decomposes into CO and either 2 Cl or  $Cl_2$ . The OH vibrational distribution is more excited than that of the HCl, indicating that it is likely formed in a simple, direct abstraction process. A secondary reaction, forming HCl with strong vibrational excitation, is observed at later times in this system. The identity of the latter reaction is presently unknown.

Results of experiments of the  $CHF_3$  reaction are broadly similar to these, but differ in some details. In this case, no OH is observed within the signal to noise of the present data. Since the infrared transition probabilities of OH are extremely weak, however, the abstraction reaction may

still be occurring. No CO is observed in this reaction and since this product should be observable, its absence suggests that the energetic  $\text{COF}_2$  does not decompose as readily as  $\text{COCl}_2$ . Although the initial HF vibrational excitation is low, it has substantial rotational excitation, indicating that the HF elimination involves the transfer of the H atom from an extended C-H configuration so that an orbiting motion about the F atom is created. The results of the  $\text{CHF}_2\text{Cl}$  experiments are similar in many ways to the  $\text{CHF}_3$  observations. In this case as well, HF is formed with low vibrational, but high rotational excitation. HCl is produced in substantially less than the statistically-expected amount, however, and the initial data contain no evidence for the H-abstraction channel or for any detectable secondary reaction within the time-frame available to the experiment.

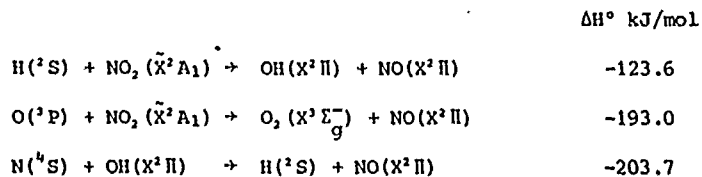
## LIF Measurements on Product State Distributions in Radical-Radical Reactions

Brian J. Orr,<sup>1</sup> Ian W.M. Smith, Richard P. Tuckett

Department of Chemistry, University of Birmingham,

P.O. Box 363, Birmingham B15 2TT, U.K.

Collisions between free radicals (species with one or more unpaired electron) are likely to proceed via a transition collision complex, since the formation of a new chemical bond can lead to a deep minimum on one of the potential energy surfaces which correlate with the reaction products. Such reactions have no activation energy, and measurements of the rovibrational product state distribution can indicate the role, if any, played in the dynamics by the formation of the complex. Measurements of this kind are rare, and we are using laser-induced fluorescence (LIF) to probe the product state distribution from a number of such reactions, especially those producing NO X<sup>2</sup>Π. We expect to report detailed vibrational, rotational, spin-orbit, and Λ-doublet distributions for the products of the following exothermic reactions:



The reactions are carried out in a low pressure chamber under near collision-free or arrested relaxation conditions, so that we try to observe the initial product state distributions prior to relaxation occurring.

The H + NO<sub>2</sub> reaction is exothermic enough to populate up to OH v''=3 and NO v''=5. We have probed both fragments by single photon LIF via the OH A<sup>2</sup>Σ<sup>+</sup> - X<sup>2</sup>Π (308 nm) and NO A<sup>2</sup>Σ<sup>+</sup> - X<sup>2</sup>Π (226 nm) band systems. This reaction has been studied by other groups (e.g. 1,2,3), but they have all only probed

the OH distribution. This is the first published observation of the NO distribution by LIF. Our initial results can be summarised as follows:

- a) The OH is produced rotationally and vibrationally hot.
- b) The OH  $X^2\Pi$  A-doublets are unequally populated, with the  $\Pi^+$  levels (from which P,R branches originate) preferentially populated over the  $\Pi^-$  levels (from which Q branches originate).
- c) The NO is produced vibrationally cold with Population ( $v=1$ )/Population( $v=0$ )  $< 0.02$ .
- d) We have not yet attained a low enough pressure to prevent rotational relaxation of NO, so NO( $v=0$ ) shows a thermalised rotational distribution.

#### References

1. R.P. Mariella, B. Lantzsch, V.T. Maxson and A.C. Luntz, 1978, J. Chem. Phys., 69, 5411.
2. J.A. Silver, W.L. Dimpfl, J.H. Brophy and J.L. Kinsey, 1976, J. Chem. Phys., 65, 1811.
3. J.C. Polanyi and J.J. Sloan, 1975, Int. J. Chem. Kinet. Symp., 1, 51.

<sup>1</sup>Permanent address: Department of Chemistry, University of New South Wales, P.O. Box 1, Kensington, Australia 2033.

## REACTIVITY OF VAN DER WAALS COMPLEXES

C. Jouvet, M.C. Duval, W.H. Breckenridge, B. Soep

Laboratoire de Photophysique Moléculaire

Bât. 213 - Université de Paris-Sud

91405 - ORSAY Cedex - France.

We have developed a method which initiates selectively a photochemical reaction. We prepare the reactants within a van der Waals complex which is then lifted into the reactive surface by tunable selective laser excitation. These reaction conditions similar to a photodissociation at the low temperatures of supersonic free jets, are experimentally simple and provide the least averaging over the various collision parameters.

This technique applied to the complex  $\text{Hg} - \text{H}_2$  has revealed an orbitally selective reaction. The reaction pathways within the excited complex ( $^3\Pi_1$ ) region depend upon the orientation of the 6p mercury orbital perpendicular or parallel to the  $\text{Hg} - \text{H}_2$  internuclear axis.

The reaction is shown to proceed directly when the 6p orbital is oriented perpendicular to the internuclear axis by an insertion mechanism through the hydrogen bond exactly as could be foresighted. On the contrary, the reaction is indirect for a non perpendicular orientation of the Hg 6p orbital.

Furthermore the method prepares the reactants with very low angular momentum thus reducing the averaging over the final distributions. The rotational distribution of the  $\text{HgH}$  fragment gives us some insight into the transition state region of the reaction.

## THE DYNAMICS OF REACTIVE COLLISIONS OF ATOMIC CARBON

G. Dorthé<sup>a</sup>, M. Costes<sup>a</sup>, C. Naulin<sup>a</sup>, Ph. Caubet<sup>a</sup>, C. Vaucaïps<sup>b</sup> and G. Nouchi<sup>b</sup>

a - Laboratoire de Photophysique et Photochimie Moléculaire

b - Centre de Physique Moléculaire Optique et Hertzienne

Université de Bordeaux I - 33405 Talence Cedex - France.

Many reactions of atomic carbon are very exoergic, presumably exhibiting pathways with no or very small activation barriers and leading to electronically excited products. These reactions could be of interest for electronic transitions chemical lasers, interstellar chemistry and combustion.

In flow experiments at 300 K the reactions with  $N_2O$ ,  $NO_2$ ,  $SO_2$ ,  $OCS$  and  $H_2S$  have been shown to give electronic chemiluminescence from  $CN$ ,  $NO$ ,  $SO$  and  $CS$ . The chemiluminescences from  $C + N_2O$  and  $C + SO_2$  appear interesting for an electronic transition chemical laser. Rate constants for these reactions at 300 K will be given.

The study of the dynamics of such reactions has been undertaken in crossed pulsed supersonic molecular beams. Atomic carbon is generated by graphite vaporisation with an excimer laser. Products are probed by laser induced fluorescence with a pulsed dye laser. Collision energies are ranging from 0.05 eV to 0.3 eV. The  $C + NO \rightarrow CN + O$  reaction has no activation barrier since  $CN$  signal remains unchanged when increasing collision energy. Conversely the  $C + N_2O \rightarrow CN + NO$  reaction has an activation barrier  $< 0.08$  eV since  $CN$  signal begins to be detected at a collision energy of 0.08 eV and increases sharply when increasing collision energy.  $CN$  vibrational distribution decreases smoothly from  $v'' = 0$  to  $v'' = 4$  with a sharp cut-off at  $v'' = 5$  for the  $C + NO$  reaction.  $CN$  produced from  $C + N_2O \rightarrow CN + NO$  exhibits a vibrational popular inversion with a maximum population at  $v'' = 4$ . The study of the dynamics of other reactions is in progress.

MOLECULAR BEAM STUDY OF THE RADICAL GROUP EFFECT IN THE K +  
RI  $\longrightarrow$  KI + R(R=CH<sub>3</sub>, C<sub>2</sub>H<sub>5</sub>, nC<sub>3</sub>H<sub>7</sub>) REACTIVE COLLISIONS(\*)

V. Sáez Rábanos, F.J. Aoiz, V.J. Herrero, E. Verdasco and A. González Ureña.

Departamento de Química Física. Facultad de Química. Universidad Complutense, Madrid-28040, SPAIN.

(\*) Support of this work by the Comisión Asesora of Spain (grant 963/81) is gratefully acknowledged.



## ABSTRACT

Differential reaction cross-section for the  $K + RI \longrightarrow$   $KI + R(R=CH_3, C_2H_5, C_3H_7)$  systems have been measured as a function of the collision energy by using our molecular beam apparatus. The analysis of the center-of-mass angular and recoil velocity distribution of the products indicated: (a) a backward peak character as correspond to a direct, rebound mechanism (b) that the average translational energy of the products  $\langle E_T' \rangle$  increases approximately linearly with (increasing) collision energy,  $\langle E_T \rangle$ , as follows  $\langle E_T' \rangle / \text{KJ.mol}^{-1} = a \langle E_T \rangle / \text{KJ.mol}^{-1} + b$  where (a,b) are (0.65, 66.5), (0.56, 58.4) and (0.28, 30.3) for the methyl, ethyl and propyl iodide reactions respectively. Whereas in the methyl and ethyl reactions the fraction of the available energy that appears in translation,  $f_T$ , is about 0.65-0.55 in the propyl case it reduces to ca. 0.3.

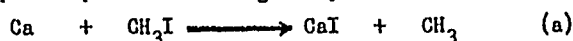
A comparison with photofragmentation studies for the alkyl iodides, RI, has shown a similar dynamics involving a "quasi-diatomic" C-I excitation followed by recoil of a "soft" radical. An information theoretical analysis of the products' recoil velocity distribution revealed that the (direct) dynamics involving the rupture of the same C-I bond can recover the experimental differential reaction cross-sections providing that the statistical contribution, associated with the degrees of freedom of the different radical groups, is properly increased. In particular the enhancement of the energy disposal for the propyl reaction could be associated to the presence of the symmetric C-C-C bending motion.

LASER INDUCED FLUORESCENCE STUDY OF REACTIONS OF Ca WITH CH<sub>3</sub>I AND  
CF<sub>3</sub>I IN THE MOLECULAR BEAM-GAS APPARATUS

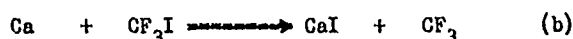
Guo-zhong He, Jue Wang, R. S. Tse\*, and Nan-quan Lou  
Dalian Institute of Chemical Physics, Academia Sinica, P.R. China

One of the major topics in molecular dynamics is to study the distribution of available energy to internal state of the nascent reaction products by the molecular beam techniques as well as the laser induced fluorescence method.

In this paper we present a beam-gas experiment on the exothermic reactions



and



for which the vibrational populations of nascent product CaI are probed by means of LIF. The beam-gas apparatus employed is shown schematically in Fig.1.

A calcium beam effuses from an orifice (0.8 mm) on the top of a cylindrical crucible, heated to 1050 K by thermal radiation from a sleeved graphite electrical resistant heating tube, and passes through a slit (2.5 mm) into the scattering chamber, which is filled with CH<sub>3</sub>I (or CF<sub>3</sub>I) at pressures of (1-20) × 10<sup>-5</sup> torr. The pulsed laser beam from a YAG:ND laser pumped tunable dye laser (Quanta Ray, DCR-1 and PDL) intersects the Ca beam perpendicularly in the center of the scattering chamber. The dye laser is scanned in wavelength to generate an excitation spectrum of the CaI product using the  $\text{CaI } A^2\Pi_{3/2} - X^2\Sigma^+$  band system. The linewidth of the dye laser beam is about 0.2 Å. The fluorescence is viewed by a photomultiplier (R943). A PAR model 162,165 boxcar integrator is used to amplify and average the fluorescence signals. The output of the boxcar drives a stripchart recorder.

Laser excitation of the  $\text{CaI } A^2\Pi_{3/2} - X^2\Sigma^+$  band system in the region 6375-6395 Å is used to determine the internal state distribution of the reaction product. Fig.2 shows the variation of total fluorescence intensity with excitation wavelength for the CaI ΔV=0 sequence of the Ca+CH<sub>3</sub>I and Ca+CF<sub>3</sub>I reactions. In the CaI  $A^2\Pi_{3/2} - X^2\Sigma^+$  band system, heads are formed in the Q<sub>2</sub> and P<sub>21</sub> branches at almost the same frequency and value of J,

$$J_{\text{head}}^{Q_2+P_{21}} = \frac{(2B'' - B_{\text{eff}})}{2(B_{\text{eff}} - B'')}, \text{ and in the } P_2 \text{ branch at } J_{\text{head}}^{P_2} = \frac{(B_{\text{eff}} + 2B'')}{2(B_{\text{eff}} - B'')},$$

For the (0,0) band of the  $\text{CaI } A^2\Pi_{3/2} - X^2\Sigma^+$  transition,  $J_{\text{head}}^{Q_2+P_{21}} = 34$  and  $J_{\text{head}}^{P_2} = 104$ .

The presence of the heads of the (0,0), (1,1), (2,2), (3,3), (4,4) bands for reaction (a) and the (8,8), (9,9), (10,10), (11,11) bands for reaction (b) indicated that the substantial rotational excitation of the product CaI occurred.

Computer simulation of the observed LIF spectra revealed that the average vibrational energy of the CaI for reaction (a) was about 10% of the total available energy, and that of the reaction (b), about 40%. The relative vibrational state distribution of CaI formed in the reactions (a) and (b) are shown in Fig.3. For reaction (a), the vibrational distribution of CaI was produced preferentially around  $V=2$ , while for reaction (b) the peak shifted to  $V=10$ .

A comparison is made of the fraction of the total energy going into vibrational energy,  $\langle f_v \rangle = E_v(\text{CaI})/E_{\text{tot}}$ , for four reactions. The results are shown in the following table:

	$\text{CH}_3\text{I}$	$\text{CF}_3\text{I}$	
Ba	41%	69%	(from reference (1))
Ca	19%	40%	

For the series of reactions  $\text{M} + \text{CH}_3\text{I}$  ( $\text{CF}_3\text{I}$ ) with  $\text{M} = \text{Ca}, \text{Ba}$ , there is an increasing  $\langle f_v \rangle$  as the atomic mass of the alkaline earth metal atom increase.

Surprisal analysis of the vibrational population suggests that the vibrational excitation of radical  $\text{CH}_3(\text{CF}_3)$  must be taken into account for reaction mechanism analysis.

DIPR model is used to calculate the  $\langle f_v \rangle$  of these two reactions.

Comparisons with other reactions, such as  $\text{K} + \text{CH}_3\text{I}$  ( $\text{CF}_3\text{I}$ ) and  $\text{Ba} + \text{CH}_3\text{I}$  ( $\text{CF}_3\text{I}$ ), are given and some similar features are pointed out.

#### Reference

- (1) G.P. Smith, J.C. Whitehead, and R.N. Zare, J.C.P. 67, 1912 (1977);  
P.J. Dagdigian, H.W. Cruse and R.N. Zare, C.P. 15, 249 (1976)

\*Visiting scientist from Dept. of Chemistry, University of Hong Kong

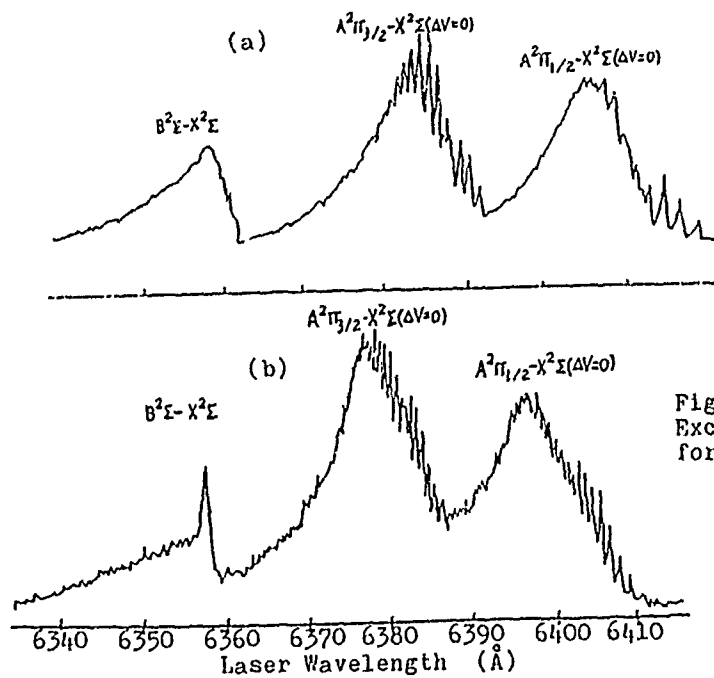


Fig. 2  
Excitation spectra  
for (a)  $\text{Ca}+\text{CH}_3\text{I}$   
(b)  $\text{Ca}+\text{CF}_3\text{I}$ .

Fig. 3 Vibrational state distribution of  $\text{CaI}$  formed in the reactions (a)  $\text{Ca}+\text{CH}_3\text{I}$  and (b)  $\text{Ca}+\text{CF}_3\text{I}$ .

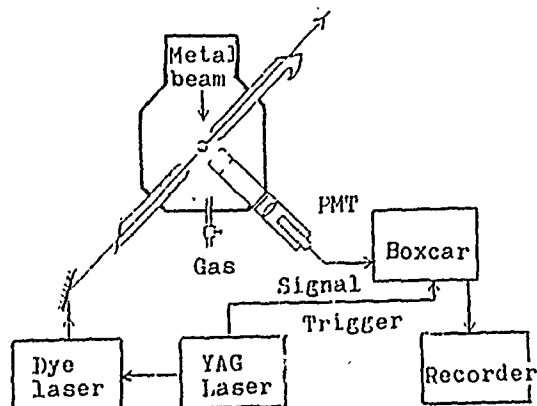
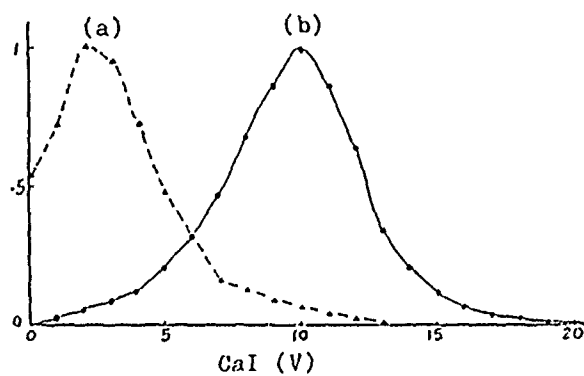


Fig. 1 Schematic of  
experimental apparatus.

Energy and Angular Momentum Disposal in Chemiluminescent Electronically  
Excited Atomic Reactions

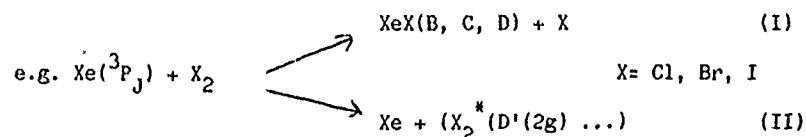
Keith Johnson, Agust Kvaran<sup>+</sup>, John P Simons and Peter A Smith

Chemistry Department, The University, Nottingham NG7 2RD, England

<sup>+</sup> Science Institute, The University of Iceland, 107 Reykjavik, Iceland

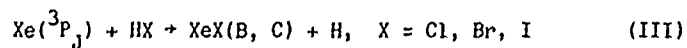
In addition to their intrinsic interest in the field of u.v./visible laser systems, the chemiluminescent reactions of electronically excited atoms have many features attractive to the student of molecular reaction dynamics. Translational energy utilisation can be probed through measurements of the intensity of the chemiluminescence excited by collision of superthermal reagent beams; internal energy disposal and product branching ratios can be determined from the analysis of resolved chemiluminescence spectra under both static and molecular beam conditions; differential cross-sections can be obtained through measurements of the depletion of elastically scattered reagent beams at large scattering angles; the influence of molecular spatial or electronic orbital alignment prior to collision can be probed by polarised laser excitation techniques; the collisional energy dependence of product rotational alignment and angular momentum disposal can be obtained through measurements of the chemiluminescence polarisation excited under molecular beam conditions; resolution of the chemiluminescence spectrum may reveal the dependence of the alignment on the product vibrational state. Many more measurements are possible when the excited atom is itself fluorescent. The chemiluminescent interaction of electronically excited rare gas atoms  $\text{Rg}(np^5(n+1)s)$  provides an ideal system for dynamical

studies which exploit this wide variety of techniques. Resembling in some ways the 'harpoon' chemistry of the alkali metal atoms [1] their dynamics are both complicated and enriched by the electronic excitation; excitation transfer channels can now compete with the alternative atom transfer reactions.



Unravelling the dynamics of such systems requires a careful and systematic analysis of the intensities of the overlapping bound  $\rightarrow$  free oscillatory spectral continua, their polarisations and their dependence on the collision energy. Interpretation of the experimental data should address the degree to which purely kinematic rather than dynamical factors govern the observed behaviour, the degree to which the competing physical channels (II) may influence the dynamics of the reactive channels (I) and an assessment of which observables are most sensitive to particular features of the potential energy surfaces. The chemiluminescence polarisation for example, reflects the degree of product rotational alignment which in turn reflects the partitioning of angular momentum between orbital and internal motion: this, in its turn, may be sensitive to the repulsive release of potential energy in the exit channel, to the preferred collision geometry at the head of the exit channel and/or to the duration of the collision.

The lecture will review recent experimental studies of the reaction dynamics in the kinematically constrained systems



and in the unconstrained systems (I) and (II)[2]. These will be compared with the analogous alkali metal atom reactions to see how far the analogy

is realistic, and measured against the predictions of a hierarchy of 'minimum detail' theoretical models. These include a purely kinematic model ('physics-free') [3], the DIPR model (exit repulsion and collision geometry) [4], a phase space model [5] (purely statistical) and a constrained phase space model ('conservation laws plus').

- [1] D W Setser, T D Dreiling, H C Brashears, Jr. & J H Kolts, Far. Discussion Chem. Soc. (1979) 67 255
- [2] K Johnson, J P Simons, P A Smith, C Washington and A Kvaran, Mol. Phys., (1986) 57 255.  
K Johnson, R Pease, J P Simons, P A Smith and A Kvaran, Faraday Trans. Chem. Soc. (1986), in press.
- [3] I R Elsum and R G Gordon, J.Chem.Phys., (1982) 76 3009.
- [4] D R Herschbach, Faraday Discussion Chem.Soc. (1973) 55 116  
M G Prisant, C T Rettner and R N Zare, J.Chem.Phys. (1984) 81 2699
- [5] D A Case and D R Herschbach, J.Chem.Phys., (1976) 64 4212

Topological study on three and four atom indirect  
exchange reactions. Application to the processes  
 $C(^3P) + NO(X^2\Pi)$  and  $C(^3P) + N_2O(X^1\Sigma^+)$

M.T. Rayez, P. Halvick, B. Duguay and J.C. Rayez  
Laboratoire de Physicochimie Théorique  
Université de Bordeaux I - 33405 Talence Cedex

Since the work of Polanyi and coworkers, it is now admitted that the location of the barrier, the inner repulsive wall and the relative values of the masses of the atoms play an important role on the nascent energetic distribution on the products of a three atom exchange reaction.

Due to the difficulty of the theoretical approach joined to the lack of experimental dynamical studies, few analogous investigations have been undertaken in the case of reactive processes involving three and four atoms and exhibiting at least one well along the route from the reactants to the products i.e. indirect processes. A recent paper of M. K. Osborn and I. W. M. Smith (Chem. Phys. 91, 13, 1984) reports a quasi classical trajectory (Q.C.T.) study of vibrational energy transfer in inelastic collisions on potential energy surfaces (P.E.S.) possessing potential minima.

In order to analyze the role played by different topological factors on the products energetic distribution of a reactional process, we present a Q.C.T. study based on three and four atom model analytical potentials describing the reactions  $A + BC \rightarrow AB + C$  and  $A + BCD \rightarrow AB + CD$  (masses :  $A = 12$ ,  $B = 14$ ,  $C = 16$  in  $BC$ ,  $C = 14$  and  $D = 16$  amu in  $BCD$ )

In the case of a three atom reaction, 1D and 3D approaches have been performed, but in the case of a four atom reaction, only a 1D study has been undertaken owing to the difficulties we encountered for the elaboration of realistic 3D analytical potentials.

The 3-atom analytical models are built by the mixing of a L.E.P.S. function and a polynomial expression containing quadratic, cubic and quartic terms which describes the well. The L.E.P.S. function simulates the asymptotic behaviours of the system.

The 4-atom analytical models are constructed on the same scheme but the polynomial expression must obey several requirements : i)- the



representation of the stable BCD system alone by an ad hoc well, ii)- the simulation of the four atom well which lies on the reaction route and iii)- the continuous passage from the first well to the second as long as the A atom approaches the BCD molecule.

These models are flexible enough to allow the change almost independently of their topological features. Therefore, we have modified the energetic difference between products and reagents, the location of the well, its concavities and its depth. In fact, the location of the well and its curvatures at the minimum (quadratic, cubic and quartic forces constants) are kept linked by an empirical relation which has been well established on real molecules. The 1D-QCT calculations are performed with the initial conditions : relative translational energy  $T = 0.1$  eV, zero point vibrational levels for BC and BCD.

Among the different topological parameters investigated at the 1D level (3 and 4-atom cases), we show that the anisotropy of the intermediate well and its location are the important factors which govern the nascent distribution of the energy of the reaction on the products, the others, playing a minor role. Hence, a mapping of the percentage of the average vibrational energy of the newly formed diatomic molecules versus the location of the well - that is to say the curvatures at the minimum - can be easily elaborated. As long as the intermediate well becomes more and more elongated in the products direction, it appears an increase of the energy channeled on the vibration of the diatomic molecule formed. A consequence of this fact is the reduction of the number of reactive outcomes since the transfer of momentum in the direction of the products is less and less efficient.

The 3-atom - 3D investigation (rotational level  $J_{BC} = 0$ ) does not change drastically the previous conclusion. In fact, we observed that the complex keeps a small bent shape associated with a less deep well than the linear structure. This change leads to a greater anisotropy of the well and consequently, favours an increase of the vibrational excitation of the AB molecule.

Ab-initio determination of the fundamental sheet potential energy implied in the reaction  $C(^3P) + NO(X^2\Sigma^+) \rightarrow CN(X^2\Sigma^+) + O(^3P)$  (exoergicity = -1.35 eV) shows an intermediate well of 4.2 eV depth (with respect to reactants energy), related to a linear structure CNO (equilibrium distances :  $r_{CN} = 1.22\text{\AA}$  and  $r_{NO} = 1.23\text{\AA}$ ) of principal force constants respectively equal to  $k_{CN} = 18$  mdyne/ $\text{\AA}$  and  $k_{NO} = 15$  mdyne/ $\text{\AA}$ . QCT calculations on an analytical surface possessing these features lead to vibrational population of  $CN(X^2\Sigma^+)$  which does not exhibit any inversion and which is in

satisfying agreement with supersonic pulsed crossed beams experiments.

Semi-empirical determination of lowest energy sheet of potential energy associated with the process  $C(^3P) + N_2O(X^1\Sigma^+) \rightarrow CN(X^2\Sigma^+) + NO(X^2\Pi)$  reveals the existence of a well of 4.65 eV depth corresponding to a structure CNNO of principal force constants equal to  $k_{CN} = 17.6$  mdyne/Å,  $k_{NN} = 12.8$  mdyne/Å and  $k_{NO} = 19.2$  mdyne/Å. QCT calculations performed on an analytical representation of the potential energy surface leads to an inversion of the vibrational population of  $CN(X^2\Sigma^+)$  around  $v'' = 2$  which is only in fair agreement with experiments (the maximum is located around  $v'' = 4$ ). Several arguments can be raised to explain this difference.

DYNAMICAL PROCESSES OF DETACHMENT IN  $\text{Cl}^-/\text{H}_2$ 

M. Barat, J.C. Brenot, M. Durup-Ferguson\*, J. Fayeton, J.C. Houver and  
J.B. Ozenne

*L.C.A.M., Bâtiment 351, Université de Paris-Sud, 91405 Orsay*

*\*L.P.C.R., Bâtiment 350*

The various channels enhanced by kinetic energy of  $\text{Cl}^-$  ion in  $\text{Cl}^-$  on  $\text{H}_2$  collision produce two independently detectable species : a fast neutral  $\text{HCl}$  or  $\text{Cl}$  and an ionized particle  $\text{H}^-$  or  $\text{e}^-$ . A coincident detection of the two detectable products allows an unambiguous analysis of the various competing channels.

In this crossed beam experiment a multicoincident detection is used fig. (1) which has been previously settled in LCAM<sup>(1)</sup>. This technique directly gives complete time and spatially resolved product distributions. At a given collision energy the ultimate result of the data processing gives the relative probability of each channel as a function of the CM deflection angle of the fast neutrals and of the amount of kinetic energy transferred to internal energy of the products. The contour map of each competing channel can be drawn fig. (2).

The main conclusions for the  $\text{Cl}^-/\text{H}_2$  system are the following : the two reactive channels giving  $\text{ClH} + \text{H}^-$  and  $\text{ClH} + \text{H} + \text{e}^-$  proceed through the same reactive path on the potential surface they are both severely peaked at the same  $\chi$  angle, the reactive detachment occurs when the trajectory would lead to  $\text{HCl}$  vibrational excitation above  $v=3$  a transition through a temporary  $\text{HCl}^- \dots \text{H}$  occurs which immediately autodetaches giving  $\text{HCl} + \text{e}^- + \text{H}$ .<sup>(2)</sup>

The generality of this competition process between reaction and reactive detachment has been checked on other halogene $^-/\text{H}_2$  systems. In  $\text{I}^-/\text{H}_2$  the transitory  $\text{IH}^-$  does not detach therefore the reactive detachment is not observed. In  $\text{Br}^-/\text{H}_2$  the reactive detachment proceeds from the reaction path for vibrational excitation of  $\text{BrH}$  of  $v \geq 2$  in agreement with the position of the surfaces crossing  $\text{BrH} + \text{H}^- \rightarrow \text{HBr}^- + \text{H}$ . At collision energy lower 10 eV the reactive detachment is the most important detachment process at higher collision energy other detachment processes compute : one involving vibrational excitation of  $\text{H}_2$  but not yet fully understood. An other one proceeding through a spectator mechanism by which just one H atom is involved in the collisional

process the other one staying at rest. The Cl atom is backward scattered and  $H_2$  molecule dissociates.

An other process still more strange where the  $H_2$  vibration is frozen. The  $H_2$  molecule reacts like an He atom of masse 2 which can be accompanied with an excitation of Cl which in this case is back scattered.

#### References

- (1) J.C. Brenot, J.A. Fayeton, J.C. Houver, Rev. Sci.Instr. 51, 1623 (1980)
- (2) M. Barat, J.C. Brenot, J.A. Fayeton, J.C. Houver, J.B. Ozenne, R.S. Berry and M. Durup Ferguson, Chem.Phys. 97, 165 (1985)

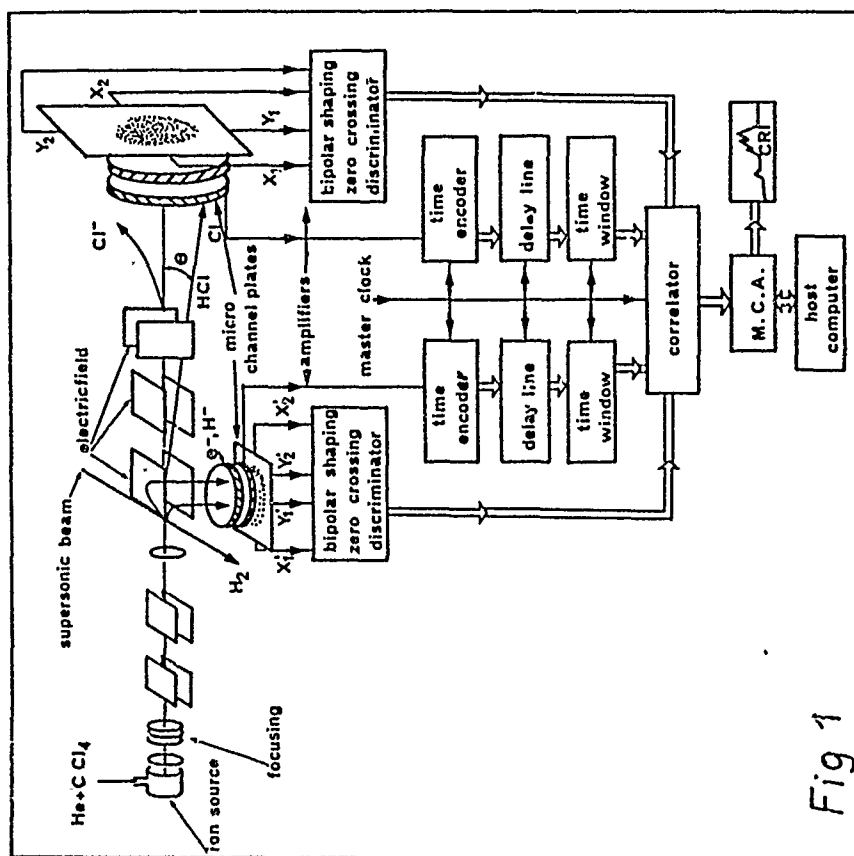


Fig 1

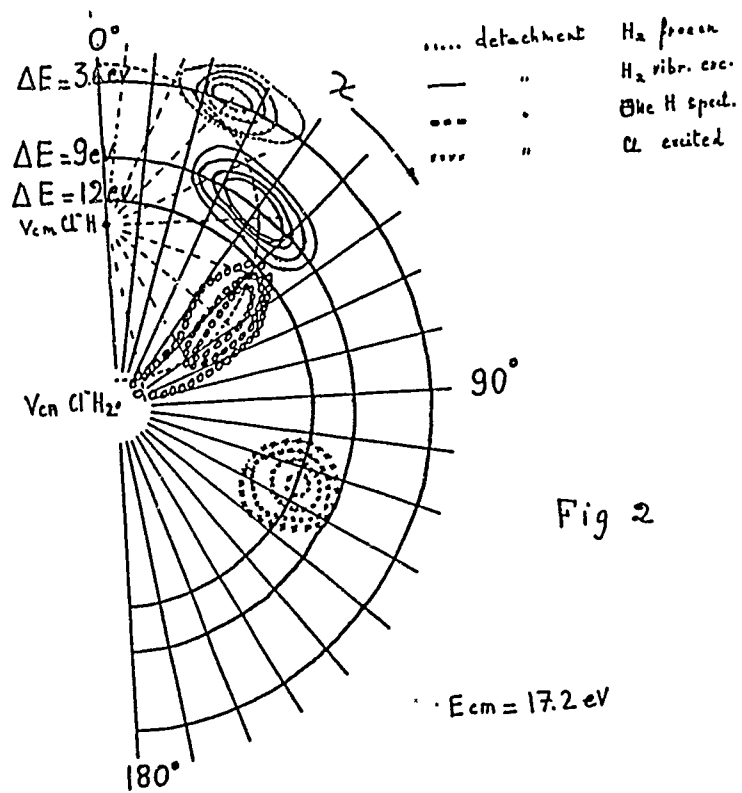


Fig 2

Some Current Problems in Atmospheric Ozone Chemistry - Role of  
Chemical Kinetics

R.A. Cox

Combustion Centre, Harwell Laboratory, Didcot, Oxon, U.K., OX11 0RA.

Atmospheric ozone is produced and removed by a complex series of elementary gas-phase photochemical and chemical reactions involving  $O_x$ ,  $HO_x$ ,  $NO_x$ ,  $ClO_x$  and hydrocarbon species. Concern about changes in the balance and distribution of ozone as a result of mans activities has led to an intense research effort to study the kinetics and mechanisms of the reactions controlling atmospheric ozone.

At the present time there is a good knowledge of the basic processes involved in ozone chemistry in the stratosphere and the troposphere and the kinetics of most of the key reactions are well defined. There are a number of difficulties in the theoretical descriptions of observed ozone behaviour which may be due to uncertainties in the chemistry. Examples are the failure to predict present day ozone in the photochemically controlled region above 35km altitude and the large reductions in the ozone column in the Antarctic Spring which has been observed in recent years.

In the troposphere there is growing evidence that ozone and other trace gases have changed appreciably from pre-industrial concentrations, due to chemical reactions involving man-made pollutants. Quantitative investigation of the mechanisms by which these changes may occur requires a sound laboratory kinetics data base.

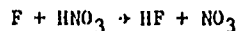
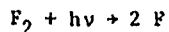
ABSOLUTE RATE CONSTANTS FOR THE GAS-PHASE REACTION OF  
NO<sub>3</sub> RADICALS WITH REDUCED SULFUR COMPOUNDS

Timothy J. Wallington, Roger Atkinson, Arthur M. Winer and James M. Pitts, Jr., Statewide Air Pollution Research Center, University of California, Riverside, California 92521, U.S.A.

In-situ long pathlength spectroscopic studies have shown that the NO<sub>3</sub> radical is a common constituent of continental nighttime atmospheres [1], with mixing ratios of 10-100 parts-per-trillion being routinely observed at several arid/semi-desert locations in California [2]. Laboratory kinetic studies have shown that the NO<sub>3</sub> radical reacts rapidly with the more highly alkyl-substituted alkenes (including the monoterpenes), hydroxy-substituted aromatics and dimethyl sulfide, and that these reactions can be important as nighttime tropospheric loss processes for the NO<sub>3</sub> radical and/or these organic compounds [3]. Until very recently [4,5], however, the available kinetic data were all obtained from relative rate studies carried out at room temperature and atmospheric pressure of air.

In order to allow the determination of absolute NO<sub>3</sub> radical reaction rate constants, we have constructed and utilized a flash photolysis-visible absorption apparatus, and report here recently obtained rate constant data for a series of reduced sulfur compounds over the temperature range 270-350 K.

NO<sub>3</sub> radicals were generated by the flash photolysis of F<sub>2</sub>-HNO<sub>3</sub> mixtures in helium, nitrogen or argon diluent



and monitored by long pathlength visible absorption at 662 nm.



Absolute rate constants have been determined for the reduced sulfur compounds  $\text{CH}_3\text{SCH}_3$ ,  $\text{CH}_3\text{SSCH}_3$  and  $\text{CH}_3\text{SH}$  over the temperature and pressure ranges 280-350 K and 50-400 torr total pressure, respectively. These reactions are all at the high pressure limit, and the rate constants obtained are given in Table 1. In addition, upper limit rate constants were obtained at 298 K for the reactions of the  $\text{NO}_3$  radical with  $\text{H}_2\text{S}$  and  $\text{SO}_2$ , and these data are also given in Table 1.

Table 1. Absolute Rate Constants for the Gas-Phase Reaction of the  $\text{NO}_3$  Radical With  $\text{CH}_3\text{SH}$ ,  $\text{CH}_3\text{SCH}_3$ ,  $\text{CH}_3\text{SSCH}_3$ ,  $\text{SO}_2$  and  $\text{H}_2\text{S}$

Reactant	$10^{13} \times k \text{ (cm}^3 \text{ molecule}^{-1} \text{ s}^{-1})^a$		
	280 K	298 K	350 K
$\text{CH}_3\text{SH}$	$(8.0 \pm 1.4)$	$(8.1 \pm 0.6)$	$(5.4 \pm 0.7)$
$\text{CH}_3\text{SCH}_3$	$(8.8 \pm 1.2)$	$(8.1 \pm 1.3)$	$(7.7 \pm 0.7)$
$\text{CH}_3\text{SSCH}_3$	$(5.3 \pm 0.8)$	$(4.9 \pm 0.8)$	$(4.3 \pm 0.6)$
$\text{SO}_2$	-	$\leq 0.004$	-
$\text{H}_2\text{S}$	-	$\leq 0.3$	-

<sup>a</sup>Indicated errors represent two standard deviations.

Least squares analyses of these data yield the Arrhenius expressions

$$k(\text{CH}_3\text{SCH}_3) = (4.7^{+2.6}_{-1.7}) \times 10^{-13} e^{(170 \pm 130)/T} \text{ cm}^3 \text{ molecule}^{-1} \text{ s}^{-1}$$

$$k(\text{CH}_3\text{SSCH}_3) = (1.0^{+2.6}_{-0.7}) \times 10^{-13} e^{(600 \pm 400)/T} \text{ cm}^3 \text{ molecule}^{-1} \text{ s}^{-1}$$

$$k(\text{CH}_3\text{SH}) = (1.9 \pm 0.3) \times 10^{-13} e^{(290 \pm 50)/T} \text{ cm}^3 \text{ molecule}^{-1} \text{ s}^{-1}$$

where the error limits given are two least squares standard deviations. These rate constants will be compared with the available literature data, and the atmospheric implications discussed.

#### References

1. R. Atkinson, A. M. Winer and J. N. Pitts, Jr., *Atmos. Environ.*, 20, 331 (1986) and references therein.
2. U. F. Platt, A. M. Winer, H. W. Biermann, R. Atkinson and J. N. Pitts, Jr., *Environ. Sci. Technol.*, 18, 365 (1984).
3. A. M. Winer, R. Atkinson and J. N. Pitts, Jr., *Science*, 224, 156 (1984).
4. A. R. Ravishankara and R. L. Mauldin, III, *J. Phys. Chem.*, 89, 3144 (1985).
5. J. P. Burrows, G. S. Tyndall, W. Schneider and G. K. Moortgat, presented at the 17th Int. Symp. Free Radicals, Snow Mountain Ranch, CO, August 18-23, 1985.

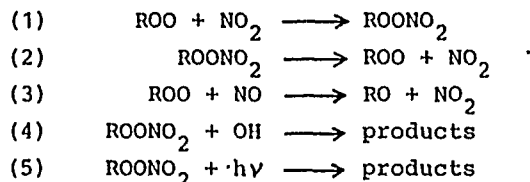
## Thermal Stability of Peroxynitrates

A. Reimer and F. Zabel

Bergische Universität - GH Wuppertal, Physikalische Chemie  
 Fachbereich 9, 56 Wuppertal 1, West Germany

Within the last ten years evidence has increased that, in the atmosphere, a large part of  $\text{NO}_x$  and of peroxy radicals may be tied up in peroxynitrates. For example, acetyl peroxynitrate (PAN) seems to be an ubiquitous compound in the troposphere, with a background mixing ratio of 50 - 100 pptv [1]. Other peroxynitrates (including peroxynitric acid,  $\text{HOONO}_2$ ) have not been detected yet in field experiments, but their existence in higher altitudes is suggested from the results of laboratory experiments (e.g. [2-4]).

The importance of peroxynitrates for the chemistry of the atmosphere will largely depend on the rate constants of reactions



and on the products of reactions (4) and (5). In this work, reaction (2) has been investigated for  $\text{R} = \text{CH}_3$ ,  $\text{CH}_3\text{CO}$ ,  $\text{CCl}_3$ , and  $\text{CCl}_2\text{F}$  in a temperature controlled 420 l reaction chamber from Duran glass which is surrounded by 20 photolysis lamps. The reaction chamber has a built-in White mirror system for long-path absorption measurements which is coupled to a Fourier-transform infrared spectrometer (NICOLET 7199). Experimental conditions include temperatures between  $-20$  and  $+50^\circ\text{C}$  and total pressures between 10 and 800 mbar.  $\text{N}_2$  and  $\text{O}_2$  were used as buffer gases. The peroxynitrates were prepared in situ by photolysis of the following gas mixtures: azomethane/ $\text{N}_2/\text{O}_2/\text{NO}_2$  (for  $\text{CH}_3\text{OONO}_2$ ),  $\text{Cl}_2/\text{CH}_3\text{CHO}/\text{O}_2/\text{N}_2/\text{NO}_2$  (PAN),  $\text{Cl}_2/\text{CHCl}_3/\text{O}_2/\text{N}_2/\text{NO}_2$  ( $\text{CCl}_3\text{OONO}_2$ ),  $\text{Cl}_2/\text{CHCl}_2\text{F}/\text{O}_2/\text{N}_2/\text{NO}_2$  ( $\text{CCl}_2\text{FOONO}_2$ ). The initially established equilibrium between reactions (1) and (2) was disturbed by addition of large amounts ( $\sim 0.3$  mbar) of  $\text{NO}$ , giving rise to reaction (3). Using high  $[\text{NO}]/[\text{NO}_2]$

ratios, the effective first order decay rate constant of  $\text{ROONO}_2$ , as measured by IR absorption, was equal to  $k_2$ .

Rate constants  $k_2$  thus obtained are strongly temperature and pressure dependent. They are presented in figures 1 and 2 for

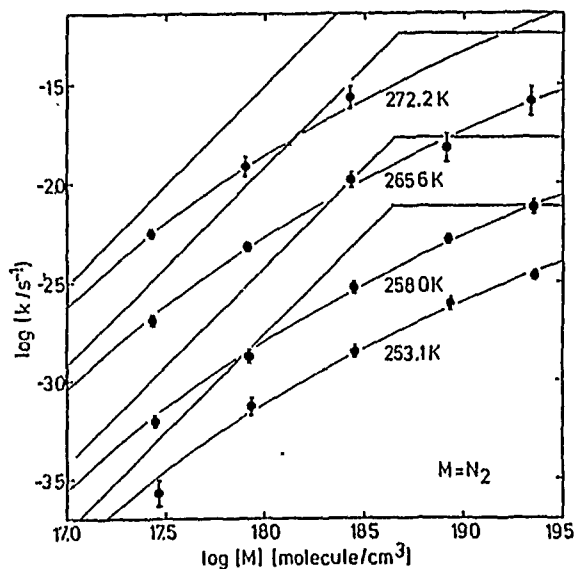


Fig. 1 Thermal decomposition of methyl peroxyxynitrate

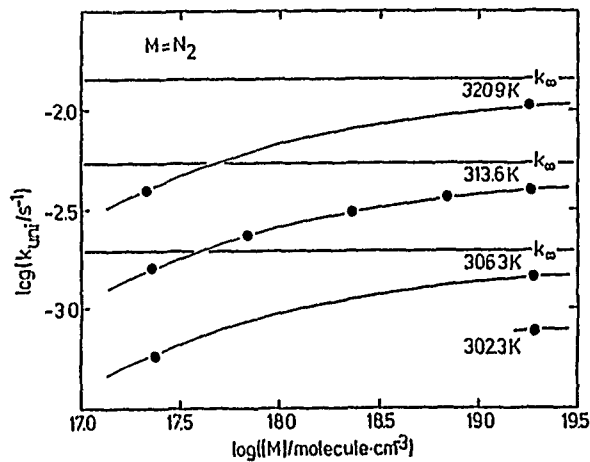


Fig. 2 Thermal decomposition of acetyl peroxyxynitrate

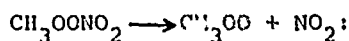
$\text{CH}_3\text{OONO}_2$  and  $\text{CH}_3\text{C(O)OONO}_2$ , respectively. Each point represents at least 4 individual measurements. The rate data were evaluated according to the modified Kassel treatment of unimolecular react-

ions as proposed by Troe [5]. Fitting the experimental data points to the 3-parameter-equation

$$\log (k/k_{\infty}) = \log \frac{k_0/k_{\infty}}{1 + k_0/k_{\infty}} + \frac{\log F_c}{1 + \left[ \frac{\log (k_0/k_{\infty})}{N_c(F_c)} \right]^2},$$

$$N_c(F_c) = 0.75 - 1.27 \log F_c,$$

with the  $F_c$  values held fixed at their theoretical strong collision values [2], the following parameters were obtained:



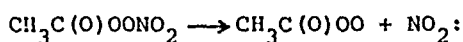
$$F_c = 0.47$$

$$k_0/[N_2] = 8.5 \times 10^{-4} \times \exp(-20.5 \text{ kcal}\cdot\text{mol}^{-1}/RT) \text{ cm}^3\text{molecule}^{-1}\text{s}^{-1}$$

$$k_{\infty} = 2.3 \times 10^{16} \times \exp(-21.4 \text{ kcal}\cdot\text{mol}^{-1}/RT) \text{ s}^{-1}$$

$$k_{\text{O}_2}^{\text{O}_2}/k_{\text{O}_2}^{\text{N}_2} = 1.2 \pm 0.4$$

$$\Delta H_{r,298}^{\text{O}} = (21.9 \pm 0.8) \text{ kcal/mol (using literature data on } k_1)$$



$$F_c = 0.27$$

$$k_0/[N_2] = 6.3 \times 10^{-2} \times \exp(-25.4 \text{ kcal}\cdot\text{mol}^{-1}/RT)$$

$$k_{\infty} = 2.2 \times 10^{16} \times \exp(-26.7 \text{ kcal}\cdot\text{mol}^{-1}/RT)$$

$$k_{\text{O}_2}^{\text{O}_2}/k_{\text{O}_2}^{\text{N}_2} = 0.9 \pm 0.2$$

Experiments on the thermal decomposition of  $\text{CCl}_3\text{OONO}_2$  and  $\text{CCl}_2\text{FOONO}_2$  are still in progress.

When these results are combined with literature data it may be estimated that in the upper troposphere mole fractions of the same order of magnitude (10 - 100 ppt) are present for the different reactive nitrogen species ( $\text{NO}+\text{NO}_2$ ),  $\text{HOONO}_2$ ,  $\text{CH}_3\text{OONO}_2$ , and  $\text{CH}_3\text{C(O)OONO}_2$ . Similarly, the halomethyl peroxy nitrates possibly represent reservoirs for reactive halogen and  $\text{NO}_x$  in the stratosphere.

#### References

- [1] H.B. Singh and L.J. Salas, Atmos. Environ. 17(1983)1507
- [2] R.A. Graham, A.M. Winer, and J.N. Pitts, Jr., J. Chem. Phys. 68(1978)4505
- [3] A. Bahta, R. Simonaitis, and J. Heicklen, J. Phys. Chem. 86(1982)1849
- [4] R. Simonaitis and J. Heicklen, Chem. Phys. Lett. 62(1979)473
- [5] J. Troe, Ber. Bunsenges. Phys. Chem. 87(1983)161

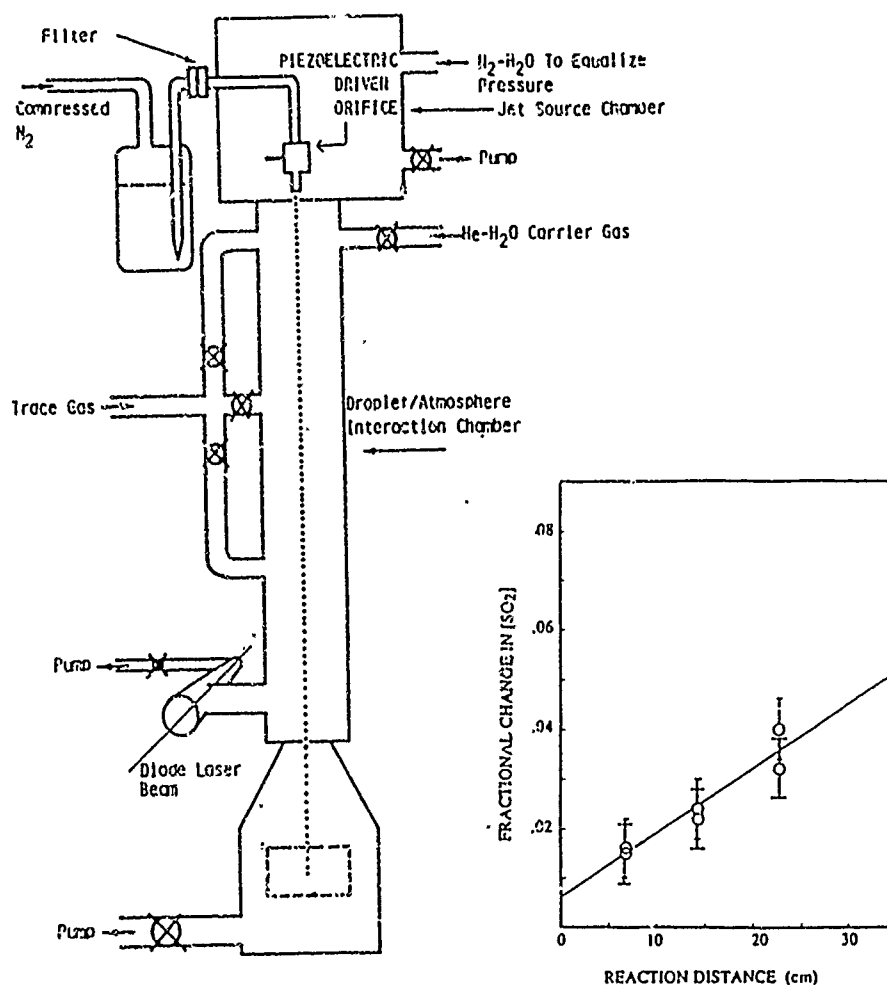
Abstract for the 9th International Symposium on Gas Kinetics,  
Bordeaux, France, July 20-25, 1986

THE STICKING OF GAS MOLECULES TO WATER SURFACES

James Gardner, Lyn Sharfman, Yusuf G. Adewusi and Paul Davidovits,  
Boston College, Department of Chemistry, Chestnut Hill, MA 02167  
U.S.A.

Mark S. Zahniser, Douglas R. Worsnop and Charles E. Kolb  
Aerodyne Research, Inc. 45 Manning Road, Billerica, MA 01821  
U.S.A.

Many important atmospheric reactions occur inside the water droplets of clouds and mists. These processes begin with the precursor gas molecules such as  $\text{SO}_2$  or  $\text{NO}_2$ , for example, hitting the surface of the droplet and crossing into the interior. The probability that a molecule striking the surface, sticks to it and enters the droplet is called the sticking or accommodation coefficient. This is the key parameter linking gas phase to liquid phase chemistry and it often governs the kinetics of heterogeneous reactions in the atmosphere. An experimental technique has been developed to measure these accommodation coefficients. The apparatus is shown schematically in figure 1. A controllable stream of mono-dispersed droplets is produced by a vibrating nozzle jet. The droplets enter a flow system containing the atmospheric trace species. The droplets are turned on and off while the density of the species is monitored spectroscopically. The details of the flow system, temperature control and droplet switching are not shown. The reacting gas can be introduced at three different points in the flow tube. In this way the length of the interaction region can be varied.  $\text{SO}_2$  was the first gas



studied in this way. In the insert of figure 1 we show a plot of the change in SO<sub>2</sub> density due to the water droplets as a function of the length of the interaction region. With the flow rates and other experimental parameters known, the accommodation coefficient can be calculated from such a plot. For SO<sub>2</sub> the value of this parameter is  $(2.4 \pm 0.4) \times 10^{-3}$ . The results of

C4

accommodation coefficient measurements. for several other gases of atmospheric interest will be presented.

A kinetic model has been developed which predicts the size of the accommodation coefficients. In this model it is assumed that a molecule which hits the water surface will enter the interior if during its residence time on the surface a hole in the liquid sufficiently large to accommodate the molecule appears at the surface site. The predictions and implications of this model will be discussed.

#### Acknowledgements

This work was sponsored by: The National Science Foundation, U.S. Environmental Protection Agency, Coordinating Research Council and the Electric Power Research Institute.



DISCHARGE FLOW DETERMINATION OF THE RATE CONSTANTS FOR THE REACTIONS



D. MARTIN, J.L. JOURDAIN and G. LE BRAS.

(Centre de Recherches sur la Chimie de la combustion et des Hautes  
Températures - C.N.R.S 45071 ORLEANS cedex 2 - FRANCE.)

The main atmospheric oxidation steps of SO<sub>2</sub> : SO<sub>2</sub> + OH + M → HOSO<sub>2</sub> + M (1) and HOSO<sub>2</sub> + O<sub>2</sub> → HO<sub>2</sub> + SO<sub>3</sub> (2) have been studied at room temperature using the discharge flow - EPR - mass spectrometric method. The rate constants of these reactions were determined by EPR monitoring of the OH decay in the presence of excess SO<sub>2</sub>, successively in the absence and presence of O<sub>2</sub>. HO<sub>2</sub> produced in reaction (2) was converted into OH by NO addition either together with the reactants SO<sub>2</sub> and O<sub>2</sub> or separately, just upstream of the EPR cavity. Heterogeneous processes were minimized by coating the wall of the reactor with halocarbon wax.

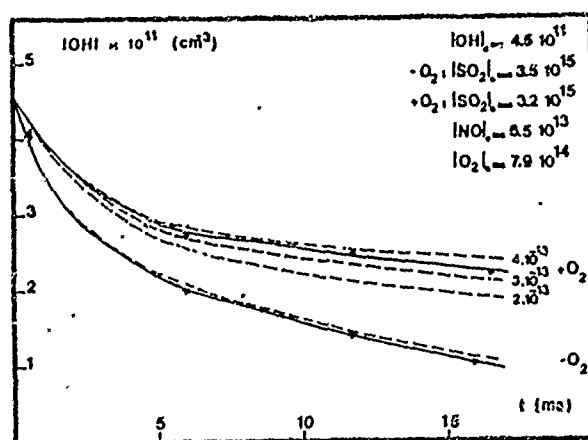
The reaction SO<sub>2</sub> + OH + M → HOSO<sub>2</sub> + M (1) was studied in the absence of O<sub>2</sub> at pressures ranging from 1 to 6.4 Torr of helium, with partial pressures of SO<sub>2</sub> in the range 0.01 - 0.15 Torr. Both graphical and mathematical treatments of the data led to the following values of the rate constants for reaction (1) with respectively SO<sub>2</sub> and He as the third body :

$$k_{III}^{SO_2} = (1.33 \pm 0.40) \times 10^{-30} \text{ cm}^6 \text{ molecule}^{-2} \text{ s}^{-1}$$

$$k_{II}^{He} = (8.1 \pm 0.2) \times 10^{-32} \times [He] + (2.4 \pm 0.4) \times 10^{-15} \text{ cm}^3 \text{ molecule}^{-1} \text{ s}^{-1}$$

The third order rate constant obtained with SO<sub>2</sub> as the third body and the apparent second order rate constant determined with He as the third body are in good agreement with the data of LEU [1]. This experimental expression of  $k_{II}^{He}$  compares well with recent theoretical calculations of WINE et al [2] which indicate that the reaction would be in the fall off regime in the pressure range considered (1 - 6.4 Torr).

The rate constant for the reaction  $\text{HOSO}_2 + \text{O}_2 \rightarrow \text{HO}_2 + \text{SO}_3$  (2) was measured from a computer fitting of the OH decay curves obtained in the absence and presence of  $\text{O}_2$  and NO. In a first series of experiments where NO was added separately, just upstream of the EPR cavity, the possible  $\text{HOSO}_2 + \text{NO}$  reaction was negligible. However a first order reaction rate of  $50 \text{ s}^{-1}$  had to be considered for  $\text{HOSO}_2$  to fit the data obtained over the entire range of  $\text{O}_2$  concentrations used ( $3.5 \times 10^{14} - 1.5 \times 10^{15}$ ). This additional sink of  $\text{HOSO}_2$  could be a wall reaction. An example of experimental data is given in the figure below (the solid lines represent the experimental decay curves of OH and the dashed lines the calculated ones).



In a second series of experiments where NO and  $\text{O}_2$  were flowed together, an upper limit of  $5 \times 10^{-13}$  was determined for the  $\text{HOSO}_2 + \text{NO}$  reaction.

From the series of experiments, the following value was obtained for  $k_2$  :

$$k_2 = (3.5 \pm 1) \times 10^{-13} \text{ cm}^3 \text{ molecule}^{-1} \text{ s}^{-1}$$

This value is in good agreement with the flash photolysis measurement of MARGITAN [3] ( $k_2 = (4 \pm 2) \times 10^{-13}$ ) also obtained from a computer simulation of his experimental data. The agreement is also good with a

further discharge flow determination of HOWARD [4] ( $k_2 = (4.4 \pm 0.9) \times 10^{-13}$ ) where  $\text{HO}_2$  and  $\text{HOSO}_2$  were respectively detected by LMR and chemical ionization.

The present value of  $k_2$  confirms the STOCKWELL and CALVERT [5] hypothesis concerning the occurrence of reactions (1) and (2) in the atmosphere and the subsequent  $\text{HO}_x$  conservation in the gas phase oxidation of  $\text{SO}_2$  in the atmosphere.

#### References

- 1- M.T. LEU : J. Phys. Chem., (1982), 86, 4558.
- 2- P.H. WINE, R.J. THOMPSON, A.R. RAVISHANKARA, D.H. SEMMES, C.A. GUMP, A TORABI, and J.M. NICOVICH : J. Phys. Chem., (1984), 88, 2095.
- 3- J.J. MARGITAN : J. Phys. Chem., (1984), 88, 3314.
- 4- C.J. HOWARD : Communication at the seventeenth symposium on free radicals, Granby, Colorado, USA, August 18-23 1985.
- 5- W.R. STOCKWELL and J.G. CALVERT : Atm. Env., (1983), 17, 2231.

HIGH RESOLUTION FOURIER TRANSFORM SPECTROSCOPY OF GAS  
PHASE RADICALS AND REACTION PRODUCTS

James B. Burkholder, Philip D. Hammer, and Carleton J. Howard

National Oceanic and Atmospheric Administration  
Aeronomy Laboratory, R/E/AL2  
Boulder, Colorado 80303  
U.S.A.

and

C.I.R.E.S., University of Colorado  
Boulder, Colorado 80309  
U.S.A.

Recent results using a high resolution Fourier transform spectrometer optically coupled to a fast flow multipass absorption cell for the spectroscopic study of gas phase radicals and reaction products will be presented.

High sensitivity infrared and microwave spectroscopic techniques are viable methods for monitoring transient species in both laboratory and field studies. For these techniques to be successful detailed spectroscopic information of the transient species is required. In the past high resolution infrared spectra of transient species have been recorded using LMR, diode laser, and difference laser techniques. To date high resolution Fourier transform spectroscopy (FTS) has been used to study relatively stable species. In this report FTS high resolution infrared absorption spectra of  $\text{HO}_2$ ,  $\text{DO}_2$ ,  $\text{FO}$ ,  $\text{ClO}$ ,  $\text{SO}$ ,  $\text{CS}$  and several other short lived radicals will be presented.

The implication of these results to atmospheric chemistry will be discussed.

KINETICS AND MECHANISM OF ATMOSPHERIC CS<sub>2</sub> OXIDATION

A.R. Ravishankara, E.R. Lovejoy, N.S. Wang, and C.J. Howard

NOAA, ERL, R/E/AL2

Boulder, CO 80303, USA

and

P.H. Wine, J.M. Nicovich, and A.J. Hynes

Georgia Tech Research Institute

Atlanta, GA 30332, USA

Oxidation of CS<sub>2</sub> in the earth's atmosphere is believed to yield COS and SO<sub>2</sub>. Previous work had indicated that the reaction of OH with CS<sub>2</sub> was too slow for it to be important. Recently we have obtained evidence to show that OH adds very rapidly to CS<sub>2</sub> to form CS<sub>2</sub>OH adduct which in the presence of O<sub>2</sub> undergoes further reactions. In the absence of O<sub>2</sub> (or other reactants) the CS<sub>2</sub>OH adduct thermally decomposes to give back OH and CS<sub>2</sub>. Using 248 nm pulsed laser photolysis of H<sub>2</sub>O<sub>2</sub> to produce OH followed by pulsed laser induced fluorescence detection of OH, we have directly observed the equilibrium,

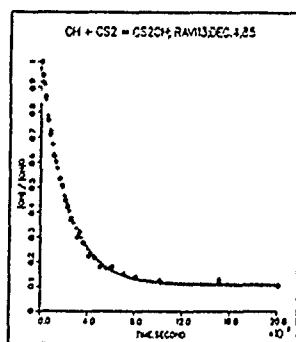
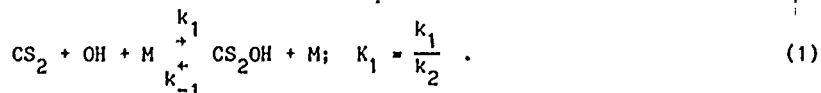


Figure 1. Temporal Profile of OH in the presence of  $1.84 \times 10^{16}$  CS<sub>2</sub> cm<sup>-3</sup>, 43 torr N<sub>2</sub>, and  $3.5 \times 10^{14}$  H<sub>2</sub>O<sub>2</sub> cm<sup>-3</sup> at 262K.

Figure 1 shows a temporal profile of OH following  $\text{H}_2\text{O}_2$  photolysis in  $\text{CS}_2$ . Using such temporal profiles, the equilibrium constant  $K_1$  has been measured as a function of temperature in the range 259-318K. Figure 2 shows a plot

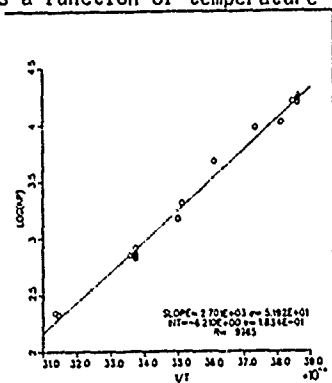


Figure 2. Temperature dependence of the equilibrium constant.

of  $\log k_p$  vs  $1/T$ . From the slope of this plot the heat of reaction 1 is calculated to be  $-(12.4 \pm 0.5)$  kcal/mole and the heat of formation of  $\text{CS}_2\text{OH}$  at 298K calculated to be 25.0 kcal/mole. In addition, using the same experimental method as above, the rate coefficient for the reaction,



has also been measured. The absolute rate coefficients for the reaction of OH with  $\text{CS}_2$  in  $\text{N}_2/\text{O}_2$  mixtures have been measured as a function of total pressure, composition, and temperature and they are listed in Table I. Lastly, experiments are underway to identify and quantify the products of reaction (2) using an LMR spectrometer coupled to a discharge flow system. When completed, this work will map out the course of  $\text{CS}_2$  oxidation in the atmosphere. It already has shown that OH indeed initiates  $\text{CS}_2$  oxidation in the troposphere.

---

Work performed at NOAA was supported by NOAA as a part of the National Acid Precipitation Assessment Program. Work performed at Georgia Tech was funded by the National Science Foundation.

Table I. The rate coefficients for the reaction of OH with CS<sub>2</sub> under various conditions of composition and Temperature.

Temp, K	Total Pressure, torr	Pressure of O <sub>2</sub> , torr	[OH] <sub>0</sub> , 10 <sup>11</sup> cm <sup>-3</sup>	[CS <sub>2</sub> ], 10 <sup>15</sup> cm <sup>-3</sup>	k' (a), 10 <sup>3</sup> s <sup>-1</sup>	k, cm <sup>3</sup> molecule <sup>-1</sup> s <sup>-1</sup>
251	690	14	4	0-2	0.07-6	~3x10 <sup>-12</sup>
253	690	345	12	0-9	0.03-68	(5.94±0.16)x10 <sup>-12</sup>
251	690	145	3	0-10	0.06-68	(5.86±0.74)x10 <sup>-12</sup>
253	280	140	16	0-12	0.5-51	(3.46±0.10)x10 <sup>-12</sup>
253	680	680	6	0-9	0.2-63	(5.80±0.20)x10 <sup>-12</sup>
253	140	140	9	0-17	0.3-43	(2.27±0.12)x10 <sup>-12</sup>
261	689	144	20	0-7	0.47-42	(4.16±0.39)x10 <sup>-12</sup>
270	690	145	7	0-7.7	0.05-31	(3.61±0.15)x10 <sup>-12</sup>
287	690	145	12	0-17	0.24-32	(1.68±0.22)x10 <sup>-12</sup>
296	685	143	3	0-25	0.08-37	(1.50±0.09)x10 <sup>-12</sup>
295	700	1.4	2	0-0.9	0.03-27	(2.56±0.18)x10 <sup>-14</sup>
295	690	14	2	0-12	0.06-2.5	(1.97±0.03)x10 <sup>-13</sup>
295	280	140	17	0-12	0.47-17	(0.96±0.04)x10 <sup>-12</sup>
295	690	345	23	0-16	0.45-35	(2.06±0.10)x10 <sup>-12</sup>
295	700	147	4	0-15	0.1-23	(1.51±0.09)x10 <sup>-12</sup>
295	690	0	3	0-60	0.06-0.09	(5±3)10 <sup>-16</sup>
295	140	140	20	0-17	0.4-13	(6.80±0.30)x10 <sup>-13</sup>
295	690	145	13	0-8.3	0.3-23	(2.63±0.19)x10 <sup>-13</sup>
303	688	144	1-3	0-20	0.08-20	(9.3±0.9)x10 <sup>-13</sup>
303	683	143	9-50	0-40	0.13-40	(9.90±0.20)x10 <sup>-13</sup>
328	686	144	5	0-27	0.13-8.4	(3.40±0.10)x10 <sup>-13</sup>
348	688	144	5	0-56	0.07-7.3	(1.48±0.08)x10 <sup>-13</sup>

a.  $k' = k \times [\text{CS}_2] + k_d$ ; and  $k_d$  is the first order loss rate of OH in the absence of CS<sub>2</sub>.

EXAMINATION OF THE TEMPERATURE DEPENDENCE FOR THE REACTION OF OH RADICALS  
WITH HETEROCYCLIC AROMATICS (IMIDAZOLE, FURAN, PYRROLE AND THIOPHENE) AND  
THE UNIMOLECULAR DECAY OF THE ADDUCTS IMIDAZOLE-OH AND THIOPHENE-OH

Franz Witte and Cornelius Zetzsch

Fraunhofer Institut für Toxikologie und Aerosolforschung  
Nikolai Fuchs Str. 1, D-3000 Hannover 61

In the reaction of OH radicals with aromatic compounds an addition of OH and a subsequent unimolecular decay of the aromatic-OH adduct back to the reactants is assumed to be the main reaction path<sup>1</sup>. We have been able to evaluate the temperature dependence of this equilibrium reaction of OH with benzene and some benzene-derivatives<sup>2,3</sup>. Since only a few investigations have been performed on the reaction of OH with aromatic heterocyclic compounds<sup>4-11</sup>, we tried to get some more information about the mechanism for the reaction of OH with imidazole, pyrrole, furan and thiophene.

We use a flash photolysis-resonance fluorescence apparatus to investigate the temperature dependence of these reactions between room temperature and 471 K. All experiments have been performed at a total pressure of 133 mbar with argon as inert gas using a water concentration of  $1.6 \cdot 10^{15} \text{ cm}^{-3}$ . A low flash energy of 2 J has been applied to avoid photolysis of the reactants. The initial OH-concentration can be estimated to be  $2 \cdot 10^{10} \text{ cm}^{-3}$  and the detection limit of OH to be  $\sim 10^7 \text{ cm}^{-3}$ .

In the presence of furan single exponential decays of OH are observed. Biexponential decays of OH are obtained in the presence of thiophene ( $442 \text{ K} < T < 471 \text{ K}$ ) and imidazole ( $353 \text{ K} < T < 425 \text{ K}$ ). Nonexponential decays of OH are observed in the presence of pyrrole within the whole temperature region, and only the initial slope of the decays was considered in the evaluation.



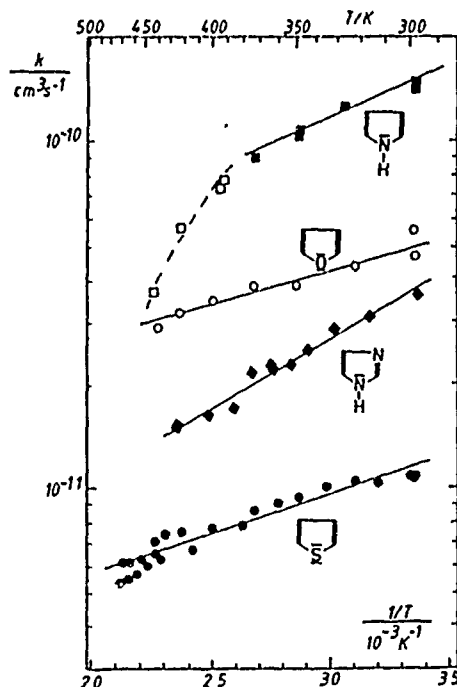


Figure 1: Arrhenius plots of the addition of OH to heterocyclic compounds pyrrole, imidazole, furan and thiophene.

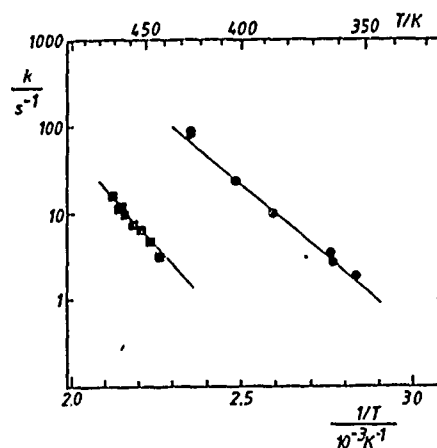


Figure 2: Arrhenius plots of the rate constants for the unimolecular decay of the adducts imidazole-OH (●) and thiophene-OH (■) back to the reactants.

Figure 1 shows Arrhenius plots of the rate constants for the primary reaction of OH with the reactants. All reactions show negative activation energies indicating an electrophilic addition of OH to the heterocyclic aromatics. The biexponential decays of OH observed in the presence of thiophene and imidazole confirm this assumption.

The evaluation of the ratio of the amplitudes of the biexponential decay curves yield equilibrium constants and hence rate constants for the unimolecular decay of the heterocyclic-OH adduct leading back to the reactants. The corresponding Arrhenius plots are shown in figure 2. Using both activation energies it is possible to derive the bond dissociation energies of these adducts forming back OH. These energies ( $\Delta H \pm 20^\circ$ ) can be determined to be  $(75 \pm 7)$  kJ/mol for imidazole and  $(92 \pm 14)$  kJ/mol for thiophene.

Reaction	Arrhenius expression
pyrrole + OH	$(1.5 \pm 0.5) \cdot 10^{-11} \exp(+ (690 \pm 120) K/T) \text{ cm}^3 \text{ s}^{-1}$
furan + OH	$(1.4 \pm 0.5) \cdot 10^{-11} \exp(+ (380 \pm 130) K/T) \text{ cm}^3 \text{ s}^{-1}$
imidazole + OH	$(1.7 \pm 0.4) \cdot 10^{-12} \exp(+ (920 \pm 80) K/T) \text{ cm}^3 \text{ s}^{-1}$
thiophene + OH	$(2.9 \pm 0.3) \cdot 10^{-12} \exp(+ (400 \pm 40) K/T) \text{ cm}^3 \text{ s}^{-1}$
imidazole-OH $\rightarrow$ imidazole + OH	$5 \cdot 10^9 \exp(- (7800 \pm 700) K/T) \text{ s}^{-1}$
thiophene-OH $\rightarrow$ thiophene + OH	$5 \cdot 10^{10} \exp(- (10300 \pm 1600) K/T) \text{ s}^{-1}$

## References

- 1 R. A. Perry, R. Atkinson, J. N. Pitts Jr., J. Phys. Chem. 81, 296 (1977)
- 2 A. Wahner, C. Zetzsch, J. Phys. Chem. 87, 4945 (1983)
- 3 F. Witte, E. Urbanik, C. Zetzsch, J. Phys. Chem. (in press)
- 4 E. C. Tuazon, R. Atkinson, A. M. Winer, J. N. Pitts Jr., Arch. Environ. Contamin. Toxicol. 13, 691 (1984)
- 5 J. H. Lee, I. N. Tang, J. Chem. Phys. 77, 4459 (1982)
- 6 R. Atkinson, S. M. Aschmann, W. P. L. Carter, Int. J. Chem. Kinet. 15, 51 (1983)
- 7 H. MacLeod, J. L. Jourdain, G. LeBras, Chem. Phys. Lett. 98, 381 (1983)
- 8 P. H. Wine, R. J. Thompson, Int. J. Chem. Kinet. 16, 867 (1984)
- 9 D. Martin, J. L. Jourdain and G. LeBras, Int. J. Chem. Kinet. 17, 1247 (1985)
- 10 T. J. Wallington, Int. J. Chem. Kinet. 18, 487 (1986)
- 11 R. Atkinson, S. M. Aschmann, A. M. Winer, W. P. L. Carter, Atmos. Environ. 18, 2105 (1984)

## The Chemical Dynamics of Highly Vibrationally Excited Molecules

F. Fleming Crim  
Department of Chemistry  
University of Wisconsin  
Madison, Wisconsin  
USA

The combination of direct excitation of overtone vibrations with time resolved spectroscopic detection is a means of probing the spectroscopy, kinetics, and dynamics of highly vibrationally excited molecules in great detail.

Spectroscopic studies, in both room temperature samples and free jets, monitor the products of a vibrational overtone initiated unimolecular reaction as a function of excitation wavelength. The resulting vibrational overtone predissociation spectra help reveal the nature of the prepared state and the types of interactions that are likely to be responsible for the structure in the spectrum. Measurements on both bound and predissociative states of molecules cooled in a supersonic expansion are particularly informative in this regard.

Kinetic measurements directly determine the rate of a vibrational overtone initiated unimolecular reaction of a fairly complex molecule (tetramethyldioxetane) that is cooled in a free jet expansion. The small initial thermal energy content of the molecules permits a particularly straightforward comparison with theory.

Dynamics studies use laser induced fluorescence detection to probe the individual quantum state populations of the OH fragments from the vibrational overtone induced reaction of hydrogen peroxide. Comparing the measured populations with theoretical predictions shows a clear distinction between different models that is most apparent near the threshold energy for the reaction.

Mode Selectivity in Reactions Induced by Vibrational Overtone Excitation

J.E. Baggott, D.W. Law, P.D. Lightfoot and I.M. Mills

Department of Chemistry, The University, Whiteknights, P.O. Box 224,  
Reading RG6 2AD, U.K.1. Introduction

Unimolecular reactions induced by direct one-photon excitation of stretching overtones of X-H bonds (X = C or O) have been studied extensively in recent years in attempts to observe mode-selective photochemistry.<sup>1</sup> The basis for the suggestion<sup>2</sup> that such states might not satisfy the requirements of rapid statistical energy redistribution, a fundamental assumption of RRKM theory, comes from the interpretation of overtone spectra in terms of the local mode model. In this model, the overtone transitions and intensities are analysed according to a diatomic Morse oscillator formalism implying localisation of excitation energy within selected bonds.

However, the problem of 'contamination' remains, i.e. it is unclear in many cases to what extent the local mode might be mixed with other molecular vibrations. Such mixing may be thought to provide channels for ultrafast relaxation from some initially prepared pure local mode state<sup>3</sup> or to simply prevent the preparation of such a state. Such contamination might explain why statistical (RRKM) behaviour has been observed in many of the reactions studied, although the sensitivity of some overtone excitation experiments to subtle deviations from statistical behaviour is open to question.<sup>4</sup>

Recent spectroscopic studies by Quack and co-workers<sup>3</sup> have revealed the presence of 'near-universal' stretch-bend Fermi resonances in molecules containing isolated C-H bonds. This is exactly the kind of interaction which may lead to contamination of local mode states and consequent rapid energy redistribution and we have, therefore, studied the C-H stretch fundamental and overtone spectra of cyclobutene in order to determine if such resonances arise in polyatomic molecules with symmetrically equivalent C-H bonds. Cyclobutene was chosen as an example of one of the few molecules which undergo unimolecular reaction following overtone excitation in the visible region.<sup>5</sup>

## 2. Experimental

Infrared spectra of gas phase cyclobutene below  $900\text{ cm}^{-1}$  were taken on a Nicolet 7199 FTIR system using Si/quartz and Ge/KBr beamsplitters and Hg-Cd-Te and In-As detectors. Overtone spectra in the near infrared and visible regions were measured using intracavity laser photoacoustic techniques as described previously.<sup>6</sup>

## 3. Results and Discussion

A portion of the infrared spectrum of gas phase cyclobutene in the region of the C-H stretch fundamentals is shown in fig. 1. We have analysed these bands in terms of separable effective vibrational Hamiltonians for the olefinic and methylenic C-H bond systems, using both a local mode and normal mode basis.<sup>7</sup> Our modelling studies reveal that the olefinic C-H stretch fundamental of  $A_1$  symmetry is in Fermi resonance with  $2\nu_3$ , where  $\nu_3$  is the ring C=C stretch. Similarly, the methylenic C-H stretch fundamental of  $A_1$  symmetry is in Fermi resonance with both  $2\nu_4$  and  $2\nu_{16}$ , where  $\nu_4$  and  $\nu_{16}$  are the in-phase and out-of-phase combinations of the  $>\text{CH}_2$  group scissor vibrations, and the stretch fundamental of  $B_2$  symmetry is in Fermi resonance with the  $\nu_4 + \nu_{16}$  combination.

Using our model vibrational Hamiltonians, we are able to predict that these resonances are of little consequence in the region of the  $\nu=4-6$  C-H stretch overtones which lie above the threshold to unimolecular reaction. However, for the methylenic C-H we do observe additional splitting at  $\nu=5$  (see fig. 2) which we have analysed in terms of a Fermi resonance with ring C-C stretch vibrations using an approximate model Hamiltonian.

With evolution operator techniques we can use our model vibrational Hamiltonians to determine the timescale of the decay of probability of an initially prepared pure local mode. For the methylenic C-H bond at  $\nu=5$  the presence of Fermi resonant ring C-C stretch vibrations causes decay of the initial state with a lifetime of ca. 0.12 ps, destroying rapidly any selectivity obtained. These results contrast with the olefinic C-H bond which, according to our modelling calculations, behaves as an 'almost' pure local mode. Further details of our calculations will be presented and the implications for mode-selective photochemistry discussed.

## References

1. F.F. Crim, Ann. Rev. Phys. Chem., 35, 657 (1984)

2. B.R. Henry, *Acc. Chem. Res.*, **10**, 207 (1977).
3. J.E. Baggott, M.-C. Chuang, R.N. Zare, H.R. Dübal and M. Quack, *J. Chem. Phys.*, **82**, 1186 (1985).
4. W.L. Hase, *Chem. Phys. Lett.*, **116**, 312 (1985); *J. Phys. Chem.*, **90**, 365 (1986).
5. J.M. Jasinski, J.K. Frisoli and C.B. Moore, *J. Chem. Phys.*, **79**, 1312 (1983).
6. J.E. Baggott, *Chem. Phys. Lett.*, **119**, 47 (1985)
7. J.E. Baggott, H.J. Clase and I.M. Mills, *Spectrochim. Acta Part A* (1986) to appear.

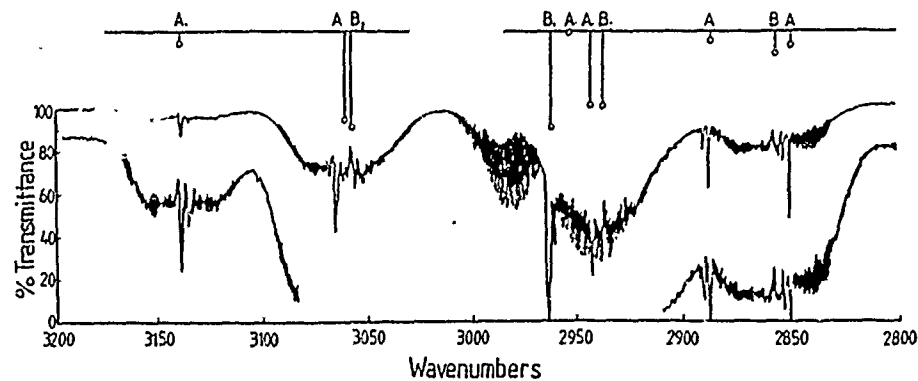


Fig. 1. Part of a FTIR spectrum of gas phase cyclobutene in the region of the C-H stretching fundamentals. The stick spectra give the band positions and intensities predicted by our model.

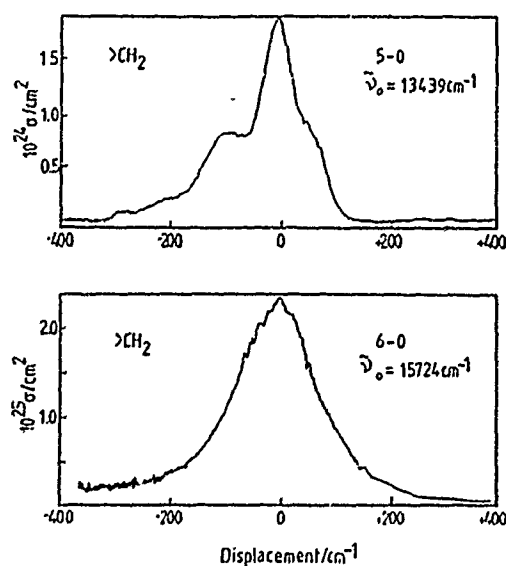


Fig. 2. Laser photoacoustic spectra of gas phase cyclobutene in the region of the  $v=5$  and  $6$  methylenic C-H stretch overtones.

ANALYTIC SOLUTION OF RELAXATION IN A SYSTEM WITH EXPONENTIAL TRANSITION  
PROBABILITIES

Wendell Forst\* and Guo-Ying Xu, Department of Chemistry and CRM,  
Laval University, Quebec, Canada G1K 7P4

Several years ago<sup>1</sup> we have obtained an analytic solution for what we call the exponential model Model B in the form of an infinite series expansion for  $c(x,t)$ , the fractional population, per unit energy, of molecules having energy  $x$  at time  $t$  (see eqs. 7-13 in ref. 1c). The number of terms which effectively contribute to the  $c(x,t)$  series increases from one (the first term) at equilibrium ( $t \rightarrow \infty$ ) to infinity at time zero ( $t \rightarrow 0$ ). Since it is obviously impractical to generate an infinite, or even very large, number of terms, the analytic solution suffers from the disadvantage that  $c(x,t)$  cannot be obtained in its infinite series expansion form at very short times. The purpose of this work is to show that the problem can be solved by an alternative approach which leads to simple and tractable expressions.

Let  $q(x,y)$  be the per-collision probability of the transition  $x \leftarrow y$ , and suppose that at  $t = 0$  the energy distribution of the molecule of interest is a delta function at  $y = y_0$ . Thus  $c(y,0) = \delta(y - y_0)$ . The first collision results therefore in the energy distribution  $c(x,n=1) = q(x,y_0)$  where the number of collisions ( $n$ ) now replaces time ( $n = \omega t$ , where  $\omega$  = collision frequency). This distribution of final energies becomes the initial distribution of initial energies for the next collision, and so on; thus the energy distribution after  $n$  collisions is

$$c(x,n) = \int c(y,n-1) q(x,y) dy \quad (1)$$

For this kind of approach to be reasonably tractable, it is necessary to take the exponential transition probability in the simple form<sup>1a,2</sup>

$$q(x,y) = \begin{cases} C \exp[-(y-x)/\alpha] & x < y \\ C \exp[-(x-y)/\beta] & x > y \end{cases} \quad (2)$$

where  $\alpha$  measures the strength of the coupling to the heat bath,  $C = 1/(\alpha + \beta)$  and  $\beta = \alpha kT/(\alpha + kT)$ . Substituting (2) into (1) yields, after some lengthy but straightforward manipulation, the result that the energy distribution after the  $n$ -th collision is

$$c(x,n) = \begin{cases} P(n) C^n \exp[-(y_0 - x)/\alpha], & x < y_0 \\ P(n) C^n \exp[-(x - y_0)/\beta], & x > y_0 \end{cases} \quad (3)$$

where  $P(n)$  is a polynomial of degree  $n-1$  given by

$$P(n) = \sum_{k=1}^n \begin{bmatrix} n-2+k \\ n-1 \end{bmatrix} \frac{z^{n-k}}{(n-k)!} C_2^{k-1} \quad (4)$$

with  $C_2 = \alpha\beta/(\alpha+\beta)$  and  $z = (x - y_0)$  or  $(y_0 - x)$  for  $x > y_0$  and  $x < y_0$ , respectively. Fig. 1 shows a plot of  $c(x,n)$  of eq. (3) for  $n = 1, 2, 3, 4, 5$  and 10, assuming  $y_0 = 5000 \text{ cm}^{-1}$ ,  $\alpha = 250 \text{ cm}^{-1}$ .

Various bulk averages can be now easily calculated, in particular the decay, after  $n$  collisions, of average energy and its square:

$$\langle\langle y \rangle\rangle = y_0 - n(\alpha + \beta) \quad (6)$$

$$\langle\langle y^2 \rangle\rangle = y_0^2 + 2ny_0(\beta - \alpha) + n(\alpha^2 + \beta^2) + n^2(\alpha - \beta)^2 \quad (7)$$

Figs. 2 and 3 show  $\langle\langle y \rangle\rangle$  and  $\langle\langle y^2 \rangle\rangle$  of eqs. (6) and (7) as the continuous line, while the dotted line represents result obtained from the more accurate series solution. It can be seen that eqs. (6) and (7) give the correct result for the first 500 collisions or so, i.e. until the energy has decayed to less than 1/10th of its initial value.

From eqs. (6) and (7) the mean square deviation of average energy is, after  $n$  collisions



$$\sigma^2 = \langle\langle y^2 \rangle\rangle + \langle\langle y \rangle\rangle^2 = n(\alpha^2 + \beta^2) \quad (8)$$

which may be used to construct a gaussian approximation to  $c(x,n)$ :

$$c(x,n) \approx (\sigma\sqrt{2\pi})^{-1} \exp[-(y - \langle\langle y \rangle\rangle)^2 / 2 \sigma^2] \quad (9)$$

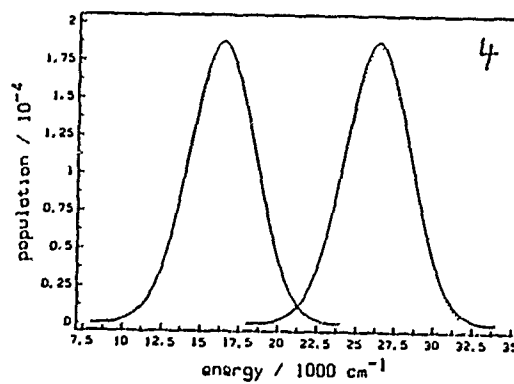
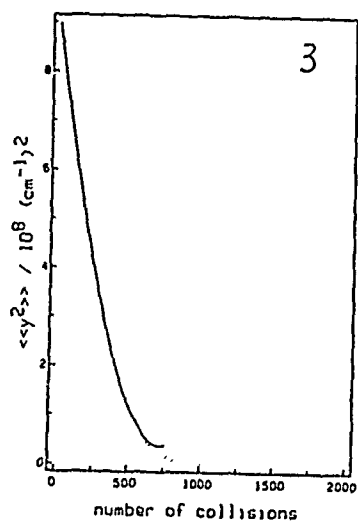
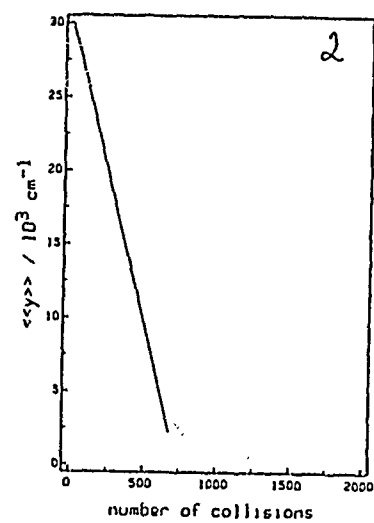
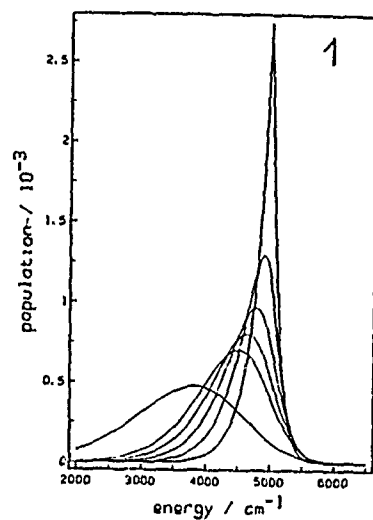
with  $\langle\langle y \rangle\rangle$  and  $\sigma^2$  from eqs. (6) and (8), respectively. This is shown in Fig. 4 which shows the population distribution after 91 collisions for an initial delta function distribution at 20,000  $\text{cm}^{-1}$  (left) and 30,000  $\text{cm}^{-1}$  (right) calculated from eq. (9) (continuous line) and compared with the more exact series solution (dotted line).

The analytic formula of eq. (3) for  $c(x,n)$  gives an accurate representation of the initial decay of the population distribution for a delta function distribution initially, and thus is useful as an adjunct to the more accurate series solution at later times. Similar comments apply to any bulk average obtained from  $c(x,n)$ . The gaussian approximation (eq.9) cannot be used very close to  $t = 0$  since  $c(x,n)$  is asymmetric on account of detailed balance (cf. Fig. 1), but as soon as energy has decayed such that the entire contribution to  $c(x,n)$  comes from the down-part ( $x < y$ ),  $c(x,n)$  becomes symmetric (see also Fig. 1), and can be usefully and simply approximated by the gaussian.

\* Present address: Département de Chimie Physique des Réactions, 1 rue Grandville, 54042 Nancy Cedex, France.

#### References

1. (a) A. P. Penner and W. Forst, J. Chem. Phys. 67, 5296 (1977); (b) W. Forst and A. P. Penner, J. Chem. Phys. 72, 1435 (1980); (c) W. Forst, J. Chem. Phys. 80, 2504 (1984).
2. J. Troe, J. Chem. Phys. 66, 4745 (1977); J. E. Dove and J. Troe, Chem. Phys. 35, 1 (1978); B. Carmeli and A. Nitzan, J. Chem. Phys. 76, 5321 (1982).



MODE SPECIFICITY IN INTRAMOLECULAR VIBRATIONAL RELAXATION AND  
UNIMOLECULAR REACTIONS: A SEMICLASSICAL ANALYSIS

V. Aquilanti, S. Cavalli and G. Grossi  
Dipartimento di Chimica dell'Universita'  
06100 Perugia, Italy

Advances in experimental techniques (in particular, laser and molecular beams, are promoting developments in the study of intramolecular vibrational relaxation and unimolecular decompositions, thus making it possible to test the statistical assumptions which underlie the current theories. An important goal also for practical purposes is to succeed in obtaining substantial deviations from statistical behavior, thus opening the experimental possibility for greater selectivity for the elementary processes of chemical kinetics and photochemistry.

An analysis of the specificity of unimolecular decompositions and of intramolecular vibrational relaxation can be developed by starting with simple models for coupled oscillators, for which different modes (and transitions between them) have been well characterized in this laboratory. The asymptotic techniques introduced, which are essentially semiclassical in nature, include: the introduction of a reaction radius as an adiabatic variable, the construction of adiabatic curves along which the system evolves in the zero approximation, the evaluation of nonadiabatic coupling terms, responsible of transitions between curves. The present investigation relates resonance lifetimes and unimolecular dissociation rates: reference problems are studied, for the inclusion of the nonadiabatic couplings which are responsible of the intramolecular redistribution of energy. Such a redistribution is localized to take place at orthogonal trajectories in the potential energy surface (ridges). Computational examples are presented.

The *a priori* calculation of collisional energy transfer  
in highly vibrationally excited molecules.

Kieran F. Lim and Robert G. Gilbert

Department of Theoretical Chemistry, University of Sydney,  
N.S.W. 2006, Australia.

Information on collisional energy transfer between a highly vibrationally excited molecule and a bath gas is important in the study of unimolecular and termolecular reactions. One wishes to find  $P(E, E')$  (the probability that a molecule with initial internal energy  $E_i = E'$ , will have a final energy  $E_f = E$ , after collision with another molecule) or its first moment ( $\langle \Delta E \rangle$ , the average energy transferred per collision).

An *a priori* calculation of  $P(E, E')$  has been carried out, based on the "biased random walk" model<sup>1</sup>. The mathematical derivation and all technical details for this model are given in Ref. 1, but can be summarised as follows.

The biased random walk model assumes that, during a collision, energy exchange between the internal degrees of freedom (of the excited molecule) and the other degrees of freedom is essentially random but for certain constraints. This implies that the time evolution of the internal energy distribution (of an ensemble of molecules) would be governed by a Smoluchowski equation. The required  $P(E, E')$  will be the value of the internal energy distribution at the end of the collision, subject to the constraint that the energy distribution before the collision is a delta function centred on  $E'$ . Two important constraints on the internal energy must be considered. First, the activation and deactivation rates are related by detailed balance: the Smoluchowski equation must contain a term which arises from this microscopic reversibility. Second, total energy (of the two body system) must be conserved: this places a boundary condition on the

Smoluchowski equation.

The Smoluchowski equation can be solved with these constraints, yielding a specific form for  $P(E, E')$  for a given impact energy of the bath gas. This form of  $P(E, E')$  is then averaged over a Boltzmann distribution of impact energies to yield the final expression for  $P(E, E')$ . This final expression is in terms of a single quantity,  $s^2 = D_e t_c$ , where  $D_e$  is an "energy diffusion coefficient" and  $t_c$  is the average duration of a collision. The value of  $s^2$  can be obtained from classical trajectory simulations by assuming that for any one trajectory, a generalised Langevin equation can be used to describe the flow of energy in and out of the molecule. The overall energy transfer,  $\langle \Delta E \rangle$ , or the downward average energy transfer,  $\langle \Delta E_{\text{down}} \rangle$ , can then be easily calculated from  $P(E, E')$ .

The assumptions given above permit  $P(E, E')$  to be evaluated *a priori* from only a small number (say, 10-50) trajectories. This use of a dynamical assumption to give a vast reduction in the number of trajectories is completely analogous to fundamental assumptions in the molecular dynamics simulation of transport properties in liquids, where the linear response formulation yields transport coefficients from only a small sample of phase space. The only difference between this method and our treatment for collisional energy transfer in gases is that our linear response hypothesis is made in "energy space".

Calculations for the deactivation of excited azulene by various monatomic bath gases, employing realistic inter- and intra-molecular potentials show good agreement with the experimental results of Rossi *et al.*<sup>2</sup> and Hippler *et al.*<sup>3</sup> This suggests that the extended model may be reliably and economically used to calculate appropriate energy transfer quantities.

Moreover, a number of general trends seen in experimental results can be rationalised with the model.

Table I:

Average downward energy transfer values<sup>4</sup> for the deactivation  
of azulene by three bath gases at 300 K. (All quantities in cm<sup>-1</sup>.)

	This work	Hippler <i>et al.</i> <sup>3</sup>	Rossi <i>et al.</i> <sup>2</sup>
$\langle E' \rangle$	17 500 30 644	17 500 30 644	17 500 30 644
He	160 225	190 184	117 190
Ne	295 353	330 332	185 279
Ar	218 344	354 360	250 366

- 1) R. G. Gilbert, J. Chem. Phys., 80, 5501 (1984);  
K. F. Lim and R. G. Gilbert, J. Chem. Phys., in press (1986).
- 2) M.J. Rossi, J.R. Pladziewicz and J.R. Barker, J. Chem. Phys., 78, 6695 (1983).
- 3) H. Hippler, L. Lindemann and J. Troe, J. Chem. Phys., 83, 3906 (1985).
- 4) "Experimental" average downward energy transfers have been calculated from published data by an exponential  $P(E, E')$ .

MULTIPHOTON IONIZATION STUDIES ON COLLISIONAL ENERGY  
TRANSFER AND UNIMOLECULAR REACTIONS OF EXCITED  
BENZENE DERIVATIVES.

H. G. Löhmannsröben<sup>†)</sup>, K. Luther, and K. Reihs

Institut für Physikalische Chemie der Universität Göttingen,  
Tammannstraße 6, D-3400 Göttingen, FRG

†) Institut für Physikalische und Theoretische Chemie der  
Universität Braunschweig, Hans-Sommer-Straße 12,  
D-3300 Braunschweig, FRG

Intramolecular reaction steps and energy transfer in collisions of highly excited molecules are observed by time-resolved resonant MPI.

Vibrationally highly excited molecules are prepared monoelectronically via laser excitation followed by a fast intramolecular step like an internal conversion or a dissociation. A detection scheme of selective ionization by kinetic control (SIKC) allows to follow the time evolution of the molecular population in a narrow section on the vibrational energy scale during the course of collisional deactivation. Thus information is gained on the average energy removal per collision and on changes in time of the energy distribution in the relaxing molecular manifold. Specific rate constants,  $k(E)$ , of intramolecular reaction steps like intersystem crossings from vibrationally highly excited states are measured in direct pump and probe experiments.

Recent results from our studies on anilin, benzene, and alkylated benzenes will be presented.

IS PROPYLENE OXIDE CATION RADICAL  
BEHAVING NON-ERGODICALLY IN ITS DISSOCIATION REACTIONS?

C. Lifshitz\*, T. Peres\*, N. Ohmichi\*, I. Pri-Bar\*\* and L. Radom\*\*\*

\*Department of Physical Chemistry

The Hebrew University of Jerusalem, Jerusalem, Israel

\*\*Radiochemistry Department

Nuclear Research Centre -- Negev, Beer Sheva, Israel

\*\*\*Research School of Chemistry

The Australian National University, Canberra, Australia

Intramolecular energy redistribution in polyatomic molecules is a topic of great current interest in chemical kinetics and dynamics. Intramolecular energy redistribution in polyatomic cations has been reviewed recently.<sup>1</sup> It has been demonstrated that isomerization can lead to nonrandom dissociation paths by channeling vibrational energy into a limited number of degrees of freedom.

We have studied the unimolecular dissociation reaction of propylene oxide cation-radical to acetyl cation plus methyl radical. We have employed carbon-13 labelling, tandem mass spectrometry techniques and *ab initio* calculations. Propylene oxide cation radical isomerizes to the methoxyethylidene radical cation,  $\text{CH}_3\text{-C-O-CH}_3^+$ , which may either dissociate directly in a reaction possessing a high reverse activation energy or in turn isomerize to acetone radical-cation, having an internal energy of ~51 kcal/mol, in large excess of the critical energy for dissociation (see Figure 1).

The main question which we have addressed is, — if acetone ion is indeed an intermediate, — is the newly formed methyl lost preferentially to the preexisting methyl. This would mean non-ergodic dissociation following isomerization — as has been observed previously for the enol



ion of acetone. In order to answer this question, we have measured the relative abundances for losses of  $^{13}\text{CH}_3$  versus  $^{12}\text{CH}_3$  from  $\text{CH}_3\text{-CH}_2\text{-}^{13}\text{CH}_2^+$  as well as kinetic energy releases for these reactions and have calculated transition state energies along the potential energy profile. The possible roles of excited electronic states and isomeric ion structures such as  $\text{CH}_3\text{OC}^+$  have also been explored.

<sup>1</sup> C. Lifshitz, J. Phys. Chem. 87, 2304 (1983).

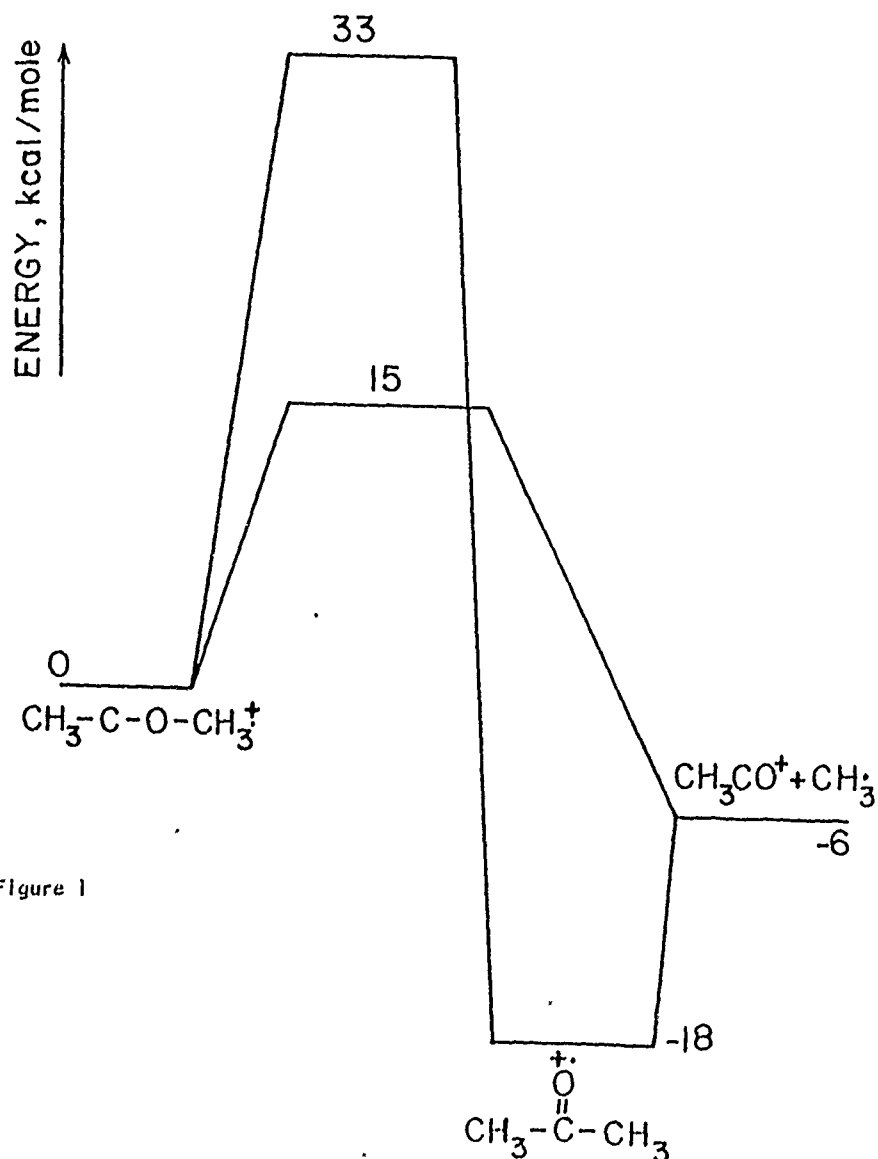


Figure 1

# Energy Selected Ion Chemistry by Photoelectron Photoion Coincidence and Laser Induced Dissociation

Tomas Baer, Thomas L. Bunn, Susan Olesik, and J.C. Morrow  
Chemistry Department  
University of North Carolina  
Chapel Hill, NC 27514

## ABSTRACT

Ions can be energy selected in photoionization experiments by detecting ions in coincidence with energy selected electrons. The electrons serve not only to identify the ions of interest, but also provide a start signal for measuring the ion time of flight (TOF). The ion TOF in turn yields information about the mass, and more interestingly, about the dissociation rate and kinetic energy released in the dissociation process. The derived microcanonical decay rate,  $k(E)$ , can be easily compared to that predicted from the statistical theory of unimolecular decay (RRKM or QET).

Recent applications to be discussed include the dissociation of halogen atom loss from the dihalobenzene ions.<sup>2</sup> The measured rates, shown in Figure 1, are in the  $10^4$  to  $10^7$  s<sup>-1</sup> range. However, extrapolation of these rates to the dissociation onset indicate that the ion lifetimes at the onset are in excess of 10 sec. The calculated rates of dissociation in conjunction with other thermochemical information are used to obtain C-X bond dissociation energies, which are listed in the Table. It is evident that the C-X bond energies in the mono- and di-halobenzenes are similar. However, the C-H bond energies are different.

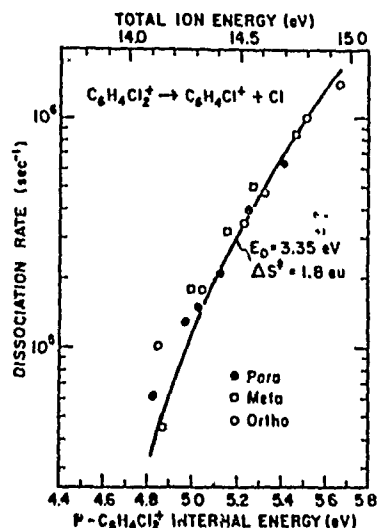


Fig. 1. Measured dissociation rates and RRKM calculations (solid line).

TABLE I. C-H and C-X Bond Energies in  $C_6H_{6-n}X_n^+$  Ions (kcal/mol)

Ion	C-H	C-Cl	C-Br
$C_6H_6^+$	85.3 <sup>3</sup>	-	-
$C_6H_5Cl^+$	89.7 <sup>2</sup>	74.8 <sup>4</sup>	-
$C_6H_5Br^+$	89.4 <sup>2</sup>	-	64.0 <sup>6</sup>
$C_6H_4Cl_2^+$	-	77.2 <sup>2</sup>	-
$C_6H_4Br_2^+$	-	-	64.6 <sup>2</sup>

Previous photoelectron photoion coincidence (PEPICO) studies of isomeric systems have demonstrated that some of these ions isomerize to the lowest energy structure prior to dissociation. This is concluded on the basis of the similarity of the dissociation rate of the various isomers, even though they have different apparent activation energies. The heights of these barriers is not known, however. A new technique for probing such barriers has been developed by combining the energy selection capability of PEPICO with laser induced dissociation. Figure 2 shows the

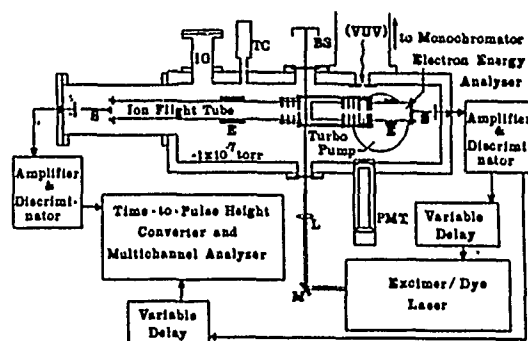


Fig. 2. Diagram of the photoelectron-photoion coincidence photodissociation spectrometer PEPICO-PDS. Taken from Reference 5.

experimental set-up. Ions are prepared in the usual PEPICO manner, by photoionization using a vacuum UV cw light source and energy selected by collecting only zero energy electrons. Although ions are formed in a distribution of internal energy states, pulsing the laser only when a zero energy electron has been detected, insures that ions of a specific internal energy are photodissociated. Both the internal energy of the ion as well as the laser wavelength can be varied thereby making this a very versatile technique for the study of ion spectroscopy and dynamics.

The initial investigations have included the photodissociation of nitrobenzene ions (see Figure 3) and  $C_4H_6^+$  ions. In the latter study, butadiene, 1-butyne, and 2-butyne ions have been photodissociated, and the results used in order to probe the ion structure as a function of the ion internal energy. Butadiene and butyne ions can be easily distinguished because the former ion has several accessible dissociative excited states that can be reached with the laser photon, where as the butyne ions have large energy gaps between the ground and excited states. However, when the butyne ions are prepared with sufficient internal energy to cause them to isomerize to the butadiene structure, they can be photodissociated. This onset for photodissociation is shown in Figure 4. This determination makes possible the construction of the energy diagram shown in Figure 5. Not surprising is the fact that the barriers for 1- and 2-butyne ion are the same, because the reaction involves just H atom transfer steps.

## References

1. Baer, T. in "Gas Phase Ion Chemistry", M.T. Bowers Ed. Vol. 1, Ch. 5, Academic Press 1979; Baer, T. in "Advances in Chemical Physics", S. Rice and Prigogine Eds., Vol. 64, p. 111, John Wiley & Sons, 1986.
2. Olesik, S., Baer, T. and Morrow, J.C. *J. Phys. Chem.* in press.
3. Rosenstock, H.M., Dannacher, J. and Liebman, J.F. *Radiat. Phys. Chem.* 40, 7 (1982).
4. Rosenstock, H.M., Stockbauer, R.L. and Parr, A.C. *J. Chem. Phys.* 71, 3708 (1979); Rosenstock, H.M., Stockbauer, R.L. and Parr, A.C. *J. Chem. Phys.* 73, 773 (1980).
5. Bunn, T.L., Richard, A.M. and Baer, T. *J. Chem. Phys.* 84, 1424 (1986).

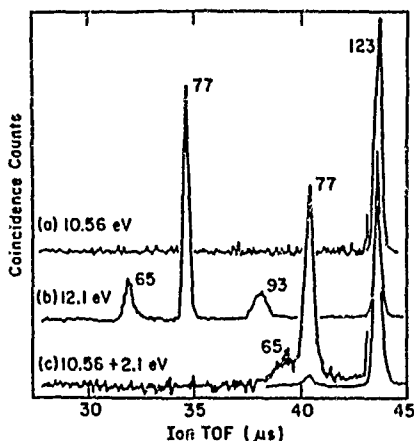


Fig. 3. Examples of ion TOF distributions for three indicated VUV and laser energies (a) and (b) are for VUV light only, while (c) includes a 2.1 eV laser photon.

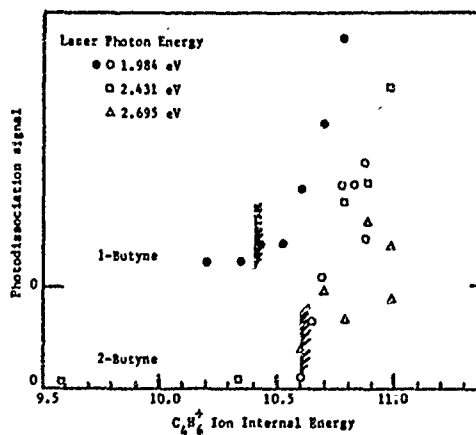


Fig. 4. Photodissociation signal as a function of  $C_4H_6^+$  internal energy.

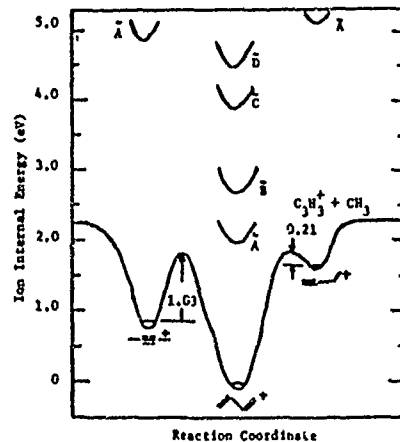


Fig. 5. Potential energy diagram derived from PEPICO-PD results.

DIRECT VERSUS INDIRECT MICROSCOPIC MECHANISMS IN THE  
Li+HF REACTION: AN ISOTOPIC AND ORIENTATIONAL STUDY

J.M. Alvarinho, Departamento de Quimica Fisica, Facultad de  
Quimica, Universidad de Salamanca, 37008 Salamanca, Spain,  
F.J. Basterrechea, Departamento de Quimica Fisica, Facultad  
de Ciencias, Universidad del Pais Vasco, Bilbao, Spain, and  
A. Laganà, Dipartimento di Chimica dell' Università, Perugia,  
Italy.

Introduction

In a previous paper /I: J.M. Alvarinho et al., J. Mol.  
Structure, 120, 187 (1985)/ we have reported a peculiar effect  
of the incoming atom orientation for the reaction  $\text{Li}+\text{HF}(v=J=0)$   
 $\text{LiF}+\text{H}$ . By running batches of quasiclassical trajectories on the  
CSCM potential energy surface /S. Carter and J.N. Murrell,  
Molec. Phys., 41, 567 (1980)/ at different collision energies  
we found, in fact, that reactive attacks onto the HF target  
preferentially occur via approaches from the H side in spite of  
the fact that the product molecule is LiF. Such an indirect  
mechanism was tentatively interpreted in paper I in terms of  
the vibrational excitation to be pumped into the HF ground  
state molecule in order to allow the overcoming of the late  
barrier. This mechanism should be influenced by changes in the  
mass of the F partner in HF, and so we extended the investiga-  
tion to the  $\text{Li}+\text{XF}(v, J=0)$  systems with  $\text{X}=\text{Mu}, {}^1\text{H}, {}^3\text{H}$  and  ${}^{10}\text{H}$ ,  $v=0$ ,  
1 and 2, and collision energy of  $15 \text{ kcal mol}^{-1}$ . The dynamical  
study was carried out by running batches of 200 trajectories  
in three dimensions starting from a given value of the approach-  
ing angle  $\phi$  ( $\phi$  called  $\theta$  in paper I is the angle included between  
Li and F distances from the centre of mass of HF and centered

on it).

## Results and discussion

A study of the angular dependence of the total cross section led us to suspect that the nature of the indirect mechanism is not exclusively related (as suggested in paper I) to the amount of vibrational energy pumped into the target molecule, but it has to do with some other quantity depending on the mass of the F partner. Therefore in order to assess in more detail the nature of the indirect reactive mechanism, we have studied the evolution of the trajectory by following step by step the variation of the internuclear distances during the integration of the motion equations.

The most important finding of the present study was evidenced in this way. In fact, by looking at the Li+MuF system starting from  $v=0$  and attack by the Mu side ( $\phi=180$  degree), it was put in evidence that during the central part of the collision the MuF molecule can easily rotate so as to end up in a geometry with  $\phi$  about 90 degree. In fact, at the beginning of the collision  $r(\text{LiF})$  equals  $r(\text{LiMu})+r(\text{MuF})$  indicating that the initial collinear configuration is kept up. However, when  $r(\text{LiMu})$  decreases to about  $2 \text{ \AA}$  the MuF molecule rotates up to about  $\phi=140$  degree. Then, after being reflected back to  $\phi<90$  degree it ends up with an orientation of about 90 degree at which the curves  $r(\text{LiMu})$  and  $(r^2(\text{LiF})+r^2(\text{MuF}))^{1/2}$  cross, and Mu can be more easily expelled into the exit channel. This explains the high reactivity of this system: the very small mass of Mu leads to a very small reduced mass and, consequently, moment of inertia of MuF which in turn facilitates the rotation of the molecule up to the perpendicular configuration. For this geometry the barrier height is minimal and slightly above the vibrational energy content of  $v=0$ , so that it can be overcome. Therefore

at least for the Mu case, it can be concluded that an energy transfer from translational to the more effective (from the point of view of reaction) vibrational motion, as we speculated in paper I, is not the leading mechanism for reaction. The role of T+V transfer is, eventually, to supply an amount of energy of few kcal mol<sup>-1</sup> needed to reactants for having, at the saddle point, enough velocity parallel to the exit channel to end into it.

An extensive graphical research of this kind undertaken for all isotopomers, vibrational energy and angles of attack leads us to the following conclusions. The unexpected reactivity at the X end (as compared to the one at the F end) of XF when X=Mu or <sup>1</sup>H and v=0 is essentially due to potential (dynamical) induced rotation of XF which brings the system into a perpendicular configuration where the vibrational energy defect is minimal and reaction can thus take place. The strong angular forces operating in this system are able to induce a considerable rotation of MuF or <sup>1</sup>HF on Li attacks by the light end of the molecules, but the rotation is only modest when the heavy (F) end is attacked. On the other hand, rotation of the heavier molecules (<sup>3</sup>HF, <sup>10</sup>HF) is very difficult and reactivity in these cases is only appreciable when no rotation (v=2) or little rotation (v=1) is necessary.

A TRAJECTORY SURFACE-HOPPING STUDY OF  $\text{Cl}^- + \text{H}_2$  REACTIVE COLLISIONS

Muriel SIZUN<sup>\*</sup>, Eric A. GISLASON<sup>\*\*</sup> and Gérard PARLANT<sup>\*\*\*</sup>

<sup>\*</sup> Laboratoire de Collisions Atomiques et Moléculaires, Bât 351,

<sup>\*\*\*</sup> Laboratoire de Résonance Electronique et Ionique, Bât 350,

Université Paris-Sud 91405 Orsay Cedex France

<sup>\*\*</sup> Department of Chemistry, University of Illinois at Chicago, Chicago, Illinois 60680, USA

The collision of  $\text{Cl}^- + \text{H}_2$  produces different accessible channels indicated in table 1. Experiments on this system were conducted recently by Barat et al(1) in the relative energy range of 5.6 to 12 eV. They observe all the various channels, except those involving the  $\text{Cl}^-$  ion. Relative cross sections are measured and normalized to the total cross-section measurements of Hug (2). The most remarkable feature of the experiment concerns the R and RD channels : products HCl were strongly peaked in the com frame near 50-60 deg, by contrast the HCl vibrational distributions were quite different in the two channels.

In our theoretical approach we want to obtain a semi-quantitative interpretation of the experimental results and a better understanding of the reaction dynamics. The first step is to construct potential energy surfaces (p.e.s.) for the  $\text{ClH}_2^-$  system. So the DIM (Diatomics -in Molecules) method is used in the zero-overlap approximation to obtain the two lowest p.e.s. of the system. The atomic basis set is restricted to the ground state of each neutral atom or atomic ion. The diabatic curves are introduced in the DIM matrix for all the diatomic fragments, neutral( $\text{HCl } 1\Sigma^+, 1\Pi$ ,  $\text{H}_2 1\Sigma_g^+$ ) or negative resonance ion ( $\text{HCl}^- 2\Pi$ , the two  $\text{H}_2^- 2\Sigma^+$  with their coupling and the two  $\text{HCl}^- 2\Sigma^+$  with their coupling given by the formula of Olson) . From the DIM matrix (5x5) it is possible to extract the adiabatic p.e.s. of  $\text{ClH}_2^-$ , or the diabatic p.e.s. which are more useful to carry out trajectory calculations : on figure 1 are represented the diabatic p.e.s correlated to the configuration  $\text{Cl}^- + \text{H} + \text{H}$  (a) and the lowest of the four p.e.s. correlated to  $\text{Cl} + (\text{H-H})^-$  (b), in the colinear geometry. The dashed curve shows the seam between the surfaces. For the neutral  $\text{ClH}_2$  surface which is needed to describe detachment products, the LEPS surface of Persky (3) is used. The seam between the neutral surface and each diabatic ionic surface



is indicated on figure 1 by the dotted line.

The set of 3 surfaces is used to calculate the reaction dynamics with the 'classical trajectory surface-hopping method'. The calculations are performed as usual except when a trajectory on either ionic surface reaches a crossing with the neutral surface. In this case, we do not allow it to continue on the ionic surface, rather we assume that the electron is immediately ejected, and consequently the trajectory remains on the neutral surface until the collision ends.

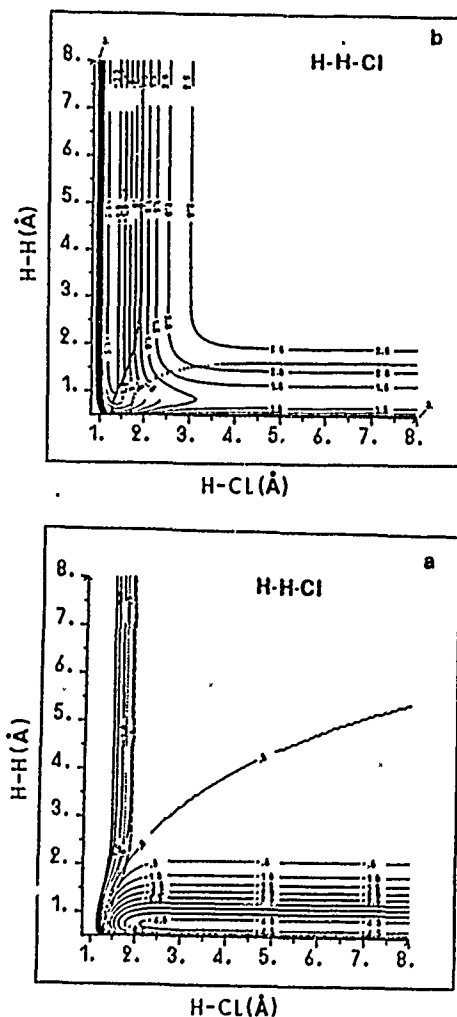


figure 1

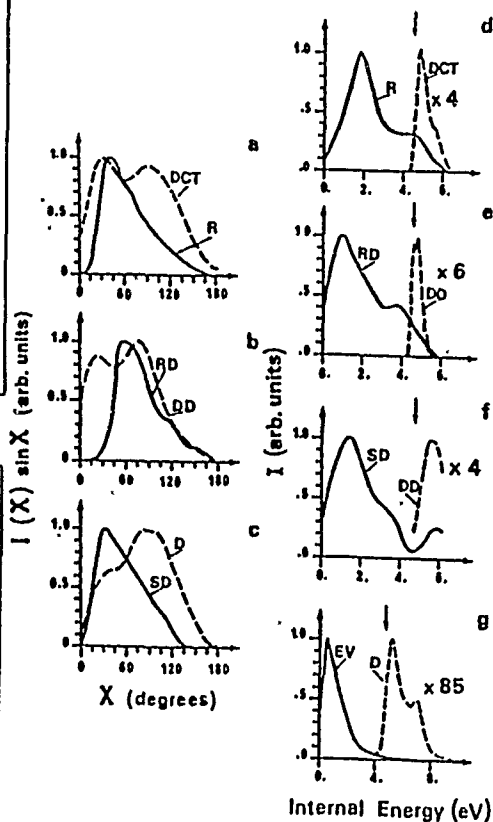


figure 2

In this way the various detachment products such as  $\text{HCl} + \text{H} + \text{e}^-$  are obtained. Our procedure assumes that all electrons are ejected with zero energy. This agrees reasonably well with the experimental values (1) which lie in the range  $\approx 0.2 \pm 0.2$  eV.

Five different sets of trajectories were run at  $E_{\text{rel}} = 9.7$  eV. The preexponential factor in the coupling between the 2 p.e.s. and the position in energy of the neutral surface relative to the ionic p.e.s. are treated as variable parameters. In each case the sum of all of the cross-sections is of the order of  $2 \text{ \AA}^2$ . The small overall reactivity is due to the fact that all product channels are endothermic by at least 2.9 eV. Our best results are obtained when the neutral surface is raised by 0.2 eV.

		$\Delta H$ eV	$\sigma_{\text{th}}$	$\sigma_{\text{exp}}$ ( $\text{\AA}^2$ )
$\text{HCl} + \text{H}^-$	R	2.91	0.46	0.3
$\text{Cl} + \text{H} + \text{H}^-$	DCT	7.34	0.04	0.0
$\text{Cl}^- + \text{H} + \text{H}$	D	4.49	0.07	
$\text{HCl} + \text{H} + \text{e}^-$	RD	3.66	0.96	0.3
$\text{Cl} + \text{H}_2 + \text{e}^-$	SD	3.60	0.26	0.3
$\text{Cl} + \text{H} + \text{H} + \text{e}^-$	DD	8.09	0.04	0.06

The overall agreement between these values and the experiments of Barat et al(1) and Huq et al (2) is fairly good. The angular and energy distributions for the six product channels were determined for each of the 5 sets of calculations. It was found that the shape of a particular distribution was rather insensitive to the particular choice of potential parameters used in the calculation. All of the computed differential cross-sections agree well with experiments as do most of the internal energy distributions (See figure 2). The one exception is  $P(E_{\text{int}})$  for the R channel which peaks at a much higher energy than the experimental distribution. Our calculations indicate that the dynamical model which appear to work the best to explain the R and RD channels results is the elastic stripping model.

(1) M. Barat, J.C. Brenot, J.A. Fayeton, J.C. Houver, J.B. Ozenne, R.S. Berry, and M. Durup-Ferguson, Chem. Phys. 97,165, (1985).

(2) M.S. Huq, D.S. Fraedrich, L.D. Doverspike, R.L. Champion and V.A. Esaulov, J.Chem.Phys. 76,4952, (1982).

(3) A. Persky, J.Chem.Phys. 66,2932, (1977).

QUASICLASSICAL TRAJECTORY STUDY OF  $X+H_2$  TYPE REACTIONS ON  
REALISTIC POTENTIAL ENERGY SURFACES

B.László, G.Lendvay and T.Bérces

Central Research Institute for Chemistry,  
Hungarian Academy of Sciences, Budapest, Hungary.

The recently proposed BSBL (Bond-Strength-Bond-Length) method [1] proved to be successful in the estimation of rate coefficients and Arrhenius parameters for  $A+BC \rightarrow AB+C$  type atom transfer reactions. The treatment defines a minimum energy path (MEP) as

$$\exp(-2\beta_{AB}X_{AB}) + \exp(-2\beta_{BC}X_{BC}) = 1$$

where  $X_{ij} = R_{ij} - R_{ij}^0$  is the extension of the bond and  $\beta_{ij}$  is the appropriate Morse parameter. The potential energy along the MEP is obtained in terms of variable  $a = \exp(-2\beta_{AB}X_{AB})$  by

$$V(a) = V_{BC}^0 + (1-a)V_{BC} + aV_{AB} + A_{AC} a^{\beta_{AC}/\beta_{AB}} (1-a)^{\beta_{AC}/\beta_{BC}}$$

where the energies for AB and BC are given by the Morse functions

$$V_{AB} = V_{AB}^0 \{a - 2a^{1/2}\} \text{ and } V_{BC} = V_{BC}^0 \{(1-a) - 2(1-a)^{1/2}\},$$

respectively and  $A_{AC}$  is a constant in the endgroup contribution term.

In this work we extended the BSBL treatment and made it suitable for the calculation of collinear potential energy surfaces (PES). Potential profiles perpendicular to the MEP were calculated from a Morse-type function in which the  $\beta$  parameter was taken as

$$\beta = a\beta_{AB} + (1-a)\beta_{BC}$$

The PES obtained by the described procedure has a triple-valued region which is normally of little importance at energies considered in trajectory calculations made for thermal rate coefficient determinations. In cases where this is not so, the deficiency can be mitigated by interpolation over the triple-valued region.

PES calculation and trajectory study was carried out for the series of  $X+H_2$  ( $X=F, Cl, Br, I$ ) reactions. As the PES is given in terms of variables  $a$  and  $\delta$  (where  $\delta$  is the least linear distance from the MEP in the  $X_{AB} - X_{BC}$  plane) and no explicit formulas exist for these variables beyond the MEP, the derivatives  $\partial V/\partial X_{AB}$  and  $\partial V/\partial X_{BC}$  were stored in a tabulation. Actual values for the forces were obtained from the data of the table by quadratic interpolation. In the trajectory calculation, the energy was conserved to 0.01%.

State-to all one dimensional rate coefficients were obtained for a vibrational level  $v$  from

$$v_{k1D}^{QCT}(T) = (2\pi\mu kT)^{-1/2} \int_0^\infty \exp(-E_{rel}/kT) v_P(E_{rel}) dE_{rel}$$

where  $E_{rel}$  is the collisional energy. As an illustration we present one dimensional Arrhenius parameters for  $v = 0$ , together with some PES characteristics in the Table below:

Reaction	$V / kJ \text{ mol}^{-1}$	$R_{HX}/A^0$	$R_{HH}/A^0$	$E_A / kJ \text{ mol}^{-1}$	$\log A$
F+HH	13.59	1.40	0.77	11.46	4.89
Cl+HH	38.17	1.38	1.03	14.30	4.80
Br+HH	92.10	1.45	1.26	68.43	4.39
I+HH	168.40	1.63	1.46	non-reactive trajectories only	

Three-dimensional rate coefficients were obtained by a method [2] called "collinear QCT transmission coefficient correction to TST". In this method, dynamical information is introduced into TST through a collinear transmission coefficient calculated as the ratio of one dimensional QCT and TST rate coefficients:

$$v_{r_{1D}}(T) = v_{k_{1D}}^{QCT}(T) / v_{k_{1D}}^{TST}(T)$$

Finally, the method which actually corresponds to a dynamical treatment for the collinear motion and a statistical treatment for all other degrees of freedom yields the corrected state-to-all TST rate coefficient:

$$v_k(T) = v_{r_{1D}}(T) v_{k_{3D}}^{TST}(T)$$

Equilibrium rate coefficients were obtained by Boltzmann averaging of state-to-all rate coefficients.

Kinetic results calculated and non-Arrhenius behavior observed for the hydrogen atom transfer reactions  $X+H_2$  will be discussed.

- [1] T.Bérces and J.Dombi, Int.J.Chem.Kinet., 12, 123 (1980).
- [2] J.M.Bowman et al., J.Chem. Phys., 75, 141 (1981).

Dynamics of Collision-Induced Dissociation

John E. Dove and M. E. Mandy

Department of Chemistry, University of Toronto,  
Toronto, Ontario, Canada M5S 1A1

and

N. Sathyamurthy and T. Joseph

Department of Chemistry  
Indian Institute of Technology,  
Kanpur 208 016, India

Quasiclassical trajectory studies have been made of collision-induced dissociation in the atom-diatom systems  $H + H_2$ ,  $He + H_2$ , and  $He + H_2^+$  over a wide range of initial translational, rotational, and vibrational energies. The dependence of the dynamics of the dissociation process on the initial energy distribution and on the interaction potential is examined. While there are substantial differences in the behavior of these three systems, in general collinear approach is disadvantageous for dissociation. A substantial contribution to the dissociation process comes from low impact parameter broadside collisions.

## A DYNAMICAL INVESTIGATION OF THE Li + HCl REACTION

A. Lagana<sup>a</sup>, E. Garcia<sup>a</sup>, J.M. Alvarino<sup>b</sup>, P. Palmieri<sup>c</sup><sup>a</sup>Dipartimento di Chimica, Universita' di Perugia (I)<sup>b</sup>Departamento de Quimica Fisica, Universidad de Salamanca (E)<sup>c</sup>Istituto di Chimica Fisica e Spettroscopia, Universita' di Bologna (I)

Crossed molecular beams measurements of reactive cross sections and product distributions for the reaction



have been reported in the literature./1/ For this reaction, a DIM potential energy surface has been suggested by Zeiri and Shapiro/2/. This PES has a collinear transition state located in the entrance channel 11.3 kcal/mol above the reactants' asymptote. Collinear quantum calculations have shown that the barrier of the DIM PES is too large for allowing a rationalization of both the low threshold energy and the large reactive cross section obtained from the experiment and that the collinearity of its transition state is in contrast with the experimental product distribution/3/.

For these reasons, we decided to perform an accurate quantum calculation of the potential energy of the Li + HCl system/4/. At each value of the approaching angle( $\vartheta$ ) considered ( $\vartheta$  is defined as the LiClH angle) the potential energy was calculated for a matrix of 56 points. Additional values were calculated for geometries close to that of the

transition state.

As anticipated in ref./4/, in order to render the calculated potential energy values suitable for scattering calculations, we fitted the computed ab initio points using a Bond Order(BO) functional form/5/. A large fraction (80%) of the fitted points deviate less than 1kcal/mol from the modified ab initio values. Larger deviations occur in the repulsive part of the BO1 surface which are of scarce relevance for dynamics. The overall rms deviation is 2.5kcal/mol. On the interpolated surface it is possible to localize the transition state and to single out its geometry. For our system it corresponds to  $\theta = 53^\circ$  and to LiCl and HCl internuclear distances of 2.30 $\text{\AA}$  and 1.55 $\text{\AA}$  respectively.

As already mentioned, experimental data of the Li + HCl reaction for reactants in the ground vibrational state and at a temperature of about 60K, show that the LiCl product is mainly scattered sideways in the forward hemisphere with respect to the incoming Li atom/1/. The strongly bent geometry of the transition state given by our calculations is in agreement with these data. Also its almost half-way location along the minimum energy path agrees with the non-negligible translational energy dependence of the reactivity upon collision energy. On the contrary, the height of the transition state of the BO1 surface is of 11.43kcal/mol (similar to the one of the ZS PES) and therefore still inadequate to explain experimental reactivity in terms



of classical trajectories.

Therefore, we decided to modify the height of the transition state to a value approximately corresponding to the lowest total energy at which the experiment gives reaction and to fit to the modified points a new BO surface. On this surface we have performed trajectory calculations. Our results show that, although the threshold energy slightly high, the dependence of the reactive cross section upon the collision energy is reasonable.

#### REFERENCES

- 1/ C.H. Becker, P. Casavecchia, P.W. Tiedemann, J.J. Valentini and Y.T. Lee - J. Chem. Phys. 73,2833(1980)
- 2/ M. Shapiro, and Y.J. Zeiri - J. Chem. Phys. 70,5264(1979).
- 3/ L. Ciccarelli, E. Garcia, and A. Lagana', Chem. Phys. Letters 120,75(1985)
- 4/ E. Garcia, A. Lagana', and A. Palmieri, Chem. Phys. Letters (in press)
- 5/ E. Garcia, and A.Lagana' - Mol. Phys. 56,629(1985)

THEORETICAL STUDY OF THE  $O(^3P) + CS_2$  GAS PHASE REACTION. POTENTIAL ENERGY HYPERSURFACE.

a) Ramón Savós, a) Miguel González, b) Josep Bofill and a) Antonio Aguilar .

a) Departament de Química Física.

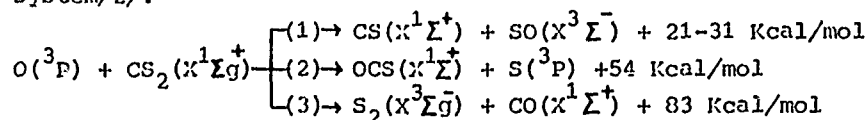
b) Departament de Química Orgánica.

Facultat de Química, Universitat de Barcelona.

Avda. Diagonal 647, 08028 Barcelona, SPAIN.

Abstract

The gas-phase reaction  $O(^3P) + CS_2$  constitutes an important step in the mechanism of  $CS_2/O_2$  chemical lasers/1/. This reaction has been widely studied experimentally, but not so theoretically. Three reaction channels have been identified for this system/2/:



with channel (1) being the most important one (~80%).

In several crossed molecular beams experiments made until now, following only the main channel, a strong forward scattering in products (~75%) has been found and a stripping mechanism has been concluded for collisional energies ranging 3.2-9.2 Kcal/mol. In addition, a considerable large fraction of the reaction energy is disposed into vibrational (~26%) and rotational (~40%) energies of CS and SO products/3,4/.

Scant attention has been given to theoretical interpretation of three reaction channels. Only collinear trajectories/3,5/ on several LEPS-like hypersurfaces and a CNDO/B study/6/ on the lowest singlet potential energy hypersurface (PEH) have been performed about this interesting system.

In order to rationalize this bulk of information, we have carried out an extensive study of the ground triplet PEH by means of the MNDO/3 UHF semiempirical method. In the search of transition states (TS's) and intermediates along minimum energy reaction paths (MERP's), connecting reactants and products on the  $OCS_2$  lowest triplet PEH, it was found that all planar structures belonged to the  $^3A''$  PEH which correlated adiabatically reac-

tants with products from all three channels (under Cs symmetry). Several intermediates, wells on the PEH, and TS connecting them each other have been located. These intermediates are connected with reactants and products along MERP's without significant TS's (barriers of potential arising only from endoergicities). It was observed that when an incoming oxygen atom approaches to CS<sub>2</sub> molecule, firstly a cis or trans planar OSCS intermediate was formed which can dissociate to CS + SO or evolve to another intermediates which originate the products of reaction channels (2) and (3). These intermediates allow to explain better the vibrational and rotational energy distributions into CS and SO products with regard to a simple MERP (only with a TS between reactants and products).

On the other hand, the short lifetimes estimated by the RRK model for the possible collision complexes are even compatible with the stripping mechanism of channel (1). Furthermore, these short lifetimes and the difficult O-migration to the carbon atom across sinuous MERP's which originates products of channels (2) and (3), seem to indicate that channel (1) will have a greater extent, as can be seen experimentally. In fact, channel (1) only implies one new bond formation and one bond breaking, while channels (2) and (3) involve many more new bond formations and breakings.

A dynamical study<sup>7/</sup>, however, would be necessary in order to account quantitatively for the different branching ratios of these three channels and other interesting dynamical features.

#### References

- /1/ M.Trtica and Z.Babarogić, Appl.Phys.B37(1985)87.
- /2/ I.R.Slagle, J.R.Gilbert and D.Gutman, J.Chem.Phys.61(1974)704.
- /3/ I.W.Smith, Discuss.Faraday Soc.44(1967)194.
- /4/ P.Å.Gorry, C.V.Nowikov and R.Grice, Mol.Phys.37(1979)329.
- /5/ H.Elgersma and G.Schatz, Chem.Phys.54(1981)201.
- /6/ L.Carlsen, J.Comput.Chem.3(1982)23.
- /7/ R.Sayós, M.González and A.Aguilar, In progress.

MOLECULAR BEAMS STUDIES OF ATOM-MOLECULE INTERACTIONS: THE  
ADIABATIC ROUTE FROM SCATTERING INFORMATION TO ANISOTROPIC  
POTENTIALS

V. Aquilanti, L. Beneventi, G. Grossi and F. Vecchiocattivi  
Dipartimento di Chimica dell'Universita'  
06100 Perugia, Italy

Detailed experimental information is being accumulated in our laboratory on scattering properties of atoms by diatomic molecules. This information, which includes absolute integral cross sections for scattering of atomic beams with magnetic analysis, and differential cross sections by crossed atomic and molecular beams, requires an accurate theoretical inversion scheme for the extraction of properties of the interaction potentials. A technique developed for this purpose is presented: it is based on the construction of adiabatic states which describe the systems in their evolution from a given molecular rotational state to the inner interaction region where the role of potential anisotropy is strongest; nonadiabatic coupling terms are also computed and their localization in terms of features of the potential energy surface is assessed. When coupling is introduced, the technique is essentially exact and tends to the Infinite Order Sudden Approximation when the latter is valid, but allows to very simply go beyond when the rotational structure of the target is important. In particular, it is possible by this technique to take into account the effect on the glory structure due to the rotational temperature of the molecule: such an effect, which has been well documented by experiments in this laboratory, cannot be dealt with by a simpler approach such as the IOS.

REACTIVE COLLISION OF O + H<sub>2</sub> PRODUCED  
WITH EXCITED STATES IN A CROSSED BEAM EXPERIMENT

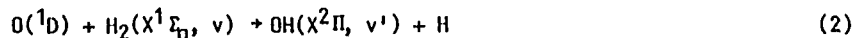
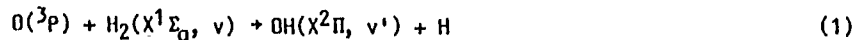
A. Lebéhot, J. Marx, F. Aguilon, and R. Campargue

Laboratoire des Jets Moléculaires

Département de Physico-Chimie

Centre d'Etudes Nucléaires de Saclay, 91191 Gif-sur-Yvette, France

The investigation of chemically reacting systems, with excited state channels, is of fundamental interest in the dynamics of molecular collisions<sup>1</sup>. In this work, the small triatomic system O + H<sub>2</sub> is investigated in the following channels which are important in the combustion of hydrogen and also in the upper atmosphere chemistry:



Reaction (2) is exothermic<sup>2</sup>, while the other reactions are possible only if a minimum amount of energy is available in the entrance channel because of a small activation barrier for reaction (1), or an endo-ergicity<sup>1</sup> which is for instance 2.2 eV for reaction (3) produced with H<sub>2</sub> (v = 0). The missing energy can be obtained by vibrationally exciting H<sub>2</sub> at least up to v = 1 for reaction (1) yielding OH with only rovibrational excitation and up to v = 5 for reaction (3) yielding OH with electronic excitation.

The reactive scattering experiment is performed by crossing O and H<sub>2</sub> molecular beams skimmed from free jet zones of silence<sup>3</sup>. The dissociation of O<sub>2</sub> is produced by radiofrequency discharge (22 MHz) in the reservoir of a quartz nozzle, with an efficiency of about 50 or 90%, in He or Ar seeded mixtures, respectively<sup>4,5</sup>. Thus, the atomic oxygen beam is generated with

at least two electronic states  $O(^1D, ^3P)$ .

Reaction (2) is produced selectively thanks to the barrier encountered for reaction (1). The internal energy distribution of the OH emitted in the direction of the O beam axis, is probed by the time-of-flight technique with a good vibrational resolution. The results (Fig. 1) derived from the TOF spectra, show that the  $OH(X^2\Pi, v')$  products are vibrationally excited up to  $v' = 4$ , with minimum populations on  $v' = 1$  or 2.

Also, reaction (3) is produced when  $H_2$  is excited vibrationally up to  $v > 5$ , by means of a low energy electron beam ( $< 100$  eV) operated coaxially to the  $H_2$  molecular beam. Thus, the vibrational levels of the ground state  $H_2(X^1\Sigma_g, v')$  are populated by radiative decay from singlet electronic states excited by electron impact<sup>6</sup>. In these conditions, reaction (3) is observed by analyzing the spontaneous fluorescence signal emitted from  $OH(A^2\Sigma^+, v')$  in the reactive collision zone. The experimental results are compared to a calculated statistical distribution (Fig. 2) taking into account the predicted populations of the vibrational levels of  $H_2$  and only the spin  $s = + \frac{1}{2}$  of OH.

Due to the difficulty of producing  $O(^1D)$  alone, reaction (1) has not yet been observed in this experiment.

#### References

1. G. Durand and X. Chapuisat, Chem. Phys. 96, 381 (1985)
2. R.J. Buss, P. Casavecchia, T. Hirooka, S.J. Sibener, and Y.T. Lee, Chem. Phys. Lett. 82, 386 (1981)
3. R. Campargue, J. Phys. Chem. 88, 4466 (1984)
4. S.J. Sibener, R.J. Buss, C.Y. Ng, and Y.T. Lee, Rev. Sci. Instrum. 51, 167 (1980)
5. J. Marx, Thesis, University of Paris-Sud (1986)
6. J. Marx, A. Lebéhot, and R. Campargue, J. Physique (Paris) 46, 1667 (1985)

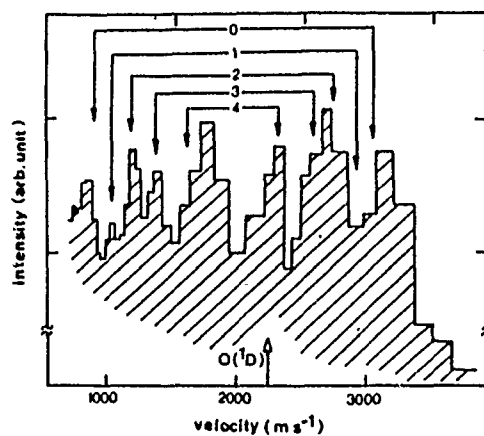


Fig.1- Typical velocity spectrum derived from TOF measurements, in the axis of the O beam, for OH obtained in reaction (2) with  $\text{H}_2(v=0)$ . The arrows show the theoretical velocities corresponding to the vibrational levels  $v' = 0$  to 4 of  $\text{OH}(X^2\Pi)$ . Also the velocity of  $\text{O}(^1\text{D})$  is indicated ( $\nabla$ ).

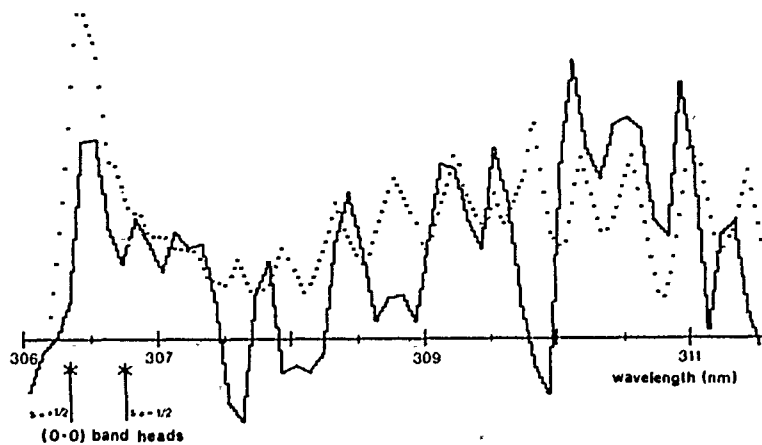


Fig.2-Fluorescence spectrum of the (0-0) band for the  $\text{A}^2\Sigma^+ \rightarrow \text{X}^2\Pi$  transition of OH obtained in reaction (3), compared to a theoretical spectrum (dashed line) derived from a statistical model with only the  $\pm\frac{1}{2}$  spin component of OH.

ROTATIONAL EXCITATION OF THE MgCl REACTION PRODUCT  
IN THE HARPOONING Mg ( $^1S$ ) + Cl<sub>2</sub> REACTION.

Bernard BOURGUIGNON, Mohammed-All GARGOURA, June McCOMBIE,  
Joëlle ROSTAS and Guy TAIEB <sup>#</sup>.

Laboratoire de Photophysique Moléculaire du C.N.R.S. <sup>\*</sup>  
Université de Paris-Sud, Bâtiment 213, 91405 Orsay-Cédex, France.

Harpooning reactions of alkali and alkaline-earth atoms with halogens are known to lead to high vibrational excitation of the reaction product. In the reactions that were experimentally studied, electron jump from the M metal atom to the X<sub>2</sub> molecule occurs at "large" internuclear distance, with respect to the equilibrium distance bondlength of the MX molecule. The dynamics of these reactions was extensively studied in the case of the alkali; although the reaction product may be electronically excited in the alkaline-earth case, experimental data (MX ro-vibrational excitation) show that the reaction dynamics is similar for alkali and alkaline-earth <sup>1</sup>. The X<sub>2</sub><sup>-</sup> ion is formed by the vertical X<sub>2</sub> + e<sup>-</sup> → X<sub>2</sub><sup>-</sup> transition, on the repulsive part of the X<sub>2</sub><sup>-</sup> potential curve. The strong electric field of the M<sup>+</sup> ion causes fast dissociation of X<sub>2</sub><sup>-</sup>, where X<sup>-</sup> takes most of the kinetic energy. The MX bond is formed by electrostatic attraction of the M<sup>+</sup> and X<sup>-</sup> ions, which allows the X<sup>-</sup> kinetic energy to be transferred into MX vibrational excitation <sup>2</sup>.

We present here a LIF study of the Mg ( $^1S$ ) + Cl<sub>2</sub> system. The A<sup>2</sup> $\Pi$  - X<sup>2</sup> $\Sigma^+$  ( $\Delta v=0$ ) bands of nascent MgCl were recorded at 0.2 cm<sup>-1</sup> resolution in a beam gas apparatus, at Cl<sub>2</sub> scattering gas pressure of 5 · 10<sup>-4</sup> Torr. The experimental spectrum was compared with simulated spectra, assuming a Boltzmann rotational population distribution. We have obtained a rotational temperature as high as 6000 ± 2000 K (56 % of the exothermicity  $\Delta E$  of the reaction). Spectrum congestion precludes more detailed analysis of the rotational population at the present resolution. The MgCl vibrational population distribution is not Boltzmann, and the vibrational excitation is only 0.13 eV (14 % the exothermicity of the reaction). Therefore the energy disposal of the Mg ( $^1S$ ) + Cl<sub>2</sub>

<sup>\*</sup> Laboratoire associé à l'Université de Paris-Sud

<sup>#</sup> and: U.E.R. Claude Bernard, Université de Rennes I, 35043 RENNES-CEDEX



system contrasts strongly with that of previously reported systems in which the reaction proceeds through the harpooning mechanism. For example, in the Ca ( $^1S$ ) + Cl<sub>2</sub> system, 70 % of the exothermicity goes into CaCl vibration and 10 % (2000 K) in CaCl rotation

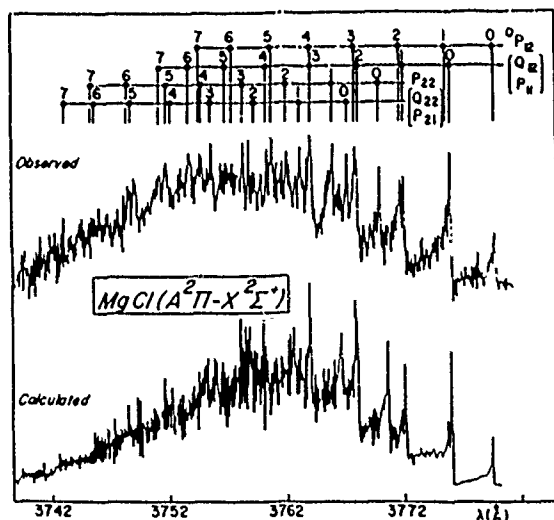


Figure 1

MgCl<sub>2</sub> or CaCl<sub>2</sub> Intermediate along the Cl-Cl<sup>-</sup> bond, providing a large impulse on the Cl<sup>-</sup> ion. This is illustrated on figure 2, where the diabatic ionic potential energy surface (PES) is represented in C<sub>∞v</sub> geometry. Entrance on the surface

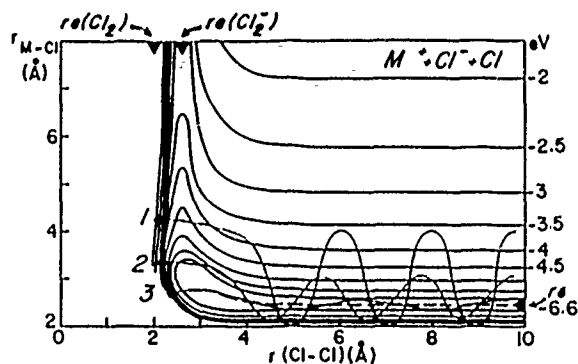


Figure 2

possibility of further stabilization of the MgCl molecule along the R<sub>Mg-Cl</sub>

3.  
For the Mg ( $^1S$ ) + Cl<sub>2</sub> system, the distance at which the electron jump occurs was estimated to be 2.7 Å, which is close to the MgCl equilibrium bondlength (2.20 Å). The corresponding distances for Ca + Cl<sub>2</sub> are 3.7 and 2.44 Å, respectively. Consequently, the MgCl vibration is restrained in the reaction intermediate. The energy is released through dissociation of the

occurs at point 2 for the Ca + Cl<sub>2</sub> system. It is clear that the reaction exoergicity is preferentially channelled into CaCl vibration, in order to attain the equilibrium CaCl bondlength (figure 3a). The Mg + Cl<sub>2</sub> system enters on the surface at point 3 and goes directly into the exit channel. There is no

coordinate, and the evolution of the system looks like a dissociation of  $\text{MgCl}_2$  along the  $\text{R}_{\text{Cl}-\text{Cl}}$  coordinate, where the affect on the  $\text{R}_{\text{MgCl}}$  distance is no greater

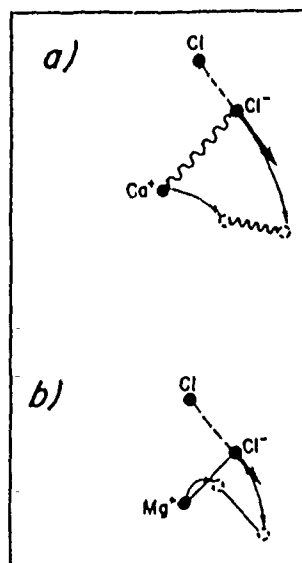


Figure 3

than the difference between the bondlength in the diatomic and the triatomic molecules. In a simple mechanical picture where  $\text{MgCl}$  is considered as a rigid rod, the  $\text{Cl}^-$  ion impulse results in rotational excitation of  $\text{MgCl}$ , equal to  $(m_{\text{Mg}} / m_{\text{MgCl}}) \Delta E \approx 40 \% \Delta E$  (figure 3b).

In conclusion, the harpooning mechanism provides an explanation for the change from vibrational to rotational excitation of the reaction product from Ca to Mg. The key factor to determine whether rotation or vibration is most excited is the electron jump distance. A more detailed analysis of the (0-0) rotational population, based on higher resolution spectra, is in progress. Reactions of other halogen molecules with Mg are also being investigated.

#### References:

1. M. Menzinger, In: *Gas Phase Chemiluminescence and Chemi-ionization*, A. Fontijn (editor), North Holland, Amsterdam, p. 25 (1985).
2. D. R. Herschbach, *Adv. Chem. Phys.*, 10, 319 (1966).
3. P. J. Dagdigan, In: *Gas Phase Chemiluminescence and Chemi-ionization*, A. Fontijn (editor), North Holland, Amsterdam, p. 203 (1985).

**A ( $^2\Sigma^+$ ) PRODUCTION BY 193 nm PHOTOLYSIS OF NITROUS ACID**

D. SOLGADI, F. LAHMANI

Laboratoire de Photophysique Moléculaire

Bât. 219 - Université de Paris-Sud

91405 - ORSAY Cedex - France

E. HONTZOPOULOS, C. TOTAKIS

Research Center of Crete

HERAKLION, (Greece).

The vibrational and rotational state distributions of the OH excited  $A^2\Sigma^+$  fragment produced by photodissociation of nitrous acid (HONO) excited at 193 nm have been investigated. The fluorescence spectrum of the OH  $A^2\Sigma^+$  fragment shows that the  $v' = 0, 1, 2$  levels are formed and the relative population has been found to be 1/0.13/0.017. The OH  $A^2\Sigma^+$  ( $v' = 0$ ) fragment exhibits a non Boltzmann rotational distribution peaking at  $N' = 12$  and levels up to  $N' = 20$  are populated.

From the linear intensity dependence of the OH  $A^+$  signal and its time evolution, a single photon dissociation process of HONO seems to be the most probable mechanism and the results show that the most of the excess energy available in the reaction ( $\sim 3000 \text{ cm}^{-1}$ ) is channelled into the internal degrees of freedom of the OH  $A$  fragment. Population of rotational levels above the limit imposed by energy conservation may result from the excitation of parent HONO molecule which possesses substantial thermal energy.

## U.V. Photoexcitation of rovibrationally excited NO.

J. DESON, C. LALO, F. LEMPEREUR, J. MASANET, J. TARDIEU de MALEISSYE.

C.N.R.S UA 40870 - Laboratoire de Chimie Générale -

Université P. et M. Curie - Tour 55 - 4 Place Jussieu

75005 PARIS - FRANCE

Absorption cross sections in the U.V. range of small molecules can be increased by modifying the rovibrational excitation of initial state.

In the experiment reported here, gas heating by a C.W. CO<sub>2</sub> laser allows the Boltzmann energy distribution in rovibrational levels of the ground state to be shaded toward higher levels.

Electronic transitions from these high rovibrational levels of the ground state molecule to excited states (dissociative or no) can then be more readily induced by U.V. absorption of the radiation at 193 nm from an ArF laser. The formation of these excited states and of excited photofragments can be observed through their emissions in the visible or near U.V.

The experimental set up allowing this double laser excitation I.R. - U.V. is described and some results are presented concerning the photoexcitation at 193 nm of rotationally excited NO.

## Experimental.

The I.R. excitation is done with a continuous wave multimode CO<sub>2</sub> laser (Cilas 260) which is grating tunable between 9 and 11  $\mu$ m with a maximum output power of 160 watts at 10,6  $\mu$ m.

The U.V. excitation is done with an excimer laser Sopra delivering pulses of 140 mJ at 193 nm (ArF) and 25 ns width at 2 Hz. Both radiations are driven into a stainlesssteel cell fitted with ClNa and MgF<sub>2</sub> windows : luminescences in visible and near U.V. are observed using quartz optics.

Time resolved spectral analysis is carried out by a Commodore CBM 4032 computer monitoring lasers triggering, monochromator Jobin et Yvon scanning and photocounting system.

### U.V. absorption of rotationally excited.

The spectroscopic analysis of the NO fluorescence induced by laser excitation at 193 nm shows that rotational levels of three excited electronic states are strongly mixed (1). It appears that at this wavelength the preparation of NO ( $A, v' = 3$ ) can be performed quasi resonantly from high rotational levels of the NO ( $X, v'' = 0, J'' = 50,5$ ).

At room temperature the population of rotationally excited NO with  $J'' \sim 50,5$  is about  $10^6$  times smaller than  $J'' = 28,5$  with an energy gap between NO ( $X, v'' = 0$ )  $J'' = 28,5$  and  $J'' = 50,5$  close to  $3000 \text{ cm}^{-1}$ .

Gas heating by an I.R. laser excitation should allow to modify the Boltzman energy distribution to the benefit of these higher rovibrational levels.

NO is not an absorber of the  $\text{CO}_2$  laser radiation. But this one operated at the  $P_{20}$  line at  $10,595 \mu\text{m}$ , is absorbed by  $\text{SF}_6$  which acts as a photosensitiser (2) in irradiated  $\text{SF}_6$ -NO mixtures. Equimolecular mixtures of  $\text{SF}_6$ -NO have been irradiated at 0,7 mbar total pressures by the two laser beams ; an important increase of the signal corresponding to the emission from NO( $B, v' = 7$ ) has been observed. Moreover a spectroscopic analysis shows that this emission is red shifted. An energy gap close to  $600 \text{ cm}^{-1}$  has been evaluated. More  $\text{SF}_6$  must be added to the gaseous mixtures in order to get an higher energy gap.

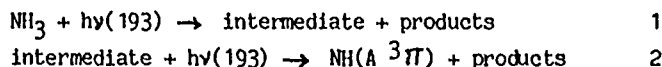
### References.

- (1) Shibuya K., Stuhl F.  
Chemical Physics 79 (1983) 367.
- (2) Tardieu de Maleissye J., Lempereur F., Lalo C., Masanet J.  
J. of Photochem., 27 (1984) 273.

193 nm PHOTOLYSIS OF AMMONIA:  
THE INTERMEDIATE IN THE 2-PHOTON FORMATION OF  $\text{NH}(\text{A } ^3\Pi)$

R. D. Kenner, F. Rohrer, R. Browarzik, A. Kaes and F. Stuhl  
Physikalische Chemie I, Ruhr-Universität Bochum  
D-4630 Bochum 1, Federal Republic of Germany

Recent results from this laboratory<sup>1</sup> have shown that the mechanism for production of  $\text{NH}(\text{A } ^3\Pi)$  in the 193 nm photolysis of ammonia is secondary photolysis of an intermediate species.



It was shown at that time that the intermediate species had a lifetime greater than 10  $\mu\text{s}$ . Consideration of the known photochemistry of ammonia (taking into account the energy restriction in reaction 2) indicates that this intermediate species must be either  $\text{NH}_2(\text{A})$  or internally-excited  $\text{NH}_2(\text{X})$ . It was previously shown<sup>2</sup> that both these species are produced in the 193 nm photolysis of  $\text{NH}_3$ .

We have measured lifetimes for the intermediates in the photolyses of  $\text{NH}_3$  and  $\text{ND}_3$  using two ArF (193 nm) excimer lasers in pump-probe experiments. The measured quenching rate constants for each of the parent molecules and for several added gases are shown in columns 2 and 3 of Table I. Note the close similarity of the results for both the protonated and deuterated species. In addition, we have obtained the zero pressure lifetimes by extrapolation of plots of the reciprocal lifetime as a function of the argon pressure at constant concentration of the parent molecules. The derived values are 250 and 600  $\mu\text{s}$  for the protonated and deuterated species respectively. Both these values have been corrected for diffusion and quenching by the residual concentration of the parent molecules.

TABLE I: Summary of Measured Quenching Rate Constants

Quenching gas	Intermediates from		$\text{NH}_2(\text{A})_1$	$\text{ND}_2(\text{A})_1$	$\text{NH}_2(\text{A})_s$
	$\text{NH}_3$	$\text{ND}_3$			
$\text{NH}_3$	110	---	190	---	500 <sup>a</sup>
$\text{ND}_3$	---	115	---	180	---
Ar	4	4	6	5	100
$\text{H}_2$	10	14	14	30	90
$\text{O}_2$	7	6	---	12	---
$\text{N}_2$	12	---	7	---	---
He	2	---	3	---	30

All values are given in units of  $10^{-12} \text{ cm}^3 \text{ s}^{-1}$ .

Entries marked --- were not measured.

<sup>a</sup>Value from reference 2.

Since the  $\text{NH}_2(\text{A})$  formed in the first photolysis step fluoresces, its kinetic properties can be easily measured and directly compared with those reported above. As has been shown previously<sup>2</sup>, this fluorescence shows a multi-exponential decay. We have investigated the species monitored by the faster decaying component of the  $\text{NH}_2(\text{A-X})$  emission (labeled  $\text{NH}_2(\text{A})_s$  in Table I) and find that it shows very different quenching behaviour than the corresponding intermediate (compare columns 6 and 2 of Table I). This "short-lived" component of the  $\text{NH}_2(\text{A-X})$  fluorescence has been attributed to emission from "pure"  $\text{NH}_2(\text{A})$  levels<sup>2</sup>. Based on our results these levels cannot be the intermediate species in reactions 1 and 2 above.

On the other hand, for both  $\text{NH}_3$  and  $\text{ND}_3$ , the species characterized by the "long-lived" component of the fluorescence (labeled  $\text{NH}_2(\text{A})_1$  and  $\text{ND}_2(\text{A})_1$  respectively in Table I) does appear kinetically similar to the intermediate (compare columns 2 and 3 to 4 and 5 in Table I). The differences in the measured results are, however, outside the combined experimental uncertainties. To study this long-lived component of the  $\text{NH}_2(\text{A-X})$  fluorescence further we have recorded emission spectra using a

delayed gate (10-160  $\mu$ s) to minimize the contribution from the fast decaying component. In the case of  $\text{NH}_3$ , the delayed spectrum seems to be dominated by emission from the  $\text{NH}_2(\text{A}) (0, \nu_2, 0) \Sigma$  states with  $\nu_2 = 5$  and 3 ( $\nu_2 = 1$  lies outside the sensitivity range of our photomultiplier). The "long-lived" component of the  $\text{NH}_2(\text{A-X})$  fluorescence has been attributed to emission from levels of  $\text{NH}_2(\text{A})$  which are weakly coupled to high levels of the ground state<sup>2</sup>. If this is true, the emission would be a monitor for a particular set of states in the ensemble of energetic ground state  $\text{NH}_2$  molecules formed in the first photolysis step. The  $\text{NH}(\text{A-X})$  fluorescence produced in the second photolysis step could be a monitor for a somewhat different set of these states. In view of the similarity observed in these experiments between the kinetic properties of the "long-lived" component of the  $\text{NH}_2(\text{A-X})$  emission and those of the intermediate species, we propose that the intermediate species in the production of  $\text{NH}(\text{A } ^3\Pi)$  in the 193 nm photolysis of  $\text{NH}_3$  are highly excited levels of the  $\text{NH}_2(\text{X})$  state (with a similar conclusion for  $\text{ND}_3$ ).

1. R. D. Kenner, F. Rohrer and F. Stuhl, Chem. Phys. Lett. 116 374 (1985).
2. V. M. Donnelly, A. P. Baronavski and J. R. McDonald, Chem. Phys. 43 271 (1979); ibid. 43 283 (1979).



PHOTODISSOCIATION OF MOLECULAR BEAMS OF  
CHLORINATED BENZENE DERIVATIVES

Teijiro ICHIMURA, Yuji MORI,  
Hisanori SHINOHARA\* and Nobuyuki NISHI\*

Department of Chemistry, Tokyo Institute of Technology,  
Ohokayama, Meguro-ku, Tokyo 152, Japan

\*Institute for Molecular Science,  
Myodaiji, Okazaki 444, Japan

Molecular beams of chlorobenzene<sup>1)</sup>, isomers of o-, m-, and p-chlorotoluene<sup>1)</sup>, dichlorobenzenes<sup>2)</sup> and pentafluorochlorobenzene<sup>3)</sup> were photodissociated using an excimer laser at 193 or 248 nm to measure the time-of-flight distributions of fragments (Cl,  $m/e=35$ ) to investigate the primary processes and the photodissociation dynamics.

A supersonic molecular beam is irradiated by 193 nm ArF or 248 nm KrF excimer laser pulses ( 50000 shots) at a frequency of 5 Hz. The time-of-flight(TOF) spectrum is generated by synchronously gating a multichannel scaler with the laser firing pulse and detecting photofragments by a quadrupole mass filter(Q-mass) as a function of time after the laser pulse. The Q-mass, operating at unit mass resolution, is separated from the reaction chamber and pumped differentially by a turbo molecular pump and an ion pump. The TOF spectrum is then converted to a center-of-mass total translational energy distribution( $P(E_T)$ ) by using a suitable Jacobian factor after subtracting the drift time in the Q-mass tube. The flight path was 16 cm and the time resolution was 1  $\mu$ s. Low energy fragments than 3 kcal/mol seems to be distorted since the detector axis is perpendicular to the molecular beam axis.

For example, fig. 1 shows the TOF signal of Cl at  $m/e = 35$  for the photolysis of p-ClC<sub>6</sub>H<sub>4</sub>Cl molecular beams at 193 nm. The total translational energy distribution,  $P(E_T)$ , of photofragments in fig. 2 has three peaks at about 3, 13 and 30 kcal/mol. The energy difference

between each two peaks of distributions is far beyond the spin-orbit splitting between  $\text{Cl}(^2\text{P}_{3/2})$  and  $\text{Cl}^*(^2\text{P}_{1/2})$ , about 2.5 kcal/mol. Thus, the fragment translational energy distributions should be assigned to the difference in dissociation processes.

The broad distribution with the peak  $E_T$  value of  $\sim 3$  kcal/mol in fig. 2 can be represented by a Maxwell-Boltzmann function ( $P(E_T) \propto E_T^{1/2} \exp(-E_T/kT)$ ) and higher energy distributions may be explained by a Gaussian function ( $P(t) \propto t^3 (t^2/t_0^2 + c)^{1/2} \exp[-(t-t_0)^2/A]$ ). Here the apparatus shape factor and the width originated in the narrow vibrational distribution around the central state 0 were considered.

The fast photofragment energy distribution ( $E_T \approx 30$  kcal/mol) may be compared to those of photodissociation of the C-Cl bond in alkyl chlorides, which are excited into the continuum of a repulsive state by the  $(\sigma^*, n)$  transition and immediately undergo direct photodissociation. The  $E_T$  value of about 30 kcal/mol observed for chlorobenzene and chlorotoluenes may be explained by a similar mechanism. This fast fragment was not observed for pentafluorochlorobenzene. This is due to the effect of fluorination to reduce the kinetic energy of fragments.

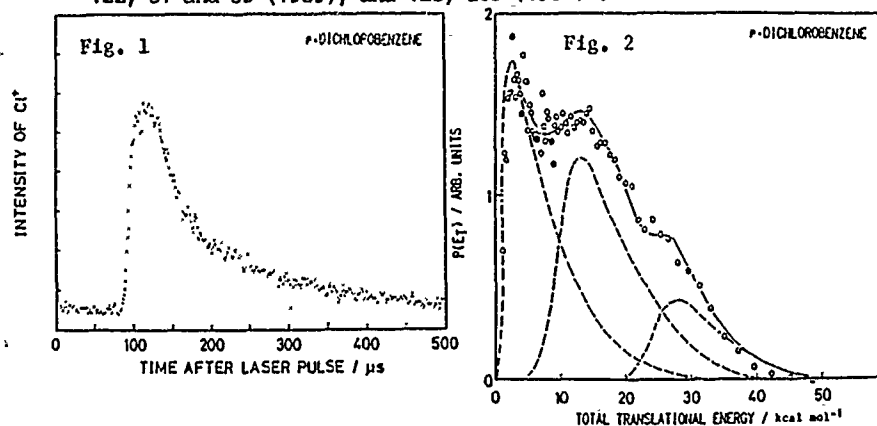
Two other lower energy components in  $P(E_T)$  observed in fig. 2 should indicate the occurrence of slow dissociation process in the photolysis of p-dichlorobenzene at 193 nm. The broad distribution with peak  $E_T$  value of 13 kcal/mol in fig. 2 cannot be represented by a Maxwell-Boltzmann distribution. Accordingly the most probable exit state to give the slower photofragments may be the highly vibrationally excited triplet state, presumably the  $(\pi^*, \pi)$  transition, generated by a fast intersystem crossing from the initial excited singlet state.

The distribution with the smallest peak  $E_T$  value of around

3 kcal/mol in fig. 2 may be represented by a Maxwell-Boltzmann distribution. The photodecomposition process to give the statistical distribution should occur after thermal randomization of the excess energy. Thus the dissociation process seems to occur from vibrationally excited  $S_0$  state to give vibrationally hot chlorophenyl radicals.

Some results obtained in this work are summarized in Table 1.

1-3) T. Ichimura, Y. Mori, H. Shinohara and N. Nishi, Chem. Phys. Lett. 122, 51 and 55 (1985), and 125, 263 (1986).



Parent molecule	$D_0(\text{C-Cl})$ (kcal/mol)	$E_{\text{avl}}$ (kcal/mol)	$E_T$ (kcal/mol)	Most probable exit state	Probability
$\text{C}_6\text{H}_5\text{-Cl}$	97	52	5.0	$S_0^* + S_3(\pi^*, \pi)$	0.39
			16	$T^* + S_3(\pi^*, \pi)$	0.34
			30	$S(\sigma^*, n)$	0.27
$p\text{-Cl}_3\text{-C}_6\text{H}_4\text{-Cl}$	97	52	4.0	$S_0^* + S_3(\pi^*, \pi)$	0.15
			16	$T^* + S_3(\pi^*, \pi)$	0.62
			31	$S(\sigma^*, n)$	0.23
$p\text{-Cl-C}_6\text{H}_4\text{-Cl}$	97	52	5.0	$S_0^* + S_3(\pi^*, \pi)$	0.33
			15	$T^* + S_3(\pi^*, \pi)$	0.41
			27	$S(\sigma^*, n)$	0.26
$\text{C}_6\text{F}_5\text{-Cl}$	97	52	6.5	$S_0^* + S_2(\pi^*, \pi)$	0.86
			15	$T^* + S_2(\pi^*, \pi)$	0.14
$\text{C}_6\text{H}_5\text{-Cl}$ (248 nm Ex.)	97	19	3.8	$S_0^* + S_1(\pi^*, \pi)$	0.64
			11	$T^* + S_1(\pi^*, \pi)$	0.36

SINGLE- AND TWO-PHOTON DISSOCIATION OF  $\text{CClF}_2\text{NO}$  IN THE VISIBLE

J.A. Dyet, M.R.S. McCoustra and J. Pfab

Department of Chemistry, Heriot-Watt University,  
Edinburgh, EH14 4AS, Scotland.

The electronic spectroscopy, photophysics and photodissociation dynamics of chlorodifluoronitrosomethane ( $\text{CClF}_2\text{NO}$ ) in the 550-710 nm region have been studied both at 300K and in a nozzle-cooled jet. Fluorescence excitation spectra of the  $\tilde{\Lambda}(^1\text{A}'') + \tilde{\chi}(^1\text{A}')(n,\pi^*)$  transition have been recorded in the 670 to 710 nm region and partially assigned to obtain information on the geometry changes and potential functions associated with the transition. From time resolved measurements of jet-cooled  $\text{CClF}_2\text{NO}$  we have obtained the non-radiative decay rates of most well defined vibronic levels active in the fluorescence excitation spectrum.

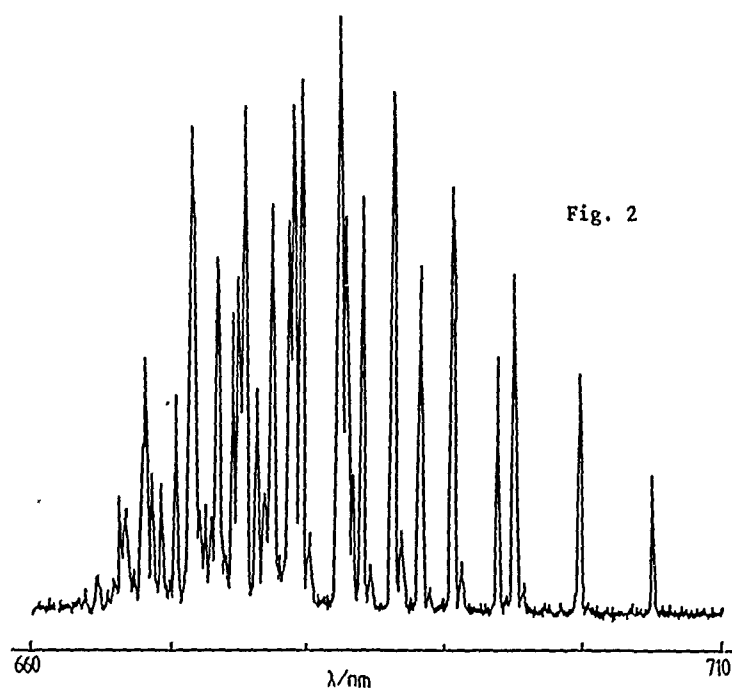
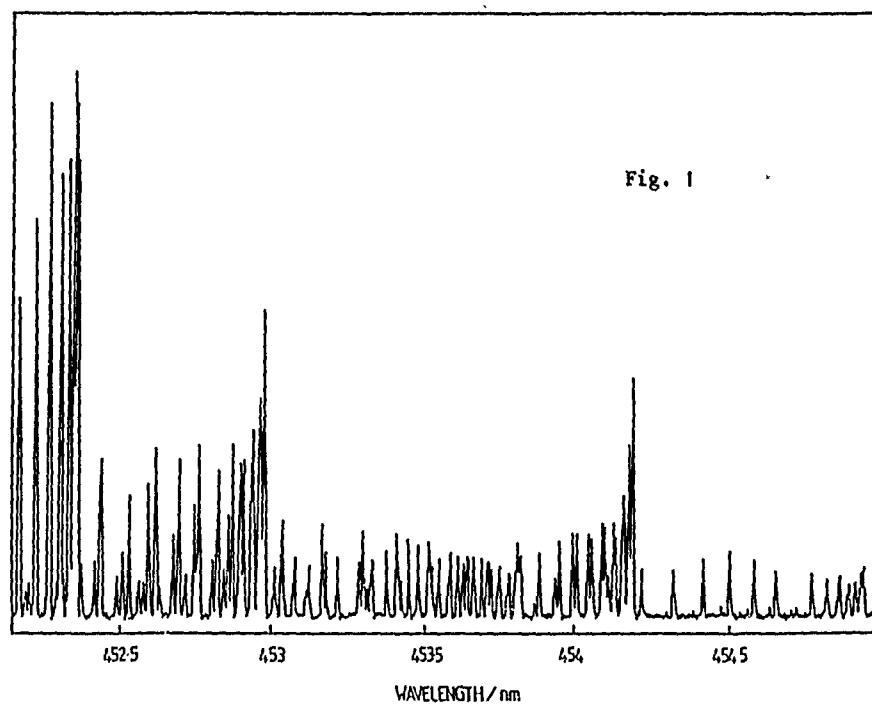
Detailed information on the electronic, vibrational and rotational population distributions of the nascent NO ground state fragment has been obtained using pulsed dye laser photolysis and delayed two-photon LIF probing of NO. Photolysis at 300K in the range 560 to 690 nm produces predominantly  $\text{NO}(v=0)$ . The proportion of nascent  $\text{NO}(v=1)$  is negligible but increases towards short wavelength where a competing two-photon dissociation becomes important leading to a non-linear increase of the NO yield with photolysis pulse power. The rotational population distributions of the nascent NO conform well to a statistical model.

State-selective photolysis of jet-cooled  $\text{CClF}_2\text{NO}$  has been performed at a number of narrow features in the fluorescence

excitation spectrum of the cold parent. Fig. 1 shows a two-photon LIF spectrum of  $\text{NO}(v=0)$  from the state-selective photolysis of cold  $\text{CClF}_2\text{NO}$  at 646.6 nm as an example. Competition between molecular fluorescence and photodissociation occurs from the electronic origin at  $14,187\text{ cm}^{-1}$  up to roughly  $15,000\text{ cm}^{-1}$  where fluorescence becomes weak due to rapid dissociation. An uncorrected NO photofragment yield spectrum is displayed in Fig. 2. Such spectra have been obtained by monitoring the production of  $\text{NO}(v=0)$  by two-photon LIF with a fixed probe wavelength while scanning the photolysis laser through the absorption of the cold parent.

The variation of the delay between the dissociation and probe laser pulses provided the appearance times of the NO fragment for several vibronic levels of the  $\tilde{\text{A}}$ -state including the origin of the system. No pronounced state-specific effects have been observed indicating that  $\text{CF}_2\text{ClNO}$  undergoes relatively slow predissociation with energy randomisation preceding the separation of the fragments.

E14



**HgBr(B → X) FLUORESCENCE EMISSION INDUCED BY KrF LASER  
MULTIPHOTON DISSOCIATION OF HgBr<sub>2</sub>**

**P. Papagiannakopoulos\* and D. Zevgolis\*\***

Research Center of Crete, Institute of Electronic  
Structure and Laser, and University of Crete,  
Heraklion, Crete, Greece

The UV multiphoton excitation and dissociation of small molecules in the gas phase with an excimer laser has been an adequate technique for generation of electronically excited free radicals [1]. In this work we studied the KrF laser (248 nm) multiphoton excitation and dissociation of HgBr<sub>2</sub> vapors, and the resulting fluorescence emission of electronically excited HgBr radicals. This strong emission in the green, corresponds to the B<sup>2</sup>Σ → X<sup>2</sup>Σ transition of HgBr radicals, and provides a good chance of achieving laser action at 502 nm, with great propagation in air and sea water.

The photolysis experiments of HgBr<sub>2</sub> vapors performed with a KrF excimer laser and with a setup described previously [2]. For an unfocused laser beam with intensity  $I \approx 30 \text{ MW/cm}^2$  and a HgBr<sub>2</sub> vapor pressure about 0.1 torr strong fluorescence emission was observed in the visible region 460-502 nm [3], Figure 1. This emission band presents discrete vibrational structure and was identified as the B<sup>2</sup>Σ → X<sup>2</sup>Σ transition of HgBr radicals. Its vibrational analysis showed good resolution for the  $v'=0 \rightarrow v''=17-22$

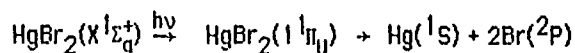
---

\* Also Department of Chemistry, University of Crete.

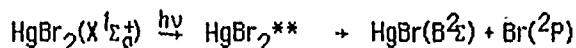
\*\*Also Department of Physics, University of Crete.

transitions, and the obtained molecular constants are in good agreement with the literature. Furthermore, the fluorescence intensity at 502 nm ( $v'=0 \rightarrow v''=22$  transition) was found to depend on the laser intensity, with a power law dependence two. This indicates that the fluorescing HgBr radical has been formed by a two-photon excitation process of the parent HgBr<sub>2</sub> molecule.

The KrF laser photodissociation of HgBr<sub>2</sub> molecules proceeds via two different channels. In the first channel the HgBr<sub>2</sub> molecules are excited by a single KrF photon absorption to a  $^1\Pi_u$  state, which correlates with a repulsive state of HgBr, and therefore undergo atomization,



In the second channel the HgBr<sub>2</sub> molecules are excited to a higher electronic state with the absorption of a second KrF photon and subsequently are decomposed to electronically excited HgBr( $B^2\Sigma$ ) radicals and Br( $^2P$ ) atoms



Therefore, the formation of electronically excited HgBr radicals takes place via the latter mechanism of two-photon excitation.

For higher laser intensities 300 MW/cm<sup>2</sup>, the HgBr(B + X) emission disappears and strong Hg emission lines are observed. Those lines correspond to the transitions ( $6^3D \rightarrow 6^3P$ ) ( $7^3P_2 \rightarrow 7^3S_1$ ) and ( $7^3S_1 \rightarrow 6^3P$ ) of excited Hg atoms.



The observed emission band  $B \rightarrow X$  of  $\text{HgBr}$  has been found to increase with the addition of an inert gas, with different efficiency depending on the nature of the gas. The obtained order of efficiency was  $\text{N}_2$ , Ar, Xe and Ne.

### References

1. P. Papagiannakopoulos and C. Fotakis, in Proceedings of Conference "Photophysics and Photochemistry above 6 eV", F. Lahmani (Ed), Elsevier, Amsterdam, 1985.
2. P. Papagiannakopoulos and C. Fotakis, J. Phys. Chem. **89**, 3439 (1985).
3. P. Papagiannakopoulos and D. Zevgolis, in Proceedings of Conference "Advances in Chemical Reaction Dynamics" ed. P. Rentzepis and C. Capellos, D. Reidel Publ., 1986.

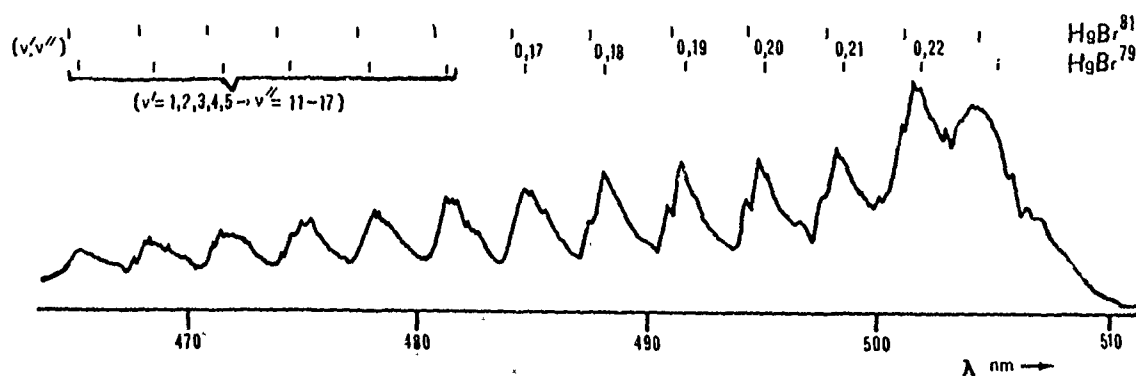


Figure 1: Emission band  $B^2\Sigma \rightarrow X^2\Sigma$  of  $\text{HgBr}$  from the KrF laser photolysis of  $\text{HgBr}_2$  vapor and 675 torr of Ar; cell temperature is  $100^\circ\text{C}$ .

PICOSECOND LASER FLUORESCENCE STUDY OF THE COLLISIONLESS PHOTODISSOCIATION OF NITROCOMPOUNDS AT 266 nm.

Jean-Claude MIALOCQ (CEA - CEN/SACLAY, IRDI/DESICP/DPC/SCM UA 331 CNRS 91191 GIF sur YVETTE Cédex, France) and John C. STEPHENSON (National Bureau of Standards, Molecular Spectroscopy Division, Gaithersburg, MD 20899, USA)

The picosecond UV photodissociation of nitroalkanes ( $R-NO_2$ ) and dimethylnitramine (DMNA) is investigated by observing excited  $NO_2^*$  fluorescence and by laser induced fluorescence (LIF) probing of ground state  $NO_2$  fragments. After photolysis by picosecond laser pulses at 266 nm, efficient monophotonic collision-free photodissociation of  $R-NO_2$  ( $R = CH_3, C_2H_5, n-C_3H_7$ , and  $i-C_3H_7$ ) or DMNA occurs within 6 ps, in good agreement with calculated RRKM lifetimes by considering that these electronically excited molecules undergo internal conversion to high vibrational levels of the ground electronic state followed by a statistical unimolecular vibrational predissociation.

Formation of excited  $NO_2^*$  from DMNA is monophotonic; for nitromethane the excited  $NO_2^*$  formation is much less efficient and increases faster than linearly with increasing energy in the UV pulse.

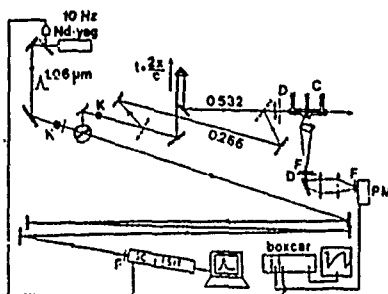


fig. 1 - Experimental Setup

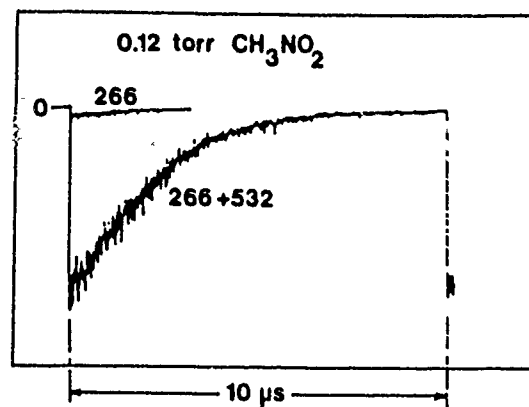
$2.7 \times 10^{-3} \text{ cm}^2$  and  $3 \times 10^{-4} \text{ cm}^2$  respectively. Maximum energies of 200  $\mu\text{J}$  (UV) and 1.0 mJ (green) were fairly constant from pulse to pulse. The zero time delay between the pump and the probe pulses was determined by probing with 532 nm pulses the photobleaching of rhodamine 6G caused by the 266 nm pulses.  $RNO_2$  or DMNA contained in a Tee shaped 4 cm diameter glass cell equipped with three fused silica windows were excited at 266 nm and the  $NO_2$  ground state fragment was probed by laser induced fluorescence (LIF) using the delayed 532 nm pulse. The fluorescence emitted in the observed 2 mm long interaction region was collected, spatially and spectrally ( $\lambda > 580 \text{ nm}$ ) filtered to discriminate against scattered laser light and analyzed with a photomultiplier. The signal was averaged with a boxcar averager-integrator, the 50 ns gate being scanned over the  $NO_2^*$  decay curve in 100 - 1000 seconds according to the nitrocompound investigated.  $NO_2$  diluted in argon was used as an actinometer. No LIF was observed when this mixture was excited at 266 nm above the  $NO_2$  dissociation limit (398 nm). Under 532 nm excitation, the initial  $NO_2^*$  fluorescence was proportional to the gas pressure and to the laser energy. The Stern-Volmer plot of the  $NO_2^*$  decay rate constant

#### EXPERIMENTAL

The laser was an active-passive mode-locked  $Nd^{3+}$ -YAG oscillator-amplifier system which delivered a 30 mJ (1064 nm) single pulse at 10 Hz. The frequency doubled 532 nm probe pulse was 31 ps duration (FWHM) as monitored by a streak camera. After frequency doubling the green pulse, the 266 nm pump was separated from the optically delayed 532 nm probe pulse. The two pulses were then collinearly recombined as in the experiment of Goldberg et al (1). The areas of the green and UV laser beams were estimated to be

versus the pressure is a straight line. The estimation of the  $\text{NO}_2$  quantum yields is based on the courageous hypothesis that the 532 nm absorption cross section of  $\text{NO}_2$  is the same for thermal and photoproduct  $\text{NO}_2$ .

#### RESULTS AND DISCUSSION



The fluorescence signal from  $\text{NO}_2^*$  formed by 266 nm photolysis of  $\text{CH}_3\text{NO}_2$  followed by (at  $t_D = 300\text{ps}$ ) 532 nm LIF probing of the ground stage  $\text{NO}_2$  photoproduct is shown in Figure 2. There is a 266-only component of the fluorescence which is about 5 % of the value caused by the 532 nm LIF of  $\text{NO}_2$  [2].

Fig. 2 - Plot of the  $\text{NO}_2^*$  fluorescence intensity as a function of time.

The picosecond kinetics of the  $\text{NO}_2$  formation follows closely that of the R-6G photobleaching observed with the same pump and probe pulses (figure 3) showing that the photodissociation occurs within 6ps. This is consistent with our RRKM lifetimes for  $\text{CH}_3\text{NO}_2$  (0.21 ps) and DMNA (4 ps) calculated from literature Arrhenius A factors and Vibrational frequencies [2].

The fluorescence signal from  $\text{NO}_2^*$  formed by 266 nm photolysis of DMNA and 532 nm probing is shown in Figure 4 [3].

The quantum yields of ground stage  $\text{NO}_2$  and excited  $\text{NO}_2^*$  formation are gathered in table. 1 [2,3].

	$\text{NO}_2$	$\text{NO}_2^*$
$\text{CH}_3\text{NO}_2$	$0.17 \pm 0.11$	$< 10^{-3}$
DMNA	$0.13 < \phi < 0.95$	$0.02 < \phi < 0.12$

Table 1 - Quantum yields of  $\text{NO}_2$  and  $\text{NO}_2^*$  formation in the photolysis of  $\text{CH}_3\text{NO}_2$  and DMNA at 266 nm.

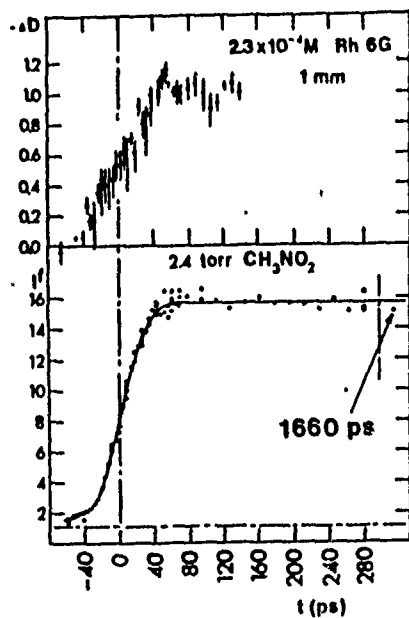


Fig. 3 - Photobleaching kinetics of a R-6G solution at 532 nm.  $\text{NO}_2^*$  LIF formation kinetics (lower curve).

In dimethylnitramine, efficient monophotonic  $\text{NO}_2^*$  formation is due to the greater available energy after the  $\text{N}-\text{NO}_2$  bond breaking ( $D(\text{N}-\text{NO}_2) = 44.1$  kcal/mole,  $D(\text{C}-\text{NO}_2) = 58.5$  kcal/mole). In the  $\text{RNO}_2$  under study, the efficiency of ground stage  $\text{NO}_2$  formation does not depend on the nature of the alkyl group.

#### References

1. L.S. Goldberg, M.J. Marrone, P.E. Schoen "Picosecond Lasers and Applications, SPIE, Vol. 322 (1982) 199.
2. J.C. Mialocq, J.C. Stephenson, Chem. Phys. (in press).
3. J.C. Mialocq, J.C. Stephenson, Chem. Phys. Lett. 123, 5 (1986) 390.

#### Acknowledgement

This work was supported by the Direction des Recherches, Etudes et Techniques under contract N° 84/819.

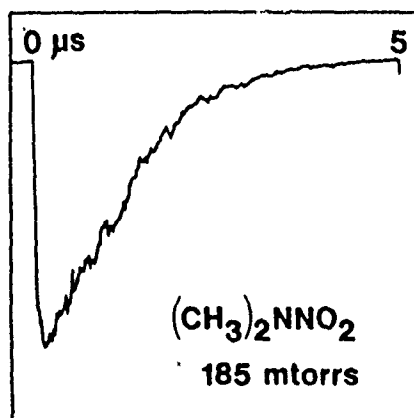


Fig. 4 - LIF signal as a function of time after pump and probe excitation of DMNA using 50  $\mu\text{J}$  (266 nm) and 350  $\mu\text{J}$  (532 nm) energies.

## Product Vibrational State Distributions in the Photodissociation

## of Iodine - Rare Gas Clusters

J.M. Philippoz and H. van den Bergh  
Laboratoire de Chimie Technique  
Ecole Polytechnique Fédérale de Lausanne  
1015 Lausanne, Switzerland

and

R. Monot  
Institut de Physique Expérimentale  
Ecole Polytechnique Fédérale de Lausanne  
CH-1015 Lausanne, Switzerland

Abstract:

The photodissociation of  $I_2M$  van der Waals clusters is studied at several wavelengths above the B state dissociation limit with  $M = He, Ne, Ar, Kr$  and  $Xe$ . The  $I_2$  product vibrational state distributions are obtained by measuring the dispersed  $B \rightarrow X$  fluorescence and analysing the resulting spectra. Excitation above the B state dissociation limit leads to significantly different reaction dynamics compared to excitation of the bound levels of the B state studied previously. Among others the recoil energies of the  $I_2$  and M fragments are much larger, and the distributions of rovibrational states in the  $I_2$  product are much wider in the present experiments. For the five rare gases studied, the photodissociation of  $I_2Ar$  leads to the smallest amount of relative translational energy in the products, in contradiction with recent quasi-classical trajectory calculations. The fragment recoil energy does not vary strongly with the excitation wavelength.

VIBRATIONAL AND ELECTRONIC COLLISIONAL RELAXATION OF  
 $C_2(d^3\Pi_g, v')$  AND  $(C^1\Pi_g, v')$  STATES

P. Bartolomé, M. Castillejo, J.M. Figuera and M. Martin, *Int<sup>o</sup> de Química Física "Rocasolano"*, CSIC, Serrano 119, 28006 Madrid, Spain.

The collisional processes of the two  $^{1,3}\Pi_g$  states of the diatomic carbon molecule, are studied for Xe,  $N_2$  and  $O_2$  as collision partners.

The  $C^1\Pi_g$  and  $d^3\Pi_g$  fragments are produced in the ArF laser multiphoton dissociation of vinyl chloride or vinyl bromide (1) and their fluorescence spectra are recorded in the presence of different pressures of the above collisional gases.

In the presence of  $N_2$ , population transfer from the higher to the lower vibrational levels is observed to compete with rotational relaxation within each vibrational state.

For Xe as the collision partner, a rate constant in reasonable agreement with previously measured values (2), is obtained for the electronic relaxation of the  $d^3\Pi_g$  state, this value being moderately dependent upon the vibrational quantum number.

More than twice faster rate constant is measured for the electronic quenching by  $O_2$ , with no measurable dependence on vibrational excitation. Faster rate constants (about 1.5 times faster) are obtained for electronic relaxation of the

observed levels of the  $C^1\Pi_g$  state, and the fastest relaxation rate is obtained for Xe, which quenches the  $C^1\Pi_g$  state at nearly every collision.

#### REFERENCES

- 1.- M. Castillejo, J.M. Figuera and M. Martín, International Conference of Multiphoton Processes III, Crete (September 1984).
- 2.- H. Okabe, R.J. Cody and J.E. Allen Jr., Chem. Phys. 92, 67 (1985).

The collisional quenching of  $\text{Ca}(4s3d(^1D_2))$  by  $\text{H}_2$  and  $\text{D}_2$ .

by David Husain and Gareth Roberts,  
 Department of Physical Chemistry,  
 University of Cambridge,  
 Lensfield Road,  
 Cambridge, CB2 1EP,  
 England.

The collisional behaviour of the low-lying, optically metastable states of the alkaline earth metal atoms, Mg, Ca and Sr ( $nsnp(^3P_J)$ ) in the gas phase, has received considerable attention during recent years from both a theoretical and experimental point of view. Characterisation of the rate of removal of these atomic states by  $\text{H}_2$  and  $\text{D}_2$  in particular, is of special interest for both quantitative and qualitative description of the appropriate potential hypersurfaces involving the triatomic species  $\text{MH}_2$  and  $\text{MD}_2$ , as such systems are clearly most amenable to theoretical investigation. In our laboratory, we have recently determined the temperature dependence of these removal processes for  $\text{Ca}(4^3P_J)$  and  $\text{Sr}(5^3P_J)$  [1,2], following the earlier studies of Breckenridge and co-workers on  $\text{Mg}(3^3P_J) + \text{H}_2, \text{D}_2$  [3,4], and have employed the results to differentiate between the competing rôles of physical energy transfer and chemical reaction. Simandiras and Handy have carried out ab initio calculations of the potential hypersurface for the  $\text{Ca}(4^3P_J) + \text{H}_2$  reaction [5], and have concluded that the activation energy is not significantly higher ( $< 5 \text{ kJ mol}^{-1}$ ) than the reaction endoergicity, in support of our earlier kinetic observations.

In this paper, we report an investigation of the collisional removal of  $\text{Ca}(4s3d(^1D_2))$ , 2.709 eV above the ground state [6], by  $\text{H}_2$  and  $\text{D}_2$  over the temperature range 750 - 1100 K.  $\text{Ca}(4^1D_2)$  atoms were generated in a slow-flow system by direct optical excitation at  $\lambda = 457.5 \text{ nm}$  via the weak electric-quadrupole allowed transition  $\text{Ca}(4s3d(^1D_2)) \leftarrow \text{Ca}(4s^2(^1S_0))$  using a pulsed dye-laser. The subsequent time-resolved emission at this resonance wavelength was optically isolated and monitored photoelectrically with boxcar integration.

The pseudo first-order decay coefficient representing overall removal of  $\text{Ca}(4^1D_2)$  by all processes may be written:

$$k' = \Sigma A_{nm} + \beta/P_{\text{He}} + k_{\text{H}_2}[\text{H}_2] \quad (\text{i})$$

with an analogous expression for  $\text{D}_2$ . The terms on the right hand side of equation (i) represent removal by spontaneous emission, diffusion and collisional quenching respectively. At a given temperature and pressure of helium buffer gas equation (i) becomes:

$$k' = K + k_{\text{H}_2}[\text{H}_2] \quad (\text{ii})$$

where K is fixed for a series of decay measurements in which  $[\text{H}_2]$  or  $[\text{D}_2]$  is varied at a given temperature and constant total pressure. Absolute second-order rate constants for the collisional removal of  $\text{Ca}(4^1D_2)$  atoms by  $\text{H}_2$  and  $\text{D}_2$ , as determined from equation (ii), are accurately



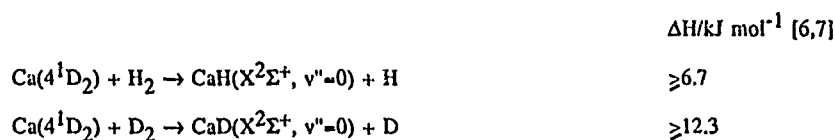
described by the following Arrhenius expressions:

$$k_{H_2} = (5.5 \pm 0.9) \times 10^{-10} \cdot \frac{\exp(-14.4 \pm 1.3 \text{ kJ mol}^{-1})}{RT} \text{ cm}^3 \text{ molecule}^{-1} \text{ s}^{-1}$$

and,

$$k_{D_2} = (3.9 \pm 0.4) \times 10^{-10} \cdot \frac{\exp(-22.2 \pm 0.8 \text{ kJ mol}^{-1})}{RT} \text{ cm}^3 \text{ molecule}^{-1} \text{ s}^{-1}$$

The activation energies so derived can be considered within the framework of chemical removal to yield electronic and vibrational ground state CaH and CaD plus H(D)( $^2S_{1/2}$ ):



Thus the present results are seen to be consistent with the hypothesis that removal of the metastable atomic state by both isotopic species is dominated by a chemical pathway in which there is a small energy barrier over and above the reaction endoergicities yielding the ground state diatomic hydride or deuteride. These measurements do not permit isolation of any quenching pathway, however minor, involving removal of  $\text{Ca}(4^1D_2)$  by physical energy transfer. Finally in this context, it is of interest to note that our earlier study of the quenching of  $\text{Ca}(4^3P_J)$  by  $H_2$  and  $D_2$  yielded activation energies for total removal which were also found to be in close agreement with the appropriate reaction endoergicities [1].

The Arrhenius pre-exponential factors also support a model based upon chemical removal of the metastable state, as seen from symmetry arguments employing the weak spin-orbit coupling approximation. We have previously observed that the pre-exponential factors for  $\text{Ca}(4^3P_J) + H_2$ ,  $D_2$  are in reasonable agreement with calculated collision numbers, in accord with a direct correlation between  $\text{Ca}(4^3P_J) + H_2(D_2)$  and  $\text{CaH(D)}(X^2\Sigma^+) + H(D)$  via a surface of  $^3A'$  symmetry [1]. Hence the significantly lower pre-exponential factors determined for the  $\text{Ca}(4^1D_2) + H_2$ ,  $D_2$  reactions may be presumed to reflect the occurrence of non-adiabatic transitions on the chemical pathways connecting the reactants with ground state products.

#### References.

- [1] D. Husain and G. Roberts, J.Chem.Soc., Faraday Trans. II, (1985), 81, 527.
- [2] D. Husain and G. Roberts, J.Chem.Soc., Faraday Trans. II, (1985), 81, 1085.
- [3] W.H. Breckenridge and W.L. Nikolai, J.Chem.Phys., (1980), 73, 2763.

E19

- [4] W.H. Breckenridge and J. Stewart, J.Chem.Phys., (1982), 77, 4469.
- [5] E.D. Simandiras and N.C. Handy, J.Chem.Soc., Faraday Trans. II, (1986), 82, 269.
- [6] 'Atomic Energy Levels', Nat.Bur.Stand.Ref.Data, Ser. 35, Ed. C.E. Moore (U.S. Government Printing Office, Washington, D.C., 1971), Vols. I-III.
- [7] K.P. Huber and G. Herzberg, 'Molecular Spectra and Molecular Structure IV. Constants of Diatomic Molecules', Van Nostrand Reinhold, New York, 1979).

Collisional Electronic Quenching of OH( $A^2\Sigma^+$ ) Radical

A. Vegiri\*, S.C. Farantos<sup>+</sup>, P. Papagiannakopoulos<sup>+</sup>, and  
C. Fotakis\*.

Research Center of Crete, Institute of Electronic Structure  
and Laser,  
Iraklion, Crete, Greece.

Abstract

Recent kinetic studies of OH( $A^2\Sigma^+$ ) colliding with CO, H<sub>2</sub>O and N<sub>2</sub> have shown the dependence of the decay efficiencies on the rotational quantum number N of the diatom [1]. In order to understand the quenching and energy transfer mechanisms of these systems we carry out quantum chemistry calculations[2]. The potential energy surfaces for the ground and excited states of OH with He and CO are constructed. The potentials of He + OH( $X^2\Pi$ ,  $A^2\Sigma^+$ ) are found to be repulsive but with interesting topology. Interaction potential of OH with CO are under investigation.

1. P. Papagiannakopoulos and C. Fotakis, J. Phys. Chem. 89, 3431, 1985.
2. S.C. Farantos, Mol. Phys. 54, 835, 1985.

---

\* Also Physics Department, University of Crete,  
Iraklion Crete, Greece

<sup>+</sup> Also Chemistry Department, University of Crete,  
Iraklion, Crete, Greece.

COLLISIONAL QUENCHING OF  $\text{OH}(A^2\Sigma^+, v'=0)$  BY  $\text{NH}_3$  FROM 250-1400K

Jay B. Jeffries, Richard A. Copeland, and David R. Crosley  
SRI International, Menlo Park, CA 94025

The rate constant for collisional removal of the  $v'=0$  level of the  $A^2\Sigma^+$  excited state of the OH radical by  $\text{NH}_3$  is measured over the temperature range 250-1400 K. The variation of this rate with collider temperature provides more insight into the mechanism than does just the magnitude of the rate at a single temperature. When long range attractive forces are important, the cross section decreases as the relative translational energy increases. When such a cross section is averaged over a thermal distribution of velocities, it will decrease with increasing temperature. We examine the temperature dependence of quenching rate constants,  $k_0$ , for OH colliding with  $\text{NH}_3$ , a quencher with a permanent dipole moment which generates a large dipole-dipole attractive term in the interaction potential. The temperature dependence observed is consistent with a quenching mechanism dominated by long range attractive forces.

Two different experimental apparatus were used to cover the range 250 to 1400 K. Between 840 and 1425 K the laser pyrolysis/laser fluorescence (LP/LF) technique<sup>1</sup> is used, and at 255 and 300 K the experiments are performed in a fast flow reactor.<sup>2</sup> The LP/LF technique uses a pulsed  $\text{CO}_2$  laser to irradiate a slowly flowing mixture of bath gas ( $\text{N}_2$  or  $\text{CF}_4$ ), infrared absorber ( $\text{SF}_6$ ), radical precursor ( $\text{H}_2\text{O}_2$ ), and quencher ( $\text{NH}_3$ ). Some of the IR energy is absorbed by the  $\text{SF}_6$  and collisional energy transfer heats the entire irradiated volume to a temperature determined by the  $\text{CO}_2$  laser pulse energy and the ratio of infrared absorber to bath gas. The low pressure flow reactor<sup>2</sup> uses Ar buffer gas; a microwave discharge in the flow reactor generates hydrogen atoms from the  $\text{H}_2$  impurity present in the Ar, and OH is produced from  $\text{H} + \text{NO}_2$ . In both apparatus, laser-induced fluorescence is used to measure a rotational temperature of the OH.

At room temperature the magnitude of the electronic quenching of  $\text{OH}(A^2\Sigma^+, v'=0)$  varies with rotational level in the A-state. Observed by McDermid and Laudenslager<sup>3</sup> for quenching by  $\text{N}_2$  and  $\text{O}_2$ , this phenomenon has

measured for a more extensive set of rotational levels and collision partners to include  $\text{NH}_3$ .<sup>4</sup> That investigation<sup>4</sup> showed that  $k_Q$  decreases as the rotational quantum number  $N'$  is increased; this produces a variation of the observed quenching rate for different rotational population distributions in the A-state. In both our high and low temperature apparatus, there is sufficient bath gas to produce, by collisional transfer, a thermal rotational population distribution in the excited  $A^2E^+$  state. Neither Ar or  $\text{CF}_4$  is an efficient quencher of the electronic state, but each is an effective collision partner for rotational relaxation of the molecules from the single rotational level initially excited into a thermal population distribution. The flow measurements are done in 8 Torr of Ar and the LP/LF measurements made between 15 and 40 Torr of  $\text{CF}_4/\text{SF}_6$  mixture. Both model calculations and diagnostic experiments verify that the quenching rates are obtained for a thermal distribution of rotational level populations of the  $A^2E^+$  state as well as a thermal distribution of collision velocities.

To measure the quenching rate, light from a pulsed, frequency-doubled dye laser excites the OH molecules to a specific rotational level in the  $A^2E^+$ ,  $v'=0$  state. Following excitation we monitor the temporal evolution of the total fluorescence. By examining the pressure dependence of the fluorescence decay, we obtain the quenching rate constant and the thermally averaged cross section,  $\sigma_Q = k_Q / \langle v \rangle$ , where  $\langle v \rangle$  is the average relative collision velocity. The eleven measurements (•) of the thermally averaged cross section between 255 and 1425 K are plotted versus temperature in Fig. 1. Two important results are evident from the data. First, the quenching cross section, thermally averaged over the rotational level distribution and collision velocity, decreases roughly a factor of two between 300 and 900 K. Second there is no observable change in the value of  $\sigma_Q$  between 850 and 1400 K.

The temperature dependence of  $\sigma_Q$  contains two distinct contributions. First,  $\sigma_Q$  may depend on relative collision velocity. The attractive interactions are modeled<sup>5</sup> by a multipole expansion; the dashed line in Fig. 1 is the temperature dependence of  $\sigma_Q$  as calculated by this model. Second, because  $\sigma_Q$  decreases as  $N'$  increases, a rotationally averaged  $\sigma_Q$  will decrease as the temperature increases because the population in the excited  $A^2E^+$  state shifts toward higher  $N'$ . With the assumption that the variation of quenching cross section with rotational level is independent of temperature, we use the data

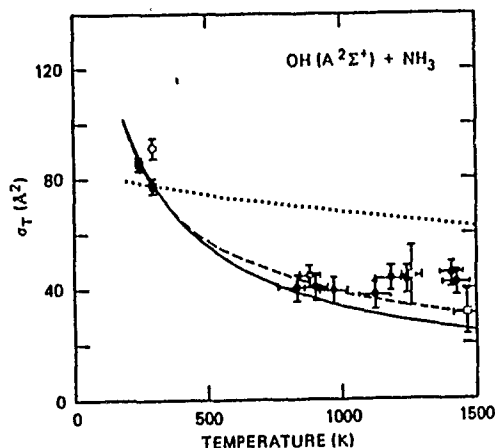
from Ref. 4 to calculate this effect. The dotted line in Fig. 1 shows the variation in  $\sigma_Q$  predicted from only the rotational level dependence.

The solid line in Fig. 1 is the prediction of  $\sigma_Q$  from the combination of the rotational level dependence and the attractive forces model. The calculation predicts a slightly greater temperature variation than we observed over the entire temperature range studied. In the high temperature region (850-1400 K), the measured  $\sigma_Q$  remains constant while the model predicts a 20% decrease. Nonetheless, the comparison between model and measured  $\sigma_Q$  represents surprisingly good agreement for such a simple model. The data indicate that the quenching mechanism is dominated by attractive forces in the temperature range 250-1400 K.

This work was supported by the Division of Basic Energy Sciences of the Department of Energy.

1. G. P. Smith, P. W. Fairchild, J. B. Jeffries, and D. R. Crosley, *J. Phys. Chem.* **89**, 1269 (1985).
2. R. A. Copeland and D. R. Crosley, *J. Chem. Phys.* **84**, 3099 (1986).
3. I. S. McDermid and J. B. Laudenslager, *J. Chem. Phys.* **76**, 1824 (1982).
4. R. A. Copeland, M. J. Dyer, and D. R. Crosley, *J. Chem. Phys.* **82**, 4022 (1985).
5. P. W. Fairchild, G. P. Smith, and D. R. Crosley, *J. Chem. Phys.* **79**, 1795 (1983).

Figure 1. Temperature dependence of the cross section for quenching of  $(A^2\Sigma^+, v'=0)$  OH by  $NH_3$ . Solid symbols are the present LP/LF ( $\bullet$ ) and flow reactor ( $\blacksquare$ ) measurements. The open squares are the previous LP/LF results (Ref. 5) and the open circle, the rotationally and thermally averaged value as computed from the state-specific cross sections (Ref. 4). The lines are calculated values, all normalized to the experimental value at 300K.



JA-3512-41

Formation of  $\text{XeCl}(B^2\Sigma_{1/2})$  and  $\text{XeI}(B^2\Sigma_{1/2})$  by Reaction  
of Electronically Excited ICl with Xe

J.P.T. Wilkinson, E.A. Kerr and R.J. Donovan  
Department of Chemistry, University of Edinburgh,  
West Mains Road, Edinburgh EH9 3JJ

D. Shaw and I. Munro  
SERC Daresbury Laboratory, Daresbury, Warrington WA4 4AD

Abstract

The ion-pair states of the halogens present an interesting challenge to the spectroscopist. They are difficult to observe using conventional techniques due to both unfavourable Franck-Condon factors from the ground state to low vibrational levels and also because the Franck-Condon accessible regions are dominated by strong transitions to Rydberg states. However, as these Rydberg states are often strongly predissociated they are not observed in fluorescence and thus by observing fluorescence excitation spectra the ion-pair states can often be studied in the absence of overlapping transitions to Rydberg states [1].

We present in Figure 1 the fluorescence excitation spectrum for ICl in the 150-190 nm region recorded using synchrotron radiation. Fluorescence from the first optically accessible ion-pair state of ICl is excited in the 170-190 nm region. When fluorescence excited in this region is dispersed we obtain a spectrum with the characteristic oscillatory continuum structure,

typical of the emission from higher vibrational levels of ion-pair states [2]. Between 160 nm and 170 nm in the fluorescence excitation spectrum we see a second, highly structured, fluorescence system which is probably the result of the interaction between a Rydberg state and an ion-pair state.

As well as direct fluorescence excitation spectra, we have also recorded action spectra for both  $\text{XeCl}(B^2\Sigma_{1/2})$  and  $\text{XeI}(B^2\Sigma_{1/2})$  formation using synchrotron radiation to excite ICl in the presence of excess xenon, see Figure 2. We find that the formation of  $\text{XeCl}(B^2\Sigma_{1/2})$ , which is thermodynamically feasible for  $\lambda < 200$  nm [3], occurs throughout both the 160-170 nm and 170-190 nm systems whereas  $\text{XeI}(B^2\Sigma_{1/2})$  is formed only when the 160-170 nm system is excited.

Further work on both the ICl fluorescence excitation spectra and the  $\text{XeI}(B^2\Sigma_{1/2})$  and  $\text{XeCl}(B^2\Sigma_{1/2})$  action spectra will be reported at the conference.

- [1] E. Kerr, M. MacDonald, R.J. Donovan, J.P.T. Wilkinson, D. Shaw and I. Munro, *J.Photochem.*, **31**, 149, 1985.
- [2] M. MacDonald, J.P.T. Wilkinson, C. Fotakis, M. Martin and R.J. Donovan, *Chem. Phys. Letts.*, **99**, 250, 1983.
- [3] G. Herzberg and K.P. Huber, *Constants of Diatomic Molecules*, Van Nostrand Reinhold, New York, 1979.



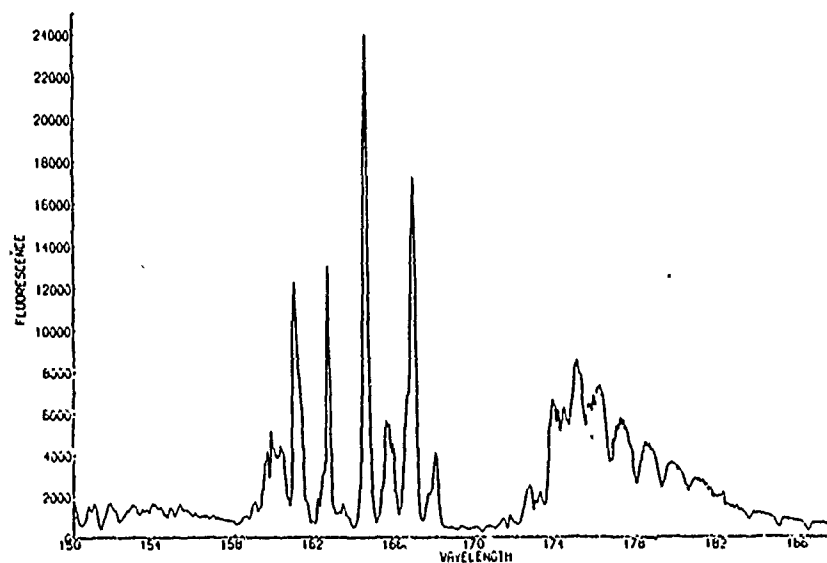


Figure 1 Fluorescence excitation spectrum for ICl  
( $P_{ICl} = 10 \text{ Nm}^{-2}$ )

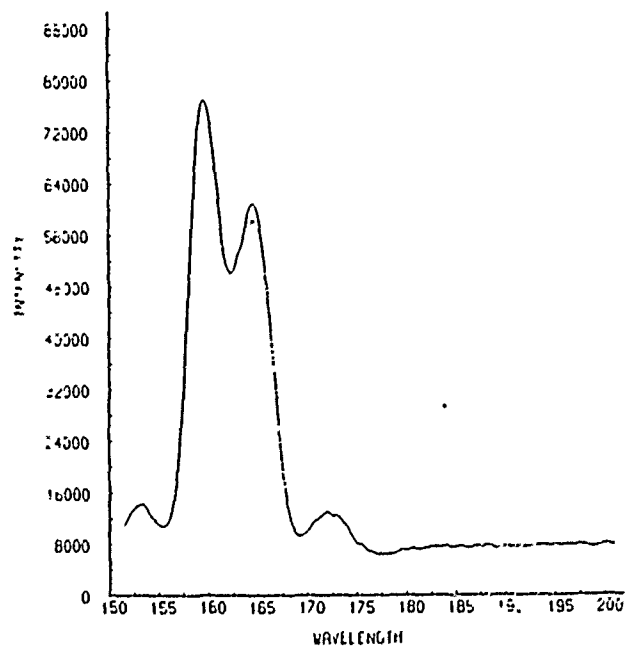
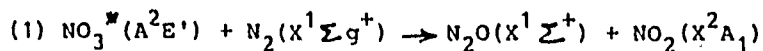


Figure 2 XeI( $\beta$ ) fluorescence excitation from reaction  
of excited ICl with excess xenon.

QUENCHING OF  $\text{NO}_3^*(^2\text{E}')$  BY  $\text{N}_2$ . A POTENTIAL  
PHOTOCHEMICAL SOURCE OF  $\text{N}_2\text{O}$ .

K.G. Pettrich, F. Ewig and R. Zellner  
Institut für Physikalische Chemie, Universität  
Göttingen, 3400 Göttingen, FRG

The origin of atmospheric  $\text{N}_2\text{O}$  is almost exclusively at the earth's surface. In-situ photochemical sources in the troposphere and stratosphere are presently unknown. However, recent evidence obtained in our laboratory suggests that a significant source of  $\text{N}_2\text{O}$  may arise from the reaction.



where the  $^2\text{E}'$ -state of  $\text{NO}_3$  is produced upon excitation of  $\text{NO}_3(^2\text{A}')^*$  by solar radiation at wavelength between 620-700 nm.

Reaction (1) is exothermic by 134 kJ/mol and spin as well as orbital symmetry allowed. However, it will be in strong competition with the simple energy transfer reaction which is usually assumed to dominate collisional electronic quenching. Direct measurements of the  $\text{N}_2\text{O}$  yield are in progress and their result will be presented at the meeting.

THE ELECTRON SWARM METHOD AS A TOOL TO INVESTIGATE  
THE THREE-BODY ELECTRON ATTACHMENT PROCESSES

I. Szamrej, I. Chrzęścik and M. Foryś

Chemistry Department, Agricultural and Teachers University,  
08-110 Siedlce, POLAND

In the recent years a large body of evidence has been collected which demonstrates the importance of the three-body processes in the electron capture in the gas phase. The electron swarm method has been widely used to investigate electron attachment. However up to date was scarcely applied to the important class of the three body processes especially those where the two molecules of the electron scavenger take a part in the reaction<sup>1/</sup>. This contribution was aimed to develop the approach which enables one to measure rate constants for such processes which occur at thermal energies.

The swarm chamber has been built basing on the experience of authors from Christophorou's laboratory and the technical details are essentially similar.

Carbon dioxide was used as a diluent gas with wide range of the thermal equilibrium region. To resolve the drift velocity /W/ problem in the presence of higher concentrations of scavengers /M/ the reaction of electron capture by SF<sub>6</sub> was applied.

First, the  $k_{e+SF_6} = 3.1 \times 10^{-7} \text{ cm}^3 \cdot \text{molec}^{-1} \cdot \text{s}^{-1}$  was measured in CO<sub>2</sub> to be constant over the 0.3-0.9 V·Torr<sup>-1</sup>·s<sup>-1</sup> of E/P using W from ref.1. Then an electron attachment coefficient / $\alpha$ / for SF<sub>6</sub> was measured in different M-CO<sub>2</sub> mixtures and W was determined as  $W = k/\alpha$ . The results are shown in Fig.1.

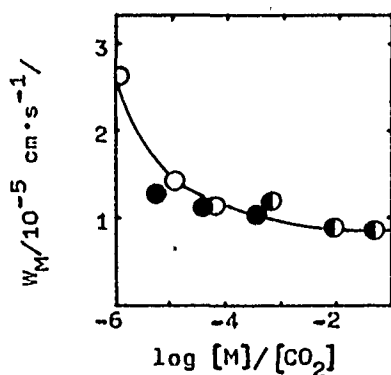


Fig.1 The influence of the scavengers concentration on the drift velocity in  $\text{CO}_2$  at  $E/P = 0.5 \text{ V} \cdot \text{Torr}^{-1} \cdot \text{cm}^{-1}$ .

○ -  $\text{CH}_3\text{Br}$   
● -  $\text{HBr}$   
◐ -  $\text{H}_2\text{S}$

It is seen that  $W$  changes strongly at lowest concentrations of admixtures and then is practically constant over the two-four-fold changes in pressure used in further experiment. Also the changes are not very specific owing to similar polarity of the admixtures.

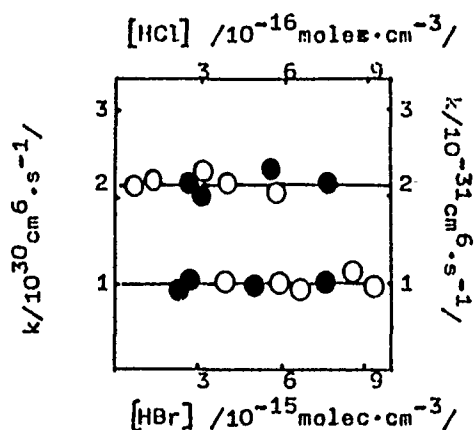


Fig.2. Three-body rate constants for  $\text{HBr}$  and  $\text{HCl}$  vs. scavenger concentrations at  $E/P = 0.5$

○ -  $p_{\text{CO}_2} = 300 \text{ Torr}$   
● -  $p_{\text{CO}_2} = 750 \text{ Torr}$

Next the  $\alpha$  values have been measured for  $\text{CH}_3\text{Br}$ ,  $\text{H}_2\text{S}$ ,  $\text{HBr}$  and  $\text{HCl}$ . The  $k$  values were calculated using  $W$  shown in Fig.1. The example results are given in Fig.2. As in the case of  $\text{SF}_6$  the  $k$  values were constant over the whole range of used  $E/P$  which means that the investigated reactions are the thermal ones.

As it is known from our<sup>2/</sup> and Armstrong's<sup>3/</sup> works by gamma

radiolysis method compounds enlisted above tend to accept thermal electrons in more than two-body reactions. Thus, the proper orders were determined by changing consecutively pressures of the participant gases. The results in Table 1 show that except  $\text{CH}_3\text{Br}$  all the processes are of the third order with  $\text{CO}_2$  or  $\text{H}_2\text{S}$  acting as the third body. This suggested that neutral van der Waals molecules can possibly be involved in the reaction.

Table 1. The rate constants for the electron capture reactions.

Reaction	$k/\text{cm}^6 \cdot \text{molecule}^{-3} \cdot \text{s}^{-1}/$	
	this work	literature
$e^- + \text{CH}_3\text{Br}^*$	$6.5 \times 10^{-12}$	$1.0 \times 10^{-9}$ 4a/, $7 \times 10^{-12}$ 4b/ $3.6 \times 10^{-12}$ 4c/
$e^- + 2\text{H}_2\text{S}$	$5.0 \times 10^{-33}$	$1.9 \pm 1.0 \times 10^{-32}$ 4d/
$e^- + \text{HBr} + \text{CO}_2$	$1.0 \times 10^{-30}$	
$e^- + \text{HCl} + \text{CO}_2$	$2.2 \times 10^{-32}$	

\* two body rate constant

#### References

1. Electron-Molecule Interactions and Their Applications, ed. L.G.Christophorou /Academic, New York, 1984/
2. I.Szamrej, I.Chrząścik, M.Foryś, Rad.Effects, 83, 291 /1984/
3. S.S.Nagra, D.A.Armstrong, J.Phys.Chem., 81, 599 /1977/
4. a/A.A.Christodoulides, L.G.Christophorou, J.Chem.Phys., 54 4691 /1971/; b/K.M.Bansal, R.W.Fessenden, Chem.Phys.Lett., 15, 21 /1972/; c/K.G.Mothes, E.Schultes, R.N.Schindler, J. Phys.Chem., 76, 3758 /1972/
5. I.Szamrej, I.Chrząścik, Rad.Phys.Chem., in press

THE ROLE OF VAN DER WAALS DIMERS IN THE ELECTRON  
CAPTURE PROCESSES

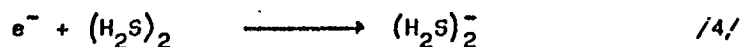
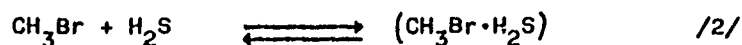
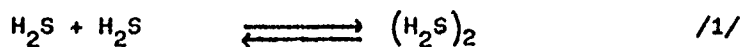
I. Szamrej, I. Chrzęćcik and M. Foryś

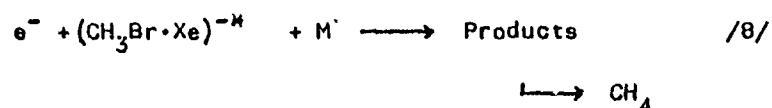
Chemistry Department, Agricultural and Teachers University,  
08-110 Siedlce, POLAND

The gamma radiolysis of the low pressure hydrogen sulphide-methyl bromide mixtures has been used as a method to investigate the three-body electron capture processes in the gas phase. Xenon has been chosen as a diluent gas as its ability to stabilize negative ions in a three-particles encounter is known to be very low while the equilibrium constant for formation of VdW dimers is comparable with that for molecular constituent.

The concentration of the final product, methane, was measured gas-chromatographically. A strong dependence of the rate of formation of negative ions on the xenon and hydrogen sulphide total pressure has been observed.

On this basis the following set of reactions has been proposed.





where M is the total concentration of the molecular components. The rate constants for the formation of the double negative ions have been calculated. They are equal to  $(2 \pm 2) \times 10^{-11} \text{ cm}^3 \cdot \text{molecule}^{-1} \cdot \text{s}^{-1}$  for  $(\text{H}_2\text{S})_2^-$  and  $(6 \pm 3) \times 10^{-28} \text{ cm}^6 \cdot \text{molecule}^{-3} \cdot \text{s}^{-1}$  and  $(8 \pm 4) \times 10^{-28} \text{ cm}^6 \cdot \text{molecule}^{-3} \cdot \text{s}^{-1}$  for  $(\text{CH}_3\text{Br} \cdot \text{H}_2\text{S})^-$  and  $(\text{CH}_3\text{Br} \cdot \text{Xe})^-$ , molecules, respectively.

Three-body kinetics of electron capture by  $H_2S$  at low hydrogen sulphide pressures shows that reaction (4) gives the stable  $(H_2S)_2^-$  dimer ion, which does not decompose as any such process should lead to hydrogen production, which was not observed. It is rather striking behaviour as it is unlikely to other known dimer ions. The observed kinetics excludes also the electron transfer from  $(H_2S)_2^-$  or  $(H_nS_m)^-$  to  $CH_3Br$  as it would lead to  $CH_4$  production and, in consequences, independence of  $G(CH_4)$  on  $CH_3Br$  concentration in the  $CH_3Br-H_2S$  mixture.

The dependence of the rate of  $\text{CH}_4$  production on the  $([\text{H}_2\text{S}] + [\text{Xe}])$  term leads to the conclusion that VdW  $(\text{CH}_3\text{Br} \cdot \text{Xe})$  and  $(\text{CH}_3\text{Br} \cdot \text{H}_2\text{S})$  molecules are responsible for the  $\text{CH}_4$  production in electron capture processes by  $\text{CH}_3\text{Br}$ . Otherwise the unlikely supposition should have been made that the effectiveness of Xe and  $\text{H}_2\text{S}$  in stabilizing the excited dimer ion is nearly equal. If the first statement is true, the used method

E25

appears to be a new one to distinguish between Bloch-Bradbury and VdW molecules ways of formation of dimer negative ions in the case when stabilizing efficiency of the species differs strongly while the equilibrium constants are similar.



Reactions of ion-pair states of  $\text{Cl}_2$ E. Nontzopoulos<sup>1</sup> and C. Fotakis<sup>1</sup>

Institute of Electronic Structure and Laser

Research Center of Crete

P.O. Box 1527, Iraklio, Crete, Greece

Chemiluminescent reactions between the  $D(^1\Sigma_u)$  ion-pair state of molecular halogens and noble gas atoms have recently received great attention [1,2]. Fluorescence from this state and intramolecular energy transfer leading eventually to the population of the lowest ion-pair state  $D'(^3\Pi_{2g})$  are competitive to reaction and have been studied in some detail. The reactivity of the  $D'$  state of  $\text{Br}_2$  has also been studied [3]. In the present work ion-pair states of  $\text{Cl}_2$  having a "gerade" parity are populated directly and selectively in a two-photon excitation process from the ground state, by means of a narrow-band tunable KrF laser. Evidence for relaxation processes and chemiluminescent reactions, which are observed in the presence of Ar, Kr and Xe will be presented and compared to those obtained in single photon excitation for the  $D(^1\Sigma_u)$  halogen state. Reaction rates are found to be fast, corresponding to a magnitude of several times the hard sphere collision cross sections. This will be interpreted on the basis of a harpooning mechanism. Finally, data will be presented for the reaction of ion-pair states of  $\text{Cl}_2$  with various hydrocarbons.

References

1. T. Müller, B. Jordan, P. Gurther, G. Zimmerer,  
D. Heaks, J. Le Calve and M.C. Castex, Chem. Phys.  
76, 295 (1983).
2. B.V. O'Grady and R.J. Donovan, Chem. Phys. Lett.  
122, 503 (1985) and references therein.
3. D.J. Ehrlich and R.M. Osgood,  
Jr. J. Chem. Phys. 73, 3038 (1980).

<sup>1</sup> Also : Dept. of Physics, University of Crete  
P.O. Box 470, Iraklio, Crete, Greece

# The association reactions of $\text{NO}^+$ with NO and $\text{N}_2$ in $\text{N}_2$ carrier gas

Rudolf R. Burke\* and Ian McLaren\*\*, LPCE, CNRS, 45071 Orleans Cedex 2

\* now at PM1, USMG & UA 844 du CNRS, CNS-CNET, BP 98, 38243 MEYLAN CEDEX

\*\* now at Department of Chemistry, Howard University, Washington, D.C.20059

The LPCE supersonic flowing afterglow permits the study of association reactions between 120 and 180 K, and from 0.4 to 0.8 mmHg. For five temperatures and three pressures, the loss rate of  $\text{NO}^+$  :  $-\text{d}[\text{NO}^+]/\text{dt} = k^1[\text{NO}^+]$  was measured as a function of NO addition. The pseudo-first-order rate constant is a linear function of  $[\text{NO}]$  with a positive intercept :  $k^1 = k^1_{\text{N}_2} + k^2_{\text{NO}}[\text{NO}]$ . The slope  $k^2_{\text{NO}}$  yields information on the  $\text{NO}^+ + \text{NO} \rightarrow \text{NO}^+(\text{NO})$  association and the intercept  $k^1_{\text{N}_2}$  on the  $\text{NO}^+ + \text{N}_2 \rightarrow \text{NO}^+(\text{N}_2)$  association (the  $\text{NO}^+(\text{N}_2)$  cluster is scavenged by the  $\text{NO}^+(\text{N}_2) + \text{NO} \rightarrow \text{NO}^+(\text{NO}) + \text{N}_2$  switch). The energy transfer mechanism (ETM) for association reactions predicts  $k^2_{\text{NO}} \sim k^3_{\text{NO}}[\text{N}_2]$ , but the experimental results give  $k^2_{\text{NO}} \propto [\text{N}_2]^{2.8}$ . If third-order is imposed on the data, one obtains  $k^3_{\text{NO}} = 4 \times 10^{-27} (150/T)^{8.3} \text{ molecule}^{-2} \text{ cm}^6 \text{ s}^{-1}$ . Extrapolation to 300 K yields the value reported by Kebarle.

The intercept  $k^1_{\text{N}_2}$  is independent of  $[\text{N}_2]$ , whereas the ETM predicts  $k^1_{\text{NO}} = k^3_{\text{NO}}[\text{N}_2]^2$ . Furthermore,  $k^1_{\text{N}_2} = 6 \times 10^3 \text{ s}^{-1}$  is independent of temperature. The mechanism proposed to account for the experimental data consists of chemical activation (ca)  $\text{NO}^+ + \text{N}_2 \rightarrow \text{NO}^+(\text{N}_2)^*$ , and radiative stabilisation (rs)  $\text{NO}^+(\text{N}_2)^* \rightarrow \text{NO}^+(\text{N}_2) + h\nu$  in competition with efficient collisional dissociation (cd)  $\text{NO}^+(\text{N}_2)^* + \text{N}_2 \rightarrow \text{NO}^+ + 2\text{N}_2$ . Applying the quasi-stationary-state approximation, one obtains  $k^1_{\text{N}_2} = k_{\text{rs}}k_{\text{ca}}/k_{\text{cd}}$ , and  $k^1_{\text{N}_2} \approx k_{\text{rs}}$  if  $k_{\text{ca}} \approx k_{\text{cd}}$ . This mechanism implies a slow unimolecular decomposition (ud)  $\text{NO}^+(\text{N}_2)^* \rightarrow \text{NO}^+ + \text{N}_2$  with  $k_{\text{ud}} \ll 10^7 \text{ s}^{-1}$ .

## HOT ATOMS IN IONOSPHERE

I.K.Larin and V.L.Talrose

Institute of Chemical Physics of the Academy of  
Sciences of the USSR, Moscow, USSR

Mechanisms and processes of hot atoms formation in ionosphere and their possible effect on chemical composition of ionosphere are discussed. The following processes are considered to be the sources of hot atoms: photodissociation, dissociative recombination and precipitation of energetic ions of  $H^+$  and  $O^+$  in high-latitudinal and medium-latitudinal ionosphere.

In particular it is shown that under conditions of magnetic storm flows of hot oxygen atoms formed as a result of a charge transfer of energetic  $O^+$  ions on oxygen atoms, may increase nitrogen oxide content in upper ionosphere of high latitudes by 3-4 orders as compared with undisturbed conditions.

Possible effect of the processes with hot atoms participation on ionic composition and total content of charged particles in ionosphere are analyzed.

The Chemistry of Sodium in the Mesosphere: Absolute Rates of the  
 Reactions  $\text{Na} + \text{O}_3 \longrightarrow \text{NaO} + \text{O}_2$  and  $\text{NaO} + \text{O} \longrightarrow \text{Na} ({}^2\text{P}_J, {}^2\text{S}_{1/2}) + \text{O}_2$

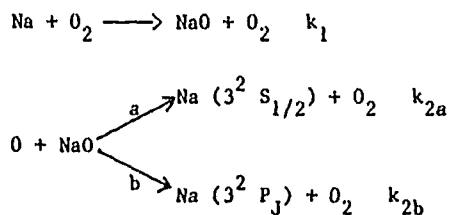
by

J.M.C. Plane, Rosenstiel School of Marine and Atmospheric Science, University  
 of Miami, 4600 Rickenbacker Causeway, Miami, FL 33149-1098, U.S.A.

D. Husain, Department of Physical Chemistry, University of Cambridge,  
 Lensfield Rd., Cambridge, CB2 1EP, U.K.

P. Marshall, Department of Chemical Engineering and Environmental Engineering,  
 Rensselaer Polytechnic Institute, Troy, NY 12180, U.S.A.

The reactions



have long been recognized as important in governing the distribution of atomic sodium in the 90km region above the earth's atmosphere, as well as the component of the air-glow emission due to the Na D-line ( $\lambda = 589\text{nm}$ ), and D-line emission in meteoric trails.

We present determination of  $k_1$  and  $k_2$  using two different and novel experimental techniques. Reaction 1 was investigated by time-resolved atomic absorption spectroscopy of Na atoms at  $\lambda = 589\text{ nm}$ , following the pulsed photolysis of NaI, in an excess of  $\text{O}_3$  that was monitored simultaneously by

steady absorption of the Hg line at  $\lambda = 253.7$  nm. We obtain a value for  $k_1 = (4^{+4}_{-2}) \times 10^{-10} \text{ cm}^3 \text{ molecule}^{-1} \text{ s}^{-1}$  at  $T = 500$  K.

The absolute rate constant,  $k_2$ , was determined by time-resolved atomic chemiluminescence at  $\lambda = 589$  nm, following reaction 2(b) as a spectroscopic marker for reaction (2), overall, subsequent to the pulsed photochemical generation of  $\text{O}(2^3\text{P}_j)$  in the presence of excess NaO.

A flow of a known concentration of NaO was created by mixing together a flow of  $\text{N}_2\text{O}$  with an excess of Na vapour entrained in a carrier gas from a heat-pipe oven. The overall rate constant was estimated to be

$$k_2 = (3.7 \pm 0.9) \times 10^{-10} \text{ cm}^3 \text{ molecule}^{-1} \text{ s}^{-1} \text{ at } T = 573 \text{ K.}$$

upper limit of 0.01 to the branching ratio of reaction (2) was also obtained, which is a rough estimate but may indicate that mechanisms other than reaction (2) are responsible for the observed D-line night-glow emission.

Parameters of Activation Barriers for Hydrogen Atom Transfer Reactions from  
Curved Arrhenius Plots

H. Furue and P. D. Pacey

Chemistry Department, Dalhousie University, Halifax, Nova Scotia, Canada B3H 4J3

Experimental data on the temperature dependence of the rates of gas phase, hydrogen atom transfer reactions have been reviewed and assembled.

The following expression, incorporating a factor,  $K$ , for tunneling through an Eckart barrier of effective height  $E_e$  and thickness,  $\Delta S_{1/2}$ , at half height, was fitted by least squares methods to the data for each reaction. Here  $A$ ,  $E_e$  and  $\Delta S_{1/2}$  were

$$k = KAT^n \exp(-E_e/RT)$$

adjustable parameters;  $n$  was fixed to match the temperature dependence contributed by other degrees of freedom. For four reactions of  $\text{CH}_3$  with organic molecules, values of  $\Delta S_{1/2}$  were found to be consistently between 0.05 and 0.06 nm. For reactions of D, O, F, Cl and  $\text{CH}_3$  with  $\text{H}_2$ , fitted values of  $A$  agreed within two standard deviations ( $\sim 20\%$ ) with values calculated from ab initio potential energy surfaces using transition state theory (TST). Similar agreement (2 to 5  $\text{kJ mol}^{-1}$ ) was obtained for effective barrier heights.

It is concluded that TST with a tunnel factor can be applied to such reactions and that curved Arrhenius plots can provide information about the barrier to reaction.

MASS SPECTROMETRIC DETERMINATION OF RATE CONSTANTS AND  
MECHANISM OF ATOMIC FLUORINE REACTIONS IN GAS PHASE

N.I. Butkovskaya, E.S. Vasiliyev, I.I. Morozov, V.L. Talrose

Institute of Chemical Physics of the Academy of Sciences  
of the USSR, Moscow, USSR

Reactions of fluorine atoms have been studied in the reactor with a diffusion cloud in flow. Reagents and reaction products, including atoms and free radicals, are directed, as a modulated molecular beam, to a focused electric or magnetic field in which particles with magnetic or dipole moments are focused onto an inlet hole of an ion source of a mass spectrometer. In such a way identification of free radicals is accomplished. It is for the first time that fluorine atoms have been identified by double-charged ions. Rate constants of a series of halogen-containing molecules with fluorine atoms have been determined at a pressure of inert gas of several torr and a room temperature.

Chemical activity of an atomic fluorine is so high that it reacts with glass and quartz walls of the reactor, yielding  $\text{SiF}_4$  and  $\text{O}_2$  into a gas phase. To eliminate this effect a discharge tube made of synthetic sapphire has been used. In most of the experiments fluorine atoms have been detected by the line  $M/e$  19.



KINETIC STUDY BY MASS SPECTROMETRY OF THE REACTION OF HYDROGEN ATOMS WITH  
ISOBUTANE IN THE RANGE 295-407 K.

by J.P. SAVERYSYN, C. LAFAGE, B. MERIAUX, A. TIGHEZZA

Université des Sciences et Techniques de Lille, Flandres Artois

Laboratoire de Cinétique et Chimie de la Combustion, UA CNRS 876

59655 VILLENEUVE D'ASCQ cedex (France)

If the reaction of hydrogen atoms with alkanes has been largely investigated, only few studies have been devoted to the reaction of hydrogen atoms with isobutane. The rate constant for this reaction has been essentially measured by indirect methods involving the addition of isobutane to a reacting  $H_2 - O_2$  system (1, 2) or investigating the radiolysis of isobutane-propylene system (3).

The present paper describes a study using a discharge-flow system coupled to a quadrupole mass spectrometer in order to make a direct measurement of the rate constant by monitoring the decay of H atoms with time and to propose a mechanism from the analysis of reaction products.

#### EXPERIMENTAL

All experiments were carried out using a conventionnal discharge-flow system coupled to a modulated molecular beam-mass spectrometric sampling technique (4). A pyrex tube (2,4 cm internal diameter and 60 cm length) was used as isothermal fast flow reactor. It was thermostatted by an oil jacket making constant to  $\pm 2K$  the temperature along the heated zone.

Hydrogen atoms were produced by a 2450 MHz microwave discharge in  $H_2$  highly diluted in He in a side tube. The He flow passed a liquid nitrogen trap to freeze traces of water.

All surfaces exposed to H atoms were coated with orthophosphoric acid in order to reduce heterogeneous recombinations. Mass spectrometric calibration of H atoms was determined by the measurement of the extent of the  $\text{H}_2$  - to - H conversion and/or by titration with  $\text{NO}_2$ .

Isobutane (purity 99,95%) was introduced into the reactor through an injector terminated by a multihole sphere. The injector could be moved along the axis of the flow reactor, varying the reaction time which was calculated from the measured flow rates using the assumption of plug flow.

The temperature of the gases was measured by means a chromel-alumel thermocouple mounted in the tip of the moveable injector. Flow rates of different reactants were measured by calibrated mass-flow controllers. The pressure in the flow tube was measured upstream by a capacitance manometer. The linear flow velocity in the reactor was set at about 20 m/s at about 1 torr.

#### RESULTATS AND DISCUSSION

The reaction between hydrogen atoms and isobutane has been investigated under pseudo-first order conditions with  $(\text{H})_0 \ll (\text{i-C}_4\text{H}_{10})_0$  over the temperature range of 295-407 K. At  $295 \pm 2\text{K}$ , the initial concentration of H atoms ranged from  $1,3 \cdot 10^{13}$  to  $1,25 \cdot 10^{14}$  atoms/cm<sup>3</sup>, while the initial concentration of  $\text{i-C}_4\text{H}_{10}$  ranged from  $1,15 \cdot 10^{14}$  to  $3,8 \cdot 10^{14}$  molecules/cm<sup>3</sup>. The ratio  $R = (\text{i-C}_4\text{H}_{10})_0 / (\text{H})_0$  was varied between 16 and 266. Results obtained at room temperature (fig.1) show an increase of the overall rate constant  $k$  for the lower values of the ratio  $R$ . For  $R$  higher than about 80,  $k$  tends to a constant value equal to  $2,2 \pm 0,4 \cdot 10^{-14}$  cm<sup>3</sup>/molecule.s at  $295 \pm 2\text{K}$ . Such a behavior of  $k$  as a function of the ratio  $(\text{i-C}_4\text{H}_{10})_0 / (\text{H})_0$  indicates the occurrence of fast secondary reactions of H atoms with products of the initial and/or secondary steps ( $\text{C}_4\text{H}_9$ ,  $\text{i-C}_4\text{H}_9$ ,...). A mechanism is proposed to interpret the formation of analyzed secondary compounds. The computer simulation of the

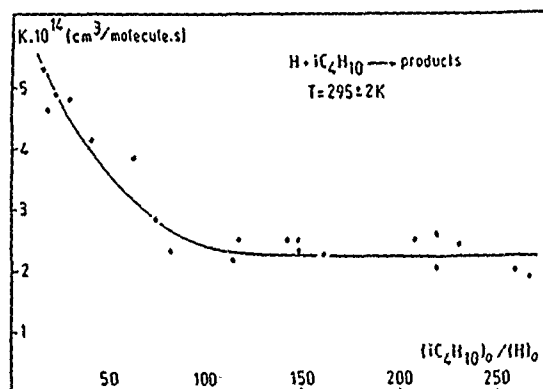


Fig.1 - Plot of the experimental values of the rate constant  $k$  as a function of the initial ratio of reactants.

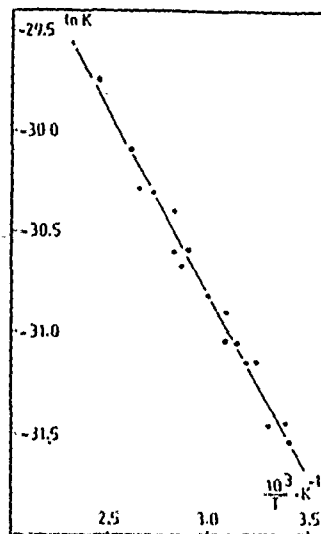


Fig.2 - Temperature dependence of the rate constant  $k$ .

mechanism enables to obtain a good agreement between the experimental and calculated curves.

In order to minimize the role played by secondary steps, the temperature dependence of  $k$  has been determined for a ratio  $(i-C_4H_{10})_0 / (H)_0$ , or about 200 (fig.2). The least squares treatment of the data yields :

$$k \text{ (cm}^3/\text{molecule.s)} = 9,3 \cdot 10^{-12} \exp(-1808/T)$$

#### REFERENCES

- 1 - N.I. GORBAN, A.B. NALBANDYAN, Zh. Fiz. Khim. 36, 1757, 1962
- 2 - R.R. BAKER, R.R. BALDWIN, R.W. WALKER, Trans. Far. Soc. 66, 2812, 1970
- 3 - K. YANG, J. Phys. Chem. 67, 562, 1963
- 4 - C. LAFAGE, These 3eme cycle Lille 1985.

Kinetics of Some Gas Phase Muonium Addition Reactions  
Between 155 and 500K

D.M. Garner, M. Senba, I.D. Reid, D.G. Fleming, D.J. Arseneau, R.J. Mikula, and L. Lee, TRIUMF and the Department of Chemistry, 4004 Wesbrook Mall, Vancouver, B. C. CANADA, V6T 2A3.

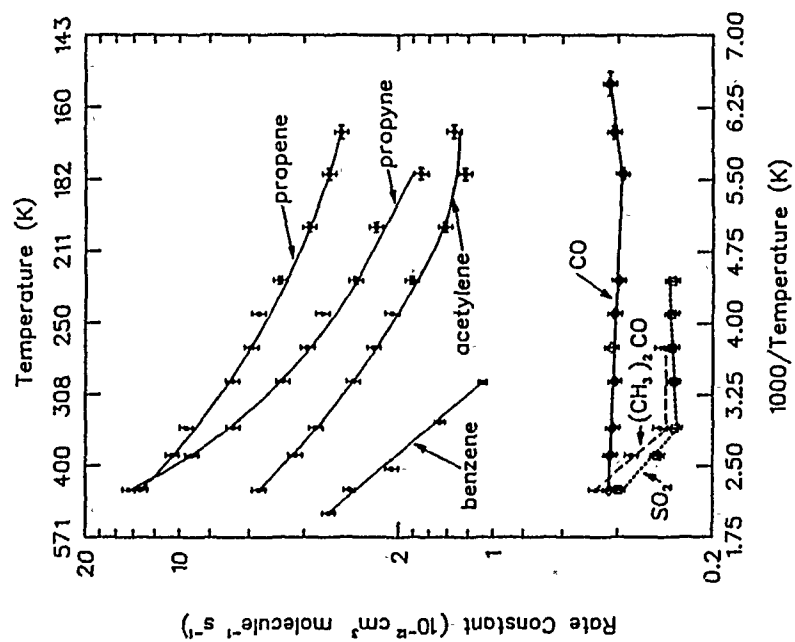
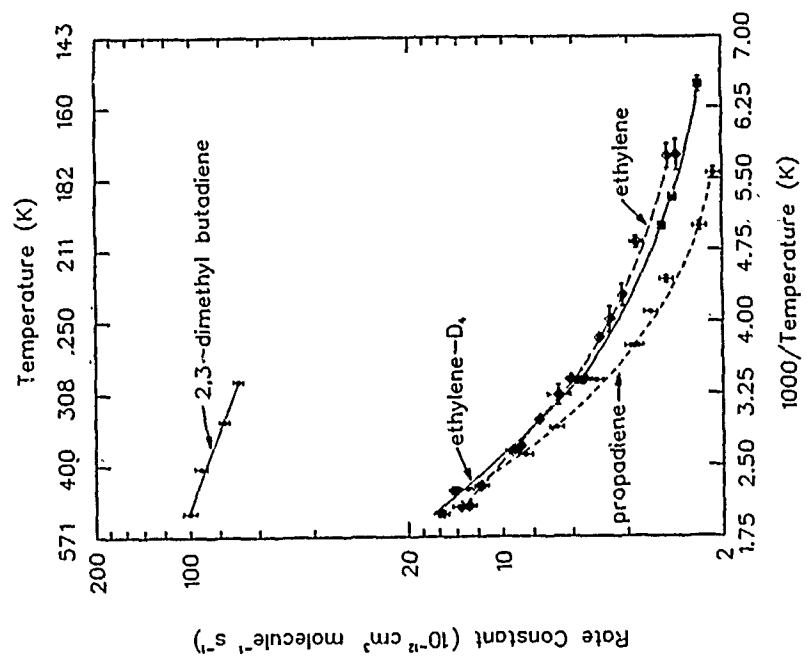
It is well established that the chemical behaviour of muonium (Mu), the neutral atom consisting of an electron bound to a positive muon, is that of a light isotope of hydrogen with an atomic mass of only 0.114 amu. We report here the bimolecular rate constants for Mu addition to ethylene, fully deuterated ethylene, propene, acetylene, propyne, allene, acetone vapour, carbon monoxide and sulfur dioxide from about 500K to 155K (or the temperature of limiting vapour pressure of the reagent in some cases). All measurements were carried out above the high pressure limit in nitrogen moderator, typically at 800 torr. No pressure dependence was detected in the rate constants at moderator pressures from 500 - 1500 torr.

The data presented in the figures are the results of preliminary analysis, except for the ethylene and ethylene-D<sub>4</sub> data which have undergone final data analysis. Final data analysis will have the effect of reducing the error bars in most cases. The lines are not fits, but are simply sketched in to guide the eye. Data for the Mu addition reactions with benzene and 2,3-dimethyl butadiene from an earlier study (Garner, Roduner, et al., unpublished) are included in the figures for comparison.

The dominant features of the data are:

1. Strong Arrhenius plot curvature in the unsaturated hydrocarbon reactions, interpreted as evidence for strong quantum tunnelling in the Mu reactions.
2. The lack of any strong secondary isotope effect in the ethylene versus fully deuterated ethylene data, consistent with the experimental data of Sugawara et al. for the analogous H atom addition reactions. However, a slight secondary isotope effect appears to be indicated with the ethylene-D4 rate constants greater than those for ethylene at high temperature probably due to the difference in vibrational partition functions; conversely, at low temperature addition to ethylene-D4 is slower than ethylene possibly due to the suppression of quantum tunnelling due an increase in reduced mass.
3. Almost perfect overlap over the whole temperature range for the rate constants for Mu addition to the isomers propyne and allene despite the naive expectation the the allene reaction would be faster due to the availability of an extra addition site and entropy considerations.
4. A negative activation energy in the CO reaction and in the low temperature acetone and SO2 reactions.
5. A strong break in the SO2 and acetone data, possibly indicative of a two component branching ratio indicative of Mu addition to O versus Mu addition to C or S.

We expect to present the results of the final data analysis at the conference.



Rate Constant Measurements for the Reactions of Ground State  
Atomic Oxygen with Tetramethylethylene,  $299\text{K} < T < 1005\text{K}$ , and  
Isobutene,  $296\text{K} < T < 1019\text{K}$

by

J. F. Smalley, R. Bruce Klemm and Fred L. Nasbitt  
Brookhaven National Laboratory  
Upton, New York 11973 (USA)

The title reactions were studied by the method of flash photolysis-resonance fluorescence. For each reaction, the photolytic source of  $\text{O}(^3\text{P})$  atoms was  $\text{O}_2$  between room temperature and  $\sim 500\text{K}$  while  $\text{NO}$  was the photolytic source of these atoms at higher temperatures.

In previous studies of the reaction of  $\text{O}(^3\text{P})$  atoms with tetramethylethylene (TME) between room temperature and  $\sim 500\text{K}$ ,<sup>1,2</sup> the rate constant was shown to decrease with increasing temperature. The results of the present study confirm this behavior. However, at the higher temperatures attained in the present study, the rate constants for this reaction first became constant between about 550 and 770K and they then began to increase at the highest temperatures (see the figure labeled TME). The curve in this figure is a fit of the bimolecular rate constant ( $k(\text{TME})$ ) data to the following sum of exponentials expression:

$$k(\text{TME}) = (1.83 \pm 0.01 \times 10^{-11} \text{ cm}^3\text{-molecule}^{-1}\text{-s}^{-1}) \exp (4.34 \pm 0.02 \times 10^2 \text{ K}/T) + \\ (1.71 \pm 0.24 \times 10^{-10} \text{ cm}^3\text{-molecule}^{-1}\text{-s}^{-1}) \exp (-2.05 \pm 0.08 \times 10^3 \text{ K}/T) \quad (1)$$

It is apparent from this figure that eq. 1 is an excellent representation of this data.

Similarly, the rate constants for the reaction of  $\text{O}(^3\text{P})$  atoms with isobutene also decrease with increasing temperature for  $T < 500\text{K}$  and increase with increasing temperature for  $T > 500\text{K}$  (see the figure labeled ISOBUTENE). The following sum of exponentials expression (see the curve in this figure) also provides an excellent

fit of the bimolecular rate constant data for isobutene:

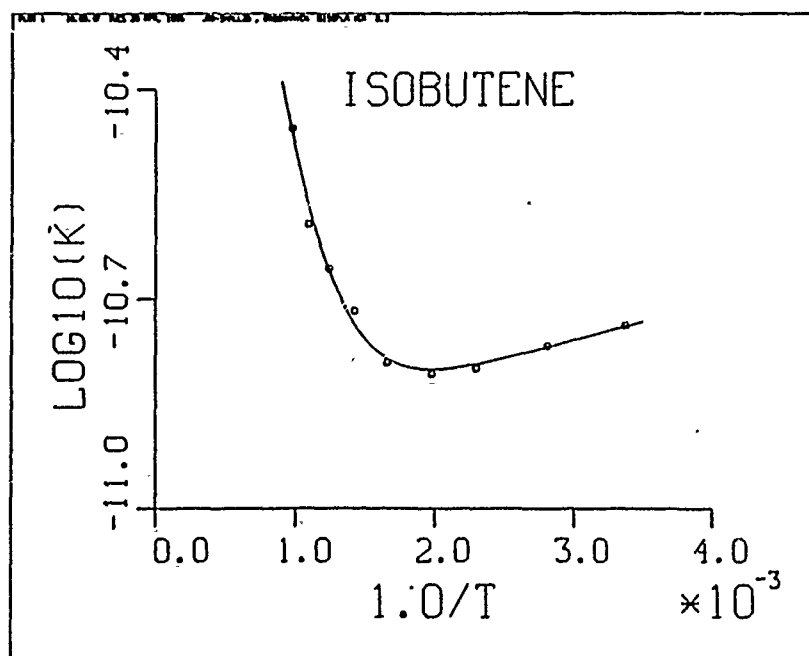
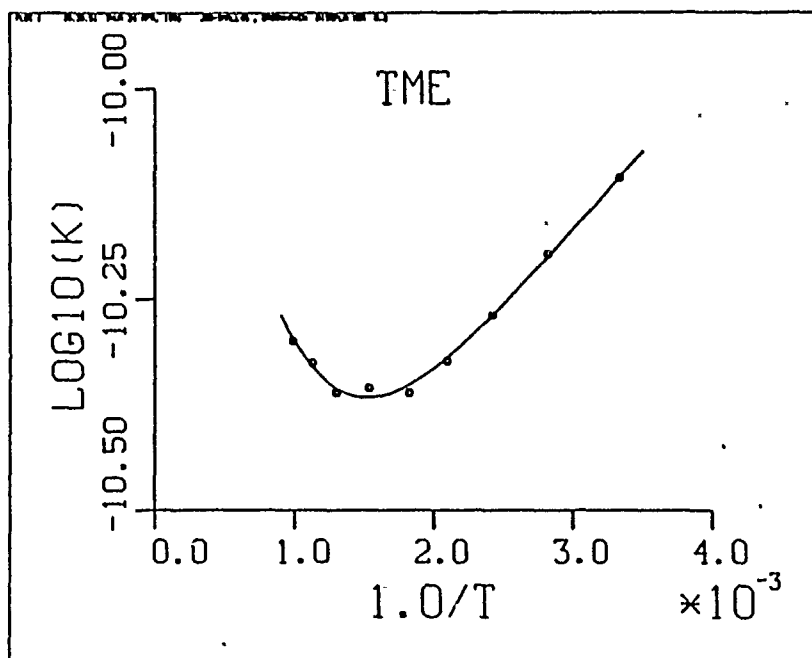
$$k(\text{Isobutene}) = (1.20 \pm 0.01 \times 10^{-11} \text{ cm}^3\text{-molecule}^{-1}\text{-s}^{-1}) \exp (1.25 \pm 0.01 \times 10^2 K/T) \\ + (8.09 \pm 1.13 \times 10^{-10} \text{ cm}^3\text{-molecule}^{-1}\text{-s}^{-1}) \exp (-3.72 \pm 0.05 \times 10^3 K/T) (2)$$

The present rate data for the title reactions will be compared to the results of previous studies. Possible reasons for the anomalous behavior of the rate constants for these reactions will be discussed.

1. Davis, D. D.; Huie, R. E.; Herron, J. T. J. Chem. Phys. 1972, 59, 628.
2. Singleton, D. L.; Furuyama, S.; Cvetanovic<sup>1</sup>, R. J.; Irwin, R. S. J. Chem. Phys. 1975; 63, 1003.

This work was supported by the Division of Chemical Sciences, U.S. Department of Energy, Washington, DC, under contract No. AC02-76CH00016.





A DISCHARGE FLOW-MASS SPECTROMETRY STUDY  
OF THE RATES OF THE REACTIONS OF  
DIACETYLENE WITH ATOMIC OXYGEN AND ATOMIC CHLORINE

M. Mitchell, J. Brunning, W. Payne and L. Stief  
ASTROCHEMISTRY BRANCH, LABORATORY FOR EXTRATERRESTRIAL PHYSICS  
NASA/GODDARD SPACE FLIGHT CENTER, GREENBELT, MD 20771, USA

The reactions of diacetylene ( $C_4H_2$ ) with atomic species are of interest for several reasons. Comparison of rate data for this molecule with the more extensive data for acetylene ( $C_2H_2$ ) may contribute to our understanding of the factors which control the kinetics of the addition of atoms to the carbon-carbon triple bond. The reactions of H and O ( $^3P$ ) with  $C_4H_2$  are important for models of the atmosphere of Titan, a satellite of the planet Jupiter, and for their roles in the combustion of acetylene.

The rate constants for the reactions  $O(^3P) + C_4H_2$  (1) and  $Cl + C_4H_2$  (2) have been determined at 298 K using a discharge flow system with collision-free sampling to a mass spectrometer.<sup>1</sup> The total pressure in the flow tube was approximately 1 Torr (He) and the flow velocity was typically  $2000 \text{ cm}^3 \text{ s}^{-1}$ . The rate constants were determined by monitoring the decay of  $C_4H_2$  in excess  $O(^3P)$  or Cl. The experiments were carried out under pseudo first-order conditions; the ratio  $[O]$  to  $[C_4H_2]$  varied from 10 to 75 while

that for  $[\text{Cl}]$  to  $[\text{C}_4\text{H}_2]$  ranged from 2 to 15. Small corrections were made to allow for depletion of the atomic species during the course of the reaction and for axial diffusion of  $\text{C}_4\text{H}_2$  in the He carrier gas. The result for  $\text{O}(^3\text{P}) + \text{C}_4\text{H}_2$  is  $k_1 = (1.49 \pm 0.17) \times 10^{-12} \text{ cm}^3 \text{ s}^{-1}$  (1  $\sigma$ ). This is in good agreement with our previous result based on the decay of  $\text{O}(^3\text{P})$  in a flash photolysis-resonance fluorescence experiment.<sup>2</sup> It is also in good agreement with the results of Niki and Weinstock,<sup>3</sup> but not with the results of Homann et al<sup>4</sup> and Homann and Wellmann<sup>5</sup> which are respectively 50% and 80% larger.

The result for  $\text{Cl} + \text{C}_4\text{H}_2$  is  $k_2 = (4.90 \pm 0.92) \times 10^{-11} \text{ cm}^3 \text{ s}^{-1}$  (1  $\sigma$ ). This study represents the first determination of  $k_2$  and the result will be compared with our results for the analogous  $\text{Cl} + \text{C}_2\text{H}_2$  reaction.<sup>6</sup> Similar comparisons will also be made for the reactions of  $\text{O}(^3\text{P})$ , H and OH with  $\text{C}_2\text{H}_2$  and  $\text{C}_4\text{H}_2$ .

The role of the reactions of  $\text{C}_4\text{H}_2$  with atomic species in the photochemistry or aeronomy of the atmosphere of Titan will be briefly discussed.

#### References

1. J. Brunning and L. J. Stief, J. Chem. Phys., **84**, 4371 (1986).
2. M. B. Mitchell, D. F. Nava and L. J. Stief, J. Chem. Phys. (submitted, 1986).

3. H. Niki and B. Weinstock, J. Chem. Phys., 45, 3468 (1966);  
errata: H. Niki, J. Chem. Phys., 47, 3102 (1967).
4. K. H. Homann, W. Schwanebeck and J. Warnatz, Ber. Bunsenges. Phys. Chem., 79, 536 (1975).
5. K. H. Homann and Ch. Wellmann, Ber. Bunsenges. Phys. Chem., 87, 527 (1983).
6. J. Brunning and L. J. Stief, J. Chem. Phys., 83, 1005 (1985).

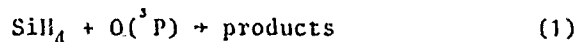
Reaction of  $O(^3P) + SiH_4$  in the Gas Phase

O. Horie<sup>a</sup>, P. Potzinger, and B. Reimann

Max-Planck-Institut für Strahlenchemie, D-4330 Mülheim/Ruhr, F.R.G.

<sup>a</sup>Present address: Max-Planck-Institut für Chemie, D-6500 Mainz, F.R.G.

Two kinetic studies<sup>1,2</sup> have been published so far for reaction (1).



However, the nature of the elementary step remains unclear. In a recent publication<sup>3</sup> we have shown that the reaction of  $(CH_3)_3SiH$  with  $O(^3P)$  proceeds via H abstraction with  $k(298\text{ K}) = (2.6 \pm 0.3) \times 10^{-12} \text{ cm}^3 \text{ s}^{-1}$ . Smaller rate constants have been measured for reaction (1), namely  $4.8 \times 10^{-13} \text{ cm}^3 \text{ s}^{-1}$  (ref.1) and  $3.3 \times 10^{-13} \text{ cm}^3 \text{ s}^{-1}$  (ref.2), although the Si-H bond dissociation energies in silane and trimethylsilane are very similar<sup>4</sup>. This suggests either that different primary processes are operating in both cases or that H abstraction by O atoms is not a direct process. A matrix isolation study<sup>5</sup> revealed that insertion of O into the Si-H bond of  $SiH_4$  is an important primary step under these conditions.

Using a discharge flow system coupled to a mass spectrometric detection system<sup>3</sup>, absolute rate constants for reaction (1) were measured and stable reaction products determined. With  $[O]_0 \gg [SiH_4]_0$  or  $[SiD_4]_0$  (at least 70 fold excess), the silane decay was exponential, yielding

$$k(O+SiH_4) = (2.1 \pm 0.4) \times 10^{-13} \text{ cm}^3 \text{ s}^{-1},$$

$$k(O+SiD_4) = (7.4 \pm 0.4) \times 10^{-14} \text{ cm}^3 \text{ s}^{-1}.$$

$\text{H}_2$ ,  $\text{Si}_2\text{H}_6$ , and  $\text{H}_2\text{O}$  were detected as stable reaction products. When the silane concentration was raised such that  $[\text{O}]/[\text{SiH}_4]_0 \leq 50$ , the system became increasingly complex. Non-exponential silane decays and O atom consumptions of up to 20 atoms per  $\text{SiH}_4$  molecule were observed.

In static experiments using mercury sensitized  $\text{N}_2\text{O}$  photolysis as a source of atomic oxygen the same products as in the flow system were found.  $\text{H}_2$  formation could be completely suppressed upon adding NO.

Of the three most likely primary processes



(1c) can be dismissed owing to the fact that  $\text{H}_2$  formation is apparently a secondary reaction. A detailed analysis shows that most experimental results can be explained by (1a); the  $\text{Si}_2\text{H}_6$  yield suggests that step (1b) contributes a maximum of 15% to the overall reaction.

The large isotope effect and the fact that the rate constant decreases from  $(\text{CH}_3)_3\text{SiH}$  to  $\text{SiH}_4$  both suggest that (1a) is not a direct abstraction reaction but proceeds rather via a complex,  $[\text{SiH}_4\text{O}]$ , that subsequently decomposes into  $\text{OH} + \text{SiH}_3$ , to a minor extent into  $\text{H}_2\text{O} + \text{SiH}_2$ , and back to  $\text{O} + \text{SiH}_4$ .

### References

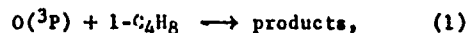
- 1) Atkinson, R.; Pitts, Jr., J.N.;  
Int. J. Chem. Kinet. 1978, 10, 1151
- 2) Mkrian, T.G.; Sarkissian, E.N.; Arutyunian, S.A.;  
Arm. Khim. Zh. 1981, 34, 3
- 3) Hoffmeyer, H.; Morie, O.; Potzinger, P.; Reimann, B.;  
J. Phys. Chem. 1985, 89, 3261
- 4) Walsh, R.;  
Acc. Chem. Res. 1981, 14, 246
- 5) Withnall, R.; Andrews, L.;  
J. Phys. Chem., 1985, 89, 3261

Rate Constant for the Reaction of  $O(^3P)$  with 1-Butene;  
 $300 < T < 900K$

by

R. Bruce Klemm, Fred L. Nesbitt and John F. Smalley  
 Brookhaven National Laboratory  
 Upton, New York 11973 (USA)

The kinetics of the elementary reaction of ground state atomic oxygen with 1-butene,



was studied using both the discharge flow-resonance fluorescence (DF-RF) method and the flash photolysis-resonance fluorescence (FP-RF) method. The FP-RF investigation was quite extensive and covered the entire temperature range from 298K to 875K. The photolytic source of  $O(^3P)$  atoms in the FP-RF experiments was  $O_2$  at temperatures between ambient and  $\sim 500K$ ; at temperatures above 500K, NO was utilized.<sup>1</sup> DF-RF experiments were performed at only two temperatures, 294K and 453K. In the range of temperature overlap, the DF-RF results are in reasonably good agreement with those from the FP-RF study although they are consistently lower by about 10-20%.

This study has attained the highest temperature to date for measuring the rate constant,  $k_1(T)$ , for reaction (1). The previous observation that  $k_1(T)$  increases very gradually with temperature and displays definite non-Arrhenius behavior was confirmed in the present study as is shown in the figure. The combined data from eight FP-RF sets and two DF-RF sets were fitted to a sum of exponentials expression to yield:

$$k_1(T) = (1.31 \pm 0.07) \times 10^{-11} \exp(-359 \pm 20/T) \\ + (5.98 \pm 0.29) \times 10^{-10} \exp(-3618 \pm 43/T),$$

where the units are  $\text{cm}^3 \text{ molecule}^{-1} \text{ s}^{-1}$  and the exponential term is in degrees Kelvin. This expression is represented in the figure as a solid line. It is

noted that the highest temperature point, at 942K, is above the extrapolation of this expression. This result remains uncertain even though the operating parameters of flash energy, premixture flow rate, total pressure and isobutene concentration were all varied extensively. Finally, over the common temperature range (298-821K), the agreement of the present results with those reported by Perry<sup>2</sup> is remarkable.

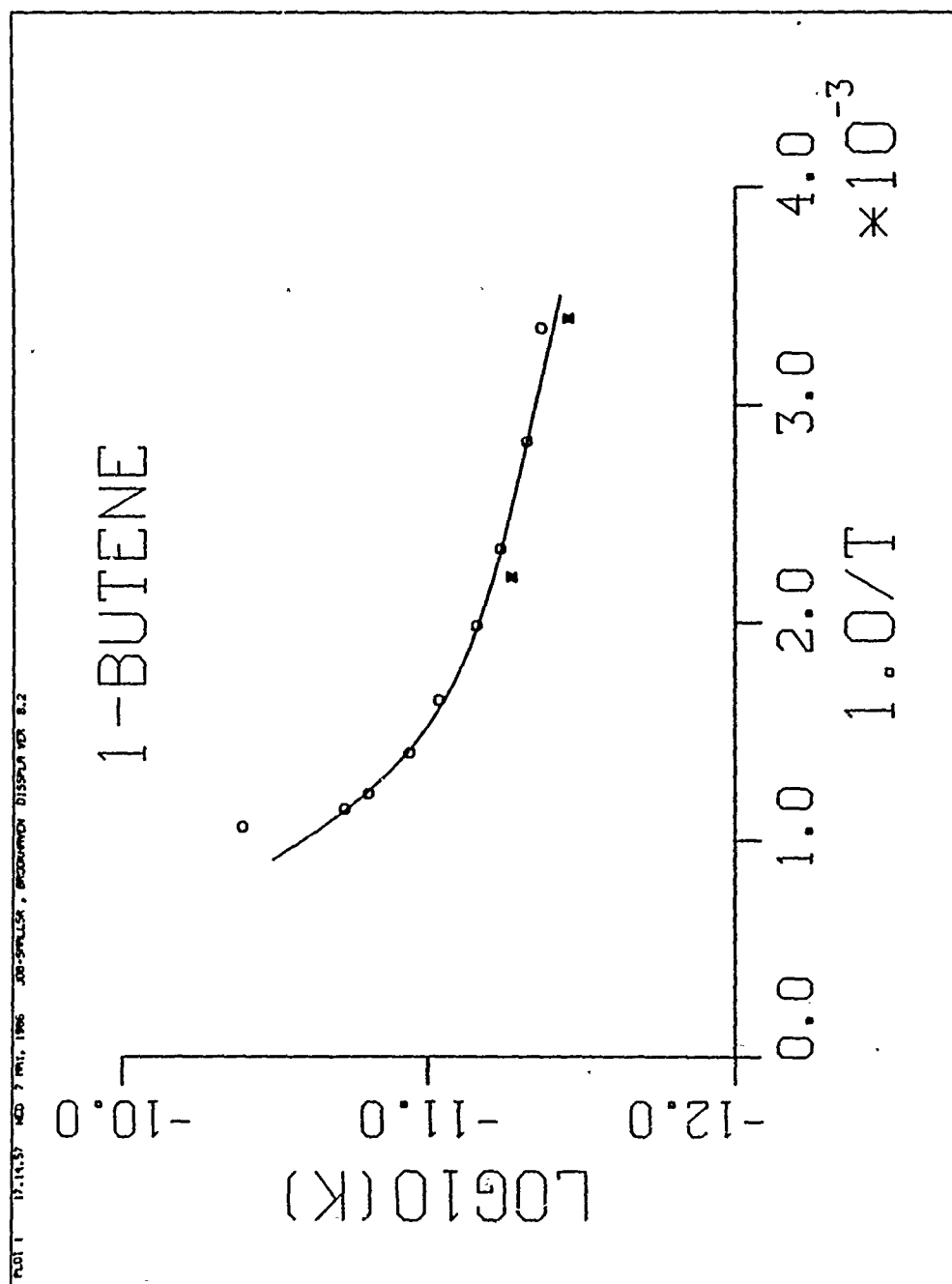
The present kinetic data for reaction (1) are thoroughly compared with previous results and the temperature dependence of  $k_1(T)$  is contrasted to the rate constant for the reaction of  $O(^3P)$  with ethylene.

#### References

1. H. H. Grotheer, F. L. Nesbitt and R. B. Klemm, J. Phys. Chem. 90, 2512 (1986).
2. R. A. Perry, private communication.

This work was supported by the Division of Chemical Sciences, U.S. Department of Energy, Washington, DC, under contract No. AC02-76CH00016.



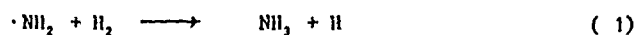


Direct Measurements of the Reactions  $\text{NH}_2 + \text{H}_2 \rightleftharpoons \text{NH}_3 + \text{H}$   
at Temperatures from 670 to 1000 K

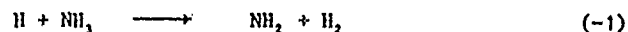
W. Hack and P. Rouveirolles

Max-Planck-Institut für Strömungsforschung  
Bunsenstr. 10, D-3400 Göttingen / West Germany

The  $\text{NH}_2$  radical reactions and the H atom reactions at high temperatures are both of theoretical and applied interest in the chemistry of ammonia combustion.<sup>(1)</sup> The knowledge of the Arrhenius parameters of the reaction



and the reverse reaction



enables a direct determination of the  $\text{H}_2\text{N-H}$  bond energy in  $\text{NH}_3$ .

The rates of the reaction (1) and (-1) were measured independently in a discharge flow system.  $k_1(T)$  and  $k_{-1}(T)$  were obtained in the temperature range  $673 \leq T/K \leq 1003$  at a pressure of  $p=4\text{mbar}$ . The main carrier gas was Helium. The surface of the quartz reactor was heated via two coaxial silver cylinders. The  $\text{NH}_2$  radicals were produced in the fast reaction  $\text{F} + \text{NH}_3 \rightarrow \text{NH}_2 + \text{HF}$ , where the H atoms were obtained in a discharge of  $\text{H}_2/\text{He}$  mixture. Pseudo-first order conditions  $[\text{H}_2]_0 \gg [\text{NH}_2]_0$  and  $[\text{NH}_3]_0 \gg [\text{H}]_0$  were applied; the  $[\text{NH}_2]$  radical profiles were measured with laser-induced fluorescence and the  $[\text{H}]$  atom profiles were followed by Lyman  $\alpha$ -absorption.

Gases with highest commercially available purity were used, where  $\text{F}_2$  and  $\text{H}_2$  were further purified by liquid  $\text{N}_2$  and/or without NaF traps, respectively.

The first-order rate constants were obtained from the slopes  $\Delta(\ln[\text{NH}_2])/[\text{NH}_2]_0/\Delta t$  and  $\Delta \ln[\text{H}]/[\text{H}]_0/\Delta t$ , respectively. The heterogeneous reactions ( $k_w(\text{NH}_2)$ ,  $k_w(\text{H})$ ), which determine the  $\text{NH}_2$  and H depletion in the absence of reactant, were followed independently for all experimental conditions.

At the experimental conditions ( $6 \cdot 10^2 \leq [\text{H}_2]_0 / [\text{NH}_3]_0 \leq 15 \cdot 10^3$ ) and ( $2.6 \cdot 10^3 \leq [\text{NH}_3]_0 / [\text{H}]_0 \leq 22 \cdot 10^3$ ) the stoichiometric factors were found to be close to unity, although  $\text{NH}_3$  and  $\text{H}_2$  were present in the system from the  $\text{NH}_3$  and  $\text{H}$  atom source, respectively.

The measurements for reaction (1) were done at 13 different temperatures. The temperature dependence of the rate constant obeyed an Arrhenius behaviour. The Arrhenius parameters:

$$k_1(T) = 3.6 \cdot 10^{12} \exp\{-(38 \pm 3) \text{ kJ mol}^{-1}/RT\} \text{ cm}^3 \text{ mol}^{-1} \text{ s}^{-1}$$

were deduced from least squares treatments of the bimolecular rate constants, obtained from the plots of the first order rate constants against the reactant concentrations for each temperature, corrected with the stoichiometric factors.

The rate of reaction (-1) was measured at 7 different temperatures in the temperature range  $673 \leq T/\text{K} \leq 1003$ . The following Arrhenius expression:

$$k_{-1}(T) = 8.1 \cdot 10^{13} \exp\{-(60.9 \pm 4) \text{ kJ mol}^{-1}/RT\} \text{ cm}^3 \text{ mol}^{-1} \text{ s}^{-1}$$

was obtained with the procedure, described above. No curvature was observed in the Arrhenius plot  $k_{-1}(T)$  versus  $1/T$ .

The Arrhenius expressions  $k_1(T)$  and  $k_{-1}(T)$ , obtained in this study, are in fair agreement with earlier determinations by DEMISSY and LESCLAUX<sup>2)</sup> and MICHAEL et al.,<sup>3)</sup> respectively.

The bond energy  $D(\text{H}_2\text{N-H})$  has been determined either from the measured activation energies  $E_{A1}$  and  $E_{A-1}$  via:

$$\Delta H^\circ(T_{\text{mean}}) = E_{A1} - E_{A-1} = D_{T_{\text{mean}}}(\text{H-H}) - D_{T_{\text{mean}}}(\text{H}_2\text{N-H}),$$

where  $\Delta H^\circ(T_{\text{mean}})$  is the enthalpy of the reaction at a mean temperature  $T_{\text{mean}}$ , and  $D_T(\text{H-H})$  and  $D_T(\text{H}_2\text{N-H})$  are the dissociation energies at that temperature, or via the equilibrium constant  $K_p(T)$ :

$$-RT \ln K_p(T) = \Delta H^\circ(T) - T\Delta S^\circ(T) = D_T(\text{H-H}) - D_T(\text{H}_2\text{N-H}).$$

Both methods give as a result:

$$D_{298\text{K}}(\text{H}_2\text{N-H}) = 455 \text{ kJ mol}^{-1}$$

and the enthalpy of formation of  $\text{NH}_2$  :

$$\Delta H_{f\text{NH}_2} (298\text{K}) = 192 \text{ kJ mol}^{-1} .$$

The bond dissociation energy  $D_{298\text{K}}(\text{H}_2\text{N-H})$  lies at the limit of the data, reported in the literature and supports the recommendation of BENSON.<sup>4)</sup>

- 1) R. Lesclaux: Reviews of Chemical Intermediates, 5, 347 (1984).
- 2) M. Demissy and R. Lesclaux: J.Am.Chem.Soc., 102, 2897 (1980).
- 3) J.V. Michael, J.W. Sutherland, and R.B. Klemm: J.Phys.Chem. 90, 497 (1986).
- 4) S.W. Benson: "Thermochemical Kinetics" 2<sup>nd</sup> Ed. A. Wiley-Interscience Publication, 1976.

Laser Studies of Gallium Atom Reaction Kinetics. S.A. Mitchell,  
P.A. Hackett, D.M. Rayner, and M. Cantin. Laser Chemistry Group,  
Division of Chemistry, National Research Council Canada, 100 Sussex  
Drive, Ottawa, Ontario K1A 0R6 Canada

Ground state  $\text{Ga}(4p^1\ ^2P_{1/2})$  atoms are produced by visible multiphoton dissociation of trimethylgallium and monitored by resonance fluorescence excitation in a pump and probe arrangement. The time dependence of the Ga concentration is observed by scanning the delay time between the pump and probe dye laser pulses. Reactions with  $\text{CF}_3\text{X}$  ( $\text{X} = \text{F}, \text{Cl}, \text{Br}, \text{I}$ ),  $\text{SF}_6$ ,  $\text{C}_2\text{F}_4$ ,  $\text{N}_2\text{O}$ ,  $\text{C}_2\text{H}_2$ ,  $\text{C}_2\text{H}_4$ , 1- $\text{C}_4\text{H}_8$  (1-butene), and  $\text{Ga}(\text{CH}_3)_3$  are studied under pseudo first-order conditions in a gas cell at room temperature. In most but not all cases an equilibrium is preserved between ground state  $\text{Ga}(4\ ^2P_{1/2})$  and metastable  $\text{Ga}(4\ ^2P_{3/2})$  (excitation energy  $826\text{ cm}^{-1}$ ) atoms. Abstraction and association reactions are observed and characterized with respect to Ar buffer gas pressure dependence.

For several of the association reactions an equilibration is observed between free Ga atoms and Ga atoms bound in complexes with the reactant molecules. A simple kinetic analysis is used to evaluate equilibrium constants from series of Ga decay traces at different pressures of reactant. From these equilibrium constants and estimated partition functions, approximate gallium atom binding energies ( $\text{kcal}\cdot\text{mol}^{-1}$ ) are obtained for  $\text{C}_2\text{H}_4$  ( $9\pm2$ ), 1- $\text{C}_4\text{H}_8$  ( $9\pm2$ ), and  $\text{Ga}(\text{CH}_3)_3$  ( $14\pm2$ ). Bimolecular and termolecular rate constants will be reported and discussed in relation to reaction products and mechanisms.

## REACTION KINETICS OF GAS-PHASE BORON ATOMS AND BORON MONOXIDE WITH OXYGEN

Richard C. Oldenborg and Steven L. Baughcum. Chemistry Division, Los Alamos National Laboratory, Los Alamos, NM 87545

The volatile boron-containing compound,  $\text{BCl}_3$ , is photolyzed in a multiple-photon process using a rare gas-halide excimer laser operating at 193 nm (ArF) to provide an essentially instantaneous source of boron atoms. The boron atoms are produced in a reactive environment containing a known concentration of  $\text{O}_2$  in an excess of argon diluent and at a controlled temperature (298 to 1300 K). The rate of oxidation of the atomic boron to  $\text{BO}$ ,



and the subsequent oxidation of  $\text{BO}$ ,



are studied by examining the temporal histories of the boron-containing species ( $\text{B}$ ,  $\text{BO}$ , and  $\text{BO}_2$ ) using laser-induced fluorescence (LIF) and chemiluminescent techniques.

The depletion of  $\text{B}$  atoms under our experimental conditions is due primarily to two reactions, namely Reaction (1) with  $\text{O}_2$  and the reaction with undissociated  $\text{BCl}_3$  precursor molecules,



The rate constant  $k_1$  is obtained from the slope of plots of the B atom decay rate vs  $O_2$  pressure and has been measured over the 298-1180 K range. No change in this rate constant is observed with variation in the Ar diluent pressure from 2.5 to 200 torr. The rate constant is large over the entire temperature range, and increases slightly at elevated temperatures. The data have been fit to both an Arrhenius expression and a  $T^n$ -type function. The results are, respectively,

$$k_1(T) = (1.19 \pm 0.04) \times 10^{-10} \exp(-158 \pm 13/T) \text{ cm}^3 \text{ molecule}^{-1} \text{ s}^{-1}$$

and

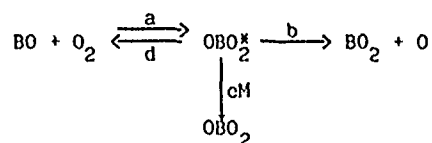
$$k_1(T) = (1.00 \pm 0.02) \times 10^{-10} (T/1000)^{0.29 \pm 0.02} \text{ cm}^3 \text{ molecule}^{-1} \text{ s}^{-1}$$

Neither form is obviously a better representation of the data. The temperature dependence of this rate constant is consistent with the results of Fontijn, Felder, and Houghton for the analogous  $Al + O_2$  reaction.

By studying the depletion of the atomic B in the absence of  $O_2$  as a function of  $BCl_3$  concentration, we obtain a room-temperature rate constant  $k_3(298 \text{ K}) = (8.5 \pm 0.9) \times 10^{-11} \text{ cm}^3 \text{ molecule}^{-1} \text{ s}^{-1}$ . To our knowledge, no previous measurements of this rate constant exist.

The depletion of BO under our experimental conditions appears to be entirely due to the reaction with  $O_2$ . In contrast to the B removal data, a dramatic change in this rate constant is observed with changes in diluent pressure. The rate constant increases rapidly with Ar pressure at low pressures, but is essentially independent of diluent pressure above 25 torr. The limiting value at high pressures is  $(2.4 \pm 0.2) \times 10^{-11} \text{ cm}^3 \text{ molecule}^{-1} \text{ s}^{-1}$ . This pressure dependence is clearly inconsistent with the simple direct atom-transfer reaction mechanism between BO and  $O_2$ . Rather, it suggests that this

This pressure dependence is clearly inconsistent with the simple direct atom-transfer reaction mechanism between BO and O<sub>2</sub>. Rather, it suggests that this is not a simple elementary reaction and may involve a stable intermediate. Our SCF/CI molecular orbital calculations show that an OBO<sub>2</sub> intermediate complex has a potential energy relative to reactants of -57 kcal/mole. This suggests a reaction mechanism analogous to that proposed for the OH + CO reaction, where collisions can stabilize the energized HOCO\* intermediate making the overall rate constant pressure dependent. Expanding Reaction (2) in this way yields,



The pressure dependent data are well fit by this expanded model, and the resulting fit parameters imply that the stabilized  $\text{OBO}_2$  is the primary product of the B0 reaction with  $\text{O}_2$  at all Ar pressures employed in our experiments (2.5-250 torr).

The temperature dependence of the BO removal rate constant by  $O_2$  at high diluent pressures ( $Ar \geq 8 \times 10^{17}$  molecules/cc) has also been investigated in the 298-1180 K range. The rate constant shows non-Arrhenius behavior and decreases with increasing temperature, which is consistent with a termolecular reaction to form a  $BOO_2$  product. The data is best fit by a  $T^{-n}$  - type function with a small activation barrier in the entrance channel.

$$k_2(T) = (1.7 \pm 0.4) \times 10^{-11} (T/1000)^{-2.23 \pm 0.5} \exp(-716 \pm 288/T) \text{ cm}^3 \text{ molecule}^{-1} \text{ s}^{-1}.$$



## PULSED LASER PHOTOLYSIS STUDY OF THE O+ClO REACTION

J. M. Nicovich, P. H. Wine, and A. R. Ravishankara\*,  
Molecular Sciences Branch, Georgia Tech Research Institute,  
Georgia Institute of Technology, Atlanta, GA 30332

\*Present address: Aeronomy Laboratory, NOAA-R/E/AL2,  
325 Broadway, Boulder, CO 80303

Recently, we reported on the development of a pulsed laser photolysis technique for studying the kinetics of radical-radical reactions at pressures up to one atmosphere and application of the technique to the O + HO<sub>2</sub> reaction [A. R. Ravishankara, P. H. Wine, and J. M. Nicovich, J. Chem. Phys. **78**, 6629 (1983)]. We have employed an extension of the same approach to investigate the temperature and pressure dependence of k<sub>1</sub>.



A Cl<sub>2</sub>/O<sub>3</sub> mixture was photolyzed at 351 nm (XeF laser) to produce Cl atoms in excess over O<sub>3</sub>. After allowing sufficient time for reaction (2) to ~~titrate~~ O<sub>3</sub> to ClO, a small fraction (typically 3%) of the ClO was photolyzed at 266 nm to produce O(<sup>3</sup>P). The decay of O(<sup>3</sup>P) in the presence of (a known concentration of) ClO was followed by time resolved resonance fluorescence spectroscopy. Two important aspects of the experimental approach are 1) small spatial non-uniformities in the 351 nm laser beam have no effect on the ClO concentration (as long as Cl atoms are in excess) and 2) the O(<sup>3</sup>P) signal strength immediately after the 266 nm laser fires can be related to the ClO concentration.

Our results are summarized in Table I. Reported rate constants were obtained from the slopes of plots of pseudo-first order O(<sup>3</sup>P) decay rate (k') versus ClO concentration. Each reported rate constant determination involved the measurement of 5-8 O(<sup>3</sup>P) temporal profiles. Within experimental uncertainty, exponential O(<sup>3</sup>P) decays and linear dependencies of k' on [ClO] were observed under all experimental conditions although, as discussed below, small systematic deviations from exponential

behavior and linear  $k'$  versus  $[ClO]$  behavior were expected, and were accounted for in the data analysis.

The "uncorrected" rate constants in Table I were obtained using measured pseudo-first order rate constants and  $ClO$  concentrations determined from the relationship

$$[ClO] = [O_3]_0(1-x) \quad (2)$$

where  $x$  is the fraction of  $ClO$  photolyzed by the 266 nm laser and  $[O_3]_0$  is the ozone concentration before the XeF laser fired. To obtain the "corrected" rate constants in Table I,  $k'$  values were corrected for slight deviations from strict pseudo-first order behavior (these corrections seldom exceeded 1%) and  $ClO$  concentrations were corrected for loss of  $ClO$  during the time period between  $ClO$  formation and the 266 nm laser pulse.  $ClO$  loss was observed to be second order and, therefore, due to the  $ClO + ClO$  reaction.  $ClO$  removal was investigated by monitoring the dependence of fluorescence signal intensity and  $k'$  on the time delay between the two lasers. For  $P \leq 50$  Torr and  $T \geq 298K$ , very little  $ClO$  loss occurred on the time scale of our experiments. However, at lower temperatures and higher pressures  $ClO$  removal became much more rapid and rather large corrections to the  $ClO$  concentration obtained from equation (2) were required.

Our results show that  $k_1$  is independent of pressure but increases with decreasing temperature. A weighted linear least squares analysis of the  $\ln k_1$  versus  $1/T$  data gives the Arrhenius expression  $k_1(T) = (1.61 \pm 0.33) \times 10^{-11} \exp[(255 \pm 60)/T]$   $cm^3 molecule^{-1} s^{-1}$ . This expression gives a value of  $3.79 \times 10^{-11} cm^3 molecule^{-1} s^{-1}$  for  $k_1(298K)$ , in good agreement with the four recent discharge flow studies. However, our results suggest that, at stratospheric temperatures, chlorine catalyzed ozone destruction may be somewhat more efficient than previously thought.

This work was supported by The Fluorocarbon Program Panel of the Chemical Manufacturers Association.

TABLE I: Summary of  $k_1$  determinations. (a)

Temperature (K)	Pressure (Torr)	$k_1 \times 10^{11}$ (uncorrected) (cc molecule <sup>-1</sup> s <sup>-1</sup> )	$k_1 \times 10^{11}$ (corrected) (cc molecule <sup>-1</sup> s <sup>-1</sup> )
231	25	4.64 $\pm$ 0.16	4.99 $\pm$ 0.17
238	25	4.25 $\pm$ 0.43	4.47 $\pm$ 0.43
252	200	3.10 $\pm$ 0.22	3.72 $\pm$ 0.24
255	25	4.15 $\pm$ 0.20	4.42 $\pm$ 0.20
255	200	3.25 $\pm$ 0.20	3.76 $\pm$ 0.28
257	25	3.86 $\pm$ 0.15	4.10 $\pm$ 0.11
257	25	4.30 $\pm$ 0.15	4.47 $\pm$ 0.19
275	25	3.94 $\pm$ 0.17	4.10 $\pm$ 0.16
298	15	3.73 $\pm$ 0.28	3.79 $\pm$ 0.27
298	15	4.17 $\pm$ 0.10	4.31 $\pm$ 0.12
298	25	3.55 $\pm$ 0.21	3.61 $\pm$ 0.21
298	25	3.47 $\pm$ 0.25	3.59 $\pm$ 0.25
298	25	3.51 $\pm$ 0.14	3.62 $\pm$ 0.13
298	25	3.87 $\pm$ 0.36	3.93 $\pm$ 0.36
298	25	3.89 $\pm$ 0.15	4.07 $\pm$ 0.17
298	50	3.91 $\pm$ 0.23	4.06 $\pm$ 0.24
298	50	3.62 $\pm$ 0.15	3.90 $\pm$ 0.11
298	50	3.70 $\pm$ 0.12	3.89 $\pm$ 0.11
298	50	3.53 $\pm$ 0.19	3.74 $\pm$ 0.14
298	50	3.76 $\pm$ 0.16	3.97 $\pm$ 0.14
298	100	3.73 $\pm$ 0.68	3.95 $\pm$ 0.67
298	200	3.39 $\pm$ 0.27	3.62 $\pm$ 0.24
298	200	3.39 $\pm$ 0.28	3.62 $\pm$ 0.31
298	200	3.55 $\pm$ 0.12	3.72 $\pm$ 0.13
298	500	3.18 $\pm$ 0.16	3.80 $\pm$ 0.12
338	25	3.16 $\pm$ 0.60	3.26 $\pm$ 0.12
359	200	2.99 $\pm$ 0.14	3.09 $\pm$ 0.15
360	25	2.89 $\pm$ 0.13	2.96 $\pm$ 0.12
367	25	3.35 $\pm$ 0.13	3.44 $\pm$ 0.13

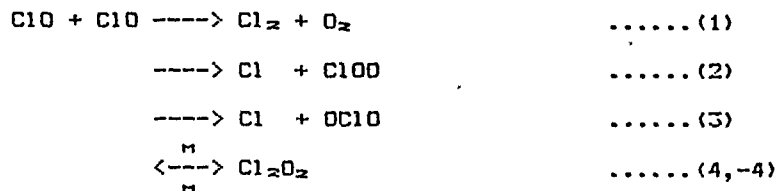
(a) Errors are  $2\sigma$  and represent precision only.

"The kinetics of ClO decay and spectroscopy of species formed."

R.A.Cox, J.M.Davies and G.D.Hayman  
Environmental and Medical Sciences Division,  
A.E.R.E. Harwell,  
Oxon., OX11 0RA.  
England.

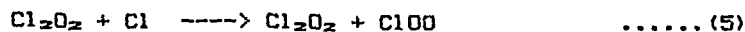
The role of ClO in the catalysis of O<sub>3</sub> decomposition in the stratosphere has been recognised since 1974 and the rate constants for the reactions involved in the ClO<sub>x</sub> catalytic cycle have been determined with good precision. In the present day stratosphere, the catalytic efficiency of the ClO<sub>x</sub> cycle has been reduced due to the coupling with the NO<sub>x</sub> chemistry. In a possible future 'high chlorine scenario', the concentration of chlorine containing species will be higher and many reactions of minor significance now may become important.

Despite the wealth of data available on the reactions of ClO, there is considerable uncertainty in the rate constants for its bimolecular and termolecular self-reactions (1-4). This program was undertaken to remove some of the uncertainty.



The kinetic experiments were performed by using a molecular modulation technique. ClO was produced by photolysis of Cl<sub>2</sub> in mixtures either with O<sub>2</sub> or with O<sub>2</sub> and N<sub>2</sub>. Total pressures from 2 to 760 torr were used at given temperatures in the range 268 to 338 K. The formation and decay of the ClO radical were followed by monitoring its ultraviolet absorption at 277.2 nm, corresponding to the 11-0 vibrational band of the A-X electronic transition.

On photolysis of Cl<sub>2</sub>, ClO was produced and reached a steady state concentration when its production and decay rates were equal. When the photolysis ceased, the ClO radicals decayed, but at a slower rate. In both cases, the decays were second order with respect to ClO. In the 'light-on' phase of the modulation cycle, there was a high concentration of Cl atoms present which scavenged Cl<sub>2</sub>O<sub>2</sub> very efficiently through reaction (5). When the photolysis



stopped, the Cl atom concentration dropped rapidly so that the back thermal decomposition reaction (-4) of the dimer became significant, leading to a slower net removal of ClO.

The observed bimolecular rate constants for the decay of ClO were plotted as a function of pressure at a fixed temperature as shown in figure 1. At low total pressures, the plots are linear. Due to the complication introduced by reaction (-4) in the 'light-off' period, the analysis concentrated on the rate constants governing the rise to and establishment of the steady state. The temperature dependences of the slope and intercept obtained from 'light-on' decays yielded the following expressions.

$$k_{\text{slope}} = (2.1 \times 10^{-10}) \times 10^{-32} \exp[(312 \pm 215)/T] \text{ cm}^6 \text{ molecule}^{-2} \text{ s}^{-1}$$

$$k_{\text{intercept}} = (1.4 \times 10^{-12}) \exp[(-1644 \pm 400)/T] \text{ cm}^3 \text{ molecule}^{-1} \text{ s}^{-1}$$

The slope of the plots of the observed rate constant versus the total pressure can be tentatively assigned to the termolecular rate constant,  $k_4$ . The zero pressure intercept is the sum of the rate constants for the effective bimolecular reactions removing ClO.

Complementary to the kinetic experiments, spectroscopic studies were undertaken in an attempt to record the ultraviolet absorption spectrum of Cl<sub>2</sub>O<sub>2</sub>.

The apparatus used in the kinetic experiments was modified to allow mixtures to flow through the reaction vessel. Ultraviolet absorption spectra were recorded using a diode array camera which allowed intensities in the wavelength range from 220 to 300 nm to be sampled simultaneously. Three systems were chosen for study.

- (1) Cl<sub>2</sub> / O<sub>3</sub> (O<sub>2</sub>) / N<sub>2</sub>
- (2) Cl<sub>2</sub>O / Cl<sub>2</sub> / N<sub>2</sub>
- (3) OCIO / N<sub>2</sub>

In each case, the differences in absorption with and without photolysis were obtained. After correction for the characteristic absorptions due to O<sub>3</sub>, OCIO etc and the ClO produced by photolysis, a residual absorption was seen in all three systems (Figure 2). The absorption, which became stronger as the temperature was reduced, is similar to ClOO, but is shifted some 10 nm to the blue. The most conclusive evidence for assigning the spectrum to Cl<sub>2</sub>O<sub>2</sub> was the dependence of the absorption on the square of the [ClO]. In the three systems used, the Cl atom concentration was kept low by the presence of an efficient scavenger (O<sub>3</sub>, Cl<sub>2</sub>O<sub>2</sub> or OCIO). This allowed the equilibrium between ClO and Cl<sub>2</sub>O<sub>2</sub> to become established and for high concentrations of the dimer to be produced in contrast to the kinetic experiments.

Current and future work will concentrate on quantifying the absorption spectrum to obtain cross-sections for the dimer in this wavelength region.

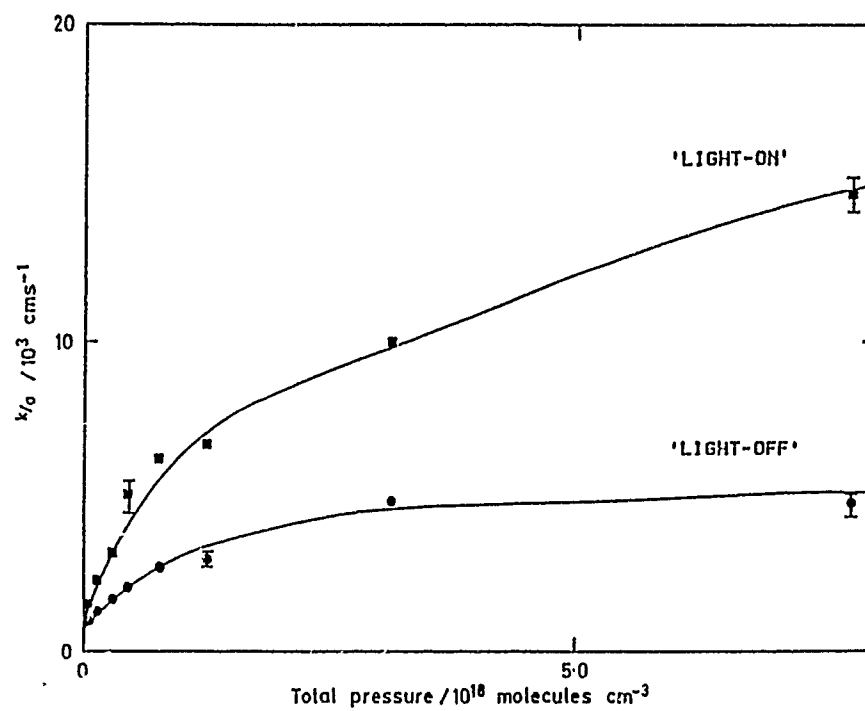


FIGURE 1 - PRESSURE DEPENDENCE OF THE OBSERVED BINOLECULAR RATE CONSTANTS AT 308K

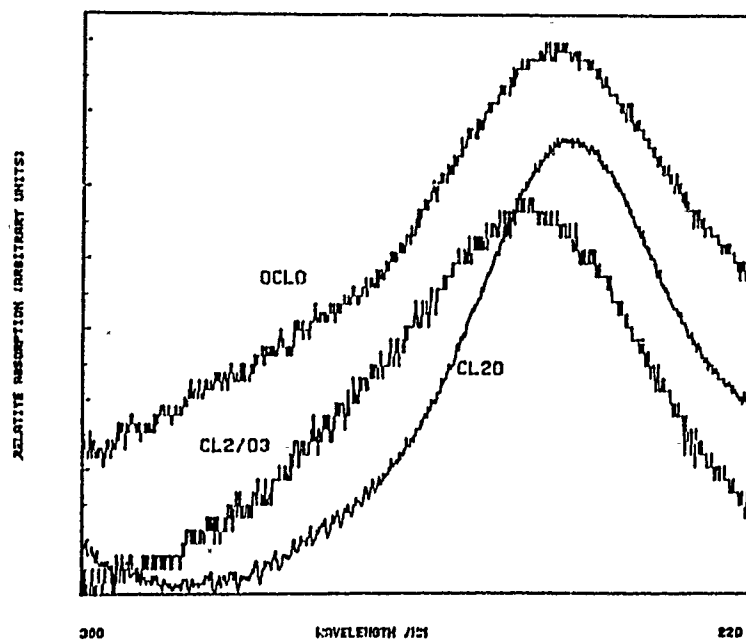


FIGURE 2 - RESIDUAL ABSORPTIONS FROM THE THREE SYSTEMS AT 263K

KINETIC STUDY OF THE REACTIONS OF  $\text{N}_2\text{O}_5$   
WITH OH,  $\text{HO}_2$ , Cl and ClO

A. Mellouki, G. Poulet and G. Le Bras

Centre de Recherches sur la Chimie de la Combustion  
et des Hautes Températures

C.N.R.S.

45071 Orléans Cedex 2 - France

Recently,  $\text{N}_2\text{O}_5$  has been detected in the stratosphere (1) at concentrations fully consistent with model predictions (2). If the thermal dissociation of  $\text{N}_2\text{O}_5$  is the main tropospheric fate of  $\text{N}_2\text{O}_5$  in day-time, in the stratosphere where the  $\text{N}_2\text{O}_5$  photolysis is an important process, the reactions of free radicals with  $\text{N}_2\text{O}_5$  could also play a role. Speculative calculations (3) have shown that, except for the Cl +  $\text{N}_2\text{O}_5$  reaction, the other title reactions could contribute to  $\text{NO}_x$  chemistry if their rate constants were higher than  $10^{-13} \text{ cm}^3 \text{ molecule}^{-1} \text{ s}^{-1}$ .

The present study was performed using the discharge-flow method.  $\text{N}_2\text{O}_5$ , prepared from the reaction of NO with  $\text{O}_3$  (4) was used in high excess (up to  $4 \times 10^{15} \text{ molecules cm}^{-3}$ ) over the free radical concentrations. All measurements were done in helium carrier at room temperature and at low pressure (between 0.8 and 2.6 Torr) in a halocarbon wax coated reactor. Free radicals were detected by E.P.R.,  $\text{NO}_2$ , resulting from the slow decomposition of  $\text{N}_2\text{O}_5$  (1 to 10% of  $\text{N}_2\text{O}_5$ ), was also calibrated by E.P.R. after conversion into NO via the addition of excess  $\text{HNO}_3$ , which was an unavoidable contaminant in  $\text{N}_2\text{O}_5$  (3 to 7% of  $\text{N}_2\text{O}_5$ ). The side reactions of  $\text{NO}_2$  and  $\text{HNO}_3$  with the free radicals were taken into account in the data analysis. And independent experiments were done under the same conditions to re-measure the rate constants for the reactions of  $\text{NO}_2$  with the four free radicals, generally leading to a good agreement with previous literature data (Table I).

TABLE I : SUMMARY OF THE SECOND-ORDER RATE CONSTANTS  
FOR NO<sub>2</sub> REACTIONS IN HELIUM AT 293K.

Reaction	N° of experiments	P (Torr)	k (cm <sup>3</sup> molecule <sup>-1</sup> s <sup>-1</sup> )
OH + NO <sub>2</sub> → HNO <sub>3</sub>	13	0.62	(6.6 ± 1.4) × 10 <sup>-14</sup>
	13	1.34	(1.24 ± 0.11) × 10 <sup>-13</sup>
	18	1.99	(1.39 ± 0.13) × 10 <sup>-13</sup>
	15	2.44	(1.70 ± 0.20) × 10 <sup>-13</sup>
HO <sub>2</sub> + NO <sub>2</sub> → HNO <sub>4</sub>	13	2.40	(a)
Cl + NO <sub>2</sub> → ClNO <sub>2</sub>	17	2.10	(7.5 ± 1.3) × 10 <sup>-14</sup>
ClO + NO <sub>2</sub> → ClONO <sub>2</sub>	10	1.80	(8.7 ± 1.0) × 10 <sup>-15</sup>

(a) : The rate constant was obtained from computer simulation of the data (due to the interference of the recombination reaction of HO<sub>2</sub>) and agreed with the low pressure limit of ref. 5 : (7.8 ± 1.9) × 10<sup>-15</sup> cm<sup>3</sup> molecule<sup>-1</sup> s<sup>-1</sup> at 2.4 Torr in helium.

• Reaction OH + N<sub>2</sub>O<sub>5</sub> :

The apparent first order rate constant for the reaction of OH (produced from the reaction H + NO<sub>2</sub> → OH + NO) with N<sub>2</sub>O<sub>5</sub> ranged from 48 to 123 s<sup>-1</sup> at 2.44 Torr. After corrections for the interfering reactions (wall loss of OH, OH + NO<sub>2</sub> + He reaction and OH + HNO<sub>3</sub> reaction) and considering both random errors and experimental uncertainties, the upper limit of the rate constant for this reaction was : 5 × 10<sup>-15</sup> cm<sup>3</sup> molecule<sup>-1</sup> s<sup>-1</sup>.

• Reaction HO<sub>2</sub> + N<sub>2</sub>O<sub>5</sub> :

HO<sub>2</sub> radicals were produced from the chemical source Cl + CH<sub>3</sub>OH + O<sub>2</sub> and were analyzed after conversion into OH through the addition of excess NO upstream from the E.P.R. cavity. The wall loss of HO<sub>2</sub> and the reaction HO<sub>2</sub> + NO<sub>2</sub> + He were found negligible leading to the upper limit for the rate constant : 1 × 10<sup>-15</sup> cm<sup>3</sup> molecule<sup>-1</sup> s<sup>-1</sup>.

• Reaction Cl + N<sub>2</sub>O<sub>5</sub> :

The apparent decays observed for the Cl atoms, produced by microwave discharge in Cl<sub>2</sub>, were mainly due to the side reaction Cl + NO<sub>2</sub> + He. The appropriate correction for each measurement led to the upper limit for the rate constant : 5 × 10<sup>-15</sup> cm<sup>3</sup> molecule<sup>-1</sup> s<sup>-1</sup>.



. Reaction ClO + N<sub>2</sub>O<sub>5</sub> :

ClO radicals were produced from the reaction  $\text{Cl} + \text{OClO} \rightarrow 2 \text{ClO}$ , with an excess of OClO. In this case, the corrections due to secondary chemistry were negligible and the upper limit obtained for the rate constant was :  $6 \times 10^{-16} \text{cm}^3 \text{molecule}^{-1} \text{s}^{-1}$ .

All the data are summarized in Table II.

TABLE II : SUMMARY OF THE UPPER LIMITS OF THE RATE CONSTANTS FOR N<sub>2</sub>O<sub>5</sub> REACTIONS AT 293K.

Reaction	$\Delta H$ x cal/mole	N° of exp.	k (cm <sup>3</sup> mol. <sup>-1</sup> s. <sup>-1</sup> )
OH + N <sub>2</sub> O <sub>5</sub> $\begin{cases} \rightarrow \text{HNO}_3 + \text{NO}_3 \\ \rightarrow \text{HNO}_4 + \text{NO}_2 \end{cases}$	-27.3	6	< $5 \times 10^{-15}$
	-19.1		
HO <sub>2</sub> + N <sub>2</sub> O <sub>5</sub> $\begin{cases} \rightarrow \text{HNO}_4 + \text{NO}_3 \\ \rightarrow \text{HNO}_3 + \text{NO}_2 + \text{O}_2 \end{cases}$	-2.9	14	< $1 \times 10^{-15}$
	-29.6		
Cl + N <sub>2</sub> O <sub>5</sub> $\rightarrow \text{ClNO}_3 + \text{NO}_2$	-18.5	20	< $5 \times 10^{-15}$
ClO + N <sub>2</sub> O <sub>5</sub> $\rightarrow \text{ClNO}_3 + \text{NO}_3$	-4.4	19	< $6 \times 10^{-16}$

The present kinetic results indicate a very low reactivity of N<sub>2</sub>O<sub>5</sub> with free radicals. That confirms the result of a previous study of O + N<sub>2</sub>O<sub>5</sub> reaction (6) for which an upper limit of the rate constant was also given :  $3 \times 10^{-16} \text{cm}^3 \text{molecule}^{-1} \text{s}^{-1}$ .

Finally, these reactions -with the pathways indicated in Table II- cannot be significant stratospheric sources of HNO<sub>3</sub>, HNO<sub>4</sub> and ClNO<sub>3</sub> and, more generally, the reactions of N<sub>2</sub>O<sub>5</sub> with free radicals can be disregarded in atmospheric chemistry.

- References -

- (1) G.C. TOON, C.B. FARMER and R.H. NORTON, Nature, 319, 570, 1986.
- (2) N.S. SOLOMON and R. R. GARCIA, J. Geophys. Res., 88, 5229, 1983.
- (3) N.D. SZE, private communication.
- (4) J. A. DAVIDSON, A. A. VIGGIANO, C. J. HOWARD, I. DOTAN, F. S. FEHSEN FELD, D. L. ALBRITON and E. E. FERGUSON, J. Chem. Phys., 68, 2085, 1978.
- (5) C. J. HOWARD, J. Chem. Phys., 67, 5258, 1977.
- (6) E. W. KAISER and S. M. JAPAR, Chem. Phys. Lett., 54, 265, 1978.

The Reactivity of the Nitrate Radical with Alkynes and some other Molecules

C. Canosa-Mas, S.J. Smith, S. Toby and R.P. Wayne

Physical Chemistry Laboratory, Oxford University, U.K.

Recent observations on the abundances of alkynes in the atmosphere (1) has stimulated renewed interest in the interactions of these species with atmospherically reactive intermediates (2). We report for the first time the rate constants for the reactions at  $295 \pm 2$  K of the nitrate radical ( $\text{NO}_3$ ) with acetylene, propyne, 1-butyne, 2-butyne, 1-pentyne and 1-hexyne. In addition, rates were measured of the reactions of  $\text{NO}_3$  with  $\text{NO}_2$ ,  $\text{O}_2$ ,  $\text{SO}_2$ ,  $\text{C}_2\text{H}_4$ , 1,3-butadiene and 2-methyl propene (isobutene). An absolute method for determining the rate constants was used.

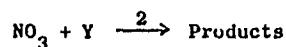
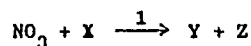
Nitrate radicals were formed in a flow system by the reaction  $\text{F} + \text{HNO}_3 \rightarrow \text{HF} + \text{NO}_3$ . Molecular fluorine diluted with helium was passed through a microwave discharge and into a stream of nitric acid vapour in a He carrier. The  $\text{NO}_3$  concentration was measured by absorption of  $\lambda = 662 \pm 2.1$  nm light using a four-pass White cell, the system being calibrated by titration with NO. In most cases  $\text{NO}_3$  reactions were studied under pseudo-first order conditions. For the fastest reactions, however, the  $\text{NO}_3$  and reactant concentrations were sometimes comparable and the data were then treated assuming second order kinetics with 1:1  $\text{NO}_3$ /reactant stoichiometry. Results using both sets of conditions were compared and computer simulation was used to investigate the influence of possible secondary reactions which could affect the stoichiometry.

We measured  $k(\text{NO}_3 + \text{NO}_2 + \text{M} \rightarrow \text{N}_2\text{O}_5 + \text{M})$  in the range 1-8 torr (He diluent) and good agreement with literature values (5) was obtained. No

direct measurements of  $\text{NO}_3$  decay along the 1 m long reaction tube were made in the absence of added co-reactant but computer simulation showed that any such loss could not have been important, as has previously been noted (3). In the presence of reactants, plots of pseudo first order constants vs reactant concentration sometimes gave small positive intercepts (typically  $\sim 0.4 \text{ s}^{-1}$ ) which may have resulted from the reaction of  $\text{NO}_3$  with adsorbed reactant.

No detectable loss of  $\text{NO}_3$  in the presence of  $\text{SO}_2$  or  $\text{O}_2$  was found which enables us to put an upper limit of  $1 \times 10^{-17} \text{ cm}^3 \text{ molecule}^{-1} \text{ s}^{-1}$  on the rate constants for these reactions, thus justifying the use of added  $\text{O}_2$  in some experiments as a check for possible radical chain reactions. Rate constants are tabulated in Table I. Comparisons between runs where reactant was used pure, was diluted with helium or was diluted with oxygen showed no significant differences.

In the cases of 2-butyne, 1,3-butadiene and isobutene, where  $[\text{NO}_3] > [\text{reactant}]$ , second order kinetic plots were curved. This curvature could be accounted for by additional consumption of  $\text{NO}_3$  according to the sequence:



where  $k_2 = (1-10) \times 10^{-14} \text{ cm}^3 \text{ molecule}^{-1} \text{ s}^{-1}$ . These values of  $k_2$  are close to those expected when the intermediate  $\text{Y} \equiv \text{NO}_2$ , and this is in accord with the postulation of epoxides and  $\text{NO}_2$  elimination when  $\text{NO}_3$  reacts with unsaturated hydrocarbons (9).

Comparisons between the rate constants for  $\text{NO}_3$  with alkynes and alkenes and those for the corresponding reactions with  $\text{OH}$ ,  $\text{O}(^3\text{P})$  and  $\text{O}_3$  are made and discussed. In addition, the relationship of  $k(\text{NO}_3 + \text{alkynes})$

and ionisation energies will be given.

Work is being continued on these systems in order to determine the temperature dependences of the rate coefficients.

Table I. Rate Constants for Reactions of  $\text{NO}_3$  at  $295 \pm 2$  K

Reactant	$k_{295\text{K}} \times 10^{16} \text{ cm}^3 \text{ molecule}^{-1} \text{ s}^{-1}$		Total pressure range, Torr
	Literature values (ref.)	This work <sup>a</sup>	
acetylene	-	$0.6 \pm 0.3$	0.6 - 8
propyne	-	$6.2 \pm 1.0$	2 - 7
1-butyne	-	$6.81 \pm 0.35$	3 - 5
2-butyne	-	$670 \pm 150$	1.5 - 10
1-pentyne	-	$11.6 \pm 1.3$	1 - 2
1-hexyne	-	$16.4 \pm 2.9$	2
sulfur dioxide	$\leq 4$ (4)	$< 0.1$	1 - 3
oxygen	-	$< 0.1$	1.7 - 5
ethylene	1.1 (6,7); 10.9 (8)	$8.8 \pm 1.1$	2 - 12
2-methyl propene	3100 (6,7); 3300 (3)	$3400 \pm 700$	2 - 5
1,3-butadiene	-	$2200 \pm 600$	2 - 4

<sup>a</sup> error limits are  $\pm 2\sigma$

#### References

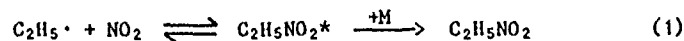
1. J.P. Greenberg and P.R. Zimmerman, *J. Geophys. Res.* 1984, **89**, 4767.
2. S. Hatakeyama, N. Washida and H. Akimoto, *J. Phys. Chem.* 1986, **90**, 173.
3. A.R. Ravishankara and R.L. Mauldin III, *J. Phys. Chem.* 1985, **89**, 3144.
4. J.P. Burrows, G.S. Tyndall and G.K. Moortgat, *J. Phys. Chem.* 1985, **89**, 4848.
5. C.A. Smith, A.R. Ravishankara and P.H. Wine, *J. Phys. Chem.* 1985, **89**, 1423.
6. R. Atkinson *et al.*, *J. Phys. Chem.* 1984, **88**, 1210.
7. E.C. Tuazon *et al.*, *J. Phys. Chem.* 1984, **88**, 3095.
8. S.M. Japar and H. Niki, *J. Phys. Chem.* 1975, **79**, 1629.
9. H. Bandow, M. Okuda and H. Akimoto, *J. Phys. Chem.* 1980, **84**, 3604.

The gas phase reaction of ethyl radicals with NO<sub>2</sub>.

SHANAHAN, I.

School of Chemical Sciences,  
National Institute for Higher Education,  
Glasnevin, Dublin 9, Ireland.

The gas phase reaction of ethyl radicals with NO<sub>2</sub> was studied at ambient temperature (298 ± 3 K). Ethyl radicals were produced by the photolysis of ethyl bromide in the wavelength range 220 - 400 nm. The major reaction products were nitroethane and acetaldehyde, but a careful search indicated that ethyl nitrite and formaldehyde were not products of the reaction. The results are interpreted in terms of a mechanism involving the production of nitroethane and ethoxy radicals:



followed by a complex reaction of C<sub>2</sub>H<sub>5</sub>O· to form acetaldehyde:



The experimental evidence is consistent with the involvement of bromine atoms in the decomposition of the ethoxy radicals, and it is proposed that CH<sub>3</sub>CHO is produced as a result of process 4a and / or 4b:



The importance of heterogeneous processes on the production of acetaldehyde will also be discussed. The relative importance of the two addition routes of C<sub>2</sub>H<sub>5</sub>· radicals to NO<sub>2</sub> was determined over a wide pressure range, providing an estimate of the high-pressure limiting value of the rate constant ratio, k<sub>1</sub>/k<sub>2</sub>.

Kinetic Measurements on the  $\text{NO} + \text{NO}_2 \rightleftharpoons \text{N}_2\text{O}_3$  Reaction using a Pulsed

## Photolysis - IR Laser Absorption Technique

Ian W.M. Smith and Gregory Yarwood

Department of Chemistry, University of Birmingham,

P.O. Box 363, Birmingham B15 2TT, U.K.

Kinetic measurements using time-resolved spectroscopic observations in the infrared are comparatively rare. They are especially useful if the ultra-violet transitions of the transient species are broad dissociative continua, particularly if overlap between such continua occur. Resonance detection methods are then impossible and standard absorption techniques are insensitive and may be difficult to interpret. On the other hand, all molecular species possess relatively narrow, characteristic infrared bands. Using a cw laser as a background source, small absorptions in infrared bands can be measured and the sensitivity is fairly independent of total pressure.

In this paper, we shall report the measurement of rate constants for the system:



at 210 K and total pressures ( $\text{M} = \text{He}, \text{Ar}, \text{CF}_4$ ) from 50 Torr to several atmospheres. Besides demonstrating the potential of the pulsed photolysis - infrared absorption technique, this investigation is the first in a series designed to study the kinetics of association-dissociation in weakly bound systems. The main components of the apparatus are (i) a conventional, low temperature, flash photolysis reaction cell, and (ii) a line-selective cw CO laser operating at ca 100 K. Mixtures are prepared containing ca 50 mTorr  $\text{NO}_2$ , 4.5-10 Torr  $\text{NO}$ ,

and diluent gas. The laser is usually operated on the  $P_{11,10}$  (14) line which is coincident with a Q branch of the  $\nu_1$  (NO stretch) mode in  $N_2O$ .<sup>1,2</sup> Pulsed photolysis (200 J flash, FWHM  $\sim 5 \mu s$ ) perturbs the equilibrium represented by equation (1) to the left and relaxation to equilibrium is observed by monitoring the transmitted intensity ( $I_t$ ) of the laser line using a room temperature InSb detector.

The single-shot traces of  $I_t$  against time are well-matched by single exponentials with the first-order constant corresponding to  $k_1[NO][M] + k_{-1}[M] = k_1[NO][M](1 + (k_{-1}/k_1[NO]))$ . The term in brackets can be calculated from the known equilibrium constant,  $K = (k_1/k_{-1})$ , with allowance being made for the small rise in gas temperature as a result of the photodissociation of  $N_2O$ . Preliminary analysis of the results yields the following third-order rate constants ( $T = 210$  K).

$$k_1^0 (M=He) = (2.0 \pm 0.5) \times 10^{-13} \text{ cm}^6 \text{ molecule}^{-2} \text{ s}^{-1}$$

$$k_1^0 (M=Ar) = (2.4 \pm 0.8) \times 10^{-13} \text{ cm}^6 \text{ molecule}^{-2} \text{ s}^{-1}$$

$$k_1^0 (M=CF_4) = (4 \pm 1) \times 10^{-13} \text{ cm}^6 \text{ molecule}^{-2} \text{ s}^{-1}$$

At the meeting we shall report (i) the results of measurements at total pressures greater than one atmosphere, in order to examine the transition into the fall-off region, and (ii) comparisons of the observed rate constants with those estimated using the methods developed by Troe.<sup>3</sup>

#### References

1. C.H. Bibart and G.E. Ewing, J. Chem. Phys., 61, 1293 (1974).
2. I.W.M. Smith and G. Yarwood, spectroscopic observations on  $N_2O$ , to be published.
3. J. Troe, J. Chem. Phys., 66, 4758 (1977); J. Troe, J. Phys. Chem., 83, 114 (1979).

Temperature and pressure dependence of the rate constant for  
the association reaction  $\text{CF}_3 + \text{O}_2 + \text{M} \rightarrow \text{CF}_3\text{O}_2 + \text{M}$

---

F. CARALP, A.M. DOGNON and R. LESCLAUX  
Laboratoire de Photophysique Photochimie Moléculaire - UA CNRS N°348  
Université de Bordeaux I - 33405 TALENCE CEDEX (France)

---

The association reaction of methyl and halomethyl radicals with oxygen are important steps in the oxidation processes occurring in the atmosphere. However the only experimental kinetic data available are limited to room temperature (see for instance : [1] for  $\text{CH}_3$  radical, [2] for  $\text{CF}_3$  and  $\text{CCl}_3$  radical, [3] for  $\text{CFCI}_2$  radical). In the case of the  $\text{CH}_3$  radicals, calculations of the fall-off parameters as a function of temperature are presented in [4].

In the scope of the study of the chlorofluoromethane oxidation, we report a detailed investigation of the reaction  $\text{CF}_3 + \text{O}_2 + \text{M} \rightarrow \text{CF}_3\text{O}_2 + \text{M}$  in the pressure and temperature range 1-12 torr and 233-473 K respectively. Measurements have been performed using pulsed laser photolysis and time resolved mass spectrometry.

The reaction was found to be in its fall-off region over our range of experimental conditions. The principal goal of this study was the determination of the temperature dependence of the fall-off parameters.

The experimental results have been modelled using the equation proposed by TROE and coworkers. The three parameters  $k_0$ ,  $k_\infty$ ,  $F_c$  have been determined by fitting this equation to our experimental data taking into account that the relative values of these parameters have the constraints imposed by the following equations :

$$k_0 = k_0^{\text{SC}} \times \beta_c \quad (1)$$



where  $k_0^{SC}$  is the low pressure limiting strong collision rate coefficient and  $\beta_c$  the collision efficiency

$$F_c = F_c^{WC} \times F_c^{SC} \quad (2)$$

where  $F_c^{WC}$  and  $F_c^{SC}$  are the strong and weak collision factors respectively

$$F_c^{WC} = \beta_c^{0.14} \quad (3)$$

$$\frac{\beta_c}{1 - \beta_c^{1/2}} = \frac{\langle \Delta E \rangle}{F_E RT} \quad (4)$$

where  $\langle \Delta E \rangle$  is the average energy removed by collision and  $F_E$  a coefficient which accounts for the energy dependence of the density of states.

$k_0^{SC}$  and  $F_c^{SC}$  have been calculated from the values of molecular parameters of  $CF_3O_2$  ( $\Delta H_{f298}^\circ = -147 \text{ kcal mole}^{-1}$  [5] and vibrational frequencies [6]) using the expression developed by TROE.

This analysis has led to a fairly good consistency between the present and previous experimental results, the theoretical approach and the molecular parameters used in the calculations. The expression obtained for the temperature dependence of  $k_0$  with  $N_2$  as buffer gas is :

$$k_0 = (1.9 \pm 0.2) \times 10^{-29} (T/298)^{(-4.7 \pm 0.4)} \text{ cm}^6 \text{ molecule}^{-2} \text{ s}^{-1}$$

The rate expression proposed for  $k_\infty$

$$k_\infty = (9 \pm 2) \times 10^{-12} (T/298)^{(0 \pm 1)} \text{ cm}^3 \text{ molecule}^{-1} \text{ s}^{-1}$$

is consistent with the calculated expression

$$F_c = \exp\{-(T/395)\}$$

and preceding values reported at room temperature.

- (1) NASA JPL Publication 85-37 (1985)
- (2) K.R. RYAN and I.C. PLUMB, Int. J. Chem. Kin. 16 (1984) 591
- (3) F. CARALP and R. LESCLAUX, Chem. Phys. Lett. 102 (1983) 54
- (4) C.J. COBOS, H. HIPPLER, K. LUTHER, R.A. RAVISHANKARA and J. TROE, J. Phys. Chem. 89 (1985) 4332
- (5) V.I. VEDENEEV, V.I. PROPOI and O.M. SARKISOV, Kinet. Catal. (Engl. Transl.) 21 (1980) 854
- (6) R. BUTLER and A. SNELSON, J. Phys. Chem. 83 (1979) 3243.

# $CX_3-O_2$ Bond Dissociation Energies

by

L. Batt and P. Stewart, University of Aberdeen,  
Aberdeen AB9 2UE, Scotland.

The experimentally observed pressure dependence for the reaction  $CX_3 + O_2 + M \rightarrow CX_3O_2 + M$ , where  $X = H$  or halogen, was modelled using a full-scale RRKM program. This involved the reverse unimolecular decomposition reaction and the employment of the principle of microscopic reversibility.

An excellent fit with experiment was obtained in each case, giving the  $CX_3-O_2$  bond dissociation energies below

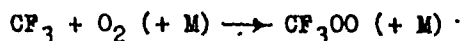
$D(CX_3-O_2) \text{Kcal mol}^{-1}$	29.9	21.6	24.8	35.6
$CX_3$	$CH_3$	$CCl_3$	$CFC1_2$	$CF_3$

DISSOCIATION ENERGY OF C-O BOND IN THE  $\text{CF}_3\text{O}_2$  RADICAL

Vedenev V.I., Goldenberg M.Ya., Teitelboim M.A.

The role of halogenated peroxide radicals in the oxidation of halogenated hydrocarbons, specifically freons, is as important as that of alkyl peroxide radicals in the oxidation of hydrocarbons. Therefore, thermochemical and kinetic data on these radicals are of considerable interest.

In the present work, <sup>by</sup> comparing new experimental data on the pressure dependence of the reaction rate constant for



with calculations performed in accordance with the RRKM theory, the C-O bond dissociation energy in the  $\text{CF}_3\text{OO}$  radical has been determined:  $D(\text{CF}_3 - \text{O}_2) = 143 \text{ kJ/mole}$ . This value differs substantially from  $D(\text{CF}_3 - \text{O}_2) = 204 \text{ kJ/mole}$ , obtained by the additivity method, and, on the whole, is in agreement with the value of  $D(\text{CF}_3 - \text{O}_2) = 134 \text{ kJ/mole}$ , previously calculated by us based on comparing the calculations performed in accordance with the RRKM theory and the kinetic data then available.

The value of C-O bond dissociation energy in the  $\text{CF}_3\text{O}_2$  radical, obtained in the present work, and the reference data on the enthalpy of formation  $\text{CF}_3$ , O,  $\text{CF}_3\text{O}$ , and  $\text{CF}_3\text{OOCF}_3$  make it possible to arrive at the following thermochemical quantities:

$$H_{f,0}^{\circ}(\text{CF}_3\text{O}_2) = -609 \text{ kJ/mole}; \quad H_{f,298}^{\circ}(\text{CF}_3\text{O}_2) = -615 \text{ kJ/mole};$$

$$D_{298}(\text{CF}_3\text{O} - \text{O}) = 209 \text{ kJ/mole}; \quad D_{298}(\text{CF}_3 - \text{OOCF}_3) = 423 \text{ kJ/mole}$$

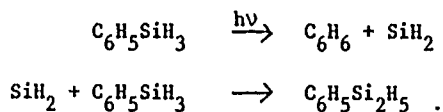
RELATIVE RATE STUDIES FOR REACTIONS OF SILYLENE

by C.D. Eley, H.M. Frey, M.C.A. Rowe, R. Walsh and I.M. Watts

Department of Chemistry, University of Reading, Whiteknights,  
P.O. Box 224, Reading RG6 2AD, England

ABSTRACT

The photochemical decomposition of gas-phase phenylsilane has been investigated at 206 nm at 298 K (and also 373 K). The formation of benzene and phenyldisilane, with and without added oxygen, supports the following mechanism



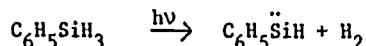
Experiments with added methylsilane give two new products, methylidisilane and phenylmethylidisilane, thus further demonstrating  $\text{SiH}_2$  trapping via



and also indicating the presence of phenylsilylene,  $\text{C}_6\text{H}_5\ddot{\text{Si}}\text{H}$  as an intermediate which is trapped via

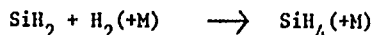


This supports earlier evidence<sup>1</sup> for a second primary process



Photolysis in the presence of added substrate gases yields rate constants for the reaction of  $\text{SiH}_2$  with these species relative to reaction with phenylsilane. These may be put on an absolute basis by use of recently measured absolute rate constants for  $\text{SiH}_2$  by Inoue and Suzuki<sup>2</sup> using LIF detection, as shown in the Table.

Further investigation of the reaction of  $\text{SiH}_2$  with  $\text{H}_2$  supports the pressure dependent process



RRKM modelling with weak collisional deactivation ( $\text{Ar}, \langle \Delta E \rangle_{\text{down}} = 200 \text{ cm}^{-1}$ ) leads to a value of  $k^\infty = 1.9 \times 10^{-12} \text{ cm}^3 \text{ molecule}^{-1} \text{ s}^{-1}$  (within a factor of 2). This is consistent with recent direct measurements by Jasinski.<sup>3</sup>

Taken in conjunction with the reverse decomposition rate constant and measured thermodynamic properties this leads to

$$\Delta H_f^\circ(\text{SiH}_2) = 65.3 \pm 1.5 \text{ kcal mol}^{-1} \quad (\text{at } 298 \text{ K})$$

The presentation will include discussion of the significance of this value in the light of previous measurements and theoretical calculations.

#### References

1. J.E. Baggott, H.M. Frey, P.D. Lightfoot and R. Walsh, Chem. Phys. Letters, 1986, 125, 22.
2. G. Inoue and M. Suzuki, Chem. Phys. Letters, 1985, 122, 361.
3. J.M. Jasinski, J. Phys. Chem., 1986, 90, 555.

Table Rate constants for reaction of  $\text{SiH}_2(^1\text{A}_1)$  at 298 K.

Reactant	$10^{12} \text{ k/cm}^3 \text{ molecule}^{-1} \text{ s}^{-1}$	Ref.
$\text{SiH}_4$	$110 \pm 20$	2
$\text{Si}_2\text{H}_6$	$570 \pm 20$	2
$\text{C}_6\text{H}_5\text{SiH}_3$	$110 \pm 16$	this work
$\text{MeSiH}_3$	$132 \pm 35^b$	this work
$\text{Me}_3\text{SiH}$	$52 \pm 9$	this work
$\text{C}_2\text{H}_4$	$97 \pm 12^a$	2
$\text{C}_2\text{H}_2$	$99 \pm 16$	this work
$\text{MeC}\equiv\text{CMe}$	$110 \pm 27$	this work
$\text{O}_2$	$1.2 \pm 0.2$	this work

a. Reference value.

b. Relative rates measured at 373 K.

## DETECTION OF RADICALS IN THE PHOTO-OXIDATION OF ALDEHYDES

G.K. MOORTGAT, J.P. BURROWS, G.S. TYNDALL, W. SCHNEIDER

R.A. COX\*, B. VEYRET\*\* and K. McADAM\*\*

Max-Planck-Inst. für Chemie, Air Chemistry Dept. D-6500 Mainz

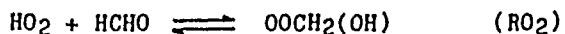
\* AERE Harwell, U.K., \*\* Université de Bordeaux I, F-Talence

A novel apparatus has been built at the MPI to study the behaviour of reactants, products and intermediates (radicals) during and after photolysis. The apparatus consists of a "double multi-path" spectrometer, combining both ir- and uv-absorption spectrometry with additional capability of modulated photolysis for transient detection. Photolysis experiments were performed in a 46 liter quartz cell equipped with two independent sets of White-optic mirrors, one being used in connection with the Bomem FTIR-spectrometer, the other for uv-visible absorption measurements. Uv-absorption-time profiles are fed into a signal averager and processed by an Apple micro-computer. A schematic diagram is shown in Figure 1.

Absorption-time profiles at selected wavelengths in the 210-275 nm region were recorded in the modulated photolysis of HCHO- and CH<sub>3</sub>CHO-air mixtures. Transient absorptions showed a characteristic rise and fall during the alternating photolysis and dark periods.

In the HCHO-air system, HO<sub>2</sub> radicals are produced in the primary photo-oxidation:  $\text{HCHO} + \text{h}\nu, \text{O}_2 \longrightarrow 2 \text{HO}_2 + \text{CO}$ . However, the observed transient absorption (see Figure 2) contained an

additional superimposed broad band spectrum with a maximum near 240 nm which was assigned to the  $\text{OOCH}_2(\text{OH})$  radical formed by the reaction of  $\text{HO}_2$  with  $\text{HCHO}$ :



Additional experiments were done in Bordeaux by flash-photolysing up to 20 torr of  $\text{HCHO}$  and observing the formation of the radicals after the flash using optical absorption at different wavelengths. A value of the equilibrium constant  $K$  was obtained:  $K = 4 \times 10^{-17} \text{ cm}^3 \text{ molecule}^{-1}$  at 305 nm. The absorption cross section at 250 nm was estimated to be near  $5 \pm 1 \times 10^{-18} \text{ cm}^2 \text{ molecule}^{-1}$ . A spectrum of the  $\text{OOCH}_2(\text{OH})$  radical obtained at Bordeaux (black dots) is shown in Figure 3, together with the uv absorption spectra of  $\text{HO}_2$  and  $\text{CH}_3\text{O}_2$ .

Measurements of absorption-time profiles at 250 nm and 220 nm during modulated photolysis of  $\text{CH}_3\text{CHO}$ -air mixtures were made using photolysis periods of 6s. Initial  $\text{CH}_3\text{CHO}$ -photo-oxidation products are  $\text{CH}_3\text{O}_2$  and  $\text{HO}_2$  radicals:



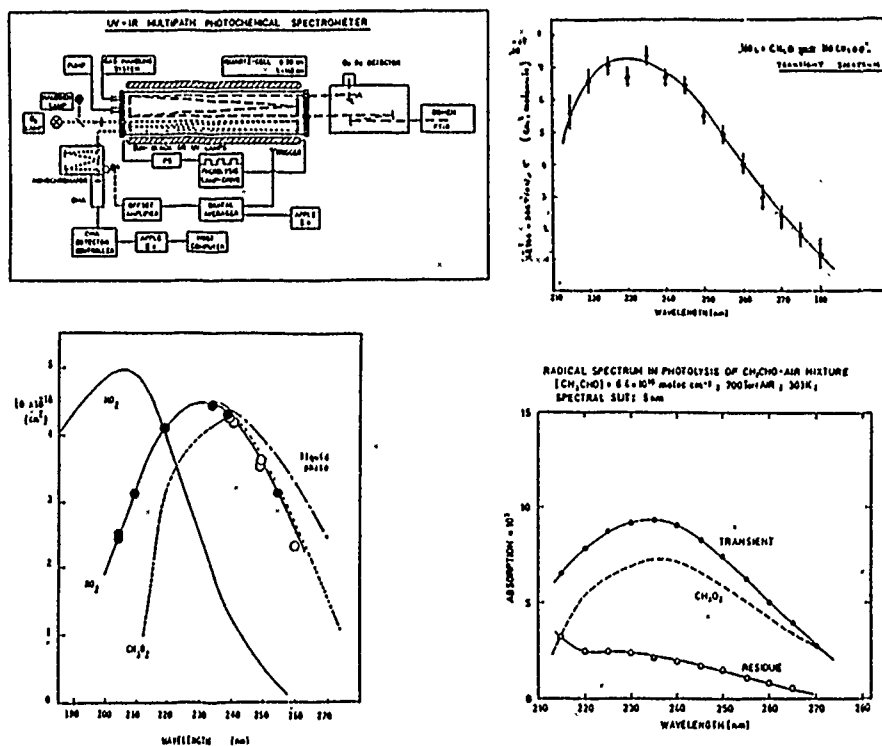
At lower concentrations (0.1 Torr  $\text{CH}_3\text{CHO}$  in 700 Torr Air) absorption at 250 nm was expected to be dominated by  $\text{CH}_3\text{O}_2$  radicals, whereas that at 220 nm was expected to contain components due to  $\text{HO}_2$  and  $\text{CH}_3\text{O}_2$ . Kinetic analysis of the data assisted by computer simulation, using several combinations of absorption cross sections of  $\text{CH}_3\text{O}_2$  (best fit =  $3.2 \times 10^{-18} \text{ cm}^2 \text{ molec.}^{-1}$ ) resulted in a value  $k = 3.7 \times 10^{-12} \text{ cm}^3 \text{ molec.}^{-1} \text{ s}^{-1}$  for the reaction





in excellent agreement with the results obtained from recent computer simulations of the photo-oxidation endproducts by FTIR-analysis.

At higher concentrations, near 10 torr  $\text{CH}_3\text{CHO}$ , the transient spectrum (see Figure 4) contained an additional component, which was attributed to the acetylperoxy radical,  $\text{CH}_3\text{COO}_2$ . This radical is formed by a chain mechanism initiated by the  $\text{CH}_3\text{O}$  radical reacting with  $\text{CH}_3\text{CHO}$ . The formation of acetic acid in the gas phase oxidation of  $\text{CH}_3\text{CHO}$  is believed to occur from the addition reaction of  $\text{HO}_2$  to  $\text{CH}_3\text{CHO}$  to form the  $\text{CH}_3\text{CH}(\text{OH})\text{O}_2$  radical. A complete mechanism of the  $\text{CH}_3\text{CHO}$  photo-oxidation will be presented.



OPTICAL DETECTION OF  $\text{OH}(\Sigma^+)$  RADICALS  
DURING OXIDATION OF ETHYLENE IN A JET-STIRRED REACTOR

A. CHAKIR, F. GAILLARD, P. DAGAUT, M. CATHONNET, J.C. BOETTNER, H. JAMES

C.N.R.S., Centre de Recherches sur la Chimie de la Combustion  
et des Hautes Températures, 45071 Orléans-Cedex, France.

The recent development in the digital computers and numerical techniques makes possible to model the kinetics of hydrocarbon oxidation. The models have to be validated through comparison with experimental results at wide ranges of operating conditions. The availability of powerful diagnostic techniques would allow to get these required experimental results.

The data we obtained in the past were from plug-flow and jet-stirred reactors. These reactors are suitable for studying the slow oxidation of hydrocarbons in the intermediate temperature range (900-1200 K) and pressures up to 1 Mpa. Up to now, kinetic models have been established for ethylene (1,2) and propane oxidation (3), and only validated through comparisons with experimental results for the molecular species concentrations.

In order to obtain more detailed information on the oxidation process, a new jet-stirred reactor, similar to that used previously (4), was built with quartz windows to allow optical access and detection of some radiative species produced during the reaction. To minimize the quenching due to collisional deexcitation, the experimental rig was designed to be operated at subatmospheric pressures.

Fluorescence light is collected, focused on the entrance slit of a monochromator Jobin-Yvon HRS 2 and detected by a photomultiplier EMI 6256 S connected to a photon counter EGG Instruments.

In the visible range, the existence of a strong continuum prevents the observation of characteristic bands of carbon containing excited species. However, in the near U.V., it has been possible to observe a significant emission whose maximum occurs at 308.9 nm, due to electronically

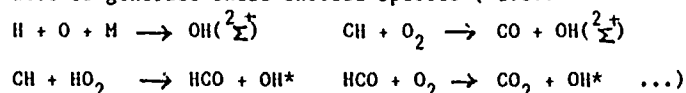
excited  $\text{OH}(\Sigma^+)$  radicals (fig. 1) The profiles of fluorescence against residence times (0.02 s  $\leftrightarrow$  0.2 s) have been obtained for pressures between 0.005 MPa and 0.02 MPa, in a wide range of equivalence ratios ( $0.4 < \phi < 2$ ); these experimental conditions allowing a good mixing of the reactor.

Gas samples were collected by a quartz sampling probe for analysis by gas phase chromatography, during the same time of optical measurements. An example of concentration profiles of main molecular compounds is given on figure 2, together with profile of emission intensity at 308,9 nm.

The ethylene oxidation at pressures above atmosphere was modelled by a comprehensive detailed kinetic mechanism (5). The same mechanism is used to reproduce the experimental results at sub-atmospheric pressures, after changing some rate coefficients. This is necessary to account for pressure dependant rate constants. A sensitivity analysis is carried out to define these reactions.

This work is in progress and satisfactory comparisons are being obtained between experiments and computations for concentrations of molecular compounds. On the basis of this agreement, computed profiles for radical species could be used to explain the origin of  $\text{OH}(\Sigma^+)$  formation in the mechanism:

- firstly, the kinetic model is investigated to select the exoenergetic processes able to generate these excited species ( i.e.:



- then, owing to the assumption that emission results from a balance between the production of  $\text{OH}(\Sigma^+)$  and their collisional deexcitation, comparison between the product of computed concentrations of the above reactant species and the level of fluorescence experimentally measured might lead to determine the part played by each process towards generation of these excited radicals.

#### REFERENCES

- (1) M. CATHONNET, F. GAILLARD, J.C. BOETTNER, P. CAMBRAY, D. KARMED, J.C. BELLET: 20<sup>th</sup> Symp. (Intern. ) on Combustion, Ann Arbor, 1985, 819.
- (2) P. DAGAUT, M. CATHONNET, F. GAILLARD, J.C. BOETTNER, J.P. ROUAN, H. JAMES: Proc. of X<sup>th</sup> I.C.D.E.R.S., A.I.A.A. Journ, 1985 (to appear).
- (3) M. CATHONNET, F. GAILLARD, J.C. BOETTNER, H. JAMES: "Propulsion and Energetics Panel" 62<sup>d</sup> Symposium, AGARD, Turquie, 1983.
- (4) P. DAGAUT, M. CATHONNET, J.P. ROUAN, R. FOULATIER, A. QUILGARS, J.C. BOETTNER, F. GAILLARD, H. JAMES: J. Phys. E: Sci. Instrum., 1986, 19.
- (5) P. DAGAUT et coll.: in progress.

Fig. 1

Detection of  $\text{OH}(\Sigma^+)$  during  
oxidation of  $\text{C}_2\text{H}_4$  in a jet-  
stirred reactor: spectrum  
of fluorescence near 308.9 nm

$P = 0.005 \text{ MPa}$   
 $T = 1110 \text{ K}$   
 $\phi = 0.4$   
 $(\text{C}_2\text{H}_4)_{\text{init}} = 1 \%$   
slit width =  $0.7 \text{ nm}$   
count rate =  $1 \text{ Hz}$   
scanning rate =  $0.017 \text{ nm.s}^{-1}$

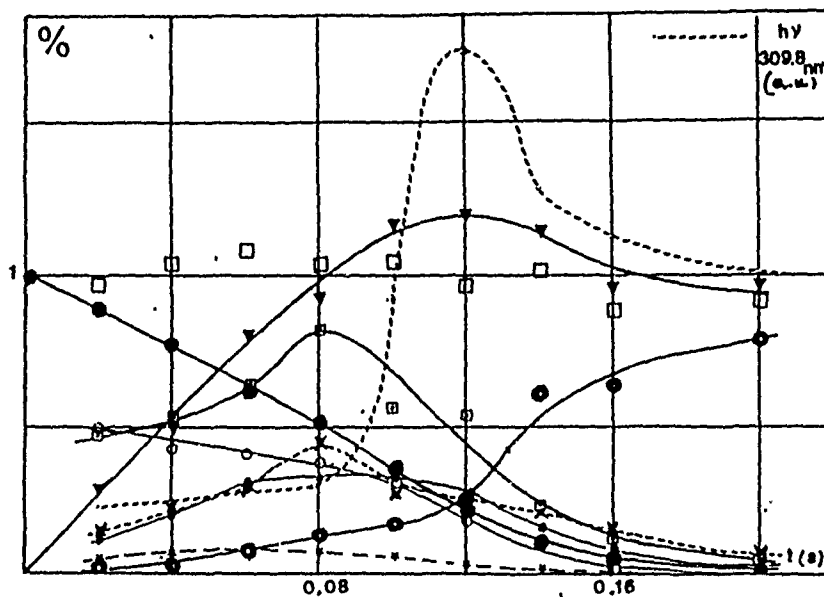
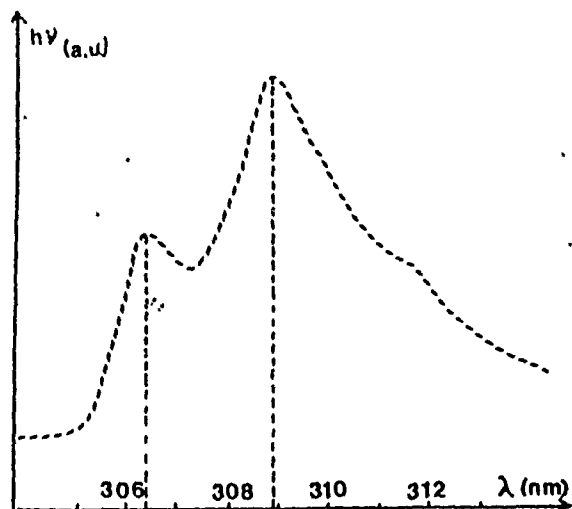


Fig. 2

Oxidation of  $\text{C}_2\text{H}_4$  in a jet-stirred reactor  
 $P \approx 0.008 \text{ MPa}$ ;  $T = 1030 \text{ K}$ ;  $\phi = 0.4$ ;  $(\text{C}_2\text{H}_4)_{\text{init}} = 1\%$

Profiles, against residence times, of:

- concentration of main molecular species ( $\text{C}_2\text{H}_4$ : ●,  $\text{CO}$ : ▼,  $\text{CO}_2$ : ○  
 $\text{CH}_4 \times 10$ : ■;  $\text{C}_2\text{H}_2 \times 100$ : □;  $\text{C}_2\text{H}_4 \times 100$ : ×;  $\text{C}_3\text{H}_6 \times 100$ : \*;  $\text{CH}_3\text{CHO} \times 100$ : ○;  $\Sigma \text{C}_2$ : □
- intensity of the fluorescence at 308.9 nm: -----

PROBE SAMPLING AND ESR DETECTION OF LABILE SPECIES  
FOR KINETICS STUDIES IN FLAMES.

J.F. PAUVELS - M. CARLIER - L.R. SOCHET

*Laboratoire de Cinétique et Chimie de la Combustion.*

*UA CNRS 876, Université des Sciences et Techniques de Lille.*

*59655 Villeneuve d'Ascq Cedex, France.*

The analysis of microstructure of flames is an important method to study the kinetics of elementary reactions at high temperature. Recently we have proposed a new development of Vestenberg and Fristrom's method to detect labile species by ESR in flames ( H, O, OH, Cl, Br, SO, SH ). The species extracted by a sampling probe are detected at a low pressure of  $3.10^{-2}$  Torr after a residence time close to 3.5 ms. In order to take into account the possible destruction of the species within the probe before ESR detection, the pressure inside the probe was changed and the quantitative measurement of the mole fraction X of the species in the flame was obtained by an extrapolation method to zero pressure.

To support the validity of this extrapolation a modelling of the main reactions occurring in the sampling probe (  $\text{OH} + \text{OH} \rightarrow \text{H}_2\text{O} + \text{O}$ ,  $k_1 = 1.08 \cdot 10^{12} \text{cm}^3 \text{mol}^{-1} \text{s}^{-1}$  ), (  $\text{O} + \text{OH} \rightarrow \text{H} + \text{O}_2$ ,  $k_2 = 1.98 \cdot 10^{12} \text{cm}^3 \text{mol}^{-1} \text{s}^{-1}$  ) with wall destruction of H, O and OH has been achieved in the case of an undoped flame. Although the contribution of homogeneous reactions may be relatively important, the results of modelling justify the validity of the linear extrapolation to zero pressure of  $\text{Log } X = f(p)$ , for the determination of the mole fraction of the species in the flame. Examples are provided for the application to the analysis of flame structure.

TWO-PHOTON LASER-EXCITED FLUORESCENCE STUDY OF H AND O ATOMS:  
TEMPERATURE-DEPENDENT QUENCHING AND LASER PHOTOLYSIS FOR  
COMBUSTION APPLICATIONS

U. Meier, K. Kohse-Höinghaus, Th. Just

DFVLR - Institut für Physikalische Chemie der Verbrennung  
Stuttgart, West Germany

The understanding of the behaviour of complicated kinetic systems like flames requires the knowledge of number densities of the reacting species and temperature. It is therefore important to obtain experimental data on absolute concentrations of atoms in a combustion environment.

Relative concentration profiles of hydrogen and oxygen atoms in a flame can be measured by laser-induced two-photon excitation followed by fluorescence detection.

To derive absolute number densities from such fluorescence measurements, we demonstrate a calibration method using the detection of known concentrations of H and O atoms produced in a discharge-flow reactor.

When this calibration technique is applied to flame conditions, the large influence of fluorescence quenching has to be taken into account. The fact that fluorescence signals in a flame are strongly affected by quenching is illustrated in fig. 1. Time-resolved fluorescence signals of H atoms in a low pressure  $H_2-O_2$  - flame are compared to those resulting from a discharge-flow reactor at about 2 mbar.

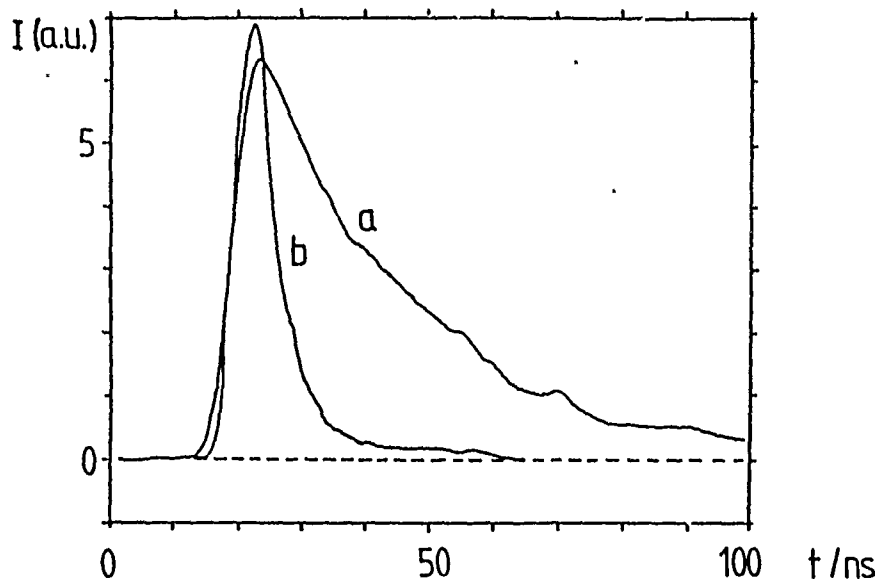


Fig. 1 Time - resolved H atom fluorescence signals;  
curve a from discharge-flow reactor at 2 mbar,  
curve b from  $\text{H}_2/\text{O}_2$  - flame at 95 mbar

The reduction of fluorescence intensity from a certain atom concentration due to quenching is taken into account by calculation of an "effective local quenching rate" under flame conditions. This rate is, in turn, derived from measurements of individual quenching rate constants for different flame-relevant collision partners in the discharge-flow system. Table 1 shows some examples for quenching of the  $n=3$  - level of H atoms which was excited by two-photon - absorption in our experiments. Similar measurements were performed for O atoms.

For  $\text{H}_2$ ,  $\text{O}_2$  and  $\text{H}_2\text{O}$  we also investigated the temperature dependence of the quenching rate constant. No noticeable temperature dependence was found within a range from 300 to 650 K. This result, together with the very high rate constants for most collision partners at room temperature suggests that long-range interactions are responsible for the

energy transfer during the collision process.

Table 1.

Quenching rate constants for the  $n=3$  state of H atoms

collision partner	$k_Q$ ( $\text{cm}^3/\text{s}$ )	collision partner	$k_Q$ ( $\text{cm}^3/\text{s}$ )
He	no effect *	H <sub>2</sub> O	$(1.1 \pm .1) \cdot 10^{-8}$
Ar	$(4.6 \pm .5) \cdot 10^{-10}$	CO <sub>2</sub>	$(3.9 \pm .2) \cdot 10^{-9}$
O <sub>2</sub>	$(2.6 \pm .1) \cdot 10^{-9}$	CH <sub>4</sub>	$(3.5 \pm .2) \cdot 10^{-9}$
H <sub>2</sub>	$(2.2 \pm .1) \cdot 10^{-9}$	C <sub>2</sub> H <sub>2</sub>	$(5.6 \pm .4) \cdot 10^{-9}$

\* within the pressure range 0.5 to 10 mbar

Two-photon excitation of atomic species requires very high laser intensities. Therefore, care must be taken to avoid production of additional atoms by laser photolysis of potential precursor molecules. Since this effect may have an influence on absolute concentration measurements, we studied the production of H and O atoms from the parent molecules O<sub>2</sub>, H<sub>2</sub>, H<sub>2</sub>O, and OH. The experiments led to the result that laser photolysis can be neglected at the wavelengths and power levels we usually employed for H and O detection; however, it may become a problem at sufficiently high intensities.

Based on the results on quenching and laser photolysis, experiments are currently under way in which absolute H atom concentrations as well as spatial concentration profiles are measured for various H<sub>2</sub>-O<sub>2</sub> - low-pressure - flames. This procedure should basically also be applicable to hydrocarbon flames.



P.B.Ayscough, D.L.Baulch and S.J.Chinnick

Department of Physical Chemistry, University of Leeds, U.K.

Two objectives of modelling complex chemical systems are

(i) to simulate an experimental or industrial process. (ii) to gain an understanding of the kinetics involved. For (i) it is often sufficient to involve a simple model with a small number of empirical parameters. The model may be conveniently derived by considering a small number of elementary reaction steps in a pseudo-mechanism. The rate parameters may then be fitted to experimental observations, but the fitted values have no fundamental significance.

In order to gain a proper understanding of a complex chemical system, it is usually necessary to construct an extensive mechanism from a systematic evaluation of all possible steps to a given order of complexity. The rate parameters for each step must be found or estimated and the mechanism translated into a set of differential equations for numerical integration.

The predicted time-concentration profiles may be compared with experiment, and further information may be obtained from a sensitivity analysis, allowing the mechanism to be refined. However, for a mechanism of 200 steps involving 50 species there are ~ 10000 1st order sensitivity co-efficients to interpret.

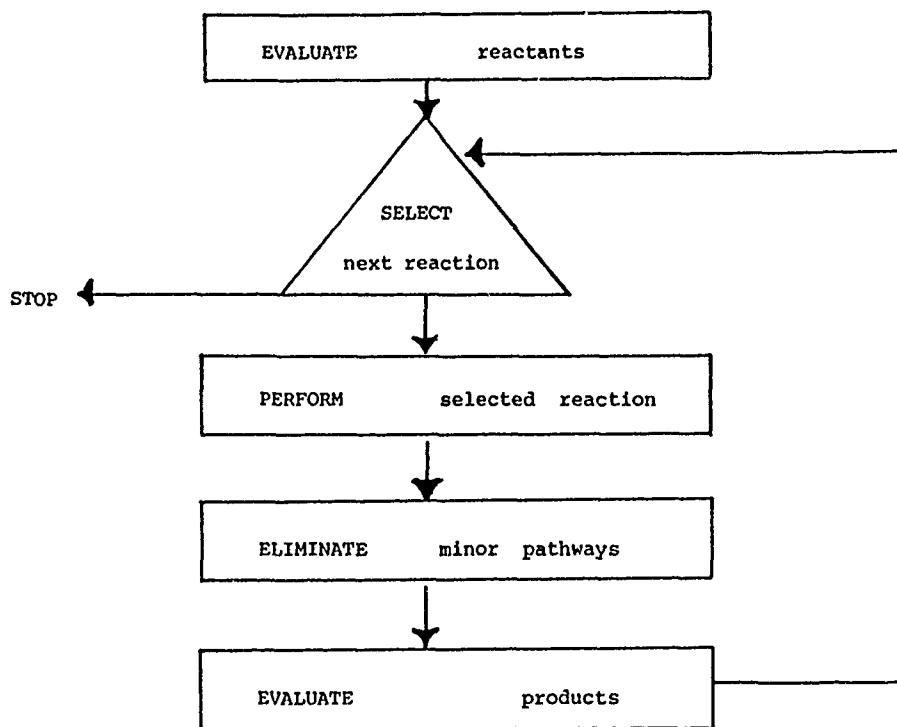
The development of computer environments for use in Artificial Intelligence has enabled an alternative approach to be explored. Using the programming language PROLOG, a computer-representation for chemical species has been derived which closely parallels simple chemical notation. It is possible to manipulate these data-structures so as to 'mirror' the rupture and formation of chemical bonds. In this manner, the following classes of (free-radical) reactions have been 'coded' :

Reaction Type

Decomposition, Molecular Elimination, Radical Decomposition, Abstraction, Addition, Isomerisation, Radical Conversion, Olefin Conversion, Recombination, Disproportionation.

In its crudest form, the computer can thus be used as a systematic generator of reaction steps in the usual process of modelling. However, it is possible to constrain the reaction generator by defining sets of rules representing chemical knowledge or intuition. This then constitutes an EXPERT SYSTEM.

The phases in which reactions are generated and expert-rules are invoked is illustrated in the following diagram :



Each distinct phase of the process is described below :

EVALUATE - For a previously unencountered species (i.e. a reactant or new product), the program finds the set of all reaction-types for which the species is a valid reactant. All feasible combinations with existing species for each reaction-type are stored (implicitly) for later consideration. Some 'embryo' reactions may be discarded at this stage using rules of the type :

"Ignore ABSTRACTIONS involving a radical X if the estimated rate of decomposition of X is considerably faster than the maximum rate of abstraction by X. "

SELECT - The order in which reactions are 'performed' can have a considerable effect upon the efficiency of the EXPERT SYSTEM. Rules are defined to give priority to the faster steps e.g :

"Decompose radicals as soon as they are generated."

"Delay termination steps until after propagation steps."

PERFORM - Once an embryo reaction has been selected, all possible products of the reaction step are generated.

ELIMINATE - For reactions with more than one possible pathway, the rate of each reaction is estimated and compared. Slow paths are not included in the mechanism e.g.

"Decomposition via C-H fission is discarded in favour of C-C fission"

An EXPERT SYSTEM for the pyrolysis of small hydrocarbons has been constructed in this manner. The program has been tested by considering ethane and propane at low pressures at around 700K since a body of good experimental data is available for these systems. On entering the structural formula for ethane, the program generated a pyrolysis mechanism involving 18 species in 44 elementary steps, without recourse to any numerical integration or sensitivity analysis. Approximately 400 reactions were considered. Similarly for propane, the program selected 140 steps involving 53 species after consideration of over 3000 possible reactions. The mechanisms produced by the EXPERT SYSTEM are comparable to, and usually form a superset of, those derived empirically in the literature.

SIMULATION OF THE THREE P-T EXPLOSION LIMITS IN THE H<sub>2</sub> - O<sub>2</sub> SYSTEM  
INCLUDING DETAILED CHEMISTRY AND MULTI-SPECIES TRANSPORT

U.Maas, J.Warnatz

Physikalisch-Chemisches Institut und Sonderforschungsbereich 123,  
Universität Heidelberg  
Im Neuenheimer Feld 294, 6900 Heidelberg, W.Germany

Since the detection of P-T explosion limits in hydrogen-oxygen mixtures in the thirtieth and fortieth, many efforts have been made to explain this phenomenon quantitatively. But all of these attempts had to include some serious restrictions like truncation of the reaction mechanism, quasi-steady state assumptions, or reduction to zero-dimensional systems etc.

The present status of knowledge on reaction kinetics in the hydrogen-oxygen system and recently developed methods for the solution of time-dependent one-dimensional partial differential equation systems now allow the simulation of all of these explosion limits, using a common detailed reaction mechanism (consisting of 37 elementary reactions /1/), a multi-species transport model /2/, and realistic surface chemistry basing on surface collision numbers and experimentally determined surface destruction efficiencies /3/. None of the restrictions mentioned above has to be applied. Solution of the partial differential equation system is done by spatial discretization by finite differences, leading to an ordinary differential/algebraic equation system, which is solved numerically using the computer codes DASSL /4/ or LIMEX /5/.

Calculated P-T explosion limits in the hydrogen-oxygen system at various conditions are presented in Fig.1. As can be seen,

these values are in quite good agreement with the experimental results. Sensitivity analysis identifies the rate-limiting processes and shows areas which should be object of further research.

#### References

1. J.Warnatz, publication in preparation
2. B.Raffel, J.Warnatz, H.Wolff, J.Wolfrum, Progr. Aeronaut. AIAA (1986)
3. U.Maas, J.Warnatz, publication in preparation
4. L.R.Petzold, A Description of DASSL: A Differential/Algebraic System Solver, Sandia Report SAND82-8637, Sandia National Laboratories, Livermore (1982), IMACS World Congress, Montreal 1982
5. P.Deuflhard, U.Nowak, Extrapolation Integrators for Quasilinear Implicit ODEs, Univ. Heidelberg, SFB 123: Tech. Rep. 332
6. H.R.Heiple, B.Lewis, J.Chem. Phys., 9 (1941) 584
7. G.von Elbe, B.Lewis, J.Chem.Phys., 10 (1942) 366
8. A.C.Egerton, D.R.Warren, Proc.Royal Soc., Ser. A, 204 (1951) 465
9. C.N.Hinshelwood, E.A.Moelwyn-Hughes, Proc. Royal. Soc. London Ser. A, 138, 311 (1932)
10. J.C.Greaves, J.W.Linnet, Trans. Faraday Soc., 54 (1958) 1323, 55, 1338-1361 (1959)
11. W.V.Smith, J. Chem. Phys., 11 (1943) 110

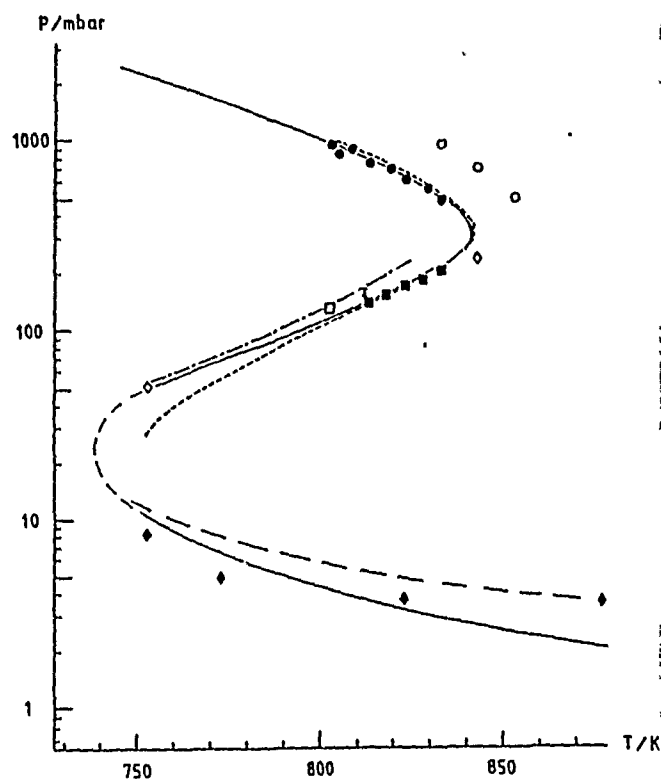


Fig.1: Calculated and experimental ignition limits for 2:1 mixtures of hydrogen and oxygen

a) spherical reaction vessel, 7.4 cm diameter;

----- calculated, surface destruction efficiency  $\gamma = 10^{-2}$  ;  
 — " ,  $\gamma = 10^{-3}$  ;  
 - - - " ,  $\gamma = 10^{-4}$  ;

■ ● experimental, thinly KCl coated vessel /6/;

○ " , heavily KCl coated vessel /6/;

◇ " , KCl coated vessel /7/;

□ " , clean Pyrex vessel /7/;

I " ,  $B_2O_3$  coated vessel /8/;

b) first explosion limit in a cylindrical silica reaction vessel, 1.8 cm diameter;

— calculated,  $\gamma = 10^{-3}$  ;

- - - " , temperature dependent  $\gamma$  , see /10,11/;

◆ experimental /9/.

## STUDY OF REACTION MECHANISMS BY SENSITIVITY ANALYSIS

T.Turányi and T.Bérces

Central Research Institute for Chemistry,  
Hungarian Academy of Sciences, Budapest, Hungary

S.Vajda

Laboratory for Chemical Cybernetics  
L.Eötvös University, Budapest, Hungary

The kinetics of homogeneous chemical processes can be described by a system of ordinary differential equations:

$$\dot{\underline{y}} = f(\underline{y}, \underline{k})$$

where  $\underline{k}$  is the vector of rate coefficients,  $\underline{y}$  designates the vector of concentrations and  $\dot{\underline{y}}$  is its derivative with respect of time. The dependence of the model's predictions on the  $\underline{k}$  parameters is usually given by the sensitivity coefficients defined as  $\partial y_i / \partial k_j$ . These sensitivity coefficients show how the solution of the system of kinetic differential equations changes as a result of variation of the parameters. The sensitivity coefficients are given by the response of the system at time  $t_2$  on the change of parameter at time  $t_1$ . The lower integration time limit in the solution of the system of kinetic differential equations and in that of the system of sensitivity equations is normally taken to be the same. The sensitivity matrix of a complex chemical reaction for time  $t_2$  is not only a function of the rate parameters and species concentrations at  $t_2$  but depends on the pre-history of the system, i.e. it depends on the concentration trajectory connecting  $t_2$  with  $t_1$ .

A sensitivity matrix which depends only on the values of kinetic parameters and on the actual concentration of the

reactive species appears to be more suitable for the analysis of the reaction mechanisms. We introduce a function of the type

$$Q(\underline{a}) = \sum_{i=1}^m \left[ \frac{\dot{Y}_i(\underline{a}) - \dot{Y}_i(\underline{a}^0)}{\dot{Y}_i(\underline{a}^0)} \right]^2$$

in order to represent the effect of kinetic parameters on the rate of reaction, where  $\underline{a} = \ln \underline{k}$ , while  $\dot{Y}_i(\underline{a}^0)$  and  $\dot{Y}_i(\underline{a})$  are the rates of formation of species  $i$  calculated with the initial ( $\underline{a}^0$ ) and with the changed ( $\underline{a}$ ) vectors of the kinetic parameters. The  $\partial \underline{f} / \partial \underline{k}$  is considered as a sensitivity matrix (designated F matrix) with elements given by

$$\frac{\partial f_i}{\partial k_j} = \frac{v_i R_j}{k_j}$$

where  $R_j$  and  $k_j$  are the rates and rate coefficients, respectively, of reaction  $j$  and  $v_i$  is the stoichiometric coefficient of species  $i$  in reaction  $j$ .

The F matrix can be obtained very simply. Principal component analysis of the matrix supplies information on the importance and on the interactions of the elementary reactions of the mechanism. The relation of the F matrix to the conventional sensitivity matrix shall be discussed.

Two complex reaction mechanisms are analysed. These are: pyrolysis of propane and oxidation of formaldehyde. Both the F matrix and the conventional sensitivity matrix have been constructed and orders of importance for the elementary steps have been derived by using the method of principal component analysis. A study of the F matrices corresponding to various



phases of the reaction (i.e. to various reaction times) supply information on the actual order of importance of the elementary steps and on the interactions of elementary reactions. Considering all results obtained for different phases of the reaction, a simplified mechanism is derived (mechanism reduction) which proves to be practically equivalent to the original one.

1. S.Vajda, P.Valkó and T.Turányi, Int.J.Chem, Kinet. 17, 55-81 (1985).
2. S.Vajda and T.Turányi, J.Phys.Chem. 90, 1664-1670 (1986).

# Implementation of the Rapid Equilibrium Approximation on a Computer for Kinetics in Complex Systems

Robert A. Alberty  
Department of Chemistry  
Massachusetts Institute of Technology  
Cambridge, Massachusetts, USA

When a complicated organic system approaches equilibrium, most of the reactions may remain very close to equilibrium while some slow reaction comes to equilibrium and eventually determines the composition of the system. An example is the conversion of methanol to gasoline using a zeolite catalyst at 700 K(1). For simpler reactions, the rapid equilibrium approximation may be used to derive the rate equation, but for the methanol conversion thousands of species and reactions are involved and so calculations must be implemented on a computer. Since many species of alkanes, alkenes, and alkylbenzenes are produced, equilibrium calculations can be greatly simplified by use of thermodynamic properties of isomer groups(2). The standard Gibbs energy of formation of an isomer group  $\Delta_f G^\circ(I)$  is given by

$$\Delta_f G^\circ(I) = -RT \ln \left[ \sum_{i=1}^{N_I} \exp(-\Delta_f G_i^\circ/RT) \right] \quad (1)$$

where  $\Delta_f G_i^\circ$  is the standard Gibbs energy of formation of isomer  $i$ .

The concept of isomer groups can be extended to whole homologous series by fixing the ethylene partial pressure so that the ratios of successive isomer groups become a function of only temperature. The Gibbs energy of formation of the alkylbenzene isomer groups at fixed partial pressure of ethylene as given by

$$\Delta_f G^*(I, C_n H_{2n-6}) = \Delta_f G^\circ(I, C_n H_{2n-6}) - ((n-6)/2)(\Delta_f G^\circ C_2 H_4 + RT \ln p_{C_2 H_4}) \quad (2)$$

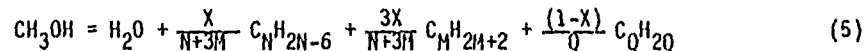
The standard Gibbs energy of formation of the homologous series is given by

$$\Delta_f G^*(HSG) = -RT \ln \left[ \sum_{n=6}^{\infty} \exp[-\Delta_f G^*(I, C_n H_{2n-6})/RT] \right] \quad (3)$$

and the equilibrium mole fractions of successive isomer groups are given by

$$Y_{C_n H_{2n-6}} = \frac{e^{-\Delta_f G^*(I, C_n H_{2n-6})/RT}}{\sum_{n=6}^{\infty} e^{-\Delta_f G^*(I, C_n H_{2n-6})/RT}} \quad (4)$$

The concept of the Gibbs energy of formation of a homologous series may be used to calculate the composition at various stages in the conversion of methanol to gasoline. In this reaction alkenes are formed rather quickly and polymerize to an equilibrium distribution of molar masses. This mixture is converted more slowly to a 1:3 mixture of alkylbenzenes and alkanes that eventually, according to thermodynamics, will yield  $C_6H_6 + 3CH_4$ . At intermediate times the stoichiometry can be represented by



where  $X$  is the extent of conversion (0 to 1) to alkanes and alkylbenzenes. In this equation the molecular formulas represent average compositions for the alkane, alkylbenzene, and alkene homologous series groups. Experimental data can be represented quite well by assuming that  $C_6H_6$  and  $CH_4$  are alkylated to equilibrium at each value of  $X$  by the ethylene that is present.

Equilibrium compositions can be computed at a series of values of  $P_{C_2H_4}$  starting with the high values that occur early in the conversion to essentially zero when the composition is represented by  $C_6H_6 + 3CH_4$ . The equilibrium composition at any stage in the conversion depends on the pressure. At a given  $P_{C_2H_4}$  the equilibrium mole fraction of ethylene is

calculated using an analog of Eq. 4. The partial pressure of the alkene homologous series group calculated from

$$P_{C_0H_{2Q}} = P_{C_2H_4} / y_{C_2H_4} \quad (6)$$

is subtracted from the total pressure of the hydrocarbons to obtain the sum of the partial pressures of the alkane and alkylbenzene homologous series groups. Each value of  $P_{C_2H_4}$  corresponds with a certain extent of conversion

X and a certain time. For a first order conversion

$$x = \left( e^{kt} - 1 \right) / e^{kt} \quad (7)$$

The Benson-group method has been used to estimate chemical thermodynamic properties of organic substances at high temperatures when data is lacking. These calculations show that within a homologous series, the chemical thermodynamic properties of isomer groups become linear functions of carbon number as the carbon number increases. Since  $\Delta_f G^\circ(l)$  is a linear function of carbon number after the first several members of a homologous series, analytic functions can be derived for N, M, Q,  $y_{C_NH_{2N-6}}$ ,  $y_{C_MH_{2M+2}}$ , and  $y_{C_QH_{2Q}}$ .

#### References

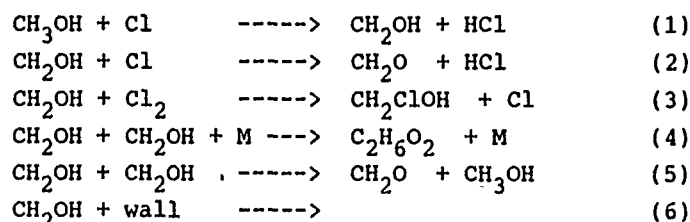
- (1) C. D. Chang and A. J. Silvestri, J. Catal. 47, 249 (1977).
- (2) R. A. Alberty, Ind. Eng. Chem. Fund. 22, 318 (1983).
- (3) R. A. Alberty, J. Phys. Chem. 89, 880 (1985).
- (4) S. W. Benson, Thermochemical Kinetics, Wiley, New York, 1976.
- (5) R. A. Alberty and I. Oppenheim, J. Chem. Phys. 84, 917 (1986).

H.H.Grotheer, G.Riekert, and Th. Just

THE SELFREACTION OF  $\text{CH}_2\text{OH}$  - RADICALS AND

THE  $\text{CH}_3\text{OH}$  -  $\text{Cl}$  -  $\text{Cl}_2$  SYSTEM

The  $\text{CH}_2\text{OH}$  selfreaction was investigated due to its potential importance particularly in the modelling of rich methanol flames. We used the mass spectrometer discharge flow technique with the fast reaction  $\text{Cl} + \text{CH}_3\text{OH} \rightarrow \text{CH}_2\text{OH} + \text{HCl}$  as a radical source ( All measurements at ambient temperature ). In that case besides the radicals there is always an excess of methanol in the reactive flow, together with  $\text{Cl}_2$  surviving the discharge. Therefore, for the measurement of the concentration dependent selfreaction of  $\text{CH}_2\text{OH}$  radicals, we had to account for the mechanism:



This complication cannot be circumvented since there is no other  $\text{CH}_2\text{OH}$  source available.

$k_1$  is up to now the only known rate coefficient in that mechanism. It has been measured by flash photolysis techniques /1/. We obtained in our flow tube for  $k_1$  the values of  $(6.2 \pm 0.9) \cdot 10^{-11} \text{ cm}^3 \text{ s}^{-1}$  in an excess of methanol and of  $(5.6 \pm 1.2) \cdot 10^{-11} \text{ cm}^3 \text{ s}^{-1}$  in an excess of chlorine atoms. The absolute chlorine concentrations were determined by titration with  $\text{Br}_2$  as well as by their reaction with  $\text{C}_2\text{H}_6$  /2/.

Reaction (2) was investigated by measuring the  $\text{CH}_2\text{OH}$  yields as a function of  $[\text{Cl}]$  and  $[\text{CH}_3\text{OH}]$  for a very short fixed residence time which was determined separately. Computed yields could be fitted to the measured data by using  $k_2 = 2 \cdot 10^{-10} \text{ cm}^3 \text{ s}^{-1}$ .

Also the reaction of  $\text{CH}_2\text{OH}$  radicals with molecular chlorine is of some importance in our system. Due to the presence of  $\text{Cl}_2$  surviving the discharge, reaction (3) cannot be measured under pseudo first order conditions in an excess of  $\text{CH}_2\text{OH}$ . On the other hand, in an excess of  $\text{Cl}_2$ , the  $\text{CH}_2\text{OH}$  decays are interfered by  $\text{CH}_2\text{OH}$  reformation via reaction (1). Therefore, we chose conditions for the chain (3) + (1) under which reaction (1) is fast compared to reaction (3), i.e.  $[\text{CH}_3\text{OH}] \gg [\text{Cl}_2] \gg [\text{CH}_2\text{OH}]$ .  $k_3$  was deduced from the measured  $\text{Cl}_2$  and  $\text{HCl}$  profiles, respectively, to be  $k_3 = 1.5 \cdot 10^{-11} \text{ cm}^3 \text{ s}^{-1}$ .

Reactions (4) to (6) were measured in a concentration range of  $5 \cdot 10^{11} \text{ cm}^{-3} < [\text{CH}_2\text{OH}] < 10 \cdot 10^{12} \text{ cm}^{-3}$  at pressures ranging between 0.3 mbar and 20 mbar. The measured decays are of mixed order, with a strong wall loss rate of  $k_6$   $20 \text{ s}^{-1}$  to  $40 \text{ s}^{-1}$  depending on the coating (usually Teflon) and the reactor diameter (19, 29 and 40 mm, respectively).

The initial radical concentrations were determined by an absolute detection of the produced formaldehyde while scavenging the radicals at the end of the flow tube via the fast reaction  $\text{CH}_2\text{OH} + \text{O}_2 \rightarrow \text{HCHO} + \text{HO}_2$  [3]. Particularly at low concentrations (about  $1 \cdot 10^{12} \text{ cm}^{-3}$ ) this method yielded results in good accord with the initial  $\text{Cl}$  concentration. Under our conditions the self-reaction (reaction 4) is in its fall off regime. By fitting our data with the expression

$$k(M) = \frac{k_O [M]}{1 + \frac{k_O [M]}{k_\infty}} \cdot 0.6 \frac{k_O [M]}{k_\infty} \left(1 + \left(\log \frac{k_O [M]}{k_\infty}\right)^2\right)^{-1}$$

we get for reaction 4:

$$k_{O4} = (2.2 \pm 0.8) \cdot 10^{-27} \text{ cm}^6 \text{ s}^{-1} \text{ and}$$

$$k_{\infty 4} = (2.4 \pm 0.6) \cdot 10^{-11} \text{ cm}^3 \text{ s}^{-1}.$$

These data are similar to current data on  $\text{CH}_3$  recombination /4/.

We could not find a significant contribution from the disproportionation channel, i.e. reaction (5).

#### References

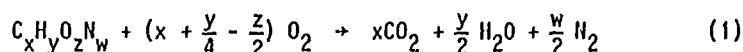
- 
- /1/ Michael J.V., Nava D.F., Payne W.A., and Stief L.J.,  
J. Chem. Phys. 70, 3652 (1979)
  - /2/ Ray G.W., Keyser L.F., and Watson R.T.  
J. Phys. Chem. 84, 1674 (1980)
  - /3/ H.H.Grotheer, G.Riekert, U.Meier, and Th.Just  
Ber. Bunsenges. Phys. Chem. 89, 187 (1985)
  - /4/ M.T. MacPherson, M.J. Pilling and M.J.C. Smith  
Chem.Phys.Lett. 94, 430 (1983)

THE ROLE OF DECOMPOSITION REACTIONS IN FLAMES  
by J. VANDOOREN, B. WALRAVENS and P.J. VAN TIGGELEN

LABORATOIRE DE PHYSICO-CHIMIE DE LA COMBUSTION  
UNIVERSITE CATHOLIQUE DE LOUVAIN  
B-1348 LOUVAIN-la-NEUVE BELGIUM

\*\*\*\*\*

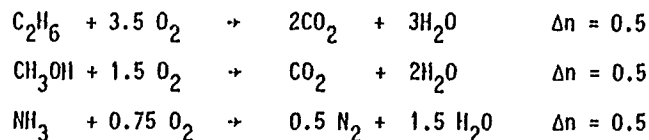
The overall stoichiometric chemical equation corresponding to the combustion process for a fuel with a formula  $C_xH_yO_zN_w$  (noncyclic compounds) can be written as follows



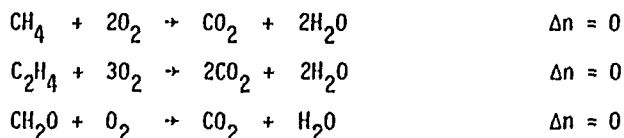
Such an overall reaction corresponds to a variation of the total number of particles  $\Delta n$ . It can refer to molecules or moles.  $\Delta n$  is the difference between the number of mole (or molecules) of products and reactants. It will be dependent on the values of  $y$ ,  $z$  and  $w$ . Three cases can be considered according the value of  $y + 2z + 2w$  :

$$\begin{aligned} \Delta n \text{ is positive if } y + 2z + 2w &> 4 \\ \Delta n \text{ is zero if } y + 2z + 2w &= 4 \\ \Delta n \text{ is negative if } y + 2z + 2w &< 4 \end{aligned} \quad (2)$$

- Most of the usual fuels will burn with an increase of the total number of particles ( $\Delta n > 0$ ) for instance



- Other fuels as  $CH_4$ ,  $CH_2O$ ,  $C_2H_4$  should burn without change of the total number of particles ( $\Delta n = 0$ ), if the overall stoichiometric equation (1) is valid



However, even when  $\Delta n = 0$ , the number of particles in the burnt gases is usually larger than those in fresh gases, since species like CO, OH, H, O are always occurring in the burnt gases.



- Nevertheless, some fuels as  $H_2$ , CO, HCN,  $C_2H_2$ , as well as polyacetylenic compounds will burn with a decrease of the total number of particles ( $\Delta n < 0$ ).

According to these considerations, it comes out that the majority of fuels burns with an increase of the total number of particles. It means that decomposition reactions must occur and a combustion mechanism has to include this kind of elementary processes besides the usual bimolecular and termolecular reactions.

The analysis of the flame structure, i.e. the measurement of profiles of concentration ( $N_i$ ) of the individual species ( $i$ ), and of the temperature profile, may provide informations on the decomposition processes. However, since for flames diffusion processes are quite important, one has to consider the mole fluxes ( $F_i$ ) of the individual species, instead. They are related to each other by  $F_i = N_i (v + V_i)$  when  $v$  stands for flow velocity and  $V_i$  for the local diffusion velocity of species  $i$ . Moreover, the total number of particles and the number of chemical bonds are connected directly. The flux of chemical bond ( $F_b$ ) can be estimated at any point throughout the flame by the expression  $F_b = \sum b_i F_i$ , where  $b_i$  is the number of bonds in the species  $i$  characterized by a mole flux  $F_i$ . If we assume that the total number of particles doesn't vary ( $\Delta n = 0$ ), the number of chemical bonds will remain also constant throughout the flame. On the contrary, any variation of  $F_b$  will lead to a gradient of the total number of bonds and will correspond to a gradient of the total number of particles. Such gradients have to be ascribed to the occurrence of both termolecular and decomposition reactions

$$\frac{dF_b}{dz} = R_t - R_d = R_b \quad (3)$$

where  $z$  is the distance,  $R_t$  the reaction rate of recombination,  $R_d$  the rate of decomposition and  $R_b$  the net reaction rate varying the total chemical bond in the system across the flame front. When  $R_b > 0$ , the recombination processes dominate. The reaction rate of decomposition, especially in the main reaction zone of low pressure flames, is faster than the reaction rate of recombination.

So, to a first approximation, we get  $R_b \approx -R_d$ .

Using this approach, the rate of decomposition has been determined in flames burning in  $\text{CH}_4/\text{O}_2$ ,  $\text{CH}_3\text{OH}/\text{O}_2$ ,  $\text{H}_2/\text{N}_2\text{O}$ ,  $\text{CH}_2\text{O}/\text{O}_2$  mixtures.<sup>(1-4)</sup>

1. For instance for  $\text{H}_2/\text{N}_2\text{O}$  flames, the elementary process

$\text{N}_2\text{O} + \text{M} \rightarrow \text{N}_2 + \text{O} + \text{M}$  (r.1) is unquestionably the unique decomposition reaction. Thus, one can write  $-R_b = k_1 [\text{N}_2\text{O}] [\text{M}]$ , and deduce therefore the value of  $k_1$ . One obtains the following expression for

$k_1 = 1.3 \cdot 10^{15} \exp(-28500/T) \text{ cm}^3 \text{ mol}^{-1} \text{ s}^{-1}$  which agrees fairly well with those measured in shock tubes.<sup>(5)</sup>

2. A similar analysis in formaldehyde flames leads to ascribe the main decomposition path of the reaction  $\text{CHO} + \text{M} \rightarrow \text{CO} + \text{H} + \text{M}$  (r.2) with

$k_2 = 2.5 \cdot 10^{15} \exp(-9300/T) \text{ cm}^3 \text{ mol}^{-1} \text{ s}^{-1}$ .

In conclusion, the analysis of the flame allows to deduce rate constants for decomposition reactions and to estimate their incidence in the combustion mechanism.

We acknowledge financial support of F.R.F.C. Contract 2.9003.82 (Belgium)

#### REFERENCES

- (1) J. PEETERS and G. MAHNEN, XIVth Symp. (Internat.) on Combustion. The Combustion Institute, 1973, p. 133
- (2) BALAKHININ, V.P. VANDOOREN, J. and VAN TIGGELEN, P.J., Comb. and Flame 28, p. 165-173 (1977)
- (3) J. VANDOOREN and P.J. VAN TIGGELEN, XVIIIth Symp. (Internat.) on Combustion, The Combustion Institute, Pittsburgh, pp. 473-483 (1981)
- (4) J. VANDOOREN, L. OLDENHOVE de GUERTECHIN and P.J. VAN TIGGELEN Comb. and Flame 64, pp. 127-139 (1986)
- (5) BAULCH, D.L., DRYSDALE, D.D., HORNE, D.G., and LLOYD, A.C., Evaluated Kinetic Data for High Temperature Reactions, Vol. 2, 1973, Butterworths, London.

PYROLYSIS OF CYCLOHEXANE / N-DECANE / STEAM MIXTURES  
AT CA. 810°C

F. BILLAUD\* and E. FREUND\*\*

\* Département de Chimie-Physique des Réactions, UA n° 328 CNRS,  
INPL-ENSIC, 1, rue Grandville 54042 NANCY Cedex

\*\* Département de Physique et Analyse, Institut Français du  
Pétrole, 1 et 4, avenue de Bois Préau, BP 311,  
92506 RUEIL-MALMAISON Cedex

The present work is a part of a more general research project aiming at understanding the reaction mechanism of the production of light olefins from naphthenic feedstocks. Such feedstocks are currently of great commercial interest because catalytic hydrogenation processes are under active consideration as a means of upgrading olefin feedstocks of high aromatic content ; such hydrogenation tends to saturate the aromatic molecules originally present without ring rupture yielding a high proportion of alicyclic compounds in the upgraded feedstock that is eventually pyrolysed.

The model reactant chosen for the present study, cyclohexane, stands for unsubstituted cycloalkanes within the naphtha boiling range.

From another practical point of view, C<sub>6</sub> cyclanes and especially cyclohexane are important elements in industrial and fuel mixtures. A better knowledge of the elementary steps and of the resulting closed sequences is thus of importance for the understanding of hydrocarbon cracking and combustion.

The naphthenes have not received nearly so much attention from the investigators of pyrolytic decomposition as the paraffins. At most, the

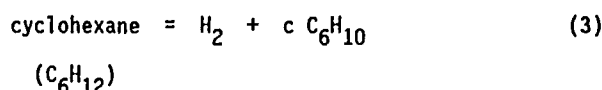
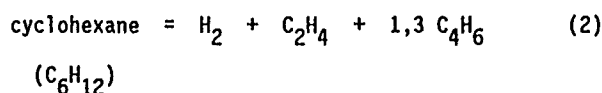
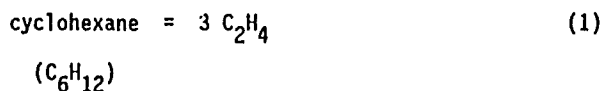
few papers found in the literature concern the 'pure reactants and never mixtures of naphthenes with alkanes ; some investigations were also performed in a shock tube by W. TSANG.

As a result of these limited experimental investigations the mechanism of decomposition of cyclanes has not been well established and published data are not sufficient to predict the distribution of the primary products even in the case of one of the simplest compounds, cyclohexane.

The apparatus and the analytical procedures have been described previously [BILLAUD (1983) (1984)] for the pyrolysis of a mixture of n-alkanes chiefly  $C_{12}$ - $C_{18}$  at 1053 K.

N-decane pyrolysis [BILLAUD (1984)] is the reference reaction and the pyrolysis of the mixture n-decane-cyclohexane is compared to it.

We describe the primary decomposition of cyclohexane by three closed sequences which lead to the following primary stoichiometries :



If we consider the yields of cyclohexene and benzene as a function of residence time, it appears that cyclohexene deshydrogenates easily into benzene and, even at very low conversions, primary stoichiometric equation (3) can be replaced by the secondary stoichiometric equation (3') :  $\text{C}_6\text{H}_{12} = 3 \text{ H}_2 + \text{C}_6\text{H}_6$ .

In order to determine the distribution of the primary stoichiometries from the yields versus residence time, we define the selectivities in the various decomposition products. As a definition, we

call selectivity of the reactant A into a product B,  $S_A(B)$ , the ratio :

$$S_A(B) = \frac{\text{number of moles of product B}}{\text{number of moles of A transformed}}$$

In order to confirm the primary mechanism of decomposition of cyclohexane in the presence of n-decane, we have made the following assumptions : the margin of selectivity for each product obtained in the pyrolysis of n-decane and in the pyrolysis of mixtures cyclohexane-n-decane is essentially due to the decomposition of cyclohexane (Hypothesis of non-interaction). Then the selectivities in  $C_3H_6$ ,  $CH_4$ ,  $1-C_4H_8$  and other products of decomposition of n-decane are the same in the presence or in the absence of cyclohexane ; therefore these products are not due to cyclohexane decomposition. On the other hand, the selectivities in  $C_2H_4$ ,  $H_2$ ,  $1,3-C_4H_6$ , and cyclohexene depend on the conversion of n-decane and we can determine for the lowest conversion of 66 % the distribution of the three above-mentioned stoichiometries, respectively 41, 43 and 16 %.  $H_2$  is representative of reactions (2) and (3),  $C_2H_4$  of reactions (1) and (2) and cyclohexene of reaction (2).

The presence of cyclohexane in a feedstock of pyrolysis is therefore not noxious towards its conversion. Cyclohexane produces  $C_2H_4$ ,  $1,3-C_4H_6$  and  $H_2$  in large yields. In a similar way, cyclohexane leads to cyclohexene which can give a secondary deshydrogenation into benzene, which is a valuable molecule, leading to an increase of octane number in gasoline (nevertheless, its toxicity might be a drawback) and above all is largely used as an intermediate in the chemical chemistry.

#### Literature cited

BILLAUD F., AJOT H. and FREUND E., 1983, Rev. Inst. Fr. Petrole, **38** (6), 763.

BILLAUD F. and FREUND E., 1984, J. Anal. and Appl. Pyrolysis, **6**, 341.

BILLAUD F. and FREUND E., 1984, 8<sup>th</sup> International Symposium on Gas Kinetics, 15<sup>th</sup>-20<sup>th</sup> July 1984, Nottingham, U.K. and Ind. Eng. Chem., Fundam. in press.

*High Temperature Pyrolysis of Toluene at Very Low Initial Concentrations**M. Braun-Unkhoff and P. Frank**DFVLR Inst. f. Phys. Chemie der Verbrennung, Stuttgart, W. Germany*

The thermal decomposition of toluene to benzyl radicals and H-atoms has been investigated behind reflected shock waves. The results reported here are from a series of investigations on aromatics carried out using a shock tube in conjunction with atomic resonance absorption spectrometry (ARAS) in the temperature range of 1400 to 1800 K and at total pressures between 1.5 and 7.8 bar. The test gas mixtures consisted of argon with relative concentrations of 2 to 30 ppm toluene which were permanently controlled by a chemical analytical method ( $\Delta c/c \leq 5$  ppm). Due to the very low initial concentrations of toluene it was possible to conduct the experiments under conditions where the influence of subsequent reactions is considerably reduced. The high sensitivity of the ARAS-technique allowed to monitor absorption signals of H-atoms with absolute concentrations of  $10^{12}$  to  $2 \times 10^{13}$  atoms  $\text{cm}^{-3}$ .

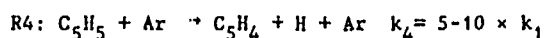
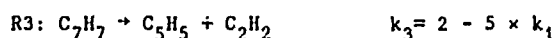
Due to the low initial concentration of toluene it was possible to evaluate the rate coefficient  $k_1$  for the initiation reaction R1:  $\text{C}_7\text{H}_8 \rightarrow \text{C}_7\text{H}_7 + \text{H}$  directly from the H-atom formation rate:  $k_1 = \left( \frac{d[\text{H}]}{dt} \right)_{t=0} \times [\text{C}_7\text{H}_8]_0^{-1}$ . The evaluated values for  $k_1$  showed within the limits of experimental scatter no dependence upon the total pressure in the investigated range. Therefore we

conclude that the reaction proceeds in the "upper part" of the fall-off regime, not far from the high pressure limit.

A least square analysis of all measured points gives rise to  $k_1 = 5.1 \times 10^{15} \exp(-45990/T) \text{ s}^{-1}$  in the temperature range of 1400 to 1700 K.

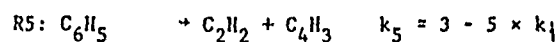
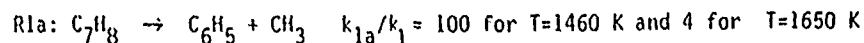
The  $k_1$ -values following from recent measurements of Mueller-Markgraf and Troe /1/ are in very good accord with our derived expression. The values derived by Rao and Skinner /2/ from D-atom measurements are about a factor of 2 smaller, but if we take corrections for isotopic effects into account, then sufficient agreement with the present values is obtained.

In the later stages of the reaction time either a maximum (at  $p_5 = 1 - 2 \times 10^{-5} \text{ mol cm}^{-3}$ ) or an only moderate increase (at  $p_5 = 5 - 6.7 \times 10^{-5} \text{ mol cm}^{-3}$ ) of the H-atom concentration was observed. For both cases a preliminary interpretation of the experimental profiles was possible with the following additional reactions:



Besides this, a second decomposition path of toluene involving cleaving of the C-C bond between the phenyl and methyl group has been discussed /3/.

By restricting our efforts on modelling the experimental profiles only in the early stages of the reaction period, it is possible to derive k-values for the reaction R1a:  $\text{C}_7\text{H}_8 \rightarrow \text{C}_6\text{H}_5 + \text{CH}_3$  with a crude reaction scheme consisting of reaction R2 and the phenyl decomposition reaction:



The methyl association reaction  $\text{CH}_3 + \text{CH}_3 \rightarrow \text{C}_2\text{H}_6 + \text{H}$ , with  $k = 1.4 \times 10^{13} \exp(-5660/T) \text{ cm}^3 \text{ mol}^{-1} \text{ s}^{-1}$  for  $T \leq 1700 \text{ K}$  /4/, has no influence under the experimental conditions. The evaluated Arrhenius expression for  $k_{1a}$  exhibits a very small value for the energy of activation ( $E_a = 10 \text{ kcal / mol}$ ), which is in severe contrast to theoretical and experimental /1,5/ findings.

Together with the results of Troe et al. /1/, who measured the decrease in the toluene concentration during the reaction time, we consider our findings as evidence against an important contribution of an unimolecular process involving cleavage of the C-C bond of the side chain to the overall dissociation reaction rate of toluene.

/1/ W. Mueller-Markgraf and J. Troe, to be published in the 21th. Symposium (Int.) on Combustion, (1986)

/2/ V.S. Rao and G.B. Skinner, J. Phys. Chem., 88, 4362 (1984)

/3/ K.H. Pamidimukkala and R.D. Kern, Int. Conf. on Chemical Kinetics, NBS, Gaithersburg, MD, poster session (1985)

/4/ P. Frank, M. Braun-Unkhoff, and Th. Just, to be published

/5/ D.L. Astholz, J. Durant, and J. Troe, Symp. (Int.) on Combustion, 18, 885 (1981)



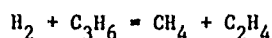
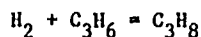
KINETIC STUDY AND MODELLING OF PROPENE HYDROGENATION-  
HYDROGENOLYSIS IN PYREX VESSELS AT ABOUT 500°C

by J.M. BERAL, C. RICHARD and R. MARTIN

Université de Nancy I, BP 239

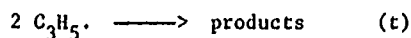
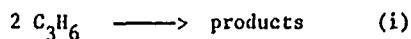
54506 VANDOEUVRE LES NANCY, France

The thermal decomposition of propene at about 500°C yields a large variety of primary products :  $H_2$ ,  $CH_4$ ,  $C_2H_4$ ,  $C_2H_6$ ,  $C_3H_4$ ,  $C_3H_8$ ,  $C_4H_8$ , 1,3- $C_4H_6$ ,  $C_5H_8$ , methylcyclopentane, methyl-3-cyclopentene,... When mixed with molecular hydrogen, propene gives rise to hydrogenation-hydrogenolysis stoichiometries :

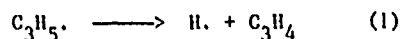


which add to the properly so-called decomposition stoichiometries. Thus, molecular hydrogen causes a selective orientation of the reaction and tends to convert propene into methane, ethylene and propane. This trend is greatly dependent on the nature of the wall reactor. For instance, the initial yields of methane + ethylene + propane in absence and presence of molecular hydrogen (190 % at 520°C) are respectively 57 and 80 in a pyrex reactor, 62 and 92 in a stainless-steel reactor, in percent of the total products.

The formation rates of several products have been studied at low extent of reaction, in Pyrex vessels. The experimental results are interpreted in terms of a free-radical chain mechanism, the processes of which are mostly homogeneous. From the rates of allene production, it is shown that the main initiation and termination steps in presence and in absence of hydrogen are :

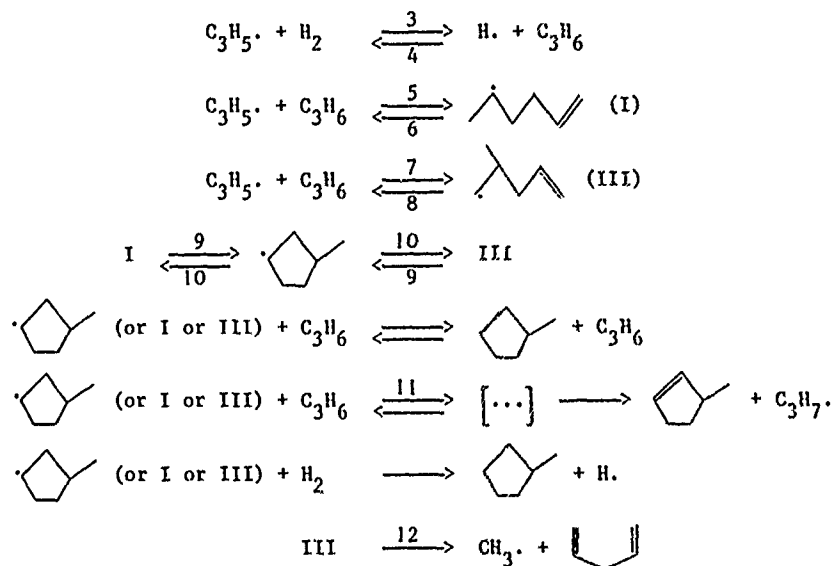


and one computes for process (1) :




$$k_1 = 10^{14} \exp(-51500/RT) \text{ s}^{-1} \quad (RT \text{ in cal.mol}^{-1})$$

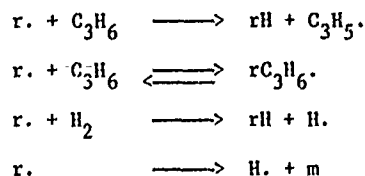
For the production rates of methylcyclopentane, methylcyclopentene and pentadiene-1,4, we write the following primary processes :



Rate constants for processes (3) (5) (9) (10) and (12) have been evaluated.

It is shown that process (10) is almost as difficult as the unimolecular deshydrogenations of (I) (III) and  and that methylcyclopentene rate is second order in propene at 518°C (process 11).

From this point, the kinetic scheme is completed in order to account for the production of methane, propane and ethylene, in presence and absence of hydrogen. Any r. free-radical ( $\text{H}\cdot$ ,  $\text{CH}_3\cdot$ , i  $\text{C}_3\text{H}_7\cdot$ , n  $\text{C}_3\text{H}_7\cdot$ , ...) gives rise to competitive processes :



A detailed modelling of the reaction is achieved by adjusting to the experi-

mental values the initial formation rates computed for methane, ethylene and propane in presence and in absence of hydrogen and in the q.s.s. and long chain approximations. An analysis of sensitivity makes it possible to isolate the determining steps and to evaluate their rate constants. A set of rate constants is obtained which is consistent with all the experimental data and with the thermochemistry or the rare values of the literature (1).

(1) C. COLLONGUES, C. RICHARD and R. MARTIN, Int. J. Chem. Kinet. 15, 5 (1983).

KINETICS OF THE HYDROGENATION OF PROPYLENE AT 950 K

D. Perrin, Université de Nancy, Nancy, France

and

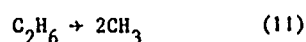
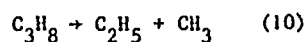
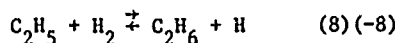
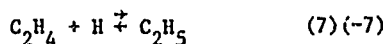
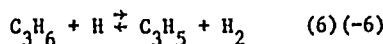
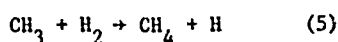
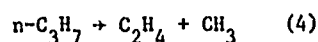
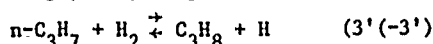
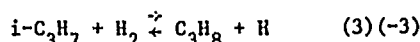
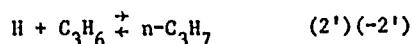
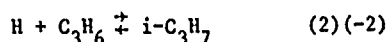
M.H. Back, Chemistry Department, University of Ottawa, Ottawa, Canada

Rate constants for atomic and radical reactions involved in hydrocarbon pyrolyses have, for the most part, been measured at temperatures below about 700 K, yet these values are often required to describe reactions occurring in the neighbourhood of 1000 K. Clearly, measurements of these rate constants in the region of temperature where they will be used would be valuable.

For this purpose the kinetics of the hydrogenation of propylene was studied in the temperature range 900 - 950 K where the reaction occurs through formation and disappearance of *n*- and iso-propyl radicals. The reaction system was similar to that described in the study of the hydrogenation of ethylene at 1150 K <sup>(1)</sup>. Mixtures of hydrogen with small quantities of propylene, 30 - 120 ppm, were admitted to a quartz reaction vessel of approximately 200 cm<sup>3</sup> and the reaction was followed by measurement of the disappearance of the reactant and the appearance of the products, methane, ethylene, ethane and propane. Acetylene was produced only in trace amounts.

In the presence of the large excess of hydrogen, the reaction is initiated by the hydrogen atoms present in thermal equilibrium with hydrogen molecules. Contrary to the situation in the previous studies at 1150 K, the establishment of the equilibrium concentration of hydrogen atoms at 950 K was not fast compared to the other radical reactions occurring in the system, and the assumption of constant concentration of hydrogen atoms throughout the course of the reaction was not valid. Under these conditions the measurement of absolute values for rate constants becomes uncertain and the system is better suited to the extraction of the relative values.

Analysis of the results was based on the mechanism given on the following page. A steady-state solution of these equations gave a series of equations for the rate of disappearance of propylene and appearance of products in terms of the concentration of hydrogen atoms. To obtain equations independent of the hydrogen atom concentration, the rates of formation of the products were expressed in terms of the rate of disappearance of propylene, according to equations A, B, C and D.



$$(A) \quad R_{\text{CH}_4} = -R_{\text{C}_3\text{H}_6} + P_1 \left( \frac{[\text{C}_3\text{H}_8]}{[\text{H}_2][\text{C}_3\text{H}_6]} \cdot \frac{R_{\text{CH}_4}}{K_2 K_3} + R_{\text{C}_3\text{H}_6} \right) - P_2 \frac{\text{C}_3\text{H}_8}{\text{C}_3\text{H}_6} R_{\text{C}_3\text{H}_6}$$

$$(B) \quad R_{\text{C}_2\text{H}_4} = -R_{\text{C}_3\text{H}_6} + P_1 \left( \frac{[\text{C}_3\text{H}_8]}{[\text{H}_2][\text{C}_3\text{H}_6]} \cdot \frac{R_{\text{C}_2\text{H}_4}}{K_2 K_3} + R_{\text{C}_3\text{H}_6} \right) - P_2 \frac{\text{C}_3\text{H}_8}{\text{C}_3\text{H}_6} \cdot R_{\text{C}_3\text{H}_6}$$

$$+ P_3 \frac{K_7 K_8 [\text{H}_2][\text{C}_2\text{H}_4] - [\text{C}_2\text{H}_6]}{\text{C}_3\text{H}_6} \cdot R_{\text{C}_3\text{H}_6}$$

$$(C) \quad R_{\text{C}_3\text{H}_8} = P_1 \left( \frac{[\text{C}_3\text{H}_8]}{[\text{H}_2][\text{C}_3\text{H}_6]} \cdot \frac{(R_{\text{C}_3\text{H}_8} + R_{\text{C}_3\text{H}_6})}{K_2 K_3} - R_{\text{C}_3\text{H}_6} \right) + P_2 \frac{\text{C}_3\text{H}_8}{\text{C}_3\text{H}_6} \cdot R_{\text{C}_3\text{H}_6}$$

$$(D) \quad R_{\text{C}_2\text{H}_6} = -P_3 \left( \frac{K_7 K_8 [\text{H}_2][\text{C}_2\text{H}_4] - [\text{C}_2\text{H}_6]}{\text{C}_3\text{H}_6} \cdot R_{\text{C}_3\text{H}_6} \right) + P_1 \frac{\text{C}_3\text{H}_8}{[\text{C}_3\text{H}_6][\text{H}_2]} \cdot \frac{R_{\text{C}_2\text{H}_6}}{K_2 K_3}$$

$$\text{with } P_1 = \frac{b_3}{b_3 + b_5} ; \quad P_2 = \frac{b_6}{b_3 + b_5} ; \quad P_3 = \frac{b_7}{b_3 + b_5}$$

$$\text{and } b_3 = k_2 \cdot \frac{k_3 [\text{H}_2]}{k_{-2} + k_3 [\text{H}_2]} + k_2 \cdot \frac{k_3 [\text{H}_2]}{k_{-2} + k_3 [\text{H}_2] + k_4}$$

$$b_5 = k_2 \cdot \frac{k_4}{k_{-2} + k_4 + k_3 [\text{H}_2]}$$

$$b_6 = k_{-3} \cdot \frac{k_4}{k_{-2} + k_4 + k_3 [\text{H}_2]}$$

$$b_7 = k_{-8} \frac{k_{-7}}{k_{-7} + k_8 [\text{H}_2]}$$

The equations were analyzed using rates and concentrations of reactants and products measured during the reaction of up to 90% of the propylene.  $P_1$  and  $P_2$  were obtained from equation C,  $P_3$  from equations B and D. Equation A was not useful because the yields of methane and loss of propylene were too close. Values were calculated over the pressure range 135 - 300 Torr and the temperature range 906 - 956 K.

The ratios of the rate constants for H-transfer from propane to H-addition to propylene may be expressed in terms of the coefficients  $P_1$ ,  $P_2$  and  $P_3$  as follows:

$$(E) \frac{k_{-3}}{k_{2'}} = \frac{P_1}{1-P_1} \cdot \frac{1}{K_2 K_3 [H_2]} \cdot \gamma$$

where the fraction  $\gamma$  may be shown, under the present conditions to be close to one.

$$(F) \frac{k_{-3'}}{k_{2'}} = \frac{P_2}{1-P_1}$$

Using the value for  $k_2$ , given by Allara and Shaw <sup>(2)</sup>,

$$k_{2'} = 10^{9.9 - 2900/\theta} \quad (R = 1.987 \text{ cal deg}^{-1} \text{ mol}^{-1})$$

the following values were obtained:

$$k_{-3} = 10^{10.36 \pm .27 - (7300 \pm 1200)/\theta} \quad (M^{-1} s^{-1})$$

$$k_{-3'} = 10^{11.07 \pm .90 - (10800 \pm 3800)/\theta} \quad (M^{-1} s^{-1})$$

Values of  $k_{-3}$  and  $k_{-3'}$  are in good agreement with expressions recommended by Allara and Shaw. Nevertheless the measurements of the relative values are possibly more useful in the application to thermal reactions of hydrocarbons in this temperature region.

1. J.-R. Cao and M.H. Back, Can. J. Chem., 60 3039 (1982).
2. D.L. Allara and R. Shaw, J. Phys. Chem. Ref. Data, 9, 523 (1980).

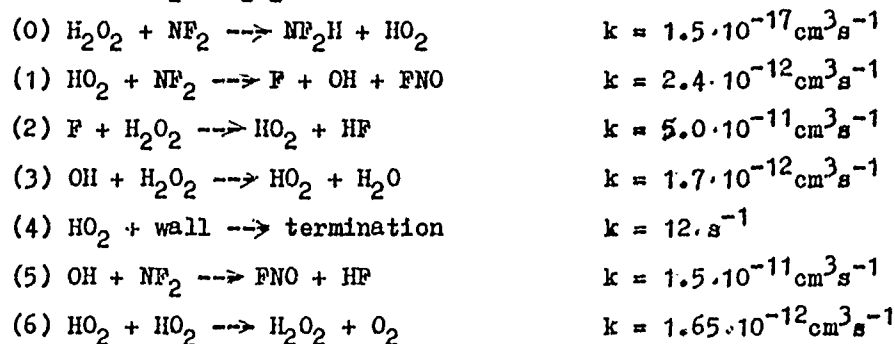
Bedjanian Yu.R., Gershenzon Yu.M., Kishkovitch O.P.  
 Rozenshtein V.B.

Institute of Chemical Physics, Moscow 117977, USSR

The study was carried out by means of EPR/LMR spectrometer combined with a flow-tube system [1].

Reaction  $\text{NF}_2 + \text{H}_2\text{O}_2$ . Recently we found that in the reaction  $\text{NF}_2 + \text{HO}_2$

$\rightarrow \text{OH} + \text{F} + \text{FNO}$  a nonactive radical  $\text{HO}_2$  interacting with a stable radical  $\text{NF}_2$  (at 300 K and ~10 Torr) gave two chemically active particles OH and F. This fact brought us to discover the branch chain reaction  $\text{NF}_2 + \text{H}_2\text{O}_2$ . Its mechanism at 300 K and 10 Torr is



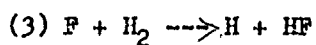
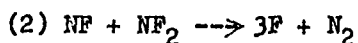
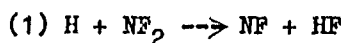
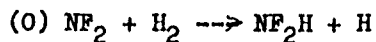
The rate constants of reactions (1), (4-6) we measured separately.

This mechanism describes very good the chain concentration limits and kinetic curves for  $\text{NF}_2$  and  $\text{HO}_2$ .

Reaction  $\text{N}_2\text{F}_4 + \text{H}_2\text{O}_2$ . The reaction was studied under the following conditions:  $p = 13$  Torr,  $[\text{N}_2\text{F}_4] = (1.0-20) \cdot 10^{14} \text{ cm}^{-3}$ ,  $[\text{H}_2\text{O}_2] = 5 \cdot 10^{15} \text{ cm}^{-3}$ . In this case the limiting stage is the decomposition of  $\text{N}_2\text{F}_4$  and therefore the stationary regime is reached during 1 s. High concentrations of the intermediate active species  $\text{NF}_2$  and  $\text{HO}_2$  are conserved during at least several seconds.

Reaction  $\text{NF}_2 + \text{H}_2$ . This reaction was investigated under the conditions:  $p = 12$  Torr ( $[\text{H}_2]/[\text{He}] = 1$ ),  $T = (500 - 850) \text{ K}$ ,  $[\text{NF}_2] =$

$\approx (0.5 - 5) \cdot 10^{14} \text{ cm}^{-3}$ . The specific kinetic features of the branch chain reactions were observed: the induction period, the ignition limit etc. The kinetic data were treated basing on the simplified scheme:



and preliminary value  $2 \cdot 10^{-10} \exp(-3000/T) \text{ cm}^3 \text{ s}^{-1}$  for  $k_2$  was obtained.

Reference. 1. Gershenzon Yu.M., Il'in S.D., Kishkovitch O.P., Lebedev Ya.S., Malkhasian R.T., Rozenshtein V.B., Trubnikov G.R. Doklady Akad.Nauk SSSR, 1980, v.255, No 3, p.620 - 622.



Abstract

Transient gain-versus-absorption laser probing of  
spin-orbit states, kinetics and dynamics

Stephen R. Leone<sup>†</sup>

Joint Institute for Laboratory Astrophysics  
National Bureau of Standards and University of Colorado  
and Department of Chemistry and Biochemistry  
University of Colorado  
Boulder, Colorado 80309-0440

A tunable F-center laser at 2710 nm and a diode laser at 1315 nm are used to probe spin-orbit populations of Br and I atoms, respectively, by time-resolved gain-versus-absorption techniques. Highly accurate quantum yields are obtained for pulsed laser photolysis of various compounds by measuring the early time gain or absorption signal relative to the final absorption amplitude when all of the excited atoms are quenched. Inherent in the method is an intrinsic normalization which eliminates many variables that usually contribute to the error in the determination. Thus the yields are insensitive to the pressure of the gas, the absorption coefficient, the tuning of the probe laser, and the power of the photolysis laser. Yields from molecules such as Br<sub>2</sub>, IBr, CH<sub>3</sub>I, and C<sub>3</sub>F<sub>7</sub>I are considered in detail.

---

<sup>†</sup>Staff Member, Quantum Physics Division, National Bureau of Standards.

In the case of  $\text{Br}_2$ , the continuum yields arising from hot bands are investigated as a function of temperature to fit the shape of the upper repulsive states. The high resolution of the probe lasers allows Doppler velocity effects to be explored. In addition, the differing reactivities of  $\text{Br}(^2p_{1/2})$  and  $\text{Br}^*(^2p_{3/2})$  are studied. For  $\text{Br} + \text{IBr}$ , the ground state atom is 40 times more reactive than the total rate of quenching plus reaction of the excited state.

These laser probe techniques and infrared fluorescence methods are used to investigate the process of collisional release in  $\text{Br}_2$ . In this process,  $\text{Br}_2$  molecules are excited with a narrowed laser to single vibration-rotation levels in the  $\text{B}^3_{\pi_0^+u}$  state at energies between 1-5 kT below dissociation. Collisional release is monitored and determined on an absolute scale by measuring the  $\text{Br}^*$  yield and the total quenching rates. The results show substantial dissociation upwards in energy, even for energies 3-5 kT below dissociation. Results for several collision partners, including He, Ar, Kr and  $\text{Br}_2$  show that all these molecules, regardless of their strength of interaction with the  $\text{Br}_2(\text{B})$  state, have essentially equal efficiencies of collisional release when compared to the quenching rate of the partner. These results will be discussed in terms of simple models.

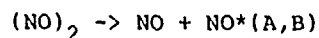
Energy Partitioning in the Electronically Excited NO  
Formed by the Photolysis of the NO Dimer

O. Kajimoto, K. Honma, Y. Achiba\*, K. Shobatake\* and K. Kimura\*

Department of Pure and Applied Sciences, College of Arts and  
Sciences, the University of Tokyo, Komaba, Meguroku Tokyo 135  
Japan

\*Institute of Molecular Sciences, Myodaiji, Okazaki, Aichi 444  
Japan

Nitric Oxide dimers, produced by a supersonic expansion  
of NO/He mixture, were photolyzed at several wavelengths between  
193 and 218 nm. The emission appearing upon irradiation were  
identified as the  $\gamma$  and  $\beta$  bands of NO monomer, indicating the  
formation of electronically excited NO in its A and B states,  
respectively.



The laser power dependences of the emission intensity and the  
 $\text{NO}^+$  ion current further revealed the mechanism of the  $(\text{NO})_2$   
photolysis as shown in Fig. 1.

The change of the emission spectra in the  $\gamma$  band region  
with varying photolysis wavelength is shown in Fig 2. By the  
photolysis at 217.8 nm only the the emission from  $v'=0$  level  
of the A state was observed whereas, at 193 nm,  $v'=3$  for the A  
state and  $v'=5$  for the B state are found to be present. On

the basis of the energetics, this observation suggests that the binding energy of the  $(\text{NO})_2$  should lie between 350 and 700  $\text{cm}^{-1}$ . The computer simulation of the observed spectra has been performed in order to derive the electronic, vibrational and rotational energy distributions in the electronically excited fragments (Fig. 3). The distributions obtained for the four photolysis wavelengths are given in Fig. 4. The vibrational distribution shows no population inversion except for the B state in the 193 nm photolysis. The total amount of the B state is greater than that of the A state. The rotational temperature for  $v'=0$  of the A state at 193 nm was also evaluated to be 1500 K from the emission spectra of higher resolution.

The above mentioned features in energy partitioning will be discussed in terms of the modified phase space theory and the crossings between various potential surfaces during the photofragmentation.

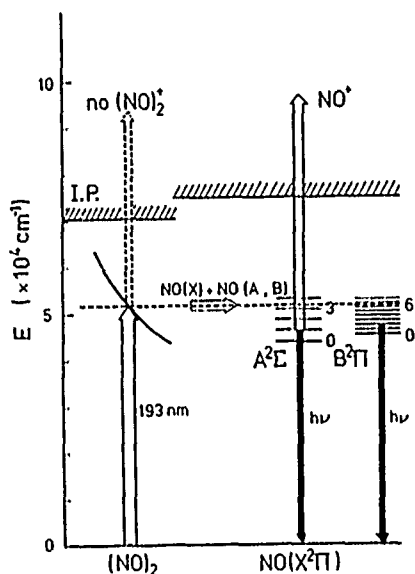


Fig. 1 A schematic representation of the mechanism of the photolysis of the NO dimer

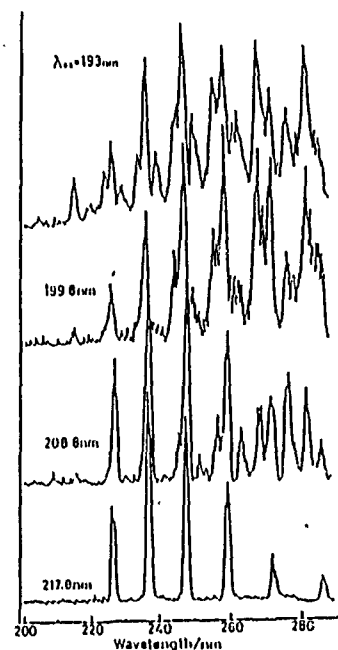


Fig. 2 The emission spectra observed by the photolysis of  $(\text{NO})_2$  at several wavelengths.

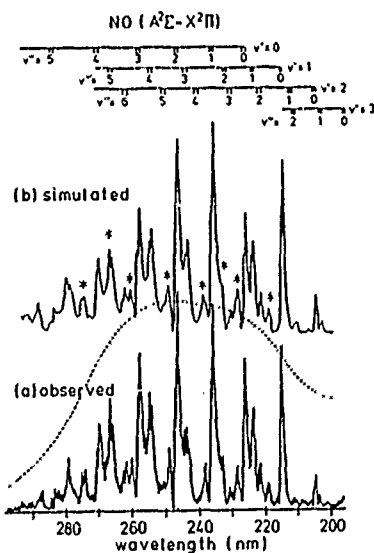


Fig. 3 The simulation of the observed spectrum.

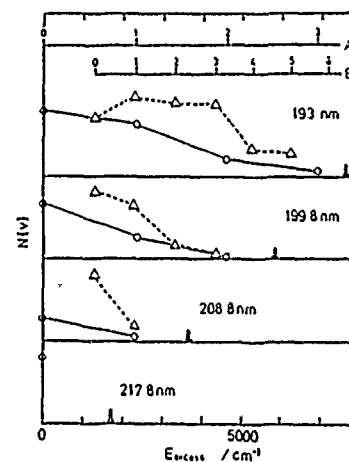


Fig. 4 The electronic and vibrational energy partitioning. O: A state,  $\Delta$ : B state.

The Raman Spectrum of Predissociating H<sub>2</sub>S

K. Kleinermanns, R. Suntz

Universität Heidelberg, Institut für Physikalische Chemie,

Im Neuenheimer Feld 253, D-6900 Heidelberg,

Federal Republic of Germany, Tel.: 06221/562508

Emission spectroscopy of photodissociating molecules provides interesting insights into the shorttime dynamics of bond ruptures /1,2/. We report here a resolved H<sub>2</sub>S photoemission spectrum after excitation at 193 nm, although its electronic spectrum in this wavelength region is diffuse. The electronic spectrum of H<sub>2</sub>S between 250 and 170 nm is nearly continuous probably due to predissociation  $\tilde{X}(^1A_1) \rightarrow ^1B_1 \rightarrow ^1A_2$  /3/.

The lifetime of H<sub>2</sub>S excited at 193 nm  $H_2S \xrightarrow{193\text{ nm}} H(^2S) + SH(X^2\Pi)$  is guessed from photofragmentation measurements to be  $\leq 10^{-14}$  s /3/, hence the re-emission efficiency is very small ( $\leq 10^{-6}$ ). A sensitive apparatus is necessary to observe such weak emission. Optimized light baffles consisting of Al/MgF<sub>2</sub> coated highly reflective scimmers as used in molecular beam experiments suppress the scattered light from the 500 mJ excimer laser pulse at 193 nm almost two orders of magnitude better than traditional baffles. The light further outside from the laser beam center is mirrored into the exit baffle system instead of being reflected back into the view region of the photomultiplier /4/. The H<sub>2</sub>S is flowed through the cell at 0.2 mbar pressure. The sidearms and the fluorescence window are purged with helium to prevent exces-

sive absorption of the pump beam and re-absorption of the Raman light.

A typical Raman spectrum of  $\text{H}_2\text{S}$  excited at 193,4 nm is dominated by the fundamentals, overtones and combinations of the bending and stretch vibrations. Up to five quanta in the bend and 6 quanta in the stretch are seen in the wavelength region 193 - 320 nm. The spectral resolution of the monochromator is 0.6 nm, while the excimer laser bandwidth is  $\sim 0.5$  nm FWHM. This spectral resolution has to be improved further to distinguish between excitation of the symmetric and antisymmetric stretch ( $\tilde{\nu}(100) = 2622 \text{ cm}^{-1} = 203,7 \text{ nm}$  and  $\tilde{\nu}(001) = 2684 \text{ cm}^{-1} = 204,0 \text{ nm}$ ). The intensities of the stretching mode overtones initially decrease in the progression, but regain intensity in combination with the bending mode  $\nu_2$  further along in the progression. The strong activity in the stretch and bend modes indicates that the corresponding normal coordinates are initially, i.e. in the Franck-Condon region, considerably displaced on the upper surface. Further experiments are directed to improve the spectral resolution of the measurements and to measure the spectrum up to the energy limit at 502 nm (with 3.91 eV as  $\text{H}_2\text{S}$ -dissociation energy).

- /1/ D. Imre, J. L. Kinsey, A. Sinka, J. Krenos, J. Phys. Chem. 88, 3956 (1984)
- /2/ E. A. Rohlfing, J. J. Valentin, Chem. Phys. Lett. 114, 282 (1985)
- /3/ G. N. A. van Veen, K. A. Mohamed, T. Baller, A. E. De Vries, Chem. Phys. 74, 261 (1983)
- /4/ J.E. Butler, Appl. Optics 21, 3617 (1982)

Vibrational and Rotational Distributions of the CO  
Product of  $\text{H} + \text{CO}(v=0, J=0)$  with Hot  
Hydrogen Atoms

Paul L. Houston  
Department of Chemistry  
Cornell University  
Ithaca, NY 14853  
U. S. A.

$\text{H}_2\text{S}$  is dissociated at excimer laser wavelengths in an pulsed nozzle beam containing CO. The H atoms produced by the dissociation make 1-2 collisions with the cold CO and excite it vibrationally and rotationally. CO products are then probed by vacuum ultraviolet laser induced fluorescence using a tunable VUV source made by four-wave mixing in Mg vapor. Because of the photolysis conditions for the  $\text{H}_2\text{S}$ , the initial translational energy is well-specified, and because of the expansion, nearly all of the CO is initially in  $v=0, J=0$ . The final product distribution can be completely determined; vibrational and rotational distributions will be reported and compared to results predicted by trajectory calculations on an ab initio surface.



ENERGY DISPOSAL IN  $O(^1D) + NH_3 \rightarrow NH_2 + OH$   
REACTION.

S.G.Cheskis, A.A.Iogansen, P.V.Kulakov, A.A.Titov,  
and O.M.Sarkisov.

The  $NH_2$  and  $OH(v)$  radicals kinetics were directly monitored by LIF-technique after laser photolysis of ozone in  $O_3:NH_3:Ar$  gas system. Room-temperature rate constant for the reaction

$O(^1D) + NH_3 \rightarrow NH_2 + OH$   $\Delta H^\circ = -40$  kcal/mole (1)  
was measured to be  $(3.3 \pm 1) \cdot 10^{-10}$  cm<sup>3</sup> molecule<sup>-1</sup> s<sup>-1</sup> by studying the ground state  $NH_2$  accumulation profiles.

A kinetic approach was employed for investigation of nascent vibrational energy distribution of  $NH_2$  and  $OH$  in the reaction (1). This approach consists in the standard kinetic measurements of collisional quenching of vibrationally excited products and subsequent restoration of their initial distributions on the basis of this kinetic data.

The detailed initial  $OH(v)$ -distribution was determined:  
 $P(v=0):P(v=1):P(v=2):P(v=3) = 0.2 : 0.32 : 0.33 : 0.15$ .

The fraction of  $NH_2$  formed in reaction (1) in the vibrationally excited states was found to be  $(58 \pm 8) \%$ .

Comparison of the obtained data with the previously reported results shows that kinetic approach is a powerful means of the vibrational energy distribution measurements.

The interaction rate constants of the vibrationally excited  $NH_2$  and  $OH$  radicals with ozone and ammonia was also obtained.

## FORMATION AND REACTIONS OF ELECTRONICALLY EXCITED HCl

M.A. Brown, P.C. Cartwright, R.J. Donovan,  
P.R.R. Langridge-Smith, K.P. Lawley

Department of Chemistry, University of Edinburgh,  
West Mains Road, Edinburgh EH9 3JJ (U.K.)

The reactions of electronically excited xenon atoms ( $\text{Xe } ^3\text{P}_{2,1,0}$ ) with ground state hydrogen chloride leading to XeCl exciplex chemiluminescence have been well studied [1,2]. However, little work has been done on the complementary reaction, namely that of electronically excited HCl with the ground state noble gas atom. Selective excitation of HCl is difficult because of the highly energetic nature of the electronic states involved. From previous high resolution V.U.V. absorption spectroscopic studies [3] and recent ab initio CI calculations [4], it is also clear that these high lying excited state potentials are complex, being dominated by considerable mixing between the valence  $\sigma \rightarrow \sigma^*$  "Ion-pair" state and "Rydberg" states of the same symmetry [5]. Recently Zimmerer et al [6] have reported single photon excitation of HCl using tunable V.U.V. synchrotron radiation. Our approach has been to use laser multiphoton excitation, with tunable U.V. radiation in the region 230-240 nm, produced by optical non-linear frequency doubling and mixing techniques.

Figure 1(a) shows a [2+1] multiphoton ionisation spectrum of HCl for two typical vibronic levels near 10.5 eV. One vibronic level being  $v' = 11$  of the "Ion-pair" state and the other, the  $v' = 0$  level of a "Rydberg"-like state that is strongly vibronically coupled to the "Ion-pair" state [5]. Dispersed fluorescence spectra following excitation at the Q(3) feature of each vibronic band are shown in Figure 1(b). Fluorescence to the vibrational continuum and highly excited vibrational levels of the ground state is observed. The appearance of XeCl exciplex ( $\text{B}^2\Sigma^+ + \text{X}^2\Sigma^+$ ) chemiluminescence is seen (Figure 1(c)) following excitation of HCl in the presence of Xe (10 torr). The XeCl exciplex action spectrum (monitored at 308 nm) follows that of the HCl MPI spectrum, showing that electronically excited HCl is responsible for the reactive channel. This and additional results involving reactions with both other electronic states of HCl and different rare gases will be further discussed.

## References

- (1) K. Johnson, J.P. Simons, P.A. Smith, C. Washington and A. Kvaran, *Mol. Phys.*, **57** (1986), 255.
- (2) M. de Vries, G.W. Tyndall, C.L. Cobb and R.M. Martin, *J. Chem. Phys.*, **84** (1986), 3753.
- (3) A.E. Douglas and F.R. Greening, *Can. J. Phys.*, **57** (1979), 1650.
- (4) M. Betterdorff, S.D. Peyerimhoff and R.J. Buenker, *Chem. Phys.*, **66** (1982), 261.
- (5) M.A. Brown, P.C. Cartwright, R.J. Donovan, P.R.R. Langridge-Smith, and K.P. Lawley, unpublished results.
- (6) G. Zimmerer, "Kinetics of Excited States Produced by Synchrotron Radiation" in *Photophysics and Photochemistry above 6 eV*. Ed. F. Lahmani.

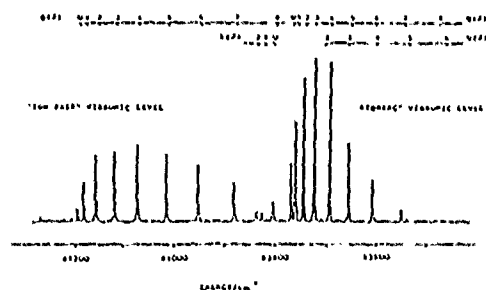


Figure 1(a)  $[2+1]$  MPI spectrum of electronically excited HCl.

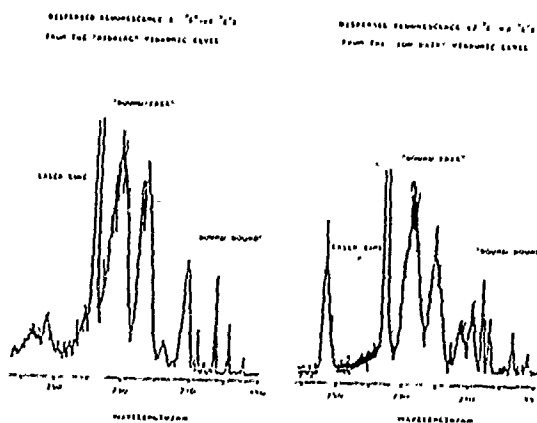


Figure 1(b) Dispersed fluorescence spectra of electronically excited HCl.

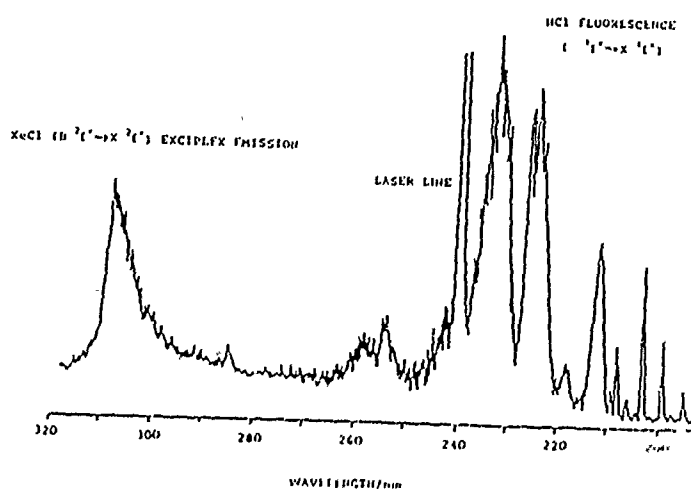


Figure 1(c) Dispersed fluorescence showing  $\text{XeCl}(B^2_{1/2} - X^2_{1/2})$  exciplex chemiluminescence.

ArF-Laser Photolysis of Hydrazoic Acid:  
Formation and Kinetics of  $\text{NH}(\text{c}^1\pi)$

F. Rohrer and F. Stuhl

Physikalische Chemie I, Ruhr-Universität Bochum, D-4360 Bochum 1,  
Federal Republic of Germany

Long Abstract

Recently we have observed the generation of four different excited  $\text{NH}(\text{a}^1\Lambda, \text{b}^1\Sigma^+, \text{c}^1\pi, \text{A}^3\pi)$  states in the ArF-laser photolysis of  $\text{HN}_3$ . Since kinetic data on the quenching of  $\text{NH}(\text{c}^1\pi)$  is scarce<sup>1)</sup> and details of the quenching mechanisms of excited small molecules are not well understood we have used this photolysis system to investigate its kinetics in the presence of a number of added gases.

In these experiments, gaseous  $\text{HN}_3$  at pressures ranging from 0.013 to 13 Pa was irradiated by the unfocussed ArF-laser beam (30  $\text{mJ}/\text{cm}^{-2}$ ; 15 ns; 193.3 nm). Excited  $\text{NH}(\text{c})$  radicals were detected by emissions from their  $\text{NH}(\text{c} \rightarrow \text{a}$  and  $\text{b})$ -transitions. The  $\text{NH}(\text{c}, v'=0$  and  $1, J')$  radicals were produced with a rotational distribution close to that corresponding to  $T_{\text{rot}}=800$  K. About 10% of the available energy appears as rotation and  $\sim 1\%$  as vibration. The quantum yield for the production of  $\text{NH}(\text{c})$  was estimated to be 0.0005 assuming no ground state  $\text{NH}(\text{X})$  is formed.

Lifetimes of the  $\text{NH}(\text{c})$  fluorescence were determined using a time constant of 30 ns. The zero pressure lifetimes of  $v'=0$  and  $1$  were measured to be  $470 \pm 15$  and  $65 \pm 20$  ns, respectively. The value for  $v'=0$  is taken to represent the radiative lifetime while that for  $v'=1$  is shortened by predissociation.

Rotational relaxation was observed to be very efficient. In the presence of Ar, for example, the addition of 6600 Pa was sufficient to generate a rotational distribution corresponding to room temperature within 50 ns. Quenching cross sections were determined in the presence of Ar, hence, to render a completely relaxed rotational distribution ( $T_{\text{rot}}=300$  K). This way, the measured quenching cross sections represent a weighted average over the collisionally coupled, rotational states at room temperature.

Table 1. Cross sections/ $10^{-16} \text{ cm}^{-2}$  for the quenching of several excited hydrides

Gas	NH(c) <sup>a)</sup>	NH(A) <sup>b)</sup>	CH(A) <sup>c)</sup>	
He	$\leq 0.0004$	$\leq 0.0046$	$< 0.0007$	a) this work
Ar	$\leq 0.001$	$\leq 0.011$	$< 0.005$	b) Ref. 2
Kr	2.58		2.44 <sup>a,d)</sup>	c) Ref. 3 for $N'=0-7$
Xe	32.9	6.0	15.6 <sup>a,d)</sup>	d) for the rotational distribution given in Ref. 4
SF <sub>6</sub>	0.032		0.026 <sup>a,d)</sup>	
N <sub>2</sub>	1.64	$\leq 0.0061$	6.7-2.5	
H <sub>2</sub>	8.01	4.4	11.6-6.5	
D <sub>2</sub>	7.63		11.0-5.9	
CO	41.8	6.4	49.6-27.6	
O <sub>2</sub>	24.2	4.3	21-10.5	
NO	71.6	17	47.7-30	
CO <sub>2</sub>	27.4	0.97	69-20.9	
H <sub>2</sub> O	88.9		92.9-73.9	
D <sub>2</sub> O	58.0		70.7-28.2	
CH <sub>4</sub>	27.3	8.0	34.4-26.3	

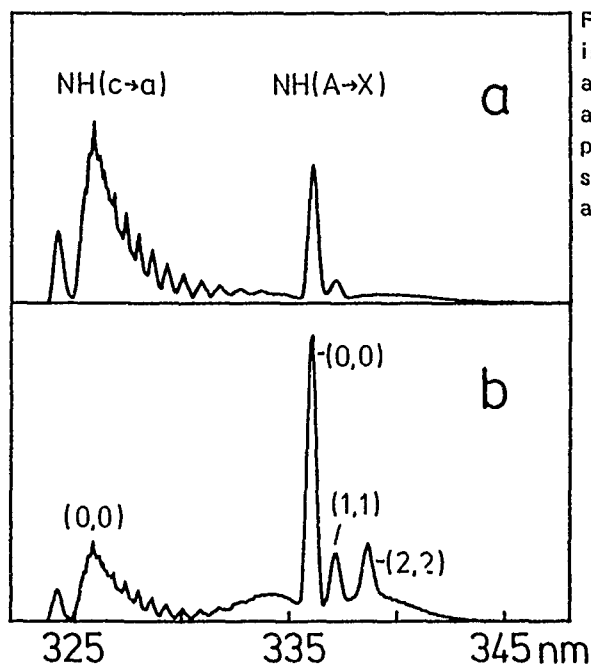


Fig. 1. Fluorescence intensities of NH(c) and NH(A) in (a) the absence and (b) the presence of O<sub>2</sub>. Pressures: 0.27 Pa HN<sub>3</sub> and 53.2 Pa O<sub>2</sub>.

The values obtained are listed in Table I together with those previously reported on the quenching of  $\text{NH}(\text{A}^3\Pi^2)$  and  $\text{OH}(\text{A}^2\Sigma^3)$ . Similarities and differences in Table I will be discussed in terms of attractive forces and calculated potential curves.

The quenching of the unrelaxed original rotational distribution (in the absence of Ar) was observed to be slightly less efficient for several added gases. This trend was found to be reversed for the addition of  $\text{O}_2$  and NO. For these quenchers, the removal rate for  $\text{NH}(\text{c})$  can be correlated with the growth rate observed for the  $\text{NH}(\text{A})$  fluorescence. Fig. 1 shows the resulting overall fluorescence intensity changes during a time interval 1  $\mu\text{s}$  after the laser shot. While the intensity of the  $\text{NH}(\text{c} \rightarrow \text{a})$  fluorescence significantly decreases by the efficient quenching by  $\text{O}_2$ , the intensity of the  $\text{NH}(\text{A})$  increases in spite of some quenching by the added  $\text{O}_2$ . Figure 1 additionally shows that  $\text{NH}(\text{A})$  is formed also as a primary product. The relative quantum yields for the primary production of  $\text{NH}(\text{c})$  and  $\text{NH}(\text{A})$  and the appropriate quenching constants were taken into account to calculate the efficiency of the collision induced intersystem crossing to be close to one for both  $\text{O}_2$  and NO.

For the addition of  $\text{O}_2$ , Fig. 1 clearly demonstrates the enhancement of  $\text{NH}(\text{A})$  in  $v=2$  and 1 (besides  $v=0$ ). We propose  $\text{O}_2(\text{a}^1\Delta)$  in the vibrational states  $v=0, 2$ , and 4 to be formed in the reaction  $\text{O}_2 + \text{NH}(\text{c})$ . For this set of products, total spin is conserved and near resonances exist being slightly endothermic.

The authors acknowledge financial support by the Deutsche Forschungsgemeinschaft (SFB 42).

#### References

- 1) T.G. Slanger in "Reactions of Small Transient Species", A. Fontijn and M.A.A. Clyne, Eds., Academic Press, 1983.
- 2) A. Hofzumahaus and F. Stuhl, J. Chem. Phys. 82, 3152 (1985).
- 3) R.A. Copeland, M.J. Dyer, and D.R. Crosley, J. Chem. Phys., 82, 4022 (1985).
- 4) R.D. Kenner, F. Rohrer, Th. Papenbrock, and F. Stuhl, J. Phys. Chem. 90, 1294 (1986).

RECENT ADVANCES IN FREE RADICAL KINETICS OF OXYGENATED HYDRO-  
CARBON SPECIES

Reinhard Zellner

Institut für Physikalische Chemie, Universität Göttingen,  
Tammannstraße 6, 3400 Göttingen

The kinetics of oxygenated hydrocarbon radicals are a central element of hydrocarbon oxidation at both low and high temperatures. Among the large variety of such radicals a few of them are accessible to isolated generation and direct time resolved detection using presently available laser techniques. In this presentation recent results obtained for the kinetics and energetics of reactions involving such radicals will be reviewed.

Methoxy ( $\text{CH}_3\text{O}$ ) and methylperoxy ( $\text{CH}_3\text{O}_2$ ) are the simplest oxygenated hydrocarbon radicals that appear in methane oxidation. From their chemical behaviour they may be considered as the hydrocarbon analogues of  $\text{OH}$  and  $\text{HO}_2$ , respectively. The kinetics of their reactions therefore deserves special attention both in view of the absolute rate coefficients as well as their theoretical interpretations. As an example for which there is thorough comparative information available for the corresponding reactions of  $\text{HO}_x$  we will present recent results obtained for reactions of  $\text{CH}_3\text{O}_x$  with  $\text{O}$  atoms and  $\text{NO}$ . Although the hydrocarbon system has in general more than one product channel, it will be shown that the gross features of the kinetics can well be represented by assuming the reactions to occur via bound intermediates.

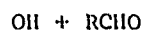
Unlike  $\text{OH}$ , oxy-radicals of the hydrocarbon system also react with  $\text{O}_2$ . As a representative example we will first present recent results for  $\text{CH}_3\text{O} + \text{O}_2$ , for which we have measured  $k(T)$  and the yield of  $\text{CH}_2\text{O}$ . Both quantities indicate that the reaction is more complex than simple  $\text{H}$  atom abstraction.

Possible alternatives will be discussed. A mechanism of still larger complexity is observed for the reaction of vinoxy ( $\text{CH}_2\text{CHO}$ ) with  $\text{O}_2$ . Here the primary process is probably the addition of  $\text{O}_2$  to the carbon radical center. This is reflected by the pressure dependence of the overall rate coefficient and its negative activation energy. However, the formation of "bimolecular" products, including OH and  $\text{CH}_2\text{O}$ , is also observed. These probably result from the unimolecular break-up of the 1,4-H atom-shifted vinoxy- $\text{O}_2$  adduct. A potential diagram accounting for these observations will be presented.

Reactions of OH radicals with aromatics at low temperatures are assumed to form the corresponding adducts. For OH + benzene we have recently succeeded to directly monitor the formation of hydroxy-cyclohexadienyl (HCND) by long-path UV-laser absorption. The same technique has also been used to study reactions of HCND in isolation. Results will be presented for direct investigations of the thermal stability of HCND and for its reactions with NO,  $\text{NO}_2$ , and  $\text{O}_2$ . The consequences of these results for the low temperature oxidation of benzene will be discussed.



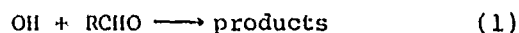
## STRUCTURE-REACTIVITY RELATIONSHIPS IN THE REACTION SERIES



S.Dóbbé, T.Bérces and F.Márta

Central Research Institute for Chemistry,  
Hungarian Academy of Sciences, Budapest, Hungary

The kinetics of OH radical reactions



has been investigated in an isothermal fast flow reactor. The OH radicals are generated in the reaction of H-atoms with excess  $\text{NO}_2$  and the decay of OH is monitored by resonance fluorescence technique. The reaction temperature has been varied in a wide range using oil thermostating jacket and electric heating.

Rate coefficients and Arrhenius parameters have been determined for reaction (1) for R groups  $\text{R} = \text{CH}_3, \text{CCl}_3, \text{CF}_3$ .

Reactivities and activation energies follow a trend expected on the basis of the strengths of the formyl C - H bonds. Comparison of experimental kinetic data with estimations based on semiempirical schemes indicate, however, that the correlation with bond energies is only qualitative. Polarity effect appear to play some role in these reactions.

The Arrhenius activation energies were found to be small and to change with temperature. Reasons of deviations from the Arrhenius law are discussed and experimental temperature dependences of the rate coefficients are compared with theoretical results.

CN GAS PHASE KINETICS PROBED BY A DIODE LASER

R. Jeffrey Balla and Louise Pasternack, Chemistry Division, Naval Research Laboratory,  
Washington, D.C. 20375-5000.

The room temperature kinetics of CN with H<sub>2</sub>, D<sub>2</sub> and CH<sub>4</sub> have been studied using a diode laser as a probe for both CN disappearance and HCN appearance. CN is produced by ArF excimer laser (193 nm) photolysis of cyanogen. The P(7)  $v=0 \rightarrow v=1$  absorption of CN ( $X^2\Sigma^+$ ) at 2015.2 cm<sup>-1</sup> is monitored as it decays following photolysis under pseudo-first-order conditions. We also measure the rise of HCN by monitoring the  $\nu_3$  vibration near 3311 cm<sup>-1</sup>. Buffer gases are added to ensure vibrational and rotational equilibration. A typical time resolved scan of the CN absorption is shown in Figure 1.

Absolute rate constants for CN+H<sub>2</sub>, CN+D<sub>2</sub>, and CN+CH<sub>4</sub> have been measured and are shown in Table 1.

Table 1: Reaction rates of CN

Reaction	Rate constant (cm <sup>3</sup> s <sup>-1</sup> ) (+2 $\sigma$ )	Pressure Range (Torr)
CN+H <sub>2</sub>	(2.58 $\pm$ 0.28) x 10 <sup>-14</sup>	10-100
CN+D <sub>2</sub>	(7.15 $\pm$ 0.86) x 10 <sup>-15</sup>	10-200
CN+CH <sub>4</sub>	(7.82 $\pm$ 0.86) x 10 <sup>-15</sup>	1-10

These rates are constant over the pressure range shown in Table 1. A typical plot of the  $\text{CN}+\text{D}_2$  pseudo-first-order reaction rate vs  $\text{D}_2$  pressure is shown in Figure 2. The reaction of  $\text{CN}+\text{H}_2$  has been studied using ab initio calculations by Bair and Dunning<sup>1</sup> and Wagner and Bair.<sup>2</sup> In cooperation with the NRL Laboratory for Computational Physics, we have extended these calculations to the  $\text{CN}+\text{D}_2$  reaction in order to determine the predicted kinetic isotope effect. The predicted value of  $k(\text{H}_2)/k(\text{D}_2)$  is 3.5, in excellent agreement with our experimental results.

We have also measured the integrated line strength for the  $P(7) \nu=0 \rightarrow \nu=1 \text{ CN}(X^2\Sigma^+)$  absorption. These experiments are performed under low pressure conditions to ensure only Doppler broadening. A value of  $S=(1.5 \pm 0.5) \times 10^{-19} \text{ cm}^2 \text{ molecule}^{-1} \text{ cm}^{-1}$  is measured.

#### REFERENCES:

- <sup>1</sup> R.A. Bair and T.H. Dunning, Jr., J. Chem. Phys., 82, 2280-2294 (1985).
- <sup>2</sup> A.F. Wagner and R.A. Bair, Int. J. of Chem. Kinetics, to be published.

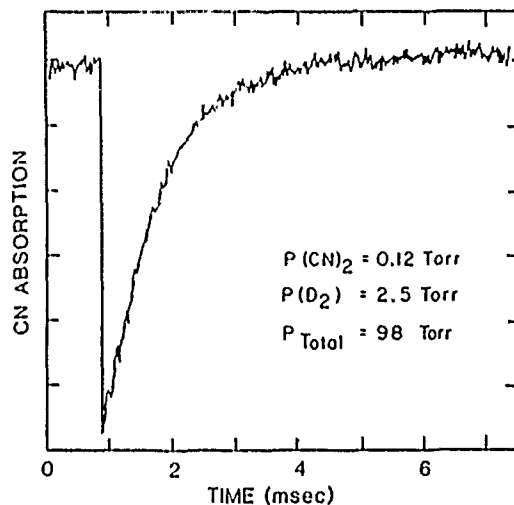


Figure 1. Time resolved scan of CN absorption. In this scan,  $P(\text{CN})_2 = 0.12 \text{ Torr}$ ,  $P(\text{D}_2) = 2.5 \text{ Torr}$ , and total pressure = 98 Torr.

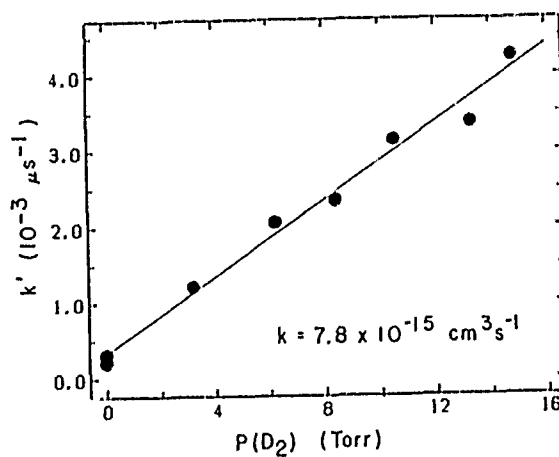


Figure 2. A plot of the pseudo-first-order reaction rate constant,  $k'$ , versus reactant pressure for the reaction of  $\text{CN} + \text{D}_2$ . The slope corresponds to a second-order rate constant of  $7.8 \times 10^{-15} \text{ cm}^3 \text{ s}^{-1}$ . The intercept reflects CN removal by diffusion and reaction with the precursor.

## Kinetic Microwave Spectroscopy of Reaction Intermediates:

## Atomic Oxygen Reactions with Olefins

Seiichiro KODA<sup>\*</sup>, Soji TSUCHIYA<sup>\*\*</sup>, Yasuki ENDO, Chikashi YAMADA  
and Eiichi HIROTA

Institute for Molecular Science, Okazaki 444, JAPAN

<sup>\*</sup> Department of Reaction Chemistry, Faculty of Engineering,  
University of Tokyo, Hongo, Bunkyo-ku, Tokyo 113, JAPAN

<sup>\*\*</sup> Department of Pure and Applied Sciences, College of Arts and  
Sciences, University of Tokyo, Komaba, Meguro-ku, Tokyo 153,  
JAPAN

A microwave spectroscopic method has been developed for kinetic studies of elementary reactions, in which reaction intermediates such as free radicals with lifetimes as short as 1 ns are directly analysed in situ condition. This method was applied to clarifying the primary mechanism of the atomic oxygen  $O(^3P)$  reactions with ethylene and tetrafluoroethylene.

Recent studies<sup>1)</sup> on the reaction of  $O(^3P)$  with ethylene have shown that both of channel (a) to yield vinoxy + H and channel (b) to yield  $CH_3 + HCO$  play important roles. But the pressure-dependency of the branching ratio has not been fully investigated. A low-pressure experiment is invaluable in order to clarify whether channel (b) is induced by intermolecular collisions or not. Microwave kinetic spectroscopy can pursue the reaction progress at a low pressure such as 0.1 Torr or less by observing the spectra of transient species as well as products in real time.

The reaction was initiated by pulsed irradiation of the

253.7 nm mercury resonant line onto an  $\text{N}_2\text{O}$ /ethylene mixture containing a trace amount of mercury vapor. A quartz tube of 1 m in length and 9 cm in inner diameter was used as a reaction/absorption cell, which was surrounded by 15 germicidal lamps of 30 W each. The light pulse was chosen to be typically of 4 ms duration. Sample gases were passed over a mercury reservoir to be saturated with mercury vapor and were then passed through the cell. The time evolution of vinoxy, HCO and  $\text{H}_2\text{CO}$  during and after the light pulse was pursued in terms of the absorption of the  $17_{0,17}-16_{0,16}$  (342311.5 MHz),  $4_{0,4}-3_{0,3}$  ( $J=4.5-3.5$ ,  $F=5-4$ , 346708.5 MHz), and  $5_{1,5}-4_{1,4}$  (351768.6 MHz) transition, respectively. The effective absorption coefficients were estimated on the basis of the dipole moment and the measured line-width at the cell pressure.

Both vinoxy and HCO were found to be formed right after the onset of the light pulse. After some kinetical treatments, the branching ratio was determined to be  $0.4 \pm 0.1$  and  $0.5 \pm 0.1$  for (a) and (b), respectively, at the pressure of 30 mTorr. In the presence of additional argon up to 300 mTorr, the branching ratio remained almost the same within experimental uncertainty. Taking into account the previous studies<sup>1)</sup> altogether, the ratio seems to be almost insensitive to the pressure over the wide range from 30 mTorr to 760 Torr. Moreover, the present pressure of 30 mTorr corresponds to the collision frequency of about  $3 \times 10^5 \text{ s}^{-1}$  assuming a hard-sphere collision cross section, and a collision complex of O and ethylene, if exists, is unlikely to survive as long as  $3 \times 10^{-6} \text{ s}$ . Therefore, channel (b) is not collisionally induced but may take place through an intramolecular path. An

intramolecular conversion between the potential surfaces leading to channels (a) and (b) may easily proceed if these two surfaces come close each other at some reaction coordinates.

In the reaction of  $O(^3P)$  with tetrafluoroethylene, the production of  $^3CF_2$  was established on the basis of its phosphorescent emission,<sup>2)</sup> but its quantum yield is not determined. Though we have not yet succeeded in detecting  $^3CF_2$  with the present microwave spectroscopic method, the time evolution of the ground state  $^1CF_2$  was pursued in terms of the absorption of the  $14_{1,14}-13_{0,13}$  transition at 343135.4 MHz. It was strongly suggested that the  $^1CF_2$  was mostly produced via quenching of the primarily produced  $^3CF_2$ . The reaction of O with tetrafluoroethylene is thus considered to proceed on a triplet reaction surface.

#### References

- 1) J. F. Smalley, F. L. Nesbitt, and R. B. Klemm, J. Phys. Chem. 90, 491 (1986), and lit. cited therein.
- 2) S. Koda, J. Phys. Chem. 83, 2065 (1979).



Kinetics of the  $\text{CH}_3 + \text{D}$  reaction : an anomalous  
isotope effect

M. Brouard and M.J. Pilling

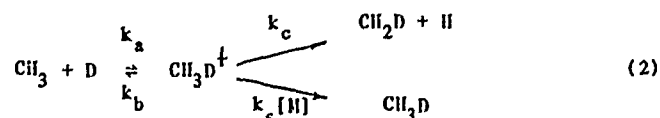
Physical Chemistry Laboratory, South Parks Road,  
Oxford, OX1 3QZ, U.K.

We recently developed a laser flash photolysis technique for measuring atom plus radical reactions, in which the atom is monitored by time-resolved resonance fluorescence and the radical by time-resolved absorption spectroscopy<sup>1</sup>. The technique has been applied to the  $\text{CH}_3 + \text{H}$  reaction,



over the temperature and pressure ranges  $300 \leq T/\text{K} \leq 600$ ;  $25 \leq P/\text{Torr} \leq 600$  (Fig. 1)<sup>2</sup>. Under these conditions the reaction is well into the fall-off regime and, whilst  $k_1^\infty$  may be obtained by extrapolation using, for example, the Troe factorisation technique, the uncertainty in  $k_1^\infty$  is significant but difficult to assess.

Over the past few years, considerable theoretical effort has been devoted to reaction (1) and, in particular, to the calculation of  $k_1^\infty$ . Precise experimental data are required for comparison with these calculations. We have investigated the reaction between  $\text{CH}_3$  and D:



using the technique employed for reaction (1). Because of zero point energy differences  $k_c \gg k_b$  and the overall rate constant for deuterium atom loss,  $k_2$ , should be close to  $k_a$ . The determination of  $k_a$  should enable the limiting high pressure rate constant for reaction (1),  $k_1^\infty$ , to be evaluated by simple correction for mass differences.

As expected,  $k_2$  was found to be independent of pressure over the range  $50 \leq P/\text{Torr} \leq 600$  and it is also independent of temperature over the range  $289 \leq T/K \leq 401$  with a mean value of  $(1.75 \pm 0.045) \times 10^{-10} \text{ cm}^3 \text{ molecule}^{-1} \text{ s}^{-1}$ . The corresponding value for  $k_1^\infty$  is  $(2.47 \pm 0.06) \times 10^{-10} \text{ cm}^3 \text{ molecule}^{-1} \text{ s}^{-1}$  and Fig. 2 shows an attempt to fit the 300 K fall-off data for  $k_1$  with this high pressure limit. The data are clearly incompatible with such a value. Fig. 2 also shows a fit to the data with  $k_1^\infty = 4.7 \times 10^{-10} \text{ cm}^3 \text{ molecule}^{-1} \text{ s}^{-1}$ , which is much more satisfactory. It appears from these experimental data that the limiting high pressure rate constant for reaction (1) may not be evaluated from  $k_2$  by a simple transition state calculation.

#### References

1. M. Brouard, M.T. Macpherson, M.J. Pilling, J.M. Tulloch and A.P. Williamson, Chem. Phys. Letters, 1985, 113, 413.
2. M. Brouard, M.T. Macpherson and M.J. Pilling, in preparation.
3. See, for example, R.J. Duchovic and W.L. Hase, J. Chem. Phys., 1985, 83, 3448; J.F. LeBlanc and P.D. Pacey, J. Chem. Phys., 1985, 83, 4511; C.J. Cobos and J. Troe, Chem. Phys. Letters, 1985, 113, 419.

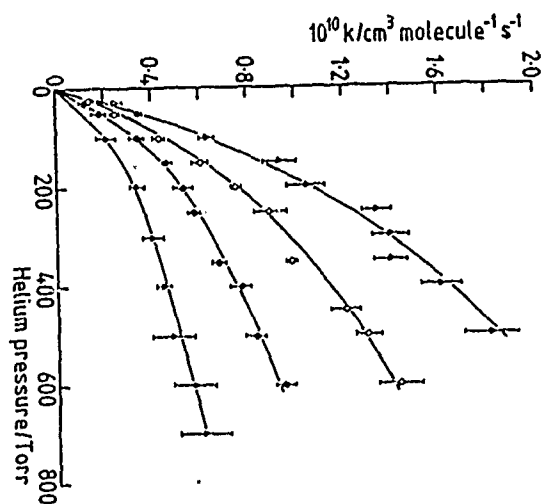


Fig. 1 Fall-off data for reaction (1) in a helium diluent:  $\Delta$ , 300 K;  $\circ$ , 400 K;  $\bullet$ , 500 K;  $\triangle$ , 600 K. The error bars represent 95% confidence limits.

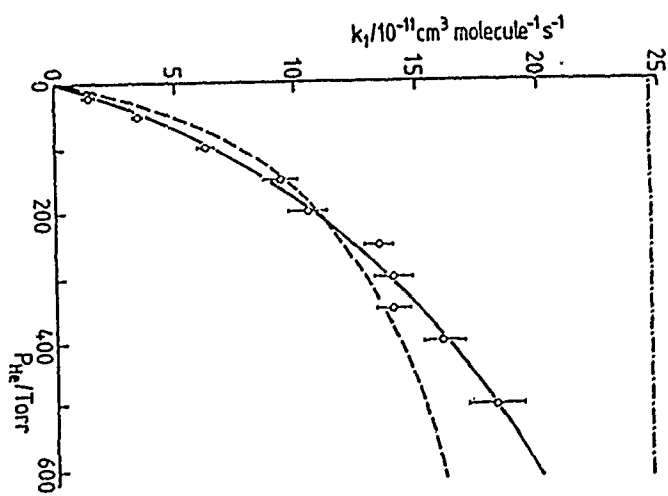


Fig. 2 Comparison of the experimental fall-off curve for reaction (1) at 300 K with the best fit curve calculated with  $k_1^{\infty}$  calculated from  $k_1^{\infty} = 2.47 \times 10^{-10} \text{ cm}^3 \text{ molecule}^{-1} \text{ s}^{-1}$ ;  $\text{---}$ , best fit curve with  $k_1^{\infty} = 2.47 \times 10^{-10} \text{ cm}^3 \text{ molecule}^{-1} \text{ s}^{-1}$ ;  $\text{---}$ , best fit curve with  $k_1^{\infty}$  fixed (optimal fit at  $k_1^{\infty} = 4.68 \times 10^{-10} \text{ cm}^3 \text{ molecule}^{-1} \text{ s}^{-1}$ ).

The Reaction  $O_2^+ + CH_4 \rightarrow H_2COOH^+ + H$ 

Eldon E. Ferguson

Aeronomy Laboratory

National Oceanic and Atmospheric Administration

Boulder, Colorado 80303

There have been a number of studies of the reaction between  $O_2^+$  and  $CH_4$  during the past 20 years. Recent studies at Colorado University have established the product ion to be methylene hydroperoxy cation,<sup>1</sup> in contrast to published reports that it is protonated formic acid. The  $H_2COOH^+$  product ion undergoes  $H^-$  transfer from alkanes larger than ethane and other hydrocarbons. It transfers the  $OH^+$  group to  $CS_2$  and many other neutrals and it proton transfers to  $H_2O$ ,  $NH_3$  and other neutrals of large proton affinity. The ion follows all three of these reaction paths with  $CH_3C(O)H$  and  $C_2H_5C(O)H$ . The ion does not exchange H atoms with  $D_2O$ . This chemistry is completely different than that of the very much more stable protonated formic acid in  $HC(OH)_2^+$ . The value of  $\Delta H_f(H_2COOH^+)$  is found to be  $185 \pm 3 \text{ kcal mol}^{-1}$ .

The reaction rate constant has been measured<sup>2</sup> over the temperature range 20-560K and as a function of relative kinetic energy from 0.01 eV to 2 eV.<sup>3,4</sup> The reaction rate constant has been determined for the five  $CH_nD_{4-n}$  isotopes.<sup>5</sup>

From this wealth of experimental data it has been possible to deduce the reaction mechanism in great detail. The reaction proceeds over a double potential minimum surface. A reversible electrostatically bound complex (well depth  $9 \text{ kcal mol}^{-1}$ ) with a lifetime  $\sim 10^{-10}$  sec at 300K is

formed initially. On  $\sim 0.5\%$  of the collisions (at 300K) an irreversible hydride ion transfer occurs over an  $8 \pm 1$  kcal mol $^{-1}$  barrier, yielding the stable (but highly excited) ion  $\text{H}_3\text{COOH}^+$ . The electrostatic well-depth and the barrier height are deduced from recent measurements of Böhrringer and Arnold.<sup>6</sup>

Following the irreversible  $\text{H}^-$  transfer from  $\text{CH}_4$  to  $\text{O}_2^+$  to produce  $\text{H}_3\text{COOH}^+$ , an H atom is rapidly ejected from carbon to yield the final product  $\text{H}_2\text{COOH}^+ + \text{H}$ . The overall reaction is  $22 \pm 3$  kcal mol $^{-1}$  exothermic.

The product ion is stable against exothermic (by 49 kcal mol $^{-1}$ ) decomposition into  $\text{HCO}^+ + \text{H}_2\text{O}$  or the even more exothermic (by 74 kcal mol $^{-1}$ ) decomposition into  $\text{H}_3\text{O}^+ + \text{CO}$ . A barrier of  $23 \pm 5$  kcal mol $^{-1}$  exists for decomposition into  $\text{HCO}^+ + \text{H}_2\text{O}$ . This leads to a proton bonding energy of  $\sim 162$  kcal mol $^{-1}$  for  $\text{H}_2\text{COOH}^+$ . We believe the neutral products of proton transfer are  $\text{CO} + \text{H}_2\text{O}$ . A simple proton transfer leaving  $\text{H}_2\text{COO}$  would be very endothermic.

The reaction rate constant increases almost linearly with number of H atoms going from  $\text{CD}_4$  to  $\text{CH}_4$  due to the H/D isotope effect of 3 for  $\text{H}^-/\text{D}^-$  transfer in the rate-controlling hydride ion transfer step. The product ion composition, however, is almost statistical (or random) due to the fortuitously off-setting H/D isotope effect in the ejection rate in the final step. Eleven measured isotopic parameters (including internal isotopic distributions for  $\text{CHD}_2\text{O}_2^+$  and  $\text{CH}_2\text{DO}_2^+$ ) are explained with the two isotopic parameters, one of which is a theoretically determined parameter.

The reaction rate constant dependence on temperature is well fit by a statistical theoretical model.

## References

1. J.M. Van Doren, S.E. Barlow, C.H. DePuy, V.M. Bierbaum, I. Dotan, and E.E. Ferguson, J. Phys. Chem., May 1986.
2. B.R. Rowe, G. Dupeyrat, J.B. Marquette, D. Smith, N.G. Adams and E.E. Ferguson, J. Chem. Phys. 80, 241 (1984).
3. N.G. Adams, D. Smith and E.E. Ferguson, Int. J. Mass Spectrom. and Ion Processes, 67, 67 (1985).
4. M. Durup-Ferguson, H. Böhrringer, D.W. Fahey, F.C. Fehsenfeld and E.E. Ferguson, J. Chem. Phys. 81, 2657 (1984).
5. S.E. Barlow, J.M. Van Doren, C.H. DePuy, V.M. Bierbaum, I. Dotan, E.E. Ferguson, N.G. Adams, D. Smith, B. Rowe, J.B. Marquette, G. Dupeyrat and M. Durup-Ferguson, J. Phys. Chem. (to be published).
6. H. Böhrringer and F. Arnold, J. Chem. Phys. 84, 2097 (1986).

KINETICS OF ION MOLECULE REACTIONS AT VERY LOW  
TEMPERATURE : THE CRESU TECHNIQUE

C. Rebrion, J.B. Marquette, B.R. Rowe, G. Dupeyrat  
Laboratoire d'Aérothermique du C.N.R.S.  
4ter, route des Gardes, 92190 Meudon (France)

1 - INTRODUCTION

A detailed understanding of the formation of complex molecules in dense interstellar clouds requires a good knowledge of ion-molecule reaction kinetics at extremely low temperatures (in the range 10-100K). From a fundamental point of view, very low levels are involved in the reaction at such temperatures, leading to a more tractable theoretical problem. Also, this could allow the determination of the rotational state influence on the reactivity. When the formation of an excited complex is involved, its lifetime is considerably enhanced at the lowest temperatures yielding large effects on the kinetics.

The CRESU technique that we have developped in our laboratory is able to measure rate coefficients with condensable species under true thermal conditions in the range 8-160K. Detailed descriptions of the technique are published elsewhere /1-3/. The low temperature is obtained by the isentropic expansion of a buffer gas, containing both ion parent and neutral reactant gases, through a suitably contoured Laval nozzle. Ions are created close downstream from the nozzle exit by an electron beam. Primary and product ions are monitored by means of a moveable quadrupole mass spectrometer associated with a particle counting system.

2 - RESULTS

In case of fast reactions all theories assume that they are dominated by long-range intermolecular forces /4/. For non-polar molecules the Langevin ion-induced-dipole theory predicts no variation in the rate

coefficient with temperature ; for these molecules quadrupole moments or anisotropy of polarizability yield additional terms in the interaction potential, which may cause variations of the kinetics with temperature. In the case of polar molecules various theories (ADD, AADD /4/, ACCSA /5/) predict an increase of the rate coefficient at the lowest temperatures.

Three sets of experimental data have been obtained concerning fast reactions of  $\text{He}^+$ ,  $\text{N}^+$  and  $\text{C}^+$  ions occurring with non-polar or slightly polar molecules ( $\text{O}_2$ ,  $\text{CH}_4$ ,  $\text{CO}$ ) /6/, with very polar molecules ( $\text{H}_2\text{O}$ ,  $\text{NH}_3$ ) /7/ and with non-polar molecules presenting very large quadrupole moments ( $\text{C}_6\text{F}_6$ ,  $\text{C}_6\text{H}_{12}$ ).

It follows from these experiments that, within the stated experimental uncertainty ( $\pm 30\%$ ), there is no significant change in the reaction rate coefficient for neutrals with important anisotropic polarizabilities or very large quadrupole moments. In contrast the rate coefficients largely increase at the lowest temperatures for polar molecules. This is qualitatively in agreement with ADD theory. For some reactions ( $\text{C}^+$ ,  $\text{N}^+$  +  $\text{H}_2\text{O}$ ) there is a very good agreement with the ACCSA theory (D.C. Clary, private communication).

Several other reactions have been studied using our technique : association reactions of  $\text{N}_2^+$  with  $\text{N}_2$  and  $\text{O}_2^+$  with  $\text{O}_2$  leading respectively to  $\text{N}_4^+$  and  $\text{O}_4^+$  /2/ and slow reactions at room temperature like  $\text{N}_2^+ + \text{O}_2 \rightarrow \text{O}_2^+ + \text{N}_2$  and  $\text{O}_2^+ + \text{CH}_4 \rightarrow \text{CH}_3\text{O}_2^+ + \text{H}$  /1/. In this case the large increase of the rate coefficient towards the lowest temperatures can be seen as a result of the much longer reaction complex lifetime at very low temperatures.

For  $\text{O}_2^+ + \text{CH}_{4-n}\text{D}_n$ ,  $0 \leq n \leq 4$  a joint research by various groups including our low temperature measurements has led to a very detailed understanding of this reaction /10/.

The reaction of  $\text{N}^+$  with  $\text{H}_2$  and  $\text{D}_2$  is a striking exception to the general



behavior. The rate coefficient dramatically decreases from 300K to 8K. This has been interpreted as a very slight endothermicity /10/.

### 3 - CONCLUSIONS

The CRESU measurements yield new insights on ion-molecule reaction kinetics. Our present program includes the study of the influence of rotational states on the reactivity using deuterated neutrals to vary the rotational states populations.

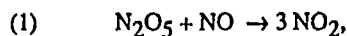
### REFERENCES

- /1/ B.R. Rowe, G. Dupeyrat, J. B. Marquette, D. Smith, N.G. Adams and E.E. Ferguson, J. Chem. Phys., 80, 241, 1984.
- /2/ B.R. Rowe, G. Dupeyrat, J.B. Marquette and P. Gaucherel, J. Chem. Phys., 80, 4915, 1984.
- /3/ G. Dupeyrat, J.B. Marquette and B.R. Rowe, Phys. of Fluids, 28, 1273, 1985.
- /4/ T. Su and M.T. Bowers in Gas phase ion chemistry, Vol 1, Ed. M.T. Bowers, Academic Press, N-Y, 1979, p. 84.
- /5/ D.C. Clary, D. Smith and N.G. Adams, Chem. Phys. Letters, 119, 320, 1985.
- /6/ B.R. Rowe, J.B. Marquette, G. Dupeyrat and E.E. Ferguson, Chem. Phys. Letters, 113, 403, 1985.
- /7/ J.B. Marquette, B.R. Rowe, G. Dupeyrat, G. Poissant and C. Rebrion, Chem. Phys. Letters, 122, 431, 1985.
- /8/ D.L. Albritton, At. Data Nucl. Data Tables, 23, 1, 1978.
- /9/ S.E. Barlow, J.M. Van Doren, C.H. Depuy, V.M. Bierbaum, I. Dotan, E.E. Ferguson, N.G. Adams, D. Smith, B.R. Rowe, J.B. Marquette, G. Dupeyrat, M. Durup-Ferguson, J. Chem. Phys. (to be submitted).
- /10/ J.B. Marquette, B.R. Rowe, G. Dupeyrat and E. Roueff, Astron. Astrophys., 147, 115, 1985.

## Neutral Reactions on Ions

A.A. Viggiano, C.A. Deakyne and J.F. Paulson  
AFGL/LID, Hanscom AFB 01731-5000

Several years ago Rowe et al.<sup>1</sup> observed for the first time an interesting set of reactions in which a neutral clustered to an alkali ion reacts with another neutral. In these reactions, the alkali ion acts mainly as a bystander providing a large electric field in which the reaction can take place. Rowe et al.<sup>1</sup> found that the reaction (1),



proceeds at a rate at least 9 orders of magnitude faster when the  $\text{N}_2\text{O}_5$  is clustered to a  $\text{Li}^+$  ion than does the purely neutral reaction. Several reasons can be suggested for the origin of this rate enhancement: (1) the kinetic energy gained during the acceleration in the ion-dipole or ion-induced dipole field is sufficient to overcome the activation energy barrier; (2) the electric field alters the potential energy surface; (3) the lifetime of the complex is enhanced.

In the present work we studied experimentally several systems for which the rate enhancement is seen. We tried to pick systems that would help to distinguish between the various mechanisms for the enhancement. Molecular orbital calculations on the energies and structures of the cluster ions were also performed to aid in understanding the rate enhancement.

The measurements were done in a variable temperature flowing afterglow. The alkali ions were made by heating rhenium filaments coated with a mixture of alkali nitrate,  $\text{Al}_2\text{O}_3$  and  $\text{SiO}_2$ . This resulted in good pure signals of the alkali ion of interest after several hours of use. Clustering was enhanced by adding a diaphragm (5 mm hole diameter) between the ion source region and the flow tube. The pressure in the ion source region was on the order of 10 torr and the flow tube pressure was approximately 0.5 torr. The neutral to be clustered to the alkali ion was added downstream of the filament and upstream of the diaphragm. In order to get the best signal of the cluster ion of interest without interference from other ions, the temperature, pressure and buffer gas were varied. Three buffers were used; He, Ar and  $\text{N}_2$ .

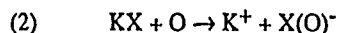
The preliminary rate constants measured in this study are given in Table 1. These rate constants are all considerably larger than those for the corresponding neutral reactions<sup>2</sup>. The largest enhancement is seen for the reaction of  $\text{Li}^+(\text{NO}_2) + \text{CO}$ , whose rate is augmented by 30 orders of magnitude over that for the gas phase reaction of  $\text{NO}_2$  and  $\text{CO}$ . The other rate enhancements are not so dramatic as this, but all are at least four orders of magnitude larger in the presence of the alkali ion.

The reaction of  $\text{NO}_2$  with  $\text{CO}$  has a gas phase activation energy<sup>2</sup> of  $28 \text{ kcal mol}^{-1}$ . The energy-gained during collision of  $\text{CO}$  with a  $\text{Li}^+$  (radius= $0.6\text{\AA}$ ) ion due to the ion-induced dipole interaction is  $108 \text{ kcal mol}^{-1}$ . Thus, the kinetic energy gained during the collision is sufficient to overcome the activation barrier in this case. In the case of  $\text{Na}^+$  (radius= $0.95\text{\AA}$ ), the energy gained from the ion-induced dipole force is only  $17 \text{ kcal mol}^{-1}$ , which is not sufficient to overcome the barrier. To

this one must add the ion-dipole term. The latter is harder to estimate due to the fact that the dipole is rotating. For a locked dipole the energy gained is  $9 \text{ kcal mol}^{-1}$ . Therefore, the energy gained during the collision is at most  $26 \text{ kcal mol}^{-1}$ . This is not quite sufficient to overcome the activation barrier, yet the rate is still enormously enhanced.

We have performed molecular orbital calculations on  $\text{Li}^+(\text{NO}_2)$ . The equilibrium geometry shows that one of the N-O bond lengths has increased compared to its value in  $\text{NO}_2$ , indicating that the bond strength has decreased. A similar effect can be expected for  $\text{Na}^+(\text{NO}_2)$ . This decrease in bond strength may well translate into a decrease in the activation energy barrier. The latter decrease may be sufficiently large for the kinetic energy gained during the collision to overcome the reduced activation barrier. The fact that the rate is slower in the presence of  $\text{Na}^+$  than  $\text{Li}^+$  supports the above suggestion. Decreasing rate constants with increasing size of the alkali ion have also been seen by Rowe et al.<sup>1</sup> The activation barriers (for the neutral reaction) for the reactions studied with O as the reactant neutral are also smaller than the energy gained during a collision of O with  $\text{Na}^+$ . We conclude from this that the major reason for the rate enhancement may be the kinetic energy gained during the collision, although it is not the only effect.

Unfortunately, it has been impossible to study reactions of O with neutrals clustered to  $\text{K}^+$ , which would give further insight into the reaction mechanism. The reaction,



where the negative ion has a mass of either  $246 \pm 2$  or  $79 \text{ amu}$ , produces 20 times more  $\text{K}^+$  than is seen before O is added. The unknown neutral KX is emitted from the K filament. The rate constant for reaction 2 is  $1.4 \times 10^{-10} \text{ cm}^3 \text{ s}^{-1}$ .

The products in the reaction of  $\text{Li}^+(\text{NO}_2)$  with CO deserve further attention. In He and Ar buffers the major product is  $\text{Li}^+(\text{CO})$ , with a small amount of  $\text{Li}^+(\text{CO}_2)$  formed. In a  $\text{N}_2$  buffer, the only product is  $\text{Li}^+(\text{CO}_2)$ . The most likely explanation for this is that the  $\text{Li}^+(\text{CO}_2)$  product is formed in an excited state (electronic or vibrational), since the reaction is exothermic by  $54 \text{ kcal mol}^{-1}$  (neglecting the difference in cluster bond strengths). The excited  $\text{Li}^+(\text{CO}_2)$  is quenched in a  $\text{N}_2$  buffer but not in the atomic buffers<sup>3</sup>. In the atomic buffers the  $\text{CO}_2$  can then be switched out of the cluster by CO, even though the switching reaction of the ground state ions would be endothermic.

It is also interesting to note that for the reaction of  $\text{H}_2\text{S}$  with O the product is different depending upon whether one or two  $\text{H}_2\text{S}$  ligands are attached to the alkali metal ion. When two are attached, an association to form  $\text{H}_2\text{SO}$  occurs; and when only one is attached, reaction to form HSO and H occurs.

In conclusion, we have studied a number of reactions that proceed faster in the presence of an inert alkali ion. The enhancement is enormous, being on the order of  $10^{30}$  for the most dramatic case. The main reason for the enhancement appears to be that the kinetic energy gained during collision is sufficient to overcome the neutral activation barrier. This appears to be a necessary but not sufficient condition for the rate enhancement to occur. Secondary causes, such as bond weakening in the presence of the alkali ion also appear to play a role.

Table 1. Rates of Ion Enhanced Reactions

Reaction	Rate Constant (cm <sup>3</sup> s <sup>-1</sup> )	Temp(K) Enhancement <sup>c</sup>	Rate
$\text{Li}^+(\text{NO}_2) + \text{CO} \rightarrow \text{Li}^+(\text{CO}_2) + \text{NO}^{\text{a}}$	7(-12) <sup>b</sup>	213-294	10 <sup>30</sup>
$\text{Na}^+(\text{NO}_2) + \text{CO} \rightarrow \text{Na}^+(\text{CO}_2) + \text{NO}$	1(-12)	213-289	10 <sup>29</sup>
$\text{Li}^+(\text{NO}_2) + \text{H}_2 \rightarrow \text{products}$	<1(-14)	219	-
$\text{Li}^+(\text{HBr}) + \text{O} \rightarrow \text{Li}^+ + \text{HBrO}$	2(-10)	178-219	10 <sup>5</sup>
$\rightarrow \text{Li}^+ + \text{Br} + \text{OH} \rightarrow$			
$\text{Li}^+(\text{HBr})_2 + \text{O} \rightarrow \text{Li}^+ + \text{HBrO} + \text{HBr}$	2(-10)	178	10 <sup>5</sup>
$\text{Na}^+(\text{HBr}) + \text{O} \rightarrow \text{Na}^+ + \text{HBrO}$	1(-10)	219	2x10 <sup>4</sup>
$\rightarrow \text{Na}^+ + \text{Br} + \text{OH}$			
$\text{Li}^+(\text{H}_2\text{S}) + \text{O} \rightarrow \text{Li}^+(\text{HSO}) + \text{H}^{\text{a}}$	2(-10)	219	5x10 <sup>4</sup>
$\rightarrow \text{Li}^+ + \text{H}_2\text{SO}$			
$\text{Li}^+(\text{H}_2\text{S})_2 + \text{O} \rightarrow \text{Li}^+(\text{H}_2\text{SO}) + \text{H}_2\text{S}^{\text{a}}$	2(-10)	219	5x10 <sup>4</sup>
$\rightarrow \text{Li}^+ + \text{H}_2\text{SO} + \text{H}_2\text{S}$			
$\text{Na}^+(\text{H}_2\text{S}) + \text{O} \rightarrow \text{Na}^+(\text{HSO}) + \text{H}^{\text{a}}$	1(-10)	178-219	1.5x10 <sup>5</sup>
$\rightarrow \text{Na}^+ + \text{H}_2\text{SO}$			
$\text{Na}^+(\text{H}_2\text{S})_2 + \text{O} \rightarrow \text{Na}^+(\text{H}_2\text{SO}) + \text{H}_2\text{S}^{\text{a}}$	2(-10)	178	3x10 <sup>5</sup>
$\rightarrow \text{Na}^+ + \text{H}_2\text{SO} + \text{H}_2\text{S}$			
$\text{Li}^+(\text{N}_2\text{O}) + \text{O} \rightarrow \text{Li}^+ + \text{N}_2 + \text{O}_2$	5(-13)	219	10 <sup>25</sup>

a. for detailed information on the products see text. b. 7(-12) means  $7 \times 10^{-12}$ . c. the rate constant in the presence of the alkali ion divided by the rate constant for the corresponding neutral reaction at the coldest temperature listed.

### References

1. B.R. Rowe, A.A. Viggiano, F.C. Fehsenfeld, D.W. Fahey, and E.E. Ferguson, *J. Chem. Phys.* **76**, 742 (1982).
2. Handbook of Bimolecular and Termolecular Gas Reactions, ed. J.A. Kerr and S.J. Moss, CRC Press Inc., Boca Raton, Florida (1981).
3. E.E. Ferguson in "Swarms of Electrons and Ions in Gases", ed. W. Lindinger, T.D. Mark., and F. Howorka, Springer Verlag, Vienna (1984).

INTEGRATION OF THEORY AND EXPERIMENT IN HIGH-TEMPERATURE  
CHEMICAL KINETICS

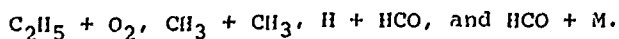
David Gutman

Department of Chemistry, Illinois Institute of Technology  
Chicago, Illinois 60616, U.S.A.

The technical difficulties associated with most experimental investigations of free-radical reactions at high temperatures usually impose significant restrictions on the range of conditions which can be covered and the degree of detail which can be obtained. Interpretation of results, particularly extrapolating laboratory findings far outside of the range of experimental conditions covered, requires not only a clear conceptual picture of the reaction dynamics but also quantitative information on the reaction energetics as well as properties of reactants and products along the reaction coordinate.

Today modern theoretical studies of chemical reactions are providing this kind of basic information on larger and larger systems. Through close cooperation between theoretical and experimental programs, knowledge on elementary reactions is being merged to develop more insightful and more comprehensive understandings of many free-radical reactions. In addition this cooperation is providing guidance for planning future theoretical and experimental studies of free-radical reactions in those directions where these efforts will be mutually supportive.

Examples of this kind of cooperation and the results it is producing will be presented. Particular emphasis will be placed on recent investigations of the following reactions:



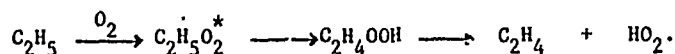
The Mechanism of the Reaction  $C_2H_5 + O_2 \longrightarrow C_2H_4 + HO_2$

by Roy R. Baldwin, Kevin McAdam, and Raymond W. Walker.

Chemistry Department, Hull University, Hull, N. Humberside,

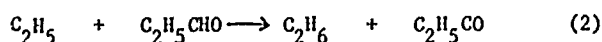
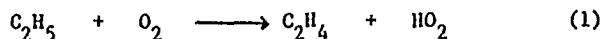
HU6 7RX, England.

There is considerable interest in the mechanism of the reaction of  $C_2H_5$  radicals with  $O_2$ , which at low temperatures gives mainly  $C_2H_5O_2$  but at higher temperatures ( $>300^\circ C$ ) gives  $C_2H_4 + HO_2$ . Gutman et al have suggested that  $C_2H_4$  is formed in the scheme



Although their experimental results are supported by one experimental study at Hull, another suggests that their mechanistic interpretation requires modification.

1. The relative yields of  $C_2H_4$  and  $C_2H_6$  from the oxidation of  $C_2H_5CHO$  have been measured over the temperature range  $320-500^\circ C$ . In the early stages of reaction, these products are formed solely in reactions (1) and (2).



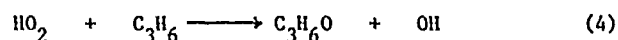
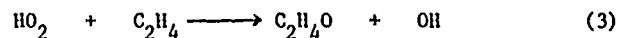
The initial values of the relative rate of formation are given by equation (1)

$$d[C_2H_4]/d[C_2H_6] = k_1[O_2]/k_2[C_2H_5CHO] \quad (i)$$

which gives an excellent interpretation of the results over a wide range of mixture composition. Accurate values of  $k_1/k_2$  are obtained, from which Arrhenius plots give  $E_2 - E_1 = 38 \pm 2 \text{ kJ mol}^{-1}$  and  $A_2/A_1 = 20.0 \pm 4.5$ . Use of literature values for  $E_2$  and  $A_2$  gives  $E_1 = (-8 \pm 5) \text{ kJ mol}^{-1}$  and  $A_1 = (1.58 \pm 0.7) \times 10^7 \text{ dm}^3 \text{ mol}^{-1} \text{ s}^{-1}$ , which provide strong evidence that

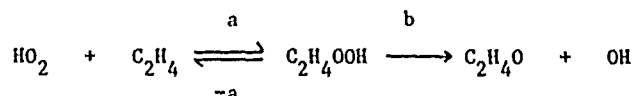
$C_2H_4$  is not formed by a direct bimolecular process involving simple H atom transfer.

2. The decomposition of tetramethylbutane in the presence of  $O_2$  has been used as a source of  $HO_2$  radicals to study the competition between reactions (3) and (4).



Measurement of the relative yields of ethylene oxide and propene oxide, and use of (4) as the reference reaction give  $A_3 = 10^{9.45 \pm 0.35} \text{ dm}^3 \text{ mol}^{-1} \text{ s}^{-1}$  and  $E_3 = 71.6 \pm 5 \text{ kJ mol}^{-1}$  between 400 and 500°C.

The formation of ethylene oxide is likely to take place in two stages

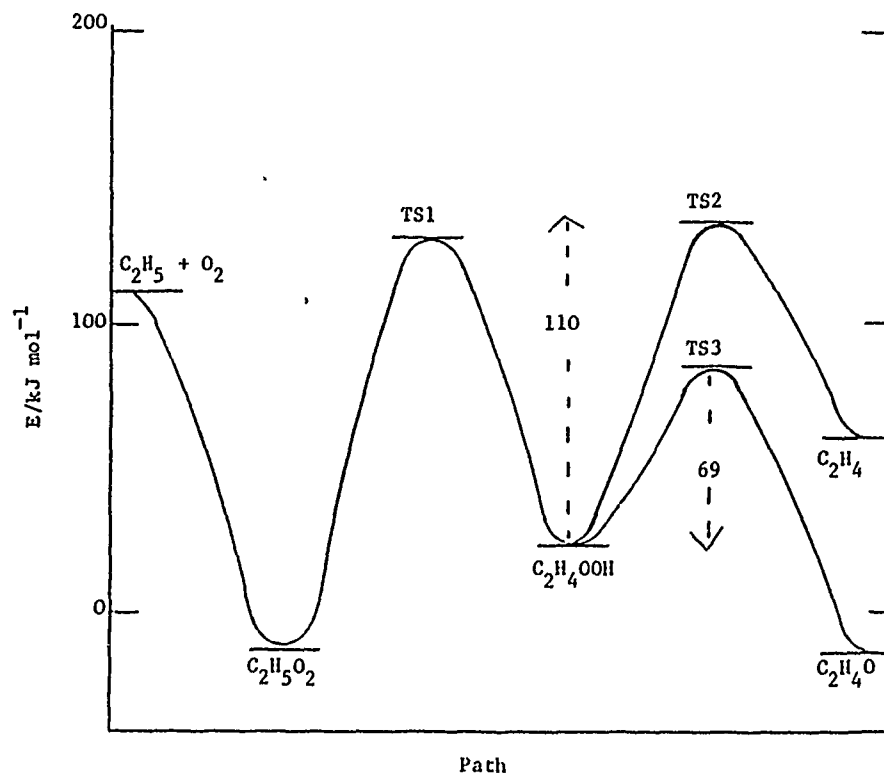


Taken in conjunction with independent work, there is ample evidence to suggest that the above Arrhenius parameters do refer to the addition step (a), so that  $k_b \gg k_{-a}$ . Similar conclusions have been reached in related reactions. This is not unexpected because as the energy diagram below shows ethylene oxide is formed exothermically ( $\Delta H$  ca  $-40 \text{ kJ mol}^{-1}$ ) whereas ethylene is formed endothermically ( $\Delta H$  ca  $40 \text{ kJ mol}^{-1}$ ). As indicated by the diagram, the decomposition (-a) to give  $C_2H_4 + HO_2$  has a very high energy barrier of about  $110 \text{ kJ mol}^{-1}$ , which raises difficulties for the explanation given by Gutman's group for the negative temperature coefficient for  $C_2H_5 + O_2$  at the higher temperatures. In contrast, a value of only  $69 \text{ kJ mol}^{-1}$  is suggested for the energy barrier of reaction (b), the formation of ethylene oxide. The effect of the much lower value of  $E_b$  could be balanced by a very adverse A factor. However, transition state calculations suggest that  $A_{-a}/A_b \nlessgtr 30$ , so that at 500°C

$k_b/k_{-a}$  is at least 16, and negligible amounts of  $C_2H_4$  would be formed from the decomposition of  $C_2H_4OOH$ . As in the range 350–550°C, the product ratio  $[C_2H_4]/[C_2H_4O]$  is about 100, then clearly  $C_2H_4$  must arise from another source than  $C_2H_4OOH$ .

It is suggested therefore that  $C_2H_4$  is not formed in the direct bimolecular reaction nor from the  $C_2H_4OOH$  radical, but is formed directly from the  $C_2H_5OO^*$  or  $C_2H_5OO$  radical.

Energy Diagram for  $C_2H_5 + O_2$





## HYDROXYL-RADICAL REACTIONS WITH UNSATURATED HYDROCARBONS: EFFECTS OF DEUTERIUM SUBSTITUTION\*

Frank P. Tully, August T. Droege<sup>†</sup>, and J. E. M. Goldsmith

Combustion Research Facility

Sandia National Laboratories

Livermore, California, 94550

U. S. A.

Detailed kinetic studies of the reactions of OH with ethene, propene, and acetylene are reported. Reactions are initiated by 193-nm photolysis of N<sub>2</sub>O in N<sub>2</sub>O/ H<sub>2</sub>O/ hydrocarbon/ helium gas mixtures, and monitored via time-resolved OH fluorescence excited using an intracavity-doubled, single-mode, cw ring dye laser. The dependences of the rate coefficients on pressure and temperature are being investigated over the ranges 3-700 torr of helium and 295-1000 K, respectively. Complex chemical mechanisms, involving OH addition, atom migration, adduct dissociation, and direct hydrogen-atom transfer, are observed. Deuterium substitution in the unsaturated hydrocarbons produces several interesting effects. The pressure-falloff behavior for the reactions OH + C<sub>2</sub>H<sub>4</sub> and OH + C<sub>2</sub>D<sub>4</sub> are significantly different; efforts to model these using the Troe formalism are underway. Significant OD concentrations are detected in the reactions of OH with C<sub>2</sub>D<sub>2</sub> and C<sub>3</sub>D<sub>6</sub>; the [OD] profiles are compatible with a mechanism involving OH addition, H- and D-atom intramolecular migration, and redissociation of OD. At high temperatures, significant kinetic isotope effects are observed in H (and D)-atom abstraction reactions.

\* This research is supported by the Division of Chemical Sciences, the Office of Basic Energy Sciences, the U. S. Department of Energy.

<sup>†</sup> Sandia National Laboratories Postdoctoral Research Associate.

## OH + OLEFIN REACTION RATES AT HIGH TEMPERATURES

Gregory P. Smith  
Chemical Physics Laboratory  
SRI International, Menlo Park, CA 94025 USA

There are many studies of OH reactions with olefins in the 250-500 K temperature range, where a pressure-dependent addition mechanism dominates, but very few direct determinations of rate constants at temperatures important in combustion, above 1000 K. We recently reported measurements for OH plus acetylene<sup>1</sup> and propylene<sup>2</sup> at 900-1300 K, which indicate a new mechanism replaces addition, perhaps hydrogen abstraction. These measurements have now been extended to ethylene and a series of butenes.

The laser pyrolysis/laser fluorescence technique<sup>2</sup> uses a pulsed infrared CO<sub>2</sub> laser beam, 1 cm in diameter, to irradiate the center of a thin, cylindrical gas cell containing 10 torr SF<sub>6</sub> infrared absorber, up to 30 torr CF<sub>4</sub> bath gas, 2 mtorr H<sub>2</sub>O<sub>2</sub> radical source, and varying amounts of olefin reactant. Within the first 40  $\mu$ s, the gas is heated by absorption and energy transfer, OH is produced by thermal decomposition, and partial cooling occurs as the result of a shock-driven expansion. There follows a quiescent period of over 150  $\mu$ s during which bimolecular kinetics can be measured, using a variably delayed, frequency doubled, YAG pumped dye laser to excite laser-induced fluorescence in the OH(A-X) (0,0) band near 308 nm. Temperature is measured by scanning several OH rotational lines, and the pressure is assumed to return to its initial value. Plots of the pseudo first-order decay rates of OH versus olefin concentration give the rate constant.

Table 1  
SUMMARY OF HIGH TEMPERATURE OH + Olefin RATE CONSTANTS

Reactant	T(K)	Number Expt.	Number Decays	$k(10^{-12}\text{cm}^3/\text{s}) \pm 1 \sigma$
ethylene	900	7	25	$2.54 \pm 0.38$
	1220	6	24	$2.49 \pm 0.5$
propylene <sup>2</sup>	1150	2	8	$8.0 \pm 1.2$
1-butene	1225	3	9	$19.7 \pm 4.2$
2-butene	1275	2	8	$27.0 \pm 3.6$
iso-butene	1260	1	5	$29.6 \pm 6.8$
dimethyl-butene	1237	1	5	$37.0 \pm 5.6$

Averaged results are given in the table above. Our previous propylene results<sup>2</sup>, those of Tully and Goldsmith<sup>3</sup>, and the observation of no abstraction products at 300 K<sup>4</sup>, indicate a surprisingly large barrier for abstraction of weakly bound allylic hydrogens. The much larger butene rate constants suggest this unexpected barrier is absent for larger alkenes. Note also that the rate constants increase with the number of allylic hydrogens. The transition state theory approach applied by Cohen<sup>5</sup> to butane and propane was applied to the alkenes. The predicted rate constants for 1- and 2-butene are 95% and 80% of those measured, with no energy barrier. The propylene barrier so determined by fitting the 1200 K data is 1.5 kcal/mol, surprisingly about the same as that for propane.

Our RRKM calculations and Tully's measurements<sup>6</sup> indicate the addition reaction of OH to ethylene to form an adduct is insignificant above 800 K. The rate constants measured above represent a direct process, either abstraction of vinylic hydrogens or some rearrangement channel. It is believed the

apparent lack of a temperature dependence is inaccurate, since no significant direct reaction was observed at low pressure at 300 K.<sup>7</sup> A transition state theory fit for abstraction to our data at 1200 K gives a barrier of 2 kcal/mol, which is somewhat below that expected, given the ethylene bond energy and known correlations for alkanes.<sup>5</sup> There is, however, other conflicting evidence concerning this reaction,<sup>8</sup> and rearrangement cannot be ruled out without high temperature product studies. The various mechanisms and available data on OH plus ethylene will be discussed in more detail, from the perspective of transition state and RRKM theories.

This work was supported by the Office of Basic Energy Sciences, U.S. Department of Energy, Contract No. DE-AC03-81ER10906.

#### References

1. G. P. Smith, P. W. Fairchild, D. R. Crosley, J. Chem. Phys. 81, 2667 (1984).
2. G. P. Smith, P. W. Fairchild, J. B. Jeffries, D. R. Crosley, J. Phys. Chem. 89, 1269 (1985).
3. F. P. Tully, J.E.M. Goldsmith, Chem. Phys. Lett. 116, 345 (1985).
4. H. W. Blermann, G. W. Harris, J. N. Pitts, J. Phys. Chem. 86, 2958 (1982).
5. N. Cohen, Int. J. Chem. Kinetics 14, 1339 (1982).
6. F. Tully, Chem. Phys. Lett. 96, 148 (1983).
7. C. J. Howard, J. Chem. Phys. 65, 4771 (1976).
8. M. Bartels, K. Hoyer mann, R. Sievert, 19th Symp. (Intl.) on Combustion, 61 (1982).

The ketenyl yield of the elementary reaction of ethyne  
with atomic oxygen at  $T = 280 - 550 \text{ K}$

J. Peeters, M. Schaekers and C. Vinckier

Department of Chemistry  
Katholieke Universiteit Leuven  
Celestijnenlaan 200F, B-3030 Heverlee, Belgium

In a previous study <sup>1</sup> of the  $\text{C}_2\text{H}_2 + \text{O}$  reaction, it was shown that both  $\text{HCCO}$  and  $\text{CH}_2$  are important primary products :



the kinetics of subsequent reactions of  $\text{HCCO}$  with both  $\text{O}$ - and  $\text{H}$ -atoms was also investigated.

The purpose of the present work was to determine the absolute  $\text{HCCO}$  yield of the elementary  $\text{C}_2\text{H}_2 + \text{O}$  reaction, at  $T = 290 - 540 \text{ K}$ . The determination was carried out using the discharge-flow technique, combined with molecular-beam mass spectrometry (MBMS). The total pressure in the flow reactor was 2 torr, with He as the diluent gas.

The total rate constant  $k_1$  of the  $\text{C}_2\text{H}_2 + \text{O}$  reaction being known, the  $\text{HCCO}$  yield  $k_{1b}/k_1$  can be obtained from an absolute measurement of the quasi-stationary  $\text{HCCO}$  concentration in a  $\text{C}_2\text{H}_2/\text{O}$  system :

$$[\text{HCCO}]_{\text{st}} = k_{1b} [\text{C}_2\text{H}_2] [\text{O}] / \sum_i k_i [X_i] \quad (\text{Eq. 1})$$

where  $\sum_i k_i [X_i]$  is the total removal frequency  $\nu_r$  of  $\text{HCCO}$  due to the various destruction reactions with the coreagents  $X_i = \text{O}, \text{H}, \text{O}_2$  and  $\text{C}_2\text{H}_2$ ; the associated rate constants  $k_i$  are known from previous work.

It is clear that the crucial factor in the determination of  $\beta = k_{1b}/k_1$  along these lines is the absolute sensitivity of the MBMS apparatus for the  $\text{HCCO}$  radical  $S(\text{HCCO}) = i(\text{HCCO})/[\text{HCCO}]$ , with  $i(\text{HCCO})$  the MBMS signal for  $\text{HCCO}$ .

A large part of the work reported here was invested in the measurement of the calibration factor  $S(\text{HCCO})$ , with the reaction



used as HCCO source. Reaction (2), which has been investigated extensively by Faubel et al.<sup>2</sup>, is a "clean" source of HCCO, all other pathways being highly endoergic.

Establishing the absolute HCCO concentration in a  $\text{C}_3\text{O}_2/\text{H}$  system requires knowledge of  $k_2$  as well as of the total HCCO removal frequency  $\nu_r' = \sum k_j[X_j]$ . The rate constant  $k_2$  at 535 K was derived from the first-order decay of  $[\text{C}_3\text{O}_2]$  at excess  $[\text{H}]$ :  $k_2 = (9.1 \pm 0.7)10^{11} \text{ cm}^3 \text{ mole}^{-1} \text{ s}^{-1}$ , in good agreement with Faubel et al.<sup>2</sup>. The sensitivity  $S(\text{HCCO})$  was obtained in experiments where the time-dependent HCCO removal frequency  $\nu_r'(t)$  was derived from the known time-dependent HCCO formation rate and from the observed time history of the  $i(\text{HCCO})$  signal; the method can be regarded as an extension of the well-known "approach to the stationary state" technique. Once  $\nu_r'(t)$  is known, the absolute  $[\text{HCCO}]$  can be calculated at each point in time; combination with the corresponding  $i(\text{HCCO})$  signals yields the calibration factor sought here.

In the actual procedure, HCCO-removal was attributed to the known<sup>1</sup> reaction



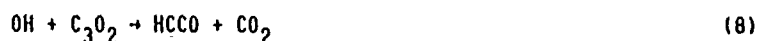
as well as to a (pseudo-)first-order process



that includes termination on the wall; the unknown parameters  $S(\text{HCCO})$  and  $k_4$  in the equation

$$d i(\text{HCCO})/dt = S k_2 [\text{C}_3\text{O}_2][\text{H}] - (k_3[\text{H}] + k_4) i(\text{HCCO}) \quad (\text{Eq. 2})$$

were evaluated simultaneously by means of the non-linear-least-squares "DUD" algorithm<sup>3</sup>. The result for  $S$  was found to be only slightly affected by the inclusion of secondary HCCO formation via



with OH generated in reactions of  $\text{O}_2$ -traces with products of reactions (3) and (4).

The sensitivity factor  $S(\text{HCCO})$  having been determined in this way, the ketenyl yield  $\beta = k_{1b}/k_1$  of the  $\text{C}_2\text{H}_2 + \text{O}$  reaction was determined from measured  $i(\text{HCCO})$  signals in  $\text{C}_2\text{H}_2/\text{O}$  systems at quasi-stationary  $(\text{HCCO})$ , as expressed by (Eq. 1) :

$$\beta = [\text{HCCO}]_{\text{st}}(k_5[\text{O}] + k_3[\text{H}] + k_6[\text{O}_2])/k_1[\text{C}_2\text{H}_2][\text{O}] \quad (\text{Eq. 3})$$

The value of the rate constants  $k_3$ ,  $k_5$  and  $k_6$  of the HCCO-reactions with H, O, respect.  $\text{O}_2$ , were taken from previous work <sup>1,4</sup>. The results :  $\beta = 0.59 \pm 0.20$  at 287 K and  $\beta = 0.64 \pm 0.19$  at 535 K (with  $2\sigma$  uncertainties) show that the elementary  $\text{C}_2\text{H}_2 + \text{O}$  reaction leads for the larger part to HCCO formation and that the HCCO-yield is nearly independent of temperature. Both these findings agree with the recent theoretical predictions by Harding and Wagner <sup>5</sup>.

#### References

1. C. Vinckier, M. Schaekers and J. Peeters, J. Phys. Chem. 89, 508 (1985).
2. C. Faubel, H. Gg. Wagner and W. Hack, Ber. Bunsenges. Phys. Chem. 81, 689 (1977).
3. M.L. Ralston and R.I. Jenrich, Technometrics 20, 7 (1978).
4. M. Schaekers, Ph. D. Thesis, Faculty of Sciences, K.U. Leuven (1985).
5. L.B. Harding and A.F. Wagner, Annual Report Theoretical Chemistry Group Argonne National Laboratory, p. 17, 1985.

THE REACTION OF CH RADICALS WITH H<sub>2</sub> FROM 372 TO 675 KS. Zabarnick\*, J.W. Fleming and M.C. LinChemistry Division  
Naval Research Laboratory  
Washington, D.C. 20375-5000

Two-laser photolysis/LIF probe experiments have been performed to measure absolute rate coefficients for the reaction of CH radicals with H<sub>2</sub>. Multiphoton photolysis of CHBr<sub>3</sub> produces CH(X<sup>2</sup>Π) radicals. The CH radicals are probed by LIF at 429.8 nm. These experiments have been performed over the temperature range 297 to 675 K at 100 torr argon total pressure in order to better characterize the abstraction reaction



At low temperatures the insertion reaction predominates



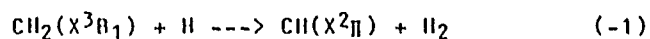
Subtraction of this low temperature insertion channel results in data that covers the temperature range 372 to 675 K for reaction (1). An Arrhenius plot yields the expression  $k_1 = (2.38 \pm 0.31) \times 10^{-10} \exp[-(1760 \pm 170)/T]$  cm<sup>3</sup>/s, as shown in Fig. 1. Also shown in Fig. 1 is a transition-state theory fit which yields a value for E<sub>0</sub>, the barrier height at 0 K, equal to 3.0 ± 0.3 kcal/mole. With this value and the known heats of formation of CH and H, we obtain an independent value for the heat of formation of CH<sub>2</sub>, ΔH<sub>f0</sub>(CH<sub>2</sub>) = 92.6 ± 0.4 kcal/mole.

---

\*NRC/NRL Postdoctoral Research Associate



The principle of microscopic reversibility allows calculation of  $k_{-1}$  if  $k_1$  and  $K_{eq}$  are known.



The results are plotted in Fig. 2. The data is well fit by the form,  $k_{-1} = (4.7 \pm 0.6) \times 10^{-10} \exp[-(370 \pm 60)/T] \text{ cm}^3/\text{s}$ . Also shown are the other literature measurements of the rate constant for this reaction. The broken line in Fig. 2 presents results of a transition-state theory calculation for reaction (-1). The calculation predicts an upward curvature at temperatures above  $\sim 1000 \text{ K}$  and leveling off of the rate constant at lower temperatures.

#### REFERENCES

1. M.R. Berman and M.C. Lin, J. Chem. Phys. 81, 5743 (1984).
2. J. Grebe and K.H. Homann, Ber. Bunsenges. Phys. Chem. 86, 581 (1982).
3. T. Bohland and F. Temps, Ber. Bunsenges. Phys. Chem. 88, 459 (1984).
4. R. Lohr and P. Roth, Ber. Bunsenges. Phys. Chem. 85, 153 (1981).

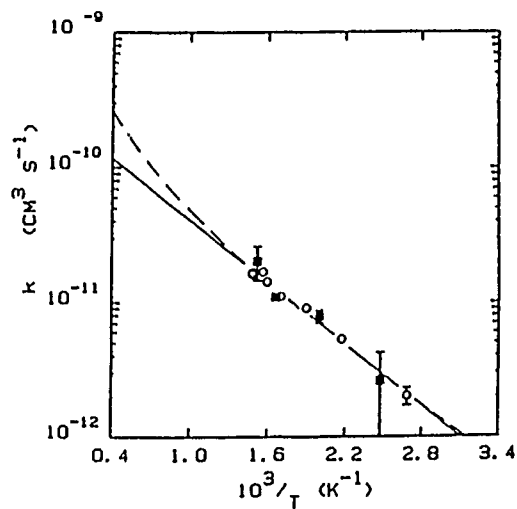


Fig. 1 Arrhenius plot for  $\text{CH} + \text{H}_2 \rightarrow \text{CH}_2 + \text{H}$ : O this work, ■ Berman and Lin (Ref. 1). Solid line is Arrhenius fit, broken line is transition-state theory calculation fit.

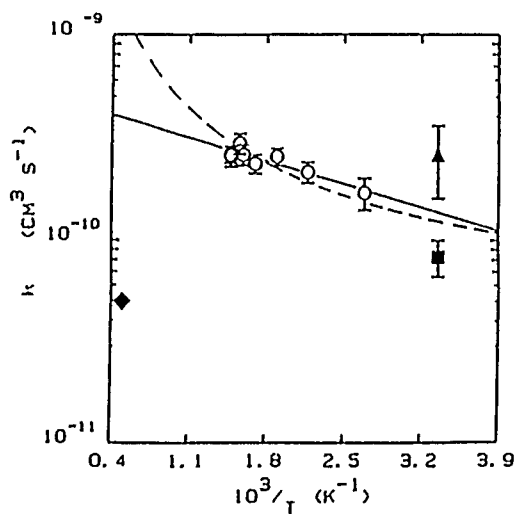


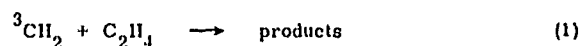
Fig. 2 Arrhenius plot for  $\text{CH}_2 + \text{H} \rightarrow \text{CH} + \text{H}_2$ : O this work, ■ Grebe and Homann (Ref. 2), ▲ Bohland and Iemps (Ref. 3), ♦ Lohr and Roth (Ref. 4). Solid line is Arrhenius fit, broken line is transition-state theory calculation fit.

A Direct Study of the Reaction  
 $\text{CH}_2 (\tilde{\text{X}}^3\text{B}_1) + \text{C}_2\text{H}_4$  in the Temperature  
 Range  $296 \text{ K} \leq T \leq 728 \text{ K}$

T. Böhland, F. Temps

Max-Planck-Institut für Strömungsforschung, Bunsenstraße 10,  
 D - 3400 Göttingen, West-Germany

**1. Introduction:** The reactions of methylene-radicals ( $\text{CH}_2$ ) with unsaturated hydrocarbons proceed via electrophilic addition to the  $\pi$ -bond system of the alkene. The low-lying singlet first excited state ( $^1\text{CH}_2$ ) has been found to add stereospecifically to  $\text{C}=\text{C}$  double bonds, whereas reactions of the triplet electronic ground state ( $^3\text{CH}_2$ ) are non-stereospecific. Direct investigations of reactions between  $^3\text{CH}_2$ -radicals and alkenes have not yet been carried out. In two recent publications we have reported on the kinetics of  $^3\text{CH}_2$ -radicals and selected saturated hydrocarbons<sup>1,2)</sup>, data for the reaction of  $^3\text{CH}_2$  with acetylene<sup>3)</sup> will be reported elsewhere. The present results are published in<sup>4)</sup>. The reaction



was investigated in the gasphase at temperatures between  $296 \text{ K} \leq T \leq 728 \text{ K}$  using a far-infrared Laser Magnetic Resonance (LMR)-spectrometer<sup>5)</sup> for direct detection of  $^3\text{CH}_2$ . The reaction mechanism was studied by observing the pressure dependence of the rate constant and by studying the isotope labelled reaction of  $^3\text{CD}_2$  with  $\text{C}_2\text{H}_4$ .

**2. Experimental:** Reaction (1) was investigated in an electrically thermostated pyrex flow reactor of 1 m length and 4 cm i.d. equipped with a moveable probe. Helium served as the main carrier gas. The temperature was measured directly within the gas stream using a calibrated thermocouple. All gases were of highest commercially available purities, ketene ( $\text{CH}_2\text{CO}$ ,  $\text{CD}_2\text{CO}$ ;  $\approx 99\%$  purity) was prepared by pyrolysis of acetone. Radicals were generated either in the moveable probe using a chemical source or photolytically in a cell attached to the upper end of the flow tube.  $^3\text{CH}_2$  ( $^3\text{CD}_2$ ) was de-

tected with the far-infrared LMR-spectrometer at  $\lambda = 157.9 \mu\text{m}$  ( $103.5 \mu\text{m}$ ) and  $B_0 = 0.323 \text{ Tesla}$  ( $0.606 \text{ Tesla}$ ), both with  $\pi$ -polarisation.

**3. Results:** The rate constant  $k_1$  was determined under pseudo-first order conditions by following the  $[\text{CH}_2]$ -decay along the reaction distance in the presence of a large excess of  $\text{C}_2\text{H}_4$ . The first  $\text{CH}_2$ -source was the reaction  $\text{O} + \text{CH}_2\text{CO} \rightarrow \text{CH}_2 + \text{CO}_2$ . Q-atoms in He were admixed to a large excess of  $\text{CH}_2\text{CO}$  within the probe, where  $\text{CH}_2$ -radicals are generated at low concentrations, i.e.  $[\text{CH}_2] \approx 2 \cdot 10^{-13} \text{ mol/cm}^3$ . The second source was the photodissociation of  $\text{CH}_2\text{CO}$  with an exciplex laser at  $\lambda = 193 \text{ nm}$ . At inert gas pressures around 1 mbar  $\text{CH}_2$ -radicals formed in excited states are rapidly quenched to the ground state. At laser pulse energies of 100 mJ and  $[\text{CH}_2\text{CO}]_0 = 10^{-10} \text{ mol/cm}^3$  around  $[\text{CH}_2]_0 \approx 10^{-13} \text{ mol/cm}^3$  was produced.

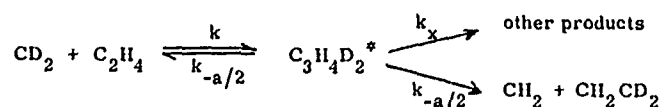
In the absence of  $\text{C}_2\text{H}_4$  the reactions of  $\text{CH}_2$  with the wall and, at higher temperatures, also with  $\text{CH}_2\text{CO}$  can be described by an "effective wall rate constant" which could be measured directly. A second minor  $^3\text{CH}_2$  depletion channel arises due to partial thermal equilibration between the two spin states of  $\text{CH}_2$  followed by the very fast reaction of  $^1\text{CH}_2$  with  $\text{C}_2\text{H}_4$ . Using the rate constants for collisional deactivation of  $^1\text{CH}_2$  to  $^3\text{CH}_2$  and for its reaction with  $\text{C}_2\text{H}_4$ , which was measured separately, small corrections ( $< 30\%$ ) were applied for each experiment.

The rate constant for the direct triplet reaction is described by the Arrhenius expression

$$k_1 = 10^{(12.50 \pm 0.10)} \exp \{(-22.1 \pm 1.0) \text{ kJ mol}^{-1} / RT\} \text{ cm}^3 / \text{mol s}.$$

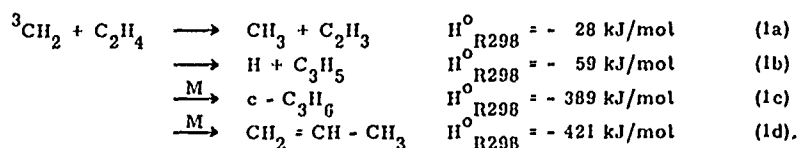
No pressure dependency of the rate constant was found in a series of experiments at  $T = 535 \text{ K}$  over a pressure-range of  $0.48 \text{ mbar} \leq p \leq 7.52 \text{ mbar}$ .

A complementary study was performed of the isotopically labelled reaction



The experiment lead to an upper limit for the channel distribution of  $k_{-a}/k_x < 0.04$ .

4. Discussion: In previous studies of reaction (1) only upper limits for the room temperature rate constant had been established. Laufer and Bass, and Frey et al. reported  $k_1 \leq 2 \cdot 10^{10}$  and  $k_1 \leq 3 \cdot 10^8$  cm<sup>3</sup>/mol s, respectively. Calculations of the energy barrier by Dewar et al. have lead to  $E_A = 21$  kJ/mol very close to the experimental value [Refs. in <sup>3</sup>]. Under our conditions the measured rate constant is independent of pressure and corresponds to its high-pressure value. Concerning the products the following channels are possible:



Stabilisation to cyclopropane and propene (1c, 1d) can play a role only at significantly higher pressures than used here. For the direct abstraction reaction (1a) an activation energy of  $E_A = 50$  kJ/mol can be estimated from the Evans-Polanyi correlation in <sup>1)</sup>, much higher than the experimental value found here. Fragmentation of chemically activated cyclopropane to H + C<sub>3</sub>H<sub>5</sub> - radicals was observed to be the major channel (> 90 %) in the reaction of H-atoms with cyclopropyl-radicals at T = 298 K and p = 0,3 mbar <sup>6)</sup>. Hence, channel (1b) is expected to be of major importance under the experimental conditions used here.

#### References

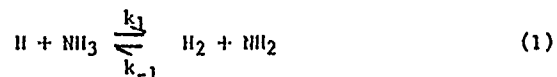
- 1) S. Dóbé, T. Böhland, F. Temps, and H. Gg. Wagner, Ber. Bunsenges. Phys. Chem. 89, 432 (1985)
- 2) ---, Ber. Bunsenges. Phys. Chem. 89, 1110 (1985)
- 3) T. Böhland, F. Temps, and H. Gg. Wagner, 21<sup>st</sup> Symposium (International) on Combustion, Munich 1986
- 4) ---, Ber. Bunsenges. Phys. Chem., in press
- 5) ---, Z. Phys. Chem. Neue Folge 412, 129 (1984)
- 6) M. Bartels, P. Heinemann, and K. Hoyer mann, 20<sup>th</sup> Symposium (International) on Combustion, pp 81, Ann Arbor 1984

Kinetics and Thermodynamics of the Reaction,  
 $\text{H} + \text{NH}_3 \xrightleftharpoons[k_{-1}]{k_1} \text{NH}_2 + \text{H}_2$  by the Flash Photolysis-Shock Tube Technique.

J. W. Sutherland, and J. V. Michael

Department of Applied Science  
 Brookhaven National Laboratory  
 Upton, New York 11973

In a previous study<sup>1</sup> the forward rate constant,  $k_1(T)$ , for the reaction,



was measured over the temperature range 908K - 1777K by the flash photolysis-shock tube technique using atomic resonance absorption to monitor the [H]. The Arrhenius rate expression was,

$$k_1(T) = (3.02 \pm 0.30) \times 10^{-10} \exp(-8067 \pm 117/T) \text{ cm}^3 \text{ molecule}^{-1} \text{ s}^{-1}.$$

If the equilibrium constant for reaction (1),  $K_1(T)$ , were known, then the rate constant for the reverse process  $k_{-1}(T)$  could be calculated.

Unfortunately, present uncertainties<sup>2</sup> in  $\Delta H_{f\text{NH}_2}^0$  lead to large variations in  $K_1(T)$  and, hence, in  $k_{-1}(T)$ . The values of  $K_1$ , that are calculated at 1000K from the tabulated thermodynamic functions<sup>3</sup> for H,  $\text{NH}_3$  and  $\text{H}_2$  and from  $S^0$  for  $\text{NH}_2$ , range from 0.52 to 17.8 depending on the value chosen for  $\Delta H_{f298}^0$ . These values have been discussed recently by Lesclaux<sup>2</sup>. (Table IV reference 2).

This paper reports experimental measurements of  $K_1(T)$  obtained over the temperature range 900-1620K with the flash photolysis-shock tube (FP-ST) technique. From these results, values for  $\Delta H_{f\text{NH}_2}^0$  and  $k_{-1}(T)$  are determined.

Mixtures of  $\text{H}_2$  and  $\text{NH}_3$  were shock heated to the desired temperature and were immediately flash photolyzed in the reflected regime to produce equal

concentrations of H-atoms and  $\text{NH}_2$ -radicals. The temperature, density and pressure in the reflected shock regime were calculated from velocity measurements of the incident shock wave, initial conditions and ideal shock theory. Corrections for non-ideal shock wave behavior were made using a method based on experimentally measured pressures and the isentropic equation of state.<sup>1,4,5</sup> The concentration of H-atoms, which ranged from  $1.0 \times 10^{11}$  -  $2.0 \times 10^{12}$  atoms/cc, was monitored by the sensitive atomic resonance absorption technique. At these low atom and radical concentrations, depletion of [H] by atom-atom, or atom-radical reactions can be neglected during the time of the experiment (0.15 - ~1.5 msec).

Since the  $[\text{NH}_3]$  and  $[\text{H}_2]$  are always maintained in a large excess the kinetics of reactions (1) and (-1) are pseudo-first order; i.e., reaction (1) simplifies kinetically to a first order relaxation process that is described by the following expression,

$$A_t = \frac{2k_{-1}' A_0}{k_1' + k_{-1}'} - \frac{(k_{-1}' - k_1')}{k_1' + k_{-1}'} A_0 \exp(-(k_1' + k_{-1}')t) \quad (2)$$

where  $A_0$  = initial absorbance by H-atoms,  $A_t$  = absorbance at time  $t$ ,  $k_1' = k_1 [\text{NH}_3]$ ,  $k_{-1}' = k_{-1} [\text{H}_2]$  and  $A_e = 2k_{-1}' A_0 / (k_1' + k_{-1}')$ , at equilibrium. If the initial concentration of  $\text{H}_2$  and  $\text{NH}_3$  in the reflected regime are the equilibrium concentrations, there will be no net change in the H-atom concentration with time,  $k_1' = k_{-1}'$ , and  $K_1 = [\text{H}_2]_0 / [\text{NH}_3]_0$ .

At any other initial ratio of  $[\text{H}_2] / [\text{NH}_3]$  the absorbance will either increase or decrease to the  $A_e$  value according to equation (2). Hence by varying the  $[\text{H}_2] / [\text{NH}_3]$  ratio at a fixed temperature until no net change in absorbance with time is observed,  $K_1$  can be simply determined from the known initial concentrations of  $\text{H}_2$  and  $\text{NH}_3$ . Too high a ratio results in an

increase in  $A_t$  whereas too low a ratio results in a decrease of  $A_t$  with time to the equilibrium values.

The experimental values of  $K_1(T)$  ranged from 1.0 at 900K to 2.2 at 1620K. The results were analyzed according to the second law of thermodynamics to give  $\Delta H^\circ_1 = 3.1 \text{ kcal/mole}$  from 900-1600K. The analysis by the third law gave a value of  $\Delta H^\circ_1 = 4.2 \text{ kcal/mole}$ . This value is independent of temperature in the range 900-1620K within experimental error. The results lead to a value of  $\Delta H^\circ_{f298}(\text{NH}_2)$  of 45.3 kcal/mole and a  $D(\text{NH}_2\text{-H})$  value of 107 kcal/mole. The Arrhenius rate expression derived for reaction (-1) in the temperature range 900 - 1620K is

$$k_{-1}(T) = 5.40 \times 10^{-11} \exp(-6496/T).$$

#### References

1. J. V. Michael, J. W. Sutherland, and R. B. Klemm, J. Phys. Chem., 90, 497 (1986).
2. R. Lesclaux, Review of Chemical Intermediates, 5, 347 (1984).
3. M. W. Chase, Jr., J. L. Curnutt, J. R. Downey, Jr., R. A. McDonald, A. N. Syverud, and E. A. Valenzuela, J. Phys. Chem. Ref. Data, 11, No. 3 (1982).
4. J. V. Michael and J. W. Sutherland, Int. J. Chem. Kinet. 18, 409 (1986).
5. J. W. Sutherland, J. V. Michael, and R. B. Klemm, J. Phys. Chem., (in press.).

Acknowledgement: We thank Mr. A. N. Pirraglia for his help with some of the FP-ST experiments. This work was supported by the Division of Chemical Sciences, U.S. Department of Energy, Washington, DC, under Contract No. DE-AC02-76CH00016.



REACTION OF ATOMIC HYDROGEN WITH MONOSUBSTITUTED HALOMETHANES.  
A MINDO ANALYSIS OF THE IMPORTANCE OF THE DIFFERENT CHANNELS.

a) a) b) a)  
Miguel González, Ramón Sayós, Josep Bofill and Margarita Albertí.

a) Departament de Química Física.

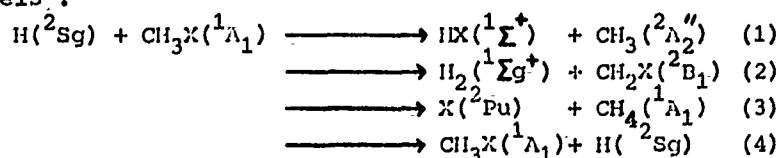
b) Departament de Química Orgánica.

Facultat de Química, Universitat de Barcelona.

Avda. Diagonal 647, 08028 Barcelona, SPAIN.

Abstract

The reactions of atomic hydrogen with monosubstituted halo-methanes ( $X=F, Cl, Br, I$ ) and with some of the isotopically substituted species, have been extensively studied experimentally/1-3/, many of these works being directed towards the characterization of the reactions in terms of the Arrhenius' kinetic parameters. In these works, it is thought that the reaction which produces methyl radical and the corresponding hydrogen halide is the principal one in the temperature range 300-1000 K. The same consideration has been employed by the present authors in recent theoretical studies on the reactions of atomic hydrogen with chloro- and bromo-methane by means of quasiclassical trajectory method /4-5/. However, in the system considered here, when only a single chemical bond breaks, a total of four primary reactions can occur. Assuming that these reactions lead to products in their electronic ground states, we have the following reaction channels:



The very limited experimental information available on competitive reactions (2)-(4) in the thermal energy range, and the general belief that reaction (1) is the principal one in these energy conditions, led us to study the  $H + CH_3X$  system using the semiempirical MINDO-UHF method in order to clarify the relative importance of the different reaction channels at thermal energies.

The calculations were performed using an improved version of MOPAC program/G/ with standard parameters. It appears that

INDO-UMF method can be used to obtain saddle point structures (TS) and energies for the reactions studied (disregarding of reaction (4) whose TS was not located); but in the case  $X=F$ , however, it seems that INDO standard parameters are not suitable for the type of reactions considered.

Once the TS's for the different channels were located, the Arrhenius' parameters were determined within the TST framework. Due to the scarcity and dispersion of published experimental data on  $E_a$  and  $A$ , the checking of our calculated results has been seriously curtailed. This experimental information is only available on reaction (1) /1-3/, and even for this one, iodine data are lacking.

For reaction (1), INDO predicts activation energies that are underestimated and frequency factors overestimated, but their relative values are in reasonable agreement with experimental ones. Moreover, this method predicts that at thermal energies only abstraction reactions ( (1) and (2) ) are important, with reaction (1) predominating; the substitution reactions ( (3) and (4) ) becoming important, probably, at much higher energies, in good accord with the general belief of experimentalists.

#### References

- /1/ L.W.Hart, C.Grunfelder and R.H.Fristrom, Comb.Flame, 23 (1974) 109.
- /2/ A.A.Westenberg and H. deHaas, J.Chem.Phys. 62 (1975) 3321.
- /3/ W.K.Aders, D.Pangritz and H.Gg.Wagner, Ber.Bun.Phys.Chem. 79 (1975) 90.
- /4/ R.Sayós, A.Aguilar, J.H.Lucas, A.Sold and J.Virgili, Chem. Phys. 93 (1985) 265.
- /5/ R.Sayós, M.González and A.Aguilar, Chem.Phys. 98 (1985) 409.
- /6/ S.Olivella, QCPE 486 (Indiana University, 1984).

EXPERIMENTAL DETERMINATION OF THE ENERGY DISTRIBUTION IN PHOTODECOMPOSITION. DIAZIRINES AND DIAZOCOMPOUNDS.

M.J. Avila, Dept<sup>o</sup> Quim. Inorgánica, Facultad de Ciencias, Universidad a Distancia, Ciudad Universitaria, 28040 Madrid.

J.M. Figuera, J. Medina and J.C. Rodríguez, Int<sup>o</sup> de Química Física "Rocasolano", CSIC, Serrano 119, 28006 Madrid, Spain.

The initial aim of the present work was to study the partitioning of energy between the fragments produced by photodissociation of complex molecules. We selected for this study a group of diazirines and diazocompounds whose experimental photolysis has been reported. We planned to use the recently developed "exact" deconvolution method (1,2,3) in order to determine the energy distribution on the hydrocarbon fragment. As the initial energy "pumped" into the system can be known we expected that some conclusions about the energy partition could be obtained.

Preliminary calculations showed an apparent "loss" of activated molecules. Therefore, we decided to investigate theoretically this problem before going on with the initial project. We have studied two cases. The first was the production of deactivated molecules by parallel reaction mechanism. Wall and manipulation induced decomposition may be very severe in highly unstable systems as those investigated here. The second was the extension of the energy distribution below  $E_0$ , the minimum energy required for an excited molecule to react. The two causes origin slightly different effects. In the first

case only the area under the normalized energy distribution function was changed while in the second case, both the area and the profile of the curve were altered. With this information in mind we proceed to deconvolute the experimental results and obtain the hydrocarbon fragment energy distributions for the following photodecompositions: diazoethane (250 nm and 436 nm) (4), diazopropane (436 nm) (5), methyldiazirine (313 nm) (6) and dimethyldiazirine (313 nm) (7). The recently reported results of 3,3' chloromethyldiazirine at 416, 365 and 337 nm have also been included (3).

Analyses of the experimentally obtained energy distribution functions have shown that no statistical distribution ( 8,9 ) alone can explain the origin of the distributions obtained. Using purely impulsive models we have arrived to similar conclusions.

Finally we have developed another model based on the individuality of the phase space of each fragment at the time of fragment separation or immediately after. We consider that the molecule enters the volume of phase space corresponding to the transition state; then, fragmentation occurs and two phase spaces corresponding one to the hydrocarbon fragment and the other to the rest molecule (transition modes, and nitrogen) are formed, but they are still able to interact and transfer energy statistically to and fro.

The model seems to be able to give a reasonable interpretation of the photodecomposition results.

## REFERENCES

- 1.- J.M. Figuera, V. Menéndez y J.C. Rodríguez, An. Quim., 80, 490 (1984).
- 2.- J.M. Figuera, V. Menéndez and J.C. Rodríguez, Int. J. Chem. Kin. 17, 583 (1985).
- 3.- M.J. Avila, R. Becerra, J.M. Figuera, J.C. Rodríguez, A. Iobar and R. Martínez-Utrilla, J. Phys. Chem. 89, 5489 (1985).
- 4.- C.L. Kibby and G.B. Kistiakowsky, J. Phys. Chem. 70, 126 (1966).
- 5.- J.M. Figuera, E. Fernández and M.J. Avila, J. Phys. Chem. 78, 1348 (1971).
- 6.- H.M. Frey and I.D.R. Stevens, J. Chem. Soc. 1700 (1965).
- 7.- H.M. Frey and I.D.R. Stevens, J. Chem. Soc. 3514 (1963).
- 8.- R.V. Serauskas and Schlag, J. Chem. Phys. 42, 3009 (1965) and 43, 898 (1965).
- 9.- Y.U. Lin and B.S. Rabinovitch, J. Phys. Chem. 74, 1769 (1970).

A STUDY OF ENERGY TRANSFER PROCESSES AT THE COLLISION OF A POLY-  
ATOMIC MOLECULE WITH AN INERT GAS ATOM BY THE METHOD OF CLASSICAL  
TRAJECTORIES

Vedenev V.I., Goldenberg M.Ya., Levitsky A.A.,  
Polak L.S., Umansky S.Ya.

A technique based on the method of classical trajectories has been developed for studying the energy transfer processes taking place at the collision of highly excited tetrahedral molecules of the methane type with the atoms of an inert gas.

Detailed characteristics were calculated for the energy transfer processes: the mean squares of the total internal vibrational and rotational energy, <sup>change</sup> as well as the correlator of the variation of rotational and vibrational energies,

These values were calculated for different models of tetrahedral molecules and collision partners. The influence exerted on the energy transfer processes by the symmetry of molecules, the presence of low-frequency internal degrees of freedom and the weight ratio of molecules and the inert gas atom was investigated.

The V-R exchange is shown <sup>to be</sup> the most effective energy exchange process in the case under consideration, its effectiveness increasing in the presence of low-frequency vibrations, characteristic, e.g., for <sup>hindered</sup> ~~impeded~~ rotations. With an increase in inert gas weight, direct V-T exchange becomes effective, which is associated with the kinematic condition of the conservation of the system's total angular momentum. It has been established that in the systems in question intensive <sup>V-R</sup> ~~energy~~ energy exchange can be observed at a relatively low variation of the total energy of the molecule, which substantially modifies the consideration of energy relaxation and molecular dissociation processes in diffusive <sup>on</sup> approximation.

TRANSITION-STATE THEORY CALCULATIONS FOR  
REACTIONS OF OH WITH HALOALKANES. II. HALOETHANES

N. Cohen

Aerophysics Laboratory

The Aerospace Corporation

P. O. Box 92957

Los Angeles CA 90009

U. S. A.

ABSTRACT

A method previously used for extrapolating rate coefficients for reactions of OH radicals with halomethanes is extended to reactions of OH with eighteen halogen-substituted ethanes. The model for the activated complex is the same for all the reactions except for two difference between the  $\alpha$ -hydrogen and the  $\beta$ -hydrogen atom abstractions: (1) In the former case, there are two new low-frequency bends in the activated complex, while in the latter there is only one. (2) There is a much larger increase in entropy due to internal rotations in the  $\beta$ -hydrogen abstractions. In both models the internal rotations are assumed to be free. These two models for activated complexes, when combined with experimental data at 298 K, give good temperature extrapolations for the rate coefficients for the 12 different reactions for which data at higher temperatures exist. For all the  $\alpha$ -hydrogen

abstraction reactions (including the halomethanes of Part I),  $\Delta S^\ddagger(298)$  could be fitted, with a maximum error of  $1.4 \text{ cal mol}^{-1} \text{ K}^{-1}$  (entropy units, or eu) and an average error of 0.3 eu, by  $\Delta S^\ddagger(298) = -2.2 \ln M - 18.0 + R \ln n_H$ , where  $M$  = molecular weight of the haloalkane and  $n_H$  = the number of  $\alpha$ -hydrogen atoms. The activation energy at 300 K,  $E(298)$ , can be fitted, with an average error of 0.3 kcal/mol and a maximum error of 1.0 kcal/mol, by

$$E(298)/R = 2100 - 85n_F - 515n_{Cl} - 950n_{CH_3} - 600n_{CH_2X} - 650n_{CHX_2} - 250n_{CX_3},$$
 where the  $n_i$  indicate the number of H atoms on  $CH_4$  replaced with the indicated substituents, and X is either Cl or F. These two relations for  $\Delta S^\ddagger(298)$  and  $E(298)$  have been used to generate a "universal" rate coefficient expression that depends only on the molecular weight and the number of abstractable H atoms in the reagent haloalkane:

$$k(T) = 10^{6.53} M^{-1} T^{1.5} \exp-[E(298)/R - 450]/T$$

where  $E(298)/R$  is given by the preceding equation. This expression in most cases predicts rate coefficients within a factor of 3 of the experimental data and offers promise as a predictive tool when no reliable data are available.



**Theoretical Studies of Hydrogen Atom Addition to Carbon Monoxide  
and the Thermal Dissociation of the Formyl Radical**

A. F. Wagner and L. B. Harding  
Argonne National Laboratory  
Argonne, IL 60439  
USA

A global *ab initio* potential energy surface has recently been calculated for HCO including both the H+CO asymptote and the high energy isomer COH. This calculated surface is used in an RRKM study of both the addition reaction H+CO and the HCO thermal dissociation as a function of temperature and pressure for buffer rare gases. The calculation incorporates tunneling through an Eckhart formalism and explores the effect of semi-empirical corrections to the *ab initio* surface. Comparison is made with the few low pressure addition rate constant measurements and with the many indirect measurements of the thermal dissociation rate constant.

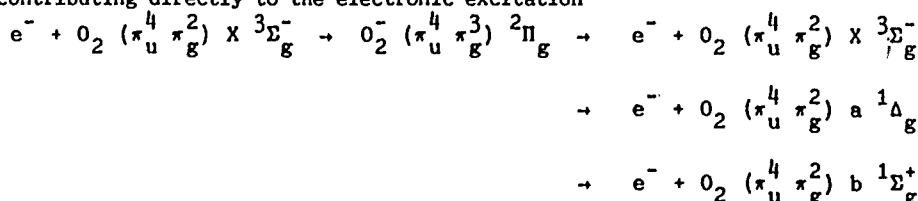
# RESONANT ELECTRONIC EXCITATION IN ELECTRON-O<sub>2</sub> COLLISION

*D. Teillet-Billy*<sup>\*</sup>, *L. Malegat*<sup>\*\*</sup> et *J.P. Gauyacq*<sup>\*</sup>

<sup>\*</sup>L.C.A.M., Bât. 351, Université Paris-Sud, 91405 ORSAY Cedex, France

<sup>\*\*</sup>ER 261, Observatoire de Paris, 92195 MEUDON, France

Scattering via the O<sub>2</sub><sup>-</sup> (<sup>2</sup>Π<sub>g</sub>) shape resonance is well known to dominate the vibrational excitation process of the ground state of O<sub>2</sub>(X<sup>3</sup>Σ<sub>g</sub><sup>-</sup>). However, three different electronic states, X<sup>3</sup>Σ<sub>g</sub><sup>-</sup>, a<sup>1</sup>Δ<sub>g</sub> and b<sup>1</sup>Σ<sub>g</sub><sup>+</sup>, are associated to the ground configuration of O<sub>2</sub>(π<sub>u</sub><sup>4</sup>π<sub>g</sub><sup>2</sup>), and can be considered as parents of the O<sub>2</sub><sup>-</sup>(π<sub>u</sub><sup>4</sup>π<sub>g</sub><sup>3</sup>)<sup>2</sup>Π<sub>g</sub> resonance. As a consequence, the resonant <sup>2</sup>Π<sub>g</sub> scattering is contributing directly to the electronic excitation



through the ejection of a π<sub>g</sub> electron, and also to the electronic excitation of the O<sub>2</sub>(π<sub>u</sub><sup>3</sup>π<sub>g</sub><sup>3</sup>) excited states through the ejection of a π<sub>u</sub> electron.

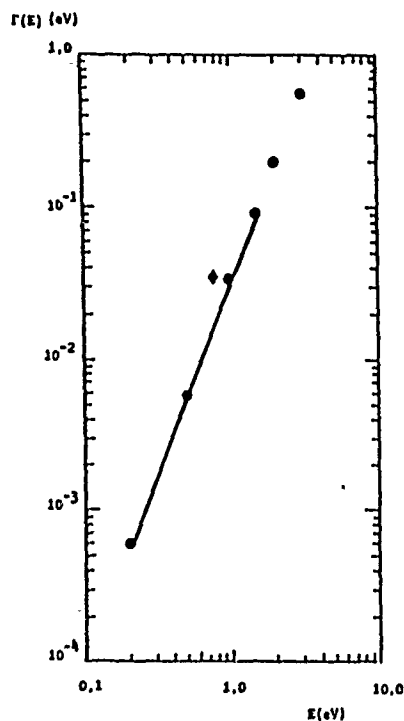
However the O<sub>2</sub><sup>-</sup> (<sup>2</sup>Π<sub>g</sub>) resonance is located at a rather low energy (≈100meV) whereas the excitation cross section have their maximum around 7 eV ; the resonant contribution thus comes from the far wings of the resonance. The proposed theoretical description is based on the extension of the effective range approximation -ERT-(3) that can handle this multichannel resonant process far from the resonance position, associated with an ab initio calculation of the O<sub>2</sub><sup>-</sup> system. In the ERT approximation, the space for the electron is separated in two regions : in the internal region r < r<sub>c</sub>, the system is described by the O<sub>2</sub><sup>-</sup> (<sup>2</sup>Π<sub>g</sub>) resonance wave function, in the external region r > r<sub>c</sub>, the system is described as a superposition of channel wave functions (e<sup>-</sup>+O<sub>2</sub>). In this region, the outer electron is assumed to interact with the molecule via the local potential V<sub>l=2</sub>(r) (V<sub>l=1</sub>(r)) of the first adiabatic angular mode (4) of the V(**r**) potential experienced by a π<sub>g</sub>(π<sub>u</sub>) electron of the O<sub>2</sub><sup>-</sup> (<sup>2</sup>Π<sub>g</sub>) system. The ERT method then reduces to the

matching of the inner and outer region wave functions at the border  $r=r_c$ .

The  $O_2^- (\pi_u^4 \pi_g^3) {}^2\Pi_g$  resonance width is calculated through the Siegert definition of a resonance -pure outgoing wave condition in all channels-, taking into account all the electronic channels coming from the detachment of a  $\pi_g$  and  $\pi_u$  electron. It appears that the width follows, over an extended energy range, a  $E^{2.5}$  energy law corresponding to a dx Wigner threshold law. The absolute value of the width is in very good agreement with the value (2) that fit the vibrational excitation cross sections of  $O_2$  ( $\times {}^3\Sigma_g^-$ ) (1). The theoretical resonant electronic excitation cross sections are presented in fig.2, together with previous experimental (1,5,6,) and theoretical (7) results. The  ${}^2\Pi_g$  resonant contribution dominates the electronic excitation to the  $a {}^1\Delta_g$  and  $b {}^1\Sigma_g^+$  states, since our results are typically lying inside the experimental error bars. It is worthnoting that this resonance, located below the excitation threshold, dominates the excitation process over a large energy range (3-15 eV). This resonant approach results are also consistent with the R-matrix results of Noble and Burke (7) that include the non-resonant contribution to the processes.

Fig 1 Resonance width:

● this work, — (2), ♦ (7).



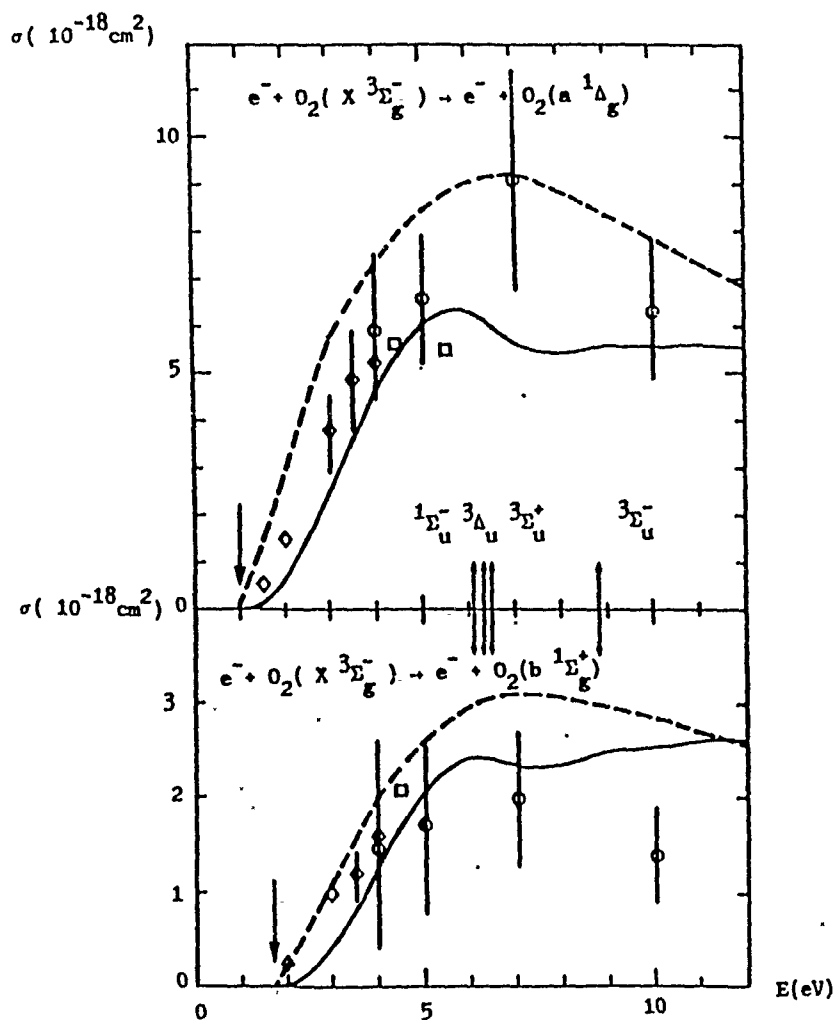


Fig 2 Cross sections:—this work,---(7),  $\diamond$  (1),  $\circ$  (5),  $\square$  (6).

- (1) F. Linder and Schmidt 1971 Z. Naturf. a 26 1617-25 ;
- (2) G. Parlant and F. Fiquet-Fayard 1976 J. Phys. B 9 1617-28 ;
- (3) J.P. Gauyacq 1983 J. Phys. B 16 4049-58 ;
- (4) M. Le Dourneuf, Vo Ky Lan and J.M. Launay 1982 J. Phys. B 15 L685 ;
- (5) S. Trajmar, D.C. Cartwright and W. Williams 1971 Phys. Rev. A4 1482-92 ;
- (6) R.I. Hall and S. Trajmar 1975 J. Phys. B 8 L393-6 ;
- (7) C.J. Noble and P.G. Burke 1986 J. Phys. B 19 L35-9.

VAN DER WAALS, CHARGE TRANSFER AND "MIXED" STATES OF MOLECULAR  
COMPLEXES FORMED IN SUPERSONIC JETS.

M. CASTELLA\*, A. TRAMER\*\*, and F. PIUZZI\*.

\* Commissariat à l'Energie Atomique, IRDI/DESICP,  
Département de Physico-Chimie, CEN/Saclay  
91191 Gif-sur-Yvette Cedex, France.

\*\* Laboratoire de Photophysique Moléculaire,  
Université Paris-Sud,  
91405 Orsay Cedex, France.

The spectroscopic and dynamic properties of molecular complexes involving a large aromatic hydrocarbon (perylene, anthracene), acting as an electron acceptor, and different large size molecules, acting as electron donors, with decreasing ionization potentials (dimethylaniline-DMA, monomethylaniline-MA-, aniline, anisole and phenol), have been studied by the supersonic jet technique.

The analysis of the electronic (excitation and fluorescence) spectra and of the lifetimes allows us to explain the different systems behaviours by the relative position of the molecular excited Van der Waals state and of the charge transfer state. Then, we can distinguish schematically three complexes classes :

a) the perylene-phenol and perylene-anisole complexes : they behave as typical Van der Waals complexes. In this case, the molecular excited state, having an energy lower than the charge transfer state, gives rise to a perylenic type emission.

b) the perylene-DMA complex : for this system, the position of both states is inversed : the lower ionic state is responsible for the exciplexic type emission. The anthracene-aniline complex also belongs to this category.

c) the perylene-aniline and perylene-MA complexes : they present an intermediary behaviour between the precedent complexes ones, mainly characterized by an emission which is neither resonant, nor exciplexic but rather "quasi-exciplexic". The molecular excited and charge transfer states are close, and this strong coupling results in a "mixed" state shifted to smaller intermolecular distance values, with a potential energy well shallow and strongly anharmonic.

The lifetimes measurements are in agreement with this interpretation. For the perylene-anisole and phenol systems, the fluorescence lifetimes, characteristic of the excited molecular state, is the same as the bare molecule one ( $\sim 11$  ns). It is much larger for the fluorescence issued from the charge transfer state of the perylene-DMA complex ( $\sim 94$  ns) (large fluorescence lifetimes characterize emission from pure charge transfer states). Perylene-aniline and -MA systems present intermediary values (respectively  $\sim 16$  and  $\sim 50$  ns).

On the other hand, we have observed for some of the complexes (anthracene-DMA and perylene-MA) the existence of isomers with drastically different spectral properties. In fact, the main features can be explained by the simultaneous presence of two isomeric complexes of the a and b classes, separated by a potential energy barrier.

To verify the precedent hypothesis, we have performed theoretical calculations giving the binding energy between the complex acceptor and donor molecules in different states. These calculations are based upon an exchange perturbation treatment, allowing to express the interaction energy as the sum of four components : electrostatic, polarization, dispersion and repulsion energies. Every term itself is the sum of interactions between small sub-units of the complex. For the perylene-DMA and -aniline complexes ground states, the results show that these systems are mainly maintained by the dispersion forces. The interaction energies obtained are large (about  $2000 \text{ cm}^{-1}$ ) : they support the experimental observations, especially the lack of predissociation in the perylene-DMA case. The more stable configurations have been determined : the donor prefer positions parallel to the longitudinal and transversal axes, as well as the central ring of the perylenic molecule. The calculations about the molecular excited Van der Waals and charge transfer states are in progress. The major difficulty comes from the refinement of the dispersive term for the molecular state, which has never been performed up to now.

## ELECTRONIC STRUCTURE OF MERCURY-ARGON COMPLEXES

O. BENOIST d'AZY, W.H. BRECKENRIDGE,  
M.C. DUVAL, C. JOUVET and B. SOEP.

Laboratoire de Photophysique Moléculaire  
Bâtiment 213 - Université de Paris-Sud  
91405 - Orsay Cedex France

The Hg-Ar complex formed in a supersonic expansion has been studied by laser double resonance and emission spectroscopy. It can be shown as a prototype for the study of electronically excited diatomic van der Waals complexes.

The emission from the upper Hg ( $7^3S_1$ ) - Ar states to the metastable  $\sim a$ ,  $\sim b$ ,  $\sim c$ ,  $\sim d$  states of Hg-Ar correlated with Hg ( $6^3P_0$ ) and Hg ( $6^3P_2$ ) provides a wealth of information on their spectroscopic constants and potentials, difficult to obtain experimentally by other methods, as those states are not optically accessible from the ground state. A simple model has been developed which allows the description of the relevant potentials by electrostatic interactions between the argon in the ground state and the excited  $6^3P$  mercury, where the average orientation of the 6p mercury orbitals with respect to the complex internuclear axis, accounts for the binding.

In addition the observation of other electronic states, such as the Rydberg Hg ( $7^3S_1$ ) states, offers even more insight in the electrostatic binding nature of the complex. The argon atom can either be nested in the last node of the 7s orbital and closely resembles to the Hg-Ar<sup>+</sup> ion or, outside the 7s cloud forms a van der Waals molecule very lightly bound.

Reactions of Metastable Rare Gas Atoms with  $N_2O$ ;  
Chemiluminescence of  $RgO^*$ ;  $Rg = Xe, Kr, Ar$ .

Aqúst Kvaran and Auðunn Lúðvíksson,  
Science Institute, University of Iceland,  
Dunhaga 3, 107 Reykjavík, Iceland.

and

William S. Hartree and John P. Simons,  
Department of Chemistry, University of Nottingham,  
Nottingham NG7 2RD, England.

Chemiluminescence spectra of rare gas oxides due to reactions of metastable  $Xe$ ,  $Kr$  and  $Ar$  with  $N_2O$  have been recorded in the UV/VUV region using a discharge flow system. Spectra due to electronic transitions from bound excited ionic states to repulsive ground states<sup>1</sup> ( $X^3\Pi$ ) were identified for  $XeO$  peaking at 235 nm (see fig. 1),  $KrO$  at 180 nm and  $ArO$  at 150 nm. The  $ArO$  spectrum is overlapped with nitrogen emission spectrum. An absence of fine structure in the tail of the  $XeO$  and  $KrO$  spectra suggests that the excited states are formed with low vibrational excitation, but significant rotational excitation<sup>2,3</sup>. Broad continua, due to transitions to  $A^3\Sigma$  states have also been found for  $XeO$  and  $KrO$  on the long wavelength side of the peak spectra. Analyses of the  $XeO$  (235 nm) and  $KrO$  (180 nm) spectra were carried out in order to determine vibrational energy disposals. Spectra were analysed by systematic simulations<sup>2</sup> and by the inversion technique<sup>4</sup>, using calculated vibrational contributions assuming fixed rotational energy<sup>2</sup>. Ground state potential curves calculated by S.R. Langhoff<sup>5</sup> were used, while upper state potential curves were varied as Rittner potentials. Transition moment functions, decreasing with increasing internuclear distance, were used. The analyses led to evaluation of spectroscopic parameters for the excited states:



	$\omega_e/\text{cm}^{-1}$	$r_e/\text{\AA}$	$T_e/\text{cm}^{-1}$
XeO	$360 \pm 20$	$2.59 \pm 0.04$	$45920 \pm 350$
KrO	$365 \pm 25$	$2.43 \pm 0.05$	$59600 \pm 400$

-as well as vibrational population distributions. Boltzmann distribution functions, valid up to maximum vibrational levels, determined by the energetics of  $\text{Rg}(^3\text{P}_2)/\text{N}_2\text{O}$ ;  $\text{Rg} = \text{Xe}, \text{Kr}$  for  $T = 3000 \pm 1000$  K (XeO) and  $T = 3500 \pm 1500$  K (KrO) gave best fits in the simulation calculations (fig. 1). Vibrational distributions determined as histogram representations by inversion showed fair agreement (fig. 2). Analogous to the rare gas halide formation reactions,  $\text{RgO}^*$  formation follows electron transfer from  $\text{Rg}^*$  to  $\text{N}_2\text{O}$ .  $\text{N}_2\text{O}$  is an efficient electron scavenger and  $\text{N}_2\text{O}^-$  is believed to be quite stable<sup>6</sup> ( $D(\text{N}_2\text{-O}^-) = 0.43$  eV<sup>7</sup>). The reactions with  $\text{Rg}^*$  therefore may proceed via long lived complexes. The vibrational distributions obtained are consistent with such a mechanism. That would contrast with findings for BaO formation reaction from  $\text{Ba} + \text{N}_2\text{O}$ , which occurs by direct reaction<sup>8</sup>.

1. M.F. Golde and B.A. Thrush, Chem. Phys. Lett., 29, 486, (1974).
2. M.F. Golde and A. Kvaran, J. Chem. Phys., a) 72, 434, (1980), b) 72, 442, (1980).
3. a) J.H. Kolts, J.E. Velasco and D.W. Setser, J. Chem. Phys., 71, 1247, ('79), b) K. Tamgake, J.H. Kolts and D.W. Setser, J. Chem. Phys., 71, 1264, ('79).
4. K. Johnson, A. Kvaran, J.P. Simons, Mol. Phys., 50, 981, (1983).
5. S.R. Langhoff, J. Chem. Phys., 71, 2379, ('80).
6. H. Shimamori and R.W. Fessenden, J. Chem. Phys., a) 68, 2757, ('78), b) 69, 4732, ('78), c) 70, 1137, ('79).
7. D.G. Hopper, A.C. Wahl, R.L.C. Wu and T.O. Tiernan, J. Chem. Phys., 65, 5474, ('76).
8. T.P. Parr, A. Freedman, R. Behrens and R.R. Herm, J. Chem. Phys., 67, 2181, ('77).

Fig. 1

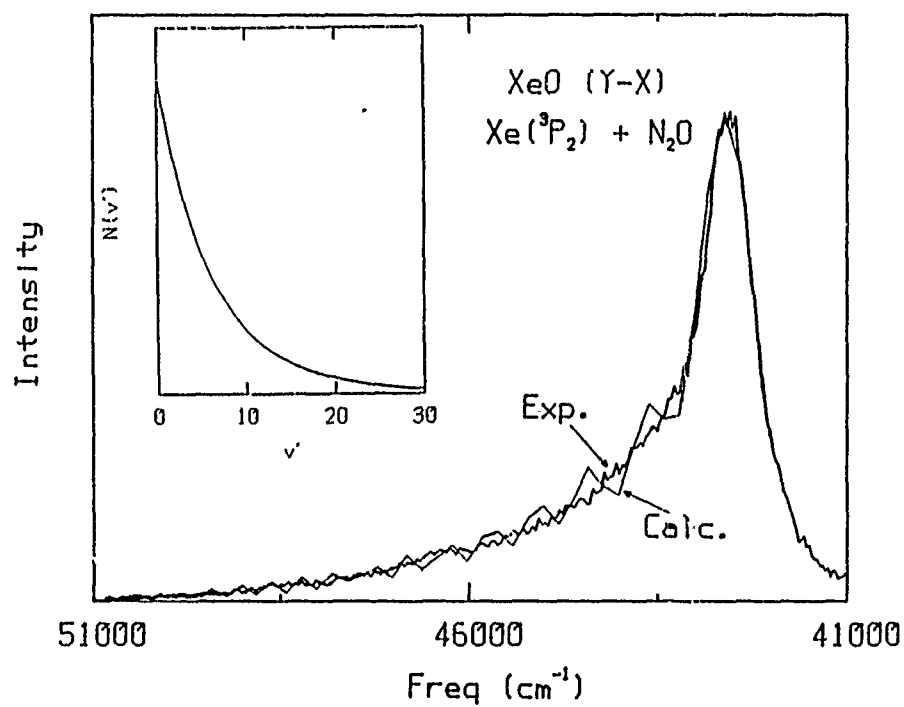
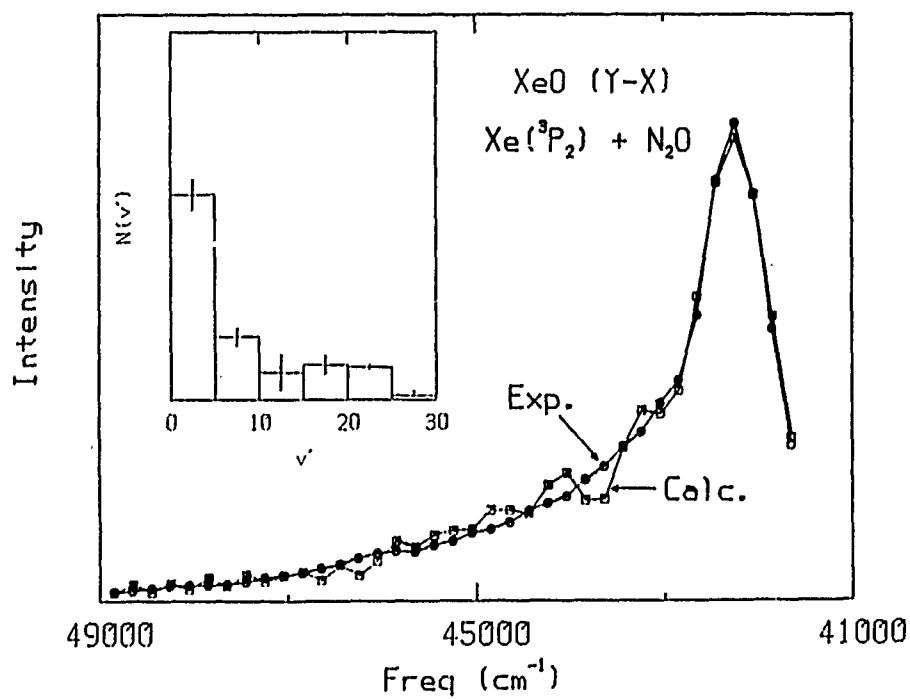


Fig. 2



A LIFETIME STUDY ON THE SECOND MAXIMUM OF PREDISSOCIATION OF  
THE IODINE  $B^3\Pi(O_u^+)$  STATE.

by F.Castaño, E.Martínez and M.T.Martínez

Departamento de Química Física. Facultad de Ciencias.

Universidad del País Vasco. Apartado 644. Bilbao. SPAIN.

The natural and magnetic predissociation of the iodine  $B^3\Pi(O_u^+)$  state have been studied extensively in the last few years (1-5). The nature of the spontaneous predissociation has been attributed to the rotational and hyperfine coupling between the  $B^3\Pi(O_u^+)$  state and the  $^1\Pi(1_u)$  repulsive state. Lehmann et al. (6) showed that the decay rate for a given hyperfine sublevel can be given by  $\Gamma = \Gamma_{\text{rad}} + \Gamma_{\text{col}} + \Gamma_{\text{IJF}}$ , where  $\Gamma_{\text{rad}}$  and  $\Gamma_{\text{col}}$  stand for the radiative and collisional decay rates, and  $\Gamma_{\text{IJF}}$  takes into account the gyroscopic and hyperfine predissociation rates plus an interaction term,

$$\Gamma_{\text{IJF}} = C_{v,J}^2 \cdot (J(J+1)) + a_{v,J}^2 \cdot f(I \cdot J) - a_{v,J} \cdot C_{v,J} \cdot g(I \cdot J)$$

where the explicit forms of the functions  $f$  and  $g$  are given in reference 6a.

No precise information of the predissociation parameters  $C_v^2$  and  $a_v^2$  is available for levels near the second maximum of predissociation, i.e.  $v' \approx 24-25$ . The aim of the present work is to get the values of the coefficients  $C_v^2$  and  $a_v^2$  for gyroscopic and hyperfine interactions, from fluorescence decay rate measurements of these levels.

Fluorescence decay lifetimes for specific rovibrational levels of the  $I_2$   $B^3\Pi(O_u^+)$  state, have been obtained by time-resolved laser induced fluorescence. Laser excitation spectra of the  $I_2$  B-X system were obtained between 545 and 555 nm by using a pulsed ( $\sim 15$  ns-FWHM) Quantel dye laser. In this wavelength region, sections of the relatively intense 24-0, 25-0, 26-0, 26-1 and 27-1 bands were observed.

Lifetime measurements were usually made at 30 mTorr of iodine, and collision free lifetimes were obtained by extrapolation to zero iodine pressure, using a collision cross-section of  $65 \text{ \AA}^2$  (7), which is coincident with our value of  $65.8 \pm 0.4 \text{ \AA}^2$  obtained for the level (24,40). Table 1 shows the collision free lifetimes obtained for selected (24, $J'$ ) and (25, $J'$ ) levels of the iodine B state.

Table 1- Collision free lifetimes for ( $v',J'$ ) levels of  $I_2$  (B)

EXCITED LEVEL			EXCITED LEVEL		
$v'$	$J'$	$\tau_0$ (ns)	$v'$	$J'$	$\tau_0$ (ns)
24	38	$745 \pm 21$	24	73	$682 \pm 17$
24	40	$785 \pm 22$	24	94	$638 \pm 18$
24	46	$796 \pm 50$	24	102	$662 \pm 37$
24	50	$800 \pm 37$			
24	55	$844 \pm 20$	25	0-5	$745 \pm 25$
24	56	$740 \pm 30$	25	30	$745 \pm 21$
24	60	$754 \pm 32$	25	88	$625 \pm 15$
24	62	$756 \pm 18$	25	95	$653 \pm 27$
24	67	$772 \pm 30$	25	106	$625 \pm 11$

The predissociation parameters  $C_V^2$  and  $a_V^2$  have been obtained from the time evolution of the fluorescence intensity for specific rovibrational levels. See table 2. Assuming the Franck-Condon approximation,  $a_V^2$  and  $C_V^2$  should be proportional to the same Franck-Condon Densities (FCD) between the  $B^3\Pi(O_u^+)$  and  $^1\Pi(1_u)$  states, times the corresponding electronic matrix elements involved. However such a dependence for  $C_V^2$  is not observed for levels near the second maximum of predissociation (8).

Table 2- Best fitted predissociation parameters  $C_V^2$  and  $a_V^2$ .

$v'$	$\Gamma_{\text{rad}}$ ( $10^6 \text{s}^{-1}$ )	$C_V^2$ ( $\text{s}^{-1}$ )	$a_V^2$ ( $10^3 \text{s}^{-1}$ )
24	0.61	$67 \pm 7$	$95 \pm 10$
25	0.60	$55 \pm 10$	$115 \pm 12$

#### REFERENCES

- 1 A.Chutjian, J.Chem.Phys. 51 (1969) 5414.
- 2 J.Tellinghuisen, J.Chem.Phys. 57 (1972) 2397.
- 3 G.D.Chapman and P.R.Bunker, J.Chem.Phys. 57 (1972) 2951.
- 4 J.Vigué, M.Broyer and J.C.Lehmann, J.Chem.Phys. 62 (1975) 4941.
- 5 M.Broyer, J.Vigué and J.C.Lehmann, J.Chem.Phys. 63 (1975) 5428.
- 6 J.Vigué, M.Broyer and J.C.Lehmann, J.Physique (a) 42 (1981) 937;  
(b) 42 (1981) 949; (c) 42 (1981) 961.
- 7 G.A.Capelle and H.P.Broida, J.Chem.Phys. 58 (1973) 4212.
- 8 F.Castaño, E.Martínez and M.T.Martínez, Chem. Phys. Lett. in press

Measurement of Rotational Energy Transfer Rates for HD ( $v = 1$ ) in  
Collisions With Thermal HD\*

David W. Chandler and Roger L. Farrow

Combustion Research Facility  
Sandia National Laboratories  
Livermore, CA. 94550

\* Work supported by the U. S. Department of Energy, Office of Basic Energy Sciences, Division of Chemical Sciences.

Abstract

We report state-to-state rotational energy transfer rates for HD excited to the first excited vibrational level of the ground electronic state. Stimulated Raman scattering is used to produce the rotationally selected, vibrationally excited HD. Subsequent collisional energy transfer from the prepared state, upon collision with a thermal distribution of HD, is monitored by multiphoton ionization through the E,F electronic state. The data are analyzed by solving the rate equations coupling the lowest six rotational states of the first excited vibrational level. In this manner, both the absolute rate constants and the optimum shape of the energy transfer probability density function are determined. The best fit of the data to trial probability density functions indicates that the HD-HD collisions preserve the magnetic sublevel,  $m$ . The total rotational energy transfer rate out of a particular rotational level is compared to high resolution Raman linewidth measurements in order to determine the degree to which the rotational energy transfer rate contributes to the linewidth.

In this paper, we report the state-to-state measurement of rotational energy transfer from one rotational energy state of the first excited vibrational level of the ground electronic state of HD to another rotational level of the same vibrational level in collisions with a Boltzmann distribution of ground state HD molecules at 298 K. The technique of stimulated Raman pumping is used to prepare a single rotational-vibrational level of HD. The multiphoton ionization technique is then used to monitor the population of states occupied as a result of collisions with the initially prepared state. By temporally delaying the lasers with respect to each other, we determine the details of the dynamics of rotational energy transfer.

Most previous studies of rotational energy transfer have been performed on upper electronic states, due to the utility of the technique of state-selective preparation by a narrowband lamp source or laser followed by resolved emission. By monitoring satellite emission bands as a function of pressure, rotational energy transfer in the upper electronic state can be readily measured. This resonance lamp technique was used by Moore and

coworkers to study the rotational energy transfer in the electronically excited B state of HD. Data from these excited state studies have been instrumental in determining empirical scaling and fitting laws. An excellent discussion of the proposed laws is contained in Reference 6. In this study we use several forms of an exponential energy gap scaling law, to parameterize our results. Procaccia and Levine have shown the exponential gap model to be successful at fitting close coupling calculations of Green for HD collisions with He and calculations of Chu for collisions of HD with  $H_2$ .

There have been very few studies performed on ground electronic state surfaces. This is primarily due to the difficulty of preparing a single rotational level and detecting rotational energy transfer on a time scale short enough to resolve the relaxation process. Previous ground-state studies have utilized an infrared double-resonance technique. This technique has been applied to heteronuclear-diatomics: To HF ( $v=1$ ) and DF ( $v=1$ ) by Hinch and Hobbs; to CO ( $v=1$ ) by Bréchnignac *et al*; to HCl ( $v=1$ ) by Menard-Bourcin *et al*; and to HF ( $v=2,3$  and 4) by Crim and coworkers. These studies rely on infrared absorption to monitor rotational states not initially populated. The use of this technique limits the sensitivity and time response of detection. In our work, these problems are minimized by using stimulated Raman pumping and multiphoton ionization detection. Both processes occur on the time scale of the laser pulses (nanoseconds). The preparation scheme is a very efficient process for HD when moderately narrowband lasers are used, and the detection scheme is highly sensitive.

Recently, variations on this scheme have been used to study rotational and vibrational energy transfer in polyatomic molecules. Orr *et al* have used a Raman excitation/laser-induced fluorescence (LIF) method to study rotational and vibrational energy transfer in ground state formaldehyde and glyoxal. A resonant variation of the Raman-LIF scheme has been used by Knight and coworkers to study energy transfer in even larger polyatomics. We have selected the hydrogenic systems to study, due to their historical and theoretical importance. Previous studies of energy transfer in hydrogen have been hampered due to the inherent difficulty of state-selective detection of a molecule with no dipole (or very small dipole in the case of HD) and whose first excited electronic state is 11 eV above the ground state. Recently, three coherent laser techniques have shown great promise for detection of hydrogen: (1) Coherent anti-Stokes Raman scattering (CARS), (2) two-photon resonantly enhanced, three-photon ionization (2+1 REMPI), and (3) direct laser-induced fluorescence, using non-degenerate four-wave mixing in a rare gas to produce the necessary tunable UV radiation. We have used the 2+1 REMPI technique due to its relative simplicity and high sensitivity.

Other non-laser based techniques have been used to study rotational energy transfer in hydrogen molecules. Of particular relevance to our study are the impressive series of molecular beam experiments of Buck and co-workers, and those of Gentry and Giese. Both groups use time-of-flight measurements of scattering distributions from crossed molecular beams to determine the differential cross-section for rotational energy transfer from  $J=0$  or  $J=1$  hydrogen molecules (depending upon the isotope and whether the ortho or para form was used) to other rotational states upon collision with various partners (rare gases or other isotopes of hydrogen). In this

manner, they are able to obtain extremely detailed information (i.e., angular resolved differential scattering cross sections) at a few relative collision energies. In contrast to our measurements, however, they are unable to determine total cross-sections. Although our measurements are thermally averaged, in contrast to the crossed molecular beam studies, they are capable of providing a wealth of data for elementary systems to which theory can be directly applied.

Additionally, the linewidths of high-pressure Raman spectra are dominated by relaxation phenomena and give an upper limit to the rotational relaxation rate. Our measurements are compared to the recent room temperature, high pressure line widths of Rosasco and May.



Laser Induced Fluorescence of  $\text{SiH}_2 \tilde{A}^1B_1 - \tilde{X}^1A_1$   
in the Supersonic Free Jet.

Kinichi Ogi and Shinya Mayama

Department of Chemistry, Tokyo Institute of Technology,  
Ohokayama, Meguro, Tokyo, Japan 152

The pulsed supersonic free jet of  $\text{SiH}_2$  was generated in the ArF laser photolysis of phenylsilane. The fluorescence and its excitation spectra of the  $\tilde{A}^1B_1 - \tilde{X}^1A_1$  transition and the fluorescence lifetimes of single rovibronic levels (SRVL) in the  $\tilde{A}^1B_1$  state have been measured.

The fluorescence excitation spectra have been observed in the region 466 ~ 640 nm. The spectra only consist of the P-type subband from the  $K_a''=0$  level,  $P_{P_1}(N)$ ,  $P_{Q_1}(N)$  and  $P_{R_1}(N)$ , of the  $(0,n,0) + (0,0,0)$  progression. The  $(0,7,0)$  band is first assigned in this work. With increase of the vibrational energy of the bending mode, the line intensities for rotationally excited levels, such as  $P_{Q_1}(1)$ ,  $P_{R_1}(1)$ ,  $P_{P_1}(2)$ , become weak in comparison with the  $P_{P_1}(1)$  line of the rotationally ground state and finally the spectra are reduced to only one rotational line  $P_{P_1}(1)$  for  $n \geq 4$ . These facts indicate the presence of the predissociation which strongly depends on J values in the excited state rotational levels.

The fluorescence spectra have revealed the vibrational energy levels of the bending mode ( $v_2$ ) in the  $\tilde{X}^1A_1$  state up to  $v_2''=7$ . The potential parameters of the bending vibration of the ground state have been determined from the fluorescence spectra:

$$\omega_2 = 1007.6 \pm 4.1 \text{ cm}^{-1}$$

$$x_{22} = -3.7 \pm 0.7 \text{ cm}^{-1}.$$

The Franck-Condon factors of the  $\tilde{A}-\tilde{X}$  system have been calculated using the molecular constants obtained. The calculated Franck-Condon factors have well reproduced the observed fluorescence spectra.

The SRVL fluorescence lifetimes of the  $\tilde{A}^1B_1$  state slowly decreased from 1.2  $\mu\text{s}$  of the (0,1,0) level to 0.54  $\mu\text{s}$  of the (0,6,0) level. The fluorescence lifetime of 0.35  $\mu\text{s}$  for the newly assigned (0,7,0) level obtained is short with respect to other lower vibrational levels. In Fig. 1, the fluorescence decay rates are plotted against cube of transition energy corrected by the Franck-Condon factors. The presence of intercept and the shortening of the fluorescence lifetime for

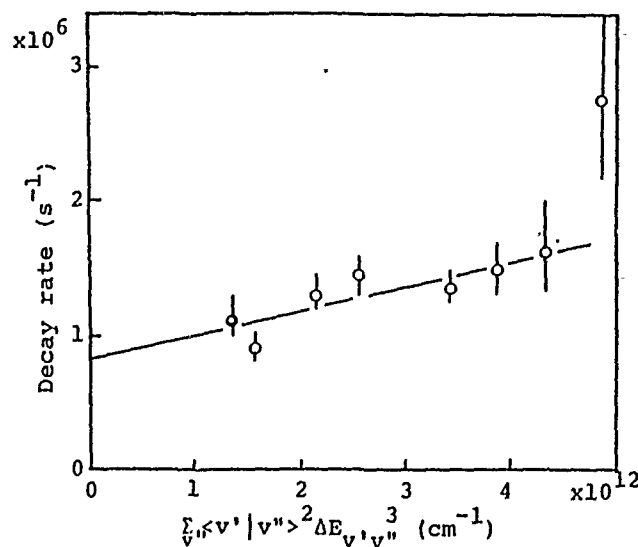


Fig. 1. Plots of the fluorescence decay rate vs. the cubic transition energy

(0,7,0) indicate that (1) non-radiative process occurs in all vibronic levels studied and (2) another non-radiative channel opens at (0,7,0). The first non-radiative channel is explained as predissociation to  $\text{Si}(^3\text{P}_g) + \text{H}_2(^1\Sigma_g^+)$  and the second is predissociation to  $\text{Si}(^1\text{D}_g) + \text{H}_2(^1\Sigma_g^+)$ . This mechanism leads the upper limit of the dissociation energy  $D_0(\text{SiH-H})$  of 26600  $\text{cm}^{-1}$  (318 kJ/mol).

**HIGH TEMPERATURE COLLISIONAL ENERGY  
TRANSFER IN HIGHLY VIBRATIONALLY EXCITED  
MOLECULES. II: ISOTOPE EFFECTS IN *iso*-PROPYL  
BROMIDE SYSTEMS**

Trevor C. Brown and Keith D. King

*Department of Chemical Engineering,  
University of Adelaide, Adelaide, S.A. 5001, Australia*

and

Robert G. Gilbert

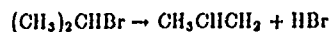
*Department of Theoretical Chemistry,  
University of Sydney, Sydney, N.S.W. 2006, Australia*

Of fundamental importance in interpreting rate data for unimolecular and termolecular reactions in the fall-off regime is the determination of the form of the probability distribution function for collisional energy exchange between a highly vibrationally excited reactant and a bath gas [1]. The development of models for this process requires experimental energy transfer data under conditions where the dependent parameters (eg. temperature and bath gas mass) can be varied and effectively interpreted. This paper is a continuation of our studies into the effects of deuteration of both the reactant and bath gas on collisional energy transfer quantities [2]. Deuteration changes the masses of the species, but leaves unchanged the potential function governing the interaction dynamics.

The technique of pressure-dependent very low-pressure pyrolysis [3,4] combined with conventional very low-pressure pyrolysis (VLPP) [5] has been used here to initially create thermal systems of highly vibrationally excited undeuterated and per-deuterated *iso*-propyl bromide molecules, and then collide these reacting systems with the inert bath gases - Ne, Xe, C<sub>2</sub>H<sub>4</sub>, and C<sub>2</sub>D<sub>4</sub>. Measurements of the increase in reaction rates of the *iso*-propyl bromide decompositions with these bath gas collisions, and a comparison of these rates with the deuterated analogues give valuable insights into the collisional probability distribution function.

The overall experimental technique is well established [3,4,5]. Briefly, the temperature dependence of the reaction rate under conditions where only gas/wall collisions occur (ie., in the absence of any reactant/reactant or reactant/bath gas collisions) is firstly obtained. These data is then fitted with RRKM theory, taking into account the temperature-dependent non-unit gas/wall collision efficiency,  $\beta_w(T)$  [3,6]. The energy dependences of the microscopic reaction rate,  $k(E)$  are consequently calculated. By maintaining the temperature constant, and increasing the pressure of bath gas in the system so that reactant/bath gas collisions compete with reactant/wall collisions the pressure-dependent rate coefficients are obtained. These values are fitted by solution of the reaction-diffusion master equation [1], using the parameters from the RRKM calculations and varying  $\langle \Delta E_{down} \rangle$  - the average downward collisional energy transfer.

The *iso*-propyl bromide systems decompose thermally via HBr elimination, e.g. for the undeuterated system:



The extrapolated high pressure rate coefficient ( $k_\infty$ ) for  $\text{C}_3\text{H}_7\text{Br}$  decomposition is given by  $k_\infty = 10^{13.6 \pm 0.3} \exp(-200 \pm 8 \text{ kJ mol}^{-1}/RT)$ . This is in excellent agreement with the high-pressure parameters reported by other authors [7]:  $A_\infty = 10^{13.70 \text{ s}^{-1}}$ ,  $E_\infty = 197.5 \text{ kJ mol}^{-1}$ . For  $\text{C}_3\text{D}_7\text{Br}$  the high-pressure parameters are  $A_\infty = 10^{13.9 \pm 0.3 \text{ s}^{-1}}$ ,  $E_\infty = 207 \pm 8 \text{ kJ mol}^{-1}$ . There is no previously reported study of  $\text{C}_3\text{D}_7\text{Br}$  decomposition, however our results are in accord with the expected isotope effect.

The average downward collisional energy transfer ( $\langle \Delta E_{down} \rangle$ ) values ( $\text{cm}^{-1}$ ) for  $\text{C}_3\text{H}_7\text{Br}$  at ca. 870 K are 486 (Ne), 539 (Xe), 825 ( $\text{C}_2\text{H}_4$ ), and 743 ( $\text{C}_2\text{D}_4$ ), and for  $\text{C}_3\text{D}_7\text{Br}$ , 442 (Ne), 570 (Xe), 729 ( $\text{C}_2\text{H}_4$ ), and 812 ( $\text{C}_2\text{D}_4$ ). Reactant internal energies to which the data are sensitive are in the range 170 - 250  $\text{kJ mol}^{-1}$ . The  $\langle \Delta E_{down} \rangle$  values for the inert bath gases Ne and Xe show good agreement with the theoretical predictions of Gilbert's biased random walk model for monatomic/substrate collisional energy exchange [8]. The relative effects of deuteration of the reactant molecule on  $\langle \Delta E_{down} \rangle$  also compare favourably with the predictions of this theoretical model. The energy transfer parameters resulting from the undeuterated and per-deuterated ethene bath gases suggest the vibrational frequencies of the polyatomic colliders will play an important role in any future model.

# References

- [1] B. S. Rabinovitch and D. C. Tardy, *Chem. Rev.*, **77**, 369 (1977).
- [2] T. C. Brown, K. D. King, and R. G. Gilbert, *Int. J. Chem. Kinet.*, **16**, 1455 (1984).
- [3] K. D. King, T. T. Nguyen, and R. G. Gilbert, *Chem. Phys.*, **61**, 223 (1981); T. T. Nguyen, K. D. King, and R. G. Gilbert, *J. Phys. Chem.*, **87**, 491 (1983); R. G. Gilbert and K. D. King, *Chem. Phys.*, **49**, 367 (1980).
- [4] R. G. Gilbert, B. J. Gaynor, and K. D. King, *Int. J. Chem. Kinet.*, **11**, 317 (1979).
- [5] D. M. Golden, G. N. Spokes, and S. W. Benson, *Angew. Chem., Int. Ed.*, **12**, 534 (1973).
- [6] P. G. Dick, R. G. Gilbert, and K. D. King, *Int. J. Chem. Kinet.*, **6**, 1129 (1984).
- [7] D. Gutman, W. Braun, and W. Tsang, *J. Chem. Phys.*, **67**, 4291 (1977).
- [8] R. G. Gilbert, *J. Chem. Phys.*, **80**, 5501 (1984).

UNIMOLECULAR REACTIONS FOLLOWING SINGLE UV-PHOTON AND MULTI  
IR-PHOTON EXCITATION

B. Abel, B. Herzog, H. Hippler and J. Troe

Institut für Physikalische Chemie der Universität Göttingen,  
Tammannstraße 6, D-3400 Göttingen, West-Germany

Unimolecular reactions are governed by two dynamically different processes. The activation of molecules above the reaction threshold and the real reaction. In thermal systems the activation occurs via intermolecular energy transfer between highly excited molecules in collisions with the heat bath. The reaction itself is determined by the intramolecular time evolution of molecules excited above the reaction threshold. The intermolecular energy transfer can be characterized by the averaged amount of energy transferred per collision  $\langle \Delta E \rangle$ . The intramolecular dynamics are described by the specific rate constant  $k(E)$ . Both quantities present key quantities in unimolecular rate theory. We present a method to directly measure under collision free conditions the specific rate constants and in the presence of collisions the  $\langle \Delta E \rangle$  values.

In our experiments vibrationally highly excited polyatomic molecules are produced in the electronic ground state by two different ways. First, absorption from a pulsed UV-laser followed by fast internal conversion is a very elegant way to create an almost microcanonic ensemble of vibrationally highly excited molecules. In the past, we have intensively used this technique for studies of the dynamic prop-

erties of these molecules. Second, IR multiphoton absorption from a pulsed  $\text{CO}_2$  laser may produce an ensemble of vibrationally highly excited molecules with different properties. Populations of excited states are monitored directly by time resolved hot band UV absorption spectroscopy. A calibration of the UV spectra by shock wave experiments allows for an analysis of the absorption changes during the laser pulses in terms of excited state populations and dissociation. Under collision free conditions the rate of unimolecular reaction of isolated molecules are measured. A comparison of the results of the two methods will be presented. For bond fission reactions the influence of total angular momentum  $J$  on the specific rate constant  $k(E,J)$  is discussed. In the presence of collisions with an inert bath gas, collisional deactivation is observed and analyzed via the dependence of the hot UV absorption spectra on the excitation energy. We conclude that time resolved hot band UV absorption spectroscopy after pulse excitation provide a particularly attractive access to the specific rate constant and to collisional energy transfer. It also allows to obtain in situ information of the energy distribution of the ensemble of vibrationally highly excited molecules produced in IR multiphoton excitation experiments.



## LASER PYROLYSIS OF DIMETHYLNITRAMINE AND DIMETHYLNITROSAMINE

S. Esther Nigenda, Alicia C. Gonzalez,  
Donald F. McMillen, and David M. Golden  
Department of Chemical Kinetics, Chemical Physics Laboratory  
SRI International, Menlo Park, CA 94025 U.S.A.

Laser-powered homogeneous pyrolysis (LPHP) has been used to study the gas-phase thermal decomposition of dimethylnitramine (DMNA) and dimethylnitrosamine (DMNO) as models for the decomposition of the cyclic nitramines. In the LPHP technique a pulsed  $\text{CO}_2$  laser is used to indirectly heat the substrate via an absorbing but unreactive gas (e.g.,  $\text{SF}_6$ ), in a bath of an inert polyatomic such as  $\text{CO}_2$ . Under these conditions there is no surface component to the reactions, since only a small portion of the cell volume is heated by the laser and the reaction time before cooling by the expansion wave is about 10  $\mu\text{s}$ , far shorter than the millisecond time scale for diffusion to the walls. The rapid cooling tends to minimize secondary reactions; however, as in shock-tube studies, hydrogen atoms and other very reactive species need to be chemically scavenged or trapped.

The cell is incorporated in a flow system that can be heated to temperatures well below substrate decomposition temperatures, but high enough to maintain low vapor pressure materials in the vapor phase. Operation of the system involves flowing the reaction mixture through the cell while the laser is pulsed at a constant repetition rate, typically about 0.2 Hz. The flow rate and irradiated volume are such that during the residence time of the substrate in the cell, the laser will have been pulsed 20 to 40 times (with complete diffusional mixing in the cell between laser pulses), and the average molecule will have been heated two to four times. The product mixture flows continuously from the cell through a heated gas sampling valve from which samples are periodically sent to a capillary GC/MS system.

The need to explicitly measure the temperature corresponding to any particular measurement of  $k$  is eliminated by concurrent determination of the

fractional decomposition of a temperature standard. Modeling of anticipated time-temperature-location variations as well as tests on substrates whose parameters are already known have shown that this "comparative rate" method accommodates wide temperature fluctuations in accurately reproducing the literature values. In the present case, Arrhenius parameters have been determined relative to isobutylbromide and tert-butylbromide decomposition, respectively.

The DMNO decomposition proceeds, between 950 and 1050K, via the simple N-N bond cleavage. The dimethylamino radical thus formed rapidly eliminates an H-atom and is detected as N-methylmethyleimine. The H-atoms are scavenged by reaction with ortho-fluorotoluene. Preliminary results yield Arrhenius parameters of  $\log k/s^{-1} = 15.0 - 46.0/\theta$ . These yield, when corrected for pressure dependence,  $\log k^\infty/s^{-1} = 15.4 - 48.3/\theta$ . These values are completely consistent with the expectation of reaction via unimolecular bond scission and a N-N bond strength in the vicinity of 48 kcal/mol.

The DMNA decomposition is more complex in that both unimolecular bond scission and HONO elimination are expected to be accessible pathways. Since both of these pathways lead to the imine, they are difficult to distinguish. Furthermore, the major product is DMNO, leading to the conclusion that the imine adds NO in the cooling period after the laser pulse. DMNA was pyrolyzed between 845 K and 970 K, leading to  $\log k/s^{-1} = 10.4 - 28.2/\theta$ . These parameters are difficult to reconcile with the expected values for the two above pathways, and the kinetic measurements are being repeated with a different internal standard.

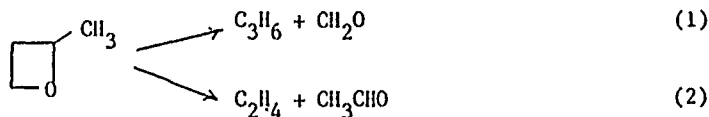
IR laser-induced decomposition of oxetanes and alkanols

by K.A. Holbrook, G.A. Oldershaw and C.J. Shaw  
Department of Chemistry, University of Hull

and P.E. Dyer  
Department of Applied Physics, University of Hull

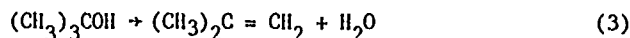
Following earlier work on the infrared laser-induced decomposition of 2,2-dimethyloxetane<sup>1</sup> we have examined the infrared laser-induced decomposition of 2-methyloxetane and of tertiary butanol, two molecules of similar molecular complexity.

The products of the decomposition of 2-methyloxetane caused by absorption of pulses from a TEA CO<sub>2</sub> laser (R34, 10 μm line) are the same as those observed in the thermal decomposition,<sup>2</sup> namely propene plus formaldehyde and ethene plus acetaldehyde.



Measurements have been made of the energy absorbed by 2-methyloxetane and of the extent of decomposition as a function of the gas pressure and laser fluence. The effect of added inert gases helium, xenon and cyclohexane has also been examined.

Similar experiments have been carried out with tert-butanol (P30, 10 μm line) for which the major decomposition product is isobutene



In both cases it is found that, for irradiation under 'collision-free' conditions ( $5 \times 10^{-2}$  Torr), the decomposition is much less in dilute mixtures of the absorber with an inert gas than in the pure reactant. We have modelled the decomposition as a function of absorbed energy by using specific rate coefficients calculated from RRKM theory. In both cases it is concluded that a large fraction of the irradiated molecules interact with the laser radiation. Results obtained for other alkanols and oxetanes may also be discussed.

References

1. K.A. Holbrook, G.A. Oldershaw, C.J. Shaw and P.E. Dyer, submitted for publication.
2. P. Hammonds and K.A. Holbrook, J.C.S. Faraday I, **78**, 2195 (1982).

Use of Doppler Broadening by the 254nm Hg Absorption Line to Monitor v-r,t Energy Transfer in Vibrationally Excited Gases

Walter Braun\*, Milton D. Scheer\*\*, R. J. Cvetanovic\*\*  
and Victor Kaufman\*\*\*

\*Center for Chemical Physics

\*\*Guest Scientists in the Center for Chemical Physics

\*\*\*Center for Radiation Research

National Bureau of Standards

A new method for measuring v-r,t energy transfer rates has been developed. It involves the use of Hg atoms as a tracer for translational energy in a vibrationally excited gas. Absorption by Hg of its 254nm resonance radiation, derived from an extensively self-reversed Hg resonance lamp, is dependent upon the line width and hence the translational temperature. By matching the hyperfine spectrum of a Hg resonance lamp in the neighborhood of 254nm with a computer model that takes into account Doppler and Lorentz line broadening (Fig. 1), a temperature calibration is readily attained (Fig.2). The method was tested by vibrationally exciting a 500:1 mixture of SF<sub>6</sub> and Hg with varying fluences from a CO<sub>2</sub> TEA laser employing the apparatus shown schematically in Fig.3. By measuring the initial slopes of the temporal changes in the 254nm absorption by the Hg tracer, which is related to changes in temperature and thus energy, energy transfer rates could be measured as a function of initial vibrational excitation energy. For vibrational excitations between 400 and 10,500cm<sup>-1</sup>, the energies transferred (v-r,t) per SF<sub>6</sub>\*-SF<sub>6</sub> collision was found to increase

approximately as the square of the excitation energy. These results are shown in Fig. 4. and are compared with recent results by Dove, Hippler and Troe<sup>(1)</sup>. The present method complements techniques recently reported by other workers<sup>(2-4)</sup>.

#### References:

- 1) J. E. Dove, H. Hippler and J. Troe, J. Chem. Phys. 82, 1907 (1985)
- 2) M. J. Rossi, J. R. Pladzievicz, and J. R. Barker, J. Chem. Phys. 78, 6695 (1983); W. Forst and J. R. Barker, J. Chem. Phys. 83, 124 (1985)
- 3) N. Selamoglu and C. Steel, J. Phys. Chem. 87, 1133 (1983)
- 4) T. Ichimura and Y. Mori, J. Chem., Phys. 83, 117 (1985)
- 5) H. Hippler, J. Troe and H. J. Wendelken, J. Chem. Phys. 78, 5351, 6709 (1983)
- 6) H. Hippler, L. Lindemann and J. Troe, J. Chem. Phys. 83, 3906 (1985)

#### Figure Captions:

Figure 1: An experimental tracing of the high resolution spectrum emitted by an extensively self-reversed capillary Hg lamp operated at 450v and 9ma (dashed curve) compared with the calculated lamp profile (solid curve).  $X_1=1$ =Doppler width.

Figure 2: Computed fractional absorption vs. temperature curves for various resonance lamp (current) conditions: 1, 8ma; 2, 10ma; 3, 15ma; and 4, 20ma.

Figure 3: Schematic diagram of apparatus used to excite vibrationally  $SF_6$  and measure its translational temperature. LS= $CO_2$  laser; L=Hg light source; M=monochromater; D=fast digitizer; MP=microprocessor; C=gas cell; PM=photomultiplier; CB=carbon block used to trigger sweep; L=lens; M1&M2=mirrors.

Figure 4: The dependence of the average energy transferred per collision vs. the average excitation energy for  $SF_6^+ + SF_6^+$  collisions compared with literature  $CS_2^+ + CS_2$ , and  $CS_2^+ + Ar$  results.

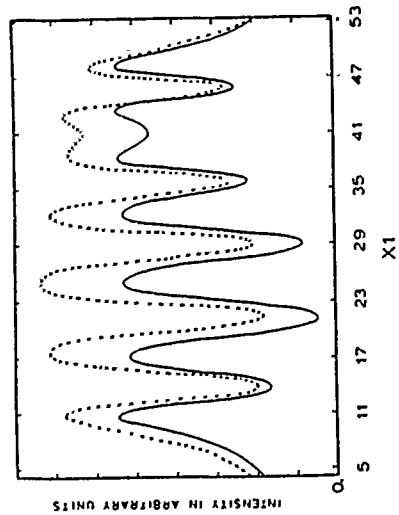


Figure 1:

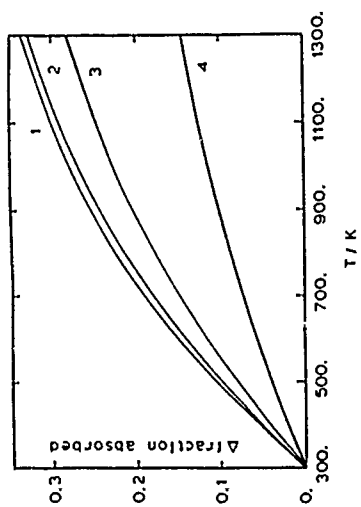


Figure 2:

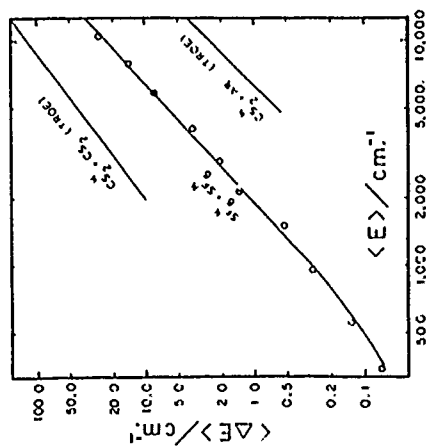


Figure 4:

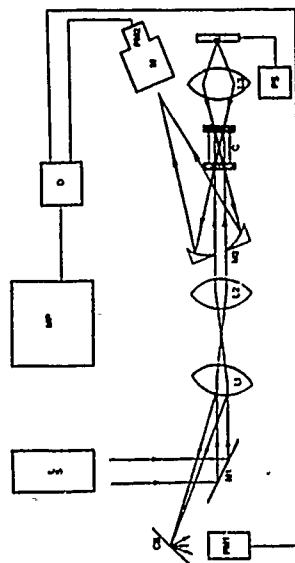


Figure 3:

Analysis of Multiple Decompositions in Chemically Activated  
Reactions.

Phillip R. Westmoreland, Jack B. Howard, and John P. Longwell

Department of Chemical Engineering  
Massachusetts Institute of Technology  
Cambridge, MA 02139 USA

Secondary decomposition can occur in a chemically activated reaction if all the excess energy in the chemically activated adduct is not dissipated by the initial decomposition. Thus, a bimolecular reaction could lead to three products by the processes  $A+B \rightarrow C^* \rightarrow D^*+E^*$ ,  $D^* \rightarrow D$ , and  $E^* \rightarrow F+G$ . Such three-product channels have been inferred from data in the past, but either the observation has not been rationalized or it has been attributed to a sequence of thermal reactions  $A+B \rightarrow D+E$  and  $E \rightarrow F+G$ . Unlike a thermal sequence, chemically activated secondary decomposition is not microscopically reversible because the reverse reaction would require excited  $E^*$  (from  $F+G$ ) and  $D^*$  to react.

Apportioning the excess energy between  $D^*$  and  $E^*$  is the difficulty in calculating the apparent rate constant. If  $D$  is an atom and  $E$  contains vibrational degrees of freedom, all the excess energy may be reasonably assigned to the species  $E^*$ . The rate constant for  $^3CH_2+^3CH_2 \rightarrow C_2H_2+2H$  is estimated by bimolecular QRRK to illustrate the quantitative analysis, but more sophisticated unimolecular reaction theories may be applied similarly.

WAVELENGTH DEPENDENT ISOMERIZATION OF ALLYL  
ISOCYANIDE

J. Segall and R.N. Zare, Department of Chemistry,  
Stanford University, Stanford, CA 94305 USA

The isomerization of allyl isocyanide (AIC) to allyl cyanide by excitation of CH vibrational overtone inside the cavity of a cw dye laser is studied at several excitation wavelengths (598-640 nm). The unimolecular reaction rate is seen to vary nonmonotonically as a function of photolysis photon energy, both with a given overtone band as well as from overtone band to overtone band. Previous workers on AIC<sup>1</sup> noted the latter effect and attributed it to a nonstatistical distribution of vibrational energy in the reacting molecules. The current results strongly indicate inhomogeneous broadening is important in the overtone spectrum of AIC and that overtone excitation may lead to a more complex distribution of excited reactants than previously thought.

\*\*Supported by AMOCO, Standard Oil (Indiana)

<sup>1</sup>K. V. Reddy and M. J. Berry, Chem. Phys. Lett. 66, 223 (1979).



A STUDY OF THE EFFECT OF EXCESS ENERGY ON THE COLLISIONAL DEACTIVATION OF  
HIGHLY VIBRATIONALLY EXCITED 7-ETHYLCYCLOHEPTATRIENE

Gui-Yung Chung and Robert W. Carr, Jr.

Department of Chemical Engineering and Materials Science  
University of Minnesota  
Minneapolis, Mn. 55455

Collisional self deactivation of 7-ethylcycloheptatriene photoactivated to total internal energies of 123 kcal/mol (240nm), 111 kcal/mol (265nm), 105 kcal/mol (280nm), and 100 kcal/mol (295nm) has been investigated. The reaction products consisted of the positional isomers 1-, 2-, and 3-ethylcycloheptatriene, and methyl-ethyl substituted benzenes formed by aromatization. The pressure dependence of reaction products resulting from positional isomerization and aromatization were determined at each wavelength in series of experiments without added bath gases. The total product yield decreased with increasing pressure, indicative of collisional stabilization of photoactivated 7-ethylcycloheptatriene. The ratio of positional isomerization products to aromatic products increased with increasing pressure at fixed wavelength, and increased with increasing wavelength at fixed pressure, consistent with a shorter lifetime for positional isomerization than for aromatization. Master equation calculations were done using RRKM theory and a stepladder model for deactivation. The model calculations predict that the average energy removed per deactivating collision,  $\langle \Delta E \rangle$ , increases with increasing excess energy of photoactivated 7-ethylcycloheptatriene. When the RRKM computed values of  $k(E)$  were normalized to an experimental value determined by direct detection (Hippler, Luther, Troe and Wendleken, J. Chem. Phys., 79, 246, (1983)), the values of  $\langle \Delta E \rangle$  obtained were 1.5 kcal/mol at 295nm, 1.8 kcal/mol at 280nm, 2.2 kcal/mol at 265 nm and 5 kcal/mol at 240 nm.

A simple FTIR instrument for emission studies

by

P. Biggs, F.J. Holdsworth, G. Marston and R.P. Wayne  
Physical Chemistry Laboratory, South Parks Rd., Oxford., U.K.

Abstract

Fourier Transform spectrometry was originally introduced to deal with the energy shortage problems endemic in working in the far-infrared. However, FT spectrometry has been successfully applied in the mid- and near-IR and is even finding uses in the visible and UV region of the electromagnetic spectrum. Employment of this technique in the IR can result in dramatic increases in the signal-to-noise ratio or resolution of spectral measurements, or both.

Two important advantages of interferometry over conventional spectrometry were pointed out by Fellgett in England and Jaquinot in France:

- i) In 1951, Fellgett recognised the so called Multiplex advantage, in that data from all the spectral frequencies present are measured simultaneously; thus, the whole of the spectral band is observed for the entire duration of the experiment. The result of this 'Multiplex' advantage is a reduction in measurement time of the spectral information.
- ii) The second advantage, pointed out in 1954 by Jaquinot, is that the optical energy throughput of an interferometer is greater than that of a monochromator for a given resolution. Radiation is transferred more efficiently in an interferometer, where the beam of radiation has cylindrical symmetry, than in a conventional spectrometer which employs slits and produces a beam of planar symmetry. The increased throughput thus results in an increased S:N ratio due to the increased signal at the detector.

The interferometer used in these studies is a low cost

Michelson type designed to be used as a teaching instrument. The interferometer was modified to allow the mirror position to be altered using a stepper motor. A He-Ne laser and associated optics were also added to allow us to guide a laser beam down the center of the main optics.

The data acquisition and control of the interferometer were performed using a small 'home' computer (Acorn BBC 'B' microcomputer). The only additional circuitry required was the power control circuit for the stepper motor and the amplifiers for the various detectors employed. The laser beam was used to provide a reference, the data acquisition being triggered using the laser fringes.

The same computer, along with a co-processor to speed up the processing, was used to perform the Fourier transform calculations. Two different FT calculation methods were employed : a 'slow' transform based on the Fourier integral, and the Fast Fourier Transform (FFT) algorithm developed by Cooley and Tukey in 1965.

Various computational techniques were used to increase both the speed of calculation and the resolution of the instrument. The use of a small computer limits the number of interferogram points to approximately 8000, which corresponds to a resolution of approximately  $3.9\text{cm}^{-1}$  (at a sampling interval of  $\Delta x = 0.3165\mu\text{m}$ ). The use of single sided interferograms increases the effective resolution to  $1.9\text{cm}^{-1}$ , but can introduce some phase errors into the spectrum, resulting in distorted peak shapes.

The method finally developed to increase the resolution was to use aliased spectra. Aliasing comes about from using discrete sampling intervals, and is manifested by the spectral function exhibiting mirror symmetry about the sampling frequency ( $\nu_n$ ). It is usually classed as a disadvantage of FT since both spectral information and noise above the folding frequency are reflected back into the fundamental range, and care must be employed to ensure that features in the spectrum are real and not aliased. If we take longer sampling intervals, we can make the mirror move a longer distance for the same number of interferogram points, thus increasing resolution, however  $\nu_n$  also decreases. If we ensure that there are no spectral peaks in the fundamental range ( $0 < \nu < \nu_n$ ), then we can use the aliased

version of the peak of interest for our studies. Thus by sampling at 3 times the normal distance ( $\Delta x = 0.949 \mu\text{m}$ ) we were able to increase the resolution to  $1.3 \text{ cm}^{-1}$  and at 5 times ( $\Delta x = 1.58 \mu\text{m}$ ), the resolution had increased to  $0.8 \text{ cm}^{-1}$  (2 and 4 times were not used because these values put  $\nu_n$  in the middle of the peak of interest).

The spectrometer was used in conjunction with a germanium detector and discharge flow system to study reactions leading to chemiluminescence in the  $1\text{-}2 \mu\text{m}$  region. Of particular interest was the  $\text{N} + \text{O}_2$  reaction,



from which emission had already been observed under low resolution. Under the greater resolution afforded us by the FT spectrometer, we were able to identify the emissions as being due to  $\text{O}_2$ ,  $\text{a}^1\Delta_g \rightarrow \text{X}^3\Sigma_u$  ( $1.27 \mu\text{m}$ ),  $\text{NO}$   $\text{C}^2\Pi \rightarrow \text{A}^2\Sigma$  ( $1.22 \mu\text{m}$ ) and the (2,0), (3,1) and (4,2) vibrational overtone transitions of OH ( $1.40\text{-}1.55 \mu\text{m}$ ).

The presence of OH emission downstream of the mixing region showed us not only that H was present as an impurity, but that it was being regenerated in the flow tube. A mechanism is presented to explain this regeneration. The presence of  $\text{O}_2$  ( $^1\Delta_g$ ) was also found to be due to H atom impurities and is explained in terms of formation of excited  $\text{HO}_2$  followed by energy transfer to  $\text{O}_2$ . The formation of  $\text{NO}(\text{C})$  was attributed to reaction between N and O atoms and computer simulations were able to match observed concentration - time profiles quite well.

Kinetic measurements were made using conventional spectrometry. N atoms were monitored by following the (0,0) band of the  $\text{N}_2(\text{B} \rightarrow \text{A})$  transition at  $1.05 \mu\text{m}$ . Again the presence of H atoms was felt, resulting in non-linear pseudo-first order decay plots. However, after taking precautions to remove traces of water from our system the rate constant for the above reaction was measured as  $k = (8.8 \pm 1.0) \times 10^{-17} \text{ cm}^3 \text{ molecule}^{-1} \text{ s}^{-1}$ . This value is in excellent agreement with the latest NASA recommendations.

MULTIPHOTON IONIZATION AS A KINETIC PROBE

H.H. NELSON and Brad R. Weiner, Chemistry Division, Naval Research Laboratory,  
Washington, DC 20375-5000, USA

The methyl radical ( $\text{CH}_3$ ) plays an important role in hydrocarbon combustion systems. Kinetic studies of the methyl radical, especially as a reaction product, have been hampered by the lack of a sensitive, convenient detection scheme. It has been monitored in kinetic systems previously using infrared<sup>1</sup> and ultraviolet<sup>2</sup> absorption spectroscopy. These techniques require the use of long path lengths, which introduces difficulties in reactant preparation, or relatively high  $\text{CH}_3$  concentrations, which leads to interference from radical-radical reactions. We are developing resonance-enhanced multiphoton ionization (REMPI) as a concentration probe for  $\text{CH}_3$  under typical laboratory kinetic conditions. The methyl radical is ionized via the  $3p\ ^2A_2''$  state resonance at 333.4 nm, as discussed by Hudgens et al.<sup>3</sup>, using the fundamental output of an excimer-pumped dye laser focussed by a 30-cm f.l. lens. The electron current produced is collected by a pair of parallel plates biased at  $\sim 300\text{V}$ , amplified and detected using a gated integrator. Using  $\text{CH}_3\text{I}$  photolysis at 266 nm as a source of methyl radicals to characterize the system, we are able to detect kinetically useful concentrations of  $\text{CH}_3$  at pressures up to 50 Torr of He. At 5 Torr total pressure, our limit of detection of  $\text{CH}_3$  in this system is  $\sim 2 \times 10^{11}\text{ cm}^{-3}$ . We will report kinetic measurements of  $\text{CH}_3$  as a product of the reaction of F atoms with  $\text{CH}_4$ . Studies of the reaction,  $\text{O} + \text{C}_2\text{H}_4$ , are underway and we will present the results available from this system.

## References:

- 1) G.A. Laguna and S.L. Baughcum, Chem. Phys. Lett., **88**, 568 (1982)
- 2) M.T. Macpherson, M.J. Pilling and M.J.C. Smith, Chem. Phys. Lett., **94**, 430 (1983)
- 3) J.W. Hudgens, T.G. DiGiuseppe and M.C. Lin, J. Chem. Phys., **79**, 571 (1983)

Intracavity Detection Applied to Reaction Rate Measurements<sup>\*</sup>J. E. Allen, Jr. and W. D. Brobst<sup>+</sup>Astrochemistry Branch, NASA, Goddard Space Flight Center  
Greenbelt, MD, USA 20771

Intracavity laser detection of atoms and molecules was first observed over fifteen years ago<sup>1,2</sup> and has steadily matured as a spectroscopic tool. However, it has seen only limited use in chemical kinetics, despite its demonstrated sensitivity and obvious applicability for the detection of weakly absorbing or predissociated species. Previous kinetic studies<sup>3,4,5</sup> were performed with pulsed lasers which are inherently less sensitive than cw lasers for intracavity detection. In addition these experiments were performed for radical species in a static cell which complicated the kinetics and therefore the rate measurement. As a consequence while these measurements are in good agreement with each other, they are all lower than the recommended value.<sup>6</sup> To demonstrate the applicability and accuracy of cw intracavity absorption, we measured the rate for the termolecular reaction  $\text{NO} + \text{NO} + \text{O}_2 \rightarrow 2\text{NO}_2$ . This reaction is ideal since it has a well known rate and can appropriately be performed in a static cell. Because the reactants are stable molecules, concentration can easily and accurately be measured with a capacitance manometer. The product is stable, thereby making calibration of the detection system straightforward, and

secondary reactions are slow enough not to unduly complicate the measurement.

The intracavity spectrometer was built around a commercially available folded cavity dye laser which was optically pumped by the 514.5 nm line of an argon ion laser. The dye laser cavity was extended to 1.8 m by removing the standard output coupler and placing a new output coupler at an appropriate distance from the dye laser housing. Cavity tuning was accomplished by laterally translating a coated wedge. A cell 0.5 m long, which had wedged windows mounted on arms cut a Brewster's angle, was placed inside the cavity and connected to a vacuum system. Pressure measurements were made with capacitance manometers. The output from the extended cavity laser was directed to a 0.75 m focal length monochromator and detected with a photomultiplier tube. The PMT signal was processed by an electrometer and subsequently displayed on a strip chart recorder.

Since the reaction was to be followed by monitoring the appearance of the  $\text{NO}_2$  product, the system was calibrated by accurately metering varying quantities of  $\text{NO}_2$  into the cell and measuring the depth of the resultant hole produced in the dye (laser output profile. Plots of this apparent absorbance vs. absorber concentration were linear over a substantial range, indicating a Beer - Lambert law type of relationship.

Kinetic experiments were performed with NO in excess of O<sub>2</sub> which can be shown to be a pseudo first order condition. Analysis indicated that NO<sub>2</sub> absorbance is a linear function of time; a plot of NO<sub>2</sub> absorbance vs. time in fact yielded a straight line whose slope is related to the desired rate. A number of experiments were performed for various laser powers, reactant concentrations and absorption transitions. From these experiments the rate was determined to be  $(2.4 \pm 0.4) \times 10^{-38} \text{ cm}^6 \text{ molec}^{-2} \text{ sec}^{-1}$  which is an excellent agreement with the recommended rate of  $(2 \pm 1) \times 10^{-38} \text{ cm}^6 \text{ molec}^{-2} \text{ sec}^{-1}$ .<sup>7</sup> This clearly demonstrates the utility of intracavity absorption for chemical kinetic studies.

\* Work supported by the NASA Upper Atmosphere Program.

+ NASA Graduate Student Researcher from Johns Hopkins University

#### References

1. L. A. Pakhomycha, E. A. Sviridenkov, A. F. Sukov, L. A. Titova and S. S. Churilov, Sov. Phys. JETP Lett 12, 43 (1970).
2. N. C. Peterson, M. J. Kurylo, W. Braun, A. M. Bass and R. A. Keller, J. Opt. Soc. Am. 61, 746 (1971).
3. J. D. Reilly, J. H. Clark, C. B. Moore and G. C. Pimentel, J. Chem. Phys. 69, 4381 (1978).



4. V. A. Nadtochenko, O. M. Sarkisov and V. L. Vedeneev, Doklady Akademii Nauk SSSR 244, 152 (1979).
5. R. J. Gill, W. D. Johnson, and G. H. Atkinson, Chem. Phys. 58, 29 (1981).
6. NASA Panel for Data Evaluation "Chemical Kinetic and Photochemical Data for Use in Stratospheric Modeling, Evaluation No. 7," JPL Publication 85-37, 1985, p. 59.
7. D. L. Bauch, D. D. Drysdale, D. G. Horne and A. C. Lloyd, Evaluated Kinetic Data for High Temperature Reactions Volume 2: Homogeneous Gas Phase Reactions of the H<sub>2</sub>-N<sub>2</sub>-O<sub>2</sub> System, Butterworths, London, 1973, p.285.

ON THE ERRORS OF ARRHENIUS PARAMETERS AND ESTIMATED RATE  
CONSTANT VALUES

Károly Héberger, Sándor Kemény<sup>1</sup> and Tamás Vidóczy

Central Research Institute for Chemistry of the Hungarian  
Academy of Sciences, H-1525 Budapest, Pf. 17. Hungary

<sup>1</sup> Department of Chemical Engineering, Technical University  
of Budapest, Budapest, Hungary

Papers on chemical kinetics usually present numerical values of rate coefficients (determined over a range of temperature) described by some form of Arrhenius-type equation. Though several papers suggest correct and useful methods for the fitting procedure and for calculating the uncertainties<sup>1-3</sup>, these methods are not universally utilized. Our aim was to show the effect of possible errors, and to emphasize the statistically correct way of data presentation.

1. Two-parameter problem using the equation  $k=A \cdot \exp(B/T)$

The problem to be solved is the minimization of

$$F = \sum_{i=1}^N w_i [k_i - A \cdot \exp(B/T_i)]^2 \quad (1)$$

where  $k_i$  is the measured rate coefficient at temperature  $T_i$ ,  $w_i$  is the statistical weight of the  $i$ -th measurement,  $N$  is the number of measurements and  $A$  and  $B$  are the two parameters to be determined. The possibilities for the determination of the two parameters are well known<sup>4</sup> (e.g. by solving the normal equation  $\partial F/\partial A = 0$ ,  $\partial F/\partial B = 0$ ). All the necessary information about the uncertainties of the fit can be found in the covariance matrix

$$\underline{COV(A,B)} = S^2 \cdot \underline{G}^{-1} \quad (2)$$

where  $S^2 = F/(N-2)$  and the elements of matrix  $\underline{G}$  are defined in the following way:

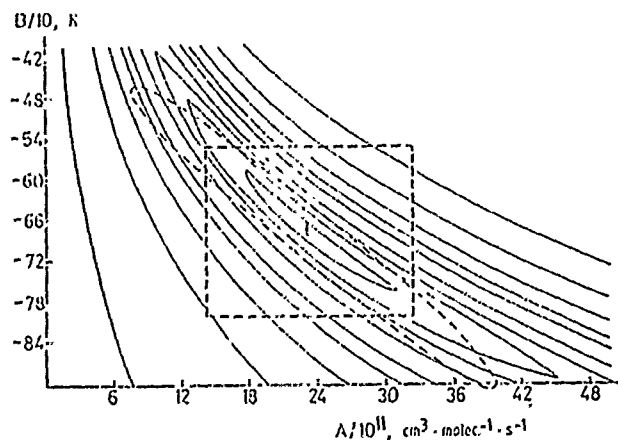
$$g_{A,A} = \sum w_i \left( \frac{\partial \hat{k}_i}{\partial A} \right)^2 \quad g_{A,B} = g_{B,A} = \sum w_i \frac{\partial \hat{k}_i}{\partial A} \frac{\partial \hat{k}_i}{\partial B} \quad g_{B,B} = \sum w_i \left( \frac{\partial \hat{k}_i}{\partial B} \right)^2 \quad (3)$$

where  $\hat{k}_i$  means the estimated rate coefficient at  $T_i$ . The best estimate of the variance of  $\hat{k}_i$  is given by

$$\text{Var}(\hat{k}_i) = \left( \frac{\partial \hat{k}_i}{\partial A} \right)^2 \text{cov}_{A,A} + 2 \frac{\partial \hat{k}_i}{\partial A} \frac{\partial \hat{k}_i}{\partial B} \text{cov}_{A,B} + \left( \frac{\partial \hat{k}_i}{\partial B} \right)^2 \text{cov}_{B,B} \quad (4)$$

As the off-diagonal element of  $\text{COV}(A,B)$  is always negative, the uncertainty of the rate coefficient will be always overestimated if the full covariance matrix is not taken into account.

To illustrate the difference between giving only the diagonal elements of  $\text{COV}(A,B)$  (thus defining a rectangular box in the parameter space), or giving the full covariance matrix (which defines an ellipse) we plotted the contour map of  $F$  for



a simulated set of data in Fig. 1. It can be seen that the ellipse is a good approximation to a section of the true error surface.

The importance of correct weighting should be emphasized. Theoretically  $w_i = 1/\sigma_i^2$  where  $\sigma_i$  is the standard deviation of  $k_i$ . If the linearized problem is solved using  $F' = \sum w'_i (\ln k_i - \ln A - B/T_i)^2$ , then  $w'_i = w_i/k_i^2$  should be applied. Inappropriate weighting can result in not only the overestimation of uncertainties, but also biased estimated mean values, as can be seen from Table 1, where the results of 20 simulated

fittings are summarized: Table 1

Parameter	True value	Average value obtained in fitting with	
		correct weighting	incorrect weighting
A	$2 \cdot 10^{-10}$	$2,0062 \cdot 10^{-10}$	$2,3328 \cdot 10^{-10}$
B	-620	-620,05	-671,52

## 2. Three-parameter problem using the equation $k=A \cdot T^n \cdot \exp(B/T)$

Due to the presence of a third parameter (n), the correlation between the parameters is even more pronounced. Therefore, a physically meaningful estimation of all three parameters is impossible.<sup>2</sup> Our work was aimed to show how the errors of measurement can influence the calculated parameters. Using simulated measurements with known errors, we will present data sets in which the calculated parameters hardly resemble the input values. In one set where the rate coefficients were calculated exactly (i.e. contained no error), but one  $k_i$  had an error of 1%, the calculated A factor deviated 50% from its true value. All these simulations indicated that the error of measurement has a detrimental effect on the determination of the parameter value. Nevertheless, if the aim of the fitting is to interpolate or extrapolate the rate coefficient value, the three-parameter fitting is the best possible solution, provided that the uncertainty of the estimated rate coefficient is given in accordance with Eq. (2-4) applied for the three parameter case.

For the estimation of activation parameters A and B the value of "n" should be constrained on the basis of theoretical considerations, and this is followed by a two-parameter fitting.

1. R. J. CVETANOVIC; D. L. SINGLETON; G. PARASKOVOPOULOS: J. Phys. Chem. 83, 50 (1979)

2. K.-M. JIANG; K.-J. HSU; J. B. JEFFRIES; F. KAUFMAN: J. Phys. Chem. 88, 1222 (1984)

3. J. C. LOPEZ; S. C. MARCH; F. C. GARCIA: Ingeneria Quimica (Madrid) 13, 147 (1981)

4. D. M. HINCHMAN: Process Analysis by Statistical Methods, Chapter 6.

176-200 pp. John Wiley & Sons, Inc. New York. 1970

The National Bureau of Standards Chemical Kinetics Data Base

John T. Herron and Robert J. Cvetanovic

Chemical Kinetics Division

National Bureau of Standards, Gaithersburg, Maryland, 20874 USA

The need for large scale chemical kinetic data bases for use in computer simulation studies of complex chemical phenomena such as combustion, atmospheric chemistry and plasma chemistry has focussed attention on the mechanics of developing such data bases as well as the more general problem of data evaluation. At NBS we have been working on the development of a data base for gas phase chemical reactions. The initial area of application is combustion chemistry, but the goal is to provide coverage for the whole range of gas phase reactions.

A data base starts with the identification and acquisition of relevant articles from the archival literature followed by the abstracting and entry of numerical data into the data base. The design of the data base management system is a crucial element in the effectiveness of the system. The NBS data base management system uses five functionally and logically interrelated data bases to handle chemical kinetic data:

DB CHEM (dictionary of chemical species) identifies reactant or product chemical species through the use of unique identifiers. Each species is assigned a CHEM Access Number, and is described by the Chemical Abstracts Service chemical name and registration number, common synonyms, molecular formula in a standard order of

arrangement, and an assigned isomer index number.

DB RDIC (dictionary of chemical reactions) identifies chemical reactions through the use of search codes automatically generated from CHEM Access Numbers. Each reaction is assigned an RDIC Access Number.

DB KDAT (kinetic data) contains the values of kinetic parameters for individual reactions identified by their RDIC Access Numbers.

DB BIBB (bibliography) contains the bibliographic citations to the data and can be searched by author, year, journal, etc.

DB JRNS (chemical journals) contains information on the standard abbreviations used for journals.

These five data bases are supported by various application programs to allow easy searching and updating of the numerical data base. Searching strategies can be based on chemical species, classes of reactant or product species, or kind of data (experimental, theoretical, etc.).

A primary objective of the data base design is to allow flexibility in output format based on a simple input format procedure. Table 1 is an example of an output formatted data sheet which accurately reflects the input format.

The data evaluation activities of the Chemical Kinetics Data Center are concerned primarily with the general area of combustion chemistry. Because of the wide range of temperature and pressure encountered in combustion systems, evaluation requires not only an examination of the validity of reported data, but also the use of a theoretical framework for fitting and extrapolating the data. Examples of data evaluation in the form

or data sheets for individual reactions in the methane oxidation system will be shown (Tsang and Hampson, 1986).

Table 1. Example of Input Data Format

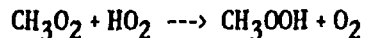
Reaction, Reference Code and Notes	Ph- Data ase type	Temp.	k, k/k(ref), A, A/A(ref)	n	B, B-B(ref)	k, A k err. units factor
<b>OH + O → H + O<sub>2</sub></b>						
<i>Hydroxyl + Oxygen atom</i>						
83 BRU/SCH2 Reaction of OH radicals with O atom in a fast-flow reactor. Laser-magnetic resonance. Resonance-fluorescence. Resonance-absorption. P = 1-5 Torr. (He, or Ar)	G EX	298	(1.87±0.30)(13)	-	-	2
83 TEM Reaction of Hydroxyl radicals with O atoms by Far-Infrared Laser-Magnetic-Resonance Spectrometry.	G EX	296	(4.0±1.2)(13)	-	-	2
<b>OH + HO<sub>2</sub> → H<sub>2</sub>O + O<sub>2</sub></b>						
<i>Hydroxyl + Hydroperoxo</i>						
83 SCH Reaction of OH with HO <sub>2</sub> in a fast-flow reactor. Laser-magnetic resonance. Resonance-fluorescence. Resonance-absorption. P = 1-5 Torr. (He, or Ar)	G EX	298	(4.46±0.12)(13)	-	-	2
83 TEM Reaction of Hydroxyl radicals with Hydroperoxo radicals by Far-Infrared Laser-Magnetic-Resonance Spectrometry.	G EX	296	(4.0±1.2)(13)	-	-	2
<b>OH + H<sub>2</sub>O<sub>2</sub> → HO<sub>2</sub> + H<sub>2</sub>O</b>						
<i>Hydroxyl + Hydrogen peroxide</i>						
83 LAM/HOL 1)	G EX	241-413	(4.22±1.20)( 4)	2.5	-838±86	2
83 LAM/HOL 2)	G EX	294	(1.08±0.18)(12)	-	-	2
1) Reaction of OH with H <sub>2</sub> O <sub>2</sub> in a Pyrex reaction cell. Flash-photolysis. Resonance-fluorescence. OH radicals generated by Flash-photolysis of H <sub>2</sub> O <sub>2</sub> or HONO <sub>2</sub> . Curved Arrhenius plot. P(H <sub>2</sub> O <sub>2</sub> ) = 0.7-1.2 Torr. P(HONO <sub>2</sub> ) = 5-10 Torr. P(He) = 760 Torr.						
83 TEM Reaction of Hydroxyl radicals with Hydrogen peroxide by Far-Infrared Laser-Magnetic-Resonance Spectrometry.	G EX	296	(1.0±0.2)(12)	-	-	2

## SPECTROSCOPY OF HO<sub>2</sub> AND CH<sub>3</sub>O<sub>2</sub> RADICALS AND THE KINETICS OF THEIR MUTUAL REACTION

K. McADAM, H. FORGES, and B. VEYRET  
LABORATOIRE DE CHIMIE PHYSIQUE A  
UNIVERSITE DE BORDEAUX I  
33405, TALENCE, CEDEX, FRANCE

### INTRODUCTION:

The reactions of peroxy radicals play an important role in atmospheric and combustion chemistry. For example, the competition between NO and HO<sub>2</sub> for methyl peroxy radicals is known to be one of the most important factors determining the rate of production of ozone in the troposphere. While there have been many kinetic studies of the reactions of these radicals, in particular the self-reactions of CH<sub>3</sub>O<sub>2</sub> and HO<sub>2</sub> radicals<sup>1</sup>, there is a need for another direct determination of the rate constant for the cross reaction:



The only direct study, by Cox and Tyndall<sup>2</sup>, revealed a reaction with a large negative temperature coefficient, similar to that of the HO<sub>2</sub> + HO<sub>2</sub> reaction, and a room temperature rate constant of  $6.0 \times 10^{-12} \text{ cm}^3 \text{ molecules}^{-1} \text{ s}^{-1}$  at 760 Torr pressure. However, recent work by Moortgat et al.<sup>3</sup>, and the product analysis results of Kan et al.<sup>4</sup>, produced values of  $3.7 \times 10^{-12}$  and  $1.3 \times 10^{-12} \text{ cm}^3 \text{ molecules}^{-1} \text{ s}^{-1}$  respectively. In view of the importance of this reaction and of this disagreement, we have started a detailed study of this reaction.

### EXPERIMENTAL:

All experiments have been carried out using our flash photolysis-U.V. absorption apparatus. Reactant gas mixtures flow through a thermostated Pyrex reaction cell. HO<sub>2</sub> and CH<sub>3</sub>O<sub>2</sub> radicals are produced by competition between CH<sub>3</sub>OH and CH<sub>4</sub>, respectively, for the Cl atoms generated by flashing Cl<sub>2</sub> / CH<sub>3</sub>OH / CH<sub>4</sub> / O<sub>2</sub> / N<sub>2</sub> mixtures. The analysing beam (from a D<sub>2</sub> lamp) passes through the cell, via quartz windows, and impinges onto a monochromator. The signal from the photomultiplier is fed through a transient recorder to a microcomputer for accumulation and subsequent analysis by computer simulations.

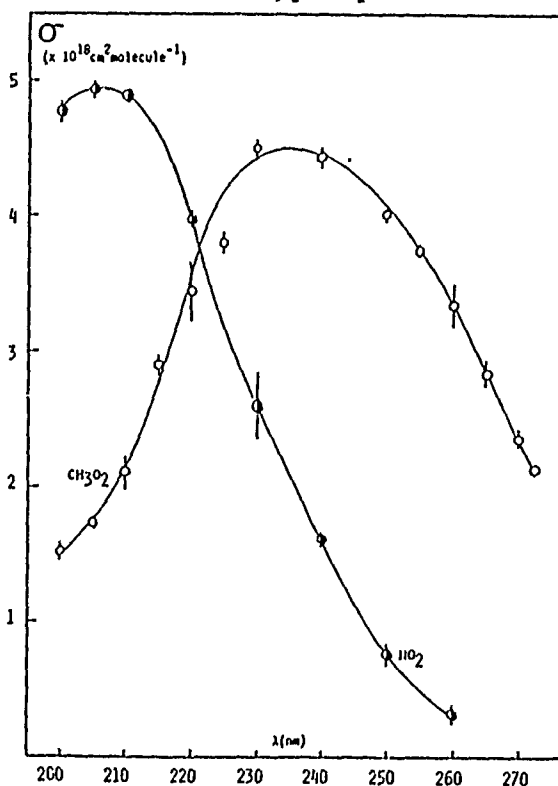


**RESULTS:**

There have been a number of studies of the U.V. spectra of the two radicals. While there is good agreement on the shape and magnitude of the  $\text{HO}_2$  spectrum, there is some uncertainty over the magnitude of the  $\text{CH}_3\text{O}_2$  spectrum<sup>5</sup>. For example, at 250nm the values available for  $\sigma$  range from  $2.5$  to  $5.0 \times 10^{-18} \text{ cm}^2 \text{ molecule}^{-1}$ . We therefore started our study by determining the spectra of  $\text{HO}_2$  and  $\text{CH}_3\text{O}_2$  over the wavelength range 200 - 270 nm.

By using the same conditions of flash intensity and  $\text{Cl}_2$  concentration, for each of the radical sources, we were able to obtain spectra for the two radicals ( fig.1 ), with an absolute measurement of their relative cross-sections. The  $\sigma$ -axis scale was obtained by normalising our value at 210nm for  $\text{HO}_2$  to the value given in the latest NASA report<sup>1</sup>.

FIG. 1 : U.V. SPECTRA OF  $\text{CH}_3\text{O}_2$  AND  $\text{HO}_2$ .



Separate studies of the  $\text{CH}_3\text{O}_2 + \text{CH}_3\text{O}_2$  and  $\text{HO}_2 + \text{HO}_2$  reactions gave rate constants consistent with the results of previous workers. Analysis of results from the  $\text{CH}_3\text{O}_2 + \text{HO}_2$  reaction reveal that the reaction has a

pressure dependant component ( fig.2 ). Our present values, between 100 and 600 torr, lead to a preliminary expression for the rate constant, at 298K, of

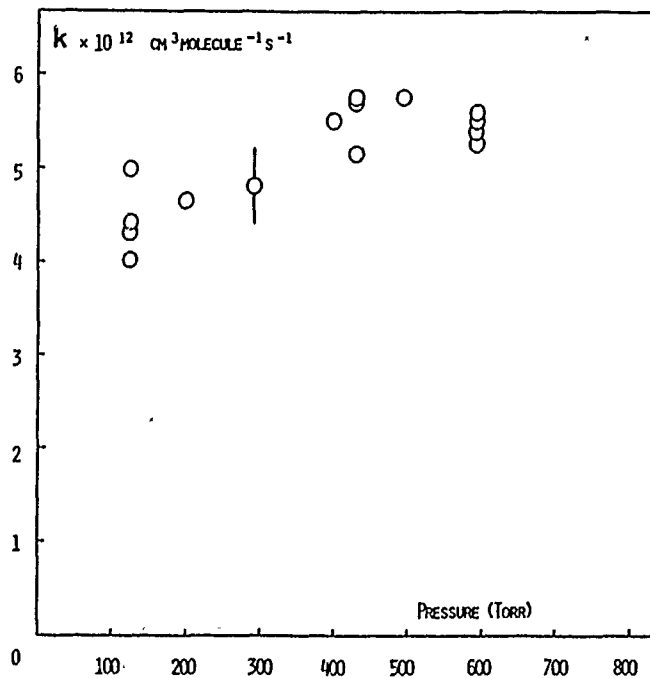
$$k = 4.3 \times 10^{-12} + 6.7 \times 10^{-32} \times [M] \text{ cm}^3 \text{ molecule}^{-1} \text{ s}^{-1},$$

although the value from 400 Torr up to atmospheric pressure appears to be constant at  $(5.5 \pm 0.5) \times 10^{-12} \text{ cm}^3 \text{ molecule}^{-1} \text{ s}^{-1}$ , in agreement with the value of Cox and Tyndall. Further experiments are currently underway to provide more information about the temperature and water vapour dependencies of this reaction.

### References

1. DeMore et. al., Evaluation No.7 of the NASA Panel for Data Evaluation. JPL Publication 85-37 ( 1985 ).
2. R.A. Cox and G.S. Tyndall, 1980, J. Chem. Soc., Faraday Trans. II, 76 p.153.
3. Moortgat et al. This meeting.
4. Kan et. al., 1980, J. Phys. Chem., 84 p. 3411.
5. S.P. Sander and R.T. Watson, 1981, J. Phys. Chem., 85, p. 2964.

FIGURE 2: VARIATION OF k WITH TOTAL PRESSURE



THE KINETICS OF HYDROXYL RADICAL REACTIONS WITH ALKANES  
STUDIED UNDER ATMOSPHERIC CONDITIONS

S J HARRIS and J A KERR

Department of Chemistry  
University of Birmingham  
Birmingham B15 2TT  
ENGLAND

ABSTRACT

A photolytic flow system has been constructed to study the reactions of hydroxyl radicals under tropospheric conditions (synthetic air mixture at atmospheric pressure) and over a range of atmospherically relevant temperatures (-30 to +50°C). The hydroxyl radicals were generated from the photolysis of methyl nitrite in the presence of added nitric oxide and they have been reacted with pairs of alkanes. The relative rates of the two hydroxyl-alkane reactions were monitored by following the rates of decay of the alkanes.

These reactions have been studied to provide additional data on the temperature coefficients of OH + alkane reactions, which will enable the development of more sophisticated bond additivity schemes for the rate constants of these reactions, which are needed in computer modelling of tropospheric systems.

RATE CONSTANT AND MECHANISM OF THE REACTION OH+HCOOH

G.S. Jolly, D.J. McKenney, D.L. Singleton, G. Paraskevopoulos  
and A.R. Bossard, Division of Chemistry, National Research  
Council of Canada, Ottawa, Canada, K1A 0R9.

Formic acid consisting of mixtures of monomer and dimer was photolysed at 222 nm using a pulsed KrCl excimer laser. The monomer yields OH with a quantum yield  $\phi(\text{OH})=1.00\pm0.08$ , whereas the dimer does not yield OH. This indicates that the dominant, if not the only, path of photolysis of the monomer is,



The kinetics of the subsequent reaction of OH with the monomer and dimer of formic acid was studied at 296K by following the pseudo-first-order decay of OH,  $[\text{HCOOH}] \gg [\text{OH}]$ , by time resolved resonance absorption at 308.2 nm. Pseudo-first-order rate constants,  $k_1$ , were obtained for a range of formic acid pressures from the slopes of linear plots of  $\ln([\text{OH}]/[\text{OH}]_0)$  against time. The apparatus and technique have been described before.<sup>1</sup>

A plot of  $k_1$  against the concentration of formic acid, [monomer+dimer], is shown in figure 1, and is clearly non linear, indicative of different rates of reaction of the monomer and dimer of formic acid with OH. The values of the second-order rate constants, for the reactions of OH with the monomer,  $k_2$ , and the dimer,  $k_3$ , were obtained by non-linear least squares fitting of equation I to the data in fig. 1.

$$k_1 = k_2[\text{monomer}] + k_3[\text{dimer}] \quad (\text{I})$$

where the concentrations of the monomer and dimer were calculated at each pressure of formic acid from the literature value of the equilibrium constant,  $K=(\text{HCOOH})^2/(\text{HCOOH})_2$ , taken at 296K as  $K=1.09 \times 10^{-7}$  mol/cm<sup>3</sup>. The resulting values in cm<sup>3</sup>/mol s at the 95% confidence intervals are:  $k_2=(2.95 \pm 0.07) \times 10^{11}$  and  $k_3=0 \pm 0.15 \times 10^{11}$ . Our value is in excellent agreement with the recent value of Wine *et al.*,<sup>2</sup>  $(2.78 \pm 0.47) \times 10^{11}$ , but is ~50% greater than the value of Zetzsch and Stuhl.<sup>3</sup> There was no significant concentration of dimer in both previous studies because of the very low pressures of formic acid.

Computer simulations of experiments with 0.5 torr of O<sub>2</sub> indicate that H-atoms are formed during the reaction in agreement with ref. 2. Our results and those of ref. 2, i.e., a) dimer much less reactive than monomer, b) rate constant essentially constant from 298 to 430K,<sup>2</sup> and c) little isotope effect for DCOOH,<sup>2</sup> are consistent with a complex mechanism in which H is preferentially abstracted from the OH rather than the CH bond of the acid, despite its being ~14 kcal/mol stronger. The resulting HCOO radical dissociates to H+CO<sub>2</sub>. A BEBO calculation indicates an activation energy of 1-2 kcal/mol less for abstraction from the OH bond compared to the CH bond. The lower activation energy may be attributed to reversible formation of a hydrogen bonded adduct between OH and formic acid, followed by transfer of the hydroxylic hydrogen in the adduct.

#### References

1. G.S. Jolly, G. Paraskevopoulos and D.L. Singleton, Chem. Phys. Letters 117, 132 (1985).

2. P.H. Wine, R.J. Astalos and R.L. Mauldin III, J. Phys. Chem. 89, 2660 (1985).
3. C. Zetzsch and F. Stuhl, "Physicochemical Behaviour of Atmospheric Pollutants".. Proceedings of the Second European Symposium; Reidel: Dordrecht, 1982, p. 129.

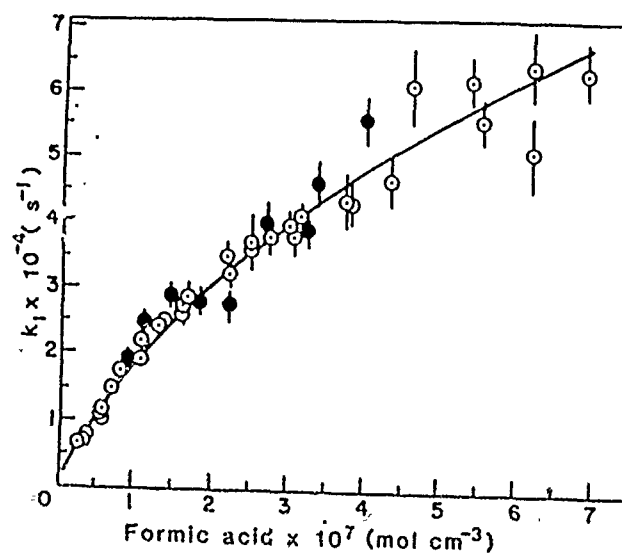


Fig. 1

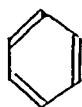
THE REACTIONS OF HYDROXYL RADICALS WITH AROMATIC COMPOUNDS

D.L.Baulch, I.M.Campbell and S.M.Saunders

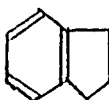
Department of Physical Chemistry, University of Leeds, U.K.

Rate constants for the gas phase reactions of the hydroxyl radical with aromatic hydrocarbons are of fundamental importance for modelling the chemistry of polluted urban atmospheres, combustion processes, and soot formation.

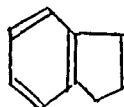
In the present study rate constants for the reaction of OH with benzene (I), indane (II) and indene (III) were measured at 295K and over the pressure range 0.30 - 4.76 Torr.



I



II



III

Experimental

A conventional fast-flow discharge system was used. OH was generated by the fast reaction of H atoms with NO, and changes in OH concentration were monitored by resonance fluorescence using microwave-powered discharge lamps. Helium was used as the carrier gas.

All of the reactions were studied under pseudo-first order conditions. Concentrations of OH were in the range  $1.1 \times 10^{-10}$  -  $2.5 \times 10^{-9}$  mol dm<sup>-3</sup> and of the aromatic compounds in the range  $1 \times 10^{-9}$  -  $6 \times 10^{-7}$  mol dm<sup>-3</sup>. The possible effects of potential competing reactions of radicals produced in the reaction were checked by computer simulation. Values of the pseudo-first order rate constant,  $k'$ , were obtained from the temporal decays of [OH]. Plots of  $k'$  versus [Aromatic] were linear, the slope yielding the second order rate constant, and all gave intercepts,  $k_w$ , which agreed with the independently measured values of the wall decay constant.

Results and Discussion

The measured values of the second order rate constant are shown in Table 1.

Compound	<u>Table 1</u>	
	$10^{-8} \text{ k/dm}^3 \text{ mol}^{-1} \text{ s}^{-1}$	Pressure/Torr.
Benzene	0.321 $\pm$ 0.027	0.45
	0.879 $\pm$ 0.045	1.17
	2.18 $\pm$ 0.27	2.91
	3.13 $\pm$ 0.18	4.76
Indane	54.4 $\pm$ 8.0	0.3
	56.9 $\pm$ 8.4	1.2
Indene	68.4 $\pm$ 10.0	0.24
	99.4 $\pm$ 11.5	0.42
	207.0 $\pm$ 30.0	1.14
	307.0 $\pm$ 46.0	1.81

Benzene

The rate constant for reaction with benzene is pressure dependent as would be expected if the reaction involves primarily addition to the ring followed by decomposition or collisional stabilization of the adduct. The dependence on pressure is linear within experimental error over the range studied and linear extrapolation to zero benzene concentration yields only a very small intercept on the ordinate suggesting little, if any, contribution from abstraction pathways.

The values of  $k$  obtained are significantly lower (factor of 1.5-2.0) than obtained in the only other comparable work by others overlapping the pressure range studied here. In that work, by flash photolysis, the bath gas used was argon and the work did not extend to as low a pressure as the present study.



When unimolecular reaction rate theory is applied to the present results together with those obtained by others at high pressures the outcome suggests that the high pressure limiting value for  $k$  is larger than hitherto suggested and at the highest pressures used (600 Torr.) the reaction is still far from its high pressure limit.

#### Indane

The reaction with indane was studied at only two pressures but the constancy of  $k$  over this range suggests that the reaction mechanism involves hydrogen abstraction from the five membered ring rather than addition. The high value of  $k$  is comparable with values for abstraction from other polycyclic compounds.

#### Indene

The results for indene also show a pressure dependent  $k$ . If plots of  $k$  versus [Indene] are extrapolated linearly to zero indene concentration a substantial intercept is obtained suggesting that both pressure dependent and pressure independent pathways are operative corresponding to addition and abstraction. However such an interpretation can only be tentative since the existing data are too sparse to be sure that a linear interpretation is valid.

The high values of  $k$  obtained for the pressure dependent pathway suggest that addition is occurring at the double bond in the five membered ring which is behaving as an olefin rather than part of the aromatic system.

MEASUREMENT OF THE RATE CONSTANT OF THE REACTION  $\text{OH} + \text{H}_2\text{S} \rightarrow \text{PRODUCTS}$   
IN THE RANGE 243-473 K BY DISCHARGE FLOW LASER INDUCED FLUORESCENCE

P. DEVOLDER - C. LAFAGE - L.R. SOCHET

*Laboratoire de Cinétique et Chimie de la Combustion.*

*UA CNRS 876. Université des Sciences et Techniques de Lille.*

*59655 Villeneuve d'Ascq Cedex. France.*

The reaction 1,  $\text{OH} + \text{H}_2\text{S} \rightarrow \text{HS} + \text{H}_2\text{O}$  is an important step in the combustion process of fossil fuels and is believed to represent a major sink for  $\text{H}_2\text{S}$  in earth's atmosphere. In contradiction to older measurements, recent measurements of  $k_1$  suggested the existence of an unexpected minimum of the rate constant near room temperature, which is difficult to interpret on the basis of a simple abstraction mechanism. We have performed a new investigation of the reaction 1 in the range 243-473 K with the discharge flow technique associated with the sensitive detection of OH by laser induced fluorescence. Our results confirm the existence of a flat minimum of  $k_1$  in the range 263 - 296 K :  $k_1 = (30 \pm 8) \cdot 10^{-13} \text{ cm}^3\text{s}^{-1}$  with a slight increase towards larger temperatures.

## Reactions of OH Radicals with Reduced Sulphur Compounds

I. Barnes, V. Bastian and K.H. Becker

Physikalische Chemie/FB 9

Bergische Universität-Gesamthochschule Wuppertal

D 5600 Wuppertal 1

Presented here are results on the kinetics and products of the reactions of OH with a number of aliphatic thiols, aliphatic sulphides, dimethyl disulphide,  $\text{CH}_3\text{SSCH}_3$ , (DMS), dimethyl sulphoxide,  $(\text{CH}_3)_2\text{SO}$ , (DMSO), thiophenol and tetrahydrothiophene. The experiments were carried out in glass reaction chambers of different volumes at 1 atm total pressure and room temperature using either the photolysis of methyl nitrate ( $\text{CH}_3\text{ONO}$ ) in the presence of NO or  $\text{H}_2\text{O}_2$  as a  $\text{NO}_x$  free OH radical source. The competitive kinetics method was used to determine the OH rate constants and in situ long-path Fourier transform absorption spectroscopy (FTIR) was employed for the product analyses. Experimental details can be found elsewhere /1,2,3/.

Experiments performed in 1 atm air using the photolysis of  $\text{CH}_3\text{ONO}$  as the OH source led to erroneously high rate constants for all of the thiols and sulphides investigated with the exception of  $\text{H}_2\text{S}$  and DMS /4/. Recent work has shown that radical chains, possibly involving oxygenated  $\text{CH}_3\text{S}$  radicals, are responsible for the high rate constants and it has been concluded that kinetic studies by the relative method in the presence of nitric oxides will not yield reliable rate constants for the reaction of OH with thiols and sulphides /2/.

Because of the above difficulties the rate constants for the above mentioned reactions were determined in 1 atm  $\text{N}_2$  using the photolysis of  $\text{H}_2\text{O}_2$  as the OH source. The rate constants obtained using this method were in good agreement with the available literature values /5/. Table 1 lists the OH rate constants obtained for various sulphur compounds.

When the reactions of OH with the thiols were investigated in 1 atm air using  $\text{H}_2\text{O}_2$  as the OH source the rate constants were between 20-30% higher than the corresponding rate constants determined in  $\text{N}_2$ . Wine et al. /8/ failed to detect an  $\text{O}_2$  effect for these reactions and secondary chemistry involving  $\text{CH}_3\text{SO}_x$  is probably responsible for the effect observed here. For DMS the rate constant rose from  $(4.4 \pm 0.4) \times 10^{-12} \text{ cm}^3/\text{s}$  in  $\text{N}_2$  to  $(8.0 \pm 0.5) \times 10^{-12} \text{ cm}^3/\text{s}$  in air. A small oxygen effect has been reported for the reaction of OH with DMS using an absolute method /6/.

However, in the present work it is not clear whether the observed increase is due to an oxygen effect as has been found for  $\text{OH} + \text{CS}_2$  /7/ or is caused by secondary chemistry.

Existing product analyses to date of the reaction of OH with thiols and sulphides have been carried out in the presence of relatively large concentrations of nitric oxides which are unrealistic and which could influence the product distributions of these reactions. Under these conditions  $\text{SO}_2$  (~30%) and methane sulphononic acid (~50%) were observed to be the major products for the reactions of OH with DMS, DMDS and  $\text{CH}_3\text{SH}$  /5,9/.

Preliminary product analyses have been carried out in this laboratory on the reaction of OH with DMS, DMSO and  $\text{CH}_3\text{SH}$  in  $\text{NO}_x$  free systems in air using the photolysis of  $\text{H}_2\text{O}_2$  as the OH source. For DMS the yield of  $\text{SO}_2$  was found to be as high as 70±10%. Dimethyl sulphone ( $\text{DMSO}_2$ ) was also formed, however its origin is not fully certain at present. It is formed partly in a dark reaction between DMS and  $\text{H}_2\text{O}_2$  but the observed concentration can not be explained solely by this source. DMSO was not observed but other products which were qualitatively identified included  $\text{HCOOH}$ ,  $\text{HCHO}$  and CO. After spectral stripping and an unidentified peak remained at  $1050\text{ cm}^{-1}$ . The reaction of OH with DMS yielded  $\text{DMSO}_2$  as the major product. For  $\text{CH}_3\text{SH}$  the yield of  $\text{SO}_2$  was 80% and other products included  $\text{HCOOH}$ ,  $\text{HCHO}$  and CO. As for OH + DMS an unidentified peak was observed at  $1050\text{ cm}^{-1}$ . From these results and the product formation observed during experiments on the photolysis of DMDS it can be concluded that  $\text{CH}_3\text{S}$  and its  $\text{O}_2$  adducts determine the product spectrum. In the presence of NO,  $\text{CH}_3\text{SO}$  is probably being formed leading subsequently to the formation of  $\text{CH}_3\text{SO}_3\text{H}$ .

#### References

- /1/ I. Barnes, V. Bastian, K.H. Becker, E.H. Fink and F. Zabel  
Atmos. Environ., 16(1982)545.
- /2/ I. Barnes, V. Bastian, K.H. Becker, E.H. Fink and W. Nelsen  
J. Atmos. Chem., (1986) in press.
- /3/ I. Barnes, V. Bastian, K.H. Becker, E.H. Fink, Th. Klein, V. Kriesche,  
W. Nelsen, A. Reimer and F. Zabel (1984)  
Untersuchung der Reaktionssysteme  $\text{NO}_x/\text{ClO}_x/\text{HO}_x$  unter troposphärischen  
und stratosphärischen Bedingungen, Gesellschaft für Strahlen- und  
Umweltforschung mbH, ISSN 0176/0777 BPT-Bericht 11/84.
- /4/ I. Barnes, V. Bastian, K.H. Becker and E.H. Fink (1984)  
Physico-Chemical Behaviour of Atmospheric Pollutants B. Versino, G.  
Angeletti, editors, D. Reidel Publ. Comp., Dordrecht, p149-157.

- /5/ J. Heicklen, Rev. Chem. Intermediates, 6(1985)175.  
 /6/ R. Atkinson, Chem. Rev. 85(1986)69.  
 /7/ I. Barnes, K.H. Becker, E.H. Fink, A. Reimer, F. Zabel, H. Niki  
 Int. J. Chem. Kinetics 15(1983)631.  
 /8/ P.H. Wine, R.J. Thompson and D.H. Semmes  
 Int. J. Chem. Kinetics, 16(1984)1623.  
 /9/ S. Hatakeyama and H. Akimoto, J. Phys. Chem., 87(1983)2387.

Table 1. Collected rate constants for the reactions of OH radicals with  $H_2S$ , aliphatic thiols and sulphides, DMS, DMSO, thiophenol and tetrahydrothiophene.

Reactant	Ref	Chamber Volume(l)	300 K	313 K
			$k(10^{-11} \text{ cm}^3/\text{s})$	$k(10^{-11} \text{ cm}^3/\text{s})$
$H_2S^*$	ethene	40	0.52±0.08	
$CH_3SH$	propene	20	3.6±0.4	3.3±0.4
$C_2H_5SH$	"	"	4.5±0.5	4.4±0.4
$n-C_3H_7SH$	"	"	5.3±0.6	5.0±0.7
$i-C_3H_7SH$	"	"	3.9±0.4	3.6±0.3
$n-C_4H_9SH$	"	"	5.6±0.4	5.4±0.5
$i-C_4H_9SH$	"	"	4.6±0.5	3.7±0.5
$sec-C_4H_9SH$	"	"	3.8±0.6	3.1±0.3
$tert-C_4H_9SH$	"	"	2.9±0.4	2.3±0.4
$C_5H_{11}SH$	"	"	5.2±0.3	4.2±0.5
(2-methyl-butanethiol) $C_6H_{13}SH^*$	n-hexane		1.1±0.2	-
$(CH_3)_2S$	ethene	420	0.44±0.04	-
$(C_2H_5)_2S$	"	"	1.1±0.2	-
$(C_3H_7)_2S$	"	"	1.9±0.2	-
$(CH_3)_2SO^*$	cis-butene	"	5.8±2.3	-
$CH_3SSCH_3$	trans-butene	"	21 ±2	-

\*)  $H_2S$ , thiophenol and DMSO were measured in 1 atm air using the photolysis of  $CH_3ONO$  as the OH source and the remainder were measured in 1 atm  $N_2$  using the photolysis of  $H_2O_2$  as the OH source.

REACTIONS OF HYDROXYL RADICALS WITH SULPHUR CONTAINING COMPOUNDS

P Pagsberg and O J Nielsen

Risø National Laboratory, Denmark

J Treacy, L Nelson and H Sidebottom

University College Dublin, Ireland

Biogenic and anthropogenic emissions of sulphur compounds are thought to be about equal. In order that the contribution of anthropogenic emissions to acid deposition can be precisely defined it is clear that an understanding of the natural sulphur cycle is desirable. Reduced sulphur compounds such as  $\text{H}_2\text{S}$ ,  $\text{CS}_2$ ,  $\text{CH}_3\text{SCH}_3$  and  $\text{CH}_3\text{SSCH}_3$  are considered to be the most important biogenic sources of sulphur in the troposphere. These compounds are thought to be oxidized by homogeneous reactions involving hydroxyl radical initiated processes, however detailed reaction mechanisms remain obscure. Numerous experimental studies have been reported concerning the kinetics of these reactions, however, there is often conflict between rate constant data determined using absolute methods at low pressure and relative techniques under simulated atmospheric conditions.

The reaction of hydroxyl radicals with a number of reduced sulphur containing compounds have been studied using both a relative rate method and by a pulsed radiolysis-kinetic spectroscopy technique. In the relative rate measurements hydroxyl radicals were generated either by the photolysis of nitrous acid or methyl nitrite in synthetic air,

The decay of the sulphur compounds was measured relative to a reference hydrocarbon and the rate constant derived from the integrated rate equation.  $\ln [S]_0/[S]_t = k_S/k_R \ln [R]_0/[RH]_t$ . It was evident from the results that in all the runs the concentration time data plotted in the form of the above equation showed significant curvature. Also the measured rate of reaction of HO with alkyl sulphides was found to increase with increases in the concentration of added NO. Product analysis studies showed that, apart from HO radicals, a reaction product is involved in the removal of sulphides in static photolysis systems involving  $NO_x$  species. It would appear, therefore, that rate data obtained from the relative rate method using either nitrous acid or methyl nitrite as the hydroxyl radical source are unreliable.

Absolute rate constant data for the reaction of HO radicals with a range of reduced sulphur compounds have been determined at atmospheric pressure. Hydroxyl radicals were produced by pulse radiolysis of water vapour-argon mixtures and the decay rate monitored by transient light absorption at 309 nm. Under the experimental conditions used,  $[S]_0 \gg [HO]_0$ , the hydroxyl concentration followed a simple exponential decay over at least three half-lives. Rate constant data obtained for a series of alkyl sulphides can be rationalized in terms of a mechanism involving hydrogen abstraction.

RATE CONSTANTS FOR THE REACTIONS OF OD WITH DNO<sub>3</sub> AND NO<sub>2</sub>

A.R. Bossard, D.L. Singleton and G. Paraskevopoulos, Division of Chemistry, National Research Council of Canada, Ottawa, Canada, K1A 0R9.

Absolute rate constants for the reactions of OD radicals with DNO<sub>3</sub> and NO<sub>2</sub> have been measured at 297K and over a range of pressures of SF<sub>6</sub>. OD radicals were generated by pulsed laser photolysis of DNO<sub>3</sub> at 222 nm (KrCl excimer laser) and their decay was followed by time resolved resonance absorption at 307.6 nm. Pseudo-first-order rate constants,  $k_1$ , for [DNO<sub>3</sub>] or [NO<sub>2</sub>] >> [OD], were calculated from the slopes of linear plots of  $\ln([OH]/[OH]_0)$  against time. Second-order rate constants,  $k_2$ , were calculated from the values of  $k_1$ , obtained over a range of reactant concentrations. The concentration of DNO<sub>3</sub> was measured in the cell either manometrically (when alone), or spectrophotometrically at 210 nm (in mixtures with SF<sub>6</sub>). NO<sub>2</sub>, which was always present (0.05 to 0.15%), or was added in the rate measurements of OD+NO<sub>2</sub> (2 to 3%), was also measured in the cell spectrophotometrically at 405 nm. The apparatus, technique and treatment of the data have been described before.<sup>1</sup>

OD+DNO<sub>3</sub>. Rate constants were measured over a range of pressures (1.2 to 30 torr) of DNO<sub>3</sub> alone, and in the presence of 107 torr SF<sub>6</sub>. The values were corrected for the contribution to the rate constant of the reaction OD+NO<sub>2</sub>+M. The corrections ranged from 5 to 25% of the measured rates at low pressures and from 28 to



43% at 107 torr of  $\text{SF}_6$ . The corrected values in  $\text{cm}^3/\text{mol s}$  were:  $k(1.2-30 \text{ torr}) = (5.67 \pm 0.75) \times 10^9$ , and  $k(107 \text{ torr}) = (8.58 \pm 0.75) \times 10^9$  where the indicated uncertainties are the 95% confidence intervals. However, because the reaction is slow, small values of  $k_1$  requiring large corrections were measured for the available pressure range of  $\text{DNO}_3$ . Therefore, confirmation of our values by different techniques should be useful.

The present results show a marked pressure effect (51% increase for 107 torr  $\text{SF}_6$ ), in contrast to the reaction with  $\text{HNO}_3$  for which 600 torr of  $\text{SF}_6$  increased the rate constant by  $\leq 10\%$  at room temperature.<sup>1</sup> This indicates that the reaction proceeds through an excited intermediate and is in line with the prediction, by Lamb et al,<sup>2</sup> of a weak pressure dependence for  $\text{OH} + \text{HNO}_3$  and a larger one for  $\text{OD} + \text{DNO}_3$ . Combined with our value of the rate constant of the reaction  $\text{OH} + \text{HNO}_3$   $(7.57 \pm 0.64) \times 10^{10}$ ,<sup>1</sup> our results indicate a very large isotope effect for the reaction of hydroxyl radicals with nitric acid,  $k_H/k_D \sim 13$ .  $\text{OD} + \text{NO}_2 + \text{SF}_6$ . The rate constant of this reaction was needed in order to correct for its contribution to the reaction  $\text{OD} + \text{DNO}_3$  above. It was measured, for the first time, in the presence of 5 to 500 torr  $\text{SF}_6$ , by adding  $\text{NO}_2$  to  $\text{DNO}_3$  so that the reaction with  $\text{NO}_2$  dominates. The values obtained are in good agreement with those reported for the reaction  $\text{OH} + \text{HNO}_3$ , in the same pressure range of  $\text{SF}_6$ .<sup>3</sup> As expected there is no isotope effect for the addition reaction.

References

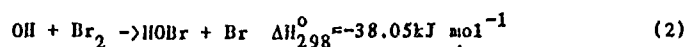
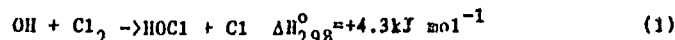
1. G.S. Jolly, G. Paraskevopoulos and D.L. Singleton, Chem. Phys. Letters 117, 132 (1985).
2. J.J. Lamb, M. Mozurkewich and S.W. Benson, J. Phys. Chem. 88, 6441 (1984).
3. a) C. Anastasi and I.W.M. Smith, J. Chem. Soc. Faraday II, 72, 1459 (1976);  
b) P.H. Wine, N.M. Kreutter and R. Ravishankara, J. Phys. Chem. 83, 3191 (1979).

THE KINETICS OF THE REACTIONS  
OF THE HYDROXYL RADICAL WITH  
MOLECULAR CHLORINE AND BROMINE.

Razmik B. Boodaghians, Ian W. Hall  
and Richard P. Wayne\*.

Physical Chemistry Laboratory, South Parks Road,  
Oxford, OX1 3QZ, England.

The rate constants for the reactions



have been measured over a range of temperatures between 253K and 333K by using a discharge flow resonance fluorescence technique.

The rate constant for the reaction of OH with  $\text{Cl}_2$  increases with temperature, and the results fit a simple Arrhenius expression. In contrast, no significant temperature dependence could be detected for the reaction of OH with  $\text{Br}_2$ .

Experimental.

In these investigations, the discharge flow method was used to generate H atoms which were reacted with excess  $\text{NO}_2$  to produce OH. The concentration of OH was kept below  $5 \times 10^{11}$  molecule  $\text{cm}^{-3}$  to minimise the effect of secondary reactions. Time resolution was achieved by adding the molecular halogens at different points in the flow tube via a sliding injector. The rate of reaction was determined by monitoring the pseudo first order decay of OH, using an EMI 9757B photomultiplier to observe the resonance fluorescence at 308 nm.

The walls of the Pyrex flow tube and the stainless steel fluorescence cell were coated with halocarbon wax to minimise wall losses of reactive species. With this coating, wall loss rates of OH were typically 5 to 10  $\text{s}^{-1}$ . Temperature regulation was achieved by circulating liquid from a thermostatically-controlled reservoir through the outer jacket of the flow tube.

Results.

At 293K, the rate constants for the reaction of OH with  $\text{Cl}_2$  and  $\text{Br}_2$  are

$$k_1 = (6.84 \pm 1.01) \times 10^{-14} \text{ cm}^3 \text{ molecule}^{-1} \text{ s}^{-1}$$

$$k_2 = (3.36 \pm 1.23) \times 10^{-11} \text{ cm}^3 \text{ molecule}^{-1} \text{ s}^{-1}$$

These results compare favourably with previously reported values in the literature [1]. The Arrhenius expression for the OH +  $\text{Cl}_2$  reaction between 253K and 333K is

$$k_1 = (1.68 \pm 1.22) \times 10^{-12} \exp[-(911 \pm 373)/T] \text{ cm}^3 \text{ molecule}^{-1} \text{ s}^{-1}.$$

For the reaction of OH with  $\text{Br}_2$ , the measured rate constants at various temperatures are

T/K	$k_2 / \text{cm}^3 \text{ molecule}^{-1} \text{ s}^{-1}$
262	$(2.05 \pm 1.18) \times 10^{-11}$
273	$(2.45 \pm 1.01) \times 10^{-11}$
293	$(3.36 \pm 1.23) \times 10^{-11}$
303	$(3.03 \pm 1.40) \times 10^{-11}$

As the table shows, the rate constants are much less dependent on temperature than are those for reaction (1), and the errors produced by least squares fitting are correspondingly large. One may regard reaction (2) as being temperature independent over the range 262K to 303K.

Discussion.

We believe these are the first reported studies of the temperature dependences of the title reactions. The Arrhenius parameters presented in this report permit us to investigate possible trends in reactivity between radicals and molecules that may shed light on the detailed mechanism of reaction, as well as offering predictive possibilities. Krech and McMadden [2] have found that the activation energy is inversely related to the polarizability of the co-reactant for several different series of radical reactions. We find evidence for such a relationship in the reactions of OH with the halogens [1]. We also find evidence for a correlation between radical-molecule reactivity and the

electron affinity of the radical partner [1], as previously suggested by Loewenstein and Anderson [3].

References

1. R.B. Boodaghians, I.W. Hall, and R.P. Wayne, To be published in J. Chem. Soc. Farad. Trans. 2
2. R.H. Krech and D.L. McFadden, J. Am. Chem. Soc., 99, 8402 (1977)
3. L.M. Loewenstein and J.G. Anderson, J. Phys. Chem., 88, 6277 (1984)

## REACTIONS OF OH RADICALS WITH ACETATES AND GLYCOLS

\*

D. Hartmann, D. Rhäsa, A. Gédra, and R. Zellner

Institut für Physikalische Chemie, Universität Göttingen,  
3400 Göttingen, Fed. Rep. of Germany

Rate constants for the reactions of hydroxyl radicals with (1) n-butyl-acetate, (2) 2-ethoxyethanol, (3) 2-butoxyethanol, and (4) 1-acetoxy-2-ethoxyethane over the temperature range  $T = 298 - 516$  K have been measured by a combined laser photolysis/resonance fluorescence (LPRF) technique. An excimer laser (EMG 100, Lambda Physik) was used as a monochromatic light source for the photolytic generation of OH from  $\text{HNO}_3$  at 193 nm (ArF). The detection of OH was by time resolved A - X resonance fluorescence excited by a microwave discharge of  $\text{H}_2\text{O}$  in Ar. All experiments were carried out under pseudo-first order kinetic conditions with the hydrocarbon concentration in excess over OH ( $> 10$ ). Second order rate coefficients were obtained from plots of  $k_{1st}$  vs. the reagent concentration. The results can be represented by the Arrhenius expressions:

$$k_1 (T) = (3.1 \pm 0.7) \cdot 10^{-11} \exp(-594 \pm 126/T) \text{ cm}^3 \text{ s}^{-1}$$

$$k_2 (T) = (1.8 \pm 0.4) \cdot 10^{-11} \exp(-120 \pm 30/T) \text{ cm}^3 \text{ s}^{-1}$$

$$k_3 (T) = (1.4 \pm 0.3) \cdot 10^{-11} \text{ cm}^3 \text{ s}^{-1}$$

$$k_4 (T) = (3.6 \pm 0.8) \cdot 10^{-12} \exp(383 \pm 80/T) \text{ cm}^3 \text{ s}^{-1}$$

The rate constants at 298 K have been compared with semi-empirical predictions based on individual C-H bond reactivities (Heicklen, a)) or characteristic group reactivities (Atkinson, b)). One of these predictive techniques is based on measured or estimated C-H bond dissociation energies and considers only the effects of substituent groups or atoms on

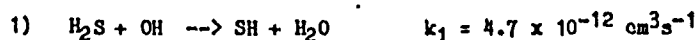
\* on leave from Central Research Institute for Chemistry,  
Budapest, Hungary

the  $\alpha$ -carbon (a), whereas the other technique is based on the estimation of  $\text{CH}_3-$ ,  $-\text{CH}_2-$ , and  $-\text{CH}=\text{}$  group rate constants and takes into account the effects of  $\beta$ -substituents (b). The difference between the predicted and observed rate coefficients is within about a factor of 2.5 and 1.5 for methods (a) and (b), respectively. It is found that the primary reaction is dominated in all cases by the H atom abstraction from the  $-\text{O}-\text{CH}_2-$  moiety (C-H bond dissociation energy =  $377 \text{ kJmol}^{-1}$ , except compound (1)). The subsequent route of atmospheric degradation is similar to the known atmospheric  $\text{CH}_4$  oxidation scheme. The atmospheric lifetime with respect to the reaction with OH radicals has been estimated to be about two days (2, 3, 4) and one week (1) for an average tropospheric OH concentration of  $10^6 \text{ cm}^{-3}$ .

KINETICS OF THE REACTIONS OF SH WITH NO<sub>2</sub> AND O<sub>2</sub>

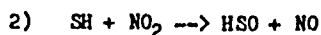
R. A. Stachnik and M. J. Molina  
 Jet Propulsion Laboratory, California Institute of Technology,  
 Pasadena, California, USA

Substantial effort has been directed in recent years toward understanding the chemistry of atmospheric sulphur compounds. H<sub>2</sub>S, a significant form of biogenic sulphur emission, is believed to be removed from the troposphere primarily by reaction with hydroxyl radical:

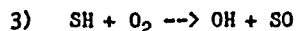


The atmospheric chemistry of the mercapto radical, SH, has been the subject of several recent kinetic and modelling studies; however, the details of the subsequent oxidation of this radical remain to be elucidated. This work examines the reactions of SH with NO<sub>2</sub> and O<sub>2</sub>.

Rate constant values for the reaction



reported by Black<sup>(1)</sup> [ $k_2 = (3.5 \pm 0.4) \times 10^{-11} \text{ cm}^3\text{s}^{-1}$ ] and by Friedl et al.<sup>(2)</sup> [ $k_2 = (3.0 \pm 0.8) \times 10^{-11} \text{ cm}^3\text{s}^{-1}$ ] differ substantially from the determination by Howard<sup>(3)</sup> ( $k_2 = 6.7 \times 10^{-11} \text{ cm}^3\text{s}^{-1}$ ). The reaction



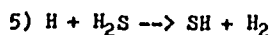
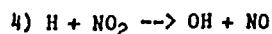
has not been observed. Upper limits for the rate constant imposed by Ties et al.<sup>(4)</sup> ( $k_3 < 3.2 \times 10^{-15} \text{ cm}^3\text{s}^{-1}$ ), Black<sup>(1)</sup> ( $k_3 < 4 \times 10^{-17} \text{ cm}^3\text{s}^{-1}$ ), and Friedl et al.<sup>(2)</sup> ( $k_3 < 1 \times 10^{-17} \text{ cm}^3\text{s}^{-1}$ ) do not eliminate reaction 3 as a significant removal process for tropospheric SH.

SH radicals were generated in this study by photodissociation of H<sub>2</sub>S with pulsed ArF excimer laser emission at 193 nm. This process



produces SH radicals with negligible vibrational excitation. The subsequent decay of the initial SH concentration was measured by monitoring the transient absorption due to the  $\Lambda^2\Sigma^+(v'=0) \leftarrow X^2\Pi(v''=0)$  band near 324 nm.

The rate constant for the reaction of SH with  $\text{NO}_2$  was determined by measuring the pseudo-first order decay rate,  $k^I$ , of SH ( $[\text{SH}]_0 = 4 \times 10^{12} \text{ cm}^{-3}$ ) with  $\text{NO}_2$  present ( $[\text{NO}_2] = 0.3 - 4.0 \times 10^{14} \text{ cm}^{-3}$ ).  $\text{O}_2$  was added to sequester the H atom photofragment and, thereby, eliminate secondary generation of SH by the reactions:



Values of  $k_2^I$  were determined at 100 torr and 730 torr total pressure with  $\text{N}_2$  as the diluent gas at 298 K from plots of  $k^I$  versus  $[\text{NO}_2]$ . The result is  $k_2 = (4.8 \pm 1.0) \times 10^{-11} \text{ cm}^3 \text{ s}^{-1}$ , independent of total pressure.

A slow reaction between SH and  $\text{O}_2$ , reaction 3, followed by reaction 1 would be a zero net loss for SH since  $k_3[\text{O}_2] \ll k_1[\text{H}_2\text{S}]$ . Evidence for SH removal by reaction with  $\text{O}_2$  was distinguished from radical-radical and other second order chemistry by measuring the increase in decay rate upon addition of CO, which removes OH, over a range of initial SH concentration. An upper limit for  $k_3$  of  $4 \times 10^{-19} \text{ cm}^3 \text{ s}^{-1}$  was obtained upon extrapolation to zero initial SH concentration. This value is smaller by a factor of 25 than the previously reported bound.

The research described in this paper was carried out by the Jet Propulsion Laboratory, California Institute of Technology, under contract with the National Aeronautics and Space Administration.

References

- (1) G. Black, J. Chem. Phys. 1984, 80, 1103.
- (2) R. R. Friedl, W. H. Brune, and J. G. Anderson, J. Phys. Chem. 1985, 89, 5505
- (3) C. J. Howard, 17th International Symposium on Free Radicals, Granby, Colorado, USA, 1985
- (4) J. J. Tise, F. B. Wampler, R. C. Oldenberg, and W. W. Rice, Chem. Phys. Lett. 1981, 82, 80

## ABSTRACT

LASER-INDUCED FLUORESCENCE STUDIES OF THE  $\text{CH}_3\text{S}$  RADICALGraham Black and Leonard E. Jusinski

Chemical Physics Laboratory

SRI International

Menlo Park, CA 94025 USA

Alkyl thiyl radicals (RS) are intermediates in combustion and atmospheric chemistry of organosulfur compounds of both natural and anthropogenic origins. These compounds, although minor constituents, may play a role in the atmospheric sulfur cycle and contribute to the acid precipitation problem. It is, therefore, important to determine the atmospheric chemistry of these radicals.

Until recently, the only reported absolute rate coefficient studies involved the HS radical.<sup>1-3</sup> Recently, the emission and laser-induced fluorescence (LIF) spectra of  $\text{CH}_3\text{S}$  were reported.<sup>4,5</sup> This has led to the first measurements<sup>6</sup> of the rate coefficients for the reactions of  $\text{CH}_3\text{S}$  with  $\text{NO}$ ,  $\text{NO}_2$  and  $\text{O}_2$ . This paper reports further LIF studies of  $\text{CH}_3\text{S}$  and a study of its reaction with  $\text{O}_3$ .  $\text{CH}_3\text{S}$  radicals were generated by the 248 nm photodissociation of dimethyl disulfide [ $(\text{CH}_3)_2\text{S}_2$ ] and 193 nm photodissociation of methyl mercaptan ( $\text{CH}_3\text{SH}$ ). Fluorescence was excited on the  $\tilde{\text{A}}^2\text{A}_1 \sim \tilde{\text{X}}^2\text{E}$  transition using a Nd:Yag-pumped dye laser. The transitions excited were  $3_0^2$  at 366.0 nm,  $3_0^1$  at 371.3 nm and  $0_0^0$  at 377.0 nm. Vibrational relaxation and electronic quenching of the upper state have been studied and the results are summarized in Table I (estimated errors are  $\pm 10\%$  for  $v_3 = 2$  and 0 and  $\pm 20\%$  for  $v_3 = 1$ ).

Table 1

RATE COEFFICIENTS FOR REMOVING  $\text{CH}_3\text{S}(\tilde{\text{A}}^2\text{A}_1)$  in  $\nu_3 = 2, 1$  and 0

<u>Gas</u>	<u>Rate Coefficients (<math>\text{cm}^3\text{molec}^{-1}\text{s}^{-1}</math>)</u>		
	$\nu_3 = 2$	$\nu_3 = 1$	$\nu_3 = 0$
He	$7.6 \times 10^{-12}$	$2.0 \times 10^{-12}$	$<1 \times 10^{-13}$
Ar	$4.9 \times 10^{-12}$	$1.7 \times 10^{-12}$	$<1 \times 10^{-13}$
H <sub>2</sub>	$8.4 \times 10^{-11}$	$5.9 \times 10^{-11}$	$5.3 \times 10^{-11}$
N <sub>2</sub>	$2.3 \times 10^{-11}$	$1.3 \times 10^{-11}$	$6.9 \times 10^{-12}$
O <sub>2</sub>	$2.1 \times 10^{-11}$	$1.4 \times 10^{-11}$	$5.7 \times 10^{-12}$
CO <sub>2</sub>	$4.7 \times 10^{-11}$	$2.4 \times 10^{-11}$	$<1 \times 10^{-13}$
CH <sub>4</sub>	$8.2 \times 10^{-11}$	$4.7 \times 10^{-11}$	$2.1 \times 10^{-11}$
SF <sub>6</sub>	$2.3 \times 10^{-11}$	$1.0 \times 10^{-11}$	$<1 \times 10^{-13}$

For He, Ar, CO<sub>2</sub> and SF<sub>6</sub>, removal of  $\nu_3 = 2$  with these gases results in  $\nu_3 = 0$  emission confirming that only vibrational relaxation can occur with these gases. For H<sub>2</sub>, N<sub>2</sub>, O<sub>2</sub> and CH<sub>4</sub> vibrational relaxation and electronic quenching are both occurring.

By varying the delay between the excimer and dye laser pulses, it was also possible to measure a rate coefficient for vibrational relaxation into the ground state ( $\nu_3 = 0$ ) of CH<sub>3</sub>S. These results are summarized in Table 2 (estimated errors are  $\pm 10\%$ ).

Table 2

VIBRATIONAL RELAXATION INTO GROUND STATE ( $v_3'' = 0$ ) OF  $\text{CH}_3\text{S}$ 

<u>Gas</u>	<u>Rate Coefficient (<math>\text{cm}^3 \text{ molec}^{-1} \text{ s}^{-1}</math>)</u>
He	$2.3 \times 10^{-12}$
Ar	$2.9 \times 10^{-12}$
$\text{N}_2$	$5.3 \times 10^{-12}$
$\text{O}_2$	$9.7 \times 10^{-12}$
$\text{H}_2$	$2.2 \times 10^{-11}$
$\text{CO}_2$	$1.4 \times 10^{-11}$
$\text{CH}_4$	$1.8 \times 10^{-11}$
$\text{SF}_6$	$3.0 \times 10^{-11}$

Experiments were then performed to measure the rate coefficient for  $\text{CH}_3\text{S}$  reacting with several gases. Most of the experiments involved photodissociation of  $\text{CH}_3\text{SH}$  at 193 nm in a high pressure of  $\text{SF}_6$ . This avoided problems with  $\text{O}_3$  absorption at 248 nm. The  $3_0^2$  transition was pumped at 366.0 nm and  $0_0^0$  reemission was monitored at 449 nm ( $3_6^0$  transition). The time delay between the excimer and dye lasers was varied to determine the decay of the  $\text{CH}_3\text{S}$  radical. No reaction with either  $\text{O}_2$  or  $\text{O}_3$  could be found ( $k_{\text{O}_3} < 8 \times 10^{-14} \text{ cm}^3 \text{ molec}^{-1} \text{ s}^{-1}$ ) and the fast reaction<sup>6</sup> with  $\text{NO}_2$  was confirmed.

#### References

1. G. Black, J. Chem. Phys. 80, 1103 (1984)
2. G. Black, R. Patrick, L. E. Jusinski and T. G. Slanger, J. Chem. Phys. 80, 4065 (1984)
3. R. R. Friedl, W. H. Brune and J. G. Anderson, J. Phys. Chem. 89, 5505 (1985)
4. K. Ohbayashi, H. Akimoto and I. Tanaka, Chem. Phys. Lett. 52, 47 (1977)
5. M. Suzuki, G. Inoue and H. Akimoto, J. Chem. Phys. 81, 5405 (1984)
6. R. J. Balla, H. H. Nelson and J. R. McDonald, J. Phys. Chem. (to be published)

OXIDATION OF THE  $\text{H}_2\text{S}$  BY THE ATMOSPHERE COMPONENTS.

V.P.BULATOV, M.Z.KOZLINER, O.M.SARKISOV.

Institute of Chemical Physics, Academy of Sciences,  
Moscow, USSR.

Absorption spectra of  $\text{HSO}_2$  radicals were detected after flash photolysis of the mixtures of  $\text{H}_2\text{S} + \text{NO}_2$  and  $\text{H}_2\text{S} + \text{O}_2$ . Intracavity laser spectroscopy technique was used for  $\text{HSO}_2$  spectra observation.

It was deduced from kinetics of  $\text{HSO}_2$  in a system  $\text{H}_2\text{S}/\text{NO}_2$  that the formation and decay of  $\text{HSO}_2$  is due to the reactions (1) and (2) respectively:

$$\begin{aligned} (1) \text{SH} + \text{NO}_2 &\xrightarrow{k} \text{HSO}_2 + \text{NO} & k = (2.4 \pm 0.4) 10^{-11} \text{ cm}^3 \text{ s}^{-1}; \\ (2) \text{HSO}_2 + \text{NO}_2 &\xrightarrow{k} \text{SO}_2 + \text{HNO}_2 & k = (4 \pm 0.4) 10^{-12} \text{ cm}^3 \text{ s}^{-1}. \end{aligned}$$

The SH radicals were formed under flash photolysis of hydrogen sulphide. The reaction (3)  $\text{SH} + \text{HO}_2 \xrightarrow{k} \text{HSO}_2 + \text{OH}$  is assumed to be the most probable source of  $\text{HSO}_2$  for the  $\text{H}_2\text{S}/\text{O}_2$  system, with  $k = 4 \cdot 10^{-11} \text{ cm}^3 \text{ s}^{-1}$ .

The  $\text{HSO}_2$  radicals kinetics dependence on  $\text{NO}_2$ ,  $\text{O}_2$  and  $\text{CO}$  concentration for the  $\text{H}_2\text{S}/\text{NO}_2$  system was studied. The rate constants of the following reactions were measured:

$$\begin{aligned} &\text{HSO}_2 + \text{HSO}_2 \xrightarrow{k} \text{products}, & k = 3 \cdot 10^{-11} \text{ cm}^3 \text{ s}^{-1}; \\ \text{SH} + \text{NO}_2 + \text{M} &\xrightarrow{k} \text{HSNO}_2 + \text{M}, & k = 5.5 \cdot 10^{-13} \text{ cm}^3 \text{ s}^{-1} \text{ (at 13 torr)}; \\ \text{HSO}_2 + \text{NO}_2 &\xrightarrow{k} \text{HNO}_2 + \text{SO}_2, & k = (2.6 \pm 0.4) 10^{-14} \text{ cm}^3 \text{ s}^{-1}; \\ \text{HSO}_2 + \text{O}_2 &\xrightarrow{k} \text{SO}_2 + \text{OH}, & k = (1.7 \pm 0.4) 10^{-15} \text{ cm}^3 \text{ s}^{-1}; \\ \text{SH} + \text{CO} &\xrightarrow{k} \text{products}, & k < 5 \cdot 10^{-16} \text{ cm}^3 \text{ s}^{-1}; \\ \text{HSO}_2 + \text{CO} &\xrightarrow{k} \text{products}, & k < 2 \cdot 10^{-16} \text{ cm}^3 \text{ s}^{-1}. \end{aligned}$$

The rate constant of the reaction  $\text{SH} + \text{O} \xrightarrow{k} \text{HSO}_2 + \text{O}$  is estimated to be  $\approx 1.3 \cdot 10^{-14} \text{ cm}^3 \text{ s}^{-1}$ .

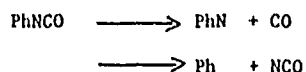
Basing on our results we suggest the following mechanism of  $\text{H}_2\text{S}$  transformation in the troposphere:

$$\text{H}_2\text{S} \xrightarrow{\text{OH}} \text{SH} \xrightarrow{\text{NO}_2} \text{HSO}_2 \xrightarrow{\text{O}_2} \text{SO}_2.$$

Relaxation and Reactions of NCO ( $\tilde{X}^2\Pi$ )

C.J. Astbury, G. Hancock and K.G. McKendrick  
Physical Chemistry Laboratory, Oxford University, Oxford, U.K.

The pulsed infrared multiple photon dissociation of phenyl isocyanate PhNCO, results in two dissociation channels :

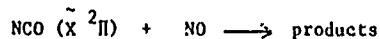


Both PhN and NCO radicals have been detected in their ground electronic states by laser induced fluorescence. For the NCO ( $\tilde{X}^2\Pi$ ) radical, this production and detection method can be used to study its removal rate constants, but before this can be done, the behaviour of any vibrationally excited states of the radical produced by IRMPD needs to be studied, as relaxation of these levels into the probed ground vibrational state will affect the overall removal rate measured. The time dependent behaviour of the first three bending vibrational levels,  $^2\Pi(00^1_0)$ ,  $^2\Delta(01^2_0)$  and  $^2\Phi(02^3_0)$  has been studied at a fixed total pressure of 5 Torr of He, Ne, Ar and Kr, with 5m Torr PhNCO precursor. Figure 1 shows the behaviour in Ar and Kr. The population of the lowest vibrational level,  $(00^1_0)$ , rises substantially after the termination of the infrared laser pulse ( $\sim 5\mu\text{s}$ ) : the higher levels show an initial increase and a significant decline, with the timescale becoming compressed and the extent of decline greater for successively higher levels. This behaviour suggests collisional relaxation of the nascent vibrational distribution in a cascade fashion proceeding towards a room temperature distribution. What however is clear is that the collisional processes are faster in Kr than in Ar (seen, for example, in the rates of decline of the signals for the vibrationally excited levels of Fig. 1) : from measurements in Ne and He the efficiencies of the relaxation processes were found to be in the order  $\text{Ne} < \text{He} \sim \text{Ar} < \text{Kr}$ . Numerical values were found from a simple model of the

relaxation processes, and fig. 1 shows the fits of this model to the data.

The relative rates of the processes with rare gases are not the same as those observed for vibrational relaxation of similar closed shell molecules, OCS and CO<sub>2</sub> [1], in which a monotonic decrease in quenching rate constant with mass of rare gas is seen, as predicted by theories of energy transfer controlled by short range repulsive forces. An electronically non-adiabatic mechanism, similar to that proposed for quenching of OH (X<sup>2</sup>Π) by Ar [2], may occur with the heavier rare gases, with the approaching atom splitting the degenerate vibronic state so that a curve crossing mechanism ensues, possibly induced by spin-orbit coupling and thus increasing in efficiency with mass of rare gas.

Vibrational relaxation of the nascent NCO species was found to be extremely rapid in the presence of N<sub>2</sub>O, the ν<sub>2</sub> frequency of which is almost resonant with that of NCO. Kinetic measurements of the removal rate of NCO with NO were carried out in the presence of 5 Torr N<sub>2</sub>O, and yielded straightforward kinetic behaviour. The rate constant at 298K for the process



was measured to be  $(3.4 \pm 0.3) \times 10^{-11} \text{ cm}^3 \text{ molecule}^{-1} \text{ s}^{-1}$ , agreeing well with a recent direct determination by Perry [3].

#### References

1. M.L. Mandrich & G.W. Flynn, J. Chem. Phys. 73 (1980) 3679;  
N.J.G. Smith, C.C. Davis & I.W.M. Smith, J. Chem. Phys. 80 (1984) 6122;  
F. Lepoutre, G. Louis & J. Taine, J. Chem. Phys. 70 (1979) 2225;  
S.L. Lunt, C.T. Wickham-Jones & C.J.S.M. Simpson, Chem. Phys. Letters  
115 (1985) 60.
2. Ch. Zuhrt, L. Zulicke & S. Ya. Umansky, Chem. Phys. Letters  
111 (1984) 408.
3. R.A. Perry, J. Chem. Phys. 82 (1985) 5485.



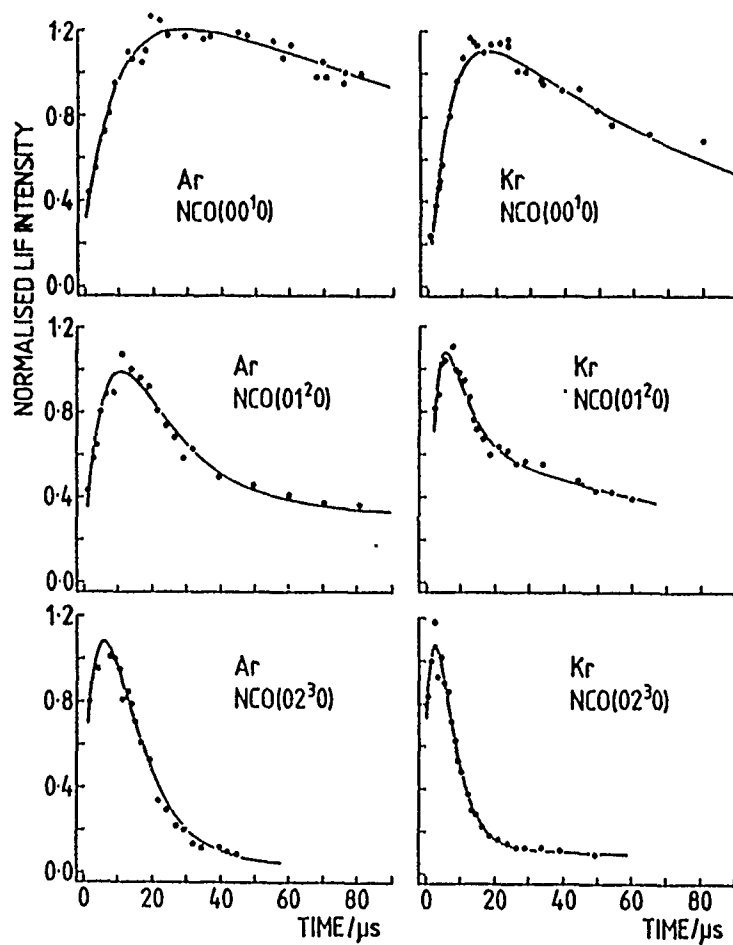


Fig. 1. Time dependences of the populations of the  $(00^1_0)$ ,  $(01^2_0)$  and  $(02^3_0)$  of NCO (X) in the presence of 5 Torr Ar and Kr. Open circles are experimental observations, full lines are predictions of a simple cascade relaxation model. The relaxation processes can be seen to be faster in Kr than in Ar.

KINETIC MEASUREMENTS OF THE NCO RADICAL REACTION WITH  
ETHENE OVER AN EXTENDED TEMPERATURE RANGE\*

Robert A. Perry

Combustion Research Facility  
Sandia National Laboratories  
Livermore, California 94550, USA

This paper describes current research that employs a laser photolysis/laser-induced fluorescence technique to measure absolute rate constants for reactions of NCO radicals with ethene. Few studies are presently available for the reaction of NCO with combustion species. Ethene is an interesting species to study because of both the major role it plays in combustion chemistry and its role as a model unsaturated hydrocarbon.

NCO radicals are produced using a fluorine, or ArF, excimer laser to photodissociate HNCO in a flowing gas mixture of HNCO:Ar:Reactant at total pressure (primarily argon) of 10-400 torr. An argon-ion-pumped ring dye laser operating with stilbene-3 dye at 416.8 nm (100 mW) is used to pump the  $A^2E(1,0,0) \leftarrow X^2\Pi(0,0,0)$  transition. The resulting fluorescence, measured at right angles to the crossed laser beams, is monitored at 438.5 nm (FWHM=8.0 nm).

Absolute rate constants for the reaction of NCO radicals with ethene were measured as a function of temperature and pressure. The rate in the high-pressure limit for the reaction of NCO with ethene was observed to decrease with increasing temperature with the best fit to the data (T=295-447 K) given by the following expression:

$$k = 3.0 \times 10^{-12} e^{(230 \pm 300)/RT} \text{ cm}^3 \text{ molecule}^{-1} \text{ s}^{-1}$$

At temperatures greater than 447 K a rapid reduction in the rate was observed, and was interpreted as a rapid decomposition of the adduct formed. Continuing experiments will address the reaction mechanism at temperatures greater than 650 K. I will discuss these measurements and their implications.

\*Research supported by Office of Basic Energy Sciences, U.S. Department of Energy.

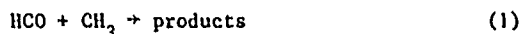
### Direct Rate Studies of HCO Radical Reactions

J.E. Baggott, H.M. Frey, P.D. Lightfoot and R. Walsh

Department of Chemistry, The University, Whiteknights, P.O. Box 224,  
Reading RG6 2AD, U.K.

#### 1. Introduction

The formyl radical is an important intermediate in the atmospheric chemistry of pollutants and in combustion systems. Numerous direct rate studies have been reported<sup>1,2</sup> and reliable rate constants are available for many of the more important HCO radical reactions. However, apart from HCO radical recombination, few radical-radical reactions involving HCO have been studied. We present here an investigation of the reaction



using a combination of 308 nm excimer laser flash photolysis of acetaldehyde and CW dye laser resonance absorption. Two conflicting values for the room-temperature rate constant of reaction (1) have been reported. Nadtochenko et al.<sup>3</sup> obtained the value  $(2.3 \pm 1.0) \times 10^{-10} \text{ cm}^3 \text{ molecule}^{-1} \text{ s}^{-1}$  for  $k_1$ , which should be contrasted with the value  $(4.4 \pm 1.6) \times 10^{-11} \text{ cm}^3 \text{ molecule}^{-1} \text{ s}^{-1}$  reported more recently by Mulenko.<sup>4</sup> Our preliminary results indicate a value for  $k_1$  between these extremes.

#### 2. Experimental

The experimental arrangement follows closely that used in recent direct rate studies by Langford and Moore,<sup>2</sup> with the exception that we used a different photolysis geometry. 308 nm radiation from a XeCl excimer laser passed through the sample cell at right angles to the dye laser beam which was multipassed (typically 48 passes giving a total path length of ca. 6 m). The dye laser radiation was tuned to the rotational band head of the  $(0,9^0_0) \leftarrow (0,0^1_0)$  band in the  $\tilde{A}-\tilde{X}$  system of HCO at 614.5 nm,<sup>5</sup> and its intensity was monitored by a fast photodiode. The production and subsequent decay of HCO from the flash photolysis of acetaldehyde was captured on a transient recorder and passed to a microcomputer for signal averaging. Fig. 1 gives an example of a decay trace obtained by averaging signals resulting from 100 excimer laser shots.

### 3. Results and Discussion

The decay of HCO radicals produced in the photolysis of acetaldehyde is determined by reaction (1) and the radical recombination reactions of HCO and of  $\text{CH}_3$ . The resulting decays cannot be integrated analytically. In order to extract values for  $k_1$  we have therefore combined numerical integration routines with non-linear least-squares fitting, requiring input values for the rate constants of both HCO and  $\text{CH}_3$  radical recombination appropriate to the conditions of temperature and pressure in our experiments. HCO radical recombination rate constants have been determined by Veyret et al.<sup>6</sup> and appear to be independent of both temperature and pressure. We have performed separate experiments using 308 nm photolysis of glyoxal to determine HCO radical recombination rates on our own apparatus. Our preliminary results are in good agreement with those of Veyret et al.<sup>6</sup> For methyl radical recombination, we have used the extensive data of Pilling and co-workers.<sup>7</sup>

Our analyses yield a value for  $k_1$  of  $1.0 \times 10^{-10} \text{ cm}^3 \text{ molecule}^{-1} \text{ s}^{-1}$ , which lies between the results of Nadtochenko et al. and Mulencko. We will present full details of our experimental techniques and the results for both HCO radical recombination and  $\text{HCO} + \text{CH}_3$  as a function of pressure.

### References

1. J.E. Baggott and M.J. Pilling, Ann. Rep. Chem. Soc. Sect. C, 80, 199 (1982).
2. A.O. Langford and C.B. Moore, J. Chem. Phys., 80, 4211 (1984).
3. V.A. Nadtochenko, O.M. Sarkisov and V.I. Vedenev, Izv. Akad. Nauk. SSSR, Ser. Khim., 3, 651 (1979).
4. S.A. Mulencko, Zh. Prikl. Spectrosk., 33, 35 (1980).
5. R. Vasudev and R.N. Zare, J. Chem. Phys., 76, 5267 (1982).
6. B. Veyret, P. Roussel and R. Esclaux, Chem. Phys. Lett., 103, 389 (1984).
7. M.T. Macpherson, M.J. Pilling and M.J.C. Smith, J. Phys. Chem., 89, 2268 (1985).

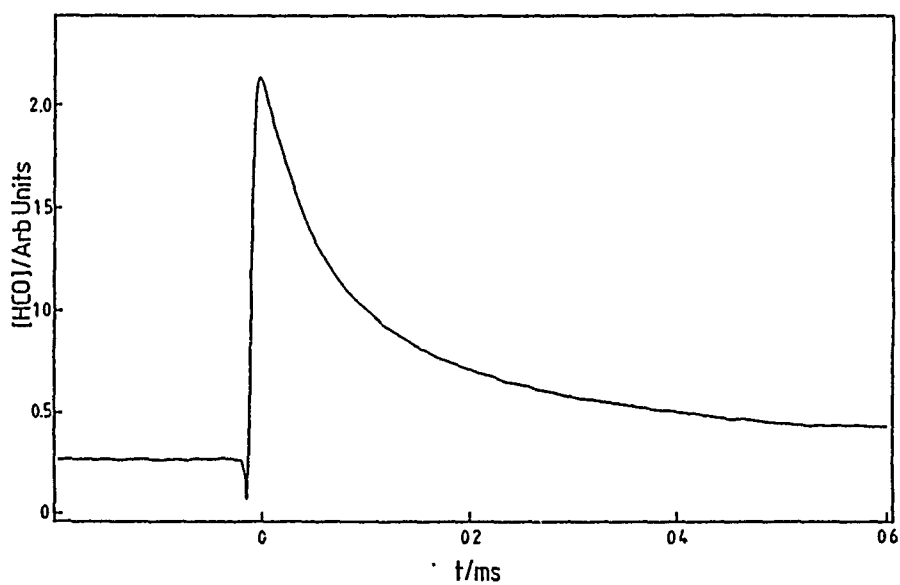


Fig. 1. Time dependence of the concentration of HCO radicals produced in the 308 nm photolysis of 50 Torr of acetaldehyde. Average of 100 excimer laser shots.

Reactions of  $\text{CH}(X^2\Pi)$  radicals with selected species at low pressure

K.H. Becker and P. Wiesen

Physikalische Chemie / FB 9

Bergische Universität - Gesamthochschule Wuppertal

D-5600 Wuppertal 1, FRG

and

K.D. Bayes

Department of Chemistry and Biochemistry

University of California

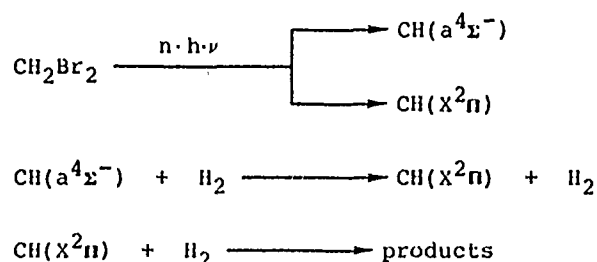
Los Angeles, CA 90024, USA

The methyne radical plays an important role as a very reactive intermediate in hydrocarbon combustion processes /1/ as well as in planetary atmospheres /2/. It is thought responsible for soot-formation /4,5/, chemiionization /7,8/ and the prompt NO-formation /9/ occurring in hydrocarbon oxidations.

The present work is concerned with direct measurements of bimolecular rate constants of  $\text{CH}(X^2\Pi)$  reactions at a total pressure of 2 Torr.

$\text{CH}$  radicals in their ground state  $X^2\Pi$  were generated by 248 nm laser photolysis of  $\text{CH}_2\text{Br}_2/\text{Ar}$  mixtures under flow conditions and detected by LIF as described previously /10/. H atoms were generated in a microwave discharge of  $\text{H}_2/\text{Ar}$  mixtures. Their concentrations were calibrated by titration with  $\text{NO}_2$ . The  $\text{CH}$  decay was followed under pseudo first order conditions by varying the delay time between the photolysis and the probe laser. Table 1 presents the obtained bimolecular rate constants at  $295 \pm 3\text{K}$  and a total pressure of 2 Torr in comparison with literature data.

In the case of  $H_2$  as reactant, the semi-log plots of the CH decay show a non-linearity that can be explained by a double exponential decay due to an additional population of the CH ground state from a precursor, which could be the metastable  $CH(a^4\Sigma^-)$  state, according to the following reaction scheme:



The obtained rate constants show that at lower  $H_2$  concentrations the depletion of CH is controlled by the reaction of  $CH(a^4\Sigma^-) + H_2$  after a certain time period.

The reaction of hydrogen atoms with  $CH(X^2\Pi)$  radicals was predicted to form carbon atoms via reaction (1) /8,25/.



In this work, for the first time, the over all rate constant for the reaction of  $CH + H$  was determined. The obtained value of  $5 \cdot 10^{-12} \text{ cm}^3 \text{ s}^{-1}$  supports reaction (1) because the approximately calculated 3rd order rate constant of  $10^{-28} \text{ cm}^6 \text{ molecule}^{-2} \text{ s}^{-1}$  would probably be too large for the recombination step at a total pressure of 2 Torr.

Table 1:

Rate constants for the reactions of  $\text{CH}(X^2\Pi)$  radicals with selected species R at a total pressure of 2 Torr

R	k. ( $10^{-11} \text{ cm}^3 \text{ molecule}^{-1} \text{ s}^{-1}$ )		Ref.
	this work	literature values	
$\text{O}_2$	$4.7 \pm 0.1$	$5.9 \pm 0.08$	/14/
		$5.1 \pm 0.50$	/17/
		$0.21 \pm 0.02$	/19/
		$8.0 \pm 3.0$	/21/
		$3.3 \pm 0.4$	/23/
$\text{N}_2$	$0.008 \pm 0.003$	$0.0072^a)$	/11/
		0.1	/12/
		$0.093 \pm 0.001^b)$	/14/
		$0.0076 \pm 0.0005^c)$	/15/
		0.008	/18/
		$0.0071 \pm 0.0006^c)$	/19/
		$0.02 \pm 0.0015^d)$	/20/
$\text{N}_2\text{O}$	$0.68 \pm 0.10$	$7.8 \pm 1.4$	/15/
		0.58	/18/
$\text{C}_2\text{H}_2$	$18 \pm 2$	7.45	/12/
		$22 \pm 4^b)$	/14/
		$42 \pm 2^b)$	/16/
$\text{H}_2$	$3 \pm 1$	$0.1^a)$	/11/
		$1.74 \pm 0.2$	/12/
		$2.3 \pm 0.5^b)$	/13/
		$2.6 \pm 0.5^b)$	/14/
		$0.79 \pm 0.22^e)$	/22/
		$1.40 \pm 0.10^b)$	/22/
$\text{H}$	0.5	4	/24/
		16	/25/
		$1.21^i)$	/26/
		$0.075^f)$	/27/
		$0.000295^g)$	/28/
		$1.29^h)$	/28/

Foot notes to table 1:

a) estimated total pressure 10 Torr

b) total pressure 100 Torr

c) total pressure 10 Torr

d) total pressure 2 Torr

e) total pressure 25 Torr

f) estimated at 4500 K

g) estimated at 4000 K for the reaction  $\text{CH} + \text{H} \longrightarrow \text{C} + \text{H}_2$

h) estimated at 4000 K for the reaction  $\text{CH} + \text{H} \longrightarrow \text{CH}_2$

i) estimated from self-absorption experiments of CH generated in pulsed discharge of methane



## References:

- / 1/ C.P. Fenimore, 13th Symposium (International) on Combustion (The Combustion Institute, Pittsburgh, 1971) p.373
- / 2/ E.W. Duley and D.A. Williams, Interstellar Chemistry (Academic Press, London, 1984)
- / 3/ Interstellar molecules (Symposium - International Astronomical Union; no. 87), 1979
- / 4/ A.G. Gaydon, The Spectroscopy of Flames, 2nd edition (Wiley, New York, 1974)
- / 5/ A.G. Gaydon and H.G. Wolfhard, Flames (Wiley, New York, 1979)
- / 6/ H.F. Calcote, 8th Symposium (International) on Combustion (The Combustion Institute, Pittsburgh, 1962) p.184
- / 7/ S.L.N.G. Krishnamachari, H.P. Broida, J. Chem. Phys. 34(5), 1709 (1961)
- / 8/ K.H. Becker, D. Kley and R.J. Norstrom, 12th Symposium (International) on Combustion (The Combustion Institute, Pittsburgh, 1969) p.405
- / 9/ D. Iverach, 14th Symposium (International) on Combustion (The Combustion Institute, Pittsburgh, 1973) p.767
- /10/ K.H. Becker, H.H. Brenig and T. Tatarczyk, Chem. Phys. Lett. 71, 242 (1980)
- /11/ W. Braun, J.R. McNesby and A.M. Bass, J. Chem. Phys. 46, 2071 (1967)
- /12/ H.W. Boshall and D. Perner, Z. Naturforsch. 26a, 1768 (1971)
- /13/ J.E. Butler, L.P. Goss, M.C. Lin and J.W. Hudgens, Chem. Phys. Lett. 63(1), 104 (1979)
- /14/ J.E. Butler, J.W. Fleming, L.P. Goss and M.C. Lin, Chem. Phys. 56, 355 (1981)
- /15/ S.S. Nagal, T. Carrington, S.V. Filseth and C.M. Sadowski, Chem. Phys. 69, 61 (1982)
- /16/ H.R. Herman, J.W. Fleming, A.B. Harvey and M.C. Lin, Chem. Phys. 73, 27 (1982)
- /17/ H.R. Herman, J.W. Fleming, A.B. Harvey and M.C. Lin, 19th Symposium (International) on Combustion (The Combustion Institute, Pittsburgh, 1982) p.73
- /18/ F.L. Nembitt, Ph.D.thesis, West Virginia University, Morgantown, 1982
- /19/ J.A. Duncanson Jr. and W.A. Guillory, J. Chem. Phys. 78(8), 4958 (1983)
- /20/ M.R. Herman and M.C. Lin, J. Phys. Chem. 87(20), 3933 (1983)
- /21/ D.A. Lichtin, M.R. Herman and M.C. Lin, Chem. Phys. Lett. 108(1), 18 (1984)
- /22/ M.R. Herman and M.C. Lin, J. Chem. Phys. 81(12), 5743 (1984)
- /23/ I. Mossing, C.M. Sadowski and S.V. Filseth, Chem. Phys. Lett. 66(1), 95 (1979)
- /24/ J.N. Murrell and L.J. Dunne, Chem. Phys. Lett. 102, 155 (1983)
- /25/ J. Peeters and C. Vinckler, 15th Symposium (International) on Combustion (The Combustion Institute, Pittsburgh, 1976) p.969
- /26/ H. Lango, R. Sobczynski and J.F. Behnke, Pol. J. Chem. 57, 169 (1983)
- /27/ A.O. Eschenroeder and J.A. Lord, 9th Symposium (International) on Combustion (The Combustion Institute, Pittsburgh, 1963) p.241
- /28/ S.W. Mayer, L. Schlofer and H.S. Johnston J. Chem. Phys. 32, 1105 (1966)

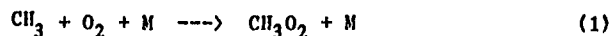
The temperature and pressure dependence of the reaction



N. Keiffer, M.J. Pilling and M.J.C. Smith

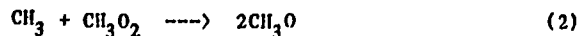
Physical Chemistry Laboratory, South Parks Road,  
Oxford, OX1 3QZ.

The reaction between the methyl radical and oxygen is an important process in combustion and is implicated in the transition from low temperature to high temperature mechanisms. The aim of the present work is to determine the pressure and temperature dependence of the low temperature peroxy radical formation process:



and hence allow good estimates to be made of  $k_1$  under combustion conditions.

In a recent investigation<sup>1</sup>, we demonstrated that previous flash photolysis studies had overestimated  $k_1$  because of interference from the reaction:



We devised a technique to enable data to be obtained by laser flash photolysis/absorption spectroscopy, at low  $[\text{CH}_3]_{t=0}/[\text{O}_2]$  concentrations, where reaction (2) makes only a small contribution, and extrapolated to  $[\text{CH}_3]_{t=0}$  where this contribution is zero. When the resulting values of  $k_1$ , obtained in an argon diluent over the pressure range

$32 \leq P/\text{Torr} \leq 488$ , were combined with the low pressure data of Selzer and Bayes<sup>2</sup>, and analysed using the Troe factorisation technique, they gave a limiting high pressure rate constant,  $k_1^\infty$ , of  $1.05 \times 10^{-12} \text{ cm}^3 \text{ molecule}^{-1} \text{ s}^{-1}$ , significantly below the value obtained by Cobos et al. at very high pressures<sup>3</sup>.

This technique has been applied to the determination of  $k_1$  over the temperature and pressure ranges  $298 \leq T/\text{K} \leq 582$ ,  $20 \leq P/\text{Torr} \leq 600$ . A preliminary analysis of the data at temperatures up to 474 K gives a temperature independent high pressure limit,  $k_1^\infty$ , of  $1.12 \times 10^{-12} \text{ cm}^3 \text{ molecule}^{-1} \text{ s}^{-1}$ , whilst  $k_1^0$ , the low pressure limit may be represented by  $k_1^0 = 1.29 \times 10^{-25} T^{-2.23} \text{ cm}^6 \text{ molecule}^{-2} \text{ s}^{-1}$ . At higher temperatures,  $k_1^\infty$  appears to fall, although it is obtained with reduced precision, because the data are further into the fall-off region. Techniques for analysing the T,P dependence of a combination reaction of this type will be discussed.

Data obtained at higher  $[\text{CH}_3]_{t=0}/[\text{O}_2]$  ratios enable  $k_2$  to be determined. Two techniques have been employed, one relying on an approximate analytic solution at low ratios and one employing numerical integration at higher ratios, where the analytic solution becomes invalid.

#### References

1. M.J. Pilling and M.J.C. Smith, J. Phys. Chem., 1985, 89, 4714.
2. E.A. Selzer and K.D. Bayes, J. Phys. Chem., 1982, 87, 392.
3. C.J. Cobos, H. Hippler, K. Luther, A.R. Ravishankara and J. Troe, J. Phys. Chem., 1985, 89, 4334.

KINETICS OF THE REACTIONS OF POLYATOMIC FREE RADICALS  
WITH MOLECULAR CHLORINE<sup>†</sup>

Raimo S. Timonen,\* John J. Russell, and David Gutman  
Department of Chemistry, Illinois Institute of Technology  
Chicago, Illinois 60616, U.S.A.

The kinetics of twelve reactions between carbon-centered polyatomic free radicals with molecular chlorine have been studied as a function of temperature. The free radicals were generated by the pulsed 193 nm photolysis of suitable precursors in a tubular reactor coupled to a photoionization mass spectrometer. Free-radical decay profiles were monitored as a function of chlorine concentration in real-time experiments to obtain the rate constant for the reaction under study. Rate constants were also measured as a function of temperature (up to 712 K) to obtain Arrhenius parameters. With one exception (the  $\text{CH}_3 + \text{Cl}_2$  reaction), this study is the first to isolate these  $\text{R} + \text{Cl}_2$  reaction for direct investigation.

The reactions of different groups of free radicals were studied: those involving alkyl radicals ( $\text{CH}_3$ ,  $\text{C}_2\text{H}_5$ ,  $i\text{-C}_3\text{H}_7$ , and  $t\text{-C}_4\text{H}_9$ ), halogenated methyl radicals ( $\text{CF}_3$ ,  $\text{CF}_2\text{Cl}$ ,  $\text{CFCl}_2$ , and  $\text{CCl}_3$ ), unsaturated hydrocarbon free radicals including ones which are resonance stabilized ( $\text{C}_2\text{H}_3$ ,  $\text{C}_3\text{H}_3$ , and  $\text{C}_3\text{H}_5$ ), and one reaction involving an acyl radical ( $\text{HCO}$ ). The results obtained are presented in the table below and are plotted in Figure 1.

The Arrhenius parameters are consistent with the formation of a polar transition state whose energy is raised or lowered by the presence of electron withdrawing or donating groups

attached to the radical center. The activation energies are determined in part by the exothermicity of the reaction. Details of the experiments, the results obtained, and their interpretation will be presented.

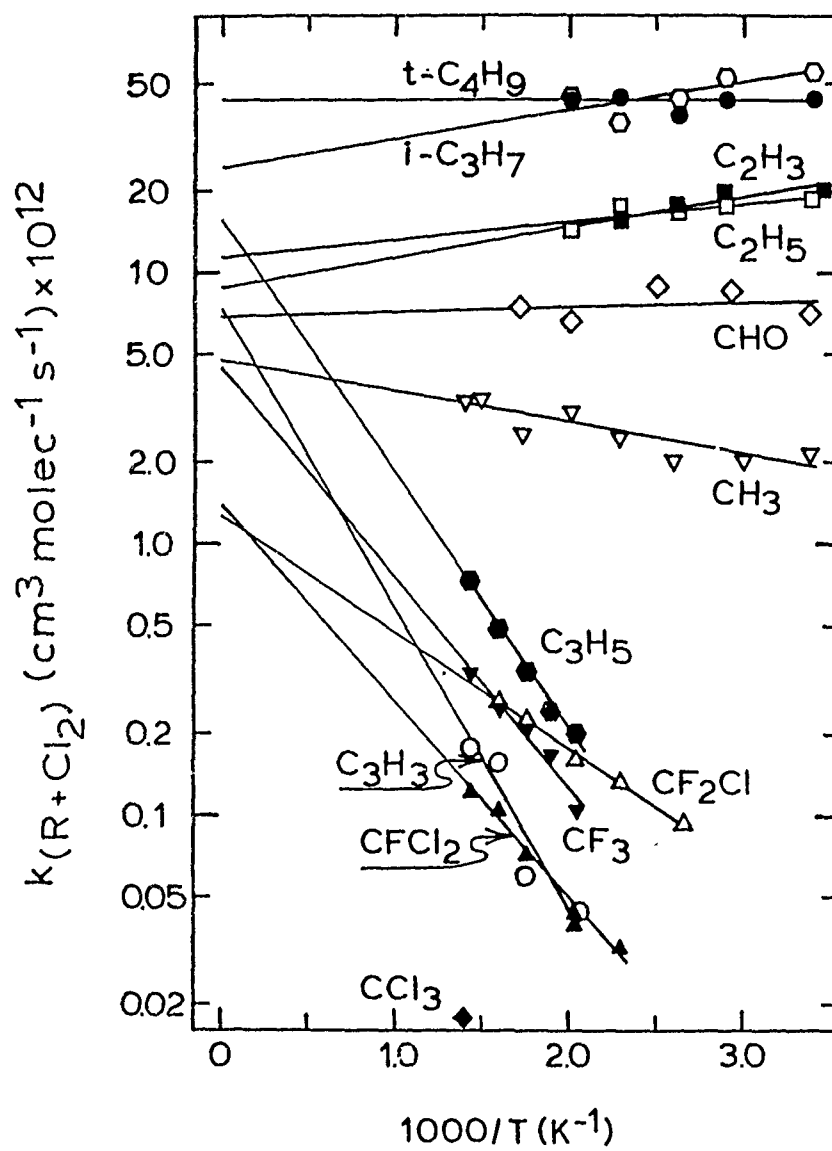
\* Permanent address, Department of Physical Chemistry,  
University of Helsinki, Finland.

+ Research supported by the Chemistry Division, National Science  
Foundation

SUMMARY OF ARRHENIUS RATE CONSTANT PARAMETERS FOR THE REACTIONS  
OF POLYATOMIC FREE RADICALS WITH MOLECULAR CHLORINE

R	$\Delta H^\circ$ (kJ/mole)	T Range (K)	$\log(A/$ $\text{cm}^3\text{molec}^{-1}\text{s}^{-1})$	$E_a$ (kJ/mole)
t-C <sub>4</sub> H <sub>9</sub>	-108	298-498	-10.40 $\pm$ 0.26	0 $\pm$ 2
i-C <sub>3</sub> H <sub>7</sub>	-112	298-498	-10.60 $\pm$ 0.26	-2 $\pm$ 3
C <sub>3</sub> H <sub>3</sub>	-62	487-693	-11.14 $\pm$ 0.31	21 $\pm$ 4
C <sub>3</sub> H <sub>5</sub>	-49	487-693	-10.81 $\pm$ 0.26	18 $\pm$ 3
C <sub>2</sub> H <sub>5</sub>	-110	295-498	-10.90 $\pm$ 0.33	-1 $\pm$ 3
C <sub>2</sub> H <sub>3</sub>	-147	298-435	-11.06 $\pm$ 0.21	-2 $\pm$ 2
CHO	-110	296-582	-11.16 $\pm$ 0.24	0 $\pm$ 2
CH <sub>3</sub>	-108	296-712	-11.32 $\pm$ 0.24	2 $\pm$ 2
CF <sub>3</sub>	-117	487-693	-11.35 $\pm$ 0.35	15 $\pm$ 5
CF <sub>2</sub> Cl	-103	376-626	-11.89 $\pm$ 0.24	8 $\pm$ 3
CFCl <sub>2</sub>	-68	435-693	-11.86 $\pm$ 0.31	14 $\pm$ 4
CCl <sub>3</sub>	-54	693 only	(-12.17)	(21)

$k = A \exp(-E_a/RT)$ . Error limits on Arrhenius parameters indicate maximum uncertainties. Most probable uncertainty in each measured rate constants is  $\pm 20\%$ .

Figure 1 Arrhenius plot of Rate Constants of Twelve R + Cl<sub>2</sub> Reactions

ON THE METHYL RADICAL-INITIATED THERMAL  
REACTION OF 2,3-DIMETHYLBUTENE-2

T. Körtvélyesi and L. Sereš

Institute of General and Physical Chemistry,  
József Attila University, Szeged, Hungary.

Investigation of the radical-initiated gas-phase thermal reactions of highly-branched olefins is relatively simple since the higher oligomer radicals are formed in kinetically insignificant concentrations due to the intramolecular non-bonding interactions present in these radicals.

The methyl radical-initiated thermal reaction of 2,3-dimethylbutene-2 (DMB) was investigated in the temperature range 389-459 K. Preliminary results are described here.

The experiments were carried out in a conventional high-vacuum static system. Di-tert-butyl peroxide (DTBP) was used as the methyl radical source. The initial concentration ranges were  $1.13 \cdot 10^{-3} \leq [\text{DMB}] / \text{mol dm}^{-3} \leq 1.50 \cdot 10^{-3}$  and  $1.27 \cdot 10^{-4} \leq [\text{DTBP}] / \text{mol dm}^{-3} \leq 2.54 \cdot 10^{-4}$ . The reaction products were analysed with an HP 5730A GC equipped with FID. Methane, ethane, acetone, 2,3-dimethylpentene-2 (DMP), 2,2,3,3-tetramethylbutane (TMB), 2,3,3,4,4,5-hexamethyl-1,5-hexadiene (HMH), 2,3,3,5,6-pentamethyl-1,5-heptadiene (PHH) and 2,3,6,7-tetramethyl-2,6-octadiene (TMO) were identified as the main products. tert-Butanol, 2,3-dimethylbutene-1, 2,2,3-trimethylbutene-3 (TB) and some  $\text{C}_{12}$  and  $\text{C}_{13}$ -monoolefins were shown to be formed in minor amounts. The initial rates of formation of the products were determined by the linear least squares method from the product accumulations.

The mechanism of the reaction was proposed on the basis of the product composition. The suggested mechanism was supported by computer simulation.

Most of the products formed in the radical recombination reactions were identified.

The radical concentrations used in the kinetic equations were calculated from the initial rates of formation of these products

$$[M] = \frac{r_o(C_2H_6)^{1/2}}{k_c(M,M)^{1/2}} \quad [A] = \frac{r_o(TMO)^{1/2}}{k_c(A,A)^{1/2}}$$

$$[MOMB] = \frac{r_o(TMB) k_c(M,M)^{1/2}}{r_o(C_2H_6)^{1/2} k_c(M,MOMB)} \quad (I)$$

where  $M = \dot{C}H_3$ ,  $A = \text{isopropyl radical}$ ,  $MOMB = \text{isobutyl radical}$ , and  $k_c$  is the radical recombination rate coefficient.

The A radical is formed in a H-abstraction reaction (H-abstraction by MOMB comprises less than 10%):



The rate of reaction (1) was calculated from the initial rates of formation of all the products incorporating the a radical, i.e.:

$$r_1 = k_1 [DMB] [M] = 2(r_o(HMH) + r_o(PMH) + r_o(TMO)) + r_o(TB) + r_o(DMP)$$

For the rate coefficient ratio,  $k_1/k_c(M,M)^{1/2}$ , we obtained:

$$\log(k_1/k_c(M,M)^{1/2}) = (3.1 \pm 0.2) - (30.9 \pm 2.7) \text{ kJ mol}^{-1}/\theta,$$

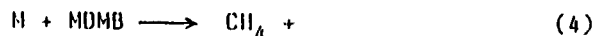
where  $\theta = RT \ln 10$ .

The MOMB radical is formed by M radical addition to DMB:



The activation energy of reaction (2) can be calculated from the rate of formation of ethane, TMB and the initial concentration of DMB.

The MOMB radical formed in reaction (2) disappears predominantly in the following two reactions:





From the rate expressions for reactions (3) and (4) and the expression for [M] (equation I)) we obtain:

$$\frac{r_o(\text{TMB})}{r_o(\text{C}_2\text{H}_6)^{1/2} [\text{DMB}]_o} = \frac{k_2 k_3}{(k_3 + k_4) k_c (\text{M}, \text{M})^{1/2}} \quad (11)$$

! From the temperature-dependence of the expression on the left-hand side we get the Arrhenius activation energy of methyl radical addition to DMB:  $E_2 = (33.2 \pm 0.8) \text{ kJ mol}^{-1}$ .

# RATE CONSTANTS FOR SOME HYDROCARBON RADICAL COMBINATIONS

L. Seres and Á. Nacsá

Institute of General and Physical Chemistry,  
A.J. University, Szeged, Hungary.

The di-tert-butyl peroxide (DTBP)-initiated reaction of 2-methylpropene (B) was studied in the temperature range 392.5-442.6 K and the concentration ranges  $3.26 \cdot 10^{-3} \leq [B] / \text{mol dm}^{-3} \leq 4.35 \cdot 10^{-3}$  and  $3.62 \cdot 10^{-4} \leq [\text{DTBP}] / \text{mol dm}^{-3} \leq 6.09 \cdot 10^{-4}$ .

The products of the reaction up to  $C_{10}$  were identified as methane, ethane (ETH), ethene, propene, 2,2-dimethylpropane, 2-methylbutane, 2-methylbutene-2, 2,2-dimethylbutane (DMBA), 2,5-dimethylhexadiene-1,5, 2,4,4-trimethylhexene-1, 2,2,4,4-tetramethylhexane, 3,3,4,4-tetramethylhexane (TMHA), acetone and tert-butanol.

The initial rates of formation of all of the above products were determined from measurements in the early stages of the reaction, where the product concentration vs. time plots are linear. Most products are formed in different reactions of methyl (M), 1,1-dimethylpropyl (MB), 1,1,3,3-tetramethylpentyl (MBB) and 2-methylallyl (MA) radicals.

The radicals MB and MBB are formed in the first two steps of the oligomerization:



while MA is a product of H abstraction by radicals:



Rate expressions were derived for product formation, based upon a mechanism involving all the possible combination, disproportionation and H abstraction reactions of the above radicals. (See e.g. the simplest model we were studying,

Scheme 1, where  $k_c$  is the rate coefficient of recombination.)

The systems of algebraic equations relating to the various models were solved, using nonlinear least squares (by the Simplex method), to yield the kinetic quantities of the rate expressions.

#### Scheme 1



$$v(ETH) = k_c(M,M)_p [M]^2 \quad (1')$$



$$v(DMBA) = 2 \{k_c(M,M)_\infty k_c(MB,MB)\}^{1/2} [M][MB] \quad (2')$$



$$v(TMHA) = k_c(MB,MB) [MB]^2 \quad (3')$$

Let us focus our attention on the simple model shown in Scheme 1. The rate coefficients of cross-combination reactions of small radicals are known to obey the "geometric mean rule". However, no information is available on the validity of this rule for sterically hindered radicals such as MB or MBB. Furthermore, reaction (1) is in its pressure-dependent region under the present conditions ( $\sim 13$  kPa overall pressure), while reactions (2) and (3) are believed to be in the high-pressure region.

Consequently,  $k_c(M,M)$  would have different values in equation (1') and equation (2'). In order to overcome these difficulties, we chose to retain the square-root dependence of  $k_c(M,MB)$  on  $k_c(M,M)$  and  $k_c(MB,MB)$ , but in order to allow for the above effects a new parameter ( $G$ ) is used instead of 2 in equation (4'), i.e.

$$k_c(M,MB) = G \{k_c(M,M)_p k_c(MB,MB)\}^{1/2} \quad (4')$$

All the radical concentrations and kinetic quantities were treated as parameters in the systems of algebraic equations, and the optimization was made by using Box's method.

If we assume that the "geometric mean rule" holds for the

radicals present in this system at high pressures (i.e. steric hindrance does not influence its validity), we have an easy way to calculate the high-pressure recombination rate constants from the data obtained at any pressure:

$$G\{k_c(M,M)_p k_c(MB,MB)\}^{1/2} = 2\{k_c(M,M)_\infty k_c(MB,MB)\}^{1/2}$$

where the indices  $p$  and  $\infty$  refer to the low-pressure and the high-pressure rate coefficients, respectively.

On rearrangement we obtain

$$k_c(M,M)_\infty = \left(\frac{G}{2}\right)^2 k_c(M,M)_p$$

In order to acquire information on the correlated errors involved in the evaluation of a large number of parameters simultaneously, different models were used. (The model shown in Scheme 1 has 21 parameters calculated from 27 equations, while the largest one has 71 parameters calculated from 99 equations.) Also, some input parameters (the initial values, the higher and lower limits of the parameters, and the number of iterations) were used with different values in different runs for each model.

Most of the rate coefficients obtained are close to the average (i.e. within 20 p.c. for the model shown in Scheme 1), except for those obtained in the 71-parameter model (50 p.c.), where all the combination and disproportionation reactions were considered to be temperature-dependent.

The high-pressure recombination reaction rate coefficients obtained are:

Radical	$\log k_c / \text{dm}^3 \text{ mol}^{-1} \text{ s}^{-1}$
methyl	$10.43 \pm 0.20$
1,1-dimethylpropyl	$9.2 \pm 0.3$
1,1,3,3-tetramethylpentyl *	$8.9 \pm 0.6$
2-methylallyl	$9.8 \pm 0.4$

Since these rate coefficients are in good agreement with those obtained for similar radicals, the assumption made, i.e. that the "geometric mean rule" is valid for bulky and unsaturated radicals, seems justified.

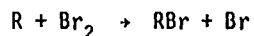
\* assuming  $G(M,MBB) = G(M,MB)$

Kinetics of the Chlorination of  $C_2H_5Br$  and the Competitive  
Bromination of  $C_2H_5Cl$ ,  $CH_3CHCl_2$ ,  $C_2H_5Br$ , and  $CH_3CHBr_2$ .

E. Tschuikow-Roux, D.R. Salomon, F. Faraji, and K. Miyokawa

Department of Chemistry, University of Calgary,  
Calgary, Alberta, Canada T2N 1N4

The competitive photobromination of  $C_2H_5Cl$ ,  $CH_3CHCl_2$ ,  $C_2H_5Br$ , and  $CH_3CHBr_2$  against  $C_2H_6$  as primary standard has been investigated between 32 and 95°C. Over this range of temperature bromine atom attack in all cases occurs almost exclusively at the halogen substituted site, leading to very simple kinetics:



where R represents  $CH_3CHX$  or  $CH_3CX_2$  ( $X = Cl, Br$ ) radicals. Using the revised rate parameters for the bromination of ethane reported by Amphlett and Whittle<sup>1</sup>, absolute Arrhenius parameters for  $\alpha$ -hydrogen abstraction have been obtained and are listed in Table I.

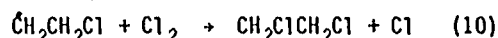
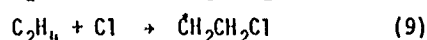
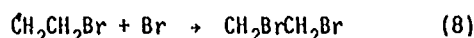
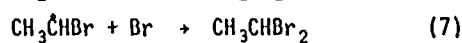
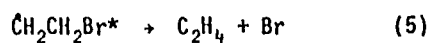
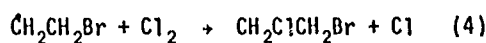
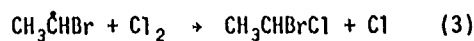
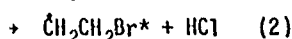
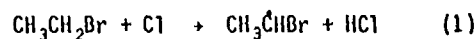
TABLE I. Hydrogen Abstraction by Bromine Atoms

Reactant	$\log_{10}(A/\text{cm}^3 \text{ mol}^{-1} \text{ s}^{-1})$	$E/\text{kcal mol}^{-1}$
$\text{C}_2\text{H}_6^{\text{a}}$	14.135	13.66
$\text{CH}_3\text{CH}_2\text{Cl}$	12.182	9.14
	12.545	9.65
$\text{CD}_3\text{CH}_2\text{Cl}$	12.535	9.65
$\text{CH}_3\text{CHCl}_2$	11.806	8.00
$\text{CH}_3\text{CH}_2\text{Br}$	12.645	10.58
$\text{CH}_3\text{CHBr}_2$	11.475	8.11

<sup>a</sup> Primary standard, Ref. 1.

In a companion study the photochlorination of  $\text{C}_2\text{H}_5\text{Br}$  has also been investigated in the temperature range 0 to 90°C, and shows a different mechanism than that observed in the chlorination of chloro- and fluoroethanes<sup>2,3</sup>.

The bromoethyl radical produced from Cl atom attack on the primary hydrogen in  $\text{CH}_3\text{CH}_2\text{Br}$  is found to be unstable even at 0°C and decomposes to  $\text{C}_2\text{H}_4$  plus Br. This causes a chain transfer which propagates parallel to the 'normal' chlorination mechanism. The principal products observed are  $\text{CH}_3\text{CHBrCl}$ ,  $\text{C}_2\text{H}_4$ ,  $\text{CH}_3\text{CHBr}_2$ , and  $\text{CH}_2\text{ClCH}_2\text{Br}$ , the yields of the latter three being pressure dependent. Trace amounts of  $\text{CH}_2\text{ClCH}_2\text{Cl}$  and  $\text{CH}_2\text{BrCH}_2\text{Br}$  were also observed. These results may be interpreted in terms of the reaction scheme:



Application of the usual stationary state approximation yields the relationships

$$\frac{[\text{CH}_3\text{CHBrCl}]}{[\text{C}_2\text{H}_4]} = \left( \frac{k_1}{k_2} - 1 \right) + (k_1 k_6 / k_2 k_5) [\text{M}]$$

$$\frac{[\text{C}_2\text{H}_4]}{[\text{CH}_2\text{ClCH}_2\text{Br}]} = \frac{k_5}{k_6} \frac{1}{[\text{M}]}$$

Plots of these product ratios against  $[\text{M}]$  or  $1/[\text{M}]$ , respectively, where  $[\text{M}]$  is an inert additive ( $\text{C}_2\text{F}_6$ ) present in excess, yielded straight lines. From the slopes and intercept we obtained at  $50^\circ\text{C}$ ,  $k_5/k_6 = 2665 \text{ Torr}$ , and  $k_1/k_2 = 3.41$ , a reasonable value for  $\alpha$  vs.  $\beta$  hydrogen abstraction.

#### References

1. J.C. Amphlett and E. Whittle, *Trans. Faraday Soc.*, **64**, 2130 (1968).
2. E. Tschuikow-Roux, T. Yano, and J. Niedzielski, *J. Chem. Phys.*, **82**, 65 (1985).
3. E. Tschuikow-Roux, J. Niedzielski, and F. Farajl, *Canad. J. Chem.*, **63**, 1093 (1985).

The Chemistry of Triplet Vinylidene Radicals: Reaction with  
Molecular Oxygen

Askar Fahr, Chemical Kinetics Division, National Bureau of Standards, Gaithersburg, Md. 20899 and Allan H. Laufer, Chemical Sciences Division, U.S. Department of Energy, Washington, D. C. 20545

Chemical reactions of small electronically excited hydrocarbon radicals, aside from those of the low-lying singlet methylene species, have not been extensively studied probably because these species are difficult to prepare and characterize. Methylene, of course, is the smallest of the series of unsaturated hydrocarbon radicals. However, the existence and identification of a long-lived carbene, i.e., the electronically excited vinylidene radical ( $\text{H}_2\text{C}=\text{C}$ ), has been documented in recent work from this laboratory<sup>1</sup>. The chemistry of vinylidene remains virtually unknown. The ground state singlet ( $^1\text{A}_1$ ) has a lifetime to isomerization to acetylene of less than 1 ps and is unlikely to be involved in chemical reactions. The first excited triplet state has a large potential barrier to isomerization that has been calculated to be about 45 kcal/mol and may be expected to be long-lived. In earlier experiments the quenching of triplet vinylidene to the ground singlet state has been examined for a series of non-reactive collision partners. In addition, efforts were made to search for a chemical reaction with several possible reactive quenching partners such as  $\text{H}_2$  and  $\text{CH}_4$ . There was no evidence for an abstraction reaction.

It is well known that ground state molecular oxygen reacts rapidly with hydrocarbon free radicals, particularly the spin-allowed reaction with triplet species. If the excited triplet



vinylidene species has properties similar to that of its methylene homolog, then we might expect a relatively rapid reaction with oxygen. In the work to be reported here we have concluded a rate constant and mechanistic investigation of the title reaction using the vacuum ultraviolet flash photolysis of vinyl chloride in to produce the triplet vinylidene species. Vacuum ultraviolet kinetic absorption spectroscopy of CO in its strong Fourth Positive system was used to monitor product formation from which it was possible to derive the rate constant of the reaction. The ( $^3B_2$ )  $H_2C=C$  was monitored in absorption at 137 nm, acetylene at 152 nm and CO, as noted above, in its (0,0) transition of the 4+ system at 154 nm.

There are several possible reaction paths, in this photolytic system, that may lead to CO formation. They include the reaction of product  $C_2H_2$  with  $O(^3P)$  that may be formed in the initial photolytic process as well as the reaction of ( $^3B_2$ )  $H_2C=C$  with molecular  $O_2$  or with  $O(^3P)$  atoms. The various processes could be discerned through a combination of temporal profiles, intensity dependencies and reaction energetics.

We will discuss the rate constant for the title reaction, possible production of vibrationally excited CO product and some comments about the nature of the transition state.

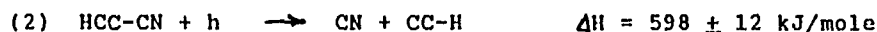
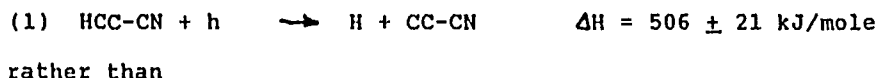
1. A. Fahr and A. H. Laufer, "Photodissociation of Vinyl Chloride: Formation and Kinetics of Vinylidene  $H_2C=C(^3B_2)$ ", J. Phys. Chem., 89, 2906(1985) and references therein

Acknowledgement: This work was supported, in part, by the Planetary Atmospheres Program of the NASA, and carried out at the National Bureau of Standards.

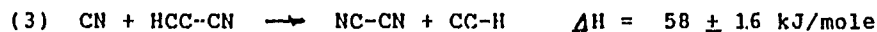
ON THE KINETICS AND THERMOCHEMISTRY OF CYANOACETYLENE AND THE  
ETHYNYL RADICAL

Joshua B. Halpern, and George E. Miller, Department of Chemistry,  
Howard University, Washington, DC, USA and Winston Nottingham,  
Department of Chemistry, University of the District of Columbia,  
Washington, DC, USA

The cyanoacetylenes are important odd nitrogen species found in interstellar space (1). Recently, ethynyl has also been observed (2). Moreover, the Voyager mission showed that HCC-CN is the second most important odd nitrogen species in the atmosphere of Titan (3). We report here on a measurement of the bond strength of dicyanoacetylene, which can be used to find the heat of formation of the ethynyl radical. The lowest energy channel for dissociation of cyanoacetylene is then found to be



We also report on a measurement of the reaction rate constant for



of the order of  $1 \times 10^{-11}$  cm<sup>3</sup>/molecule-sec. This was proposed as the source of C<sub>2</sub>N<sub>2</sub> in Titan's atmosphere to replace (4,5)



The rate of reaction 4 was originally estimated to be of the order of  $10^{-11}$  cm<sup>3</sup>/molecule-sec, but measured to be of the order of  $10^{-14}$  cm<sup>3</sup>/molecule-sec (6). Work is continuing on measurement of the branching ratios of reactions 1 and 2, and measurement of

the absorption coefficient of cyanoacetylene between 250 and 190 nm.

We used the photodissociative excitation method to measure the bond strength of  $C_4N_2$ . The apparatus was described in Reference 7. The VUV light source was formed by a short, high voltage discharge in argon, which was dispersed through a small VUV monochromator. The threshold for photodissociative excitation of  $CN (B^2_{\Sigma^+})$  is found to be  $141 \pm 2$  nm. The cutoff is not due to the absorption of  $C_4N_2$  rising suddenly at this point, or the lamp output suddenly increasing. Using the measured value of 535 kJ/mole for the heat of formation of  $C_4N_2$  (8) and 101 kJ/mole for the heat of formation of  $CN$  (9), we obtain  $648 \pm 21$  kJ/mol for the heat of formation of  $C_3N$ . This compares with a heat of formation of  $533 \pm 4$  kJ/mol for  $C_2H$ .

With the heat of formation of  $HC_3N$  of 355 kJ/mole (10) we obtain the heat of reaction 1. Thus, ethynyl will be produced by photodissociation considerably below the energetic threshold for reaction 2. We are currently measuring the branching ratio between reactions 1 and 2 at 193 nm.

The reaction rate constant of reaction 3 was measured in generally the same manner as in Reference 7. A mixture of 1%  $C_2N_2$ , 1%  $HC_3N$  and 98 % argon was passed through the photolysis cell.  $C_2N_2$  was used as the  $CN$  source because the yield of  $CN$  radicals at 193 nm was many orders of magnitude higher than for  $HC_3N$ . Decay rates were measured under pseudo-first order conditions at several pressures. The rates were plotted as a

function of the cyanoacetylene pressure to extract the rate constant for reaction 3.

This work was sponsored by NASA. GEM acknowledges the support of the United States National Science Foundation.

References

1. B. E. Turner, *Astrophys. J. Letters* 163 (1971) L35.
2. *Astrophys. J. Letters* 212 (1977) L81, L87.
3. *Science* 212 (1981), *Nature* 292 (1982), *J. Geophys. Res.*, 87 (1982).
4. Y. L. Yung, private communication 1986.
5. Y. L. Yung, M. Allen and J. P. Pinto, *Astrophys. J. Supp.* 55 (1984) 465.
6. X. Li, N. Sayeh and W. M. Jackson, *J. Chem. Phys.*, 81 (1984) 833.
7. G. E. Miller, J. B. Halpern and W. M. Jackson, *J. Chem. Phys.*, 71 (1979) 4625.
8. G. T. Armstrong and S. Marantz, *J. Phys. Chem.*, 64 (1960) 1776.
9. H. Okabe, *The Photochemistry of Small Molecules*, (Wiley, New York, 1978) p. 376.
10. H. Okabe and V. H. Diebler, *J. Chem. Phys.*, 59 (1973) 2430.

THE RADICAL-RADICAL  $\text{NF}_2$  REACTIONS

Bedjanian Yu.R., Gershenzon Yu.M., Kishkovitch O.P., Rozenshtein V.B.

Institute of Chemical Physics, Moscow 117977, USSR

The experiments were carried out in a flow-tube apparatus combined with EPR/LMR - spectrometer [1]. The  $\text{NF}_2$ -radicals were obtained in the furnace (500 K).

$\text{NF}_2 + \text{OH}$ . The experimental conditions were:  $p = (1-6)$  Torr,  $T = 300$  K,  $[\text{OH}] \sim 10^{12} \text{ cm}^{-3}$ ,  $[\text{NF}_2] = (0.6 - 3.7) \cdot 10^{13} \text{ cm}^{-3}$ .

The OH-radicals were produced in the  $\text{H} + \text{NO}_2$  reaction. One can put down the obtained rate constant  $k_1 = (1.55 \pm 0.35) \cdot 10^{-11} \text{ cm}^3 \text{ s}^{-1}$  to the only exothermic channel  $\text{OH} + \text{NF}_2 \rightarrow \text{HF} + \text{FNO}$ .

$\text{NF}_2 + \text{HO}_2$ . The experiments were carried out at  $T = 300$  K,  $p = (10 - 16)$  Torr ( $[\text{He}]/[\text{O}_2] = 1$ ),  $\text{HO}_2 = (2-20) \cdot 10^{11} \text{ cm}^{-3}$ ,  $\text{NF}_2 = (0.5 - 10) \cdot 10^{13} \text{ cm}^{-3}$ . The  $\text{HO}_2$  - radicals were produced in  $\text{H} + \text{O}_2 + \text{M}$  reaction. The rate constant  $k_2 = (2.4 \pm 0.6) \cdot 10^{-12} \text{ cm}^3 \text{ s}^{-1}$  was measured and the main channel  $\text{NF}_2 + \text{HO}_2 \rightarrow \text{F} + \text{OH} + \text{FNO}$  was determined.

$\text{NF}_2 + \text{NO}_2$ . The reaction was studied at  $T = (300 - 530)$  K,  $p = (0.8 - 60)$  Torr,  $\text{NO}_2 = (0.3 - 8.6) \cdot 10^{16} \text{ cm}^{-3}$ . The rate constant obtained for a channel  $\text{NF}_2 + \text{NO}_2 \rightarrow 2\text{FNO}$  is  $k_3 = 8.6 \cdot 10^{-11} \exp(-2450/T)$ .

$\text{NF}_2 + \text{NF}_2 + \text{M} \rightarrow \text{N}_2\text{F}_4 + \text{M}$ . The reaction was studied for  $\text{M} = \text{He}, \text{O}_2, \text{NO}, \text{N}_2\text{F}_4$  at  $p = (19 - 110)$  Torr. The following results were obtained:  $k_{\text{He}} = (0.6 \pm 0.1) \cdot 10^{-32} \text{ cm}^6 \text{ s}^{-1}$ ,  $k_{\text{O}_2} = (1.0 \pm 0.3) \cdot 10^{-32} \text{ cm}^6 \text{ s}^{-1}$ ,  $k_{\text{NO}} = (1.2 \pm 0.2) \cdot 10^{-32} \text{ cm}^6 \text{ s}^{-1}$ ,  $k_{\text{N}_2\text{F}_4} = (4.8 \pm 1.0) \cdot 10^{-32} \text{ cm}^6 \text{ s}^{-1}$ .

Reference. †. Gershenzon Yu.M., El'in S.D., Kishkovitch O.P., Lebedev Ya.S., Malkhasian R.T., Rozenshtein V.B., Trubnikov G.R. Doklady Akad.Nauk SSSR, 1980, v.255, No 3, p. 620 - 622.

Formation of molecular hydrogen by the thermal decomposition of n-dialkylperoxides in oxygen.

K.A. SAHETCHIAN, A. HEISS, R. RIGNY, J. TARDIEU de MALEISSYE

Laboratoire de Chimie Générale, C.N.R.S. UA 40870, Tour 55,  
E 4, Université P. et M. Curie, 4 Place Jussieu,  
75252 PARIS CEDEX 05 - FRANCE.

The self-reaction of  $\text{HO}_2$  radicals in the gas phase plays a crucial role in atmospheric chemistry, in low temperature combustion and generally in all systems where these radicals are present.

It is established that the recombination rate, at 298 K, depends on the overall pressure and may be modified by some additives such as  $\text{H}_2\text{O}$  vapor or  $\text{NH}_3$ . Moreover the recombination rate presents a significant negative temperature coefficient,  $-1.2 \text{ kcal.mol}^{-1}$ . The effective rate constant [1] appears as the sum of a bimolecular component and a pressure dependent termolecular one. The yield of  $\text{H}_2\text{O}_2$  measured in flash-photolysis experiments [2,3] could vary from 29 % of the self-reaction expected value (at 760 torr and 278 K in presence of  $\text{H}_2\text{O}$ ) to 93 % at low pressures (10-25 torr). In order to explain the difference between the expected and the observed values of  $\text{H}_2\text{O}_2$ , several authors have suggested that the formation of  $\text{H}_2$  was thermodynamically possible.

Previous investigations [4], carried out in quartz vessels coated by  $\text{B}_2\text{O}_3$  and treated with the slow reaction  $\text{H}_2/\text{O}_2$ , pointed out that the thermal decomposition in  $\text{O}_2$  of some di-n-alkylperoxides produced  $\text{HO}_2$  radicals ; the self-reaction of these radicals produced simultaneously  $\text{H}_2\text{O}_2$  and  $\text{H}_2$ . Alkylperoxides as  $n(\text{C}_7\text{H}_{15}\text{O})_2$ ,  $n(\text{C}_5\text{H}_{11}\text{O})_2$  or  $n(\text{C}_4\text{H}_9\text{O})_2$  were investigated by this way at concentrations ranging from 10 to 100 p.p.m.

The present work was undertaken to support the homogeneous formation of  $\text{H}_2$  by a reactive pathway parallel to the  $\text{H}_2\text{O}_2$  formation. Therefore we have studied the ratio  $[\text{H}_2]/([\text{H}_2] + [\text{H}_2\text{O}_2])$  at atmospheric pressure, as a function of 1) the temperature, 2) the ratio  $P_{\text{O}_2} / (P_{\text{O}_2} + P_{\text{N}_2})$

$P_{O_2}$  and  $P_{N_2}$  being partial pressures of  $O_2$  and  $N_2$ , 3) the concentration of peroxide ROOR (mainly  $n(C_4H_9O)_2$ ).

An overall  $6 \text{ l.h}^{-1}$  flow rate of  $N_2 + O_2$  was maintained inside the vessel at  $\Delta T = \pm 0.5^\circ\text{C}$  with a residence time of 130 s. The concentration of ROOR being constant, we have studied the influence of  $O_2$  upon the formation of  $H_2O_2$  and  $H_2$ , when  $O_2$  was substituted progressively to  $N_2$ . At vessel outlet, a flow of  $4.2 \text{ l.h}^{-1}$  was pumped through a microprobe and the condensable species were trapped at 77 K on the finger of a dismantable Dewar. Concentration measurements were performed by using H P L C for ROOR, spectrophotometry at 380 nm for  $H_2O_2$  and GC (coupled with a zirconia cell) for  $H_2$ . The detection threshold of  $H_2$  in  $O_2$  was lower than 0.1 p.p.m.

The data for six temperatures ranging from 150 to  $200^\circ\text{C}$ , obtained with different compositions, exhibit no clear dependence of the ratio  $[H_2] / ([H_2] + [H_2O_2])$  with the vessel temperature. However a slight decrease can be noticed in the range 150 -  $180^\circ\text{C}$ , followed by an apparent increase of this ratio between 180 and  $200^\circ\text{C}$ .

The intermediate temperature range from 170 -  $180^\circ\text{C}$  appears the most convenient to study the influence of  $O_2$  and ROOR on the formation of  $H_2$ . With ratios  $P_{O_2} / (P_{O_2} + P_{N_2})$  ranging from 1/6 to 5/6 as well with concentrations of ROOR from 30 to 120 p.p.m., no dependence of partial pressures of  $O_2$  or peroxide concentration was observed on the relative amount of  $H_2$  formed. An average value of  $(7.9 \pm 0.8) \%$ , with an error of 1 standard deviation, was obtained for the ratio  $[H_2] / ([H_2] + [H_2O_2])$ .

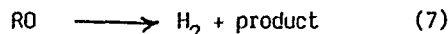
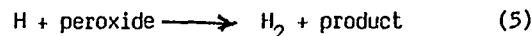
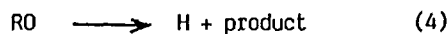
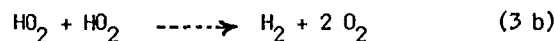
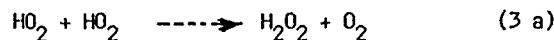
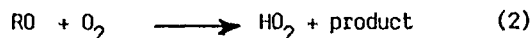
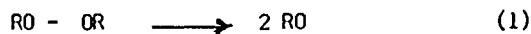
Some experiments were made with mixtures of  $O_2$  and di-tertiary-butylperoxide at concentrations ranging from 100 to 200 p.p.m. and temperatures from 170 to  $190^\circ\text{C}$ . Molecular hydrogen was also generated jointly with  $H_2O_2$  but the ratio  $[H_2] / ([H_2] + [H_2O_2])$  was lower, about 1 %.

Recently, static mixtures of  $H_2O_2$  80 % with  $N_2$  or  $O_2$  were irradiated by using an ArF exciplex laser at 193.3 nm. Fluences between 1 and  $16 \text{ mJ.cm}^{-2}$  with pulses of 30 ns were used during exposure times from 5 to 35 min. In linear photochemistry, heavy absorption of  $H_2O$  vapor occurs at 185 nm and extends through shorter wavelengths. The  $H_2O_2$  vapor absorption occurs to longer wavelengths, with an absorption coefficient  $\beta \sim 60.10^{-20} \text{ cm}^2 \text{ molec}^{-1}$  at 193 nm. In these conditions, a specific photochemical

decomposition of  $\text{H}_2\text{O}_2$  should be possible without  $\text{H}_2\text{O}$  modification ; the expected subsequent hydrogen formation proceeding from  $\text{H}_2\text{O}_2$  exclusively. Unfortunately, under non linear irradiations which correspond to the laser pulses, important quantities of molecular hydrogen are detected indifferently in presence of pure  $\text{H}_2\text{O}$  vapor or in  $\text{H}_2\text{O}/\text{H}_2\text{O}_2$  vapor mixtures. This formation of  $\text{H}_2$  is likely due to a complicated radical mechanism resulting from a not well clarified multiphotonic UV absorption by  $\text{H}_2\text{O}$  and  $\text{H}_2\text{O}_2$ .

#### Discussion.

The reactions likely to occur in this system are presented in the following mechanism :



The ratio  $[\text{H}_2]/([\text{H}_2] + [\text{H}_2\text{O}_2])$  is both independent of oxygen and ROOR concentrations ; So :

- 1) Even if H is formed during decomposition of ROOR, it would be transformed into  $\text{HO}_2$  by reaction (6) and not into  $\text{H}_2$  by reaction (5), which presents a negligible rate as compared to that of reaction (6) [4] ;
- 2) The later observation rules out the possibility that H or  $\text{H}_2$  could arise from RO radicals, according to reactions (2), (4) and (7).
- 3) Finally, the temperature having no influence on the above ratio, the formation of H or  $\text{H}_2$  from RO radicals is also excluded ; the decomposition steps (4) and (7) should have high activation energies, whereas the competitive reaction (2) has a much lower one.

In conclusion, our results are in favor of the fact that the self-reaction of  $\text{HO}_2$  radicals occurs through 2 parallel pathways (3 a) and (3 b), which may be complex and indirect.



References.

- 1) Chemical Kinetics and Photochemical Data for Use in Stratospheric Modeling, NASA, JPL Publication July 1, 1985.
- 2) C.J. HOCHANADEL, J.A. GHORMLEY, P.J. OGREN, J. Chem. Phys., 56 (1972) 4426 ;  
C.J. HOCHANADEL, T.J. SWORSKI, P.J. OGREN, J. Phys. Chem., 84 (1980) 3274.
- 3) R.A. COX, J.P. BURROWS, J. Phys. Chem., 83 (1979) 2560.
- 4) K.A. SAHETCHIAN, R. RIGNY, A. HEISS, R.I. BEN-AIM , Chem. Phys. Lett., 87 (1982) 333 ;  
K.A. SAHETCHIAN, A. HEISS, R. RIGNY, J. Canad. Chim., 60 (1982) 2896.

## Reaction Mechanisms for Decomposition of Energetic Materials\*

Carl F. Melius and J. Stephen Binkley  
Sandia National Laboratories  
Livermore, California 94550

### Introduction

The mechanism for decomposition of energetic materials at the molecular level has been investigated theoretically using the BAC-MP4 quantum chemistry method. The BAC-MP4 method provides accurate thermochemical properties of molecular species, including radicals as well as stable species and can also determine the thermochemistry of transition state structures. We have applied this method to the decomposition of C- and N-nitro compounds.

### HONO Elimination

The initial step in the decomposition process is the unimolecular bond breaking of the molecule. The heats of formation  $\Delta H_f^\circ$  and free energies  $\Delta G_f^\circ$  of nitroethane ( $\text{CH}_3\text{CH}_2\text{NO}_2$ ) and methyl-nitramine ( $\text{CH}_3\text{NHNO}_2$ ) and their possible decomposition products as well as transition state structure complexes have been calculated. The important  $\Delta H_f^\circ$ 's and  $\Delta G_f^\circ$ 's are given in Table I. The results indicate that the weakest bond is that of the  $\text{NO}_2$  group, being 48 kcal-mol<sup>-1</sup> for methyl-nitramine and 58 kcal-mol<sup>-1</sup> for nitro-ethane. For both molecules, the five-centered elimination of HONO can occur, with an activation barrier of ~41 kcal-mol<sup>-1</sup> in both cases. For nitroethane, the resulting rate constant as a function of temperature for the five-centered HONO elimination



is given in the figure and is compared with various experimental data. As one can see from the figure, the agreement is excellent. At higher temperatures, direct C-N bond scission occurs



causing an increase in the decomposition rate constant.

### II Atom Catalyzed Decomposition

The resulting unimolecular rate constants for HONO elimination at 600K obtained from Table I are 0.0025 and 0.003 sec<sup>-1</sup> respectively for methyl-nitramine and nitroethane. While the nitroethane results are in excellent agreement with experiment, for methyl-nitramine, the rate constant is significantly smaller than the overall thermal decomposition rate constants measured for nitramines. This indicates that HONO elimination is not the rate determining step in the decomposition of nitramines, and that a more complicated, non-unimolecular

\*This work supported by the U.S. Department of Energy and the U.S. Department of Defense

process is controlling the thermal decomposition of nitramines. Initial bond scissioning of the nitro group, with an activation energy of  $\sim 48 \text{ kcal}\cdot\text{mol}^{-1}$ , leading to radical formation is therefore an important unimolecular mechanism and plays a more important role. (The larger bond strength in nitroethane of  $\sim 58 \text{ kcal}\cdot\text{mol}^{-1}$  causes the HONO elimination to be more important in nitroethane.) We therefore propose a new H atom assisted decomposition pathway to explain the experimental data. The reaction pathways for H atom attack on methylnitramine are shown in Figure 2. The BAC-MP4 results indicate that H atom can readily add to the nitro group to form an intermediate complex,  $\text{CH}_3\text{NIIN}(\text{O})\text{OH}$ , which can decompose either by OH elimination, HONO elimination, or by C-N bond scission.

### Internal Hindered Rotors

The proper treatment of hindered rotors is important in these decomposition processes since both the methyl group as well as the nearly free-rotor nitro group are constrained at the five-center elimination transition state. In order to extend the BAC-MP4 thermochemistry at 0 K to finite temperatures, it is necessary to include the effects of the temperature dependence of internal hindered rotors. We therefore have derived approximate analytical functions for the energy  $E_{\text{hr}}$ , the heat capacity  $C_{\text{hr}}$ , and entropy change  $\Delta S_{\text{hr}}$  for the internal hindered rotor. These expressions extend the analytic expressions derived by Pitzer and Gwinn for infinite moment of inertia with parameters chosen to approximately fit their tabulated data for finite moments of inertia. The resulting analytical expressions are given by

$$E_{\text{hr}} = RT (0.5 + Y - g(Y)) (x (e^x - 1)^{-1})$$

$$C_{\text{hr}} = R (0.5 + Y^2 - g(Y) - g(Y)^2) (x^2 e^x (e^x - 1)^{-2})$$

$$\Delta S_{\text{hr}} = R (\ln(SI_0) + Y - g(Y)) (z^2 e^z (e^z - 1)^{-2})$$

where

$$g(Y) = Y (S_1/SI_0), \quad S_1 = \text{Modified Bessel Function}$$

$$Y = V/RT, \quad x = (1.67/I_r) (V/RT)^{1/2}, \quad z = 3.8/I_r$$

$$V = \text{barrier height}, \quad I_r = \text{reduced moment of inertia}$$

The barrier heights are estimated from the Hartree-Fock scaled frequencies  $\nu$  by

$$V = (\nu/134n)^2 I_r$$

where  $n$  is the foldedness of the barrier. The constant was adjusted to give reasonable barrier heights for the methyl radical. This treatment of hindered rotors appears to work satisfactorily for the lowest frequency hinder rotor of a molecule but breaks down for multiple hindered rotors which are coupled, thereby mixing the frequencies as well as the axis of the reduced moments of inertia.

Table I. Calculated heats of formation  $\Delta H_f^\circ$  and free energies of formation  $\Delta G_f^\circ$  at various temperatures using the BAC-MP4 method for various molecular species and transition state activated complexes involved in the decomposition of methyl-nitramine and nitro-ethane. (Energy in kcal-mole<sup>-1</sup>, temperature in K.)

<u>Molecular species</u>	$\Delta H_f^\circ$		$\Delta G_f^\circ$			
	<u>0</u>	<u>300</u>	<u>300</u>	<u>600</u>	<u>1000</u>	<u>1500</u>
CH <sub>3</sub> NHNO <sub>2</sub>	6.2	1.5	26.2	51.9	86.9	130.3
CH <sub>3</sub> CH <sub>2</sub> NO <sub>2</sub>	-19.2	-24.2	-2.5	20.0	51.1	90.0
NO <sub>2</sub>	7.2	6.5	10.9	15.4	21.5	29.0
CH <sub>3</sub> NH	47.7	45.0	52.7	61.2	73.8	90.0
CH <sub>3</sub> CH <sub>2</sub>	31.7	29.0	34.3	40.5	50.1	62.8
HONO	-17.9	-19.5	-11.3	-2.9	8.6	22.7
CH <sub>2</sub> NH	23.9	21.9	26.7	31.9	39.9	50.3
CH <sub>2</sub> CH <sub>2</sub>	15.0	12.8	16.5	20.5	27.3	36.4
CH <sub>3</sub> NHNO <sub>2</sub>						
→ CH <sub>2</sub> NH + HONO	46.8	41.9	68.0	95.0	131.7	177.3
CH <sub>3</sub> CH <sub>2</sub> NO <sub>2</sub>						
→ C <sub>2</sub> H <sub>4</sub> + HONO	21.9	17.0	40.8	65.6	99.6	142.0
H <sub>2</sub> NN(O)OH						

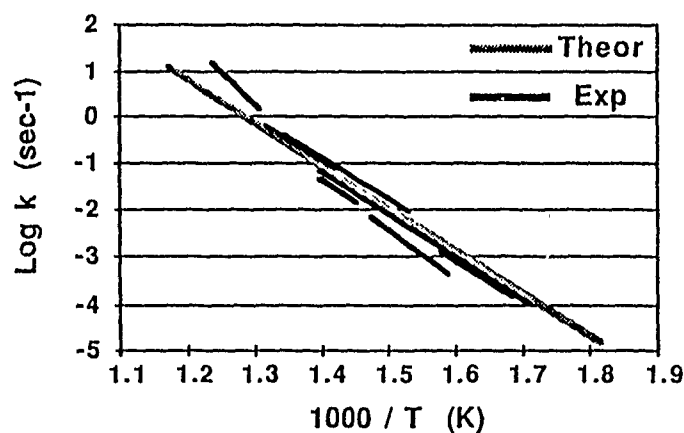


Figure 1. Rate constant for five-centered elimination of HONO from nitroethane. Shaded curve is calculated using BAC-MP4 thermochemistry. Solid curves are various experimental results.

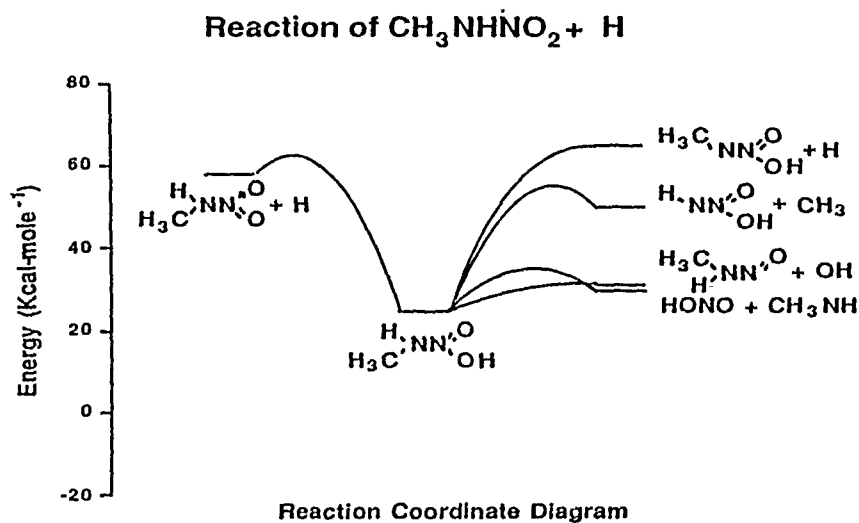


Figure 2. Calculated reaction pathways for the reaction of  $\text{CH}_3\text{NHNO}_2 + \text{H} \rightarrow$  products, based on BAC-MP4 heats of formation at 0K for stable and transition state activated complexes. Vertical energy scale in  $\text{kcal-mole}^{-1}$ .

The Pressure Dependent Decomposition of the Trifluoromethoxy  
Radical

by

L. Batt, M. MacKay, I.A.B. Reid\* and P. Stewart,

University of Aberdeen, Meston Walk, Aberdeen AB9 2UE, Scotland.

A re-examination of the decomposition of bis trifluoromethyl peroxide<sup>1</sup> allowed a value to be determined for the rate constant of the decomposition of the trifluoromethoxy radical over the temperature range 509 - 545K:



Excellent agreement was obtained from RRKM theory and experiment for the computer modelling of the pressure dependence of reaction (1) at 532.8K. The Arrhenius parameters under high pressure limiting conditions are given by:

$$\log[k_1(\infty)/\text{s}^{-1}] = 13.7 - (14300/2.303 T)$$

Some of the parameters for reaction (1) were then applied to the decomposition of the methoxy radical (2)



This led to a value for  $k_2(\infty)$  given by

$$\log[k_2(\infty)/\text{s}^{-1}] = 13.38 - (14450/2.303 T).$$

Reference

1. L. Batt and R. Walsh, Int. J. Chem. Kinet., 14, 933 (1982).

\* Present address: British Gas, London Research Station, Fulham, London, England.

# Synthesis and Pyrolysis of Perfluoroazo-2-propane

by

K.V. Scherer Jr., University of Southern California,  
Los Angeles, CA. 90089 -1062, U.S.A.

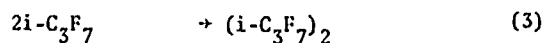
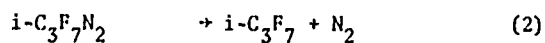
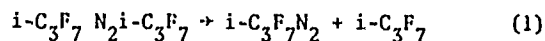
and

L. Batt and P. Stewart, University of Aberdeen,  
Aberdeen AB9 2UE, Scotland.

An improved method has been used to synthesise perfluoroazo-2-propane. Pyrolysis over the temperature range 450 -514K in a static system has been shown to be a homogeneous, first order process. No pressure dependence was observed in the presence of excess inert gas ( $\text{SF}_6$ ). The only products were nitrogen and perfluoro-2,3-dimethylbutane. The rate constant (k) for the decomposition process is given by:

$$\log(k/\text{s}^{-1}) = 16.74 \pm 0.20 - (22700 \pm 252/2.303 T)$$

These results lead to a straightforward mechanism for the decomposition process.



Comparison is made for results with other azo compounds.

# EXPERIMENTAL AND THEORETICAL STUDY OF THE ETHYL RADICAL UNIMOLECULAR DISSOCIATION

Y. SIMON, J.F. FOUCAUT and G. SCACCHI

Département de Chimie Physique des Réactions  
UA CNRS 328, INPL (ENSIC) et Université de Nancy I  
1, rue Grandville 54000 NANCY (France)

In the literature, the kinetic data on the unimolecular process of dissociation of ethyl radical are somewhat old [Lin and Back 1966 <sup>(1)</sup> ; Loucks and Laidler 1967 <sup>(2)</sup>] and rather scattered. We have considered it would be interesting to return to the study of this elementary reaction. The pyrolysis of  $C_2H_6$ , which includes it, had been studied in the following conditions : conventional static system, initial pressure between 1 and 300 torr, temperature between 793 and 813 K. The rate constant  $k$  is evaluated by the expression :  $k = \sqrt{2k_t} r_o^{C_2H_4} (r_o^{CH_4})^{-1/2}$  where  $r_o^{CH_4}$  and  $r_o^{C_2H_4}$  are the initial rates of formation of  $CH_4$  and  $C_2H_4$  and  $k_t$  the rate constant of the termination process ( $2 C_2H_5 \cdot$ ).

The experimental results (fall-off curves) are interpreted by the RRKM theory and two approaches of TROE.

## 1 - RRKM treatment.

We have used the R.R.K.M. program of R.G. Gilbert (Q.C.P.E. n° 460) <sup>(3)</sup>.

- chosen parameters for  $C_2H_5 \cdot$  radical : frequencies : 2995 (5), 1432 (4), 1037 (2), 988 (2), 540 (1) ; external symmetry number : 1 ; optical isomer : 1 ; internal rotation :  $B = 14.1 \text{ cm}^{-1}$  and internal symmetry number : 6.
- Details of the activated complex employed : frequencies : 3047 (4), 1466 (3), 1023 (2), 933 (3), 400 (2) ; external symmetry number : 1 ; optical isomer : 1.
- Other details : moments of inertia ratio : 1.14 to 1.20 (depending of T) ; collision diameter : 2.9 Å ; activation energy at 0K :  $E_0 = 38.8 \text{ kcal.mole}^{-1}$ .

These parameters give an excellent agreement between theoretical and experimental fall-off curves at any temperature. Arrhenius expressions for  $k_\infty$  and  $k_{bim}$  (the low pressure second order rate constant) can be derived (see further).



2 - First approach of TROE.

The modification of Kassel integral made by TROE <sup>(4)</sup> leads to the following expression :

$$I = \frac{k_{uni}}{k_{\infty}} = \frac{1}{\Gamma(S_K)} \cdot \int_{x=0}^{\infty} \frac{x^{S_K-1} \exp(-x) dx}{1 + \frac{k_{\infty}}{k_0} I_0(S_K, B_K) \left(\frac{x}{x+B_K}\right)^{S_K-1}}$$

$$\text{with } I_0(S_K, B_K) = \frac{1}{\Gamma(S_K)} \int_{x=0}^{\infty} (x+B_K)^{S_K-1} \exp(-x) dx \text{ and } k_0 = k_{bim} P$$

The "effective" values  $S_K$  and  $B_K$  of Kassel parameters  $S$  and  $B$  are estimated from the 15 frequencies of  $C_2H_5$ . [14 frequencies of RRKM theory +  $350 \text{ cm}^{-1}$  instead of internal rotation] and  $E_0 = 40.0 \text{ kcal.mole}^{-1}$ .

The method of determination of  $k_{\infty}$  and  $k_{bim}$  is the following one :

the theoretical curve :  $\log I$  vs  $\log \left( \frac{k_{bim} P}{k_{\infty}} \right) - \log I$  can be rewritten :

$\log k_{uni} - \log k_{\infty}$  vs  $\log P - \log k_{uni} + \log k_{bim}$  and can be derived from the experimental curve :  $\log k_{uni}$  vs  $\log P - \log k_{uni}$  by two translations leading to  $k_{\infty}$  and  $k_{bim}$  (least square method). The fitting between the two curves is very good and allows us to propose Arrhenius expressions for  $k_{\infty}$  and  $k_{bim}$ .

3 - Second theoretical approach of TROE.

The Lindemann-Hinshelwood theory leads to the "switching function"

$F_{LH}$  :

$$\frac{k_{uni}}{k_{\infty}} = \frac{x}{1+x} = F_{LH}(x) \quad \text{with } x = \frac{k_0}{k_{\infty}} = \frac{k_{bim} P}{k_{\infty}}$$

TROE <sup>(5)</sup> has shown that realistic reduced fall-off curves can be represented well by adding a broadening factor  $F(x)$  to the above expression :

$$\frac{k_{uni}}{k_{\infty}} = \frac{x}{1+x} F(x) \quad \text{with } \log F(x) = \frac{\log F_{cent}}{1 + \left( \frac{\log x}{0.75 - 1.27 \log F_{cent}} \right)^2}$$

$F_{cent}$  is evaluated from the effective parameters  $S_K$  and  $B_K$  and the collisional deactivating efficiency  $\beta_c$ .

To present experimental and theoretical results in  $\log \frac{k_{uni}}{k_{\infty}}$  vs  $\log P$  scales it is necessary to have transformed  $P$  into  $x$  :  $k_{\infty}$  can be evaluated by any extrapolation method and  $k_{bim}$  by an expression, proposed by TROE, which is a product of different factors calculable from parameters relative to reactant radical.

Chosen parameters : frequencies (those of RRKM) ;  $E_0 = 40.0 \text{ kcal.mole}^{-1}$  ; collision diameter  $4.4 \text{ \AA}$  ; number of oscillators : 14 ; number of internal rotations : 1 ; number of oscillators which disappear during the reaction : 3 ; moment of inertia ratio : 1.14 to 1.20 ; Lennard-Jones interaction energies  $c = 1.79 \times 10^3 \text{ J.mole}^{-1}$  ; average energy transferred per collision :  $\langle \Delta E \rangle = 10 \text{ KJ.mole}^{-1}$ .

The theoretical fall-off curve calculated a priori from the above expressions do not fit very well with the "experimental" points  $\log \frac{k_{uni}}{k_\infty}$  vs  $\log P$ . By a method of trial and error we have successively modified the values of  $k_\infty$  and  $k_{bim}$  until we obtained the best agreement. Again the fitting is excellent at any temperature and we can deduce Arrhenius expressions for  $k_\infty$  and  $k_{bim}$ .

#### 4 - Best Arrhenius expressions for $k_\infty$ and $k_{bim}$ .

Taking into account the thermochemistry, the best Arrhenius expressions for  $k_\infty$  and  $k_{bim}$  are obtained by RRKM method :

$$k_\infty = 10^{14} \exp \left( - \frac{41\,000}{RT} \right) \text{ s}^{-1} \text{ and } k_{bim} = 10^{18.3} \exp \left( - \frac{34\,900}{RT} \right) \text{ cm}^3 \text{ mole}^{-1} \text{ s}^{-1}.$$

The best RRKM treatment in the literature is that of Lin and Laidler <sup>(6)</sup> on the experimental results of Lin and Back and Loucks and Laidler :  $k_\infty = 10^{14.5} \exp \left( - \frac{41\,100}{RT} \right) \text{ s}^{-1}$  and  $k_{bim} = 10^{18.54} \exp \left( - \frac{34\,600}{RT} \right) \text{ cm}^3 \text{ mole}^{-1} \text{ s}^{-1}$ , in very good agreement with our work. The study of Michael and Suess <sup>(7)</sup> leads to  $E_\infty = 44\,500 \text{ cal.mole}^{-1}$  which is undoubtedly too high.

<sup>(1)</sup> M.C. LIN and M.H. BACK - Canad. J. Chem., 44, 2357 (1966).

<sup>(2)</sup> L.F. LOUCKS and K.J. LAIDLER - Canad. J. Chem., 45, 2795 (1967).

<sup>(3)</sup> R.G. GILBERT - Program QCPE n° 460.

<sup>(4)</sup> for example : J. TROE, Ber. Bunsenges. Phys. Chem., 78, 472 (1974).

<sup>(5)</sup> for example : W.C. GARDINER Jr and J. TROE - Chap. 4 in "Combustion Chemistry" - W.C. GARDINER Ed., Springer Verlag (1984).

<sup>(6)</sup> M.C. LIN and K.J. LAIDLER - Trans. Faraday Soc., 64, 79 (1968).

<sup>(7)</sup> J.V. MICHAEL and G.N. SUESS - J. Chem. Phys., 58, 2807 (1973).

THE PHOTOCHEMICAL AND THERMAL DECOMPOSITION OF SOME  
SIMPLE  $\alpha$ -DICARBONYL COMPOUNDS IN THE GAS PHASE

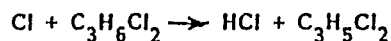
R.A. Back,  
Division of Chemistry,  
National Research Council of Canada.

Recent studies are described of the photochemical and thermal decomposition of a number of simple  $\alpha$ -dicarbonyl compounds in the gas phase, including glyoxal (cis and trans), oxalic acid, glyoxylic acid, pyruvic acid, 1,2-cyclobutanedione, and 1,2-dimethyl-cyclobutene-3,4-dione. A variety of mechanisms of decomposition is observed; where it is possible, internal transfer of H is the preferred path, in other cases concerted molecular decomposition occurs. Rate constants and Arrhenius parameters are presented for the thermal reactions, and mechanisms are discussed and compared for both the thermal and the photochemical decompositions.

## UV-Laser Induced Decomposition of 1,2-Dichloropropane

M. Schneider, R. Weller, J. Wolfrum  
Physikalisch-Chemisches Institut  
Universität Heidelberg

The thermal dehydrochlorination of 1,2-dichloropropane is known to run predominantly by unimolecular four-center elimination leading to a characteristic pattern of the product distribution (3-chloropropene, cis-1-chloropropene, trans-1-chloropropene, 2-chloropropene). 2-chloropropene is only a minor product while the cis/trans ratio of 1-chloropropene is much higher than unity. We were interested in the alternative radical chain process which is strongly inhibited by the products. The experiments were carried out at temperatures between 570 and 670K using an excimer laser (XeCl,  $\lambda = 308\text{nm}$ , 400mJ/ pulse, 80Hz maximum repetition rate) to start the chain by photolysis of the substrate. At low conversion the quantum yield was in the order of one hundred but decreased drastically with formation of the chloropropenes. From the product distribution it was possible to deduce the relative abstraction rates of the reaction



at the three differently substituted carbon atoms. In contrast to the thermal reaction 2-chloropropene is the main product, but the cis/trans ratio of 1-chloropropene remains high. The results are compared with other dehydrochlorination reactions and a computer model in order to simulate inhibition effects.

## The Thermal Decomposition of Unsymmetrical Dimethylhydrazine

K. Brezinsky and F.L. Dryer  
Princeton University  
Princeton, N.J. 08544, U.S.A.

D. Schmitt and D. Lourme  
Office National d'Etudes et de Recherches Aeronautiques  
92320 Chatillon, France

A short study of unsymmetrical dimethylhydrazine (UDMH) decomposition in the Princeton flow reactor in the temperature range 761-799K and at one atmosphere indicates that the overall conversion of UDMH to products proceeds through the initial formation of formaldehyde dimethyl hydrazone (FDH) with subsequent decomposition of FDH into smaller products. This sequence has not been observed and reported before in any of the published high temperature studies of UDMH decomposition. However, the present observations are the only existent direct measurements of intermediates formed as a function of extent of reaction, and the UDMH conversion to FDH is so rapid as to have been missed in previous studies. The conversion to FDH proceeds isoergically, i.e. without overall chemical energy release. Heat release in the UDMH decomposition appears to occur from the subsequent decomposition of UDMH into smaller products.

Using three flow reactor experiments at three different initial temperatures and the same initial UDMH concentration a first order rate constant for the conversion process to FDH has been generated. A series of three flow reactor experiments at the same temperature but different initial concentrations of UDMH has indicated that the decomposition is very near first order. The Arrhenius rate parameters developed and the experimentally observed first order nature of the reaction have been used in calculation of UDMH droplet burning characteristics.

# Oxidation of formaldehyde at low oxygen concentration.

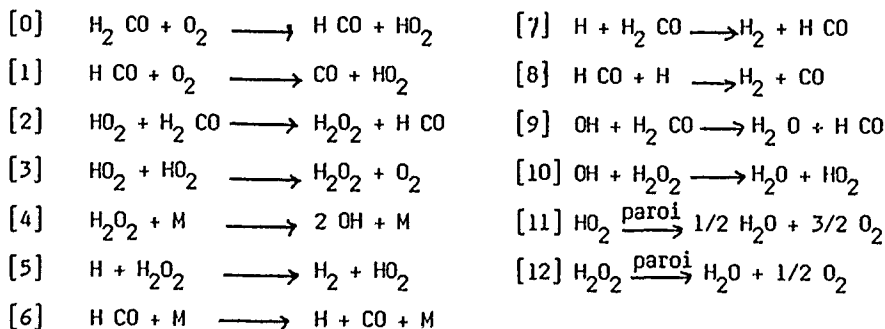
M. VANPEE\*, K. SAHETCHIAN<sup>x</sup>, V. VIOSSAT<sup>x</sup>, J. CHAMBOUX<sup>x</sup>.

\* Department of chemical Engineering, Universty of Massasuchetts, Amherst, Ma. 01003.

<sup>x</sup> Laboratoire de Chimie Générale, Université P. et M. Curie C.N.R.S. UA 40870, 4 Place Jussieu, 75252 PARIS CEDEX 05.

One of the authors studied the slow oxidation of formaldehyde at temperature about 400°C in pyrex vessels treated with acid boric and in untreated vessels (1-2). When CH<sub>2</sub>O/O<sub>2</sub> mixtures contain low oxygen amount, a clear break is observed in the course of the reaction when oxygen consumption is complete. Until this moment the behaviour of the curves (CO formation, pressure change and temperature) is the same as those for mixtures containing higher oxygen amounts. After the break, the CO formation rate increases, the hydrogen begins to appear with a rate similar to CO one ; a break is also observed on the pressure change curve, and at the same time, the temperature falls abruptly (fig. 1-2).

From the scheme proposed :



The observations can be interpreted by the existence of two distinct mechanisms. In the presence of oxygen the reactions 0 → 5 and 9 → 12 occur involving HO<sub>2</sub> and H<sub>2</sub>O<sub>2</sub> ; the reaction is a degenerated branching reaction with homogeneous and heterogeneous terminations : reactions 11 and 12 have to be included to obtain a good agreement with experimental pressure change

curves. In the second mechanism, in absence of oxygen, the reaction may be considered as a linear chain reaction with formation of CO and  $H_2$  (réactions  $4 \rightarrow 12$ ).

From the proposed mechanism, simulated curves ( $CH_2O$ ,  $O_2$ , CO,  $H_2$ ,  $H_2O$ ,  $H_2O_2$  evolution, pressure change, temperature) have been obtained with computer (fig. 3). The rate constants for reactions  $0 \rightarrow 10$  are the recommended values of literature (3-8),  $k_{11}$  and  $k_{12}$  are "fitted" according to experimental conditions.

The agreement with experimental curves is good for different conditions of temperature, mixture richness, wall treatment.

#### Bibliographie.

- (1) M. VANPEE Bull. Soc. Chim. Belge, 62, 1953, 285.
- (2) M. VANPEE Thèse - Louvain (Belgique) 1956.
- (3) K. SAHETCHIAN and col. Int. J. of Chem. Kin. Vol VII, 1975, 23.
- (4) J. PETERS, G. MAHNEN, 14<sup>th</sup> symposium (International) on combustion. The combustion Institute, Pittsburgh, 1973, 133.
- (5) C.K. WESTBROOK Combustion Science Technology 20 (5), 1979.
- (6) D.L. BAULCH and col. Evaluated Kinetic Data for high temperature reactions. Butterworths London, 1972, vol. I.
- (7) A. FONTIJN, M.A. CLYNE. Reactions of small transient species. Academic Press, 1983.
- (8) Chemical kinetics and photochemical data for use in stratospheric modeling, NASA, 1985, J.P.L. publication 85-37, C.I.T., Pasadena California.

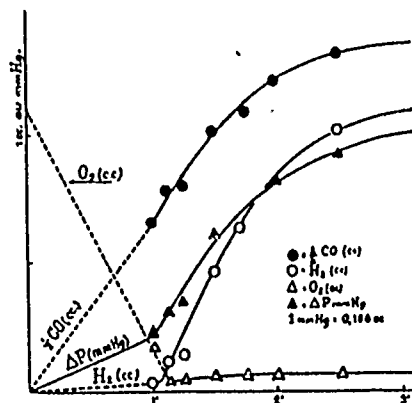


Fig. 1 — Analyse des produits de la réaction du mélange 8,7 mm  $O_2$  + 44,3 mm  $CH_2O$  à  $870^\circ C$ . Chambre de réaction pyrex :  $\phi$  : 4,6 cm, longueur 20 cm. Les quantités de gaz sont exprimées en cc ramené à  $0^\circ C$  et 760 mm Hg. La pression est exprimée en mm Hg à la température de  $870^\circ C$ .

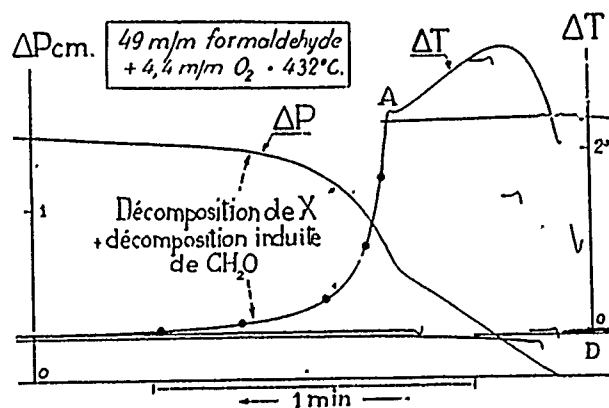


Fig. 2. — Combustion du mélange  $11CH_2O + 1 O_2$  ( $CH_2O$ ) : 40 mm Hg — ( $O_2$ ) : 4,4 mm Hg —  $T$  :  $432^\circ C$ .  $\Delta T$  et  $\Delta P$  : courbes expérimentales.

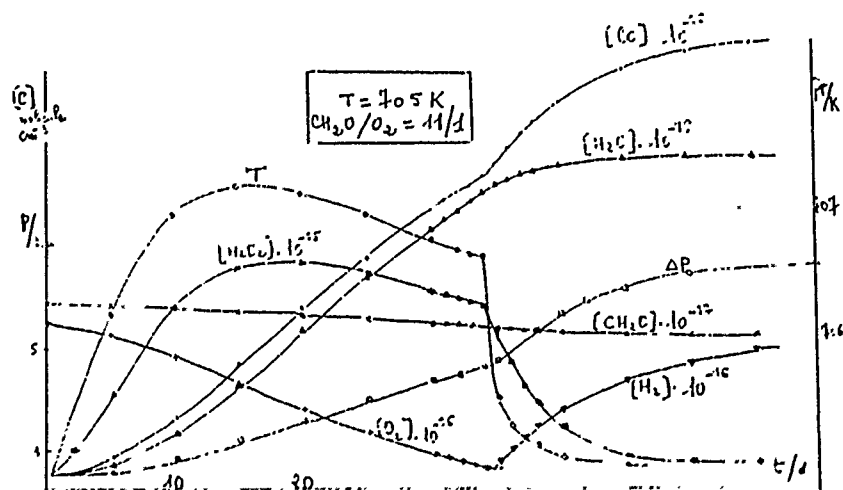


Fig. 3 — Combustion calculée



## PSEUDOFAME FRONT FOR METHANE IN A LEAN METHANE AIR MIXTURE

Marcel Vanpee  
Chemical Engineering Department  
University of Massachusetts  
Amherst, MA 01003

This paper deals with the ignition phenomena observed when a hot laminar jet of inert gases is injected into an air fuel combustible mixture. The paper concentrates especially on the air methane mixtures where a special and interesting phenomenon has been observed.

The normal ignition process is a series of reactions in the center of the jet which produce enough heat to prevent the lowering of the jet temperature owing to heat losses by conduction. A luminous column always precedes the actual ignition.

Methane does not follow this normal ignition process. Figure 1 shows that the ignition diagram is quite different from a normal one. First there is no preignition glow region. The region where no luminosity is observed changes abruptly to the point where the column branches into explosion. Secondly the limit of ignition no longer has a minimum in the flammable range but continuously decreases with decreasing concentration of methane and is prolonged to the lean side by a curve which limits a new zone. In this zone a luminous region of special shape appears in the jet. This luminous zone is shown in Figure 1. Unlike the usual preignition glow, this glow has sharp edges. The glow is strongest not at the axis of the jet but at its outside boundary, giving the impression of an inverted flame front with its apex anchored at the center of the jet. The analogy of this pseudoflame with a true flame is superficial since the luminous reaction zone is self-propagating only under the critical conditions of the experiment.

In order to get insight into the pseudoflame phenomenon, radial and longitudinal concentrations and temperature profiles were taken within the

jet. These profiles demonstrated that the luminous zone is a zone of fast reaction and that no reaction at all occurs in the dark zones. To explain the sharpness of the transition between these two zone, a branching chain mechanism is postulated and the boundary between the two zone is interpreted as being the geometrical locus where the branching probability ( $\alpha$ ) of the chain reactions equals the probability ( $\beta$ ) of rupture:  $\alpha = \beta$  (1)

If this locus and the temperature and concentration field are known, equation (1) can be expressed in terms of concentration and temperature alone. This program was carried out experimentally and led for equation (1) to the following expression:

$$\frac{[O_2]}{[CH_4]} = k \exp E/RT \quad (2)$$

with  $E = 40,000$  cal/mole and  $k = 4.2 \times 10^{-6}$ .

In terms of a branching chain mechanism, equation (2) indicates that the oxygen molecule is in the branching chain process. Methane acts in the opposite direction and therefore would be associated with the chain breaking process. These opposite effects of the oxygen and methane molecules are illustrated by a simple experiment. If the temperature of the jet is raised and if the methane and oxygen concentration, remain unchanged, the reaction zone moves upstream in the jet. The same effect is found if the temperature of the jet is maintained constant but if the oxygen concentration is progressively raised by changing the oxygen index of the outside atmosphere. If, however, the oxygen index is maintained constant but the methane concentration raised, the reaction zone moves downstream.

This experiment shows clearly the inhibiting properties of methane on its own combustion. A search for a reaction mechanism is underway.

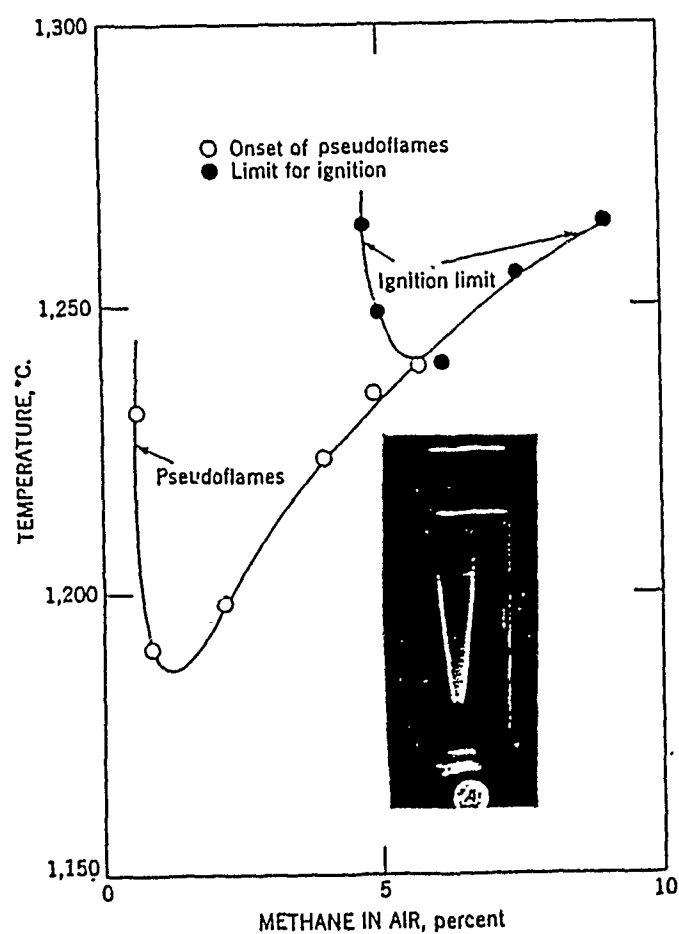


FIGURE 1. Ignition of Methane Air Mixtures by Hot Nitrogen. Jet diameter 17 mm. A: Pseudoflame in a Jet of Hot Nitrogen Flowing Into a Lean Mixture of Methane Air.

DILUTE HYDROCARBON OXIDATION IN THE PRESENCE OF THE  
CO/H<sub>2</sub>O/O<sub>2</sub> REACTION BETWEEN 960-1250 K AT 1 ATM

R.A. Yetter and F.L. Dryer

Department of Mechanical and Aerospace Engineering

Princeton University

Princeton, NJ 08544

The carbon monoxide - hydrogen - oxygen reaction, seeded with small quantities of hydrocarbons, is studied to yield information on specific elementary reaction rates and on general mechanistic behavior of the overall reaction. Experiments are conducted in an atmospheric flow reactor between 960 and 1250 K from which stable species concentrations and temperature profiles are obtained as a function of flow reactor position (or equivalently, time). Detailed modeling calculations and sensitivity analysis techniques are used to guide and analyze the experiments. The carbon monoxide reaction is used to produce a controllable bath of H, O, and OH radicals in large concentrations with which the hydrocarbon can interact. The reaction chemistry of the hydrocarbon is studied by evaluating the disappearance profiles of the hydrocarbon and its relations to and perturbations of the reacting bath characteristics. In particular, the elementary reactions of hydroxyl radical with methane and with propene were studied at 1020 K and values for the specific rate constants of  $k_{\text{CH}_4+\text{OH}} = 1.6 \times 10^{12} \text{ cm}^3 \text{ molec}^{-1} \text{ s}^{-1}$  and  $k_{\text{C}_3\text{H}_6+\text{OH}} = 8.0 \times 10^{12} \text{ cm}^3 \text{ molec}^{-1} \text{ s}^{-1}$  were obtained. The value for the  $\text{CH}_4 + \text{OH}$

rate constant is in good agreement with current literature values (e.g., Madronich, S. and Felder, W., Twentieth Symposium (International) on Combustion, 1984). Rate data for direct comparison with the measured  $C_3H_6 + OH$  rate constant is unavailable; however, the present value is in agreement with the high pressure rate constant theoretically predicted by Smith et al. (Smith, G.P., Fairchild, P.W., Jeffries, J.B., and Crosley, D.R., J. Chem. Phys. 89, 1985). The technique is presently being applied to the reaction of ethyl radicals with molecular oxygen and the ethyl thermal decomposition reaction.

KINETIC AND CHEMICAL STUDY OF THE GAS-PHASE  
OXIDATION OF ISOBUTANE AND PROPANE

by B. VOGIN, G. SCACCHI and F. BARONNET

Département de Chimie-Physique des Réactions, U.A. 328 CNRS  
INPL-ENSIC, 1, rue Grandville - F 54042 NANCY France

Despite a large number of investigations of the mechanism of gas-phase oxidations (especially of alkanes), some problems have remained unresolved. They are mentioned in a paper published a few years ago by S.W. BENSON and P.S. NANGIA (<sup>1</sup>). Among these problems, there are still controversies about the free radical mechanism, especially the reactions of HO<sub>2</sub> and the role of OH as chain carrier, the self reactions of RO<sub>2</sub>, the initiation reactions and the isomerisation steps of RO<sub>2</sub>. There is also a general lack of reliable rate data for the elementary steps and this seems to justify further experimental investigations.

The slow oxidation of light alkanes (from C<sub>2</sub> to C<sub>5</sub>) have been so far accounted for by two theoretical reaction schemes :  
- a mechanism developed by FISH and co-workers (<sup>2</sup>) emphasizing the role of the isomerisation reactions of alkylperoxy radicals RO<sub>2</sub> ;  
- the olefinic theory proposed by KNOX (<sup>3</sup>) ; according to this theory, the conjugate olefin is the dominant reaction product, up to 80 % ; the reaction products come from the subsequent reactions of the olefin.

FISH (<sup>2</sup>) tried to unify these two theories into a single general mechanism. However, the elementary steps have to be described in more detail ; it is not obvious that the oxidation of light alkanes is a purely homogeneous reactions and it is sometimes suggested that the olefin formation might be heterogeneous.

In order to contribute to a better knowledge of the oxidation mechanism of light alkanes, we have studied the slow oxidation of isobutane and propane at slow extents of reaction, at subatmospheric pressures, in the temperature range 300-350°C, in a static reaction vessel made of Pyrex. For each reaction, the major primary products are identified and measured by GLC after expansion and quenching in a sampling bulb. Trace amounts of peroxides are measured by chemiluminescence (<sup>4</sup>).

In the case of the slow oxidation of isobutane, the primary products of the reaction are : isobutene, isobutene oxide, propene, formaldehyde, propionaldehyde and acetone, peroxides and water. The product distribution is given in Table I.

DISTRIBUTION OF THE REACTION PRODUCTS EXTRAPOLATED AT ZERO TIME  
(H<sub>2</sub>O<sub>2</sub>, H<sub>2</sub>O AND CO<sub>2</sub> EXCLUDED)

PROPANE	C <sub>3</sub> H <sub>8</sub>	CH <sub>3</sub> CHO	HCHO	CH <sub>3</sub> -CH-CH <sub>2</sub>   O	C <sub>2</sub> H <sub>4</sub>	CH <sub>2</sub> -CH <sub>2</sub>   CH <sub>2</sub> -O	C <sub>2</sub> H <sub>5</sub> CHO	
% PRODUCTS	72.2	14.5	9.3	3.3	0.7	c	0	100 %
ISOBUTANE	C <sub>4</sub> H <sub>10</sub>	C <sub>2</sub> H <sub>5</sub> CHO CH <sub>3</sub> COCH <sub>3</sub>	HCHO	CH <sub>3</sub> -C-CH <sub>2</sub>   O	C <sub>3</sub> H <sub>6</sub>	CH <sub>3</sub> -CH <sub>2</sub> -CH <sub>2</sub>   CH <sub>2</sub> -O	CH <sub>3</sub> -CH-CHO   CH <sub>3</sub>	
% PRODUCTS	67.3	12.3 / 5.8	9.5	2.4	2.7	not measured	0	100 %

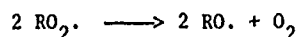
Table I

Taking into account these products and the present knowledge of radical oxidation reactions, we are able to put forward a radical scheme accounting for the formation of these products. Since, as mentioned before, there are not enough experimental rate data for these radical steps, we have estimated the Arrhenius parameters of nearly all these elementary steps by the methods of Thermochemical Kinetics proposed by BENSON<sup>(5)</sup>. The calculated values obtained in our experimental conditions have been compared to our experimental results. The agreement is generally good and the following results have been obtained :

- the chief primary product (67 %, see Table I) is isobutene and there is a parallel formation of isobutene oxide. An outline of the corresponding reaction scheme is given in figure 1. Our results are compatible, taking

into account the estimates of the rate constants, with a negligible direct route for olefin formation and also a negligible heterogeneous formation of the conjugate olefin ;

- ketones (acetone) and aldehydes (acetaldehyde) come from alkoxy radicals  $RO\cdot$ , probably formed by the disproportionation of peroxy radicals  $RO_2\cdot$ .



- the small quantities of peroxides (hydrogen peroxide, hydroperoxides) are formed by hydrogen transfer reactions of  $HO_2\cdot$  and  $RO_2\cdot$  radicals ;

- water comes from the hydrogen transfer reactions of hydroxyl radicals which become important chain carriers in the early stages of the reaction ; an accurate measurement of water formation is rather difficult to perform.

The detailed reaction mechanism and the corresponding rate constants will be given in the poster.

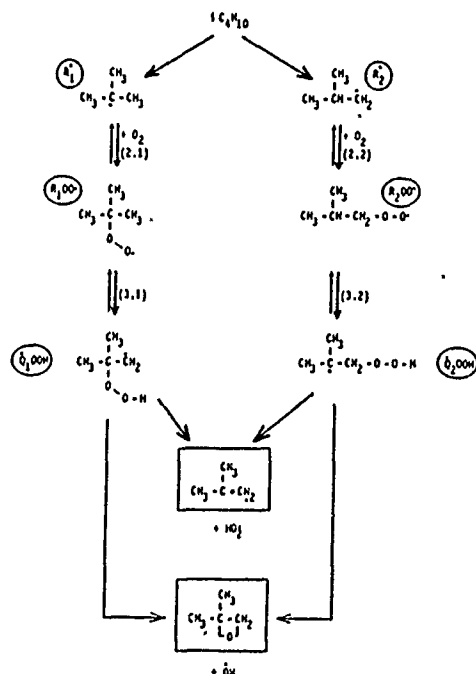


Fig. 1

Since experimental errors cannot be completely excluded and because the methods of Thermochemical Kinetics only give estimates of the rate constants, we have thought that it might be interesting to study another example according to the same methods ; we have chosen the oxidation of propane.

The slow oxidation of propane yields the following primary products: propene, propene oxide, ethylene, formaldehyde, acetaldehyde, peroxides, water and trace amounts of oxetane (trimethylene oxide). The distribution of the reaction products is given in Table I.

At first sight, it appears that the products are very similar to those obtained in the case of isobutane oxidation, which suggests that the two reactions have a substantial number of common features.

Propene is the largely dominant reaction product (72 %, see Table I) and its formation is mainly due to the decomposition of the isomerised alkyl peroxy radical ; the propene fraction due to heterogeneous steps can be neglected. There is also a parallel formation of propene oxide. Here again, the aldehydes (acetaldehyde and formaldehyde) come from the decomposition of alkoxy radicals. The substantial amounts of water are accounted for by the reaction of OH.

In this case again, we have built the proposed reaction scheme from the product distribution and estimated the corresponding rate constants by the methods of Thermochemical Kinetics.

These parallel experimental investigations of the slow oxidations of isobutane and propane show that both reactions can be described by a single reaction mechanism. The only difference consists in the numerical value of the rate constants for the elementary steps. From a mechanistic point of view, our results, corroborated by Thermochemical Kinetics calculations, show the importance of the isomerisation steps of alkyl peroxy radicals by intramolecular hydrogen abstraction. These steps are necessary if we want to account for the product distribution.

The present work stresses the role of Thermochemical Kinetics to identify the major kinetic steps in a complex reaction mechanism.

#### References

- (<sup>1</sup>) S.W. BENSON and P.S. NANGIA - Acc. Chem. Res., 12, 223 (1979).
- (<sup>2</sup>) A. FISH - Oxidation of organic compounds, vol.2, Advances in Chemistry Series, ACS, 76, 69 (1968).
- (<sup>3</sup>) J.H. KNOX - in Photochemistry and Reaction Kinetics (Editors : P.G. ASHMORE, T.M. SUGDEN and F.S. DAINTON), Cambridge University Press, Cambridge, 250 (1967).
- (<sup>4</sup>) B. VOGIN, F. BARONNET and J.C. ANDRE - Analytica Chimica Acta, 142, 293 (1982).
- (<sup>5</sup>) S.W. BENSON - Thermochemical Kinetics, 2<sup>nd</sup> ed., John Wiley, New-York (1976).



A SIMPLIFIED CHEMICAL KINETIC REACTION MECHANISM  
FOR PROPANE OXIDATION

A.Y. ABDALLA\*, J.C. BOETTNER, M. CATHONNET, P. DAGAUT, F. GAILLARD

C.N.R.S., Centre de Recherches sur la Chimie de la Combustion  
et des Hautes Températures, 45071 Orléans-Cedex, France.

The provision of a realistic accurate chemical mechanism is essential for the successful modelling of the combustion processes. The use of simplified schemes, yet still reproduce experimental data over wide ranges of operating conditions, recently has been recommended as a practicable approach (1, 2).

A simplified kinetic mechanism for the oxidation of propane was proposed. The mechanism was built up by eliminating the unimportant reactions from a comprehensive chemical kinetic reaction mechanism for the oxidation of propane (3). The elimination was based on calculating the percentage contribution of an elementary reaction to the total net rate of formation or consumption of a species. If the percentage contribution of a reaction was less than 5% over the whole working temperature range, that reaction was eliminated. The elimination process was carried out for equivalence ratios varied between 0.6-1.5.

However, it was possible to form the simplified mechanism from 23 chemical species and 55 elementary reactions instead of 41 chemical species and 168 elementary reactions in the case of the comprehensive mechanism. The simplified mechanism and the used rate coefficients in the present work are given in Table 1. Reverse reaction rates have been calculated from the equilibrium constants computed from thermodynamical data (4). In the mechanism, the propane is assumed to decompose and react thermally to form lower-molecular intermediate hydrocarbon followed by the reaction and oxidation of these intermediates to final products.

A numerical simulation to simulate the condition behind the reflected shock wave was carried out. Then, the mechanism was used to reproduce the experimental results, ignition delay time, obtained from the shock

\* On leave from Zagazig University, Egypt.

Table(1): Simplified Mechanism for Propane Oxidation , Reaction Rate Coefficients ( $\text{cm}^3 \cdot \text{mol}^{-1} \cdot \text{s}^{-1} \cdot \text{K}^{-1}$ ) and Sensitivity Coefficients

no.	Reaction						A	n	E	Reference	S
1-	H	H	INNER	H2	INNER		+.6396E+18	-1.0	+0.00	WARNA.84	-2.884
2-	H	HO2		H2	O2		+.2500E+14	+0.0	+0.69	WARNA.84	-2.884
3-	H	HO2		OH	OH		+.1500E+15	+0.0	+1.00	WARNA.84	-2.142
4-	H	OH	INNER	H2O	INNER		+.7595E+22	-2.0	+0.00	WARNA.84	-2.142
5-	O	H2		OH	H		+.1500E+08	+2.0	+7.55	WARNA.84	-2.237
6-	HO2	HO2		H2O2	O2		+.2000E+13	+0.0	+0.00	WARNA.84	-1.675
7-	H	O2	INNER	HO2	INNER		+.7875E+16	+0.0	+0.00	HACK .77	-2.884
8-	H	O2		OH	O		+.2200E+15	+0.0	+16.80	BAULC.73	-0.168
9-	H2O2	OH		H2O	HO2		+.7000E+13	+0.0	+1.43	WARNA.84	-3.315
10-	H2O2	INNER		OH	OH	INNER	+.1050E+18	+0.0	+45.41	BAULC.73	-2.884
11-	H2O2	H		H2	HO2		+.1700E+13	+0.0	+3.75	BAULC.73	-2.142
12-	HO2	O		OH	O2		+.2000E+14	+0.0	+0.00	WARNA.84	-2.884
13-	H2	OH		H2O	H		+.1000E+09	+1.6	+3.30	WARNA.84	-2.884
14-	H2O	O		OH	OH		+.1500E+11	+1.14	+17.26	WARNA.84	-2.884
15-	HO2	OH		H2O	O2		+.2000E+14	+0.0	+0.00	WARNA.84	-2.142
16-	O	O	INNER	O2	INNER		+.0997E+18	-1.0	+0.00	WARNA.84	-2.884
17-	O	H	INNER	OH	INNER		+.5425E+17	-0.6	+0.00	DIX L.81	-2.884
18-	CO	HO2		CO2	OH		+.1750E+15	+0.0	+23.60	BAULC.76	-2.884
19-	CO	OH		CO2	H		+.6220E+07	+1.5	-0.74	WARNA.84	-2.998
20-	HCO	O2		CO	HO2		+.3300E+14	-0.4	+0.00	VEYRE.81	-1.998
21-	HCO	INNER		H	CO	INNER	+.2500E+15	+0.0	+16.80	WARNA.84	-2.454
22-	HCO	OH		CO	H2O		+.5000E+14	+0.0	+0.00	WARNA.84	-2.112
23-	HCO	H		CO	H2		+.2000E+15	+0.0	+0.00	WARNA.84	-2.454
24-	HCO	O		CO	OH		+.3000E+14	+0.0	+0.00	WARNA.84	-1.897
25-	CH4	INNER		CH3	H	INNER	+.3200E+18	+0.0	+88.43	WARNA.84	-2.237
26-	CH4	OH		CH3	H2O		+.1090E+06	+2.14	+2.11	COHEN.83	-2.136
27-	CH3	O		CH2O	H		+.7000E+14	+0.0	+0.00	WARNA.84	-2.884
28-	CH2O	OH		HCO	H2O		+.3000E+14	+0.0	+1.20	WARNA.84	-2.884
29-	CH2O	H		HCO	H2		+.2500E+14	+0.0	+3.99	WARNA.84	-2.884
30-	CH2O	O		HCO	OH		+.3500E+14	+0.0	+3.51	WARNA.84	-2.202
31-	CH2O	HO2		HCO	H2O2		+.1300E+13	+0.0	+8.00	LLOYD.74	-0.959
32-	C2H6	OH		C2H5	H2O		+.8700E+10	+1.05	+1.81	TULLY.84	-2.884
33-	CH3	CH3		C2H6			+.24100E15	-0.40	0.00	WARNA.84	-2.884
34-	C2H5	O2		C2H4	HO2		+.2000E+13	+0.0	+5.00	WARNA.84	-2.884
35-	C2H4	OH		C2H3	H2O		+.3000E+14	+0.0	+2.99	WARNA.84	-0.836
36-	C2H4	OH		CH3	CH2O		+.1750E+13	+0.0	+0.96	WESTB.83	-2.884
37-	C2H3			C2H2	H		+.1600E+15	+0.0	+37.80	WARNA.84	-2.884
38-	C2H3	O2		CH2O	HCO		+.4000E+13	+0.0	-0.25	GUTHA.84	-2.884
39-	C2H2	O2		HCO	HCO		+.4000E+13	+0.0	+28.00	GARDI.68	-2.884
40-	C3H8			C2H5	CH3		+.1700E+17	+0.0	+84.84	WESTB.84	-0.335
41-	C3H8	OH		NC3H7	H2O		+.1026E+03	+2.61	+0.331	COHEN.82	-0.701
42-	C3H8	OH		IC3H7	H2O		+.1074E+02	+2.71	-1.438	COHEN.82	-0.701
43-	C3H8	HO2		NC3H7	H2O2		+.1120E+14	+0.0	+19.40	WESTB.85	-1.018
44-	C3H8	HO2		IC3H7	H2O2		+.3390E+13	+0.0	+17.00	WESTB.85	-1.018
45-	C3H8	H		NC3H7	H2		+.5620E+08	+2.0	+7.70	WESTB.84	-0.864
46-	C3H8	H		IC3H7	H2		+.8700E+07	+2.0	+5.00	WESTB.84	-0.864
47-	C3H8	O		NC3H7	OH		+.1120E+15	+0.0	+7.85	WESTB.85	-2.884
48-	C3H8	O		IC3H7	OH		+.2820E+14	+0.0	+5.20	WESTB.85	-2.884
49-	NC3H7			C2H4	CH3		+.9500E+14	+0.0	+31.00	WESTB.84	-2.884
50-	IC3H7			C2H4	CH3		+.2000E+11	+0.0	+29.50	KERR .59	-2.884
51-	NC3H7			C3H6	H		+.1250E+15	+0.0	+37.00	JACKS.61	-2.454
52-	IC3H7			C3H6	H		+.6350E+14	+0.0	+36.90	KERR .59	-2.454
53-	NC3H7	O2		C3H6	HO2		+.1000E+13	+0.0	+5.00	WESTB.84	-2.454
54-	IC3H7	O2		C3H6	HO2		+.1000E+13	+0.0	+5.00	WESTB.84	-2.454
55-	C3H6	OH		C2H5	CH2O		+.7900E+13	+0.0	+0.00	WESTB.85	-1.485

tubes (5). The comparison between the experimental and calculated results is shown in Fig. 1. A fair agreement, generally, in the testing ranges, was observed.

Then, the mechanism was subjected to a sensitivity analysis using the "brute force" method. A sensitivity coefficient,  $S$ , was defined:

$$S = \log |\Delta \tau / \tau| / \log (\Delta k / k)$$

where  $\Delta \tau$  is the change in the ignition delay time,  $\tau$ , due to  $\Delta k$  change in the rate coefficient  $k$ . The sensitivity coefficient in case of stoichiometric propane- $O_2$  mixtures was calculated and tabulated in Table 1. It can be seen that the calculated ignition delay is sensitive to the rate coefficients for the reactions involving  $C_3H_8$ , in particular the thermal decomposition step R(40). There is also a big influence of rate coefficient of chain branching reaction R(8).

The mechanism can reproduce also the burning velocity. Further, when the mechanism used to reproduce the experimental results, obtained from a jet-stirred reactor operated in intermediate temperature range up to 10 atmospheres

(3), the computed results were too far from the experimental ones. However, it can be concluded that the simplified mechanism is only suitable to reproduce global informations and not detail kinetic ones.

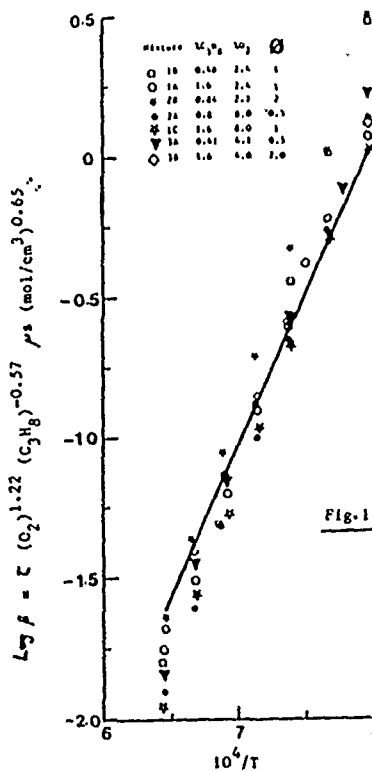


Fig. 1  
Comparison between experimental ignition delay and calculated ones. Solid line from Burcat et al. (1971). Symbols are calculated using the mechanism.

#### REFERENCES

- (1) GERSTEIN M.: NASA CP 2087, 1979.
- (2) JONES W.P. and WHITELAW J.H.: 20<sup>th</sup> Symp. (Intern) on Combustion, 233, The Combustion Institute, Pittsburgh, 1984.
- (3) DGAUT P., CATHONNET M., GAILLARD F., BOETTNER J.C., ROUAN J.P., JAMES H.: Proc. of X<sup>th</sup> I.C.D.E.R.S., A.I.A.A. Journ. to appear.
- (4) BAHN G.S.: NASA, C.R. 2178, n°73 20 932, 1973.
- (5) BURCAT A., LIFSHITZ A., SCHELLER K., SKINNER G.: 13<sup>th</sup> Symp. (Intern) on Combustion, p. 745, The Combustion Institute, Pittsburgh, 1971.

*GAS-PHASE OXIDATION OF BENZENE AND DERIVATIVES; FORMATION AND FURTHER  
CONVERSION OF PHENOLS*

R. Louw and P. Mulder  
Center for Chemistry and the Environment  
Gorlaeus Laboratories, The State University of Leiden  
P.O. Box 9502  
2300 RA LEIDEN, The Netherlands

*ABSTRACT*

The gas-phase oxidation of benzene and derivatives is important in the chemistry of the atmosphere and in combustion. Our study deals with kinetic and mechanistic features of the oxidation of arenes between 400-1000K.

A detailed thermokinetic outline is given for the formation of phenol from benzene, the major arene derived product at low degrees of conversion. Data on the kinetic H/D isotope effect support our mechanistic interpretation.

However, phenol is not a stable compound under the reaction conditions employed. At moderate degrees of oxidative degradation dibenzofuran (DBF) was found to be a major product. DBF and chlorinated DBF's are observed in stack gases of waste incinerators. The mechanism(s) of DBF's will be discussed.

## High-Temperature Propane Oxidation

R.I. Moshkina, S.S. Polyak, L.B. Romanovich

Institute of Chemical Physics, Academy of Sciences of the USSR

Propane oxidation has been studied by the kinetic tracer method (pyrex reactor,  $s/v = 0.7$  and  $12 \text{ cm}^{-1}$ ,  $T = 455^\circ\text{C}$ ,  $p = 170$  torr. About 1 % propylene differently labeled with  $^{14}\text{C}$  was added to an equimolecular propane/ oxygen mixture.

The qualitative composition of radioactive species was:  $\text{C}_3\text{H}_6$ ,  $\text{C}_2\text{H}_4$ ,  $\text{CH}_2\text{O}$ ,  $\text{CH}_3\text{OH}$ ,  $\text{CH}_3\text{CHO}$ ,  $\text{C}_3\text{H}_6\text{O}$ ,  $\text{CH}_3\text{COCH}_3$ , same as for oxidation at  $313^\circ\text{C}$ , but for  $\text{C}_3\text{H}_6$ ,  $\text{C}_2\text{H}_4$ ,  $\text{C}_3\text{H}_6\text{O}$ ,  $\text{CO}_2$  the yields were higher, and for  $\text{CH}_3\text{CHO}$ ,  $\text{CH}_3\text{OH}$  lower. Propylene oxide had one precursor - propylene, while other species were formed both from propane and propylene.

The radioactivity distribution at  $455^\circ\text{C}$  was different from that for low-temperature oxidation - a larger part of  $\text{CH}_3\text{CHO}$ ,  $\text{CH}_2\text{O}$ ,  $\text{CH}_3\text{OH}$ ,  $\text{C}_2\text{H}_4$  were generated by propylene.

Use of the differently labeled propylene revealed its reactivity in  $\text{CH}_3\text{CHO}$ ,  $\text{CH}_2\text{O}$ ,  $\text{CH}_3\text{OH}$ , and  $\text{C}_2\text{H}_4$  formation. The probability of  $\text{CH}_3\text{CHO}$  generation by groups 1-2 and 2-3 was approximately the same. At  $313^\circ\text{C}$  the probability of  $\text{CH}_3\text{CHO}$  formation from groups 1-2 and 2-3 was 0.3 and 0.7, respectively. This suggested that the subsequent propylene reactions were due to addition at the double bond, rather than to formation of allyl radicals.

At  $313^\circ\text{C}$  an increase in  $s/v$  to  $12 \text{ cm}^{-1}$  completely stopped the reaction, while at  $455^\circ\text{C}$  the maximum rate decreased  $\sim 4$ -fold, and the induction period increased  $\sim 3$ -fold. The composition of species and the radioactivity distribution were the same as for an unfilled reactor. It was found from the kinetics of the added acetaldehyde accumulation at  $313^\circ\text{C}$  that in low-temperature propane oxidation  $\text{CH}_3\text{CHO}$  was the branching agent.

## THE INITIAL STAGE OF METHANE OXIDATION AT HIGH PRESSURES

Vedeneev V.I., Goldenberg M.Ya., Gorban' N.I., Teitelboim M.A.

The kinetics of methane oxidation at high pressures has been studied in a number of works, Nobody, however, has specially investigated its initial stage. Nevertheless, the initial stage can markedly affect the course of the process as a whole.

The object of the present work is to construct and analyze on a computer an isothermal kinetic model describing the mechanism of the initial stage of methane oxidation at high pressures ( $P \geq 50$  atm.) and moderate temperatures ( $T \sim 600$  K).

A mechanism has been proposed for the initial stage of the process, represented by a combination of elementary reactions and Arrhenius' expressions for the rate constants of each one of them. The constants of controlling elementary reactions were specially analyzed based on the presently available experimental and theoretical data.

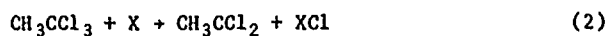
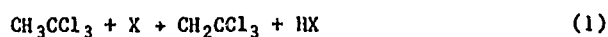
The initial oxidation stage, experimentally revealed as the induction period of a degenerated branching process, has been established to constitute a branching reaction proceeding under certain quasi-stationary conditions characterized by approximate equality of the branching and the quadratic termination rates. The combinations of reactions resulting in chain branching have been ascertained, and the influence of each one of the quadratic reactions on the kinetics of the oxidation process initial stage has been investigated.

The proposed mechanism of the initial stage of methane oxidation qualitatively describes the experimentally revealed kinetic regularities and explains the formation of the principal oxidation products: methanol, formaldehyde and water, but, naturally, does not account for their subsequent transformations, since only the very first stage of the process is involved.

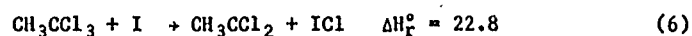
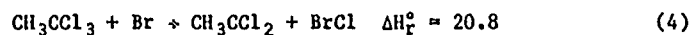
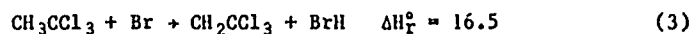
TITLE: Kinetics of the Halogen Catalyzed Elimination of HCL from 1,1,1-Trichloroethane.

AUTHORS: A.S. Rodgers and P. Jerus, Department of Chemistry, Texas A&M University, College Station, Texas 77843 U.S.A.

In the halogen catalyzed elimination of HCL from 1,1,1-Trichloroethane the rate limiting step may be either (1) or (2).

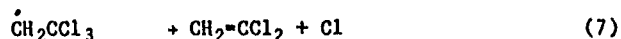
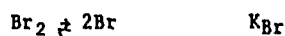


If one estimates the C-H bond dissociation energy in  $\text{CH}_3\text{CCl}_3$  as  $\sim 104$  kcal  $\text{mol}^{-1}$ , based on  $\text{CH}_3\text{CF}_3$ <sup>1</sup>; and the C-Cl bond energy as  $\sim 73$  kcal  $\text{mol}^{-1}$ , based on  $\text{C}_2\text{Cl}_6$ <sup>2</sup>; the thermochemistry of the four possible reactions for  $\text{X}=\text{Br}$  and  $\text{I}$  can be estimated as:



Based on these estimates one would expect the rate limiting steps (and thus the mechanism) to be different for  $\text{Br}_2$  catalysis compared to  $\text{I}_2$  catalysis. These reactions have been studied in the gas phase from 560 to 640 K and their kinetics determined manometrically and stoichiometry verified by g.l.c. analysis.

The reaction of bromine with  $\text{CH}_3\text{CCl}_3$  was first order in  $\text{CH}_3\text{CCl}_3$  and the first order rate constants depended on  $[\text{Br}_2]^{1/2}$ . The amount of  $\text{CH}_2 = \text{CCl}_2$  formed was in good agreement with the increase in pressure ( $\Delta P$ ) for less than 50% conversion and only traces of  $\text{CH}_3\text{CHCl}_2$  was found even when 150 torr of  $\text{HBr}$  was added to the reaction. These data are consistent with the following mechanism for the bromine catalyzed reaction.



For this mechanism; Rate =  $k_3 K_{\text{Br}}^{1/2} (\text{Br}_2)^{1/2} (\text{CH}_3\text{CCl}_3)$ .

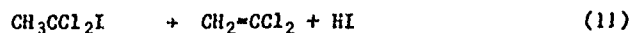
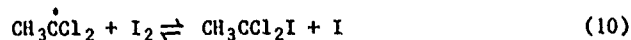
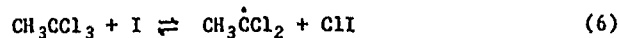
The rate of the reaction was reduced by only 7% when 145 torr of HBr was added to the initial reaction mixture which indicates that  $k_7 \gg k_3 (\text{HBr})$  under the experimental conditions.

From a consideration of similar reactions<sup>1,3-4</sup>, we have interpreted the data obtained for  $k_3$  to yield:  $\log (k_3/\text{M}^{-1}\text{s}^{-1}) = (11.30 \pm 0.3) - (19.94 \pm 0.82)/\theta$  which fits the observed rate constants with an average deviation of 8%.

One can estimate  $E_3 = 3 \pm 1.5 \text{ kcal mol}^{-1}$  from similar reactions<sup>1,3</sup> so that  $\Delta H_3(298) = 16.2 \text{ kcal mol}^{-1}$  and  $\text{DH}^\circ(\text{CCl}_3\text{CH}_2\text{-H}) = \text{DH}^\circ(\text{H-Br}) + 16.2 = 103.7 \text{ kcal mol}^{-1}$ .

In preliminary experiments at 600K it was also found that  $\text{I}_2$  catalyzed the decomposition of  $\text{CH}_3\text{CCl}_3$  to yield  $\text{CH}_2 = \text{CCl}_2$  and  $\text{HCl}$  and that, at less than 50% conversion, the agreement between  $\Delta P$  and the extent of reaction as determined by g.l.c. analysis was excellent. This showed that only the elimination of  $\text{HCl}$  was taking place. However, when  $\text{HI}$  was added to the initial reaction mixture  $d(\Delta P)/dt$  was noticeably decreased and  $\text{CH}_3\text{CHCl}_2$  was a major product. This suggested that reaction (6) rather than (5) was rate limiting and that the mechanism for the  $\text{I}_2$  catalyzed reaction was:





Making the steady state assumption and assuming that reaction(s) (12) will keep the concentration of  $ICl$  low, one then obtains: Rate =  $k_6 K_I^{1/2} (I_2)^{1/2} (CH_3CCl_3)$ .

This is the concentration dependence observed experimentally over an eleven fold variation in  $(CH_3CCl_3)/(I_2)$ . An analyses of the rate data from 565 to 610K resulted in  $\log (k_6/M^{-1}s^{-1}) = (10.65 \pm 0.16) - (23.25 \pm 0.4)/\theta$ . If one assumes that  $E_6 = 0 \pm 1$  kcal mol<sup>-1</sup> based on the results of similar reactions with  $I_2$  and  $Br_2^5$ , then  $\Delta H_6^\circ(298) = 23.5$  kcal mol<sup>-1</sup> and  $DH^\circ(CH_3CCl_2-Cl) = DH^\circ(I-Cl) + 23.5 = 73.8 \pm 1.5$  kcal/mol.

#### References

1. E.C. Wu and A.S. Rodgers, J. Phys. Chem., 78, 2315 (1974).
2. J.A. Franklin, G. Huybrechts and C. Cillien, Trans. Faraday Soc., 65, 2094 (1969).
3. J.C. Amphett and E. Whittle, Trans. Faraday Soc., 64, 2130 (1968).
4. K.D. King, D.M. Golden and S.W. Benson, Trans. Faraday Soc., 66, 2794 (1970).
5. D.F. McMillen and D.M. Golden, An. Rev. Phys. Chem., 33, 493 (1982).

## COMPUTER PROGRAMS AND DATA BASES FOR THE KINETICS OF GAS PHASE REACTIONS

G.M. CÔME, G. SCACCHI, Ch. MULLER, P.M. MARQUAIRE and P. AZAY  
CNRS (UA 328), INPL (ENSIC) et Université de NANCY I

1. Computer programs and data bases have been built for the mechanistic modelling and the simulation of gas phase reactions. Only specific comments on the system (fig. 1) will be given here.

Building the reaction mechanism is achieved by a program, which is able to write the complete list of the primary elementary processes of the reaction from the list of the reactants. Generally, the mechanism is very impressive and should be reduced at the moment by hand. Progresses in this field are expected from expert systems (see below).

The thermochemical data of molecules and free radicals are computed by the methods of the thermochemical kinetics, developed by BENSON. The only data needed for these calculations are the structural formulae of the compounds. In the future, the kinetic parameters will be found in a bibliographic data base and the methods of BENSON for the kinetics will be programmed (see fig. 2) ; the number of data will be increased and the consistency of all types of data (thermochemical, kinetic, bibliographic, computerized) will be checked and improved.

From the mechanism and the associated data, a compiler furnishes the rate laws as a function of current concentrations and temperature.

The above programs and data bases involve the usual problems encountered in computer chemistry : - external and internal coding of chemical structures, reactions and of their properties - algorithms of canonicity, searching for substructures - relational data base operating system.

The simulation of the reaction in a given reactor needs to solve the material, energy and momentum balances. As it is well known, the corresponding algebraic or differential equations remain difficult to solve, because they are very stiff, coupled and non-linear. Various numerical algorithms have been used or tested, from the simplest ones up to more sophisticated.

2. Applications of this system have been achieved in the case of the pyrolysis of neopentane and propane at high temperature, the chlorination of

ethylene (CHLOE Process, ATOCHEM), the thermal reaction of chlorine and methane (BENSON's patent), etc... It has been shown, in the case of neopentane pyrolysis, that the same mechanism accounts for experimental results in the temperature range 700-1300 K and from KNUDSEN pressures to around 1 atm. This is in favour of using such fundamental models for engineering purposes.

### 3. Which is the state of the art in this field ?

One of the first attempts to solve complex reaction mechanisms has been that of EDELSON (BELL Co.). The programs by the NASA and SANDIA laboratories for chemical kinetics (respectively NASAKIN and CHEMKIN) have been developed for simulating reactions and include thermochemical data bases ; these codes are well documented. Another program, SPYRO, specially devoted to pyrolysis reactions, has been developed by KTI. The most prominent feature of this program is its ability to cope with very complex mixtures. This is due to the central concept of lumping both components and reactions.

### 4. What are nowadays the prospects ?

They concern both the kinetic themes and the methodology.

The kinetic themes include both fundamental (elucidation of complex reaction mechanisms, determination of thermochemical data of molecules and free radicals, and of kinetic parameters of elementary processes) and engineering objectives (energy, chemicals, ecology).

The core of the elucidation of complex reaction mechanisms is the generation of the mechanism itself ; the method described here is far from being satisfactory : simultaneously, too much and not enough processes are generated, because no stoichiometric and kinetic knowledges are put in the machine, nor qualitative rules, nor quantitative laws or data, so that the generating system works blindfold. The way for doing better is an expert system, of which a general scheme is shown in the figure 3. Among others, knowledges such as stoichiometric and kinetic experimental results, thermochemical and kinetic data, rules for writing elementary reactions and building reaction mechanisms, rules of lumping, etc..., have to be taken into account.

The determination of quantitative data by the methods of BENSON has been achieved for thermochemistry, the work for kinetics is to be done.

Further more increments (see fig. 2) and improvements in the fields of oxidation and combustion are needed.

As concerns engineering prospects, the state of the art in gas phase reactions permits us to use a mechanistic modelling for solving such problems as improving conversion, selectivity and energy saving on existing plants, designing new processes for producing chemicals.

Mechanistic modelling also occurs in ecology, for example in meteorology and in safety. Regarding this last point, our thermochemical program has been extended to CHETAH calculations.

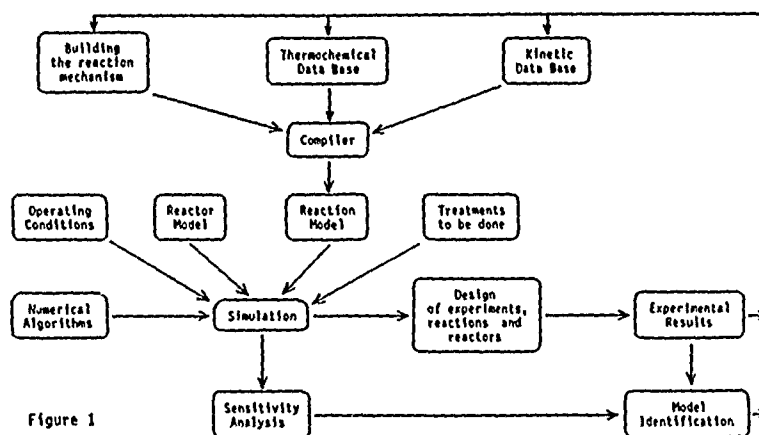


Figure 1

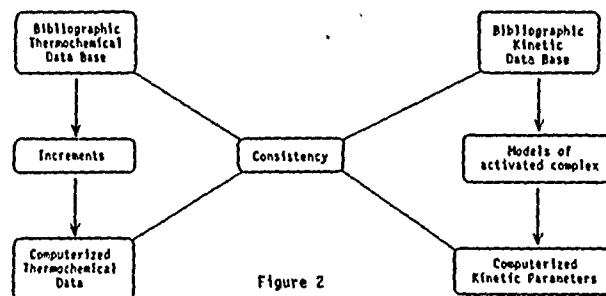


Figure 2

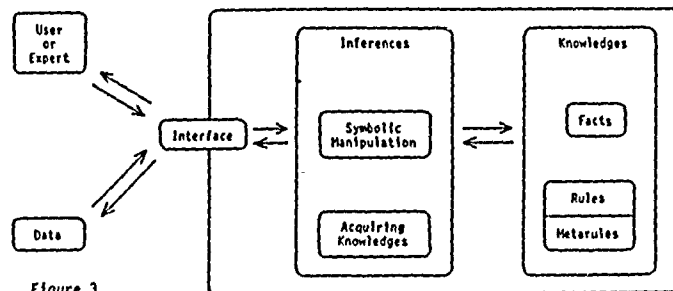


Figure 3

## THE THERMAL DECOMPOSITION OF n-HEXANE

by Freddy E. Imbert and Roger M. Marshall.

University College of Swansea, Swansea SA2 8PP. United Kingdom.

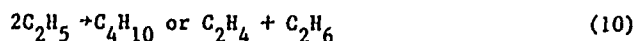
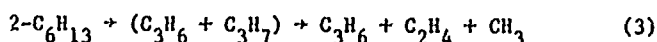
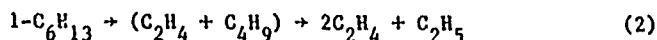
The initial stages ( $\sim 2\%$  reaction) of the thermal decomposition of n-hexane have been investigated in the ranges 723-823 K and 10-100 Torr using a conventional static system with gas chromatographic analysis of the hydrocarbon products. A typical distribution of product yields (Torr) is shown below for the pyrolysis of 50 Torr of n-hexane for 20 seconds at 798 K.

$\text{CH}_4$	$\text{C}_2\text{H}_6$	$\text{C}_2\text{H}_4$	$\text{C}_3\text{H}_6$	$1-\text{C}_4\text{H}_8$	$1-\text{C}_5\text{H}_{10}$	$\text{H}_2$
0.434	0.189	0.494	0.376	0.207	0.063	0.051

[The yield of hydrogen is calculated so as to maintain the C/H balance].

Plots of product yield against reaction time are linear, i.e. there is no sign of the self-inhibition as observed for several other alkanes.

It is shown that the overall mechanism is



From the data on the rate of ethane formation, we estimate

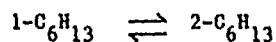
$$\log(k_g/\text{cm}^3 \text{ mol}^{-1} \text{ s}^{-1}) = 13.30 - 17.9 \text{ kcal mol}^{-1}/(2.3 \text{ RT})$$

which provides the familiar curved Arrhenius plot when combined with published data for both lower and higher temperatures. From data on product

yields, we obtain the relative yields of products from reactions (2)-(5) i.e. decompositions of  $C_6H_{13}$  isomers to be

$$(2) : (3) : (4) : (5) \simeq 1 : 9 : 1.3 : 4.7$$

with a small temperature dependence. The relative proportion of the products arising from 1- and 2- $C_6H_{13}$  is in marked contrast to the corresponding proportions in n-butane pyrolysis of about 1 : 3. We conclude that isomerisation via a strain-free, 6-membered, cyclic transition state

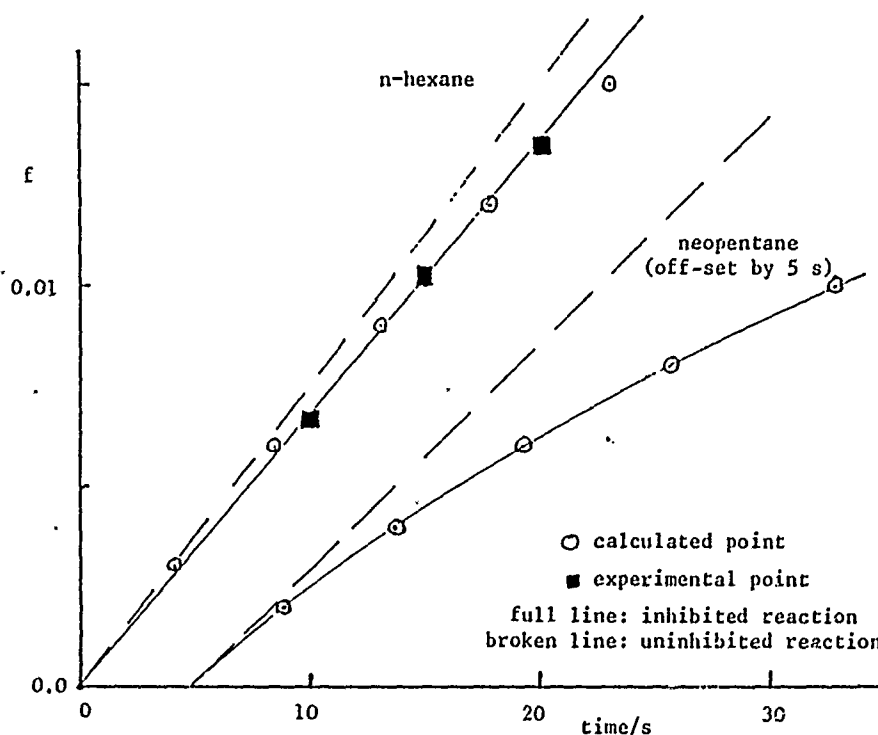


occurs giving the roughly 1:10 equilibrium proportions of 1- and 2- $C_6H_{13}$  estimated by us. This conclusion is supported by estimates which suggest that the isomerisation is about an order of magnitude faster than the competing decomposition process. Any isomerisation involving 3- $C_6H_{13}$  would, at best, involve a strained 5-membered, cyclic, transition state. Simple estimates suggest that this isomerisation has a rate comparable with or perhaps somewhat slower than the competing decomposition. Thus no definite conclusion can be drawn concerning the significance, if any, of this type of isomerisation.

The absence of self-inhibition in the pyrolysis of n-hexane and in that of n-butane is in marked contrast to the strong self-inhibition by the olefin products observed in the pyrolyses of several other alkanes. To investigate this phenomenon further we have made a detailed comparison of the pyrolyses of n-hexane and of neopentane. The self-inhibition of the latter is due mainly to the abstraction of allylic H from the product isobutene by the chain carrying radical,  $CH_3$ , the resultant resonance stabilised radical then becoming involved in termination reactions. We have calculated the effect of a similar mechanism on the pyrolysis of n-hexane. In this case only  $C_3H_6$  and 1- $C_4H_8$  are relevant products since, while 1- $C_5H_{10}$  does have allylic H, the resultant pentenyl radical can unimolecularly decompose with loss of  $CH_3$  and thus cannot lead to inhibition.

By making sensible (we hope!) assumptions about the reactivity of  $C_2H_5$  towards allylic H, we estimate for 798 K and 50 Torr n-hexane

$(\text{Inhibited rate})/(\text{Uninhibited rate}) = 1/(1 + 20f)$  where  $f$  is the fractional extent of reaction which may be compared with the ratio  $1/(1 + 117f)$  which we estimate from published data for neopentane in the same conditions. The implications of these two expressions are illustrated in the diagram as plots of  $f$  against reaction time for the stated conditions. For neopentane a pronounced curve is obtained whereas for n-hexane, the curvature is so slight that the experimental results are very well fitted by a straight line even though, as illustrated, there is some inhibition of the reaction. The fundamental reason for the difference lies in the fact that  $C_2H_5$  is much less reactive than  $CH_3$  towards abstraction of H.



Chain kinetics in igniting hydrocarbon-air mixtures studied by transient  
OH fluorescence following photolytic perturbation

C. Morley and L.J. Kirsch

Shell Research Ltd., Thornton Research Centre, P.O. Box 1, Chester,  
CH1 3SH, UK

The chemistry leading to autoignition of hydrocarbon-air mixtures is complex but a simplified model of the kinetics has been developed [1, 2] which can account for much of the observed behaviour below about 850 K. This has recently been extended [3] by improving the interpretation in terms of fundamental chemistry for alkanes but even so a number of important parameters are empirically fitted (in a non-unique way) from ignition delay measured in a rapid compression machine. The present work uses a new experimental method to verify the general features of the model and to determine its parameters experimentally.

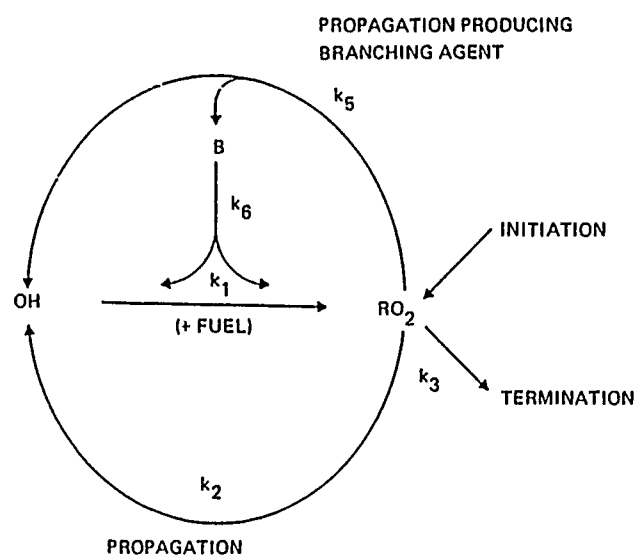
Cool flames in n-heptane air mixtures have been stabilised at atmospheric pressure on a flat flame burner. The mixture is heated in a few tens of milliseconds by passing through an electrically-heated porous board made of sintered metal fibres. A cool flame develops downstream sometimes followed by a second stage of ignition. OH was detected by fluorescence induced by an excimer pumped doubled dye laser at 282 nm. Initial experiments found unexpectedly large OH signals from the region between the cool flame and the second stage of ignition. However, the signal was found to be dependent on the square of the laser intensity suggesting that the OH was being produced photolytically. At low intensities natural OH with a fluorescence signal proportional to the laser intensity could be detected with a sharply peaking concentration in the cool flame, as expected.

By detecting the OH with a second lower powered dye laser fired a variable time after the first the decay of OH back to its steady state



concentration following its photolytic production could be observed. A similar perturbation method has previously been used in hot flames by Chou and Dean [4]. By observing the dependence of the signal on the wavelength of the photolysis laser the photolytic species was shown to be a peroxide, probably hydrogen peroxide. In the post cool flame region the OH decay could be fitted over a thousand fold drop in concentration to the sum of 3 exponentials. The interpretation is in terms of the generalised model [1, 3] shown in the figure. The initial fast decay is ascribed to the reaction of OH with the fuel ( $k_1$ ). The second slow decay is essentially determined by the termination rate ( $k_3$ ) after the OH and  $RO_2$  have equilibrated. The slowing to the third rate is caused by decomposition of the branching agent ( $k_6$ ) becoming significant. The results show that the kinetic chains are short, with the propagation, termination and branching rates all of comparable size. This contrasts with earlier formulations of the model [1-3] but is consistent with the conclusions of Baldwin et al [5]. The experimentally determined rates were consistent with those derived from literature rate constants where these were available.

1. M.P. Halstead, L.J. Kirsch, A. Prothero, C.P. Quinn, Proc. Roy. Soc. Lond. A346 515 (1975)
2. M.P. Halstead, L.J. Kirsch, C.P. Quinn, Combust. Fl. 30 45 (1977).
3. R.A. Cox, J.A. Cole, Combust. Fl. 60 109 (1985).
4. M.S. Chou, A.M. Dean, Int. J. Chem. Kinet. 17 1103 (1985).
5. R.R. Baldwin, G.R. Drewery, R.W. Walker, J.C.S. Farad II 82 251 (1986).



Chemical mechanism for initial stages of hydrocarbon oxidation

## MODELING NITRIC OXIDE FORMATION IN COMBUSTION\*

James A. Miller  
Combustion Research Facility  
Sandia National Laboratories  
Livermore, CA 94550

### ABSTRACT

Nitric oxide formation under lean combustion conditions is well understood and can be predicted accurately by the Zel'dovich, or thermal, NO mechanism. However, complications arise under rich conditions and when nitrogen is chemically bound in the fuel. These situations have in common the feature that hydrogen cyanide is formed as an intermediate.

The development of a kinetic model that accurately describes NO formation under a wide range of conditions requires a close interaction among modeling, theory, and experiment. This paper will describe such an interaction. Particular topics to be covered include

- 1) modeling nitric oxide formation in well-stirred reactors,
- 2) the conversion of  $HCN$  to  $NO$  and  $N_2$  in low-pressure  $H_2/O_2/Ar - HCN$  flames,
- 3) hydrocarbon/nitric-oxide interactions in low pressure flames,
- 4) the theoretical prediction of the rate coefficients for  $O + HCN \rightarrow$  products and  $OH + HCN \rightarrow$  products.

\* Research sponsored by the U.S. Department of Energy, Office of Basic Energy Sciences, Division of Chemical Sciences.

## MODELLING OF THE GAS PHASE FREE RADICAL CHEMISTRY OF THE PLASMA

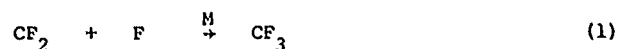
ETCHING PROCESS:  $\text{CF}_4$  AND  $\text{CF}_4/\text{O}_2$  MIXTURESI.C. Plumb and K.R. Ryan

CSIRO Division of Applied Physics, Sydney, Australia 2070

Although plasmas of  $\text{CF}_4$  and mixtures of  $\text{CF}_4$  with  $\text{O}_2$  are used widely for the etching of semiconductors, the chemistry of these plasmas is not well understood. A model has been developed which places emphasis on the gas phase free radical reactions occurring in these plasmas and the calculations of the model are compared with the experimental results of Smolinsky and Flamm [1].

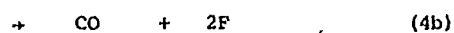
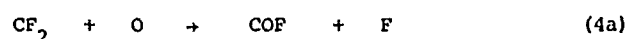
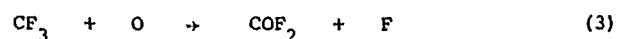
Important requirements for the model are dissociation rates and branching ratios for the dissociation paths. Electron impact dissociation rates for  $\text{CF}_4$  and  $\text{O}_2$  have been deduced from the experimental measurements of consumption of  $\text{CF}_4$  and  $\text{O}_2$  in  $\text{CF}_4/\text{O}_2$  plasmas as a function of feed gas composition and flow rate. Dissociation rates for other species have been calculated relative to  $\text{CF}_4$  where cross-section data are available, or set equal to the  $\text{CF}_4$  dissociation rate where no data are available. The dissociation paths for  $\text{CF}_4$  have been deduced from a knowledge of the free radical reaction rates and the stable product distribution observed downstream of a radio-frequency discharge by Smolinsky and Flamm. It is concluded that  $\text{CF}_2$  is a direct product of electron impact of  $\text{CF}_4$  and that its rate of production is about twice that of  $\text{CF}_3$ . This direct formation of  $\text{CF}_2$  from  $\text{CF}_4$  rather than by electron impact dissociation of  $\text{CF}_3$  is an important feature of the model.

For  $\text{CF}_4$  plasmas, the amount of  $\text{CF}_4$  consumed is low because gas phase reactions between F and both  $\text{CF}_2$  and  $\text{CF}_3$  lead to the rapid re-forming of  $\text{CF}_4$  [2]



The effect of reactions (1) and (2) under conditions appropriate to plasma etching is to hold the concentrations of  $\text{CF}_3$ ,  $\text{CF}_2$  and F virtually constant over a wide range of flow rates. When Si is added to the plasma, the model predicts only minor changes in the concentrations of the major species in the discharge but significant changes to the stable products observed downstream.

In  $\text{CF}_4/\text{O}_2$  plasmas, rapid gas phase reactions between O atoms and both  $\text{CF}_3$  and  $\text{CF}_2$  [3,4]



allow the F concentration to increase, which is in accord with experimental observations. The model is able to predict the trend of the experimental results as the mixture composition and flow rate are changed. The agreement for concentrations of the observed stable products CO,  $\text{CO}_2$  and  $\text{COF}_2$  is generally better than a factor of two over a wide range of experimental conditions. Although the molecular fluorine concentrations predicted by the model are lower than those observed experimentally, the total amount of fluorine produced (F and  $\text{F}_2$ ) is in good agreement and it is suggested that

atomic fluorine may have been combining on the surface of the sampling pinhole in the experiments of Smolinsky and Flamm.

A total of 49 gas phase reactions were included in the model for  $\text{CF}_4/\text{O}_2$  plasmas. However, it can be shown that only 13 have important effects on the results of the modelling. Five of these are electron impact dissociation processes and the remaining eight are free radical reactions. Of the eight important free radical reactions, the rate coefficients for all except one are well established.

For both  $\text{CF}_4$  and  $\text{CF}_4/\text{O}_2$  plasmas, the calculations of the model are in good agreement with the experimental data over a wide range of experimental conditions. This confirms the importance of gas phase free radical reactions in these plasmas.

#### REFERENCES

1. G. Smolinsky and D.L. Flamm, J. Appl. Phys. 50, 4982 (1979)
2. I.C. Plumb and K.R. Ryan, Plasma Chem. Plasma Process. 6, 11 (1986)
3. K.R. Ryan and I.C. Plumb, J. Phys. Chem. 86, 4678 (1982)
4. K.R. Ryan and I.C. Plumb, Plasma Chem. Plasma Process. 4, 271 (1984)

REACTION OF  $\text{CF}_3$  RADICALS ON  $\text{SiO}_2$  and Si SURFACES BETWEEN 300-600 K  
Robert Robertson, Michel J. Rossi, and David M. Golden, Department of Chemical  
Kinetics, SRI International, Menlo Park, CA 94025

The reaction between  $\text{CF}_3$  radicals and the surfaces of interest were studied in a VLP flow reactor whose total pressure was kept in the millitorr range. The  $\text{CF}_3$  radicals were generated from  $\text{CF}_3\text{I}$  both by UV (248 nm) and IR-multiphoton photolysis, and the subsequent gas-phase reaction products were followed by mass spectrometry and by in situ REMPI (resonance-enhanced multiphoton ionization) of  $\text{CF}_3$ . The surface reaction was found to yield CO, HF,  $\text{CO}_2$ ,  $\text{COF}_2$  and  $\text{SiF}_4$ . The  $\text{H}_2\text{O}$  level was greatly reduced in comparison to our earlier studies (to 1%), nevertheless, hydrogen-containing products were clearly observable, indicating that trace amounts of water readily react with  $\text{CF}_3$ .

The kinetics of homogeneous  $\text{CF}_3$  recombination, which we also measured under our conditions on an absolute basis, served as the "clock" for the surface reactions. The rates for the irreversible surface loss of  $\text{CF}_3$  and for the formation of CO and other surface reaction products were measured as a function of temperature of the substrate surface, and a simple Langmuir-type kinetic model was used to describe the heterogeneous reactions, which are competing with homogeneous gas-phase chemistry.

The REMPI studies of  $\text{CF}_3$  indicate the real-time behavior of the radical in the presence of the hot surface and directly obtain the sticking coefficient of  $\text{CF}_3$ . We believe these values to be of great fundamental and practical interest as they represent the first values for sticking coefficients of radicals that were obtained in a direct way.

Abdalla A.Y. : 163  
Abel B. : 114  
Achiba Y. : F2  
Adewuyi V.G. : C4  
Aguilar A. : E6  
Aguillon F. : E8  
Aker P.M. : A6  
Alberti M. : 11  
Alberty R.A. : E58  
Allen J.E. : 123  
Alvariño J.M. : E1, E5  
Aoiz F.J. : B3  
Aquilanti V. : D4, E7  
Arseneau D.J. : E33  
Astbury C.J. : 139  
Atkinson R. : C2  
Avila M.J. : 12  
Ayscough P.B. : E55  
Azay P. : J2  
  
Back M.H. : E64  
Back R.A. : 156  
Baer T. : D8  
Baggott J.E. : D2, 141  
Baldwin R.R. : H2  
Balla R.J. : G3  
Barat M. : B7  
Barnes I. : 131  
Baronnet F. : 162  
Bartolomé P. : E18  
Basterrechea F.J. : E1  
Bastian V. : 131  
Batt L. : E48, 153, 154  
Baughcum S.L. : E40  
Baulch D.L. : E55, 129

Bayes K.D. : 142  
Becker K.H. : 131, 142  
Bedjanian Y.R. : E65, 150  
Beneventi L. : E7  
Benoist d'Azy O. : 18  
Beral J.M. : E63  
Bércecs T. : E3, E57, G2  
Biggs P. : 121  
Billaud F. : E61  
Binkley J.S. : 152  
Black G. : 137  
Boettner J.C. : E52, 163  
Bofill J. : E6, 11  
Böhland T. : H7  
Boodaghians R.B. : 134  
Bossard A.R. : 128, 133  
Bourguignon B. : E9  
Bowman J.M. : A3  
Braun W. : 117  
Braun-Unkhoff M. : E62  
Breckenridge W.H. : B1, 18  
Brenot J.C. : B7  
Brezinsky K. : 158  
Brobst W.D. : 123  
Brouard M. : 143  
Browarzik R. : E12  
Brown M.A. : F6  
Brown N.J. : A5  
Brown T.C. : 113  
Brunning J. : E35  
Bulatov V.P. : 138  
Bunn T.L. : D8  
Burke R.R. : E27  
Burkholder J.B. : C6  
Burrows J.P. : E51



Butkovskaya N.I. : E31

Campbell I.M. : I29

Campargue R. : E8

Canosa-Mas C. : E44

Cantin M. : E39

Carlier M. : E53

Caralp F. : E47

Carr R.W. : I20

Cartwright P.C. : F6

Castafio F. : I10

Castella M. : I7

Castillejo M. : E18

Cathonnet M. : E52, I63

Caubet P. : B2

Cavalli S. : D4

Chakir A. : E52

Chamboux J. : I59

Chandler D.W. : I11

Cheskis S.G. : F5

Chinnick S.J. : E55

Chrzaścik I. : E24, E25

Cohen N. : I4

Côme G.M. : J2

Copeland R.A. : E21

Costes M. : B2

Cox R.A. : C1, E42, E51

Crim F.F. : D1

Crosley D.R. : E21

Cvetanovic R.J. : I17, I25

Dagaut P. : E52, I63

Davies J.M. : E42

Davidovits P. : C4

Deakynne C.A. : G8

Deson J. : E11

Devolder P. : I30

Dóbbé S. : G2

Dagnon A.M. : E47

Donovan R.J. : E22, F6

Dorthe G. : B2

Dove J.E. : E4

Droege A.T. : H3

Dryer F.L. : I58, I61

Duguay B. : B6

Dunning Jr. T.H. : A3

Dupeyrat G. : G7

Durup-Ferguson M. : B7

Duval M.C. : B1, I8

Dyer P.E. : I16

Dyet J.A. : E14

Eley C.D. : E50

Endo Y. : G4

Ewig F. : E23

Fahr A. : I48

Faraji F. : I47

Farantos S.C. : E20

Farrow R.L. : I11

Fayeton J. : B7

Ferguson E.E. : G6

Figuera J.M. : E18, I2

Fleming D.G. : E33

Fleming J.W. : H6

Forges H. : I26

Forst W. : D3

Foryś M. : E24, E25

Fotakis C. : E20, E26

Foucaut J.F. : I55

Frank P. : E62	Hancock G. : I39
Freund E. : E61	Harding L.B. : I5
Frey H.M. : E50, I41	Harris S.J. : I27
Furue H. : E30	Hartmann D. : I35
	Hartree W.S. : I9
Gaillard F. : E52, I63	Hayman G.D. : E42
Garcia E. : E5	Héberger K. : I24
Gardner J. : C4	Heiss A. : I51
Garner D.M. : E33	Herrero V.J. : B3
Gargoura M.A. : E9	Herron J.T. : I25
Gauyacq J.P. : I6	Herzog B. : I14
Gédra A. : I35	Heydtmann H. : A6
Gershenson Y.M. : A2, E65, I50	Hippler H. : I14
Gilbert R.G. : D5, I13	Hirota E. : G4
Gislason E.A. : E2	Holbrook K.A. : I16
Golden D.M. : I15, J7	Holdsworth F.J. : I21
Goldenberg M.Y. : E49, I3, I66	Honma K. : F2
Goldsmith J.E.M. : H3	Hontzopoulos E. : E10, E26
Gonzalez A.C. : I15	Horie O. : E36
González M. : E6, I1	Houston P.L. : F4
González Ureña A. : B3	Houwer J.C. : B7
Gorban' N.I. : I66	Howard C.J. : C6, C7
Grossi G. : D4, E7	Howard J.B. : I18
Grotheer H.H. : E59	Husain D. : E19, E29
Gui-Yung Chung : I20	Hynes A.J. : C7
Guo-Ying Xu : D3	
Guo-zhong He : B4	Ichimura T. : E13
Gutman D. : H1, I44	Ilin S.D. : A2
	Imbert F.E. : J3
Hack W. : E38	Iogansen A.A. : F5
Hackett P.A. : E39	Ivanov A.V. : A2
Hall I.W. : I34	
Halpern J.B. : I49	James H. : E52
Halvick P. : B6	Jeffries J.B. : E21
Hammer P.D. : C6	Jerus P. : J1

Johnson K. : B5  
Jolly G.S. : I28  
Joseph T. : E4  
Jourdain J.L. : C5  
Jouvet C. : B1, I8  
Jue Wang : B4  
Jusinski L.E. : I37  
Just Th. : E54, E59

Kaes A. : E12  
Kajimoto O. : F2  
Kaufman V. : I17  
Keiffer M. : G5  
Kemény S. : I24  
Kenner R.D. : E12  
Kerr E.A. : E22  
Kerr J.A. : I27  
Kimura K. : F2  
King K.D. : I13  
Kirsh L.J. : J4  
Kishkovitch O.P. : E65, I50  
Kleinermanns K. : F3  
Klemm R.B. : E34, E37  
Koda S. : G4  
Kohse-Höbginghaus K. : E54  
Kolb C.E. : C4  
Körtvélyesi T. : I45  
Kozliner M.Z. : I38  
Kucheryavii S.I. : A2  
Kulakov P.V. : F5  
Kvaran A. : B5, I9

Lafage C. : E32, I30  
Laganá A. : E1, E5  
Lahmani F. : E10

Lalo C. : E11  
Langridge-Smith P.R.R. : F6  
Larin I.K. : E28  
László B. : E3  
Laufer A.H. : I48  
Law D.W. : D2  
Lawley K.P. : F6  
Lebéhot A. : E8  
Le Bras G. : C5, E43  
Lee L. : E33  
Lempereur F. : E11  
Lendvay G. : E3  
Leone S.R. : F1  
Lesclaux R. : E47  
Levitsky A.A. : I3  
Lifshitz C. : D7  
Lightfoot P.D. : D2, I41  
Lim K.F. : D5  
Lin M.C. : H6  
Löhmansröben H.G. : D6  
Longwell J.P. : I18  
Lourme D. : I58  
Louw R. : I64  
Lovejoy E.R. : C7  
Lüdviksson A. : I9  
Luther K. : D6

Maas U. : E56  
MacKay M. : I53  
Malegat L. : I6  
Mandy M.E. : E4  
Marquaire P.M. : J2  
Marquette J.B. : G7  
Marshall P. : E29  
Marshall R.M. : J3

Marston G. : I21  
Márta F. : G2  
Martin D. : C5  
Martin M. : E18  
Martin R. : E63  
Martínez E. : I10  
Martínez M.T. : I10  
Marx J. : E8  
Masanet J. : E11  
Mayama S. : I12  
McAdam K. : E51, H2, I26  
McCombie J. : E9  
McCoustra M.R.S. : E14  
McKendrick K.G. : I39  
McKenney D.J. : I28  
McLaren I. : E27  
McMillen D.F. : I15  
Medina J. : I2  
Meier U. : E54  
Melius C.F. : A5, I52  
Mellouki A. : E43  
Meriaux B. : E32  
Mialocq J.C. : E16  
Michael J.V. : H8  
Mikula R.J. : E33  
Miller A. : J5  
Miller G.E. : I49  
Miller J.A. : A5  
Mills I.M. : D2  
Mitchell M. : E35  
Mitchell S.A. : E 39  
Miyokama K. : I47  
Molina M.J. : I36  
Monot R. : E17  
Moorgat G.K. : E51

Mori Y. : E13  
Morley C. : J4  
Morozov I.I. : E31  
Morrow J.C. : D8  
Moshkina R.I. : I65  
Mulder P. : I64  
Muller Ch. : J2  
Munro I. : E22  
  
Nacsá Á. : I46  
Nan-quan Lou : B4  
Naulin C. : B2  
Nelson H.H. : I22  
Nelson L. : I32  
Nesbitt F.L. : E34, E37  
Nicovich J.M. : C7, E41  
Niefer B. : A6  
Nielsen O.J. : I32  
Nigenda S.E. : I15  
Nishi N. : E13  
Nouchi G. : B2  
  
Obi K. : I12  
Ohmichi N. : D7  
Oldenborg R.C. : E40  
Oldershaw G.A. : I16  
Olesik S. : D8  
Orr B.J. : A7  
Ozenne J.B. : B7  
  
Pacey P.D. : E30  
Pagsberg P. : I32  
Palmieri P. : E5  
Papagiannakopoulos P. : E15, E20  
Paraskevopoulos G. : I28, I33

Parlant G. : E2  
Pasternack L. : G3  
Paulson J.F. : G9  
Pauwels J.F. : E53  
Payne W. : E35  
Peeters J. : H5  
Peres T. : D7  
Perrin D. : E64  
Perry R.A. : I40  
Pettrich K.G. : E23  
Pfab J. : E14  
Philippos J.M. : E17  
Pilling M.J. : G5, I43  
Pitts J.N. : C2  
Piuze F. : I7  
Plane J.M.C. : E29  
Plumb I.C. : J6  
Potakis C. : E10  
Polak L.S. : I3  
Polyak S.S. : I65  
Pötzinger P. : E36  
Poulet G. : E43  
Pri-Bar I. : D7

Radom L. : D7  
Ravishankara A.R. : C7, E41  
Rayez J.C. : B6  
Rayez M.T. : B6  
Rayner D.M. : E39  
Rebrion C. : G7  
Reid I.A.B. : I53

Reid I.D. : E33  
Reihls K. : D6  
Reimann B. : E36  
Reimer A. : C3  
Rhäsa D. : I35  
Richard C. : E63  
Riekert G. : E59  
Rigny R. : I51  
Roberts G. : E19  
Robertson R. : J7  
Rodgers A.S. : J1  
Rodríguez J.C. : I2  
Rohrer F. : E12, F7  
Romanovich L.B. : I65  
Rossi M.J. : J7  
Rostas J. : E9  
Rouveirolles P. : E38  
Rowe B.R. : G7  
Rowe M.C.A. : E50  
Rozenshtein V.B. : A2, E65, I50  
Russell J.J. : I44  
Ryan K.R. : J6

Sáez Rábanos V. : B3  
Sahetchian K.A. : I51, I59  
Salomon D.R. : I47  
Sarkisov O.M. : F5, I38  
Sathiyamurthy N. : E4  
Saunders S.M. : I29  
Sawerysyn J.P. : E32  
Sayós R. : E6, I1  
Scacchi G. : I55, I62, J2  
Schaeckers M. : H5  
Scheer M.D. : I17  
Scherer Jr, K.V. : I54

Schmitt D. : I58  
Schneider M. : I57  
Schneider W. : E51  
Segall J. : I19  
Senba M. : E33  
Seres L. : I45, I46  
Shanahan I. : E45  
Sharfman L. : C4  
Shaw C.J. : I16  
Shaw D. : E22  
Shinohara H. : E13  
Shobatake K. : F2  
Sidebottom H. : I32  
Simon Y. : I55  
Simons J.P. : B5, I9  
Singleton D.L. : I28, I33  
Sizun M. : E2  
Sloan J.J. : A6  
Smalley J.F. : E34, E37  
Smith G.P. : H4  
Smith I.W.M. : A7, E46  
Smith M.J.C. : G5  
Smith P.A. : B5  
Smith S.J. : E44  
Sochet L.R. : E53, I30  
Soep B. : B1, I8  
Solgadi D. : E10  
Stachnik R.A. : I36  
Stephenson J.C. : E16  
Stewart P. : E48, I53, I54  
Stief L. : E35  
Stuhl F. : E12, F7  
Suntz R. : F3  
Sutherland J.W. : H8  
Szamrej I. : E24, E25

Taieb G. : E9  
Talrose V.L. : E28, E31  
Tardieu de Maleissye J. : E11, I51  
Teillet-Billy D. : I6  
Teitelboim M.A. : E49, E66  
Temps F. : H7  
Tighezza A. : E32  
Timonen R.S. : I44  
Titov A.A. : F5  
Toby S. : E44  
Tramer A. : I7  
Treacy J. : I32  
Troie J. : A4, I14  
Truhlar D.G. : A1  
Tschuikov-Roux E. : I47  
Tse R.S. : B4  
Tsuchiya S. : G4  
Tuckett R.P. : A7  
Tully F.P. : H3  
Turányi T. : E57  
Tyndall G.S. : E51  
  
Umanskii S.Y. : A2, I3  
  
Vajda S. : E57  
Van den Bergh H. : E17  
Vandooren J. : E60  
Vanpee M. : I59, I60  
Van Tiggelen P.J. : E60  
Vasiliyev E.S. : E31  
Vaucamps C. : B2  
Vecchiocattivi F. : E7  
Vedeneev V.I. : E49, I3, I66  
Vegiri A. : E20

Verdasco E. : B3  
Veyret B. : E51, I26  
Vidóczy T. : I24  
Viggiano A.A. : G8  
Vinckier C. : H5  
Viossat V. : I59  
Vogin B. : I62

Wagner A.F. : A3, I5  
Walker R.W. : H2  
Wallington T.J. : C2  
Walravens B. : E60  
Walsh R. : E50, I41  
Wang N.S. : C7  
Warnatz J. : E56  
Watts I.M. : E50  
Wayne R.P. : E44, I21, I34  
Weiner B.R. : I22  
Weller R. : I57  
Westmoreland P.R. : I18  
Wiesen P. : I42  
Wilkinson J.P.T. : E22  
Wine P.H. : C7, E41  
Winer A.M. : C2  
Witte F. : C8  
Wofford J. : I57  
W D.R. : C4

Yamaa C 4  
Yarwood G. : .46  
Yetter R.A. : I61

Zabarnick S. : H6  
Zabel F. : C3  
Zahniser M.S. : C4

Zare R.N. : I19  
Zellner R. : E23, G1, I35  
Zetzsch C. : C8  
Zevgolis D. : E15

**THE 9th INTERNATIONAL SYMPOSIUM ON GAS KINETICS**  
**has been sponsored by :**

- Aérospatiale
- British Gas
- British Petroleum Company plc.
- Centre National de la Recherche Scientifique
- Commissariat à l'Energie Atomique (CEN-Saclay-DPC)
- Communauté Urbaine et Ville de Bordeaux
- Conseil Régional d'Aquitaine
- Electricité de France
- Elf Aquitaine - SNEA(P)
- Gaz de France
- IBM France
- ICI plc.
- Institut Français du Pétrole
- Lambda Physik
- Ministère de la Défense (DRET)
- Ministère de l'Environnement
- Photon Science Instruments
- Quantel
- Shell Research Ltd.
- Société Européenne de Propulsion
- SOPRA
- Université de Bordeaux I
- US Army - European Research Office
- USAF - European Office of Aerospace Res. and Develop.
- US Naval Research - Branch Office, London

*We gratefully acknowledge the financial assistance  
given by these organisations.*